LEABHARLANN CHOLÁISTE NA TRÍONÓIDE, BAILE ÁTHA CLIATH | TRINITY COLLEGE LIBRARY DUBLIN
Ollscoil Átha Cliath | The University of Dublin

Terms and Conditions of Use of Digitised Theses from Trinity College Library Dublin

Copyright statement

All material supplied by Trinity College Library is protected by copyright (under the Copyright and Related Rights Act, 2000 as amended) and other relevant Intellectual Property Rights. By accessing and using a Digitised Thesis from Trinity College Library you acknowledge that all Intellectual Property Rights in any Works supplied are the sole and exclusive property of the copyright and/or other IPR holder. Specific copyright holders may not be explicitly identified. Use of materials from other sources within a thesis should not be construed as a claim over them.

A non-exclusive, non-transferable licence is hereby granted to those using or reproducing, in whole or in part, the material for valid purposes, providing the copyright owners are acknowledged using the normal conventions. Where specific permission to use material is required, this is identified and such permission must be sought from the copyright holder or agency cited.

Liability statement

By using a Digitised Thesis, I accept that Trinity College Dublin bears no legal responsibility for the accuracy, legality or comprehensiveness of materials contained within the thesis, and that Trinity College Dublin accepts no liability for indirect, consequential, or incidental, damages or losses arising from use of the thesis for whatever reason. Information located in a thesis may be subject to specific use constraints, details of which may not be explicitly described. It is the responsibility of potential and actual users to be aware of such constraints and to abide by them. By making use of material from a digitised thesis, you accept these copyright and disclaimer provisions. Where it is brought to the attention of Trinity College Library that there may be a breach of copyright or other restraint, it is the policy to withdraw or take down access to a thesis while the issue is being resolved.

Access Agreement

By using a Digitised Thesis from Trinity College Library you are bound by the following Terms & Conditions. Please read them carefully.

I have read and I understand the following statement: All material supplied via a Digitised Thesis from Trinity College Library is protected by copyright and other intellectual property rights, and duplication or sale of all or part of any of a thesis is not permitted, except that material may be duplicated by you for your research use or for educational purposes in electronic or print form providing the copyright owners are acknowledged using the normal conventions. You must obtain permission for any other use. Electronic or print copies may not be offered, whether for sale or otherwise to anyone. This copy has been supplied on the understanding that it is copyright material and that no quotation from the thesis may be published without proper acknowledgement.

Front-end analogue filter design for diagnostic electrocardiographic equipment

Roberta Dozio

Thesis submitted for the degree of

Doctor of Philosophy

Department of Electronic and Electrical Engineering
University of Dublin, Trinity College



April 2013

TRINITY COLLEGE
2 4 MAY 2013
LIBRARY DUBLIN

Thesis 9900

Declaration

I declare that this thesis has not been submitted as an exercise for a degree at this or any other university and it is entirely my own work.

I agree to deposit this thesis in the University's open access institutional repository or allow the library to do so on my behalf, subject to Irish Copyright Legislation and Trinity College Library conditions of use and acknowledgement.

Summary

This thesis addresses the design of an analogue front-end filter for portable electrocardiographic equipment. The task of the filter is to eliminate as much out-of-band noise and interference as possible before the electrocardiogram is further processed. In order to guarantee that the filter does not significantly distort the input signal, the requirements specified by international standards and recommendations for the time and frequency domain characteristics of diagnostic electrocardiographic devices are strictly enforced throughout this work.

Since the spectrum of the ECG signal extends over more than two decades, the design of the lowpass and highpass sections of filter can be approached separately. As regards the lowpass filter, several all-pole transfer functions are analysed. Their performance is compared with regard to passband flatness, out-of-band rejection, in-band group delay variation and amplitude of the step response overshoots. From this analysis, it emerges that linear phase with equiripple error and equiripple impulse overshoot filters represent a suitable alternative to the Bessel characteristic commonly employed for the implementation of the lowpass filter. It is suggested that fourth or sixth order equiripple filters with 3dB-cutoff point equal to 150 Hz are employed to minimise the chance of aliasing occurring when the electrocardiogram is digitised at the minimum frequency allowed by the standards.

Attention is then focused on the highpass section. Since the specifications set by the standards and recommendations for the low-frequency response of ECG recording equipment are extremely stringent, only one analogue solution has ever been proposed for the highpass filter. It consists of a single-pole network having a 3dB-cutoff frequency of 0.05 Hz, which has become the benchmark for assessing the performance of other analogue highpass systems for electrocardiographic applications. On the other hand, numerous digital techniques have been developed over the years for the reduction of low-frequency noise in ECG records. The frequency and time domain characteristics of a number of FIR filters are tested for compliance with the standards, which surprisingly are satisfied by only one of the systems analysed.

The possibility of designing an analogue highpass filter suitable for diagnostic applications that provides better rejection of the low-frequency noise than the 0.05 Hz single-pole

network is then investigated. At first, the derivation of the highpass transfer function is attempted using lowpass-to-highpass transformations and conventional compensation techniques, but this approach does not prove successful. An optimisation procedure is therefore devised to maximise the low-frequency attenuation of second and third order highpass filters and implemented in MATLAB®. The requirements set by the standards and recommendations on the time and frequency domain responses are expressed as constraints in the optimisation algorithm and the objective function is selected in turn as: the stopband limit, the 3dB-cutoff frequency and the area subtended by the magnitude response of the filter. The results obtained in the last two cases, which are quite similar, represent an improvement over the reference 0.05 Hz system. The 3dB-cutoff frequencies of the second and third order optimised filters are as high as 0.07 Hz and 0.12 Hz, respectively.

Following this, the distortion introduced by the optimised filters into synthetic and real electrocardiographic recordings is evaluated and compared with that associated with the 0.05 Hz single-pole system. Both the test waveforms and the criteria employed to assess the distortion are derived from the standards, whereas the ECG records are taken from an annotated database available on PhysioNet. The ability of the various highpass filters to eliminate the low-frequency noise and interference is then evaluated by measuring the reduction of the power contained in electrocardiographic records at frequencies lower than the ECG spectrum. This technique is applied to three noise records accessible on PhysioNet and to the ECG recordings previously used in the distortion analysis. A third order filter designed to have a concave magnitude response over the transition region and characterised by a 0.09 Hz 3dB-cutoff frequency is found to provide the best trade-off between time domain distortion and noise rejection capabilities. The percentage reduction in noise power achieved by this filter can be up to 40% higher than that of the reference 0.05 Hz network and the distortion it introduces into synthetic ECG waveforms is lower than for any of the other highpass filters.

Finally, the possibility of employing a single-amplifier circuit for the implementation of the complex conjugate poles and zeros of this third order concave filter is examined. The sensitivity of the structure to variations in the passive components is evaluated and the values of its resistors and capacitors are selected in such a way that the variability in the location of poles and zeros is minimised. A Monte Carlo simulation of the time and frequency domain characteristics of the third order filter is then performed assuming a 1% uniformly distributed tolerance in the components. Based on this analysis, the constraints set during the optimisation procedure are revised to allow for the variability in the system responses. The third order concave filter derived from the optimisation procedure when these revised conditions are imposed is characterised by a 3dB-cutoff frequency approximately 7% lower than that of the original system.

In memory of Bernadette

Acknowledgements

I would like to express my sincere thanks to:

Dr Martin J. Burke for giving me the opportunity to work under his supervision and for his guidance and advice throughout this project;

IRCSET (Irish Research Council for Science, Engineering and Technology) for funding this work during the first three years;

Professor Frank Boland for his feedback on my transfer report;

All the technical and administrative staff in the Department of Electronic and Electrical Engineering for being so approachable and always helping me without hesitation;

Ms Bernadette Clerkin for all her help and kind support: it meant a lot to me;

Adeshina, Cedric, Gavin and Craig for sharing interesting research ideas;

Everybody who worked in the top floor lab of the Printing House for creating a great atmosphere;

My friends in Ireland and Italy for all the good times together and for making me smile when I needed it most;

My parents and sister for their constant encouragement and for being there, always;

Manuel for his strength, help and support: thanks for standing next to me every day.

Contents

List of Figures xvii

List of Tables xxvii

Nomenclature xxxv

1 Introduction 1

1.1 Importance of the electrocardiogram 1

1.2 ECG signal quality 2

1.3 Aim of the project 3

1.4 Thesis overview 4

2 ECG signal 7

2.1 The heart and cardiovascular system 7

2.2 ECG generation and measurement 8

2.2.1 Body surface potentials 9

2.2.2 Skin-electrode interface 12

2.2.3 12-lead system 14

2.2.4 Measurement equipment 18

2.3 Electrocardiographic waveform 19

2.3.1 Heart electrical activity 19

2.3.2 ECG time profile 21

2.3.3 ECG frequency content 24

2.4 Noise and interference 25

2.4.1 In-band noise 26

2.4.2 Out-of-band noise 31

2.4.3 Discussion 32

3 ECG filter characteristics and requirements 35

3.1 Introduction 35

3.2 AHA recommendations 36
3.2.1 Review of the AHA recommendations 36
3.2.2 Rationale behind the recommendations 38
3.3 Current international standards 41
3.3.1 European and American standards 41
3.3.2 Comparison of standards and recommendations 43
3.4 Analysis of the pulse response constraints 45
3.4.1 Possible relation between pulse area and constraints 45
3.4.2 Pulse response of a single-pole highpass filter 46
3.4.3 Reformulation of time domain constraints 51
3.5 Filter phase response 55
3.5.1 Review of the phase linearity requirement 55
3.5.2 Comparison of phase and pulse response requirements 57
3.5.3 Analysis of a bidirectional filter 58
3.6 Alternative test of the filter response 62
3.7 Conclusion 65

4 Lowpass filter design **67**
4.1 Introduction 67
4.2 Lowpass filter requirements 67
4.3 Overview of classic responses 69
4.3.1 Butterworth 70
4.3.2 Gaussian 72
4.3.3 Bessel 74
4.3.4 Linear phase with equiripple error 74
4.3.5 Equiripple impulse overshoot 77
4.4 Verification of the system requirements 82
4.4.1 Comparison between responses 82
4.4.2 Response to a triangular input wave 84
4.5 Considerations regarding the sampling frequency 85
4.6 Conclusion 89

5 Preliminary analysis for the highpass filter design **91**
5.1 Introduction 91
5.2 Highpass filter requirements 92
5.3 Digital techniques for baseline wander removal 95
5.4 FIR filters for ECG applications 98

5.4.1 Recursive filter with integer coefficients (Ahlstrom and Tompkins, 1985) 99
5.4.2 FIR filter with a reduced number of impulse response coefficients (Van Alste et al., 1985) . . . 102
5.4.3 FIR filter implemented without the use of multipliers (Raita-aho et al., 1994) . . . 103
5.4.4 Moving average filter . . . 106
5.4.5 Averaging $D \times N$ filter (Tabakov et al., 2008) . . . 107
5.4.6 Frequency and time domain constrained filter (Henzel, 2005) . . . 108
5.5 Analogue implementations for the reduction of low-frequency noise and interference . . . 110
5.6 Lowpass-to-highpass transformations . . . 113
5.6.1 Classic H(1/s) transformation . . . 113
5.6.2 1-H(s) transformation . . . 115
5.6.3 Discussion . . . 116
5.7 Analogue compensation techniques . . . 118
5.7.1 Allpass network . . . 118
5.7.2 Pole-zero network . . . 120
5.7.3 Lag-lead network . . . 123
5.8 Conclusion . . . 128

6 Highpass filter design **133**
6.1 Introduction . . . 133
6.2 Optimisation procedure . . . 135
6.2.1 Objective function . . . 137
6.2.2 Constraints definition . . . 139
6.2.3 Further constraints . . . 141
6.2.4 Algorithm description . . . 142
6.2.5 Starting point . . . 145
6.3 Optimisation of the stopband limit with the 3dB-cutoff frequency being fixed at 0.05 Hz . . . 148
6.4 Optimisation of the stopband limit . . . 155
6.5 Optimisation of the 3dB-cutoff frequency . . . 162
6.6 Optimisation of the overall low-frequency attenuation . . . 176
6.7 Analysis of the convergence of the optimisation algorithm . . . 181
6.8 Conclusion . . . 182

7 Validation of the highpass filter design **187**
7.1 Introduction . . . 187
7.2 Distortion analysis for synthetic ECGs . . . 189
7.2.1 Input test signals . . . 189
7.2.2 Results and discussion . . . 191
7.3 Distortion analysis for real ECGs . . . 197
7.3.1 Preprocessing of the ECG records . . . 197
7.3.2 Results and discussion . . . 201
7.4 Reduction of the low-frequency noise . . . 206
7.5 Conclusion . . . 212

8 Circuit topology for the third order highpass filter **215**
8.1 Introduction . . . 215
8.2 Analysis of the sensitivity of the time and frequency responses to changes in the filter parameters . . . 216
8.3 Friend's single-amplifier biquad topology . . . 220
8.4 Sensitivity analysis of Friend's circuit and selection of component values . . . 222
8.5 Monte Carlo simulation of the highpass filter . . . 229
8.6 Redesign of the third order highpass filter . . . 234
8.7 Conclusion . . . 236

9 Conclusion **241**
9.1 Overview . . . 241
9.2 Contributions of this work . . . 243
9.3 Recommendations for standards and test signals . . . 244
9.4 Further work . . . 246

References **249**

Publications **267**

Appendix A **269**
A.1 Study of the first derivative of the magnitude response of the second order filter 269
A.2 Chebyshev and Elliptic lowpass filters . . . 271
A.2.1 Chebyshev filter . . . 271
A.2.2 Elliptic filter . . . 272
A.3 Complete results of the optimisation procedure . . . 274
A.3.1 Optimisation of the 0.05 Hz second order filter . . . 274
A.3.2 Optimisation of the 0.05 Hz third order filter . . . 277

A.3.3 Optimisation of the stopband limit 282
A.3.4 Optimisation of the 3dB-cutoff frequency 287
A.3.5 Optimisation of selected points in the filter transition region 292
A.3.6 Optimisation of the overall low-frequency attenuation 301

Appendix B **305**
B.1 Synthetic ECG waveforms 305
B.2 Power spectrum of the bw record 308
B.3 Error introduced by the highpass filters into selected records of the QT database 309
B.4 Change in the ST segment slope introduced by the highpass filters into the records of the QT database 314
B.5 Noise reduction achieved by the highpass filters for selected records of the QT database 320

Appendix C **327**
C.1 Sensitivity of Friend's circuit 327
C.2 Results of the optimisation procedure 330

List of Figures

2.1 Diagram of the cardiovascular system. 8
2.2 Schematic diagram showing the mechanisms underlying ECG recording. . . 9
2.3 Typical waveform of the transmembrane potential of an excitable cell undergoing stimulation. 10
2.4 Equivalent dipole associated with the depolarisation of the atria. 11
2.5 Diagram of the skin-electrode interface and its equivalent electrical circuit. . 13
2.6 Lead vectors for limb and chest leads. 15
2.7 Standard placement of limb and precordial electrodes for ECG monitoring in hospital settings. 16
2.8 Circuit associated with Wilson's central terminal. 17
2.9 Schematic diagram of a single channel ECG recording system. 18
2.10 Electrical conduction system of the heart. 20
2.11 Different phases of the cardiac cycle. 20
2.12 12-lead electrocardiogram measured on a healthy subject. 22
2.13 Waves and intervals of a normal lead II ECG signal. 22
2.14 Normalised power spectrum of the overall ECG signal, QRS complex and P and T waves. 25
2.15 Spectrum of noise and artifacts in exercise electrocardiograms. 26
2.16 Power line interference. 27
2.17 Ringing artifacts introduced after the QRS complex by a steep notch filter aimed at removing power line noise. 28
2.18 Electromyographic noise. 28
2.19 Effect of a 40 Hz lowpass filter on a noisy ECG waveform. 29
2.20 Comparison between the power spectrum of motion artifacts and that of the QRS complex. 30
2.22 Electrode contact noise. 31
2.23 Respiratory artifact. 31
2.24 Baseline drift. 32

3.1 Frequency response requirements for electrocardiographic equipment, as outlined in the AHA reports. 37
3.2 Time domain requirements set by the 1990 AHA recommendations for electrocardiographic filters. 38
3.3 Error introduced by a first order 0.05 Hz highpass filter for a 3.33 mV$\times$300 ms rectangular input pulse. 40
3.4 Specifications for the magnitude response of ECG measurement systems detailed in the European standard EN 60601-2-51:2003. 42
3.5 Triangular wave for testing the high-frequency response of electrocardiographs according to the European standard EN 60601-2-51:2003. 42
3.6 Requirements for the pulse response of ECG recording systems as specified by the European standard EN 60601-2-51:2003. 43
3.7 Requirements for the amplitude response of diagnostic ECG devices as defined by the American standard ANSI/AAMI EC11:1991/(R)2001/(R)2007. . 44
3.8 Response of a 0.05 Hz first order highpass filter to a set of rectangular input pulses, having equal area but different durations. 49
3.9 Triangular pulse. 50
3.10 Response of a 0.05 Hz first order highpass filter to a set of rectangular and triangular input pulses having equal area. 52
3.11 Artifactual elevation of the ST segment produced by an ambulatory electrocardiographic device. 56
3.12 Diagram illustrating how the bidirectional filter $b(t)$ is derived from the base filter $h(t)$. 59
3.13 Magnitude response of a first order highpass filter having 3dB-point at 0.25 Hz and of the bidirectional filter constructed from it. 61
3.14 Error introduced by a 0.25 Hz first order highpass system and by the bidirectional filter derived from it when a 3.33 mV$\times$300 ms rectangular pulse is applied at the input. 61
3.15 Typical shape of a calibration ECG signal. 62
3.16 Calibration signals used to test the electrocardiograph response according to the EN 60601-2-51:2003 standard. 63

4.1 Requirements set for the magnitude response of the lowpass ECG filter. . . 68
4.2 Time and frequency domain characteristics of Butterworth filters of order 2 $\leq n \leq$ 6 with 3dB-cutoff at 150 Hz. 71
4.3 Time and frequency domain characteristics of Gaussian filters of order 2 $\leq n \leq$ 6 with 3dB-cutoff at 150 Hz. 73

4.4 Time and frequency domain responses of Bessel filters of different orders having 150 Hz 3dB-bandwidth. 75
4.5 Error function for the Chebyshev approximation of a linear phase response. 77
4.6 Time and frequency domain characteristics of filters having linear phase with equiripple error (ϵ = 0.5°) of order $2 \leq n \leq 6$ for a 3dB-cutoff frequency of 150 Hz. 78
4.7 Phase characteristic of filters having linear phase with equiripple error (ϵ = 0.5°) of order $2 \leq n \leq 6$ for a 3dB-cutoff frequency of 150 Hz. 79
4.8 Time and frequency domain characteristics of 1% equiripple impulse overshoot filters of order $2 \leq n \leq 6$ having a 150 Hz bandwidth. 80
4.9 Typical impulse response of an equiripple impulse overshoot filter of order n = 5. 81
4.10 Group delay characteristic of 1% equiripple step overshoot filters of order $2 \leq n \leq 6$ for a 3dB-cutoff of 150 Hz. 82
4.11 Input triangular test waves and corresponding output signals for a 150 Hz 6th order Bessel filter. 85
4.13 Amplitude response of different 6th order filters having 150 Hz as 3dB-cutoff. 88

5.1 Magnitude response of two single-pole highpass networks with 3dB-point located at 0.05 Hz and 0.1 Hz, respectively, and of a second order highpass filter obtained by cascading two equal first order sections and having 0.05 Hz cutoff frequency. 93
5.2 Displacement from the isoelectric line and recovery slope after the application of a 3 mV$\times$100 ms rectangular pulse at the input of two single-pole highpass networks with 3dB-point located at 0.05 Hz and 0.1 Hz, respectively, and of a second order highpass filter obtained by cascading two equal first order sections and having 0.05 Hz cutoff frequency. 94
5.3 Structure of the adaptive filter for baseline wander removal proposed by Thakor and Zhu. 96
5.4 Non-recursive implementation of an FIR filter. 98
5.5 Pole-zero configuration of a lowpass integer filter for N = 8. 99
5.6 Magnitude and phase response of the recursive filter with integer coefficients proposed by Ahlstrom and Tompkins and of the lowpass filter from which it is derived. 100
5.7 Response of the recursive filter proposed by Ahlstrom and Tompkins to a 3 mV$\times$100 ms rectangular pulse. 101
5.8 Magnitude response of the non-recursive filter designed by Van Alste et al.. 103

5.9 Pulse response of the non-recursive filter proposed by Van Alste et al.. . . . 104
5.10 Low-frequency amplitude characteristic of the recursive FIR filter proposed by Raita-aho et al. and of the intermediate filters used in its design. 105
5.11 Magnitude response of the recursive FIR filter designed by Raita-aho et al.. 105
5.12 Response of the recursive FIR filter designed by Raita-aho et al. to a 3 mV$\times$100 ms rectangular pulse. 106
5.13 Amplitude response of a highpass moving average filter with a window length N = 7601 for a sampling frequency of 500 Hz. 107
5.14 Amplitude characteristic of the averaging 10$\times$17 filter proposed by Tabakov et al. for a sampling frequency of 250 Hz. 109
5.15 Response of the 10$\times$17 averaging filter described by Tabakov et al. to a 3 mV$\times$100 ms rectangular input pulse. 109
5.16 Magnitude characteristic of the filter designed by Henzel by constraining its frequency and time domain responses. 111
5.17 Response of the filter proposed by Henzel to a 1.5 mV$\times$80 ms input triangular wave. 111
5.18 Amplitude characteristic, group delay and step response of highpass Bessel filters of order n = 2, obtained using the classic H(1/s) transformation and the 1-H(s) transform proposed by Blinchikoff and denormalised to have a 3 dB loss at 0.05 Hz. 114
5.19 Magnitude response of highpass Bessel filters of different order, obtained through the 1-H(s) transformation and denormalised so that the 3dB-point corresponds to 0.05 Hz. 116
5.20 Displacement from the isoelectric line occurring in the response of highpass Bessel filters of order n = 2 and 0.05 Hz cutoff frequency after the application of a 3 mV$\times$100 ms rectangular input pulse. 117
5.21 Phase response of highpass Bessel filters of order n = 2, obtained using the classic H(1/s) transformation and the 1-H(s) transformation and denormalised to have 3 dB attenuation at f = 0.05 Hz. 118
5.22 Group delay of first and second order allpass filters for ω_0 = 1 rad/s. 119
5.23 Passive implementation of lead and lag networks. 121
5.24 Magnitude and phase response of a lead and a lag network for α = 0.2 and $\omega' = \omega''$ = 1 rad/s. 122
5.25 Passive realisation of a lag-lead network. 124
5.26 Magnitude and phase response of a passive lag-lead network for ω_1 = 1 rad/s and ω_2 = 3 rad/s, when $C_1 = C_2$. 125

5.27 Amplitude characteristic of the system obtained by cascading a second order Bessel 1-H(s) highpass filter and a compensating lag-lead network. 129
5.28 Displacement from the isoelectric line and absolute value of the recovery slope of the response of the system obtained by cascading a second order Bessel 1-H(s) highpass filter and a compensating lag-lead network after the application of a 3 mV×100 ms rectangular input pulse. 130

6.1 Mask showing the limits imposed on the filter magnitude response during the optimisation process. 142
6.2 Magnitude characteristic of second order Butterworth and Chebyshev filters having 3dB-cutoff frequency equal to 0.037 Hz and displacement from the isoelectric line occurring after the application of a 3 mV×100 ms rectangular pulse at their inputs. 146
6.3 Magnitude characteristic of third order Butterworth, Chebyshev and Elliptic filters having 3dB-cutoff frequency equal to 0.021 Hz and displacement from the isoelectric line occurring after the application of a 3 mV×100 ms rectangular pulse at their inputs. 147
6.4 Magnitude response of the 0.05 Hz second and third order filters, optimised for a stopband attenuation of 40 dB. 150
6.5 Displacement from the isoelectric line and absolute value of the recovery slope after the application of a 3 mV×100 ms rectangular pulse at the input of the 0.05 Hz second and third order optimised filters. 151
6.6 Phase response of the 0.05 Hz second and third order filters, optimised for a stopaband attenuation A_s = 40 dB. 152
6.7 Magnitude response of the 0.05 Hz second and third order filters optimised for different values of stopband attenuation. 154
6.8 Amplitude characteristic and displacement from the isoelectric line occurring after the application of a 3 mV×100 ms rectangular input pulse for the 0.05 Hz second order filters optimised for different values of maximum allowable pulse response overshoot. 156
6.9 Amplitude characteristic and displacement from the isoelectric line occurring after the application of a 3 mV×100 ms rectangular input pulse for the 0.05 Hz third order filters optimised for different values of maximum allowable pulse response overshoot. 157
6.10 Amplitude response of the second and third order filters obtained by optimising the stopband limit for different values of minimum required attenuation. . 159

6.11 Displacement from the isoelectric line occurring after the application of a 3 mV$\times$100 ms rectangular pulse at the input of the second and third order filters obtained by optimising the stopband limit for different values of minimum required attenuation. 160
6.12 Absolute value of the slope following the application of a 3 mV$\times$100 ms rectangular pulse at the input of the second and third order filters obtained by optimising the stopband limit for different values of minimum required attenuation. 161
6.13 Magnitude response of the second and third order filters obtained by maximising the 3dB-cutoff frequency. 164
6.14 Diagram exemplifying constraint c_{10}, which requires the magnitude response of the third order filter to be lower than that of the reference 0.05 Hz single-pole system in the transition region. 165
6.15 Amplitude characteristic of the third order filter obtained by maximising the 3dB-cutoff frequency when the magnitude response is constrained to be lower than that of the 0.05 Hz single-pole network in the transition region. . . 166
6.16 Amplitude characteristic of the third order filter obtained by maximising the 3dB-cutoff frequency when its magnitude is constrained to be concave outside the passband. 168
6.17 Magnitude response of the third order concave filter and its first and second derivatives, shown for a linear frequency scale. 169
6.18 Displacement from the isoelectric line and absolute value of the recovery slope occurring after the application of a 3 mV$\times$100 ms rectangular pulse at the input of the second and third order filters derived by maximising the 3dB-cutoff frequency. 170
6.19 Phase response of the second and third order filters derived by maximising the 3dB-cutoff frequency. 171
6.20 Magnitude response of the second and third order filters obtained by maximising the frequency at which different critical attenuations are reached in the transition region. 173
6.21 Displacement from the isoelectric line occurring after the application of a 3 mV$\times$100 ms rectangular pulse at the input of the second and third order filters derived by maximising the frequency at which different critical attenuations are reached in the transition region. 174

6.22 Absolute value of the recovery slope occurring after the application of a 3 mV×100 ms rectangular pulse at the input of the second and third order filters derived by maximising the frequency at which different critical attenuations are reached in the transition region. 175
6.23 Diagram showing the area that is being maximised when the optimisation of the overall low-frequency attenuation is performed. 177
6.24 Magnitude response of the second and third order filters obtained by maximising the overall low-frequency rejection, shown for linear amplitude and frequency scales. 178
6.25 Phase response of the second and third order filters derived by maximising the overall low-frequency rejection. 178
6.26 Amplitude characteristic of the second and third order filters obtained by maximising the overall low-frequency rejection. 179
6.27 Displacement from the isoelectric line and absolute value of the recovery slope after the application of a 3 mV×100 ms rectangular pulse at the input of the second and third order filters obtained by maximising the overall low-frequency rejection. 180

7.1 Test waveform obtained from the parameters of the CAL20000 signal when the QRS complex is modelled by a triangular wave. 190
7.2 Test waveform obtained from the parameters of the CAL20000 signal when the QRS complex is modelled by a sinusoidal wave. 190
7.3 Synthetic electrocardiographic signal obtained by periodising the test ECG derived from the parameters of the CAL20000 waveform when the QRS complex is modelled by a triangular wave at a heart rate of 60 bpm. 191
7.4 Initial transient occurring when the third order concave filter is applied to the signal generated by adding a 500 μV DC offset to the synthetic test signal derived from the CAL20000 waveform. 192
7.5 Error introduced by the third order concave filter into the test signal derived from the CAL20000 parameters. 193
7.6 Magnitude characteristic of the highpass bidirectional filters derived from a 0.1 Hz single-pole network and from second and third order 0.15 Hz Butterworth filters. 198
7.7 Displacement from the isoelectric line and slope of the response of the highpass bidirectional filters derived from a 0.1 Hz single-pole network and from second and third order 0.15 Hz Butterworth filters to a 3 mV×100 ms rectangular input pulse applied at t = 10 s. 199

7.8 Excerpt from record sel47 (lead A). 203
7.9 Response of the reference 0.05 Hz first order network and of the optimised highpass filters to an input signal obtained by adding a 0.025 Hz sinusoid of 2 mV amplitude to the synthetic test ECG derived from the CAL20000 parameters 207
7.10 Power spectral density of the em record (lead A). 210

8.1 Magnitude characteristic of the third order concave filter obtained by maximising the 3dB-cutoff frequency and displacement from the isoelectric line occurring after the application of a 3 mV$\times$100 ms rectangular pulse at its input.217
8.2 Distributions of the frequency and Q-factor of the poles and zeros of the third order filter for which either the passband peak or the amplitude of the pulse response undershoot is in the 95th percentile. 219
8.3 Friend's single-amplifier circuit. 221
8.4 Maximum theoretical percentage change in the Q-factor of the poles and zeros of Friend's circuit for C_2/C_1 varying between 1 and 10 when n_2 = 0.91. 229
8.5 Magnitude characteristic of the 3000 iterations of the third order concave filter obtained by simulating a 1% uniformly distributed tolerance in the 11 passive circuit components and displacement from the isoelectric line occurring after the application of a 3 mV$\times$100 ms rectangular input pulse. 232
8.6 Magnitude characteristic of the third order concave filter designed to have a pulse response undershoot of less than 95 µV and displacement from the isoelectric line occurring after the application of a 3 mV$\times$100 ms rectangular pulse at its input. 235
8.7 Magnitude characteristic of the 3000 iterations of the third order filter designed to have a pulse response undershoot of less than 95 µV obtained by simulating a 1% tolerance in the circuit components and displacement from the isoelectric line occurring after the application of a 3 mV$\times$100 ms rectangular input pulse. 238

A.1 Amplitude characteristic of normalised Chebyshev filters with passband ripple equal to 0.5 dB. 272
A.2 Magnitude characteristic of normalised Elliptic filters having a passband ripple of 0.5 dB and a minimum stopband attenuation of 40 dB. 273

B.1 Test waveform obtained from the parameters of the CAL20002 signal when the QRS complex is modelled by a triangular wave. 305

B.2 Test waveforms obtained from the parameters of the CAL20100, CAL20110 and CAL20160 signals when the QRS complex is modelled by a triangular wave. 306
B.3 Test waveforms obtained from the parameters of the CAL20200 and CAL20500 signals when the QRS complex is modelled by a triangular wave. 307

List of Tables

3.1 Parameters employed for the triangular wave test by different European standards. 42
3.2 Specifications set on the magnitude response of the ECG filter by the 1990 AHA recommendations and current international standards. 45
3.3 Geometry of the input pulse and specifications for the output signal as described in different standards and recommendations. 46
3.4 Maximum displacement introduced by a 0.05 Hz single-pole highpass filter for different input signals. 48
3.5 Features of the calibration waveforms. 64

4.1 Amplitude of the maximum overshoot in the step response of Butterworth filters. 70
4.2 In-band group delay variation for a 1% equiripple step overshoot filter. 82
4.3 Frequency and time domain properties of the lowpass filters under analysis, for a 3dB-bandwidth of 150 Hz. 83
4.4 Output amplitude reduction of the narrow triangular wave (20 ms) with respect to the reference wave (200 ms) for various 4th and 6th order filters, all having 150 Hz 3dB-bandwidth. 85
4.5 Out-of-band attenuation characteristics of the lowpass filters under analysis, for a 3dB-bandwidth of 150 Hz. 87
4.6 Location of the poles $(-\alpha_k \pm j\beta_k)$ of the 6th order equiripple impulse and of the 4th order linear phase with equiripple error filters having 3dB-cutoff equal to 150 Hz. 90

5.1 Maximum displacement from the isoelectric line occurring in the pulse response of highpass Bessel filters of different orders, when their 3dB-cutoff frequency is equal to 0.05 Hz. 117
5.2 Sets of parameters defining the passive lag-lead network that were tested to compensate the magnitude response of the highpass filter (C_1 = 100 nF). . 127

5.3 Combinations of component values that allow the standards' requirements for ECG filtering to be fulfilled by the responses of the cascade of the lag-lead network and the highpass filter. 128

6.1 Results obtained by optimising the stopband limit of the 0.05 Hz second and third order filters for A_s = 40 dB. 149
6.2 Optimisation results obtained for the 0.05 Hz second and third order filters for different levels of minimum stopband attenuation. 153
6.3 Results obtained by optimising the stopband limit of the 0.05 Hz second and third order filters (A_s = 40 dB) for different values of maximum allowable pulse response overshoot. 158
6.4 Optimisation results obtained for the second and third order filters for different levels of minimum stopband attenuation. 162
6.5 Results obtained by optimising the 3dB-cutoff frequency of the second order filter. 163
6.6 Results derived by optimising the 3dB-cutoff frequency of the third order filter when the amplitude response is forced to be lower than that of the reference single-pole network. 167
6.7 Results obtained by maximising the frequency at which different selected attenuations are achieved by the second and third order filters in the transition region. 172
6.8 Results obtained by maximising the overall rejection of the filter at low frequencies. 177

7.1 Settling times of the second and third order filters obtained through the optimisation procedure and of the reference 0.05 Hz single-pole network. 191
7.2 Distortion introduced by the second and third order highpass filters and by the 0.05 Hz single-pole network into the test signals obtained from the parameters of the calibration waveforms when the QRS complex is modelled as a triangular wave. 194
7.3 Distortion introduced by the second and third order highpass filters and by the 0.05 Hz single-pole network into the test signals obtained from the parameters of the calibration waveforms when the QRS complex is modelled as a sinusoid. 195
7.4 Average distortion introduced by the second and third order highpass filters and by the 0.05 Hz single-pole network into the synthetic test signals. 196

7.5 Measurement of the power contained in bw record at frequencies lower than 0.5 Hz before and after the application of the bidirectional filters obtained from a 0.1 Hz first order system and 0.15 Hz second and third order Butterworth filters. 201
7.6 Statistics of the error introduced by the second and third order optimised filters and by the 0.05 Hz single-pole network into the records of the QT database. 203
7.7 Statistics of the change in the ST segment slope introduced by the second and third order optimised filters and by the 0.05 Hz single-pole network into the records of the QT database. 206
7.8 Power measured for the noise records of the MIT-BIH Noise Stress Test database. 208
7.9 Measurement of the power contained in the noise records of the MIT-BIH Noise Stress Test database at frequencies lower than 0.5 Hz after they have been filtered using the highpass systems under analysis. 209
7.10 Average low-frequency power and noise reduction obtained for the noise records of the MIT-BIH Noise Stress Test database when they are filtered using the different highpass systems. 210
7.11 Average low-frequency power and percentage noise reduction obtained for selected records of the QT database when they are filtered using the different highpass systems. 211

8.1 Parameters of the transfer function of the third order concave filter. 218
8.2 Theoretical maximum percentage changes that can affect the frequency and Q-factor of the poles and zeros of Friend's circuit for different values of the high-frequency gain n_2 and of the ratios C_2/C_1 and G_B/G_A. 227
8.3 Values of Friend's circuit components calculated for n_2 = 0.91, when C_2 = 100 nF and R_C = 1 MΩ. 228
8.4 Theoretical maximum percentage changes that can affect the frequency and Q-factor of the poles and zeros of Friend's circuit for n_2 = 0.91, $1 \leq C_2/C_1 \leq 3$ and $0.009 \leq G_B/G_A \leq 0.091$ (C_2 = 100 nF and R_C = 1 MΩ). 230
8.5 Values of Friend's circuit components calculated for n_2 = 0.91 and C_2/C_1 = 2.13, when C_2 = 100 nF and R_C = 1 MΩ. 230
8.6 Theoretical and practical resistances and capacitances required for the implementation of the third order concave filter and corresponding values for the frequency and Q-factor of the poles and zeros. 231

8.7 Frequency and Q-factor of the poles and zeros of the simulated third order filter that presents the largest pulse response undershoot. 233
8.8 Maximum and minimum values of the frequency and Q-factor of the poles and zeros measured from the 3000 simulations performed for the tolerance of the circuit components. 233
8.9 Parameters of the transfer function of the third order concave filter designed to have a pulse response undershoot of less than 95 μV. 236
8.10 Theoretical maximum percentage changes that can affect the frequency and Q-factor of the complex conjugate poles and zeros of the third order filter designed to have a pulse response undershoot of less than 95 μV (n_2 = 0.91, C_2 = 100 nF and R_C = 1 MΩ). 237
8.11 Values of Friend's circuit components calculated for the third order filter designed to have a pulse response undershoot of less than 95 μV (n_2 = 0.91, C_2/C_1 = 2.13, when C_2 = 100 nF and R_C = 1 MΩ). 237
8.12 Values of resistors and capacitors that can be employed for the implementation of the third order filter designed to have a pulse response undershoot of less than 95 μV. 238

A.1 Results obtained by optimising the stopband limit of the 0.05 Hz second order filter when A_s = 40 dB for different starting points. 274
A.2 Results obtained by optimising the stopband limit of the 0.05 Hz second order filter when A_s = 20 dB for different starting points. 275
A.3 Results obtained by optimising the stopband limit of the 0.05 Hz second order filter when A_s = 60 dB for different starting points. 275
A.4 Results obtained by optimising the stopband limit of the 0.05 Hz second order filter when A_s = 40 dB and the maximum positive overshoot allowed for the pulse response is equal to 5 μV. 276
A.5 Results obtained by optimising the stopband limit of the 0.05 Hz second order filter when A_s = 40 dB and the maximum positive overshoot allowed for the pulse response is equal to 2 μV. 276
A.6 Results obtained by optimising the stopband limit of the 0.05 Hz third order filter when A_s = 40 dB for different starting points. 277
A.7 Results obtained by optimising the stopband limit of the 0.05 Hz third order filter when A_s = 20 dB for different starting points. 278
A.8 Results obtained by optimising the stopband limit of the 0.05 Hz third order filter when A_s = 60 dB for different starting points. 279

A.9 Results obtained by optimising the stopband limit of the 0.05 Hz third order filter when A_s = 40 dB and the maximum positive overshoot allowed for the pulse response is equal to 5 μV. 280
A.10 Results obtained by optimising the stopband limit of the 0.05 Hz third order filter when A_s = 40 dB and the maximum positive overshoot allowed for the pulse response is equal to 2 μV. 281
A.11 Outcome of the stopband optimisation procedure for the second order filter when A_s = 20 dB for different starting points. 282
A.12 Outcome of the stopband optimisation procedure for the second order filter when A_s = 40 dB for different starting points. 283
A.13 Outcome of the stopband optimisation procedure for the second order filter when A_s = 60 dB for different starting points. 283
A.14 Outcome of the stopband optimisation procedure for the third order filter when A_s = 20 dB for different starting points. 284
A.15 Outcome of the stopband optimisation procedure for the third order filter when A_s = 40 dB for different starting points. 285
A.16 Outcome of the stopband optimisation procedure for the third order filter when A_s = 60 dB for different starting points. 286
A.17 Results derived by maximising the 3dB-cutoff frequency of the second order filter for different starting points. 287
A.18 Results derived by maximising the 3dB-cutoff frequency of the third order filter when A_s = 40 dB for different starting points. 288
A.19 Results derived by maximising the 3dB-cutoff frequency of the third order filter when A_s = 60 dB for different starting points. 289
A.20 Results derived by maximising the 3dB-cutoff frequency of the third order filter when no amplitude ripple is allowed in the stopband ($A_s \rightarrow \infty$) for different starting points. 290
A.21 Results derived by maximising the 3dB-cutoff frequency of the third order filter having concave magnitude characteristic outside the passband for different starting points. 291
A.22 Results derived by maximising the frequency at which an attenuation of 1.5 dB is achieved by the second order filter for different starting points. 292
A.23 Results derived by maximising the frequency at which an attenuation of 4.5 dB is achieved by the second order filter for different starting points. 293
A.24 Results derived by optimising the 6dB-point of the second order filter for different starting points. 294

A.25 Results derived by maximising the frequency at which an attenuation of 1.5 dB is achieved by the the third order filter ($A_s \to \infty$) for different starting points.295
A.26 Results derived by maximising the frequency at which an attenuation of 4.5 dB is achieved by the the third order filter ($A_s \to \infty$) for different starting points.296
A.27 Results derived by optimising the 6dB-point of the third order filter ($A_s \to \infty$) for different starting points. 297
A.28 Results derived by maximising the frequency at which an attenuation of 1.5 dB is achieved by the the third order filter having concave magnitude characteristic outside the passband for different starting points. 298
A.29 Results derived by maximising the frequency at which an attenuation of 4.5 dB is achieved by the the third order filter having concave magnitude characteristic outside the passband for different starting points. 299
A.30 Results derived by optimising the 6dB-point of the third order filter having concave magnitude characteristic outside the passband for different starting points. 300
A.31 Results obtained by optimising the overall low-frequency rejection of the second order filter for different starting points. 301
A.32 Results obtained by optimising the overall low-frequency rejection of the third order filter ($A_s \to \infty$) for different starting points. 302
A.33 Results obtained by optimising the overall low-frequency rejection of the third order filter having concave magnitude characteristic outside the passband for different starting points. 303

B.1 Power content of the `bw` record at frequencies lower than 0.5 Hz measured using different techniques. 308
B.2 Error introduced when the reference 0.05 Hz single-pole system is applied to selected records of the QT database. 309
B.3 Error introduced when the second order filter characterised by real poles is applied to selected records of the QT database. 310
B.4 Error introduced when the second order filter is applied to selected records of the QT database. 311
B.5 Error introduced when the third order filter is applied to selected records of the QT database. 312
B.6 Error introduced when the third order concave filter is applied to selected records of the QT database. 313

B.7 Number and length of the annotated ST segments employed in the analysis of the change in slope introduced by the highpass filters into the records of the QT database. 314
B.8 Change in the ST segment slope produced when the reference 0.05 Hz single-pole filter is applied to the records of the QT database. 315
B.9 Change in the ST segment slope produced when the second order filter characterised by real poles is applied to the records of the QT database. 316
B.10 Change in the ST segment slope produced when the second order filter is applied to the records of the QT database. 317
B.11 Change in the ST segment slope produced when the third order filter is applied to the records of the QT database. 318
B.12 Change in the ST segment slope produced when the third order concave filter is applied to the records of the QT database. 319
B.13 Power measured for selected records of the QT database. 320
B.14 Low-frequency power and noise reduction obtained for selected records of the QT database when they are filtered using the 0.05 Hz single-pole reference network. 321
B.15 Low-frequency power and noise reduction obtained for selected records of the QT database when they are filtered using the second order filter having real poles. 322
B.16 Low-frequency power and noise reduction obtained for selected records of the QT database when they are filtered using the second order filter. 323
B.17 Low-frequency power and noise reduction obtained for selected records of the QT database when they are filtered using the third order filter. 324
B.18 Low-frequency power and noise reduction obtained for selected records of the QT database when they are filtered using the third order concave filter. . 325

C.1 Sensitivities of the frequency and Q-factor of the poles and zeros of Friend's circuit with respect to component tolerances for n_2 = 0.82 (R_C/R_D = 2.2/10). 327
C.2 Sensitivities of the frequency and Q-factor of the poles and zeros of Friend's circuit with respect to component tolerances for n_2 = 0.91 (R_C/R_D = 1/10). . 328
C.3 Sensitivities of the frequency and Q-factor of the poles and zeros of Friend's circuit with respect to component tolerances for n_2 = 0.99 (R_C/R_D = 1/100). 329
C.4 Results obtained by maximising the 3dB-cutoff frequency of the third order concave filter when the undershoot occurring after the application of a 3 mV$\times$100 ms rectangular input pulse is constrained to be less than 95 μV for different starting points. 330

Nomenclature

AHA	American Heart Association
AV	Atrioventricular
bpm	beats per minute
CT	Central Terminal
CVD	Cardiovascular Disease
ECG	Electrocardiogram
EMD	Empirical Mode Decomposition
FIR	Finite Impulse Response
HR	Heart Rate
LA	Left Arm
LL	Left Leg
PSD	Power Spectral Density
QP	Quadratic Programming
RA	Right Arm
RL	Right Leg
SA	Sinoatrial
SQP	Sequential Quadratic Programming

Chapter 1

Introduction

1.1 Importance of the electrocardiogram

Diseases of the heart and circulatory system, i.e. cardiovascular diseases (CVDs), are the main clinical causes of death worldwide. In 2008, more than 17 million people died of CVDs, which accounted for approximately one third of all deaths [1]. Cardiovascular diseases are also the main cause of mortality in Europe and are responsible for more than 4 million deaths annually, accounting for nearly half of all deaths [2]. In Ireland, the percentage of deaths due to CVDs at 35% is about one fourth lower than the European average. Nonetheless, approximately 10,000 people died of cardiovascular diseases in Ireland in 2006, with an annual rate of 2.3 per 1,000 head of population [3].

A fundamental clinical tool for the diagnosis and treatment of cardiovascular disorders is the electrocardiogram (ECG), which is a recording of the electrical potentials associated with heart activity as detected by electrodes placed on the surface of the body [4]. One of the primary applications of electrocardiography is its use in the evaluation of myocardial ischaemia, which is caused by a narrowing of the blood vessels that supply the heart muscle itself and can lead to myocardial infarction, i.e. heart attack. The electrocardiogram is indeed the first test performed when myocardial infarction is suspected and the information derived from it plays an essential role in assessing the need for coronary surgical procedure and the selection of the most appropriate type [5, 6]. The electrocardiogram is also the most accurate tool for the detection of physiological abnormalities in the heart, such as arrhythmias, i.e. abnormal cardiac rhythms, and its analysis can reveal anomalies in the geometry of the heart or in the concentration of electrolytes in the blood [7, 8].

The development of the first ECG recording machines more than a century ago was accompanied by some initial scepticism regarding the usefulness of the electrocardiogram as a clinical tool [5]. Since then, however, considerable reduction in the size of the mea-

surement equipment and a steady improvement in the recorded signal quality have led to the electrocardiogram becoming the most commonly performed cardiovascular clinical test, with more than 100 million ECG records analysed in Europe each year [5, 9]. The success of electrocardiography can be attributed to the fact that the ECG is a non-invasive, safe, relatively inexpensive, simple-to-perform and reproducible test, yet it is an extremely powerful aid in the detection of a wide variety of adverse cardiac conditions [5].

Even though, traditionally, electrocardiographic recording has been limited to the hospital environment, ambulatory ECG monitoring has enjoyed increased popularity in recent years. The expanding ageing population, the rising number of sufferers of chronic diseases, spiralling healthcare costs, as well as a considerable change in the attitude of people towards the management of their own health, have led to a growing demand for portable medical devices. Technological advances, such as the reduction in cost, size and power consumption of electronic systems, have further fostered the widespread diffusion of ambulatory equipment outside of the clinic [10]. Introduced in the late 1950s by Holter [11], electrocardiographic recordings performed over long periods of time under daily living conditions have proven an invaluable tool in identifying cardiac diseases on subjects showing intermittent symptoms. More recently, ambulatory electrocardiography has found routine use in the monitoring of patients recovering from cardiac procedures or receiving treatment using specific drugs, during the pre-operative assessment of patients scheduled for surgery and in the verification of the correct functioning of implantable cardiac devices, such as pacemakers and miniature defibrillators [12].

1.2 ECG signal quality

The ECG signal provides a graphical representation of the electrical activity involving different regions of the heart over the duration of the cardiac cycle. An accurate analysis of the morphology and timing of its constituent waves is fundamental in assessing cardiac health status. Numerous cardiovascular disorders can produce significant changes in the ECG profile, which are related to underlying malfunctions of the heart or circulatory system [4, 7, 8].

Because even subtle variations in the shape of the ECG waveform can be indicative of severe cardiac problems [4, 8], it is essential that the ECG signal is recorded with the utmost fidelity. Distortions introduced by the measurement equipment can adversely affect the interpretation of diagnostically relevant features of the electrocardiogram and can ultimately lead to misdiagnosis of cardiac conditions [13, 14]. In order to guarantee that the electrocardiogram can be reliably employed in the diagnosis and management of heart dis-

eases, the performance requirements that ECG recording systems must satisfy have been standardised [9, 15].

One of the most critical subsystems of electrocardiographic monitoring equipment is the filter necessary to eliminate the noise and interference collected together with the ECG signal by the electrodes placed on the skin. It has been shown that considerable deformation of the ECG profile is likely to occur if the characteristics of this filter are not adequate for high quality electrocardiographic recording [16–18]. In order to prevent the filtering system from introducing significant distortion over the spectrum of the ECG signal, extremely stringent specifications are defined for the frequency response of the electrocardiograph by current international standards.

1.3 Aim of the project

The ultimate goal of this research project is to design an optimal analogue filter to be integrated into the front-end stage of portable electrocardiographic recording systems. This filter is meant to eliminate as much as possible of the out-of-band noise and interference before the ECG signal is digitised or otherwise processed. Since the frequency interval containing the principal components of the ECG spectrum extends over approximately two decades [19], the front-end filter can be considered as wide-band. It can thus be separated into two independent subsystems: a lowpass and a highpass filter. The lowpass filter is necessary to suppress the high-frequency noise and to keep aliasing from occurring in the digitisation process. On the other hand, a highpass filter is required to prevent sizeable low-frequency noise and large DC offset voltages present at the interface between the skin and the electrodes from saturating the front-end amplifier [20].

A Bessel transfer function of varying order is generally employed in the design of the lowpass filter [20–22]. It has, however, never been established if there are limitations on the minimum order of this filter nor if any other classic transfer function would be more appropriate for electrocardiographic applications. A systematic analysis of the frequency and time domain characteristics of different transfer functions needs therefore to be performed in view of the requirements specified for the ECG filter, so that the most suitable option can be identified.

Such a direct selection approach cannot, on the other hand, be applied to the design of the highpass filter. The specifications set by the standards for the low-frequency response of ECG recording systems are so strict that only one straightforward solution exists for the analogue highpass filter. This solution is given as a single-pole network with a 3dB-cutoff frequency of 0.05 Hz and it has been in use since the American Heart Association (AHA)

recommended it in 1967 [23]. Almost 50 years later, the 0.05 Hz first order filter is still employed by the vast majority of electrocardiograph manufacturers and it has also become the reference by which the performance of any other highpass filter for electrocardiographic applications is assessed [18, 24].

It should, however, be noted that the AHA recommendations and the international standards based upon them have been significantly modified since 1967 and the requirement of a low-frequency cutoff of 0.05 Hz has been lifted [9, 15, 19]. This has led, over the past 30 years, to the development of numerous digital techniques for the elimination of low-frequency noise from electrocardiographic records. On the other hand, no sensible analogue alternative to the 0.05 Hz single-pole network has ever been proposed. The design of an analogue highpass filter having better rejection properties than the 0.05 Hz first order system and yet fulfilling the performance standards specified for ECG recording equipment is the main focus of this thesis.

1.4 Thesis overview

Before the design of the front-end filter is attempted, a thorough analysis of the requirements set for ECG measurement systems by the European and American standards and the AHA recommendations is performed. Currently, the filtering specifications are expressed simultaneously in the frequency and time domains. Whereas the frequency domain requirements are simply defined as conditions on the system magnitude response, the time domain specifications are formulated in terms of the distortion introduced by the filter into set input waveforms [9, 15, 19]. Because these pulse response requirements do not appear to be consistently defined across the literature, a detailed examination is performed. Moreover, since a phase linearity requirement is often suggested as a complement to the magnitude response specifications of the highpass system [13, 18, 19, 24–26], the limits imposed on the filter characteristics by the phase condition are compared to those determined by the time domain constraints actually defined in the standards.

In order to derive an optimal transfer function for the analogue filters, traditional design and compensation techniques are initially investigated. Since this approach does not prove effective in establishing a highpass system having better rejection characteristics than the traditional 0.05 Hz single-pole network, the possibility of designing the filter directly from the specifications contained in the standards and recommendations is investigated.

When analysing possible hardware implementations of the front-end filters, emphasis is placed on the circuit complexity and on its power consumption. The intended application for the improved analogue front-end filters is in low power ambulatory monitoring devices.

In these systems, the power limitations imposed by the battery life preclude the use of complex digital filtering techniques, yet as much as possible of the out-of-band noise and interference needs to be eliminated before the storage or transmission of the ECG signal.

Thesis outline

- Chapter 1: Introdution
- Chapter 2 provides background information on the generation and measurement of the electrocardiogram. The time profile of the ECG waveform and its frequency content are presented and different sources of noise and interference affecting electrocardiographic recording are described.
- In Chapter 3, the filtering requirements established by the European and American standards and the AHA recommendations for electrocardiographic equipment and their rationale are thoroughly examined.
- Chapter 4 deals with the lowpass filter. After summarising the design requirements, the frequency and time domain characteristics of different transfer functions are illustrated and compared with respect to passband flatness, out-of-band rejection, in-band group delay and step response overshoot. The compliance with a triangular wave test specified by the current international standards is then verified.
- Chapter 5 begins by investigating the specifications for the highpass filter and illustrating the severe restrictions imposed by the time domain conditions on its magnitude response. A review of the digital techniques employed for the removal of low-frequency noise from ECG records is then proposed. Because of their relatively low complexity and widespread use, linear digital filters are presented in greater details and the responses of a number of them are tested for compliance with the standards. Attention is subsequently focused on analogue filters. Lowpass-to-highpass transformations are considered and the changes they produce in the time and frequency characteristics of the lowpass prototype are analysed in light of the requirements for diagnostic quality recording. The effectiveness of classic analogue compensation methods in improving the responses of the highpass filters obtained using these transformations is finally evaluated and their shortcomings identified.
- In Chapter 6, an optimisation procedure developed by the author for the design of the highpass filter is described. The low-frequency attenuation of second and third order filters is maximised subject to a set of constraints derived from the time and frequency

domain requirements specified by the standards and recommendations. The material presented in this chapter has been partially published in [27, 28].

- Chapter 7 presents a rigorous methodology for the measurement of the distortion introduced into electrocardiographic recordings by the highpass filters. Their ability to reduce the low-frequency noise and interference is also evaluated and the system providing the best trade-off between noise reduction and time domain distortion is identified.

- In Chapter 8, the sensitivity of this optimal highpass filter with respect to changes in the values of its coefficients is evaluated. A simple circuit topology suitable for the implementation of the filter is then analysed and its passive components derived in such a way that the variability in the location of the poles and zeros is minimised. The design of the highpass filter is finally revised to account for the variations in the system time and frequency domain responses due to component tolerances.

- Chapter 9 summarises the main findings of this study and identifies the research areas that require further investigation.

Chapter 2

ECG signal

2.1 The heart and cardiovascular system

The function of the cardiovascular system, schematically illustrated in Figure 2.1, is to carry oxygen and nutrients to the organs and tissues of the human body and to collect carbon dioxide and waste products and transport them to the lungs and kidneys for excretion. The main components of the circulatory system are the heart, the blood and the blood vessels, with the heart acting as a pump and forcing blood through the arteries and veins [29, 30].

The heart is divided into four chambers: the two upper chambers are called atria and the two lower chambers are termed ventricles. The right and left sides of the heart operate as two functionally distinct units, supplying blood to the the lungs and to all the other organs, respectively. When the heart contracts, the de-oxygenated blood in the right ventricle is forced out to the lungs where carbon dioxide is released and oxygen is absorbed. Blood flows then back from the lungs into the left atrium. This path of blood flow through the lungs is called pulmonary circulation. At the same time, the heart contraction causes the oxygenated blood contained in the left ventricle to be pumped out to the rest of the body. After oxygen and nutrients are delivered to the organs, blood is finally returned through the venous system to the right atrium. The loop is named systemic circulation [29, 30].

Two main phases can be identified during the cardiac cycle: diastole, which is the resting phase during which the heart chambers fill with blood, and systole, i.e. the period during which contraction of the heart muscle occurs and the blood is ejected into the arteries [30]. In order for the pumping action to be efficient, the contraction and relaxation of cardiac muscle fibres need to be precisely coordinated. This coordination is controlled by an electrical impulse, which triggers the contraction of each cardiac cell. The stimulus is rhythmically initiated inside the heart by a group of specialised cells and conducted by the exchange of ions between adjacent cells throughout the entire cardiac muscle [32].

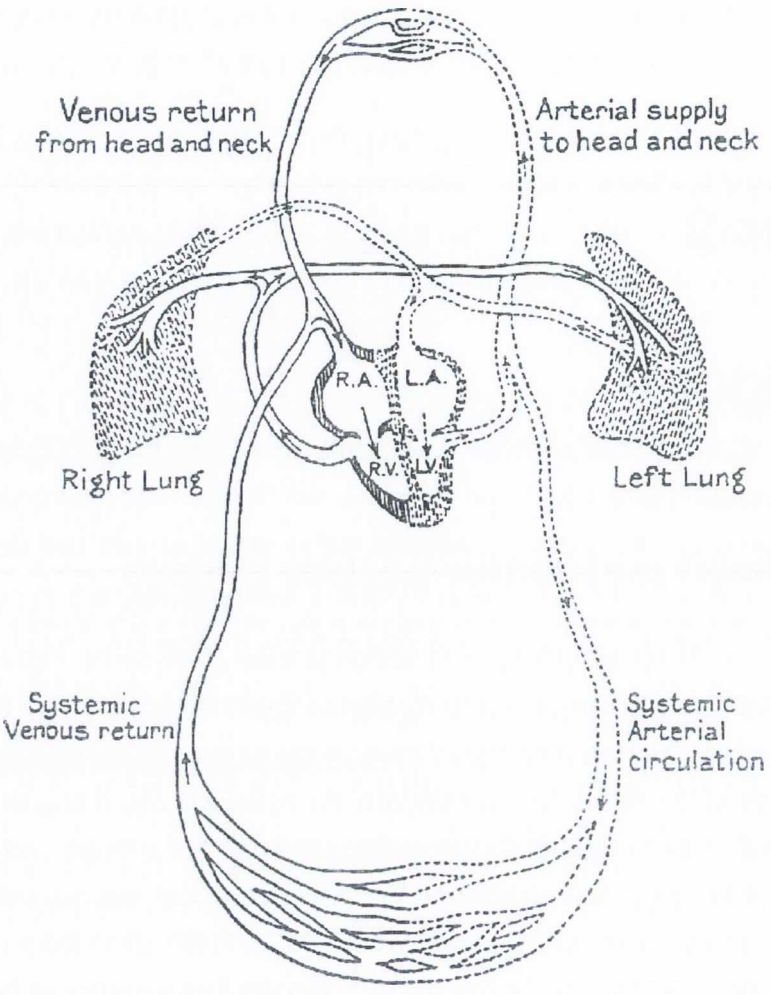


Figure 2.1: Diagram of the cardiovascular system (modified from [31]). R.A., L.A., R.V. and L.V. stand for right atrium, left atrium, right ventricle and left ventricle, respectively.

2.2 ECG generation and measurement

The ECG signal is ultimately generated by ionic currents flowing through the membranes of cardiac cells and between adjacent cells. The electric field created in and around the heart by these currents varies in intensity and direction during the cardiac cycle and can be detected by electrodes placed on the surface of the skin. The electrocardiogram is obtained by measuring the potential difference between two selected locations on the body or between one location and a reference point [8]. The differential signal is amplified and filtered to improve readability and reduce the noise and interference collected by the electrodes together with the ECG. The electrocardiographic record can then be further processed and analysed using diagnostic criteria to obtain clinical information and identify abnormalities. This sequence of physiological and technological processes leading to the recording and interpretation of the ECG signal is illustrated in Figure 2.2.

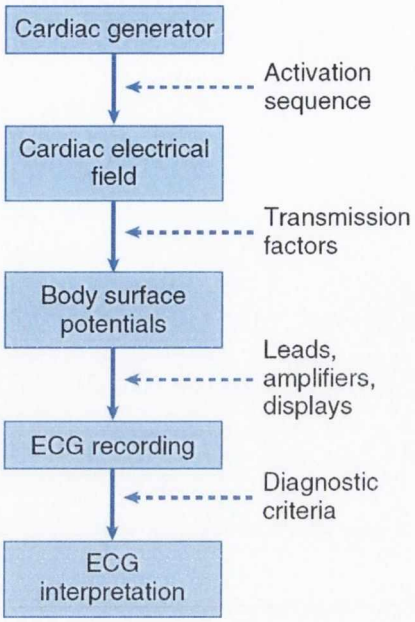


Figure 2.2: Schematic diagram showing the mechanisms underlying ECG recording [8]. The factors influencing or perturbing the measurement and analysis of the electrocardiogram are indicated by the dashed arrows.

2.2.1 Body surface potentials

Certain types of cells within the body, including cardiac muscle cells, are known as excitable cells. When at rest, these cells possess a potential difference between the inside and the outside of the cellular membrane [30]. This polarisation or resting potential is due to the difference in concentration of ions, mainly sodium, potassium, calcium and chloride [7], across the cell wall and its value lies between -70 and -90 mV [29], with the minus sign indicating a net positive ion concentration outside the cell. When the cell is appropriately stimulated, the permeability to ions of its membrane is altered, leading to a higher concentration of positively charged ions inside the cell. This mechanism of ion flow is termed depolarisation. The transmembrane potential difference after the redistribution of ions is named the action potential and is approximately equal to 20 mV [30]. Finally, the intracellular potential starts to decrease and the cell gradually returns to its resting state through the process known as repolarisation. Figure 2.3 shows the typical potential changes occurring when an excitable cell is stimulated.

In practice, a stimulus determines the sequential depolarisation of the cardiac cells along a muscle fibre. This process is termed activation and can be modelled as a current dipole moving along the fibre with an intensity proportional to the rate of change of the intracellular potential and an orientation in the direction of propagation [8, 33]. Since adjacent fibres undergo sequential depolarisation simultaneously, the instantaneous heart

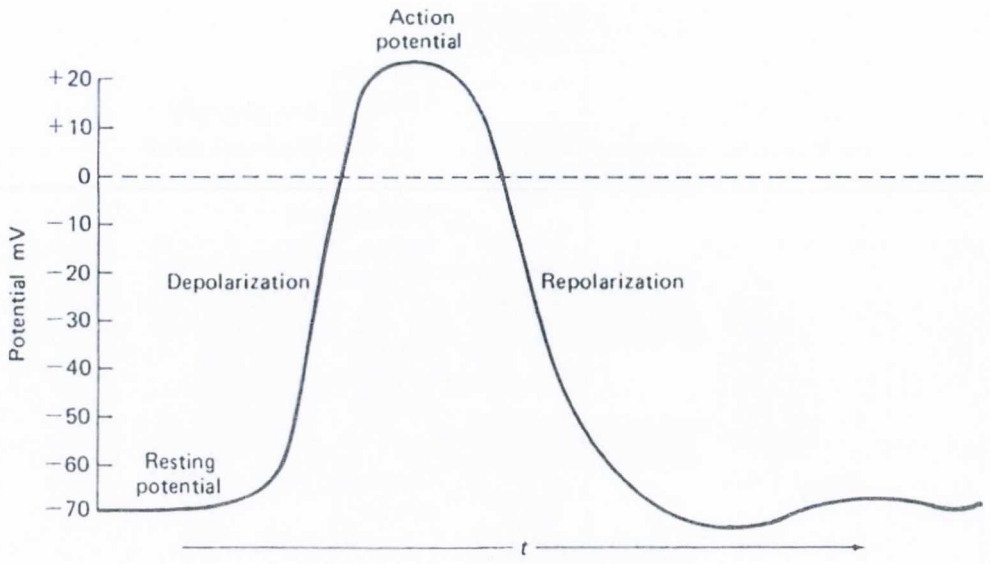


Figure 2.3: Typical waveform of the transmembrane potential of an excitable cell undergoing stimulation (modified from [30]). The wave profile and the time scale vary depending on the type of cell, with the action potential for cardiac muscle cells lasting between 150 and 300 ms.

activity can be represented as a distribution of active current dipoles [7]. This model can be further simplified by assuming that all of the current dipoles originate at a single point in space. Therefore, at each instant, the activation front can be represented by a single current dipole, determined as the vector sum of all the individual dipoles, as shown in Figure 2.4. The equivalent dipole is usually referred to as the heart vector [7, 8]. The potential field generated by this current dipole is such that an electrode placed on the body surface senses a positive potential when the activation front is moving towards its location [8].

An equivalent current dipole can also be constructed when the cardiac muscle cells undergo repolarisation, during the process termed recovery. Since the intracellular potential of repolarised cells is lower than that of the cells for which repolarisation has not begun yet, the orientation of such a dipole is opposite to the direction in which recovery is occurring [8]. The dipole magnitude is smaller than during activation because, for cardiac muscle cells, the rate of change in the transmembrane potential is lower during repolarisation than during depolarisation. Moreover, the velocity is between 10 and 100 times slower for recovery than for activation and large portions of the fibre are subject to recovery simultaneously [8, 33]. Therefore, ECG waveforms associated with the repolarisation of cardiac cells are expected to be lower in amplitude and longer in duration than those generated by the activation process [8].

The cardiac electric field, generated by the activation and recovery sequences, is significantly modified by the complex morphology of the human body. The cardiac potentials, as seen at the skin surface, depend on both the biological properties of the signal sources

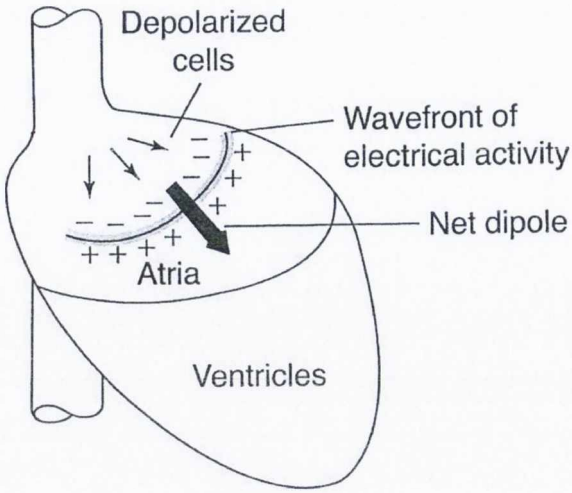


Figure 2.4: Equivalent dipole associated with the depolarisation of the atria (modified from [32]).

and on the biophysical characteristics of the structures contained in the space between the sources and the body surface. The factors influencing the surface potentials can be grouped into the following four categories [8].

- Cellular factors, such as ion concentration, alter the magnitude of transmembrane potentials and local ionic currents.
- Cardiac factors, like the anisotropy of cardiac fibres and the presence of connective tissue between them, affects the electrical coupling between cells.
- Extra-cardiac factors are related to the inhomogeneous electrical properties of the torso anatomical structure. The cardiac electric field is modified by the organs and tissues present between the depolarising/repolarising region and the body surface, such as lungs, bones and skeletal muscles, subcutaneous fat and skin.
- Physical factors, like the variable distance between the heart and the recording electrode and the eccentricity of the heart within the chest, significantly influence the amplitude of the surface potentials.

The effect of all these factors is so marked that the body surface potentials only maintain a general spatial relationship with the underlying cardiac event and they appear much smoother than the transmembrane potentials [8]. Their magnitude is also many times lower than the voltage difference measured across cell membranes. In fact, even though the peak-to-peak amplitude of transmembrane potentials is about 100 mV, the amplitude of the ECG signal is typically between 0.5 and 4 mV [34].

2.2.2 Skin-electrode interface

The measurement of cardiac potentials is enabled by surface electrodes, which operate essentially as transducers converting the ionic current within the body into electronic current in the lead wires connected to the monitoring system [35, 36]. The skin-electrode interface, where this phenomenon takes place, is classically modelled as a double time constant system with time-varying parameters [35, 37], as shown in Figure 2.5. This electrical equivalent circuit can be further subdivided into two subsystems, representing the electrode-electrolyte interface and the skin-electrolyte interface, respectively. The electrolyte layer is usually composed of a coupling gel containing chloride ions [35, 38], which comes pre-applied on the common disposable self-adhesive electrodes.

The electrode-electrolyte interface corresponds to the exact location where the conversion between ionic current and electronic current occurs. The transfer of charge between ions in the electrolyte and free electrons in the electrode is allowed by chemical reactions taking place at the boundary between the two materials. Due to these reactions, the distribution of ions in the electrolyte in the vicinity of the interface is such that an electrical double layer is formed. That is, one type of charge is dominant on the surface of the electrode, whereas the opposite charge is prevalent in the adjacent electrolyte [35, 36, 39]. The potential associated with the double layer, labelled E_{34} in Figure 2.5, is primarily dependent on the chemical composition of electrode and electrolyte, on the temperature and on the current flowing through the interface [35, 37]. The double layer at the electrode-electrolyte interface is also characterised by a capacitance and a leakage resistance, C_4 and R_4, respectively, in Figure 2.5. R_4 represents the resistance between electrode and electrolyte and is smaller than 500 Ω, whereas C_4 is the capacitance across the layer of charge and is estimated to be larger than 1 mF in conventional wet electrodes [37]. A further resistance is associated with the electrolyte itself, R_3. Its value depends on the concentration and mobility of the ions in the gel, with typical values being in the range 0.1-1 kΩ [39].

The electrical characteristic of the skin-electrolyte interface is strongly influenced by the properties of the outer layer of the skin, the epidermis. A continuous process of regeneration occurs in this layer, with cells being constantly displaced by new cells being formed underneath them. While travelling outwards, the cells die and a layer of dead material forms on the skin surface [35, 38, 39]. This outermost layer, called the stratum corneum, has electrical characteristics very different from those of live tissue and its impedance is much higher than that measured for the body fluids underneath [38]. Therefore, whereas the dermis and subcutaneous layer of the skin, as well as the tissues located deeper within the body, can be simply represented by a resistance, R_1, of a few hundred ohms [38, 39], the more complex model of a parallel RC circuit and potential E_{23} is needed to characterise

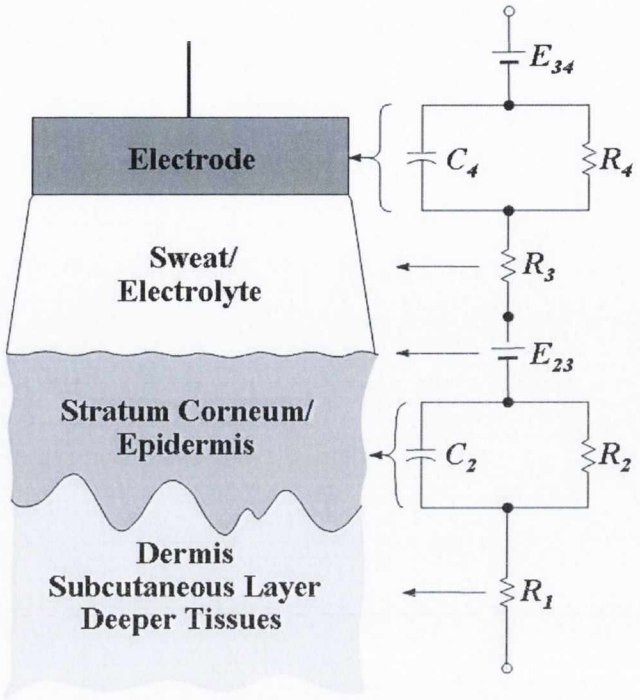


Figure 2.5: Diagram of the skin-electrode interface and its equivalent electrical circuit (modified from [35]).

the interface between the stratum corneum and the electrolyte. All of these parameters characterising the interface between the epidermis and the electrolyte are dependent on the preparation performed on the skin prior to the application of the electrodes and on the electrolyte composition [37, 39]. Moreover, the resistance R_2 is inversely proportional to the area of contact of the electrode and values ranging between a few kΩs to tens of MΩs have been measured for conventional gelled electrodes [39]. Conversely, the capacitance C_2 is directly proportional to the electrode contact area and varies between tens and hundreds of nFs [39].

As suggested earlier, the parameters in the skin-electrode interface are in reality time dependent. It takes approximately 15-20 minutes after the application of the electrolyte paste or gel for the skin impedance to reach a stable minimum [39]. During this time interval, the water and ions contained in the coupling gel diffuse through the stratum corneum, creating a conductive bridge between the gel and the dermis [38, 39]. Moreover, a non-linear relationship can be identified between the values of the elements in the equivalent circuit shown in Figure 2.5 and the density of the current flowing into the skin-electrode system [35]. The parameters in the electrical model can, however, be considered constant for current densities lower than 10 μA/cm^2 [40]. Other quantities that influence the model of the skin-electrode interface are the mechanical pressure between the electrode and the skin [41] and the level of moisture in the skin due to sweat [38, 41].

ECG recording systems employing dry or pasteless electrodes have been proposed since the 1960's [36]. This type of electrode is particularly useful for long-term monitoring because it overcomes the limitations associated with the electrolytic gel applied to facilitate the conversion between ionic and electronic current in common wet electrodes. The conductive paste tends, in fact, to dry out over time and it can cause skin irritation and even allergic reactions [36, 39, 42], especially when ECG recording is performed over an extended period. Dry electrodes can be characterised using the same electrical model derived for gelled or wet electrodes (see Figure 2.5), but the values of the circuit components are significantly different [35, 43]. The contact characteristic between the skin and the electrode is indeed deeply influenced by the fact that the sweat substitutes for the coupling electrolyte [36]. Furthermore, since a layer of sweat needs to build up under the electrode to allow current conduction between the body and the measurement system, the impedance of the skin-electrode interface usually takes longer to stabilise than for wet electrodes [43].

2.2.3 12-lead system

An electrocardiographic lead is determined either by a couple of electrodes or between a single recording electrode and a reference point and it provides a representation of the heart electrical activity as seen from a specific direction. A vector is associated with each lead and is oriented along the imaginary line connecting the two sites. When two electrodes are employed, a bipolar lead measuring the difference in surface potentials between the locations is created. One of the electrodes constitutes the positive terminal and the lead vector points towards it. For unipolar leads, the potential at one site is evaluated with respect to a reference potential, which can be calculated from the voltage readings at other electrode locations [8].

The standard clinical ECG is based on a 12-lead system consisting of three bipolar limb leads (I, II and III), three unipolar augmented limb leads (aVR, aVL, aVF) and six unipolar chest leads (V_1 to V_6). The limb leads describe the cardiac electric field in the frontal plane, whereas the chest or precordial leads provide a representation in the horizontal plane [8, 44]. The corresponding lead vectors are shown in Figure 2.6.

Bipolar limb leads were introduced in the first decade of the 20^{th} century by Einthoven [45, 46], who devised the first relevant ECG measuring system [5, 47]. For the recording to be performed, the measuring sites needed to be immersed in a saline solution and the electrodes were traditionally placed on the wrists and ankles [5, 47]. Einthoven assumed the electrode locations to be the vertices of an equilateral triangle, having the heart at its centre [44]. The three bipolar lead vectors are defined by the edges of the Einthoven's triangle and their orientation is shown in Figure 2.6. The voltage measured for each lead is

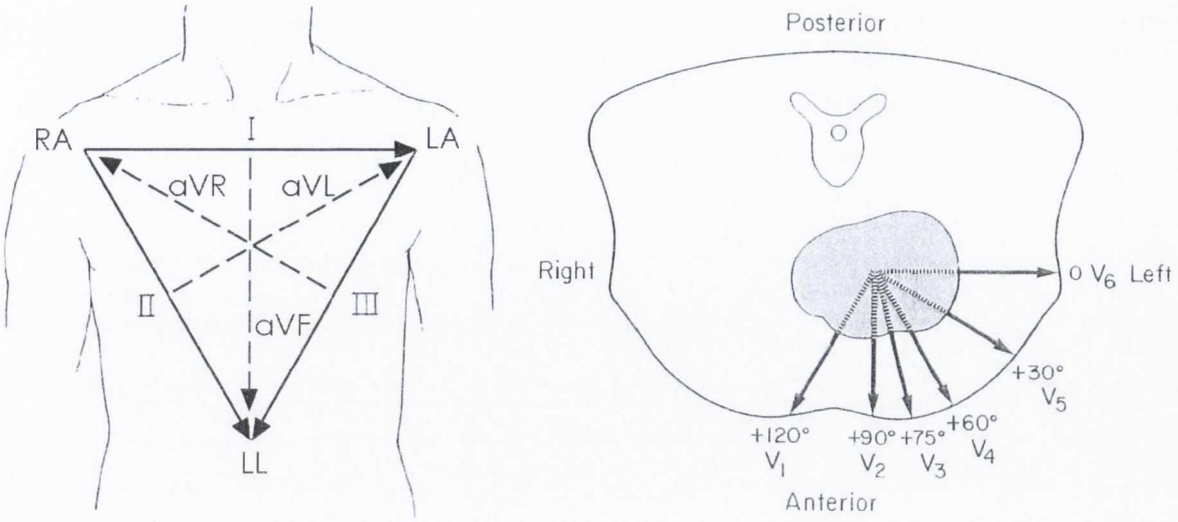


Figure 2.6: Lead vectors for the limb leads (left) and for the chest leads (right) (modified from [44]).

simply given by the difference in potential level Φ between two electrode locations:

$$\begin{aligned} V_{\mathrm{I}} &= \Phi_{\mathrm{LA}} - \Phi_{\mathrm{RA}} \\ V_{\mathrm{II}} &= \Phi_{\mathrm{LL}} - \Phi_{\mathrm{RA}} \\ V_{\mathrm{III}} &= \Phi_{\mathrm{LL}} - \Phi_{\mathrm{LA}} \end{aligned} \tag{2.1}$$

where LA, RA and LL identify the left arm, right arm and left leg, respectively. The right leg (RL) is either connected to ground [8] or to an active circuit that reduces the common-mode interference [39, 48–51]. It is easily verified by applying Kirchhoff's voltage law that the voltage reading for one lead can be derived from the other two measurements as

$$V_{\mathrm{II}} = V_{\mathrm{I}} + V_{\mathrm{III}}. \tag{2.2}$$

Electrodes located on the limbs are obviously not suitable for measurements in ambulatory settings or during exercise and, to reduce the noise induced by the subject's movement, they are substituted with electrodes on the torso, which are also used for bedside cardiac monitoring [52]. The limb electrodes are thus usually located according the Mason-Likar placement [53] as in Figure 2.7, where the sites of the precordial electrodes (leads V_1 to V_6) are also highlighted.

In order to deepen the knowledge on the cardiac electrical activity in the frontal plane, unipolar limb leads were introduced in the early 1930's by Wilson [44–46]. Each one of the limb electrodes is, in turn, used as the exploring electrode and the potential at a central terminal (CT) is taken as reference. Wilson's central terminal is determined by connecting

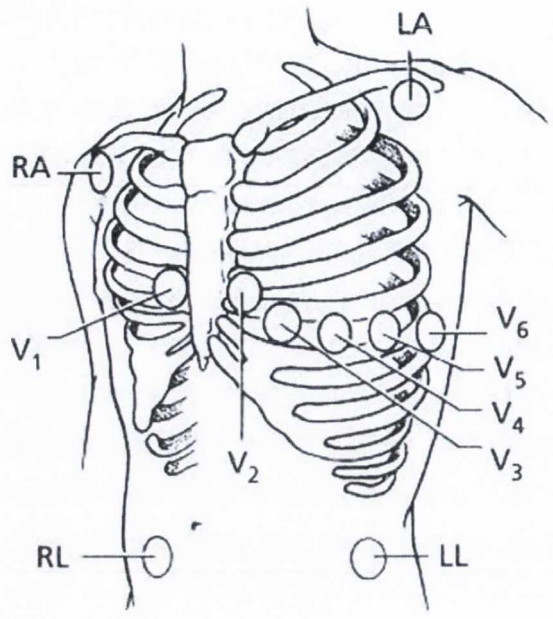


Figure 2.7: Standard placement of limb and precordial electrodes for ECG monitoring in hospital settings [52].

together all three limb electrodes. A resistor is inserted between each electrode and the central terminal to prevent currents from flowing between the electrodes [44]. To reduce the artifacts produced at the skin-electrode interface, it is advisable to employ a high value resistor, R, for this purpose [45]. As illustrated in Figure 2.8, Wilson's central terminal is located at the centre of the Einthoven triangle and the potential measured here is the average of the voltage readings at the limb locations. In fact, according Kirchhoff's current law, the sum of the currents flowing into or out of the central terminal, as shown in Figure 2.8, must equal zero:

$$I_{\mathrm{RA}} + I_{\mathrm{LA}} + I_{\mathrm{LL}} = \frac{\Phi_{\mathrm{CT}} - \Phi_{\mathrm{RA}}}{R} + \frac{\Phi_{\mathrm{CT}} - \Phi_{\mathrm{LA}}}{R} + \frac{\Phi_{\mathrm{CT}} - \Phi_{\mathrm{LL}}}{R} = 0, \tag{2.3}$$

which yields:

$$\Phi_{\mathrm{CT}} = \frac{\Phi_{\mathrm{RA}} + \Phi_{\mathrm{LA}} + \Phi_{\mathrm{LL}}}{3}. \tag{2.4}$$

Using Wilson's central terminal, three additional limb leads (VR, VL and VF) are obtained. For example, V_{VR}, the voltage measurement at the right arm, is equal to:

$$V_{\mathrm{VR}} = \Phi_{\mathrm{RA}} - \Phi_{\mathrm{CT}} = \frac{2\Phi_{\mathrm{RA}} - \Phi_{\mathrm{LA}} - \Phi_{\mathrm{LL}}}{3}. \tag{2.5}$$

In 1942, Goldberg noted that the amplitude of the unipolar limb leads could be increased by excluding the exploring electrode from the calculation of the central terminal [44–46]. The

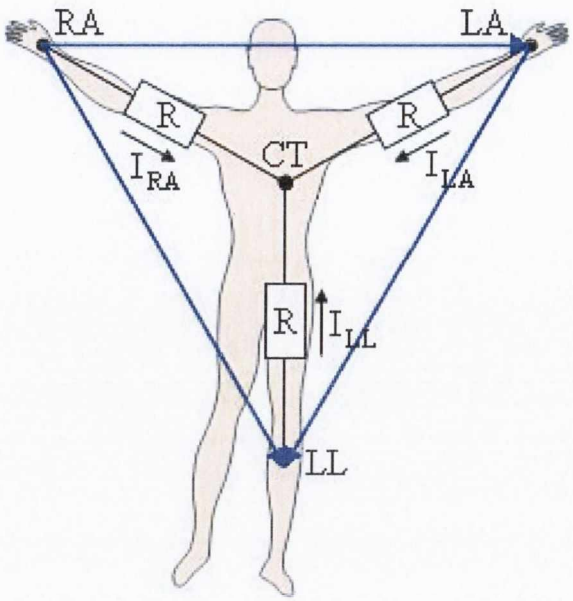


Figure 2.8: Circuit associated with Wilson's central terminal (modified from [45]).

central terminal for the right arm can thus be computed as:

$$\Phi_{CT/RA} = \frac{\Phi_{LA} + \Phi_{LL}}{2}, \tag{2.6}$$

with the augmented VR (aVR) lead reading being equal to:

$$V_{aVR} = \Phi_{RA} - \Phi_{CT/RA} = \frac{2\Phi_{RA} - \Phi_{LA} - \Phi_{LL}}{2}. \tag{2.7}$$

The augmented limb leads have the same direction as the original Wilson unipolar limb leads, but a measured voltage 50% larger is achieved by just modifying the central terminal definition, as seen by comparing Eqs. (2.5) and (2.7).

The precordial leads, introduced in the 1930's [54], record the potential at six locations on the chest referred to Wilson's central terminal. Since Φ_{CT} is relatively constant during the cardiac cycle, the signals measured by these leads are substantially determined by the potentials at the sites of the chest electrodes [8]. Precordial leads are more sensitive than limb leads in detecting ischaemia and they are quite useful in diagnosing changes in the position or geometry of the heart. In particular, leads V_3 and V_5 are very powerful in detecting ECG abnormalities that can be linked to ischaemic heart disease [52, 55], whereas V_1 is often selected for the diagnosis of arrhythmias [52].

For ECG monitoring in clinical settings a system composed by five electrodes is commonly used, since it facilitates measuring all the limb leads and one precordial lead, which is usually chosen to be V_1 [52]. For ECG recordings during exercise a reduced lead sys-

tem, consisting of leads II, V_2 and V_5, is considered adequate for detection of ischaemia and identification of arrhythmias [56].

2.2.4 Measurement equipment

The differential signals associated with the leads under study are acquired using an electrocardiograph, which conditions and displays the ECG record. The schematic diagram of a single channel ECG measurement device is shown in Figure 2.9. Three main sections can be identified: the front-end acquisition stage, the processing and analysis unit and the storage and display system. The front-end circuitry represents the most critical of these subsystems, because the input signal has very limited amplitude and is contaminated by numerous sources of noise and interference (see Section 2.4). It is essential that high signal fidelity is maintained during the amplification and filtering process, so that meaningful information about the cardiac activity can be derived either by automated analysis algorithms applied to the digitised signal or by visual inspection of the displayed ECG record.

For each channel, the first step in the measurement procedure is the amplification of the potential difference sensed between the lead terminals. The instrumentation amplifier (IA) performing this task generally comprises different stages. The first stage is characterised by a high input impedance, which compensates for the high, and often imbalanced, impedances associated with the skin-electrode interface, thus preventing attenuation and distortion. An amplifier having limited or unity gain is usually employed for this stage because DC offset voltages present at the interface between the skin and the electrodes can cause saturation of the amplifier [20, 39, 50, 57]. The skin-electrode polarisation potentials can, in fact, reach hundreds of mVs [39] and the international standards specify that ECG recorders must be able to handle imbalanced DC offsets as large as $\pm$300 mV [9, 15]. The second stage in the amplification process is constituted by a differential amplifier featuring a large common-mode rejection ratio [39, 50, 57] and therefore capable of suppressing the significant common-mode interference associated with the measurement (see Section 2.4.1). Further single-ended amplification stages can follow to guarantee that the output

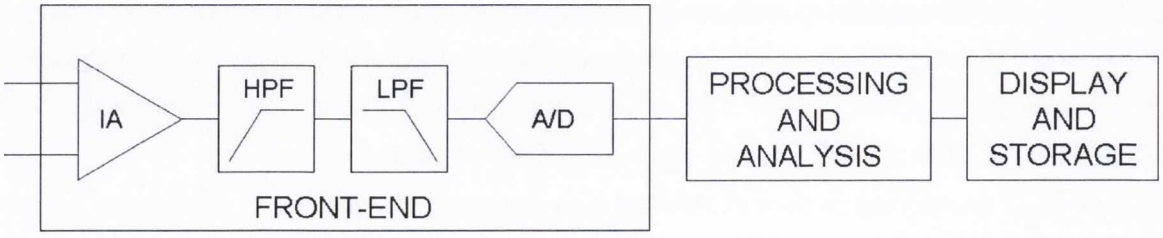


Figure 2.9: Schematic diagram of a single channel ECG recording system.

signal is sufficiently large to be displayed. The overall gain of the instrumentation amplifier is approximately 1000, that is, an output signal of about 1 V amplitude is recorded when the input signal is equal to 1 mV [39, 50].

Since the spectrum of the ECG signal is limited (see Section 2.3.3), the bandwidth of the amplifier should also be restricted so that the signal-to-noise ratio is maximised. First of all, a highpass filter (HPF) is required to reduce low-frequency noise collected during the measurement. Its main function is to suppress the DC offset voltage generated at the skin-electrode interface and prevent the saturation of the instrumentation amplifier. This filter is generally inserted after the first stage of amplification, so that any large DC potential is eliminated before the useful signal is amplified to a sufficiently high level [20, 39]. The highpass filter can, however, be located after the instrumentation amplifier provided that this circuit is AC-coupled to the lead wires. A lowpass filter (LPF) is then applied to reduce noise occurring at frequencies higher than the ECG spectrum. The fundamental function of this filter is to prevent aliasing during subsequent analogue-to-digital (A/D) conversion [20].

Once the signal has been digitised, it can be stored and displayed or transmitted to a unit performing further signal conditioning or analysis. Numerous digital techniques are available to lower the level of the noise and interference superimposed on the ECG signal. Automated analysis algorithms can then perform various tasks such as calculating the heart rate, recognising certain cardiac disorders like arrhythmia, identifying the different components of the ECG waveform and measuring their amplitude and duration [4].

2.3 Electrocardiographic waveform

2.3.1 Heart electrical activity

At each cardiac cycle, the heart's electrical activity is initiated by the spontaneous depolarisation of the cells at the sinoatrial (SA) node, which is located at the upper right corner of the right atrium, as shown in Figure 2.10. Even though cells at different cardiac sites have the ability to start the activation process, the SA node has the highest excitation frequency and, thus, acts as the cardiac pacemaker in a healthy subject [4, 7, 44, 45]. From the SA node, the activation front propagates simultaneously downwards within the right atrium and leftwards through the left atrium, finally reaching the atrioventricular (AV) node. This first activation wave is illustrated in Figure 2.11(a). Even if the depolarisation process starts in the right atrium, both atria undergo activation simultaneously during most of its time duration. Therefore, the atria can be regarded as a unit from the point of view of the cardiac electrical activity. The atria are subsequently repolarised, with the recovery proceeding in the same direction as the previous activation [8].

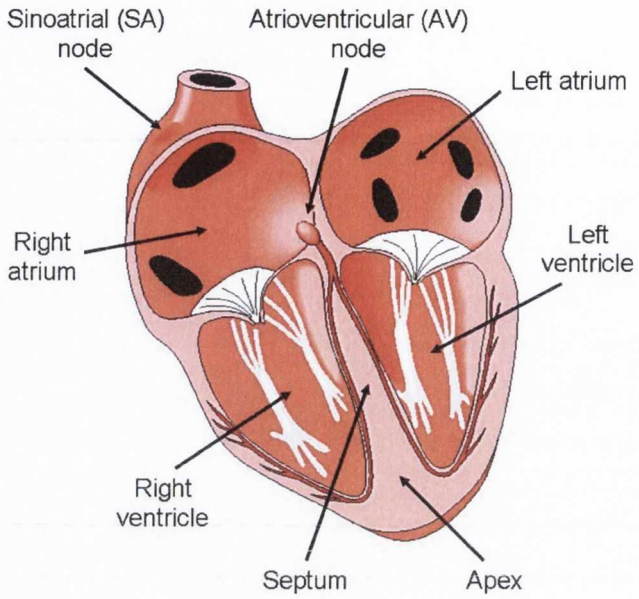
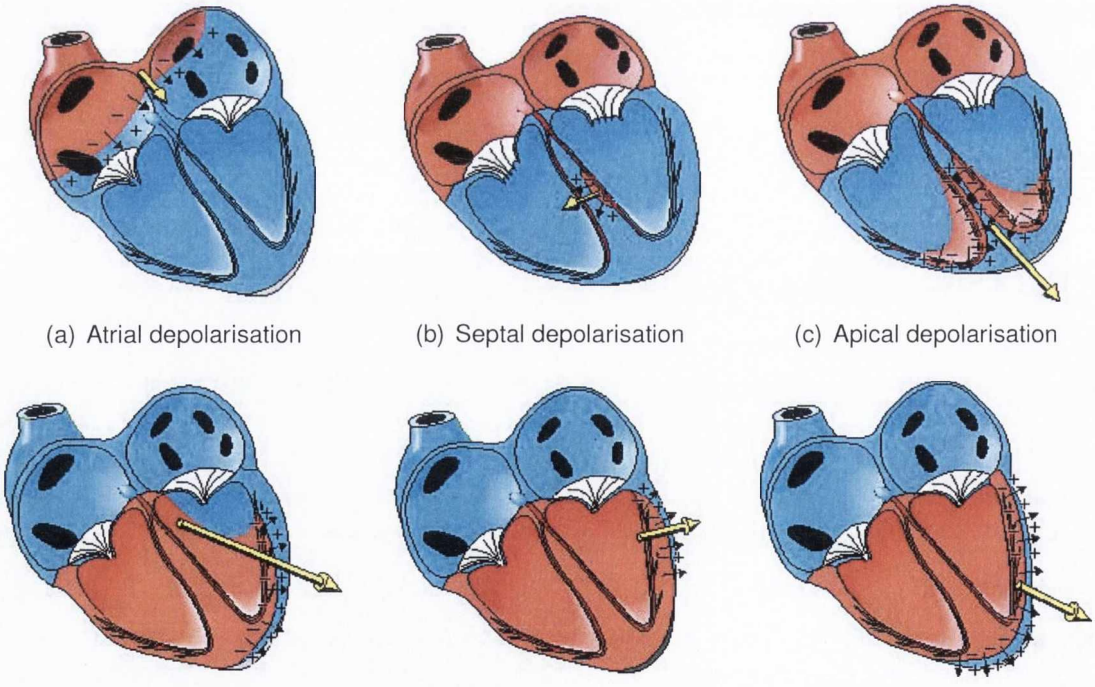


Figure 2.10: Electrical conduction system of the heart (modified from [45]).



(a) Atrial depolarisation (b) Septal depolarisation (c) Apical depolarisation

(d) Left ventricle depolarisation (e) Late ventricle depolarisation (f) Ventricles repolarisation

Figure 2.11: Different phases of the cardiac cycle (modified from [45]). The depolarisation/repolarisation wavefront and the resultant heart vector are illustrated for each phase.

The slow conduction through the tissue in the AV node, which electrically connects the atria to the ventricles, generates a delay in the activation progress, during which the atria contract and the blood is ejected into the ventricular chambers [29, 44]. The ventricular depolarisation starts in the septum between the ventricular chambers proceeding from left to right and it subsequently spreads downwards to the apex of the heart. After approximately 40 ms from the beginning of the ventricular activation, the right ventricle is completely depolarised. On the other hand, the activation front continues to propagate through the left ventricle, eventually reaching its top leftmost corner [44]. The propagation wavefront and the direction of the heart vector during the main phases of ventricular depolarisation are shown in Figures 2.11(b) to 2.11(e).

The ventricular recovery starts from the external wall of the left ventricle, that is, the region that underwent depolarisation last, and it later involves more internal areas [45]. Since the repolarisation front is directed inwardly, the corresponding heart vector points towards the outside of the ventricle. Its orientation is similar to that determined by the depolarisation of the left ventricle [7, 8, 45], as evident when comparing Figure 2.11(f) with Figure 2.11(d). Recovery does not propagate along the heart conduction fibres as was the case for the depolarising wave and extended regions of the ventricles can undergo repolarisation simultaneously instead. Therefore, the heart vector associated with it takes into account numerous contributions in different directions, which consistently vary with time [44].

2.3.2 ECG time profile

A 12-lead electrocardiogram recorded on a healthy subject is illustrated in Figure 2.12 and its major features are identified in Figure 2.13, showing the profile of a normal ECG wave as measured from lead II. The vertical deflections of the ECG signal represent the depolarisation and repolarisation of muscle fibres in different regions of the heart. The amplitude of these waves is evaluated with reference to the baseline, which is defined as the isoelectric level measured between the P wave and the QRS complex, i.e. on the PQ segment [4, 51].

P wave

Atrial activation is reflected on the ECG record by the P wave. Its length is generally less than 120 ms, as measured from the lead with the widest P wave, and its amplitude is normally less than 0.25 mV. The signal generated during the repolarisation of the atria has a very low amplitude and it is superimposed on the wave generated by the ventricular activation. Therefore, deflections due to atrial recovery cannot usually be seen on the ECG

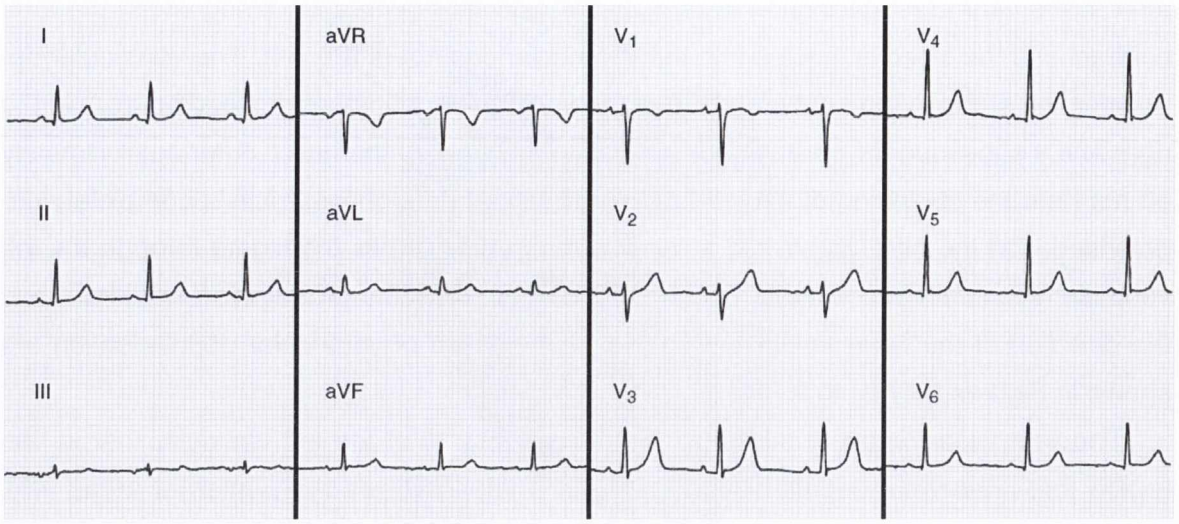


Figure 2.12: 12-lead electrocardiogram measured on a healthy subject [8].

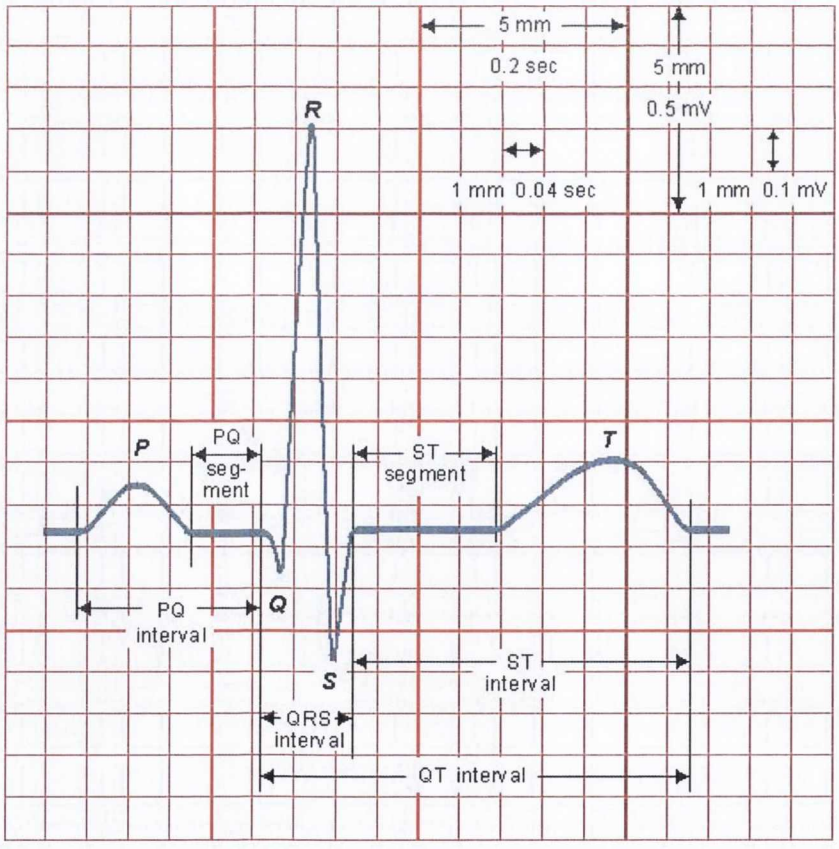


Figure 2.13: Waves and intervals of a normal lead II ECG signal (modified from [45]).

tracing [4, 8, 45].

PQ segment

The PQ segment is the isoelectric portion of the electrocardiogram that extends from the end of the P wave to the onset of the QRS complex and it represents the conduction delay that occurs at the AV node. The PQ segment is rarely measured in practice. On the other hand, the length of the PQ interval, that comprises both the P wave and the PQ segment, is considered clinically significant. The duration of the PQ interval, which is usually measured in the lead where it is shortest, is approximately 120 to 200 ms and varies slightly with heart rate [4, 8, 51].

QRS complex

The ventricular activation sequence is illustrated in the electrocardiogram by the QRS complex. Its first positive deflection is called R wave. If an initial negative deflection is present, it is termed Q wave. The negative deflection following the R wave is called S wave. The biggest deflection of the QRS complex, i.e. the R wave for the schematic ECG shown in Figure 2.13, is produced during the activation of the left ventricle, when the depolarisation process is substantially over in the right side of the heart. The QRS duration usually spans between 60 to 100 ms, with its higher limit being 120 ms in the lead showing the widest QRS complex, whereas its amplitude is generally between 1 and 2 mV in a healthy subject [4, 8, 30, 44, 51].

ST segment

When the depolarisation of the left ventricle is terminated, the ECG signal returns to the baseline in all leads. The ST segment extends from this time instant till the beginning of the T wave, that is, when the signal departs once more from the isoelectric level. This segment represents the delay between activation and recovery in the left ventricle and it is generally isoelectric in normal subjects. Any major deviation from a flat profile can be significant in the diagnosis of cardiac conditions, such as myocardial ischaemia or infarction [4, 8].

T wave

The T wave is the result of ventricular repolarisation. Since the heart vector corresponding to this phase of the cardiac cycle is approximately oriented as during the activation of the left ventricle, the polarity of the T wave is generally the same of the net polarity of the preceding QRS complex. Its average amplitude is 0.3 mV and its duration, as well as the duration of

the ST segment, is highly dependent on the heart rate. Since it accounts for the overall effect of the repolarisation of the cardiac cells, the T wave is the slowest changing wave in the ECG [4, 8, 51].

QT interval

The QT interval identifies the combined duration of ventricular activation and recovery and is measured from the beginning of the QRS complex to the end of the T wave. Since the length of the QT interval varies considerably from lead to lead, it is evaluated from the lead with the longest interval. Furthermore, the QT interval is dependent on the heart rate (HR) and its duration decreases as the rate increases. A corrected QT interval taking into account the heart rate can be calculated using Bazett's formula as:

$$QT_c = \frac{QT}{\sqrt{RR}}, \tag{2.8}$$

where RR is the time interval between two consecutive QRS peaks and can be derived from the heart rate as RR = 60/HR. The QT_c length is less than or equal to 440 ms in normal subjects [8, 44, 51].

2.3.3 ECG frequency content

As mentioned earlier, the T wave constitutes the slowest changing portion of the electrocardiographic signal (see Figure 2.14), with its main frequency components extending as low as 1 Hz [19]. However, since the ECG wave repeats almost unchanged at each heartbeat in a healthy subject, the low-frequency bound of the electrocardiogram corresponds to the minimum expected heart rate. At rest, the heart rate is normally between 60 and 100 beats per minute (bpm) [7], but lower values are sometimes measured. Because in 99% of adults, 99% of the time, the heart rate is higher than 40 beats per minute, the low-frequency limit of the ECG bandwidth can be taken as 0.67 Hz [19]. An even lower limit for the heart rate of 30 beats per minute is sometimes selected, leading to a lower boundary for the ECG spectrum of 0.5 Hz [14, 19].

On the other hand, the upper limit of the ECG bandwidth is set by the frequency components of the QRS complex. It can be seen in Figure 2.14 that the spectrum of the QRS complex shows a peak at approximately 10 Hz and then it steadily decreases, reaching a negligible amplitude at 40 Hz. Independent studies confirm both the presence of a plateau or a peak between 7 and 10 Hz in the QRS spectrum [51, 59] and the reduced content of the ECG signal at frequencies higher than 40 Hz [60, 61]. Golden et al. [60] reported that the amplitude of the ECG spectrum is a maximum at the lowest frequency measured

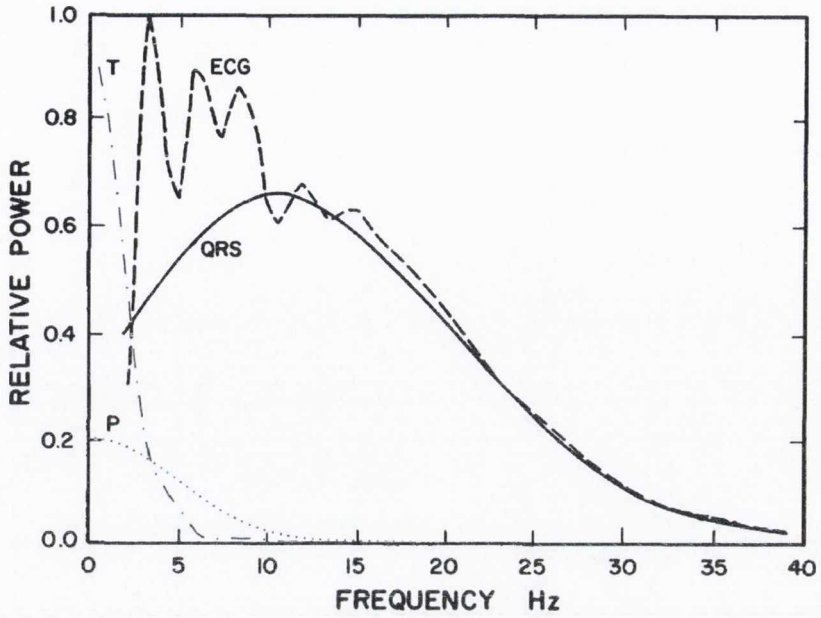


Figure 2.14: Normalised power spectrum of the overall ECG signal, QRS complex and P and T waves (modified from [4, 58]).

in their analysis, approximately 1 Hz, and that a notch is also present at about 4 Hz, as illustrated in Figure 2.14. Moreover, the frequency at which the average magnitude spectrum of a normal electrocardiogram is 20 dB lower than the peak is located by that study at 36 Hz, whereas the frequency at which the magnitude is -40 dB is identified as 105 Hz. These measurements provide a rationale for the high-frequency limit specified in the international standards for electrocardiographic equipment. The 3dB-cutoff frequency of an ECG recorder is required to be at least 40 Hz for non-diagnostic measurements [62, 63] and between 100 and 150 Hz when diagnostic quality records are needed [9, 15]. This higher limit allows accurate measurements of duration and amplitude of the constituent waves of the electrocardiogram [60] and accurate reproduction of small rapid deflections, which may occur especially in subjects affected by heart conditions [64].

2.4 Noise and interference

Due to the limited amplitude of the ECG waveform, the quality of electrocardiographic recordings is heavily influenced by the level of noise and interference superimposed on them. Numerous sources of contamination affect ECG measurements and the spectrum of the most common artifacts is shown in Figure 2.15. If we consider the frequency range of the ECG signal extending between 0.5 and 150 Hz, as discussed in the previous section, these disturbances can be broadly grouped in two categories: in-band and out-of-band.

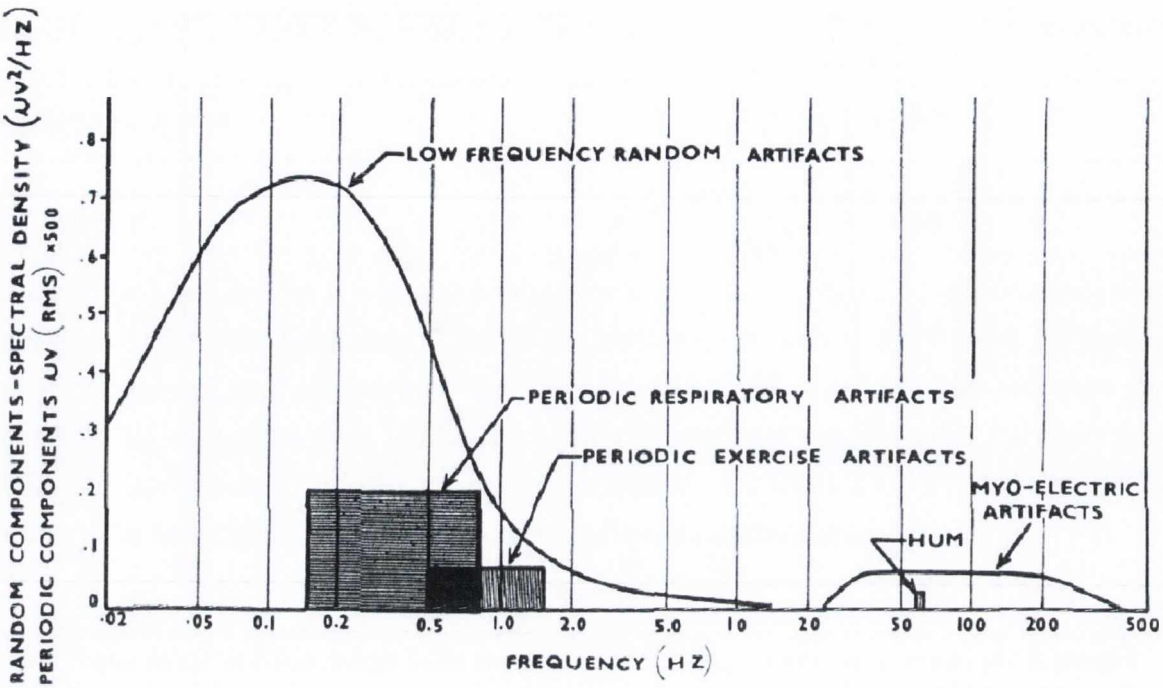


Figure 2.15: Spectrum of noise and artifacts in exercise electrocardiograms (modified from [65]).

The first class comprises power line interference, indicated as hum in Figure 2.15, electromyographic artifacts and motion artifacts, which in Figure 2.15 can be identified as the periodic exercise artifacts. The second group of interfering signals includes respiratory artifacts, baseline wander, which is named low-frequency random artifacts in Figure 2.15, and high-frequency noise.

2.4.1 In-band noise

Power line interference

The electric power system is a major source of interference in electrocardiographic recording. Power line noise manifests itself as the sum of sinusoidal signals with frequencies equal to that of the mains supply (50 or 60 Hz) and its harmonics and overall amplitude typically as high as half the peak-to-peak voltage of the ECG signal [66]. This type of interference produces a thickening in the baseline, as shown in Figure 2.16, and it can cause the appearance of false notches in the QRS complexes [67].

There are two mechanisms which produce power line interference: electric field coupling and electromagnetic induction [48, 50]. Electric fields surrounding the main power lines and the power cords that connect the electrical devices in the vicinity of the patient capacitively couple into the subject being monitored. The coupling can be reduced by designing the

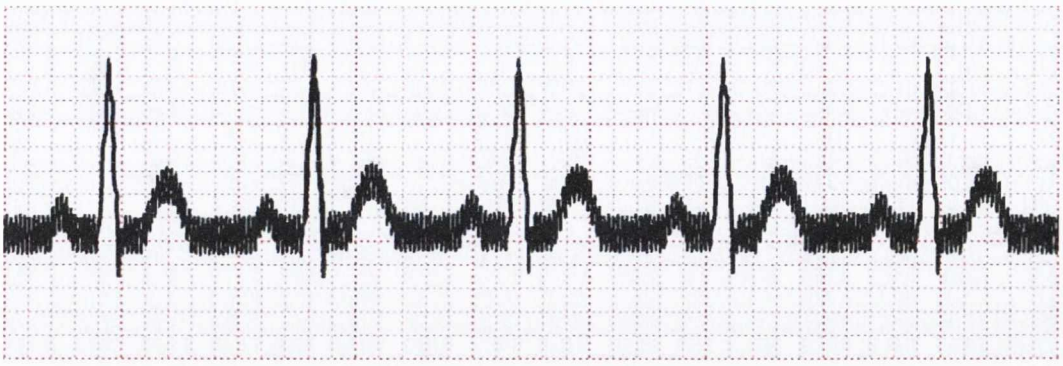


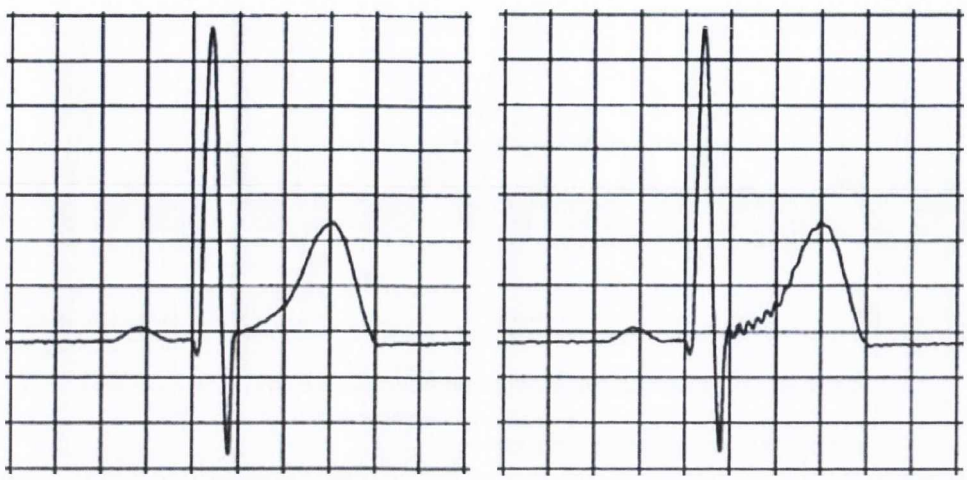
Figure 2.16: Power line interference [67].

front-end instrumentation amplifier to have an input impedance much higher than that of the skin-electrode interface and a large common-mode rejection ratio. On the other hand, varying magnetic fields, generated by the current flowing in the power lines, induce a voltage in the loop constituted by the patient, the lead wires and the electrocardiograph. Decreasing the loop area by twisting the lead wires together and keeping them as short and close to the body as possible helps to minimise the power line interference due to electromagnetic induction.

Notch filters located at the mains frequency and its harmonics are also often employed to remove any residual power line interference from the ECG recording [68–70]. No requirement is specified for the width of the stopband of these notch filters by either the European or the American standards for diagnostic electrocardiographic devices [9, 15]. However, if the bandwidth of the filter removing the power line interference is too wide, the amplitude of the QRS complex can be significantly attenuated or other relevant components of the ECG signal distorted [24]. On the other hand, if the transition between passband and stopband of the filter is too steep, ringing occurs in the output signal [9, 24], which can mimic low amplitude cardiac activity in the terminal portion of the QRS complex [4], as illustrated in Figure 2.17.

Muscle artifacts

During electrocardiographic measurements, biopotentials associated with muscle contractions appear on the skin surface along with the ECG signal, as illustrated in Figure 2.18. These electromyographic artifacts are particularly large during ambulatory monitoring and exercise ECG recording [4] and their amplitude can be as high as 0.5 mV [39]. Since the power spectrum of muscle noise contains significant components at frequencies higher than 30 Hz [39], as shown in Figure 2.15, this type of artifact cannot be filtered out of the electrocardiographic record without introducing marked distortion in the ECG signal.



(a) Input (b) Output

Figure 2.17: Ringing artifacts introduced after the QRS complex by a steep notch filter aimed at removing power line noise [24].



Figure 2.18: Electromyographic noise [4].

Nonetheless, a 40 Hz lowpass filter is often employed to remove muscle noise in non-diagnostic electrocardiographic measurements [24, 26, 49], especially when monitoring is performed in ambulatory settings [63]. The application of such a filter obviously results in a smoother-looking electrocardiographic record, but it also leads to a significant reduction in the amplitude of the QRS complex, as clearly illustrated in Figure 2.19.

Motion artifacts

Motion artifacts are periodic baseline changes caused by vibrations and patient movements [66] and are extremely common in measurements performed in ambulatory settings and during exercise [4, 71]. Movements generate a mechanical deformation of the skin underneath the electrodes, which leads to changes in the impedance and potential associated

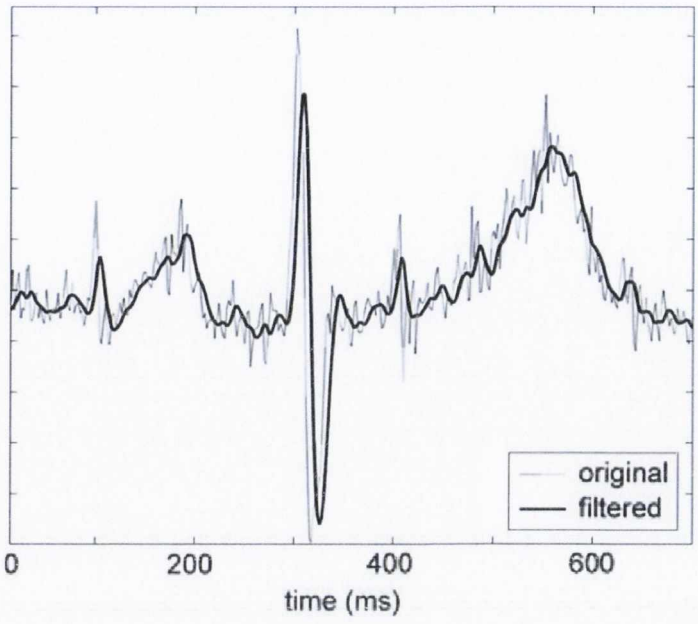


Figure 2.19: Effect of a 40 Hz lowpass filter on a noisy ECG waveform [26].

with the skin-electrode interface [72]. Even though Figure 2.15 displays periodic exercise noise only for frequencies up to 1.5 Hz, the spectrum of motion artifacts extends approximately between 1 and 10 Hz [4], as shown in Figure 2.20. The amplitude of this interfering signal can be as high as 5 times the ECG peak-to-peak voltage [66], which can render the electrocardiographic record unreadable (see Figure 2.21). Since large periodic waveforms are associated with motion artifacts, the peaks occurring in the recorded signal can be mistaken for QRS complexes by analysis algorithms [4]. For example, a heart rate of 223 bpm was reported by a monitoring system for the signal shown in Figure 2.21(b), even though the actual heart rate was only 63 bpm [73].

Electrode contact noise

Electrode contact noise is a transient interference which is caused by the loss of contact between the electrode and the skin. This disturbance manifests itself as rapid step-like transition in the ECG baseline [66], which generally causes saturation of the recorded signal at the full scale deflection level [51]. A few episodes of contact loss are shown in the ECG record in Figure 2.22. Electrode contact noise is often considered as a type of motion artifact [4, 71], even though it is non-periodic and is characterised by a higher frequency content than artifacts induced by repetitive movements.

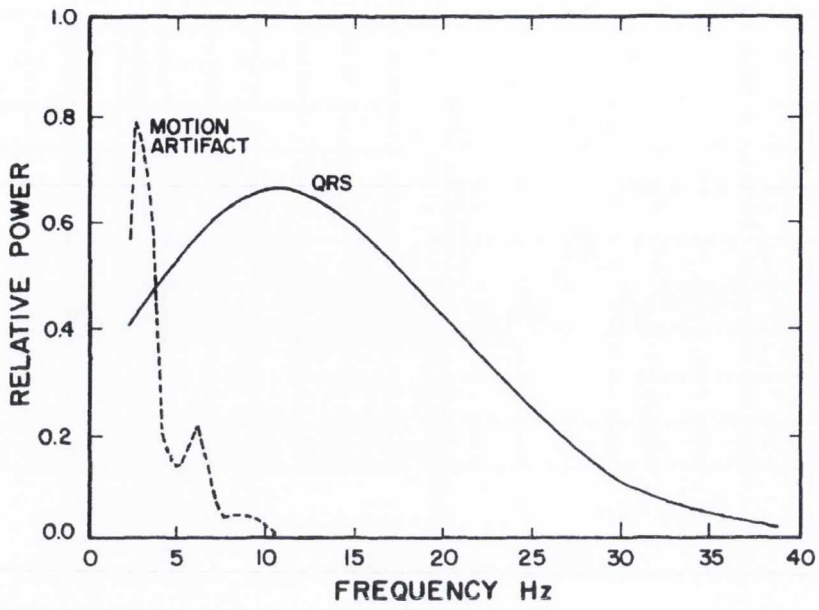
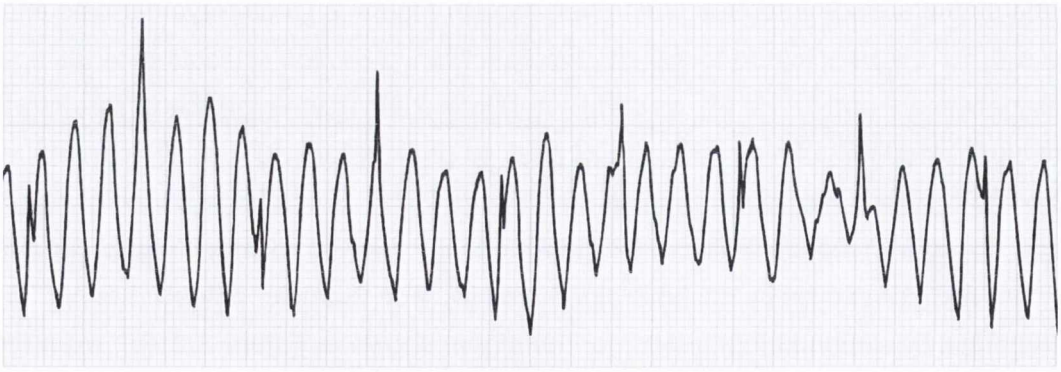
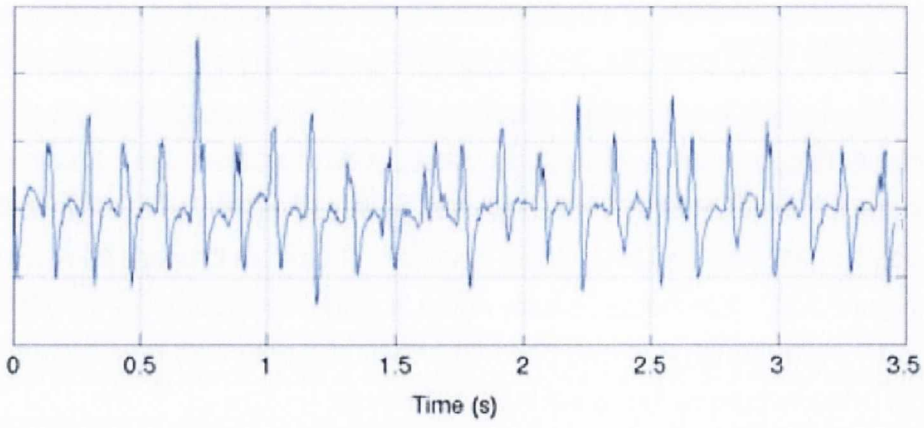


Figure 2.20: Comparison between the power spectrum of motion artifacts and that of the QRS complex (modified from [58]).



(a) Artifacts obscuring normal QRS complexes [8].



(b) Artifacts occurring during tooth brushing [73].

Figure 2.21: ECG records showing marked motion artifacts.

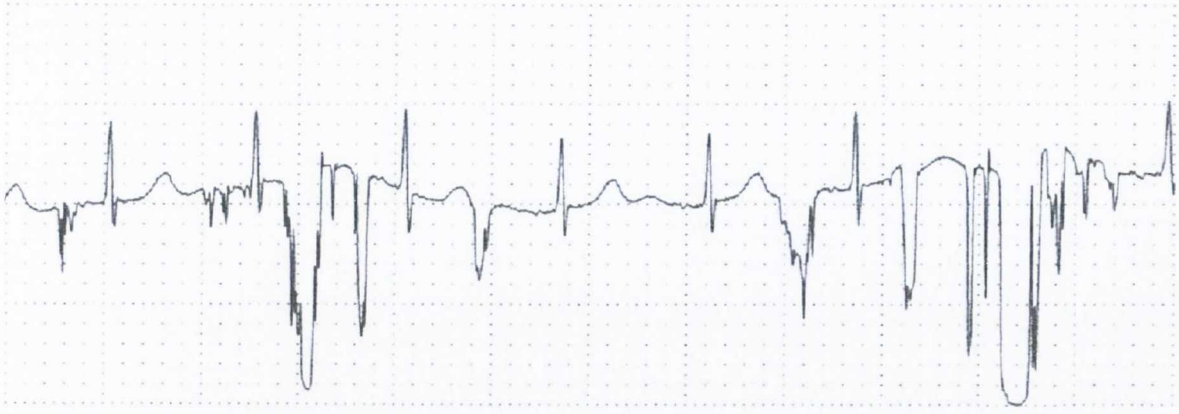


Figure 2.22: Electrode contact noise [4].

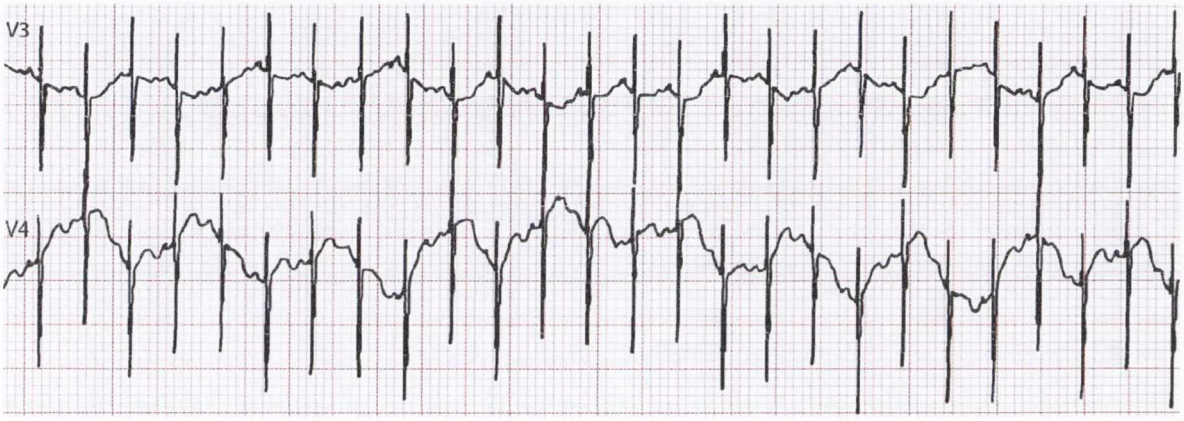


Figure 2.23: Respiratory artifact [67].

2.4.2 Out-of-band noise

Respiratory artifacts

The low-frequency drift due to respiration can be represented by an additive sinusoidal signal modulating the amplitude of the ECG baseline. The frequency of respiration generally varies between 0.15 and 0.3 Hz [66], but it can reach 0.8 Hz during exercise, as illustrated in Figure 2.15. The peak amplitude of the sinusoidal disturbance associated with respiration is reported to be approximately 15% of the ECG signal [65, 66]. An electrocardiographic record presenting respiration-induced noise is shown in Figure 2.23.

Baseline wander

Baseline wander or drift is produced by very slow changes in impedance and potential occurring at the skin-electrode interface due to variations in temperature or hydration [74, 75]. The amplitude of baseline wander can be several times larger than that of the ECG signal, as illustrated in Figure 2.24, and its spectrum is usually located at frequencies lower

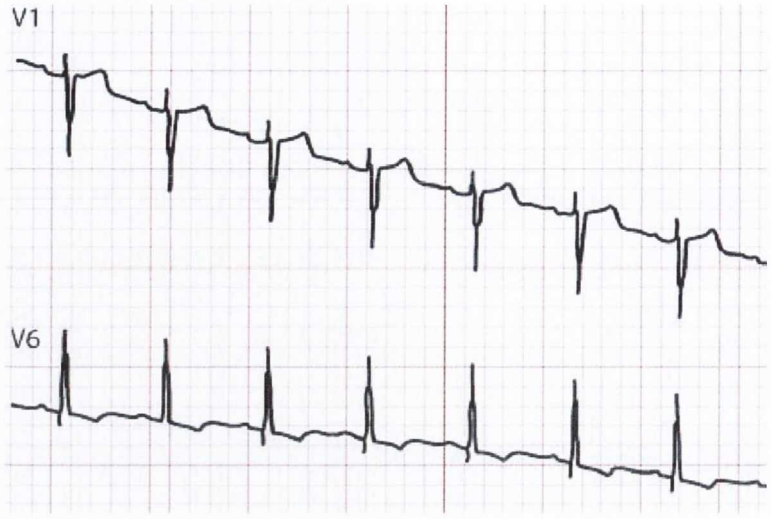


Figure 2.24: Baseline drift [67].

than the ECG spectrum [4]. The term baseline wander is also commonly used to refer to any type of noise containing only very low frequency components regardless of the source generating it. Respiratory and exercise artifacts are thus often regarded as examples of baseline wander [4, 69, 70].

High-frequency noise

Numerous different sources are responsible for high-frequency noise, which is electromagnetically coupled into the ECG recording system as described earlier for power line interference [39]. Fluorescent lighting, for example, can produce interference at a frequency equal to three times the mains frequency [67], that is, at the upper end of the ECG spectrum. Noise generated by other medical devices present near the patient can, instead, be modelled as a sinusoidal signal with frequency between 100 and 1000 kHz and amplitude approximately two times that of the ECG signal [66]. The main issue associated with high-frequency interference is that radio frequency noise is often modulated with low frequency components, which can be demodulated within the ECG spectrum in the presence of non-linearities in the amplifier circuit [39] or when the electrocardiographic record is digitised [66].

2.4.3 Discussion

As illustrated earlier for power line interference and electromyographic artifacts, in-band noise cannot be removed using linear time-invariant filters without introducing considerable distortion into the ECG signal. Even though digital techniques can be employed in the

attempt to reduce this type of disturbance [4, 76], their analysis lies beyond the scope of the project. In the remainder of this work, the attention will, therefore, be focused exclusively towards the elimination of out-of band noise.

Chapter 3

ECG filter characteristics and requirements

3.1 Introduction

In order to deliver diagnostic quality ECG records, electrocardiographic monitoring devices must reproduce the morphology of the ECG signal as faithfully as possible. In other words, the deviation of the system output from a linear representation of the input signal should be limited. The filters incorporated into electrocardiographic equipment are critically important because the electrocardiogram can be heavily distorted if their transfer function is not adequately selected [16–18]. To prevent deformation of diagnostically significant features of the ECG record, international standards define a set of requirements that electrocardiographic filtering systems must satisfy. Since these specifications are substantially based on the recommendations of the American Heart Association [9, 15], the conditions outlined in the AHA publications and the rationale behind their definition are presented first.

In recent years, the filtering characteristics of electrocardiographic devices, specified in standards and recommendations, have been simultaneously defined in the frequency and time domains [9, 15, 19, 62–64, 77]. ECG filters must comply with conditions set both on their magnitude response and on specific features of the output signals obtained for fixed input stimuli. In particular, the requirements for the highpass filter, needed to reject baseline wander and DC offset voltage generated at the skin-electrode interface, have been related to the properties of the system response to an input pulse. In order to evaluate the possibility of simplifying these specifications, the constraints that the pulse response has to satisfy to comply with the standards are analysed in detail.

In the past, a 0.05 Hz single-pole analogue highpass filter has been used to define the low-frequency characteristic of electrocardiographic equipment [23] and, based on the

frequency response of such a system, minimum requirements for the magnitude and phase response of ECG filters have been derived [63, 77]. In particular, it has been suggested that the filter phase response at low frequencies should be at least as linear as that of the 0.05 Hz first order filter [19]. Later in this chapter, this phase linearity condition and the most recent specifications imposed on the system pulse response are compared.

Finally, an alternative methodology to test simultaneously the response of the measurement equipment over the whole ECG spectrum is presented. This technique, described in one of the current European standards, employs a set of test waveforms that resemble electrocardiographic signals [9].

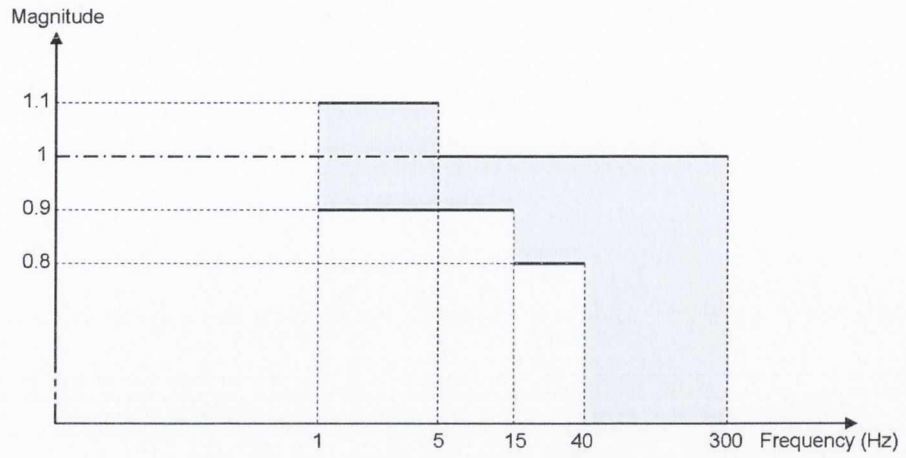
3.2 AHA recommendations

3.2.1 Review of the AHA recommendations

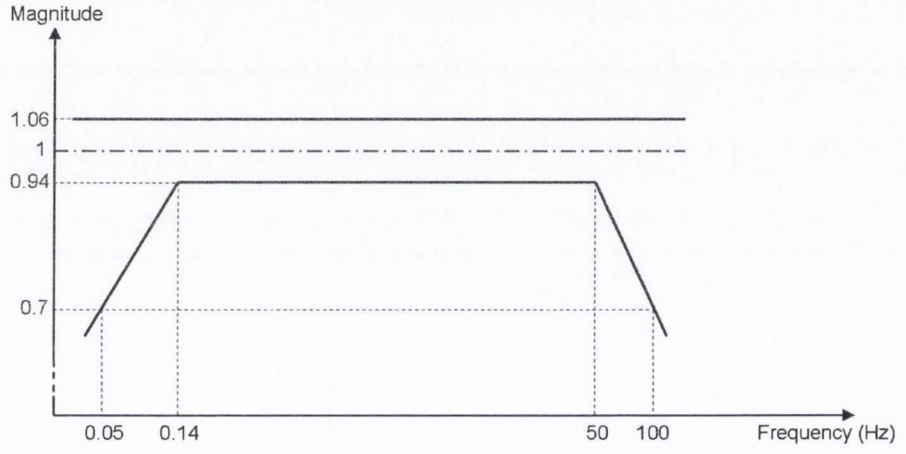
The 1954 AHA report for the standardisation of ECG leads [54] contains some of the earliest recommendations regarding the filtering characteristics of electrocardiographic equipment. The minimum requirements for the magnitude response are defined from 1 to 300 Hz as illustrated in Figure 3.1(a). Furthermore, the AHA Committee suggests that, if employed in waveform analysis, the ECG instrumentation should display a flat frequency response between 0.5 and 100 Hz.

In the following AHA report published in 1967 [23], the filter specifications are made more stringent. It is required for the magnitude response to be flat to within ± 0.5 dB from 0.14 to 50 Hz. Moreover, the amplitude at 0.05 Hz shall not be reduced by more than 3 dB compared with that measured in-band. The limits for the filter frequency response are shown in Figure 3.1(b) and, whereas the attenuation at 100 Hz should not exceed 3 dB, it is suggested that the instrumentation bandwidth should extend to at least 500 Hz to account for ECG high frequency components.

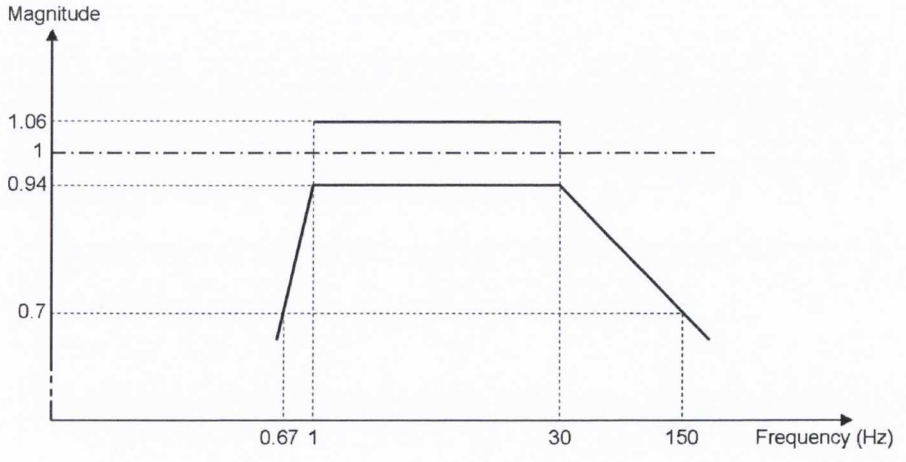
The specifications for the ECG filter then remained completely unchanged for over 20 years [78], until the publication of the AHA recommendations for automated electrocardiography in 1990 [19]. In this report, the filtering requirements are, for the first time, formulated in both the frequency and time domain. The filter amplitude response should be flat to within ± 0.5 dB from 1 to 30 Hz, with the respective 3dB-cutoff points located at frequencies lower than 0.67 Hz and higher than 150 Hz, as shown in Figure 3.1(c). The response in the time domain, which determines the system characteristic at frequencies lower than 0.67 Hz, is constrained by the maximum distortion allowable for a 1 mVs input pulse. The output should not present a displacement from the isoelectric line of greater than 0.3 mV after the pulse and the slope of the recovery response should be limited to 1 mV/s outside the pulse



(a) 1954 AHA recommendations



(b) 1967 AHA recommendations



(c) 1990 AHA recommendations

Figure 3.1: Frequency response requirements for electrocardiographic equipment as outlined in the 1954 (a), 1967 (b) and 1990 (c) AHA reports, respectively. In (a), the area allowable for the magnitude response is shaded. For comparison purposes, the graphs are drawn to scale, with the frequency axis being logarithmic.

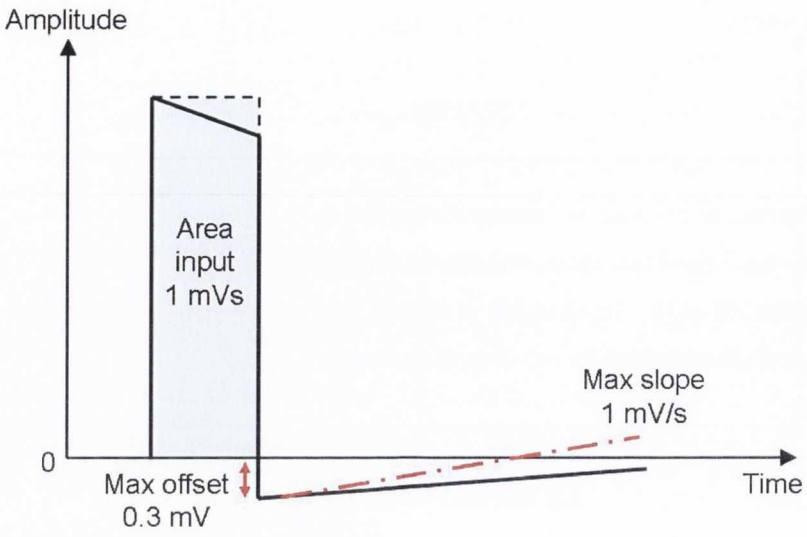


Figure 3.2: Time domain requirements set by the 1990 AHA recommendations for electrocardiographic filters.

interval, as illustrated in Figure 3.2. The current 2007 AHA scientific statement [64] reaffirms the validity of the 1990 specifications for ECG filtering. The only significant difference is the recommendation to set the high-frequency cutoff equal to 250 Hz for measurements on children and infants.

3.2.2 Rationale behind the recommendations

Comparing the characteristics in Figure 3.1, it can be noticed that, since the earliest recommendations, the frequency response of ECG recording systems is required to be effectively flat in the interval extending from 1 to 30~50 Hz. This frequency range encompasses the main components of the ECG signal, as previously described in Section 2.3.3. Therefore, the distortion introduced by the electrocardiographic instrumentation over this frequency interval must be kept to a minimum. On the other hand, the requirements for the filtering characteristic at very low frequencies as well the high-frequency cutoff specification are not so self-explanatory and their rationale is examined in the remainder of this section.

The low-frequency recommendations included in the AHA reports published since 1967 are substantially based on a study, performed in 1966 by Berson and Pipberger [16], examining the distortion of the ECG signal generated by the recording system. They analysed the effects of analogue highpass filters with different cutoff and roll-off values on the ST segments and T waves in normal and abnormal records. The cutoff frequency was varied between 0.05 and 0.5 Hz and the slope of the magnitude characteristic set at 20, 40 and 80 dB/decade. Moreover, the errors introduced into the ECG signal by a few electrocardiographs and portable recorders were also quantified. Berson and Pipberger concluded

that even measurement equipment satisfying the then current 1954 AHA recommendations led to unacceptable distortions in the interval between the end of the QRS complex and the termination of the T wave. The employment of a filter having 3dB-point equal to 0.05 Hz and roll-off of 20 dB/decade was suggested to ensure that errors due to the recording system are lower than 50 μV in the early part of the ST segment.

According to this proposal by Berson and Pipberger, a first order highpass filter with 3dB-point at 0.05 Hz has been employed to define the low-frequency behaviour of ECG measurement equipment. In the 1967 AHA report, the condition that the low-frequency characteristic of the ECG system needs to be equal to that of a 0.05 Hz single-pole high-pass filter is expressed by the requirement that the amplitude response of the electrocardiograph is at most reduced by 3 dB at 0.05 Hz and by 0.5 dB at 0.14 Hz. Furthermore, the same report also states that the time constant of the recording system should be equal to 3.2 s, which is precisely that of a first order filter with 0.05 Hz cutoff. In the 1990 AHA recommendations, the filter low-frequency characteristic is described in the time domain by its response to an input pulse, with the 3dB-point and roll-off left unspecified. Nevertheless, at least the requirement set for the displacement seems to be directly derived from the pulse response of a first order 0.05 Hz highpass filter. From Figure 3.3, it can be seen that, when a rectangular pulse 300 ms wide and 1 mVs in area is applied at the input of such a filter, the displacement from the isoelectric line occurring at the output is exactly equal to 0.3 mV, i.e. the limit specified by the AHA recommendations.

As regards the filter high-frequency response, the requirements defined in the 1967 AHA report can be similarly traced back to another study by Berson and Pipberger [17]. Different parameters related to the QRS complex, such as the peak amplitude and duration of Q, R and S waves, were analysed for normal and abnormal ECG recordings filtered with analogue lowpass systems having cutoff frequencies up to 100 Hz and roll-off values of -20 and -40 dB/decade. Filters with a resonant peak and -80 dB/decade roll-off were also employed. It emerged that wave durations are practically unaffected if the filtering system has no in-band peak and a cutoff frequency higher than 50 Hz, whereas wave amplitudes are generally decreased when the 3dB-point is reduced. Berson and Pipberger recommended a high-frequency limit for the system bandwidth above 100 Hz to avoid amplitude errors larger than 100 μV, for a filter with no amplitude peaks, and suggested the use of an even higher 3dB-point to achieve a resolution of 50 μV. Since the requirement of 100 Hz as minimum cutoff frequency was essentially due to the technological limitations of the time, the AHA 1990 recommendations revised the high-frequency 3dB-point, which was increased to 150 Hz. This allowed the AHA specifications to be harmonised with the then current Canadian standard, on which the filter implementations for marketed electrocardiographs were based [19].

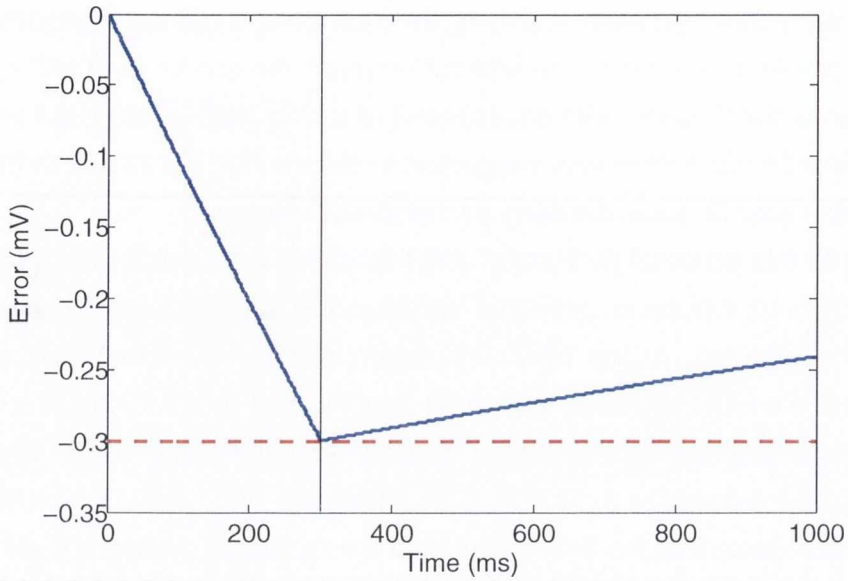


Figure 3.3: Error introduced by a first order 0.05 Hz highpass filter when a 3.33 mV×300 ms rectangular pulse is applied at the input. The difference between input and output signals is equal to the displacement from the isoelectric line for time values larger than 300 ms. The maximum allowable displacement specified by the 1990 AHA recommendations is represented on the graph by the dashed line.

The extension of the high-frequency limit for ECG recordings on infants and children recommended in the 2007 AHA statement is supported by a 2001 study by Rijnbeek et al. [79]. For each subject, the authors applied a set of digital filters with cutoff points between 50 and 300 Hz to a 12-lead average ECG and calculated the absolute error in the maximum QRS amplitude. Following the analysis of the records of more than 2000 patients, with and without cardiac abnormalities, a 250 Hz bandwidth is suggested for paediatric ECG measurements. This limits the maximum error to less than 25 μV in more than 95% of infants less than a year old. Since the upper limit of the ECG frequency spectrum decreses with age in childen, the study also points out that for adolescents, between 12 to 16 years of age, a high-frequency cutoff of 150 Hz is sufficient to guarantee amplitude errors lower than 25 μV in more than 95% of cases for most leads. This explains the AHA decision to leave the high-frequency cutoff unchanged from the previous recommendations for recordings on adults and adolescents.

3.3 Current international standards

3.3.1 European and American standards

The minimum performance requirements for diagnostic ECG devices, are currently defined by the European standard EN 60601-2-51:2003 for recording and analysing electrocardiographs [9]. The amplitude specifications of the ECG measurement system, illustrated in Figure 3.4, clearly show that its response should be as flat as possible in the frequency range extending from 0.67 to 40 Hz. Indeed, 0.67 Hz can be considered the low-frequency limit of the ECG spectrum, since it corresponds to the lowest heart rate of 40 bpm expected in adults, as previously discussed in Section 2.3.3. A further test needs to be performed to verify the high-frequency response of the electrocardiographic equipment and in particular its ability to adequately reproduce narrow R waves. The output amplitude of an input triangular wave having 20 ms duration, 1.5 mV peak amplitude and frequency lower or equal to 1 Hz, as seen in Figure 3.5, shall not be reduced by more than 12% compared to that of another triangular wave with the same peak amplitude and frequency but having 200 ms duration. On the other hand, the low-frequency characteristics of the ECG filter are, once more, detailed in terms of its response to an input pulse. These specifications, shown in Figure 3.6 for an input rectangular pulse of 3 mV amplitude and 100 ms duration, prescribe that a 300 μVs pulse shall not produce:

- An offset, or displacement, from the isoelectric line greater than 100 μV;
- A slope greater than 250 μV/s in a 200 ms interval immediately following the pulse;
- A slope greater than 100 μV/s anywhere else outside the region of the pulse.

European standards EN 60601-2-27:2006 [62] and EN 60601-2-47:2001 [63] set the requirements for the essential performance of non-diagnostic ECG monitoring equipment and ambulatory electrocardiographic systems, respectively. The filtering specifications for these types of ECG device are less strict than those contained in the EN 60601-2-51:2003 standard. For example, even though the passband of non-diagnostic electrocardiographic recording systems is still defined over the interval between 0.67 and 40 Hz, these frequencies represent the 3dB-cutoff points of the ECG filter. The low-frequency time domain requirements are also partially relaxed. The response to a rectangular 300 μVs (3 mV$\times$100 μs) pulse shall not, in fact, present a slope greater than 300 μV/s after the termination of the input wave. The constraint on the displacement from the isoelectric line is, however, unchanged, with the limit being set to 100 μV. Moreover, as it can be observed from Table 3.1, the high-frequency specifications defined for the response to input triangular waves are far less stringent than those established by the EN 60601-2-51:2003 standard.

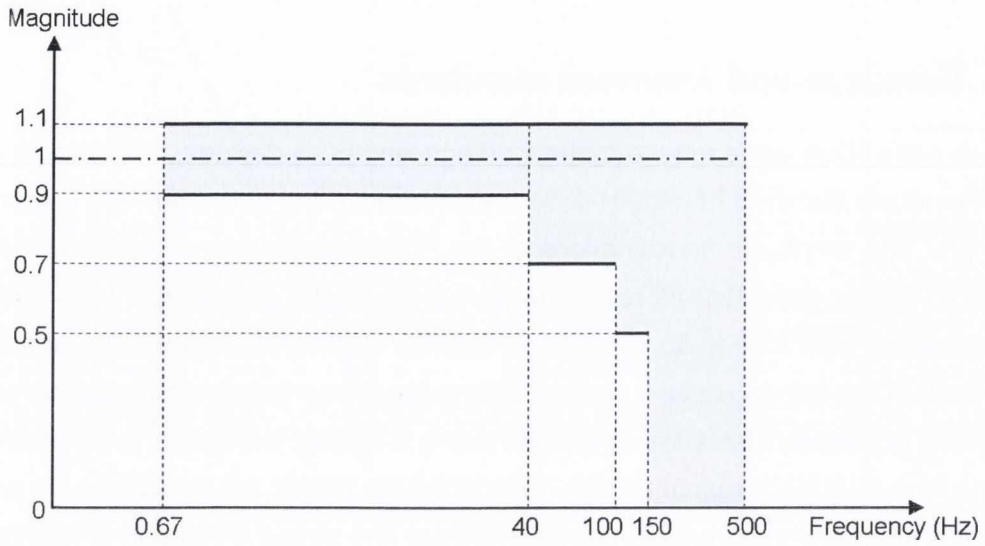


Figure 3.4: Specifications for the magnitude response of ECG measurement systems detailed in the European standard EN 60601-2-51:2003. The area allowable for the amplitude characteristic is shaded.

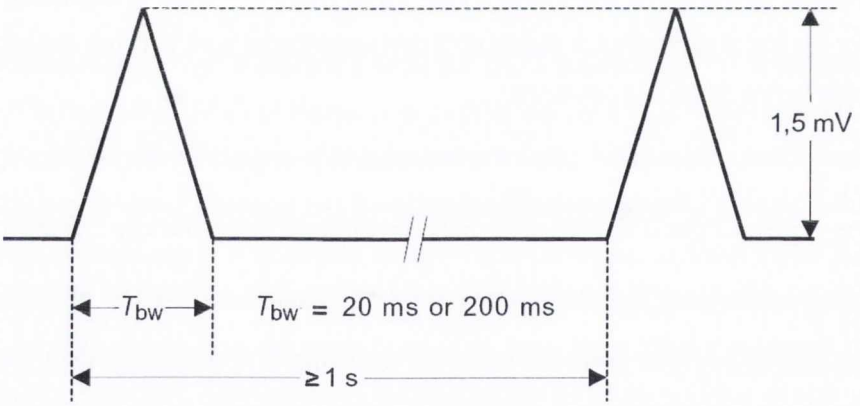


Figure 3.5: Triangular wave for testing the high-frequency response of electrocardiographs according to the European standard EN 60601-2-51:2003 [62].

Table 3.1: Parameters employed for the triangular wave test by different European standards.

	Input wave duration (ms)		Output wave amplitude ratio narrow/wide (%)	
Standard	wide	narrow	min	max
60601-2-51:2003	200	20	88	100
60601-2-27:2006	200	20	75	100
60601-2-47:2001	200	40	60	110

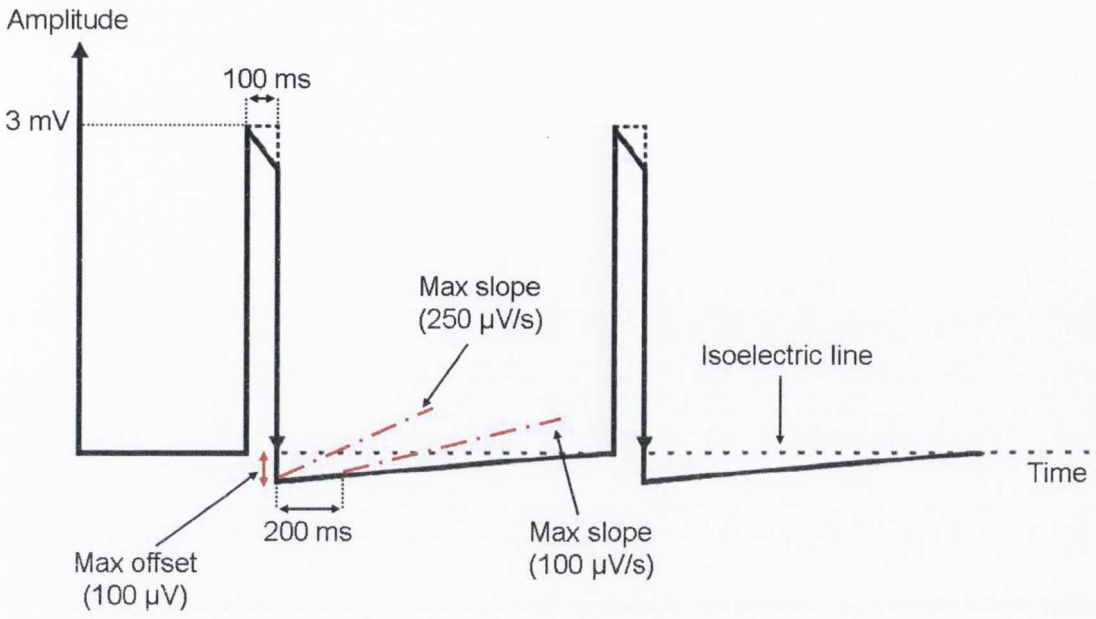


Figure 3.6: Requirements for the pulse response of ECG recording systems as specified by the European standard EN 60601-2-51:2003 (modified from [9]).

The American counterpart to the EN 60601-2-51:2003 European standard is the ANSI/AAMI EC11:1991/(R)2001/(R)2007 [15], describing the minimum performance specifications of diagnostic electrocardiographic devices. The magnitude response of the recording system is required to be flat to within $\pm$ 10% for frequencies between 0.67 and 40 Hz. Moreover, the ECG filter has to satisfy either the amplitude constraints shown in Figure 3.7 or the condition that the response to the triangular test signal illustrated in Figure 3.5 is not reduced by more that 10% when the signal duration is decreased from 200 ms to 20 ms. The pulse response requirements are exactly the same as those defined by the European standards EN 60601-2-27:2006 and EN 60601-2-47:2001 for non-diagnostic and ambulatory electrocardiographic equipment.

3.3.2 Comparison of standards and recommendations

Both European and American current standards are substantially based on the 1990 AHA recommendations, leading to very similar specifications for electrocardiographic equipment in both regions. If we consider the standards for diagnostic electrocardiographic devices, the high-frequency requirements are marginally stricter for the American standard than for its European equivalent EN 60601-2-51:2003, as seen by comparing Figures 3.4 and 3.7. In contrast, the specifications for the filter low-frequency characteristic are tighter for the EN 60601-2-51:2003. In particular, the maximum slope allowed for the response after the application of the input pulse is smaller. Furthermore, it should be noted that the European

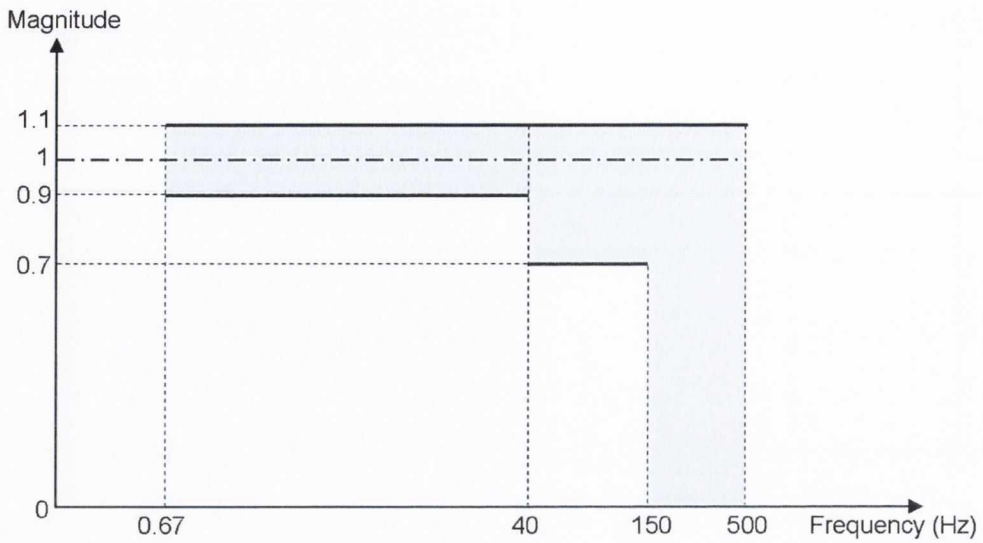


Figure 3.7: Requirements for the amplitude response of diagnostic ECG devices as defined by the American standard ANSI/AAMI EC11:1991/(R)2001/(R)2007.

standards for monitoring devices and ambulatory electrocardiographs, EN 60601-2-27:2006 and EN 60601-2-47:2001, respectively, specify a low-frequency response comparable to that required for diagnostic recording systems. The EN 60601-2-47:2001 standard even states that, for the equipment to be suitable for ST segment measurement, its low-frequency characteristic should be that of a first order highpass filter with 0.05 Hz cutoff frequency. On the other hand, there are less restrictions imposed on the high-frequency behaviour of non-diagnostic devices. The passband is, in fact, defined by the location of the 3dB-points and the requirements for the triangular wave amplitude test are more relaxed.

Analysing the differences between the standards and the 1990 AHA recommendations [19], presented in Section 3.2.1, it can be noticed that, in the latter case, no triangular wave test is specified. Nevertheless, the high-frequency cutoff frequency suggested in the AHA report is the same as that established by the American standard, as shown in Table 3.2. It can also be seen that, in the 1990 AHA report, the passband is identified by a smaller frequency range, but a stricter limit is set on the ripple allowable for the magnitude response over this interval. Regarding the ECG filter characteristics at low frequencies, the requirements are expressed in terms of the properties of the response to an input pulse in all cases. However, in the AHA recommendations, the only parameter defining the input pulse is its area, which is approximately three times larger than that of the rectangular pulse suggested for the test by the European and American standards.

In summary, the requirements detailed in the European standard for recording and analysing electrocardiographs (EN 60601-2-51:2003) are the strictest with regard to the filter low-frequency response. The boundaries specified in the 1990 AHA report for the

Table 3.2: Specifications set on the magnitude response of the ECG filter by the 1990 AHA recommendations and current international standards.

Standards/recommendations	Passband		High-frequency
	Frequency range (Hz)	Ripple (%)	3dB-cutoff (Hz)
1990 AHA report	1-30	± 6	150
60601-2-51:2003	0.67-40	± 10	100
EC11:1991/(R)2001/(R)2007	0.67-40	± 10	150

passband amplitude response are the most stringent, whereas the system high-frequency characteristic is more tightly defined in the American standard for diagnostic electrocardiographic devices (ANSI/AAMI EC11:1991/(R)2001/(R)2007). In the remainder of this thesis, the most demanding set of requirements, based on these three sources, will be taken into consideration in the design of the electrocardiographic filter.

3.4 Analysis of the pulse response constraints

3.4.1 Possible relation between pulse area and constraints

Since the publication of the 1990 AHA report [19], the low-frequency characteristic of the ECG recording system has been expressed in terms of the response to an input pulse. A brief analysis seems to indicate that the constraints which the output signal needs to satisfy are related to the area of the pulse, rather than its shape, amplitude and duration. In the EN 60601-2-51:2003 European standard [9], a rectangular waveform is given as an example of possible input pulse, but it is also stated that "another equivalent pulse" can be employed in the test. In the 1990 AHA recommendations, the input pulse is directly defined by its area and two cases involving a 2 mV$\times$100 ms rectangular and a 3 mV$\times$100 ms triangular test signal are illustrated. The amplitude k, duration t_0, and area A of the input pulse, the maximum acceptable displacement of the output signal from the isolelectric line, d, and the maximum slope allowable for the response after the pulse, m, are summarised in Table 3.3 for different standards and recommendations. From the ratios obtained dividing the maximum displacement and slope by the area of the input signal, it appears that the magnitude of the allowable offset is approximately equal to one third of the area and that, in most cases, there is a one to one relationship between the slope requirement and the area of the input pulse. If the relations between the constraints and the area are valid, it should be possible to transform the pulse response requirements into specifications for a standard impulse response. This conversion would then allow a formal definition of the low-frequency characteristic of the ECG filter, which is independent of the pulse geometry.

Table 3.3: Geometry of the input pulse and specifications for the output signal as described in different standards and recommendations.

Standards Recommend.	Shape	Amplitude k (mV)	Duration t_0 (ms)	Area A (µVs)	Displacement d (µV)	Slope m (µV/s)	d/A (1/s)	m/A (1/s^2)
60601-2-27 60601-2-47 EC11	rect	3	100	300	100	300	0.33	1
60601-2-51	rect	3	100	300	100	250 100	0.33	0.83 0.33
1990 AHA	rect	- -	- -	1000	300	1000	0.3	1
	rect	2	100	200	60	- -	0.3	- -
	triangle	3	100	150	45	150	0.3	1

3.4.2 Pulse response of a single-pole highpass filter

Let us consider a single-pole highpass filter and analyse the relationship between the dimensions of the input pulse and the characteristics of the output signal. The low-frequency specifications contained in standards and recommendations are likely to have been, at least partially, derived from the time domain response of this type of filter, as previously discussed in Section 3.2.2. The transfer function of such a first order system, having a zero at 0 Hz and a real negative pole, $-p$, is

$$H(s) = \frac{s}{s+p}. \tag{3.1}$$

If we assume an input rectangular pulse of amplitude k and duration t_0, the output of the recording system is given by

$$y_{\text{rect}}(t) = k\,[g(t) - g(t - t_0)], \tag{3.2}$$

where $g(t)$ is the filter response to a unity step:

$$g(t) = e^{-p\,t} \qquad \text{for} \quad t \geq 0. \tag{3.3}$$

Since the input signal is null after t_0, the displacement of the response from the isoelectric line after the application of the pulse is equal to both the output signal and the error introduced by the filter:

$$d_{\text{rect}}(t) = k\left[e^{-p\,t} - e^{-p(t-t_0)}\right] \qquad \text{for} \quad t \geq t_0. \tag{3.4}$$

Substituting $t = x + t_0$, the offset can be written as a function of the new variable x:

$$\begin{aligned} d_{\text{rect}}(x) &= k\left[e^{-p(x+t_0)} - e^{-p\,x}\right] \\ &= k\left[e^{-p\,x}\left(e^{-p\,t_0} - 1\right)\right] \qquad \text{for} \quad x \geq 0. \end{aligned} \tag{3.5}$$

Since p and t_0 are positive quantities, the term in parentheses in the previous equation is negative. The displacement from the isoelectric line following the pulse is also negative and its expression can be rewritten to highlight this characteristic:

$$d_{\text{rect}}(x) = -k\,e^{-p\,x}\left(1 - e^{-p\,t_0}\right) \qquad \text{for} \quad x \geq 0. \tag{3.6}$$

From Eq. (3.6), it is evident that the undershoot, or negative displacement, occurring after the application of a rectangular input to a simple first order filter is not proportional to the pulse area. Although linearly dependent on the pulse amplitude k, the offset is related to the duration t_0 through an exponential. Nevertheless, if the exponential function is expressed in terms of its power series

$$e^{\alpha} = \sum_{n=0}^{\infty} \frac{\alpha^n}{n!} = 1 + \alpha + \frac{\alpha^2}{2!} + \frac{\alpha^3}{3!} + \ldots \tag{3.7}$$

and the first two terms of the expansion are substituted into Eq. (3.6) for $\alpha = -p\,t_0$, the displacement expression becomes

$$d_{\text{rect}}(x) = -k\,t_0\left(p\,e^{-p\,x}\right) \qquad \text{for} \quad x \geq 0. \tag{3.8}$$

The error introduced by the substitution is negligible for small values of the product $p\,t_0$, that is, when the duration of the rectangular pulse is small compared with the time constant of the filter. In this case, the offset from the isolectric line can be considered proportional to the area of the input pulse, $A = k\,t_0$. Furthermore, it should be noticed that the filter impulse response,

$$h(x) = -p\,e^{-p\,x} \qquad \text{for} \quad x > 0, \tag{3.9}$$

can be identified in Eq. (3.8) and this equation rewritten as

$$d_{\text{rect}}(x) = A\,h(x) \qquad \text{for} \quad x > 0. \tag{3.10}$$

The undershoot occurring after a rectangular input pulse can, therefore, be expressed in terms of the filter impulse response scaled by the pulse area, provided the duration of the input signal is sufficiently short.

Figure 3.8(b) shows the error introduced by a 0.05 Hz single-pole highpass filter when a set of rectangular pulses is applied at the input. These pulses, illustrated in Figure 3.8(a), have different durations, but a constant area of 300 μVs, that is, the area of the pulse specified by the European and American standards (see Table 3.3). It can be observed that the error occurring after the end of the pulse converges towards the filter impulse response as the duration of the rectangular wave diminishes. On the other hand, Figure 3.8 also highlights how the approximation introduced in Eq. (3.8) loses validity when the width of the rectangular pulse is increased. Furthermore, it should be pointed out that the displacement from the isoelectric line is at a maximum if calculated from the impulse response according to Eq. (3.10). It can be seen from Table 3.4 that the maximum undershoot decreases as the duration of the input signal increases.

The slope of the response to the rectangular waveform is obtained by differentiating the filter output given by Eq. (3.2), which is equal to the offset as expressed in Eq. (3.6):

$$m_{\text{rect}}(x) = k\left(1 - e^{-p\,t_0}\right) p\, e^{-p\,x} \qquad \text{for} \quad x \geq 0. \tag{3.11}$$

For small values of the product $p\,t_0$, the exponential depending on this quantity can be substituted, once more, with the first two terms of the power series expansion in Eq. (3.7), yielding:

$$m_{\text{rect}}(x) = k\,t_0\left(p^2 e^{-p\,x}\right) \qquad \text{for} \quad x \geq 0, \tag{3.12}$$

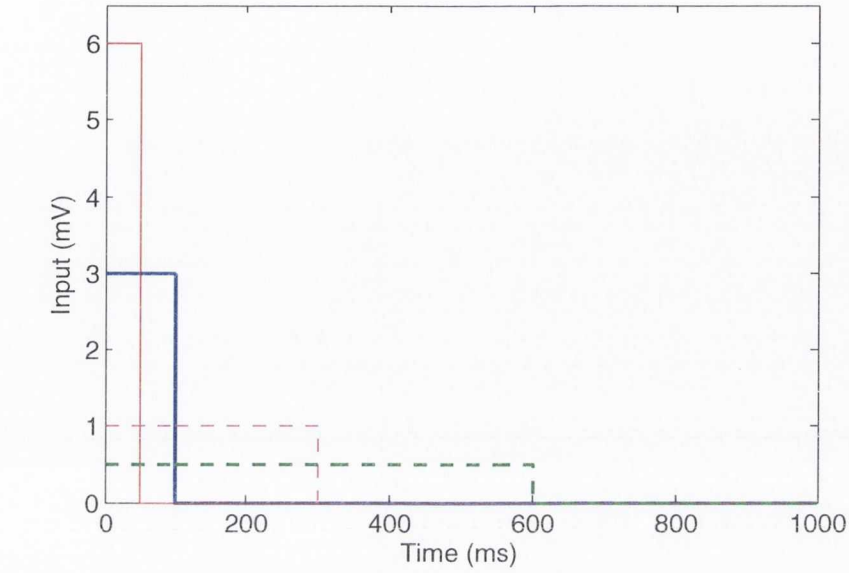
where the expression in parentheses corresponds to the derivative of the system impulse response given in Eq. (3.9). Therefore, the slope of the output signal after the termination of the input pulse can also be rewritten in terms of the system response to a Dirac delta function of area A:

$$m_{\text{rect}}(x) = A\,h'(x) \qquad \text{for} \quad x > 0. \tag{3.13}$$

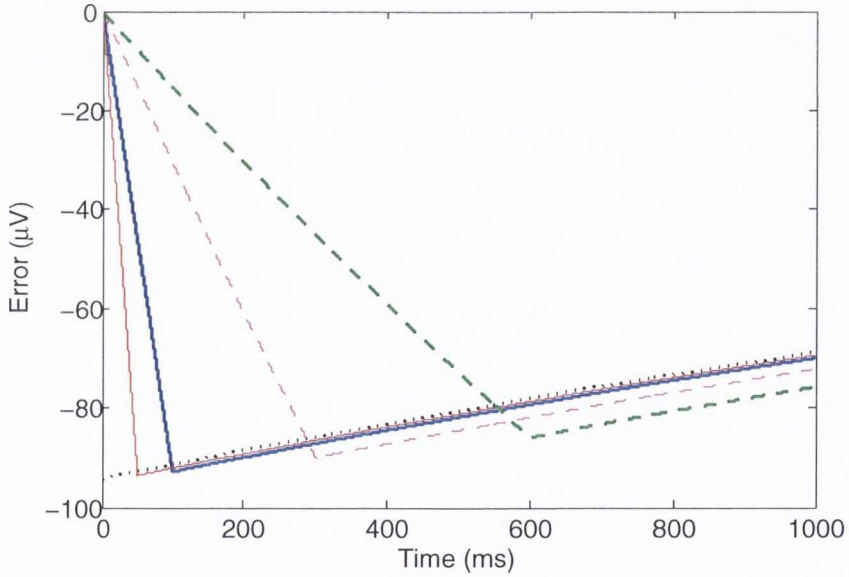
Let us now determine the characteristics of the filter response to an input triangular wave having the same area as the previously analysed rectangular pulse. The analytical expression for the triangular signal in Figure 3.9 can be obtained as the combination of

Table 3.4: Maximum displacement introduced by a 0.05 Hz single-pole highpass filter for different input signals (see Figure 3.8(b)).

Input pulse shape	Undershoot (μV)
Dirac delta 300 μVs	94.2
Rectangular 6 mV×50 ms	93.5
Rectangular 3 mV×100 ms	92.8
Rectangular 1 mV×300 ms	89.9
Rectangular 0.5 mV×600 ms	85.9



(a) Rectangular input signals



(b) Difference between output and input signals

Figure 3.8: Response of a 0.05 Hz first order highpass filter to a set of rectangular input pulses (a), having equal area but different durations. The error introduced by the system for each input signal and the filter response to an input Dirac delta having the same area of the rectangular pulses (dotted line) are shown in (b).

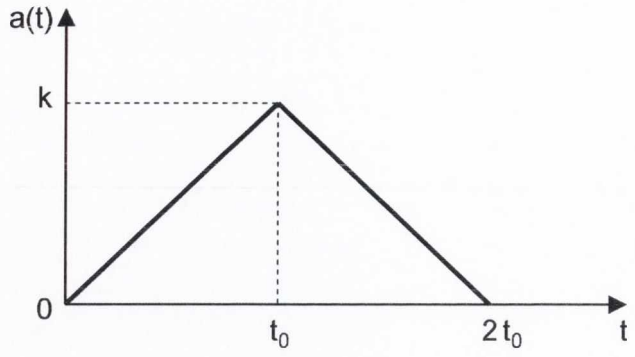


Figure 3.9: Triangular pulse.

ramp functions scaled and translated along the time axis:

$$a(t) = \frac{k}{t_0}\left[r(t) - 2r(t-t_0) + r(t-2t_0)\right], \tag{3.14}$$

where the ramp function is defined as:

$$r(t) = \begin{cases} t & \text{for} \quad t \geq 0 \\ 0 & \text{for} \quad t < 0 \end{cases} \tag{3.15}$$

and k/t_0 is the slope of the upward portion of the triangular pulse. The Laplace transform of the response of the first order highpass filter to the ramp function is:

$$F(s) = R(s)\,H(s) = \frac{1}{s(s+p)} \qquad \text{with} \quad R(s) = \frac{1}{s^2}. \tag{3.16}$$

Using the Heaviside partial fraction method, the response to the ramp in the time domain is readily found to be:

$$f(t) = \frac{1}{p}\left(1 - e^{-p\,t}\right) u(t), \tag{3.17}$$

where $u(t)$ is the unit step function. The response of the filter to the triangular pulse can thus be expressed as:

$$\begin{aligned} y_{\text{tr}}(t) &= \frac{k}{t_0}\left[f(t) - 2f(t-t_0) + f(t-2t_0)\right] = \\ &= \frac{k}{t_0}\frac{1}{p}\left\{\left(1 - e^{-p\,t}\right) u(t) - 2\left[1 - e^{-p(t-t_0)}\right] u(t-t_0) + \left[1 - e^{-p(t-2t_0)}\right] u(t-2t_0)\right\}. \end{aligned} \tag{3.18}$$

The displacement from the isoelectric line after the end of the pulse is obtained by noting that all of the step functions in the previous equation have a value of unity for $t \geq 2t_0$,

yielding:

$$\begin{aligned} d_{\text{tr}}(t) &= \frac{k}{t_0}\frac{1}{p}\left\{1 - e^{-p\,t} - 2\left[1 - e^{-p(t-t_0)}\right] + 1 - e^{-p(t-2t_0)}\right\} \\ &= \frac{k}{t_0}\frac{1}{p}\left[-e^{-p\,t} + 2e^{-p(t-t_0)} - e^{-p(t-2t_0)}\right] \qquad \text{for} \quad t \geq 2t_0. \end{aligned} \tag{3.19}$$

The substitution $t = x + 2t_0$ is performed and Eq. (3.19) becomes a function of x:

$$\begin{aligned} d_{\text{tr}}(x) &= \frac{k}{t_0}\frac{1}{p}\left[-e^{-p\,(x+2t_0)} + 2e^{-p(x+t_0)} - e^{-px}\right] \\ &= \frac{k}{t_0}\frac{1}{p}e^{-p\,x}\left(2e^{-p\,t_0} - e^{-2p\,t_0} - 1\right) \\ &= -\frac{k}{t_0}\frac{1}{p}e^{-p\,x}\left(1 - e^{-p\,t_0}\right)^2 \qquad \text{for} \quad x \geq 0. \end{aligned} \tag{3.20}$$

If the exponential dependent on t_0 is replaced with the first two terms of its power series from Eq. (3.7), then Eq. (3.20) can be rewritten as:

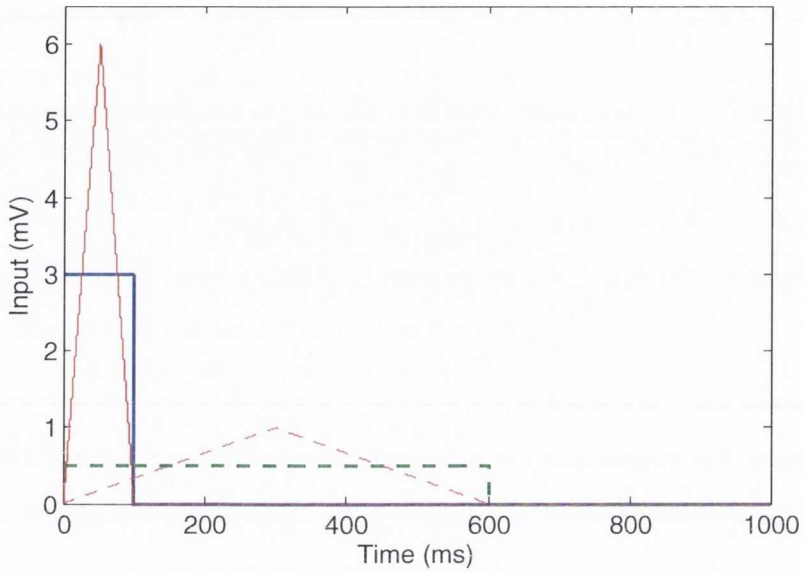
$$\begin{aligned} d_{\text{tr}}(x) &= -\frac{k}{t_0}\frac{1}{p}e^{-p\,x}(p\,t_0)^2 \\ &= -k\,t_0\left(p\,e^{-p\,x}\right) \qquad \text{for} \quad x \geq 0. \end{aligned} \tag{3.21}$$

This is the same result as was obtained for the offset following a rectangular input pulse, as is evident by comparing Eq. (3.21) with Eq. (3.8). In Figure 3.10, it can be seen that, for a 0.05 Hz first order highpass filter, the undershoot occurring after a triangular input pulse is very similar to that for a rectangular wave having the same area and duration.

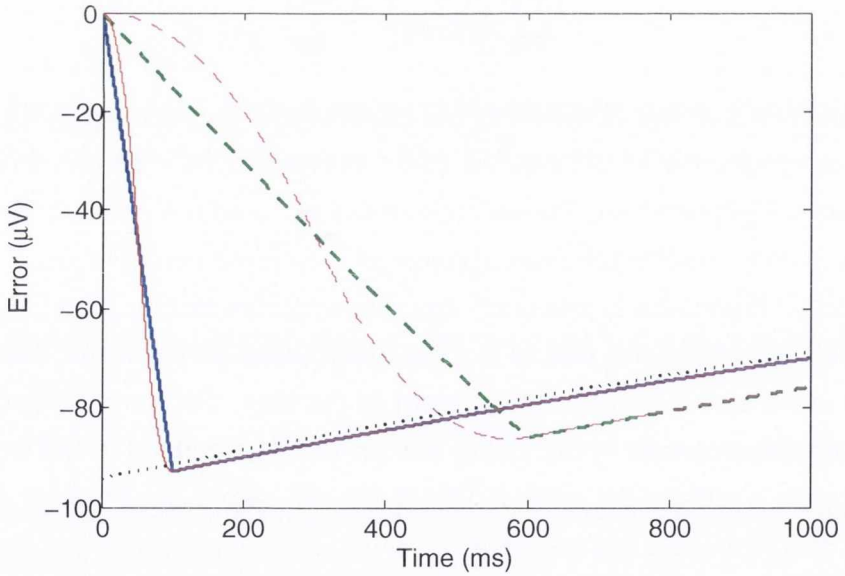
Furthermore, it is possible to prove the equivalence between the slope of the response to the triangular waveform and that to a rectangular pulse of the same area, when the duration t_0 is much less than the time constant of the filter. For small values of $p\,t_0$, the derivative of the displacement in Eq. (3.20) can, in fact, be reduced to the expression for the slope following a rectangular wave in Eq. (3.12). Therefore, the relevant properties of the response of a first order highpass filter to a triangular input pulse can be reduced to those determined for a rectangular input pulse, provided the duration of the waveforms is much less than the filter time constant.

3.4.3 Reformulation of time domain constraints

Based on the analysis performed in the previous section, it is possible to conclude that, in general terms, the pulse response of a single-pole filter depends on the shape of the input signal and that there exists a non-linear relationship between the output function and the



(a) Rectangular and triangular input signals



(b) Difference between output and input signals

Figure 3.10: Response of a 0.05 Hz first order highpass filter to a set of rectangular and triangular input pulses (a), having equal area. The error introduced by the system for each input signal and the filter response to an input Dirac delta having the same area of the input pulses (dotted line) are shown in (b).

duration of the input pulse. Nevertheless, it also emerges that both the displacement of the output response from the isolectric line and the slope of the output signal after the end of the pulse can be considered to be independent of the geometry of the input signal when the duration of the stimulus is sufficiently small. This condition seems to be fulfilled by the input rectangular signal suggested by the international standards to test the low-frequency behaviour of electrocardiographic equipment, shown in Figure 3.6. The response of a 0.05 Hz single-pole highpass filter to such a pulse is represented by the thick solid curve in Figure 3.8(b). From this figure and Table 3.4, it is evident that there is very little difference between the maximum undershoot caused by the 3 mV$\times$100 ms rectangular pulse and by a Dirac delta function of the same area. A similar argument applies to the slope of the pulse response, since the relation between this characteristic of the output signal and the derivative of the impulse response is shown in Eq. (3.13) to be linear for input signals of short duration. Therefore, if the requirements on the maximum allowable offset and slope presented in Table 3.3 are derived from the response of a 0.05 Hz first order highpass filter to a pulse of similar time duration as that specified by the standards, it is possible to transform the time domain response constraints into specifications for the impulse response of the ECG recording system.

The conversion between pulse and impulse response constraints is based on the consideration that the Dirac delta function can be seen as the limit of a rectangular waveform with unity area when its duration tends to zero. Let us consider the offset condition for a rectangular input pulse of amplitude k and duration t_0 and generalise the finding of the previous section. The requirement on the displacement of the response can be expressed as:

$$k\,|g(t) - g(t - t_0)| \leq d \qquad \text{for} \quad t \geq t_0, \tag{3.22}$$

where $g(t)$ is the response of an ECG filter of undefined transfer function to a unity input step and d is the maximum allowable offset. Both terms can be divided by the pulse amplitude and duration, yielding:

$$\frac{|g(t) - g(t - t_0)|}{t_0} \leq \frac{d}{k\,t_0} \qquad \text{for} \quad t \geq t_0. \tag{3.23}$$

Substituting $t = x + t_0$ leads to:

$$\left| \frac{g(x + t_0) - g(x)}{t_0} \right| \leq \frac{d}{A} \qquad \text{for} \quad x \geq 0, \tag{3.24}$$

where the area of the pulse, A, has been substituted for $k\,t_0$. The limit of the expression on

the left side of Eq. (3.24) can be now calculated for t_0 going to zero:

$$\lim_{t_0 \to 0} \frac{g(x+t_0) - g(x)}{t_0} = g'(x) = h(x), \tag{3.25}$$

where $h(x)$ is the system impulse response. Since the step response $g(x)$ is discontinuous at $x = 0$, its derivative is not defined here and this point excluded from the transformation. The condition on the displacement from the isolelectric line can thus be rewritten in terms of the impulse response as:

$$|h(x)| \leq \frac{d}{A} \qquad \text{for} \quad x > 0, \tag{3.26}$$

with d/A being approximately equal to 0.33 as seen from Table 3.3.

In a similar manner, the condition imposed on the slope of the pulse response can also be reduced to an inequality involving the filter impulse response. For input pulses of short duration, the requirement on the slope can, in fact, be reduced from

$$k\,[h(t) - h(t - t_0)] \leq m \qquad \text{for} \quad t \geq t_0 \tag{3.27}$$

to

$$h'(x) \leq \frac{m}{A} \qquad \text{for} \quad x > 0, \tag{3.28}$$

where m is the maximum acceptable slope and the value of the ratio m/A is given in Table 3.3 for different standards and recommendations.

As previously highlighted, the definition of the low-frequency characteristic of the ECG filter in terms of impulse response allows the time domain constraints to be simplified, which become independent of the geometry of the input signal. This type of formulation may also be beneficial to the direct design of the ECG filter from the specifications. An analytical expression of the requirements for the system transfer function is indeed more easily derived from the impulse response. Furthermore, a suitable waveform to employ in practical tests could be freely chosen, provided its duration is limited compared to the system rise time.

On the other hand, for the transformation between pulse and impulse response constraints to be fully legitimate, it would be necessary to prove that both time domain specifications have actually been derived from the response of a 0.05 Hz first order highpass filter. As regards the offset condition, the informative material accompanying the EN 60601-2-47:2001 standard [63] indicates that the displacement from the baseline allowed after the pulse is indeed representative of the undershoot occurring for a single-pole 0.05 Hz system. However, the motivation for the slope constraint is unclear and appears to be related to the clinical significance of voltage changes across the ST segment. Therefore, not being able

to determine the rationale behind the pulse response specifications, the author can only recommend that the formulation of the time domain requirements is made uniform throughout the different international standards and that the geometry of the input pulse to employ in the tests is completely defined. More specifically, a triangular wave resembling in amplitude and duration an average QRS complex could be used as input signal, as previously suggested by Heinonen [80] and Bailey [81]. The shape of the ST segment, which is a fundamental diagnostic feature of the electrocardiogram, is, in fact, primarily affected by the recovery of the electrocardiographic filter from the preceding QRS complex.

3.5 Filter phase response

3.5.1 Review of the phase linearity requirement

Even though no mention of the phase response of electrocardiographic recording systems is present in the normative section of the standards, strong relevance has been given in the literature to this characteristic of the ECG filter. Particular focus has been placed on the phase linearity of the highpass filter that determines the low-frequency behaviour of the ECG monitoring system [13, 18, 19, 24–26, 82].

The relevance attributed to the phase response of electrocardiographs at low frequencies can be traced back to the work performed in the early 1980's by Tayler and Vincent [13, 25]. They noticed that artifactual ST segment distortions, such as those shown in Figure 3.11, can occur in ambulatory ECG records, thus impairing diagnoses related to myocardial ischaemia. Consequently, they analysed the amplitude and phase response of several ECG measurement systems, finding that ST segment distortion was present, even when the magnitude characteristic of these devices satisfied the flatness requirement specified by the then current 1975 AHA recommendations [78]. Most of the electrocardiographs under study showed marked phase non-linearities, whose effect on the ST segment could be reproduced by applying an allpass filter to the ECG signal. Tayler and Vincent concluded that the phase shift introduced by the recording system delays the low frequency components of the QRS complex so that, in the time domain, they overlap the ST segment. It was thus suggested that, in order for the ECG waveform to be faithfully reproduced, electrocardiographic monitors need to have a linear phase response and a flat amplitude response for frequencies as low as 0.5 Hz. This frequency is, in fact, sometimes considered the lowest limit of the ECG signal bandwidth, since it corresponds to a heart rate of 30 beats per minute (see Section 2.3.3). This article also proposed that ideally the ECG recording devices should have zero magnitude response at frequencies lower than 0.5 Hz to eliminate baseline drift and minimise low-frequency noise and interference.

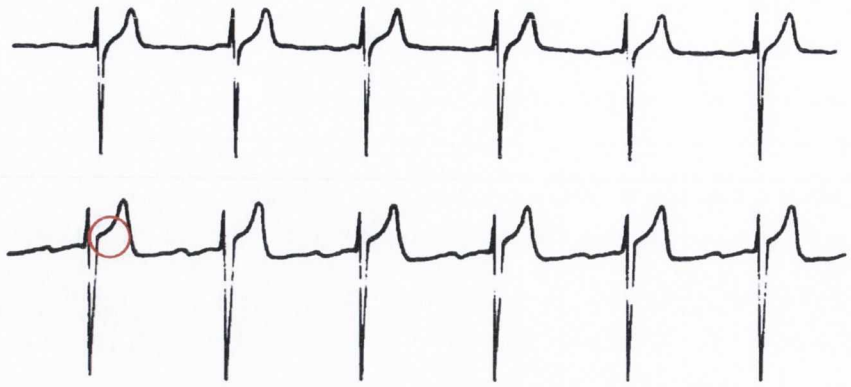


Figure 3.11: Artifactual elevation of the ST segment produced by an ambulatory electrocardiographic device (modified from [13]). An undistorted recording of a normal V_2 lead signal is presented in the upper trace. The bottom trace shows the same signal re-recorded using an ECG monitor that introduced ST segment abnormalities.

The 1990 AHA report [19] also contains references to the phase response of the electrocardiographic filter, even though the phase linearity condition is not included in the recommendations for ECG recording devices. It is stated that a single-pole highpass system with 3dB-cutoff at 0.05 Hz does not cause noticeable distortions in the ST segment, T wave or QT interval, since the phase shift introduced by the filter is less than 6° for frequencies higher than 0.5 Hz, that is, over the ECG spectrum. The AHA recommendations also suggest that a system that fulfils the amplitude response requirements shown in Figure 3.1(c) and has a phase linearity at least equal to that of a 0.05 Hz first order highpass filter is likely to meet the pulse response criteria specified in the report and presented in Section 3.2.1.

The tradition of relating the distortion of the ST segment to the lack of phase linearity is deeply rooted and even recently published articles [18, 24, 26, 82] dedicate much attention to the phase response of the ECG equipment. These studies generally present the most recent international standards for electrocardiographic devices, which quantify the distortions introduced by the ECG filtering process based on the response to an input pulse and do not contain any reference to the phase response of the system. Nevertheless, the work by Abacherli and Schmid [82] still ends up concentrating on the low-frequency cutoff of the amplitude response and on the phase linearity of the ECG filter, be it analogue or digital, whereas the articles by Burri et al. [18] and Luo and Johnston [24] continually stress how artifactual elevation or depression of the ST segment can be eliminated if the filter has a linear phase characteristic.

3.5.2 Comparison of phase and pulse response requirements

Despite the fact that the phase linearity requirement often appears alongside the specifications on the pulse response of the measurement system [18, 19, 24, 82], it should be noted that these conditions are not equivalent. In order for the ECG signal to be faithfully recorded, the phase response of the equipment needs to be linear in-band. In fact, this ensures that all of the ECG frequency components are delayed by the same amount in the time domain, minimising the overlap of contributions due to the different constituent waves of the electrocardiogram. The phase linearity condition is, however, not sufficient to guarantee that the offset and slope of the filter response to a set input pulse comply with the requirements outlined in the standards.

Generally speaking, if the shape of the input is to be preserved, the impulse response of the filter through which the signal is passing needs to have no overshoot or ringing and to be symmetrical about the time at which the peak occurs [83]. A filter satisfying these conditions should have an ideal Gaussian magnitude response and a perfectly linear phase response at all frequencies. A Gaussian magnitude response is, however, physically unrealisable, since it implies time domain responses starting at negative infinity when a input signal is applied at some finite time, that is, the system is not causal. Nevertheless, the filter amplitude should tend to approximate this type of response, which is perfectly smooth and without any abrupt change in attenuation at the cutoff frequency. The overshoot occurring in the impulse or step response of a filter is a consequence of the steepness of the amplitude response at the cutoff and is exaggerated if the phase response is not linear over the whole bandwidth, since phase non-linearity leads to a non-symmetric impulse response [84]. Therefore, a system with a sharply changing attenuation at the cutoff inevitably generates distortion in the time domain response, even when its phase response is perfectly linear.

Let us consider again the work by Berson and Pipberger [16] presented in Section 3.2.2, which examined the errors introduced in the electrocardiogram by the low-frequency response of the recording system. They concluded that the distortions generated by the highpass filter are dependent on both the cutoff frequency and the steepness of the amplitude response and, for this reason, excluded the possibility of employing a filter with a roll-off greater than 20 dB/decade, even when its 3dB-point is set as low as 0.05 Hz. The first order highpass filter proposed by this study was, however, used in the 1990 AHA report to suggest a general condition for the phase response of ECG recording devices. In abstracting a phase linearity requirement from the 0.05 Hz single-pole system, it was not considered that the properties of a first order system are completely determined by a single parameter, namely, the frequency of the pole. For a first order system, the shape of the

magnitude and phase responses is fixed, with the cutoff point defining their position on the frequency axis. Furthermore, the amplitude of its impulse response is also determined by the pole frequency, as shown in Eq. (3.9). Therefore, setting the 3dB-point lower than the lowest ECG frequency component allows the phase non-linearity to be shifted outside of the signal bandwidth and, at the same time, decreases both the undershoot and the recovery slope of the pulse response. On the other hand, for higher order analogue or digital filters, the relationship between frequency and time domain characteristics is more complex and the amplitude and phase responses need to be considered simultaneously to determine the system time domain behaviour.

The dependence of the ST segment distortion on the slope of the ECG filter magnitude characteristic was actually not recognised by Tayler and Vincent. This is substantially related to the amplitude response of the filter employed in their analysis to intentionally reduce the ECG signal components at low frequencies [13]. They performed a discrete Fourier transform on different electrocardiograms, reduced the magnitude of low-frequency harmonics and reconstructed the signal in the time domain, to compare it with the original. In particular, they attenuated the magnitude response by 10% at 2 Hz and 20% at 1 Hz. This amplitude reduction is, however, less than the loss produced by applying a single-pole highpass filter to the ECG signal. The amplitude response for the first order system described by Eq. (3.1) is given by

$$|H(f)| = \sqrt{\frac{f^2}{f^2 + f_0^2}}, \tag{3.29}$$

where $f_0 = p/(2\pi)$ is the filter 3dB-point. Inverting the above equation allows the cutoff frequency to be calculated for a given attenuation occurring at a set frequency. For a loss of 10% at 2 Hz, the 3dB-point of the first order filter turns out to be 0.97 Hz. In other words, the attenuation of the single-pole filter at 1 Hz is approximately 30%, whereas the filter employed by Tayler and Vincent only causes a loss of 20% in the signal amplitude at the same frequency.

3.5.3 Analysis of a bidirectional filter

In order to provide an example of the lack of equivalence between phase and pulse response constraints, the characteristics of a bidirectional highpass filter are examined. This type of filter is often cited as a possible non real-time improvement over the single-pole 0.05 Hz highpass filter [13, 18, 19, 24, 26, 77, 82]. In 1975 Longini et al. [85] suggested for the first time the employment of bidirectional filters in biomedical applications to overcome the problem of phase shift being introduced into physiological signals by the recording system.

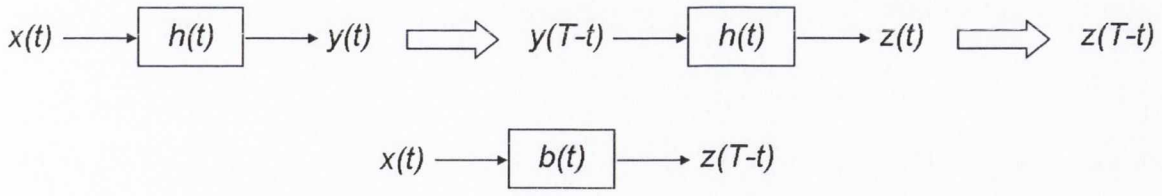


Figure 3.12: Diagram illustrating how the bidirectional filter $b(t)$ is derived from the base filter $h(t)$. T represents the total duration of the input signal.

The input signal, after being filtered in the forward direction, is inverted and passed though the filter a second time. The output data are obtained by finally inverting the time axis. This process is illustrated in Figure 3.12.

Longini et al. proved that the phase characteristic of the bidirectional filter is null at all frequencies and its attenuation in decibels is double that of the base filter. Let us derive the transfer function of the bidirectional filter in order to highlight these properties. Using the convention shown in Figure 3.12, the transfer function of the output from the first pass is equal to

$$Y(s) = X(s)H(s). \tag{3.30}$$

$y(t)$ is subsequently inverted along the time axis and shifted by the duration of the signal, T, to obtain $y(T-t)$. The time shift is introduced to allow the inverted signal to start at $t = 0$, that is, to be causal. The Laplace transform of this signal is given by

$$\mathscr{L}\left[y(T-t)\right] = -e^{sT}Y(-s) \tag{3.31}$$

The transform of the output from the second pass, $z(t)$, is

$$Z(s) = -e^{sT}Y(-s)H(s) \tag{3.32}$$

and that of the ultimate output from the system can be expressed as

$$\mathscr{L}\left[z(T-t)\right] = -e^{sT}Z(-s). \tag{3.33}$$

By substituting sequentially Eq. (3.32) and Eq. (3.30) into the previous equation, the final output of the bidirectional filter can be written as:

$$\begin{aligned}\mathscr{L}\left[z(T-t)\right] &= -e^{sT}\left[-e^{-sT}Y(s)H(-s)\right] \\ &= \left[X(s)H(s)\right]H(-s) \\ &= X(s)\left[H(s)H(-s)\right].\end{aligned} \tag{3.34}$$

Therefore, the transfer function of the bidirectional filter is $B(s) = H(s)H(-s)$. Furthermore, it should be noticed that the effect of the time shift introduced, after the first data inversion, to get a physically realisable signal, $y(T-t)$, is balanced by the second time shift applied on the $z(-t)$ signal. For $s = j\omega$, the Fourier transform of the bidirectional filter can be obtained as:

$$\begin{aligned} B(j\omega) &= H(j\omega)H(-j\omega) = H(j\omega)H^*(j\omega) \\ &= |H(j\omega)|^2 \left[\angle H(j\omega) + \angle H^*(j\omega)\right] = |H(j\omega)|^2 \left[\angle H(j\omega) - \angle H(j\omega)\right] \\ &= |H(j\omega)|^2 \angle 0. \end{aligned} \tag{3.35}$$

From the above equation, it is evident that the filter has a purely real transfer function and that no net phase shift is introduced in the filtering process:

$$|B(\omega)| = |H(\omega)|^2 \qquad \text{and} \qquad \angle B(\omega) = 0. \tag{3.36}$$

If the base filter, $H(s)$, through which the data are passed twice, is the first order highpass filter described by Eq. (3.1), the amplitude response of the bidirectional filter can be simply obtained by squaring Eq. (3.29):

$$|B(f)| = \frac{f^2}{f^2 + f_0^2}, \tag{3.37}$$

where f_0 is the 3dB-point of the single-pole filter. Let us now determine the value of f_0 needed for the bidirectional filter to achieve a loss of 0.5 dB at 1 Hz, which is the passband limit specified in the 1990 AHA recommendations for low frequencies (see Figure 3.1(c)). Inverting the above equation and substituting for an attenuation of 6% at 1 Hz, f_0 turns out to be approximately 0.25 Hz. The amplitude of both the first order highpass filter and the bidirectional filter obtained from it are shown in Figure 3.13.

The error introduced by the filters when a 3.33 mV$\times$300 ms rectangular input pulse is applied at t = 5 s is presented in Figure 3.14. Even though the output characteristic of the bidirectional filter is superior to that of the first order base filter, the displacement from the isolectric line still exceeds the limit set by the 1990 AHA recommendations to guarantee an acceptable low-frequency response for the ECG recording system. Therefore, the response of the bidirectional filter to an input pulse confirms that the phase linearity condition is not sufficient to prevent distortion in the time domain. Furthermore, it is also proven that a system fulfilling the 1990 AHA amplitude response requirements and having a better phase linearity than that of a 0.05 Hz first order highpass filter does not meet the pulse response criteria specified by the AHA recommendations, in contrast to what is stated in the 1990

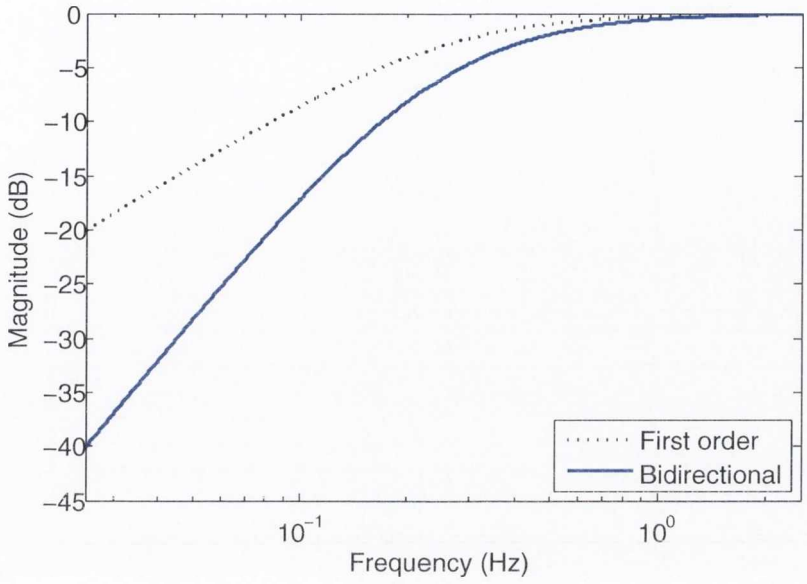


Figure 3.13: Magnitude response of a first order highpass filter having 3dB-point at 0.25 Hz and of the bidirectional filter constructed from it.

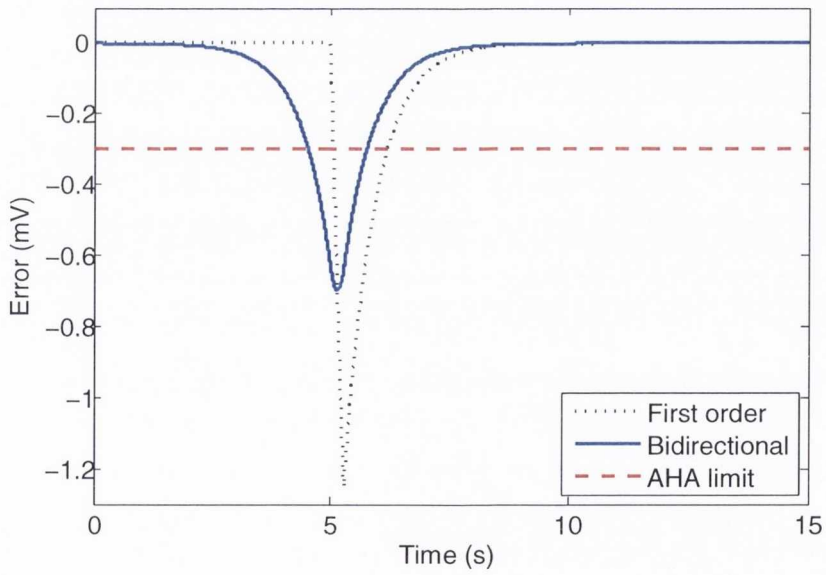


Figure 3.14: Error introduced by a 0.25 Hz first order highpass system and by the bidirectional filter derived from it when a 3.33 mV$\times$300 ms rectangular input pulse is applied at t = 5 s. The limit defined in the 1990 AHA report for the undershoot is represented on the graph by the dashed line.

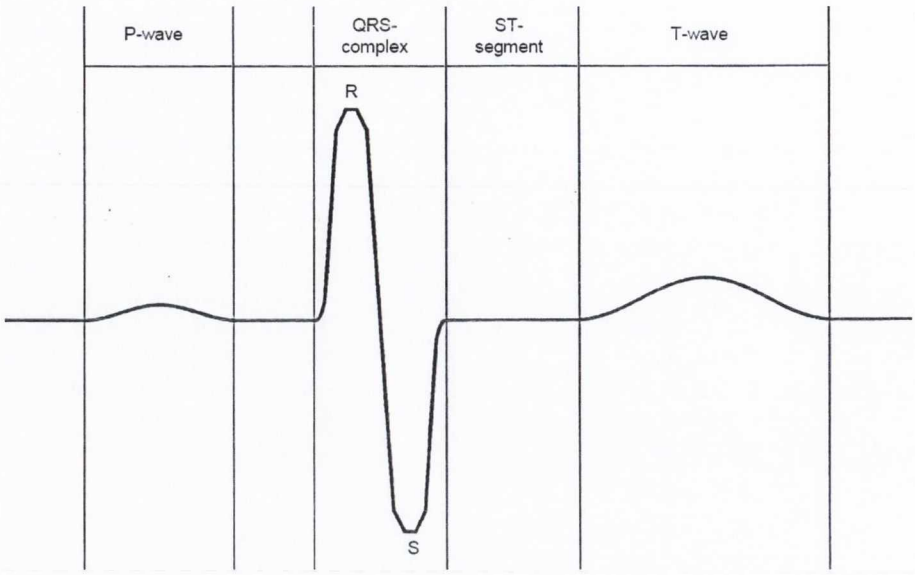


Figure 3.15: Typical shape of a calibration ECG signal [9]. The ECG terminology is used to identify the principal components of the calibration signal.

report itself.

3.6 Alternative test of the filter response

The EN 60601-2-51:2003 European standard [9] outlines an alternative method of testing an electrocardiograph response which is based on calibration waveforms. These signals have a shape similar to the ECG, with intervals and durations of the constituent waves selected to simulate real electrocardiograms, but are defined by mathematical functions. The calibration waveforms are constructed in a piecewise fashion of first and second degree polynomials and sinusoids. Furthermore, the first and second derivatives of the signal are limited so that the onset and termination of the ECG constituent waves are smooth [9]. The general shape of a calibration ECG signal is shown in Figure 3.15.

The test specified in the standard allows simultaneous verification of the responses of the electrocardiographic device at both high and low frequencies. Given a set of input calibration ECGs, the output peak amplitude of R and S waves shall not deviate by more than 5% from the input values, whereas the error on the amplitude of the ST segment, as measured between 20 and 80 ms after the end of the QRS complex, needs to be limited to ± 25 μV. Furthermore, the ST segment slope cannot exceed 50 μV/s. The calibration signals employed in the test are shown in Figure 3.16 and the main properties of their constituent waves are reported in Table 3.5. It can be noticed that the waveforms exhibit varied features, so that they are representative of both normal and abmormal recordings

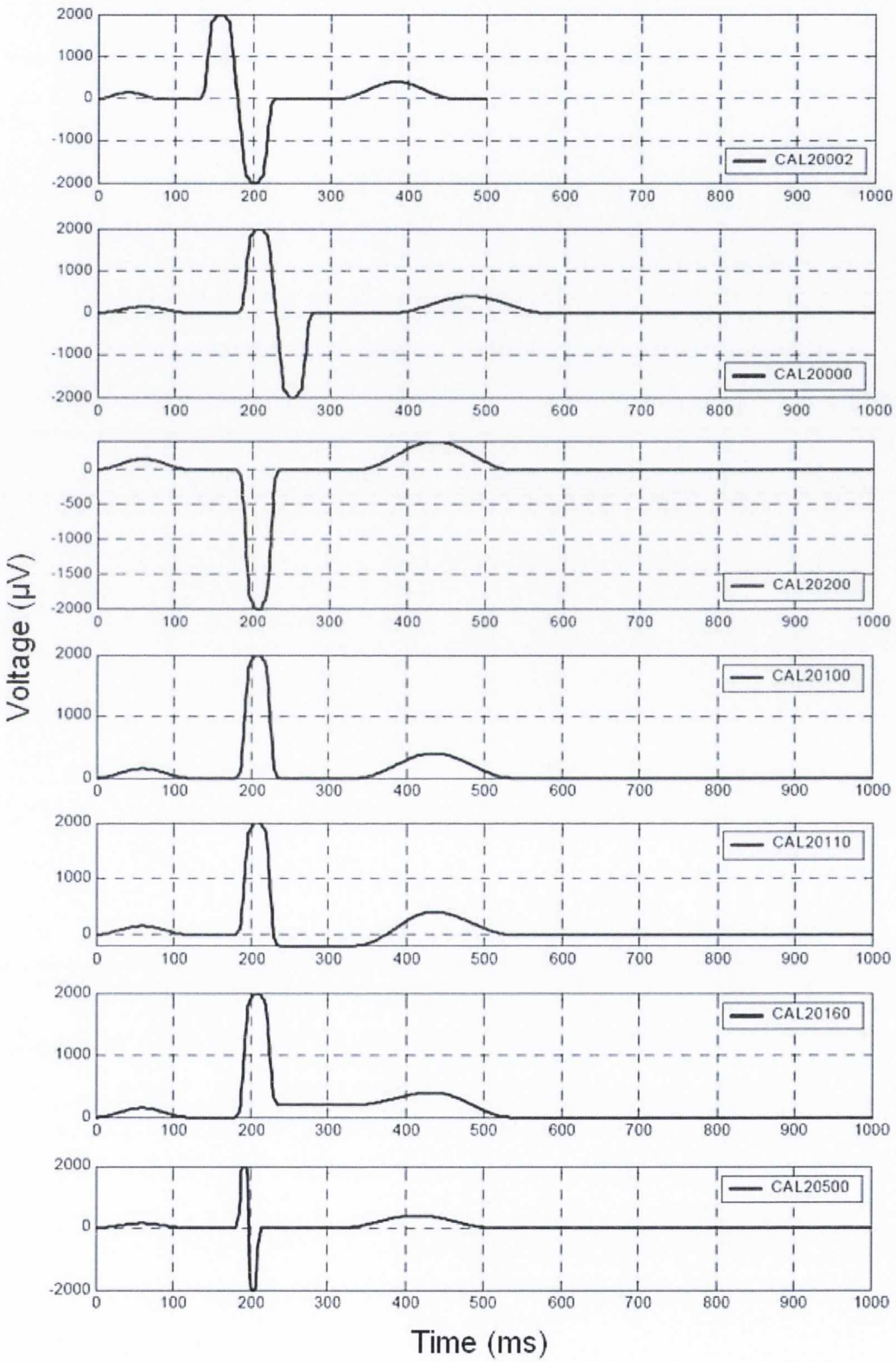


Figure 3.16: Calibration signals used to test the electrocardiograph response according to the EN 60601-2-51:2003 standard [86].

Table 3.5: Features of the calibration waveforms shown in Figure 3.16 (from [87]).

Signal	Amplitude (μV)						Duration (ms)						HR (bpm)
	P	Q	R	S	ST	T	P	PQ	Q	R	S	QT	
CAL20002	150	0	2000	-2000	0	400	76	128	0	50	50	334	120
CAL20000	150	0	2000	-2000	0	400	114	177	0	50	50	397	60
CAL20200	150	-2000	0	0	0	400	114	177	56	0	0	353	60
CAL20100	150	0	2000	0	0	400	114	177	0	56	0	353	60
CAL20110	150	0	2000	0	-200	400	114	177	0	56	0	353	60
CAL20160	150	0	2000	0	200	400	114	177	0	56	0	353	60
CAL20500	150	0	2000	-2000	0	400	114	177	0	18	18	333	60

in different leads. Monophasic, with either a positive or negative peak, and biphasic QRS complexes are present, as well as flat, depressed and elevated ST segments. Furthermore, for one of the signals the duration of the QRS complex is extremely limited, allowing the amplitude response of the system to be evaluated at the high end of the ECG frequency spectrum.

These calibration waveforms appear extremely useful for verifying the response of electrocardiographic filters or equipment. The distortion introduced by the recording device can be quantified with respect to a set of completely defined signals. Furthermore, the employment of standardised test inputs allows the performance of various ECG systems, proposed by different authors or implemented by different manufacturers, to be compared. The calibration waveforms could also find application in the design of electrocardiographic filters. The constraints imposed on the response to a mathematically defined QRS complex could be utilised to establish an appropriate system transfer function. Moreover, as previously highlighted in Section 3.4.3, synthetic curves mimicking the QRS complex can be employed to assess the distortions the ECG recording equipment could introduce into the ST segment in actual measurements.

Even though the test employing the calibration waveforms is a formal part of a current international standard, these signals have rarely been used in practice to investigate the distortion introduced by ECG monitoring devices [86, 87] or filtering methods [70]. Furthermore, in the latter case, the signal adopted to test filter performance does not have the same shape as the corresponding calibration ECG. Despite the fact that the fundamental ECG components have the same amplitude and approximate duration as those of the calibration signal, the QRS complex is modelled by a triangular wave. A possible explanation of the scarce use of these test signals is that they seem to be available only to electrocardiograph manufacturers and test institutions [9]. The author was, indeed, unable to find either the complete mathematical definition or a digital representation of the calibration waveforms. Consequently, the lack of this information seems to have greatly hindered the adoption and

use of the calibration ECG signals in research studies. Moreover, notwithstanding the benefits that could be achieved from a common set of waveforms representative of the ECG signal, it appears that the interest in the calibration signals is diminishing. The test methodology based on these standard waveforms has, in fact, been excluded from the European standard for electrocardiographic monitoring equipment (EN 60601-2-27:2006) [62], published more recently than the EN 60601-2-51:2003 which introduced them.

3.7 Conclusion

In this chapter, the evolution of the AHA recommendations for electrocardiographic equipment has been presented and the studies that have prompted modification of the ECG filter requirements over the years have also been described. Furthermore, the current international standards that need to be met by electrocardiographic devices to guarantee undistorted signal recording have been outlined. From the analysis of these standards and recommendations, it emerges that the requirements for the low-frequency response of ECG filters are particularly critical.

It appears indeed remarkable that present-day specifications for the highpass ECG filter are primarily based on a study performed in the 1960's, in which Berson and Pipberger [16] suggested the employment of a 0.05 Hz single-pole system to suppress low-frequency noise. The requirements derived from this filter are extremely stringent, but a relaxation of the specifications cannot be backed up, since there is practically no other study on the subject. Only one recent work analysing the distortion that can be introduced into the ECG signal by inadequate highpass filtering has been found by the author [18]. This study investigates how ST segment abnormalities due to inadequacies in the recording equipment can potentially be mistaken for signs of myocardial infarction. The authors recorded 12-lead electrocardiograms on 20 healthy subjects, applying different first order highpass filters with cutoff frequencies between 0.05 Hz and 1 Hz. The distortions occurring in the ST segment were then measured and it was concluded that no significant ST elevation or depression is present in the records for filters having 3dB-point as high as 0.1 Hz. It should be stressed that, even in this study, an essential role is played by the 0.05 Hz single-pole filter, which is the benchmark used to assess the performances of the other analogue highpass systems. Given the widespread relevance still attributed to the 0.05 Hz first order filter [26, 82], this system will be employed in the remainder of this thesis as a reference for the design of the highpass electrocardiographic filter.

Special attention has also been devoted in this chapter to the current formulation of the highpass specifications for the ECG filter. At present, the low-frequency characteristics of

the electrocardiographic system are detailed in terms of its response to an input pulse. However, in the 1990 AHA recommendations [19] and in the European standard for diagnostic electrocardiographic recorders (EN 60601-2-51:2003) [9], the geometry of this input signal is not thoroughly defined and only its area is specified. It has been shown that, even for a simple single-pole system, the pulse response is actually dependent on the shape of the input waveform and that there is a non-linear relationship between the duration of the input pulse and the characteristics of the output signal on which the constraints for undistorted ECG recording are imposed. It is thus suggested by the author that a unique geometry is defined across all of the international standards and it is proposed that an input waveform resembling in shape, amplitude and duration the QRS complex is employed in the test. A triangular pulse, or a modified version of the calibration ECG signals described in the EN 60601-2-51:2003 standard, could be utilised for this purpose. Furthermore, it has been demonstrated how the specifications for the pulse response could be more conveniently expressed in terms of requirements for the filter response to an input Dirac delta function. The transformation between requirements is valid provided that the time domain conditions have been derived from the response of the 0.05 Hz single-pole highpass filter to an input signal of very short duration.

Finally, it has been highlighted how the phase response of the highpass ECG filter has been given focused attention over the years, even if no requirement is specified for this characteristic by either the AHA recommendations or the international standards. It has been pointed out that the phase linearity condition suggested by Tayler and Vincent [13, 25] is less stringent than the constraints set on the pulse response to guarantee accurate ECG recording. In order to prove the difference between phase and pulse response requirements, it has been shown that a bidirectional filter, designed to fulfil the passband amplitude limits described in the 1990 AHA report, does not satisfy the time domain specifications, despite having a null phase response at all frequencies.

Chapter 4

Lowpass filter design

4.1 Introduction

Since the high-frequency requirements specified by the international standards are not very demanding [9, 15], finding a lowpass characteristic that satisfies them is quite straightforward. In fact, provided that the magnitude response does not need to be particularly steep at the cutoff frequency, some of the classic filter transfer functions guarantee a good degree of phase linearity as well as limited transient response overshoots [83, 84]. On the other hand, a thorough review of the advantages and drawbacks of using different filter families in electrocardiographic applications has never been performed.

In this chapter, the constraints employed in the design of the ECG lowpass filter are illustrated and four types of transfer function that fulfil these requirements are presented. Their frequency and time domain characteristics are compared with regard to passband flatness, in-band group delay variation and maximum amplitude of the step response overshoots. Furthermore, the responses of these filters to a triangular input pulse are tested for compliance with the specifications set by the standards. Finally, the influence of the filter out-of-band rejection on the choice of sampling frequency in a digital ECG monitoring system is investigated.

4.2 Lowpass filter requirements

The amplitude specifications for the lowpass filter, shown in Figure 4.1, are determined as the strictest combination between the high-frequency requirements for ECG recording systems detailed in the American standard ANSI/AAMI EC11:1991/(R)2001/(R)2007 [15] and in the 1990 AHA recommendations [19]. According to the latter publication, the passband ripple is restrained to ± 0.5 dB, whereas the frequencies defining the passband interval and

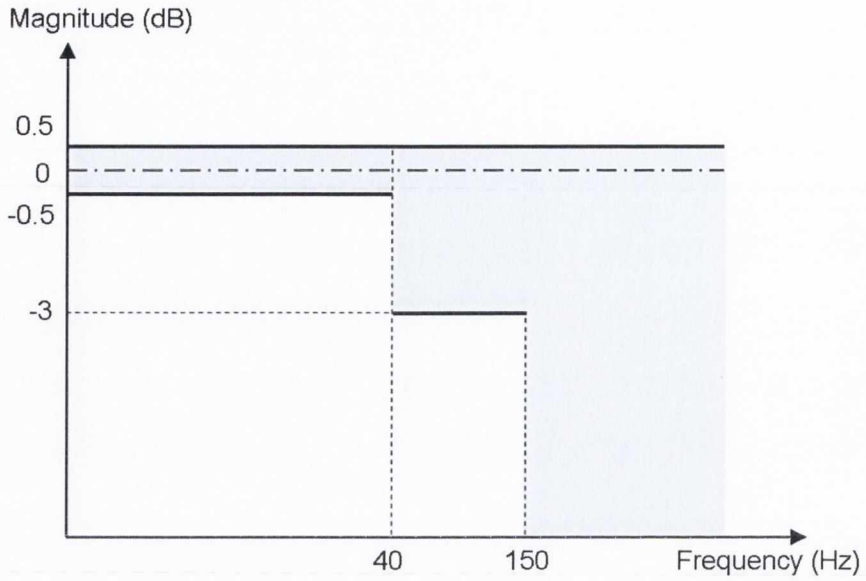


Figure 4.1: Requirements set for the magnitude response of the lowpass ECG filter.

the 3dB-cutoff are set as specified in the standard. In summary, the amplitude of the ECG lowpass filter needs to be flat to within ± 0.5 dB up to at least 40 Hz and the 3dB-point must be at least 150 Hz. These magnitude specifications are not particularly stringent and, indeed, are satisfied even by a first order filter. On the other hand, since the ECG filter should eliminate as much noise as possible outside the signal spectrum, it is advisable that the lowpass filtering system has a stopband rejection greater than that of a single-pole filter.

Furthermore, to ensure faithful reproduction of the input signal, it is essential for the filter phase response to be approximately linear over the ECG bandwidth. In other words, the filter group delay, defined as:

$$D(\omega) = -\frac{d\theta(\omega)}{d\omega}, \tag{4.1}$$

where $\theta(\omega)$ is the system phase response, needs to be constant over the ECG spectrum. This guarantees that the individual constituent waves in the ECG signal are delayed by the same amount and the time overlap of ECG components having different frequency content is avoided. Another condition necessary to minimise the distortion introduced by the recording system is the absence of excessively large overshoots or prolonged ringing in the time domain response of the filter. Since no particular requirement for the time domain response of the lowpass filter is defined by either the AHA recommendations [19, 64] or the international standards [9, 15, 62, 63, 77], a guideline for the maximum allowable overshoot can be obtained from the specifications set for the response of ECG monitoring system to a 300 μVs pulse, which were previously illustrated in Section 3.3.1. Both European and American standards require that an undershoot larger than 100 μV is not produced

when a rectangular pulse of 3 mV amplitude and 100 ms duration is applied at the input of the recording system. If the settling time of the system under consideration is much shorter than 100 ms, the rise and fall phase of the rectangular waveform can be considered independently. This appears to be the case for the lowpass filter under design. In fact, the time constant of a first order filter with 150 Hz 3dB-cutoff is approximately 1 ms and the settling time of higher order systems is expected to be of the same order of magnitude, that is, quite small compared with 100 ms. Therefore, for an input step of 3 mV amplitude, the overshoot in the output signal needs to be limited to 100 μV, i.e. the maximum percentage overshoot allowed is equal to 3.3%.

4.3 Overview of classic responses

Even though little information is available regarding the characteristics of lowpass filters for use in ECG monitoring equipment, implementations appear to be based mainly on the Bessel transfer function. In particular, fourth and eight order systems with 3dB-point between 100 and 250 Hz have been previously employed as front-end filters [20–22, 31, 88]. In the remainder of this section, the frequency and time domain characteristics of different filter families, including the Bessel type, are presented and compared to determine the optimum trade-off between stopband rejection, phase response linearity and damping of the step response. In order to keep the complexity of the implementation at a minimum, the investigation has been restricted to all-pole transfer functions.

The cutoff frequency of the filters under analysis has been fixed to 150 Hz, so that the highest reduction of frequency components outside the bandwidth of the electrocardiographic signal can be achieved. In fact, even though it has long been recognised that very high frequency components are present in the QRS complex [60, 89, 90], a passband limit of 150 Hz is considered sufficient, according to the standards and recommendations [15, 19, 64], to guarantee undistorted ECG recording. Furthermore, the use of this 3dB-cutoff frequency is quite customary in ECG recording and analysing systems. For example, the upper limit of the ECG spectrum is set to 150 Hz by the analysing algorithms utilised by Philips Medical Systems (Andover, MA) [67] and GE Healthcare (Freiburg, Germany) [91]. Moreover, both the integrated electrocardiographic device proposed by Schiller (Baar, Switzerland) [92] and the design suggested for the analogue front-end of ECG equipment by Texas Instruments (Dallas, TX) [93] contain a lowpass filter having 3dB-cutoff frequency of 150 Hz.

4.3.1 Butterworth

Let us first consider the Butterworth transfer function, which was actually employed by Van Alste et al. [94] and Vehkaoja and Lekkala [95] for electrocardiographic measurements. This family of filters is often selected for its mathematical simplicity and for the low sensitivity of its response to parameter changes [84]. The Butterworth transfer function is determined by approximating the ideal rectangular magnitude response in the Taylor sense at zero frequency. That is, the magnitude characteristic is made maximally flat for f = 0 Hz and, the higher the approximation order n, the flatter the amplitude curve is at this frequency. Butterworth polynomials [83] can be identified as the denominator of the normalised transfer function of this kind of filter. The Butterworth magnitude characteristic, which for the normalised filter is equal to [84]:

$$|H(\omega)| = \frac{1}{\sqrt{1+\omega^{2n}}}, \tag{4.2}$$

is monotonically decreasing and, the higher the order, the faster the gain is reduced with frequency in the stopband region. Indeed, the magnitude steepness is limited at the cutoff frequency, whereas for higher frequencies the gain decreases at the rate of $20n$ dB/decade, as illustrated in Figure 4.2(a). The group delay of Butterworth filters shows a maximum just below the cutoff frequency, as is evident from Figure 4.2(b), and the phase response of the system can be considered reasonably linear only for frequencies lower than half the bandwidth [84]. Furthermore, the step response, depicted in Figure 4.2(c), shows marked overshoot, whose amplitude increases with the filter order, as summarised in Table 4.1.

Overall, the features of the Butterworth phase and time domain responses prevent the employment of this type of filter in the context of ECG recording. An approximately flat group delay characteristic over the bandwidth of the electrocardiographic signal could, indeed, be achieved by doubling the cutoff frequency at the expense of a reduced rejection of the noise components in the frequency interval between desired and actual 3dB-points, i.e. between 150 and 300 Hz. On the other hand, even for n = 2, the step response overshoot is larger than the guideline maximum of 3.3% outlined in the previous section. Therefore, due to

Table 4.1: Amplitude of the maximum overshoot in the step response of Butterworth filters.

Order n	Overshoot (%)
2	4.3
3	8.1
4	10.8
5	12.8
6	14.3

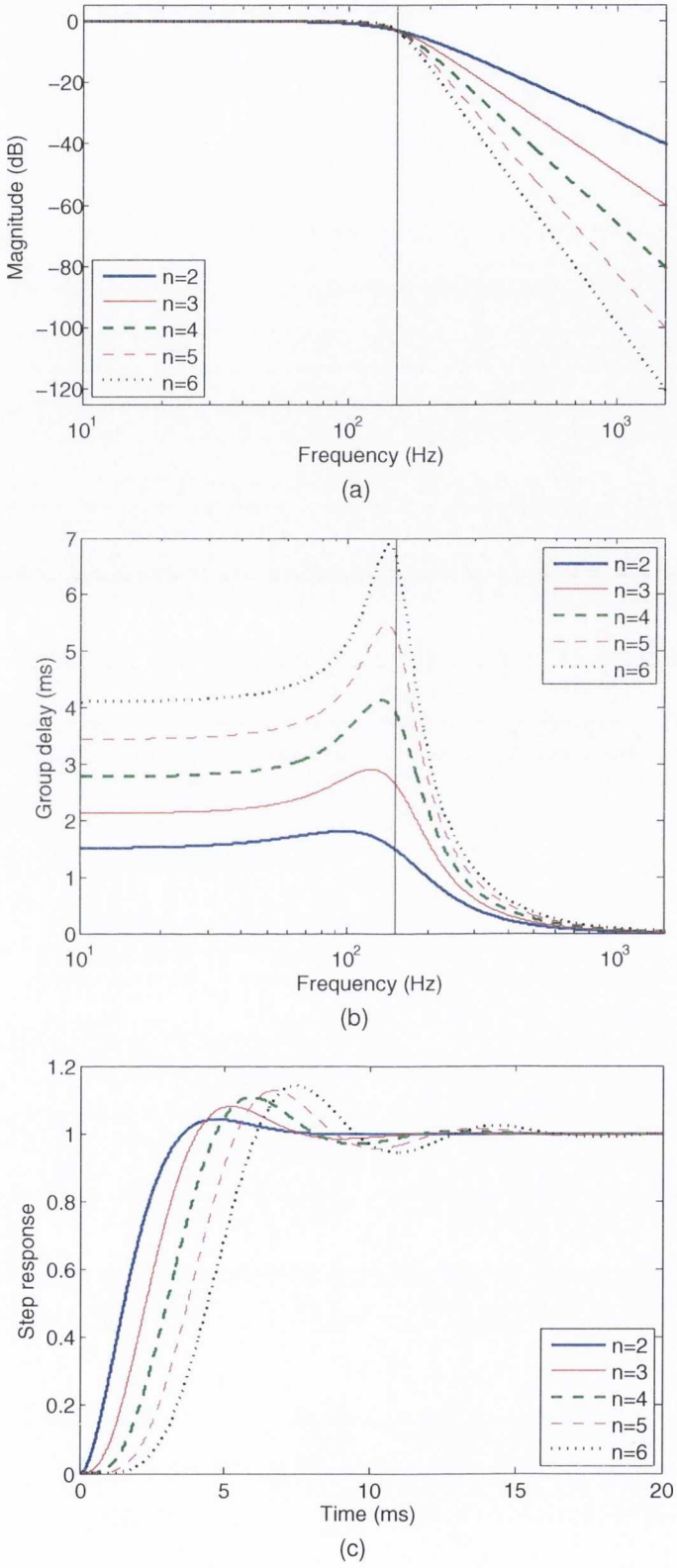


Figure 4.2: Time and frequency domain characteristics of Butterworth filters of order $2 \leq n \leq 6$ with 3dB-cutoff at 150 Hz. This cutoff frequency is identified by the vertical line in the magnitude (a) and group delay (b) plots.

its unsuitability for applications, such as electrocardiographic monitoring, that only allow for minimal time domain distortions, Butterworth filters will not be considered further in the review of classic characteristics for the design of the ECG lowpass network. Other lowpass transfer functions, such as the Chebyshev type (see Section A.2.1), that are characterised by a magnitude response steeper than that of the Butterworth filter in the transition region will also not be discussed. In fact, since the transient response overshoot is substantially linked to the rapid change in attenuation at the cutoff frequency [84], the peak occurring in the step response of this kind of filters will be even larger than that of a Butterworth network of the same order.

4.3.2 Gaussian

The magnitude response of the Gaussian transfer function is derived as an approximation of the ideal Gaussian amplitude:

$$|H(\omega)| = e^{-\omega^2/2}. \tag{4.3}$$

To obtain a physically realizable network, the exponential in the magnitude-squared ideal response is replaced with its Taylor series expansion of order n:

$$|H(\omega)|^2 = \frac{1}{e^{\omega^2}} \cong \frac{1}{1 + \omega^2 + \frac{\omega^4}{2!} + ... + \frac{\omega^{2n}}{n!}}. \tag{4.4}$$

The filter order determines the accuracy of the approximation. For example, the ideal Gaussian magnitude response is approximated within 1 dB up to the 11dB-point by the fourth order filter and to about the 18dB-point by the sixth order one [83]. The frequency and time responses, which are illustrated in Figure 4.3 for filters having a 150 Hz bandwidth, are obtained from the pole locations of normalised Gaussian filters [96]. It should be noted that the group delay, shown in Figure 4.3(b), is flat up to frequencies close to the cutoff point and that, as the order of the filter increases, this characteristic improves even further. The step response of Gaussian magnitude filters, depicted in Figure 4.3(c), does not show any appreciable overshoot either. In fact, as previously discussed in Section 3.5.2, no overshoot or ringing is present in the time domain characteristics of a system having an ideal Gaussian amplitude response, of which the Gaussian filter is an approximation.

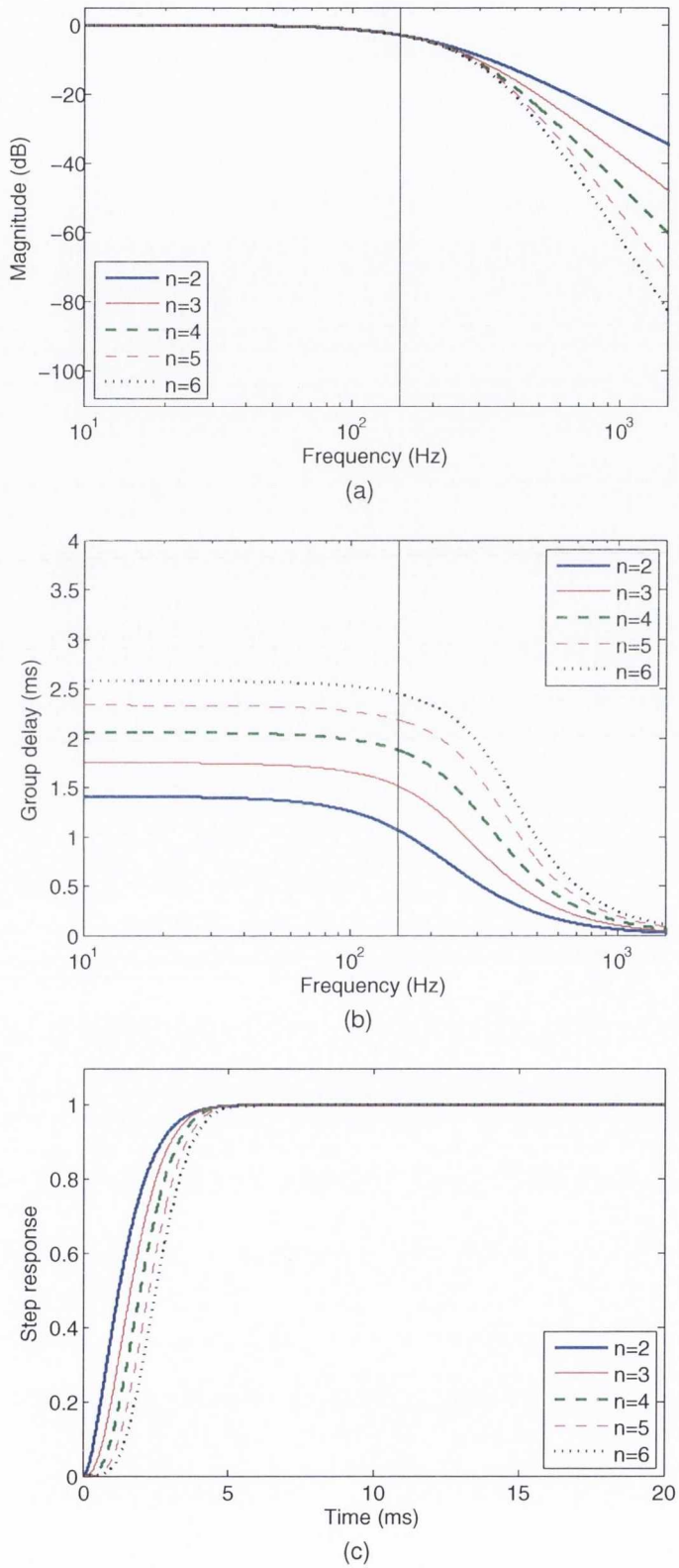


Figure 4.3: Time and frequency domain characteristics of Gaussian filters of order $2 \leq n \leq 6$ with 3dB-cutoff at 150 Hz.

4.3.3 Bessel

A Bessel filter is obtained when the group delay approximates to unity in the Taylor sense at zero frequency, that is, the group delay characteristic is maximally flat for f = 0 Hz. The phase response of the system can thus be considered linear from 0 Hz to a certain frequency determined by the order of the filter. The denominator of this maximally flat delay transfer function, which is related to a class of Bessel polynomials, can be determined from the recursive formula [84, 96]:

$$B_n(s) = (2n-1)B_{n-1}(s) + s^2 B_{n-2}(s) \quad \text{with} \quad B_0 = 1 \quad \text{and} \quad B_1(s) = s + 1 \tag{4.5}$$

and the Bessel transfer function can be expressed as:

$$H(s) = \frac{B_n(0)}{B_n(s)}. \tag{4.6}$$

The frequency and time domain characteristics of Bessel filters of order $2 \leq n \leq 6$ with 3dB-cutoff at 150 Hz are presented in Figure 4.4.

The selectivity of the Bessel filter is slightly better than that of a Gaussian filter of the same order. However, both filter types have poor attenuation characteristics and do not present a sharp rejection onset at the cutoff frequency [83], as shown in Figures 4.3(a) and 4.4(a) for Gaussian and Bessel filters, respectively. Understandably, the passband group delay is flatter for the Bessel filter than for the Gaussian and, indeed, the Gaussian filter cannot be used in certain applications due to its phase response not being sufficiently linear [83]. On the other hand, the transient overshoot of the Gaussian filter is limited compared to that of the Bessel response. Nevertheless, the Bessel characteristic will also approach the ideal Gaussian response, as the filter order goes to infinity [84].

4.3.4 Linear phase with equiripple error

A constant group delay is more efficiently approximated when an equiripple approximation is used rather than a maximally flat one. For a given filter order, the Chebyshev delay approximation can be considered constant over a wider frequency range than the Taylor one, since in the latter case all the degrees of freedom of the system are employed to shape the approximating curve to be maximally flat at zero frequency. Even though the transfer function of all-pole lowpass filters having equiripple delay has been numerically determined, the location of the poles is generally tabulated for absolute values of the delay ripple [97]. This formulation, however, is not particularly suitable for filter design and, in the literature [83, 84, 96, 98], preference has been given to an almost equivalent class of filters

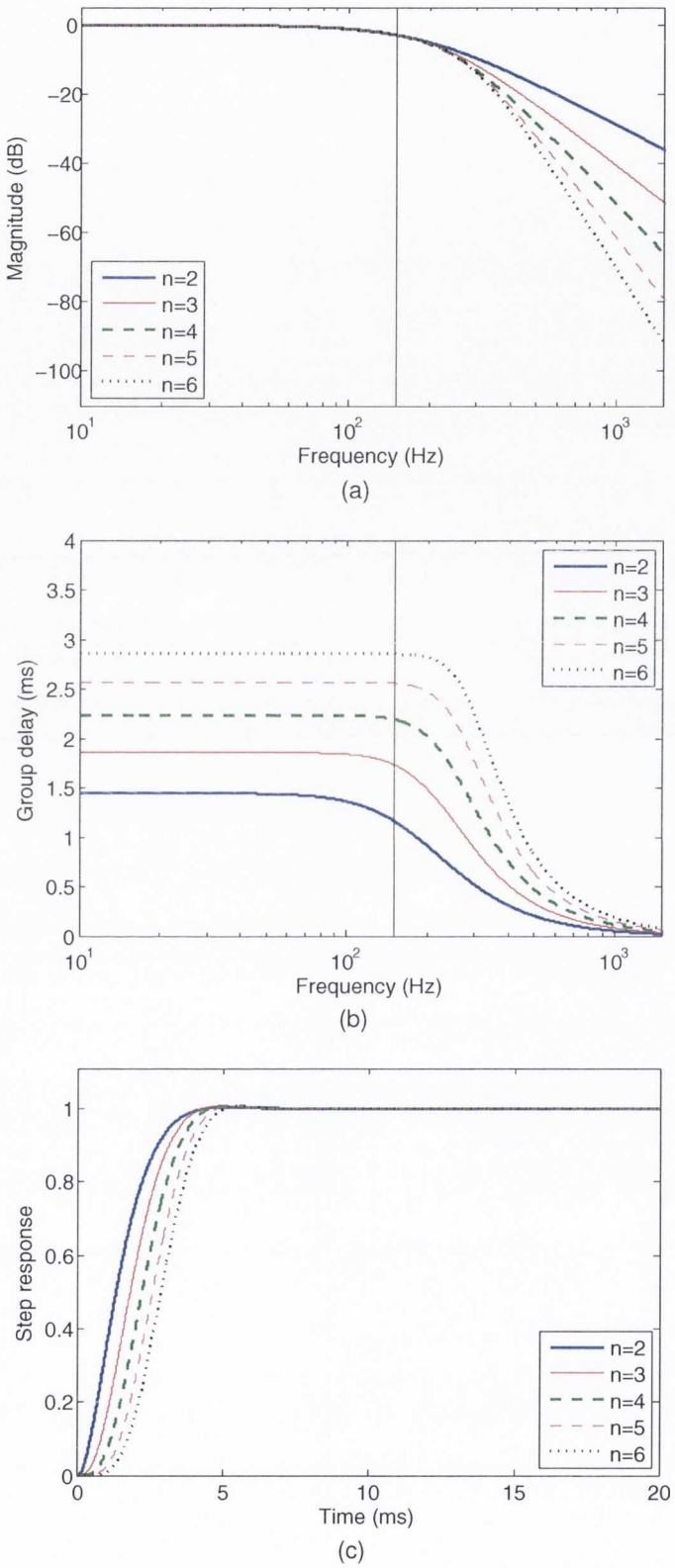


Figure 4.4: Time and frequency domain responses of Bessel filters of different orders having 150 Hz 3dB-bandwidth.

that are characterised by an approximately linear phase response. The transfer function of these filters is actually derived by applying a Chebyshev approximation to the system phase characteristics, instead of its delay response.

The procedure for determining the pole locations of the filters having linear phase with equiripple error was illustrated by Humpherys [96]. The transfer function of the all-pole lowpass filters was expressed as:

$$H(s) = \begin{cases} \dfrac{H_0}{\prod_{k=1}^{n/2}[(s+\alpha_k)^2 + {\beta_k}^2]} & \text{for } n \text{ even} \\ \dfrac{H_0}{(s+p)\prod_{k=1}^{(n-1)/2}[(s+\alpha_k)^2 + {\beta_k}^2]} & \text{for } n \text{ odd} \end{cases} \tag{4.7}$$

that is, the filters are characterised by complex conjugate poles ($\alpha_k > 0$) except for a negative real pole, $-p$, when n is odd. The phase response was derived as:

$$\theta(\omega) = \begin{cases} -\sum_{k=1}^{n/2} \tan^{-1} \dfrac{2\alpha_k\omega}{{\alpha_k}^2 + {\beta_k}^2 - \omega^2} & \text{for } n \text{ even} \\ -\tan^{-1}\dfrac{\omega}{p} - \sum_{k=1}^{(n-1)/2} \tan^{-1} \dfrac{2\alpha_k\omega}{{\alpha_k}^2 + {\beta_k}^2 - \omega^2} & \text{for } n \text{ odd.} \end{cases} \tag{4.8}$$

The error function was selected as the difference between the actual phase characteristic and the ideal linear phase response:

$$E(\omega) = -\theta(\omega) - \pi\omega, \tag{4.9}$$

where $\theta(\omega)$ is negative. A Chebyshev approximation of this error function was then obtained by defining a system of n non-linear equations of the form [96]:

$$E_i(\omega_i) = -\theta(\omega_i) - \pi\omega_i + (-1)^i \frac{\pi\epsilon}{180} = 0 \qquad \text{when} \quad i = 1, 2, \ldots, n, \tag{4.10}$$

where, according to Figure 4.5, ϵ is the maximum allowable phase deviation in degrees and ω_i the frequency of a maximum or a minimum of the error function. Since there is no closed form solution to this equiripple error approximation problem, the location of the poles in Eq. (4.7) were derived using an iterative procedure [96]. In summary, the phase response of this type of filters approximates a line over a finite frequency range, which, for a given bandwidth, is determined by the filter order n. Over the approximation interval, the number

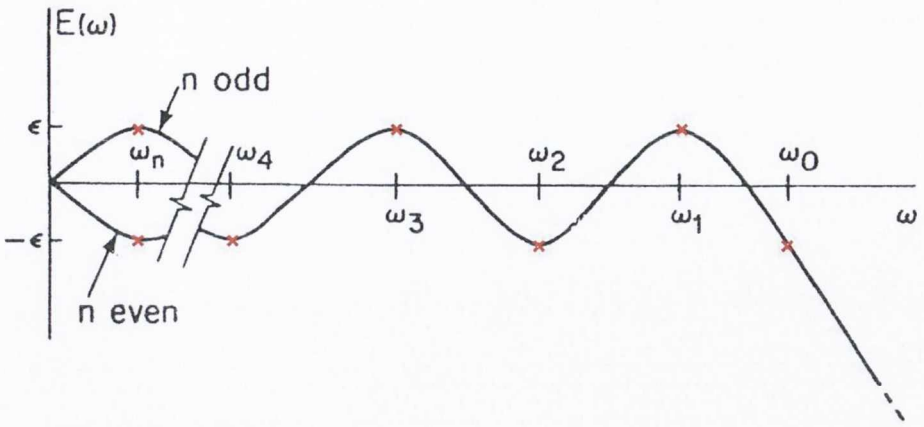


Figure 4.5: Error function for the Chebyshev approximation of a linear phase response (modified from [96]).

of points characterised by maximum phase deviation is $(n+1)$, as shown in Figure 4.5. Furthermore, increasing the phase ripple ϵ extends the region over which the group delay can be considered constant deeper into the stopband and yields a greater attenuation at high frequencies [98].

The pole locations of the filters having linear phase with equiripple error are tabulated for $\epsilon = 0.5°$ [96]. For this ripple value, the magnitude characteristics, group delays and step responses of filters of various orders are illustrated in Figure 4.6, whereas their phase responses are shown in Figure 4.7. The 3dB-passband limit is fixed to 150 Hz in these representations. Even though the filters having linear phase with equiripple error are not characterised by a sharp cutoff, their stopband attenuation is greater than that of Bessel filters of the same order and reaches $20n$ dB/decade deep into the stopband [83]. This is evident when comparing Figures 4.6(a) and 4.4(a). On the other hand, both types of filter have approximately the same amplitude response in-band and in the transition region. As regards the transient characteristics, the overshoot is generally more pronounced and the ringing is more prolonged for the filters having linear phase with equiripple error than for Bessel filters [98].

4.3.5 Equiripple impulse overshoot

The transfer functions of lowpass filters having equiripple overshoot in either the impulse or the step response were numerically derived by Jess and Schussler [99, 100]. They defined an approximation problem that forced the time domain overshoot to oscillate in an equiripple manner about its steady state value. For an all-pole filter of order n, whose transfer function is given by Eq. (4.7),$(n-1)$ degrees of freedom were employed to constrain the amplitude of the first $(n-1)$ overshoots or undershoots in either the impulse or the step response

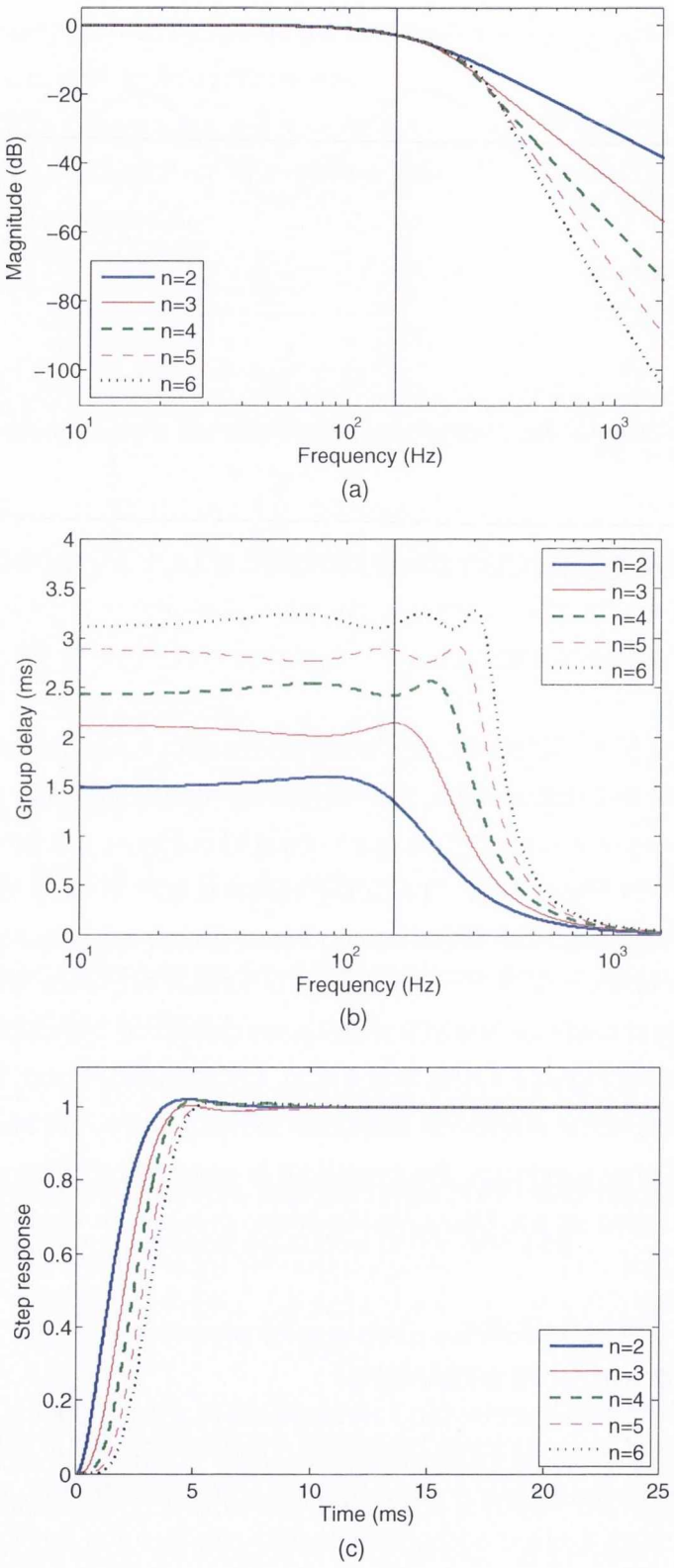


Figure 4.6: Time and frequency domain characteristics of filters having linear phase with equiripple error (ϵ = 0.5°) of order $2 \leq n \leq 6$ for a 3dB-cutoff frequency of 150 Hz.

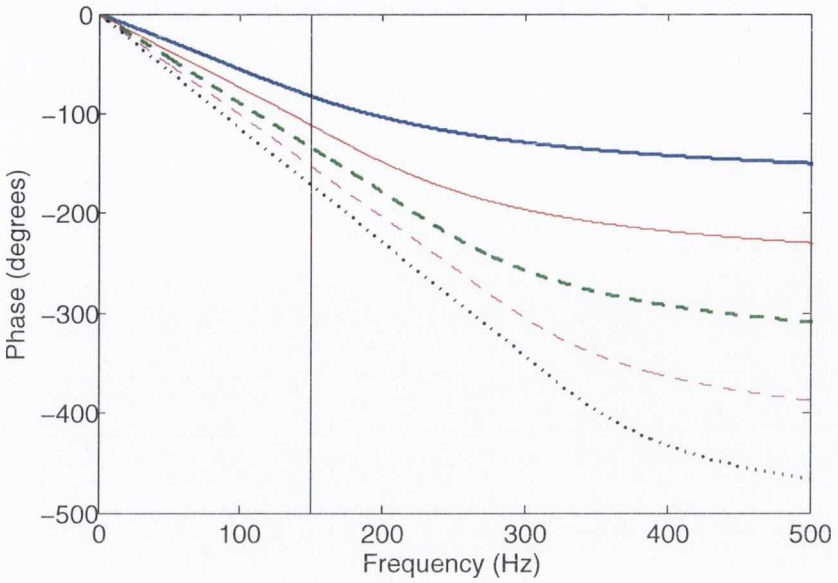


Figure 4.7: Phase characteristic of filters having linear phase with equiripple error (ϵ = 0.5°) of order $2 \leq n \leq 6$ for a 3dB-cutoff frequency of 150 Hz.

to be equal to the maximum allowable value, q_t [96]. The other two free parameters were used to make the gain of the system unity at zero frequency:

$$|H(0)| = 1, \tag{4.11}$$

and to set the magnitude response of the filter equal to a desired attenuation, q_f, at the critical frequency ω_c:

$$|H(\omega_c)| = q_f. \tag{4.12}$$

An iterative procedure was employed by Jess and Schussler to numerically solve the system of non-linear equations described by the above conditions and, thus, determine the location of the poles of the lowpass transfer function $H(s)$. The poles of both equiripple step and equiripple impulse overshoot networks were tabulated for q_t = q_f = 0.01 and ω_c = 1 rad/s [99]. That is, the amplitude of the time domain ripple is set to $\pm$1% and the attenuation of the filter is equal to 40 dB for a stopband limit of 1 rad/s.

The magnitude, group delay and step response of 1% equiripple impulse overshoot filters of different orders are shown in Figure 4.8 for a 3dB-passband limit of 150 Hz and a sketch of their impulse response is presented in Figure 4.9. When comparing Figures 4.8(a) and 4.6(a), it appears evident that the stopband attenuation of these filters is quite similar to that of the constant-delay types previously presented. From Figure 4.8(b), it should also be noticed that the group delay characteristic shows a peak in the stopband for orders $n \geq 5$. However, since the attenuation at the frequency of the peak is sizable, i.e. more than 10 dB

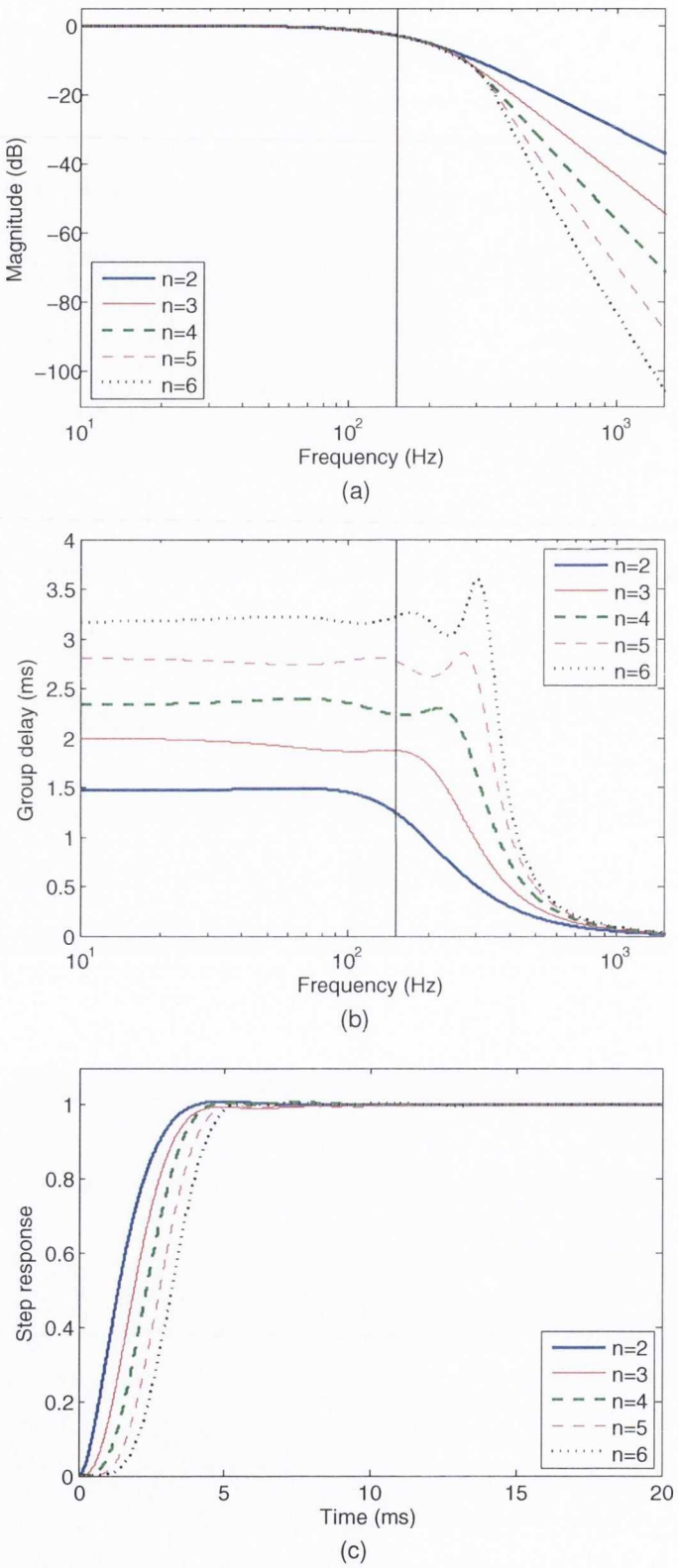


Figure 4.8: Time and frequency domain characteristics of 1% equiripple impulse overshoot filters of order $2 \leq n \leq 6$ having a 150 Hz bandwidth.

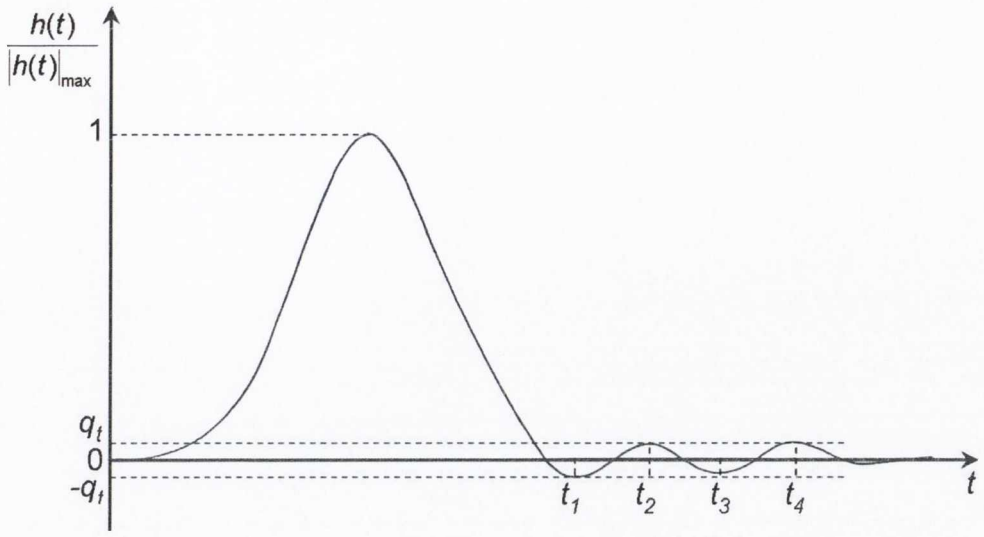


Figure 4.9: Typical impulse response of an equiripple impulse overshoot filter of order $n = 5$ (modified from [96]).

for both fifth and sixth order filters, the effect of this delay peak on the time domain overshoot is negligible [84]. Except for the case $n = 2$, the filters derived by imposing the equiripple overshoot condition on the step response are different from those obtained by constraining the impulse response overshoot [100]. The group delay response of equiripple step filters, illustrated in Figure 4.10 for a 1% overshoot, is indeed characterised by larger peak than that occurring in the response of equiripple impulse filters (see Figure 4.8(b)). The group delay variation for equiripple step overshoot filters is therefore expected to be larger than for the equiripple impulse overshoot ones. The percentage group delay variation calculated over the filter 3dB-bandwidth for a 1% equiripple step overshoot filter is presented in Table 4.2. Comparing these values with those obtained for the 1% equiripple impulse overshoot filter, illustrated in Table 4.3, shows that the in-band group delay variability is similar for $n = 3$ and $n = 4$, but considerably lower in the latter case for $n \geq 5$. Furthermore, this reduced delay variation does not appear to have a detrimental effect on the step response overshoot of the equiripple impulse filter, which can be seen from Table 4.3 to be lower than 1%. The equiripple impulse filter was, therefore, chosen for the comparison with the other transfer functions previuosly presented in this section.

Obviously, other types of all-poles transfer functions that allow a good compromise between time and frequency domain characteristics have been described in the literature [96–98]. One such transfer function was analytically derived by Rakovich et al. [101] and, similarly to the filters obtained by Jess and Schussler [99, 100], a maximum amplitude for its impulse response overshoot can be specified. In this case, however, the transient overshoot is not forced to have an equiripple behaviour and the steady state is reached faster

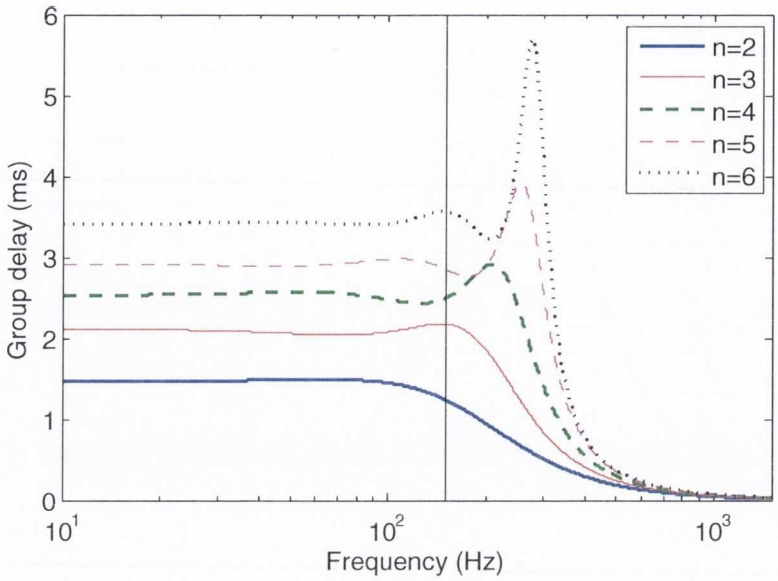


Figure 4.10: Group delay characteristic of 1% equiripple step overshoot filters of order $2 \leq n \leq 6$ for a 3dB-cutoff of 150 Hz.

Table 4.2: In-band group delay variation for a 1% equiripple step overshoot filter.

Order n	Group delay variation (%)
2	16.4
3	6.1
4	5.3
5	4.4
6	4.6

than by the equiripple impulse overshoot filter. On the other hand, when the same allowable overshoot is selected, the filter proposed by Rakovich at al. is identical to the one designed by Jess and Schussler for $n = 3$ and there is no appreciable difference between the two solutions for $n = 4$ and $n = 5$. For higher order systems, the equiripple impulse overshoot filters actually provide a higher stopband selectivity [101].

4.4 Verification of the system requirements

4.4.1 Comparison between responses

Relevant frequency and time domain characteristics for the filter responses presented in the previous section are summarised in Table 4.3. The passband limit, defined as the frequency at which the attenuation is equal to 0.5 dB, ranges from 55 to 75 Hz, with an average value dependent on the transfer function family of between 60 and 65 Hz. Therefore, since the

Table 4.3: Frequency and time domain properties of the lowpass filters under analysis, for a 3dB-bandwidth of 150 Hz.

Order n	$f_{0.5\text{dB}}$ (Hz)	Group delay variation (%)	Group delay variation (ms)	Max step response overshoot (%)
Gaussian				
2	59.5	24.1	0.3	0.1
3	60.9	13.5	0.2	0.1
4	61.1	8.8	0.2	0.0
5	61.1	6.4	0.1	0.0
6	61.1	5.1	0.1	0.0
Bessel				
2	63.3	19.1	0.3	0.4
3	64.3	6.4	0.1	0.8
4	63.5	1.8	0.0	0.8
5	62.7	0.4	0.0	0.8
6	62.5	0.1	0.0	0.6
Linear phase with equiripple error (ϵ = 0.5°)				
2	74.3	15.4	0.2	2.1
3	55.0	6.0	0.1	0.4
4	71.0	4.9	0.1	1.8
5	53.3	4.5	0.1	0.0
6	69.8	4.2	0.1	1.0
Equiripple impulse (1% overshoot)				
2	67.2	16.4	0.2	1.0
3	55.5	6.9	0.1	0.0
4	67.6	6.8	0.2	0.8
5	57.6	2.6	0.1	0.0
6	64.2	2.1	0.1	0.5

passband limit is consistently higher than 40 Hz and the 3dB-cutoff point is fixed to 150 Hz, it can be concluded that all of the systems analysed satisfy the amplitude requirements for the ECG lowpass filter illustrated in Figure 4.1. It is also worthwhile noting that the in-band amplitude behaviour of both types of equiripple filters is dependent on whether the system transfer function contains an even or an odd number of poles. Indeed, the frequency at which an attenuation of 0.5 dB occurs is much lower for odd order equiripple filters than for even order ones. The positive counterpart to this reduced passband flatness is the limited amplitude of the step response overshoot of odd order systems, as indicated by the rightmost column in Table 4.3. It should be pointed out that the maximum step response overshoot is lower than 3.3% of the steady state value for all the filters studied. That is, the transient overshoot can be considered sufficiently small according to the guideline drawn in

Section 4.2.

Regarding the linearity of the phase response, it can be noticed that for second order filters the percentage group delay variation is particularly large, i.e. about 15% to 25%. On the other hand, for all the transfer function types, the variability in group delay decreases substantially with the order and the absolute delay variation over the 3dB-passband is limited to a maximum of 0.3 ms, even for $n = 2$. Such a time shift between the maximally and minimally delayed frequency components of the ECG spectrum does not appear to be relevant when digitisation of the signal after the analogue front-end of the measurement system is performed at a sampling frequency of about 1000 Hz, which is often used in electrocardiographic recordings [18, 102–105]. In fact, as long as the sampling period is larger than the maximum difference in group delay, the lag of the time domain contribution of the maximally delayed frequency will not be sufficient for it to be superimposed onto the value of the following sample instead of adding to the current output. If high resolution records are required for specific ECG analyses, such as detection of pacemaker pulses [24, 64], the lowpass filter should be suitably chosen so that the absolute group delay variation is limited compared with the sampling period. In particular, all the 5th and 6th order systems shown in Table 4.3 would be adequate for a sampling frequency of up to 5000 Hz and Bessel filters could be employed to achieve an even higher time resolution.

In summary, excluding the second order filters, which have a large percentage group delay variation over the passband, all systems under analysis seem to be suitable for the design of the front-end lowpass filter for ECG recording equipment. The magnitude specifications set in Section 4.2 according to the current American diagnostic standard [15] and 1990 AHA recommendations [19] are satisfied. The in-band group delay variability can be considered negligible for sampling rates in the region of 1000 Hz and the maximum amplitude of the step response overshoots is at most 1.8% of the steady state value.

4.4.2 Response to a triangular input wave

As discussed in Section 3.3.1, in order to test the ability of the ECG filter to correctly reproduce the narrow R wave of an ECG signal, current European and American standards require the output amplitude of two input triangular waves to be compared [9, 15, 62, 63, 77]. Figure 4.11 shows the input waveforms, having 200 and 20 ms durations, respectively, and the corresponding responses for the 6th order Bessel filter with a 3dB-cutoff frequency of 150 Hz. The output amplitude of the narrow triangular wave is about 6.5% less than that of the wider wave. As summarised in Table 4.4, all the filters previously analysed cause approximately the same amplitude reduction on the 20 ms wave and even a first order filter with the same bandwidth would not attenuate the narrow pulse by more than 6.7% com-

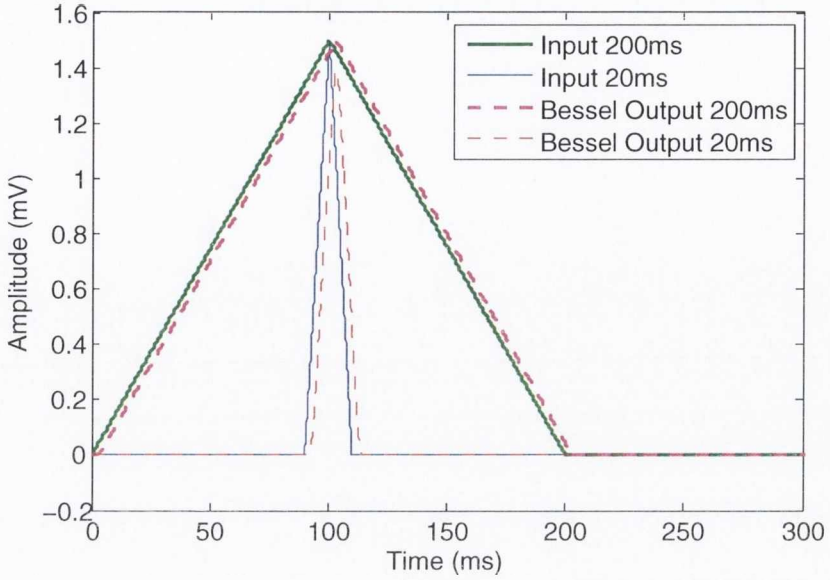


Figure 4.11: Input triangular test waves and corresponding output signals for a 150 Hz 6th order Bessel filter.

Table 4.4: Output amplitude reduction of the narrow triangular wave (20 ms) with respect to the reference wave (200 ms) for various 4th and 6th order filters, all having 150 Hz 3dB-bandwidth.

	Reduction (%)	
Filter type	4th order	6th order
Gaussian	6.4	6.4
Bessel	6.4	6.4
Linear phase with equiripple error ($\epsilon = 0.5°$)	6.0	5.9
Equiripple impulse (1% overshoot)	6.1	6.3

pared to the output amplitude of the 200 ms triangular wave. Hence, the stricter requirement of the American standard for diagnostic electrocardiographs, which specifies a maximum amplitude reduction of 10%, is satified by the different lowpass filter designs.

4.5 Considerations regarding the sampling frequency

The analysis of the lowpass characteristics performed in the previous section does not consider in detail the filter rejection in the transition region and in the stopband. As highlighted by Luo and Johnston [24], the international standards [9, 15, 62, 63, 77] and the AHA recommendations [19, 64], from which the system specifications have been derived, do not actually delineate a minimum output amplitude reduction for the ECG filter outside the passband. Nonetheless, the out-of-band rejection constitutes an essential criterion that should be evaluated together with the passband magnitude, the phase response and the transient

overshoot when the filter characteristic is chosen. In fact, a fundamental function of the analogue lowpass front-end filter, aside from eliminating the high-frequency noise outside the ECG spectrum, is to prevent aliasing when the electrocardiographic signal is sampled. According to the Nyquist theorem, the sampling frequency, f_s, should be greater than twice the bandwidth of the analogue signal [106]. Since the input signal of ECG recording devices cannot be considered truly bandlimited, the analogue front-end filter needs to achieve a substantial amplitude reduction at frequencies higher than $f_s/2$, that is, the Nyquist frequency. If the signal components at these frequencies are not adequately reduced, their spectral image, i.e. the alias, centred around the sampling frequency will interfere with the baseband spectrum of the signal, leading to distortion of the sampled ECG.

Table 4.5 presents a summary of the out-of-band rejection properties of the different filter types, when the 3dB-cutoff is set at 150 Hz. The attenuation is measured at 250 and 500 Hz, i.e. the Nyquist frequencies for sampling rates of 500 and 1000 Hz, respectively, where 500 Hz is the lower limit for the sampling frequency recommended in the 1990 AHA report [19] and the current European standard for recording and analysing electrocardiographs [9]. As outlined in Section 4.3, the filter families under consideration do not provide strong attenuation at frequencies higher than the cutoff because the reduced amplitude of the transient overshoots is only achievable at the expense of decreased steepness of the magnitude response in the transition region. It can thus be noticed that, irrespective of the filter order, the attenuation at 250 Hz lies between 7 and 10 dB, that is, the amplitude of the output signal is at most reduced to one third of its input value at this frequency. Therefore, none of the filters analysed can guarantee sufficient out-of-band rejection to allow the use of the minimum sampling frequency, as pointed out in the American standard for diagnostic electrocardiographic devices [15]. In fact, due to the limited amplitude reduction of the spectral components between 250 and 500 Hz, a consistent overlap occurs between their aliases and the baseband signal spectrum in the frequency range between zero and the 250 Hz Nyquist limit, as clearly depicted in Figure 4.12(a). On the other hand, if the sampling frequency is chosen to be 1000 Hz, then 5th and 6th order filters having either linear phase with equiripple error or impulse response with equiripple overshoot, as well as the 6th order Bessel filter, can be employed for the ECG lowpass filter. In this case, the amplitude of the output signal at 500 Hz is less than 2% of that of the input signal and the aliasing distorsion introduced on the sampled ECG can be considered negligible, as shown in Figure 4.12(b). As illustrated in Figure 4.13 for n = 6, the magnitude response of Gaussian filters after the cutoff frequency does not decrease as fast as that of the other types of transfer function. Since the output amplitude at 500 Hz is almost 4% even for the 6th order system, a higher order Gaussian transfer function might be chosen for the front-end lowpass filter. It should, however, be recognised from Table 4.5 that the increase in rejection at 500 Hz is not pro-

Table 4.5: Out-of-band attenuation characteristics of the lowpass filters under analysis, for a 3dB-bandwidth of 150 Hz.

Order n	Attenuation @ 250 Hz (dB)	Attenuation @ 500 Hz (dB)	Amplitude @ 500 Hz (%)
Gaussian			
2	7.1	16.3	15.4
3	7.8	20.7	9.2
4	8.2	24.2	6.2
5	8.3	26.9	4.5
6	8.3	28.9	3.6
Bessel			
2	7.5	17.4	13.5
3	8.7	23.4	6.8
4	9.3	28.4	3.8
5	9.4	32.5	2.4
6	9.3	35.7	1.6
Linear phase with equiripple error (ϵ = 0.5°)			
2	8.5	19.4	10.7
3	10.2	27.8	4.1
4	9.5	34.0	2.0
5	9.0	39.0	1.1
6	9.0	42.9	0.7
Equiripple impulse (1% overshoot)			
2	7.9	18.3	12.2
3	8.9	25.4	5.4
4	8.6	31.6	2.6
5	8.6	37.7	1.3
6	9.0	43.7	0.7

portional to the filter order and less than 2 dB additional attenuation would be gained for n = 7.

Overall, it can be concluded that the analogue lowpass filters under study cannot prevent aliasing if the sampling frequency is chosen lower than 1000 Hz. Since the current 2007 AHA scientific statement [64] recommends a sampling rate for the front-end analogue to digital conversion much higher than that used in later stages for the ECG processing, a different approach can be employed. The electrocardiographic signal is initially oversampled, then digitally filtered to drastically reduce the spectral content at frequencies higher than half of the final required sampling rate and lastly downsampled to a frequency as low as 500 Hz [20, 24]. Evidently, the digital filter used in this process also needs to satisfy the requirements defined in Section 4.2 for the passband amplitude, phase response and

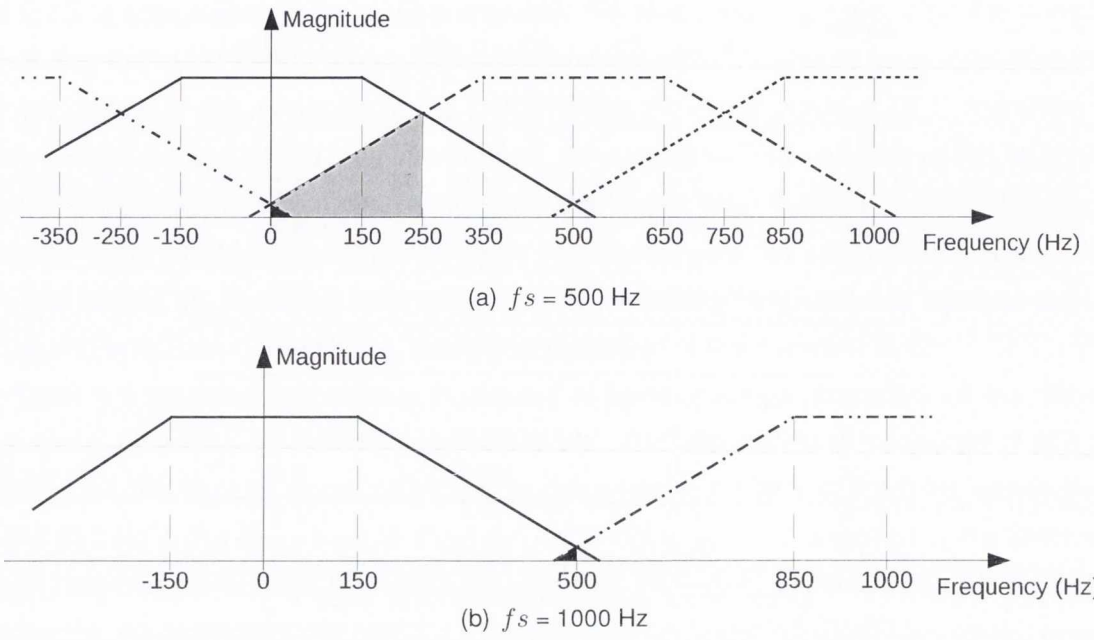


Figure 4.12: Overlap between the baseband spectrum and the spectral aliases produced by the digitisation of the ECG signal for different sampling frequencies.

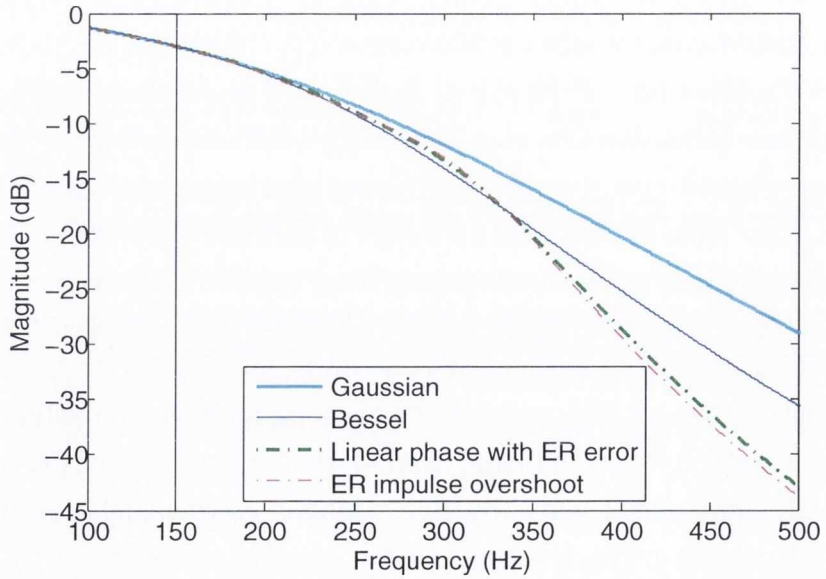


Figure 4.13: Amplitude response of different 6th order filters having 150 Hz as 3dB-cutoff.

transient overshoots, when combined with the front-end analogue filter.

4.6 Conclusion

In this chapter, different designs for the front-end lowpass filter of diagnostic ECG monitoring systems have been analysed and compared. Based on the magnitude and pulse response requirements set by the 1990 AHA recommendations [19] and the ANSI/AAMI EC11:1991/(R)2001/(R)2007 American standard [15], the constraints that the frequency and time domain characteristics of the lowpass filter need to satisfy have been established. It has then been shown that the requirement defined for the amplitude of the step response overshoot is fulfilled by Gaussian, Bessel, linear phase with equiripple error (ϵ = 0.5°) and equiripple impulse (1% overshoot) filters of any order. On the other hand, a limit on the minimum order of the lowpass system is imposed by the need for an almost flat in-band group delay characteristic. As regards the out-of-band rejection, the 3dB-cutoff point of the filters under consideration has been chosen as the lowest permitted by the current American standard of 150 Hz. This selection allows the high-frequency noise to be maximally attenuated and does not have any detrimental effect on the passband flatness of the filter amplitude response.

The time domain characteristics of the transfer functions under analysis have been tested using a triangular input pulse. It has been proven that the amplitude reduction introduced by the filter on a narrow 20 ms triangular wave compared with a 200 ms wide wave is well within the limits specified by the ANSI/AAMI EC11:1991/(R)2001/(R)2007 standard.

Overall, the author would recommend the implementation of the front-end lowpass system to be based on one of the equiripple transfer functions. For $n \geq 3$, linear phase with equiripple error or equiripple impulse overshoot filters provide a very good trade-off between stopband rejection and undistorted transmission of the ECG signal. On the other hand, even though Bessel and Gaussian characteristics present either a lower in-band group delay variation or a flatter step response, their magnitude responses decrease less sharply in the transition region.

In order for the hardware realisation to achieve the best performance in terms of power consumption, the system order should be selected to be even. In fact, unless it is feasible to place a first order section in a location of the front-end of the ECG monitoring system that does not require the employment of a buffer, the same number of active components will be needed for the implementation of even networks of order n and odd ones of order $(n-1)$. The higher order system would, however, allow better rejection of the stopband frequency components, flatter in-band group delay and lower step response overshoot.

If the front-end lowpass filter is to be safely employed for anti-aliasing purposes when the sampling rate of the ECG recording equipment is approximately 1000 Hz, the author would suggest the use of the 6th order equiripple impulse (1% overshoot) filter. The location of the complex conjugate poles of its transfer function for a 3dB-cutoff frequency of 150 Hz is given in Table 4.6, according to the nomeclature used in Eq. (4.7), where

$$H_0 = \prod_{k=1}^{n/2} \left({\alpha_k}^2 + {\beta_k}^2 \right) . \tag{4.13}$$

The group delay variation of the 6th order equiripple impulse filter is only 2.1% over the passband and the maximum amplitude of the step response overshoot is limited to 0.5% of the steady state value. At the same time, the 150 Hz equiripple impulse filter allows unwanted components at frequencies higher than 500 Hz to be reduced to less than 0.7% of their input values. Even though the out-of-band attenuation of the 6th order filters having equiripple impulse overshoot or linear phase with equiripple error are practically identical, the other relevant properties are slighly inferior for the latter. In fact, as shown in Table 4.3, the percentage group delay variation over the passband and the maximum amplitude of the step response overshoot of the filter having linear phase with equiripple error, although limited in absolute terms, are double those of the corresponding equiripple impulse filter.

If the use of three operational amplifiers is impractical or the power consumption of the front-end stage of the recording system needs to be kept at an absolute minimum, the 4th order linear phase with equiripple error (ϵ = 0.5°) filter could be employed instead. This system, whose poles are listed in Table 4.6, is characterised by a slightly higher out-of-band attenuation than the equiripple impulse filter of the same order and by a smaller group delay variation over the passband. The step response overshoot of the filter having linear phase with equiripple error is approximately twice as large as those of the equiripple impulse and Bessel systems, yet its amplitude (see Table 4.3) is well below the 3.3% limit established in Section 4.2 from the specifications defined in the international standards.

Table 4.6: Location of the poles ($-\alpha_k \pm j\beta_k$) of the 6th order equiripple impulse and of the 4th order linear phase with equiripple error filters having 3dB-cutoff equal to 150 Hz.

6th order Equiripple impulse (1% overshoot)	4th order Linear phase with equiripple error (ϵ = 0.5°)
- 391.5 $\pm$ j 1950.6	- 568.9 $\pm$ j 1412.0
- 577.8 $\pm$ j 1148.0	- 701.9 $\pm$ j 483.7
- 662.3 $\pm$ j 380.8	

Chapter 5

Preliminary analysis for the highpass filter design

5.1 Introduction

The highpass filter is probably the most critical subsection of an ECG monitoring system. Its role is to eliminate as much as possible of the low-frequency interference, that is, baseline wander and respiratory artifacts, without introducing any distortion into the low frequency components in the electrocardiographic signal. The low-frequency end of the ECG spectrum is, in fact, responsible for the preservation of the shape of the ST segment, which is an extremely clinically significant feature of the electrocardiogram. The analysis of a depression or elevation of the ST segment is essential for the diagnosis of myocardial ischaemia or infarction [4, 8].

Since the quality of the filter response greatly affects the overall performance of the ECG recording equipment, very demanding requirements are established by international standards for the characteristics of the highpass system [9, 15, 62, 63, 77]. The time domain performance requirements are especially strict and the specifications set for the maximum allowable undershoot and recovery slope of the filter response to an input rectangular pulse impose severe constraints on the design of the highpass filter.

Over the years, numerous digital solutions have been proposed for the reduction of baseline wander. The most common techniques are presented in this chapter and their suitability for low-power portable ECG monitoring systems is discussed. An analysis of the frequency and time domain characteristics of a few digital filters suggested for electrocardiographic applications is also performed. In particular, their response to an input rectangular pulse is examined for compliance with the standards' requirements.

In contrast with the wealth of digital methodologies for the elimination of low-frequency

noise described in the literature, the only analogue technique actually employed for baseline drift removal in diagnostic ECG measurement systems consists of the application of a first order highpass filter to the electrocardiographic recording. This simple filter is generally realised as a single-pole passive network having a cutoff frequency of 0.05 Hz. In order to investigate the possibility of designing a higher order analogue highpass filter having better rejection properties than the first order 0.05 Hz system and yet not distorting the ECG signal, traditional techniques for the design of analogue filters are first analysed. The classic lowpass-to-highpass transformations used to derive the transfer function of highpass filters are presented and the employment of compensation methods to modify the time and frequency domain characteristics of the analogue filters is also discussed.

5.2 Highpass filter requirements

The specifications for the highpass ECG filter are determined from the requirements detailed in the 1990 AHA recommendations [19] and the European standard EN 60601-2-51:2003 for diagnostic electrocardiographic devices [9]. As regards the amplitude response, the 1990 AHA report establishes that the passband ripple needs to be limited to ± 0.5 dB over the ECG spectrum, which is defined by the European standard to include frequencies as low as 0.67 Hz. In order to prevent excessive amplification of the low-frequency noise, it is, however, sensible to extend the 0.5 dB upper bound set for the in-band magnitude characteristic down to 0 Hz. In other words, overshoots in the filter amplitude are not allowed to exceed 6% of the high-frequency output level at any frequency.

Nonetheless, the most stringent requirements for the highpass system are specified in terms of its response to a narrow rectangular input pulse. As previously discussed in Section 3.3.1, the EN 60601-2-51:2003 standard prescribes that a 3 mV$\times$100 ms input pulse is employed to check the low-frequency distortion introduced by the filter. Limits are set for the displacement from the isoelectric line and the recovery slope after application of such a pulse. According to the standard, the maximum allowable value for the offset is equal to 100 µV, whereas two different bounds are defined for the recovery slope of the pulse response, as illustrated in Figure 3.6.

These pulse response constraints actually impose severe restrictions on the magnitude response of the highpass filter. The steepness of the out-of-band amplitude characteristic as well as the frequency of the 3dB-cutoff point need, indeed, to be limited for the specifications set on the displacement and recovery slope to be fulfilled. Let us, for example, consider a second order highpass filter obtained by cascading two equal first order RC sections and having an overall cutoff of 0.05 Hz and a single-pole network with 3dB-point at 0.1

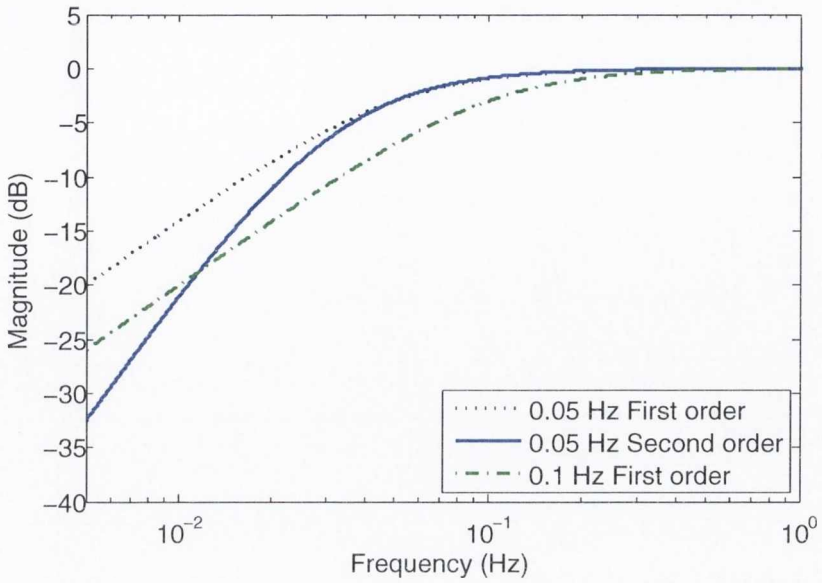


Figure 5.1: Magnitude response of two single-pole highpass networks with 3dB-point located at 0.05 Hz and 0.1 Hz, respectively, and of a second order highpass filter obtained by cascading two equal first order sections and having 0.05 Hz cutoff frequency.

Hz. Both filters were employed by Berson and Pipberger [16] when testing the distortions introduced into the ST segment and T wave by different highpass networks. The amplitude characteristic of these filters and their response to a 3 mV$\times$100 ms input pulse are presented in Figures 5.1 and 5.2, respectively. For comparison purposes, the magnitude and pulse responses of a 0.05 Hz single-pole system are also shown. It can be noticed that, for both filters under analysis, the undershoot occurring after the end of the rectangular wave is larger than the 100 µV limit. The infringement of the specification by the second order filter is limited to 20% of the maximum allowable value, whereas the response of the 0.1 Hz single-pole filter presents an undershoot almost twice as large as the bound. As regards the slope of the pulse response, it is evident from Figure 5.2(b) that for the second order filter the maximum value reached after the end of the input rectangular signal is well within the specified boundaries. On the other hand, the recovery slope in the response of the 0.1 Hz first order network marginally exceeds the 100 µV/s limit defined by the EN 60601-2-51:2003 European standard. It can be concluded that, even though a 0.05 Hz first order filter satisfies the pulse response requirements, a filter having the same cutoff frequency but higher stopband rejection does not fulfil the specification set by the international standards on the displacement from the isolectric line. Furthermore, if the cutoff frequency of the highpass filter is marginally increased from 0.05 to 0.1 Hz, not only the offset constraint is not met, but the bound set for the recovery slope of the pulse response is also exceeded.

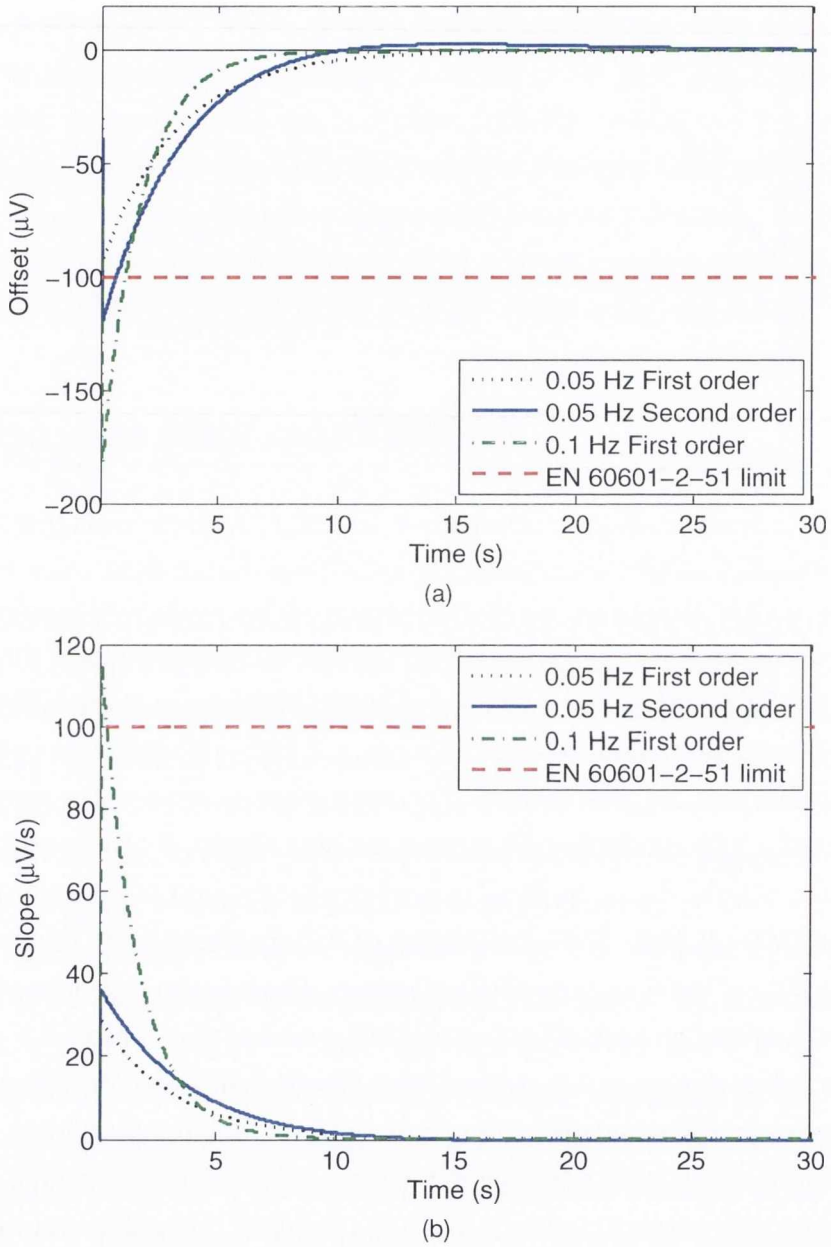


Figure 5.2: Displacement from the isoelectric line (a) and recovery slope (b) after the application of a 3 mV×100 ms rectangular pulse at the input of two single-pole highpass networks with 3dB-point located at 0.05 Hz and 0.1 Hz, respectively, and of a second order highpass filter obtained by cascading two equal first order sections and having 0.05 Hz cutoff frequency. The bounds established by the European standard for the maximum allowable undershoot and slope are represented by the dashed lines.

5.3 Digital techniques for baseline wander removal

A very large number of digital solutions for the elimination of low-frequency interference from ECG records have been proposed since the late 1970's. One of the earliest techniques devised involves estimating the baseline wander and subtracting it from the electrocardiographic signal. Cubic splines were originally employed for the determination of the baseline drift [107], but polynomial interpolation has also been suggested for the purpose [108]. The baseline wander estimation relies on finding some fiducial points on the intervals of the ECG wave that are considered isoelectric in the absence of noise, that is, the PQ or TP segments (see Section 2.3.2). Independent of the method used for the selection of the fiducial points, also called knots, their location is related to that of the R wave peak [107–110] and a QRS detector is needed for their determination. Since the amplitude of the low-frequency artifacts can be several times larger that that of the ECG signal [66], the algorithm for the R wave detection needs to be very robust to prevent miscalculation of the knots' positions, which could lead to significant errors in the drift estimation. Due to the issues related to the precise localisation of the fiducial points in a noisy environment, this technique does not appear suitable to be realised at the front-end of an ECG recording system.

Finite impulse response (FIR) filters started being employed for the conditioning of the electrocardiogram in the mid 1980's [68, 111] and they still represent a popular solution for ECG processing applications [70, 112]. This type of filter also appears to be used in practice by some electrocardiograph manufacturers. In 2006, Burri et al. [18] reported that a 0.67 Hz FIR filter was employed by Schiller (Baar, Switzerland) and an anti-drift highpass filter with 0.5 Hz cutoff frequency by Et Medical Devices (Milan, Italy). Even if the latter filter is not specifically stated to be FIR, this property can be inferred by the manufacturer's declaration that the system has a linear phase response. In fact, whereas FIR filters can be easily designed to achieve phase linearity [113], highpass analogue filters and their digital counterpart, infinite impulse response (IIR) filters, do not share this property (see Section 5.6). Due to their widespread use in electrocardiographic applications, a few examples of FIR highpass filters, including moving average filters, will be discussed in detail in the next section.

Adaptive techniques for the design of FIR filters for baseline drift removal have been proposed in the 1990's. Sornmo [114] suggested an array of digital filters having different cutoff frequencies. Two algorithms were developed for selecting the appropriate 3dB-bandwidth of this time-varying filter. One method was based on the frequency of baseline wander present in the recorded signal, the other one on the measured heart rate. Another algorithm for the determination of the variable cutoff frequency was later devised by Pandit [115]. The local

spectrum of the input signal was calculated and the frequency content in the interval between 0 and 1 Hz used to choose the 3dB-point of the digital filter applied to each portion of the recording. It is evident that these methodologies are quite computationally intensive and their implementation in a low-power ambulatory ECG measurement equipment is not practicable.

A simpler adaptive filter for the reduction of low-frequency artifacts was described by Thakor and Zhu [116]. Its structure is shown in Figure 5.3, where the primary input $s_1 + n_1$ represents the electrocardiographic signal contaminated by the baseline wander and n_2 constitutes the reference input for the noise, which was selected by Thakor and Zhu to be a unity constant. The filter error output, ϵ, is the best least-squares estimate of the noise-free ECG signal, s_1, when the mean square error between the primary and the reference inputs is minimised. Only one weight W is needed for the adaptive filter, that is, a single filter coefficient is adapted at each time step. The strength of this method lies in the fact that the clean ECG can be estimated without any *a priori* knowledge of the statistical or spectral properties of either the signal or the noise. On the other hand, Thakor and Zhu pointed out that, due to the attenuation introduced into the low frequency components of the ECG signal, the proposed filter actually produces some distortion of the ST segment. Therefore, this technique, and other adaptive filtering methods derived from it [117, 118], cannot be applied for the removal of baseline wander in diagnostic electrocardiographic applications, where the shape of the ST segment must be preserved to the highest extent possible.

Another class of digital filters often selected for the removal of low-frequency artifacts associated with the ECG recording is bidirectional filters [119, 120]. In the last decade, two different techniques in which the cutoff frequency of the bidirectional filter is adjusted according to the features of the ECG signal have been introduced [121, 122]. Both approaches are based on the misconception that a highpass zero-phase filter is suitable for processing the electrocardiogram without introducing significant time domain distortions, provided that the system 3dB-point is located at frequencies lower than the ECG spectrum. It has, however, been proven in Section 3.5.3 that a null-phase filter fulfilling the magnitude

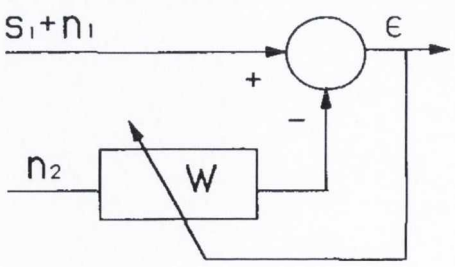


Figure 5.3: Structure of the adaptive filter for baseline wander removal proposed by Thakor and Zhu (modified from [116]).

requirements specified by the 1990 AHA recommendations [19] does not necessarily meet the pulse response constraints as well. Bidirectional filters cannot, therefore, be employed for baseline drift correction in diagnostic ECG devices, unless a sufficiently low cutoff frequency is selected (see Section 7.3.1).

In more recent years, numerous other digital techniques have been applied to ECG recordings with the aim of reducing low-frequency artifacts. In particular, several algorithms based on wavelet transforms have been developed since the end of the 1990's [118, 123–127]. Empirical mode decomposition (EMD) has also been recently proposed by Blanco-Velasco et al. [128] for the reduction of baseline drift. This methodology, however, does not appear to be very innovative. The recorded signal is decomposed through EMD into the sum of intrinsic mode functions, which are then simply passed through a bank of low-pass digital filters with different cutoff frequencies in order to estimate the baseline wander. Non-linear techniques, such as morphological filtering, have been employed for baseline drift correction, as well. A simple algorithm based on the successive application of opening and closing morphological operators was first proposed in 1989 by Chu and Delp [129] and later partially modified by other contributors [130, 131], whereas a more complex methodology was discussed by Sun et al. [132]. In morphological signal processing, the outline of the input signal is transformed using another signal, called the structuring element. The drawback of this approach is that the shape of the structuring element needs to be selected according to the characteristics of the signal to be extracted, i.e. the baseline wander, in this case. Other non-linear filtering methods for the elimination of low-frequency noise from ECG recordings have been presented by Keselbrener et al. [133] in 1997 and by Leski and Henzel [134] in 2005. These approaches, respectively, consist of a median filter and a modification of the classic moving average filter. Furthermore, Kalman filtering [135, 136], independent component analysis [137] and neural networks [138] have been suggested as solutions to the baseline wander removal issue.

Some of these novel techniques provide good suppression of the baseline drift and, from visual inspection, they do not appear to distort the electrocardiographic signal. However, these algorithms are usually not tested for compliance with the requirements specified by the international standards for ECG equipment. Indeed, only the performance of the non-linear filter described by Leski and Henzel [134] was tested using the ECG test signals of the CTS (Conformance Testing Services for Computerized Electrocardiography) database [9], which includes the calibration waveforms discussed in Section 3.6. Moreover, even though these recently proposed methodologies can easily be employed off-line on the digitised ECG signal, due to their computational requirements they do not seem to have found practical application in the design of electrocardiographic measurement systems, which must operate in real-time.

5.4 FIR filters for ECG applications

An FIR filter is characterised by an impulse response having a limited number of terms. The transfer function of this kind of filter is given by:

$$H(z) = \frac{Y(z)}{X(z)} = b_0 + b_1 z^{-1} + b_2 z^{-2} + \ldots + b_N z^{-N}, \tag{5.1}$$

where the parameters b_i, with $i = 0, 1, \ldots, N$, are the coefficients of the filter impulse response. An alternative representation of the FIR filter is provided by the difference equation, which specifies the numerical algorithm for the filter implementation [139]:

$$y(nT) = \sum_{i=0}^{N} b_i x(nT - iT), \tag{5.2}$$

where T is the data sampling period.

FIR filters are usually realised non-recursively, that is, without the use of feedback. In this case, the output signal is simply obtained as the weighted sum of the values stored by delay stages, as shown in Figure 5.4. The weights multiplying the content of the storage registers are equal to the coefficients of the filter impulse response. It should be finally noted that recursive implementations of FIR filters are also possible and that they are, indeed, more convenient when a large number of the impulse response coefficients are zero [113].

In the remainder of this section, some FIR filters proposed for the reduction of low-frequency interference in the electrocardiogram will be analysed. Particular attention will be dedicated to their frequency and time domain characteristics, which will be compared with the requirements for a highpass ECG filter illustrated in Section 5.2. Obviously many other FIR filters have been suggested for baseline wander removal. However, either the details necessary for their implementation are not provided in the literature [140, 141] or they are very similar to the filter types that will be discussed [142].

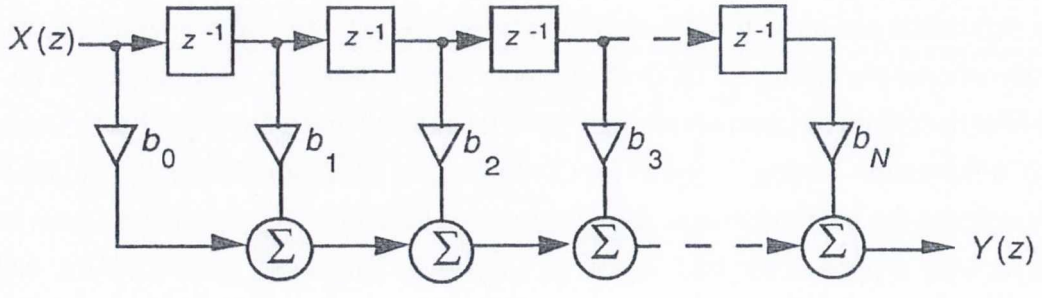


Figure 5.4: Non-recursive implementation of an FIR filter [113].

5.4.1 Recursive filter with integer coefficients (Ahlstrom and Tompkins, 1985)

Digital filters containing only integer coefficients in their difference equation were first proposed by Lynn [143] in 1970 with the aim of reducing the computational complexity of data processing in real-time applications. The transfer function of a first order lowpass integer filter is given by [144]:

$$H_{LP}(z) = \frac{1 - z^{-N}}{1 - z^{-1}}. \tag{5.3}$$

In the z-plane, $H_{LP}(z)$ is characterised by N equally spaced zeros on the unit circle. The zero located at $z = 1$ is cancelled by a pole, as illustrated in Figure 5.5. Since all the other poles are located at the origin of the z plane, Eq. (5.3) represents the recursive expression of an FIR filter. A recursive realisation is selected for this type of filter because a non-recursive implementation, although possible, would require many more digital operations. The gain of the integer filter $H_{LP}(z)$ is exactly equal to N at 0 Hz and the input signal is fully attenuated at the frequencies corresponding to the uncancelled zeros. Furthermore, the phase characteristic of the system is piecewise linear with 180° discontinuities at the frequencies of the zeros.

A highpass filter for real-time ECG signal processing was derived by Ahlstrom and Tompkins [111] from the first order integer filter described by Eq. (5.3). The highpass filter is obtained by subtracting the output of the lowpass filter from the original signal:

$$H_{HP}(z) = 1 - \frac{H_{LP}(z)}{N}. \tag{5.4}$$

Ahlstrom and Tompkins chose $N = 256$ and a sampling rate $f_s = 1/T = 200$ Hz. The magnitude response of the lowpass and highpass filters defined by these parameters are shown

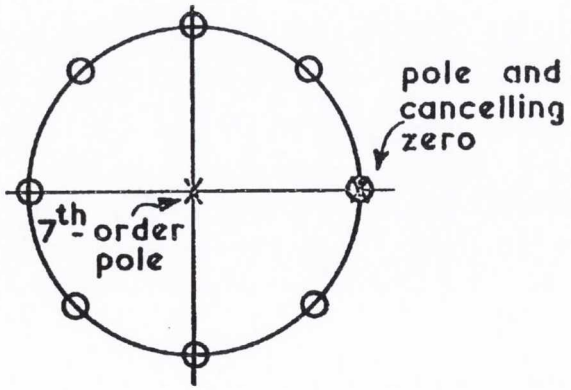


Figure 5.5: Pole-zero configuration of a lowpass integer filter for $N = 8$ [145].

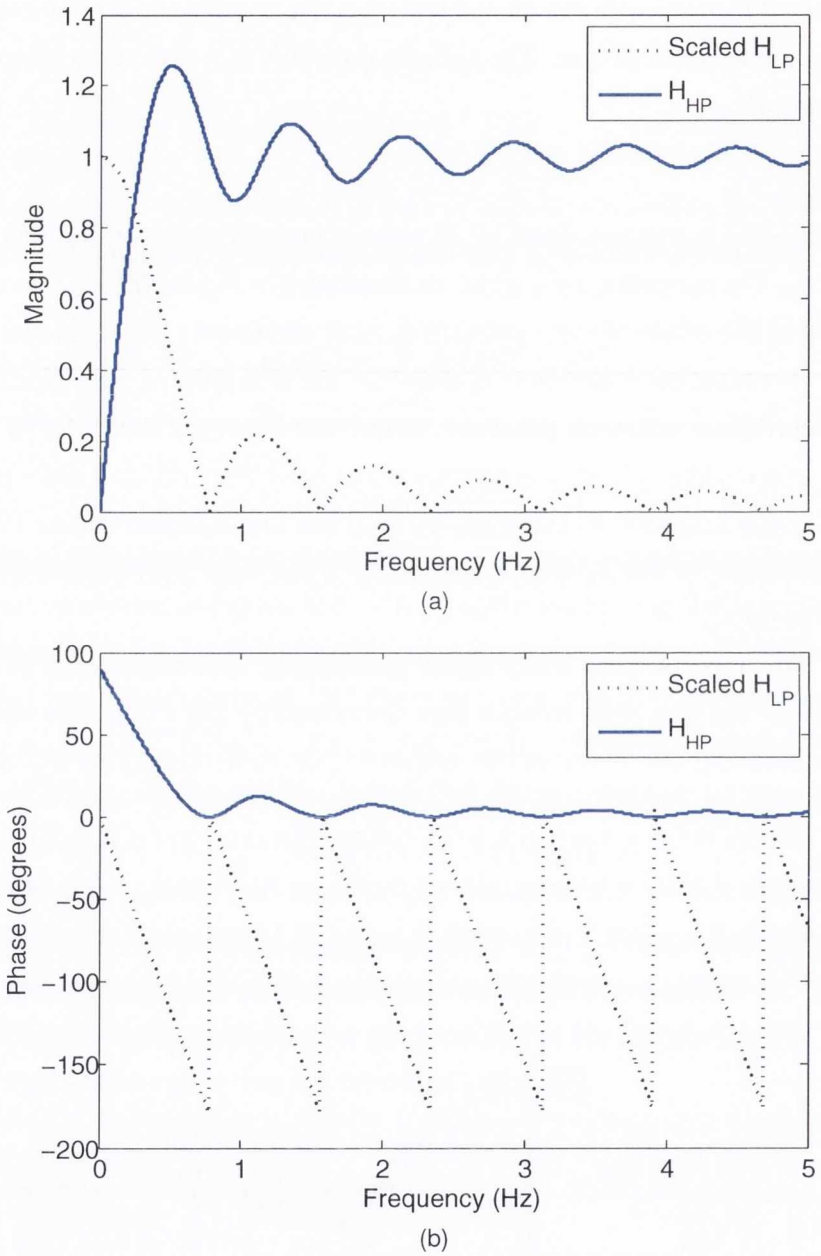


Figure 5.6: Magnitude (a) and phase (b) response of the recursive filter with integer coefficients proposed by Ahlstrom and Tompkins and of the lowpass filter from which it is derived. The lowpass filter is scaled to have unity gain at zero frequency.

in Figure 5.6(a). The frequency of the first amplitude zero of the lowpass filter is equal to f_s/N = 0.78 Hz and the 3dB-point of the lowpass magnitude response is located at 0.35 Hz. The cutoff frequency of the highpass filter is lower than that of the lowpass system and it can be measured to be 0.19 Hz. The highpass amplitude response is also characterised by a 2 dB peak at approximately 0.5 Hz and a ripple over the ECG spectrum that is as high as 12% of the high-frequency magnitude value. The amplitude of this in-band ripple is larger than both the 6% limit established by the 1990 AHA recommendations [19] and the 10% bound specified by the European and American standards for diagnostic electrocardiographic equipment [9, 15]. The phase response of the highpass filter is illustrated in Figure 5.6(b) and it can be clearly seen that its linearity is limited to the interval between 0 and 0.78 Hz, that is, the location of the first amplitude zero of the lowpass filter. The highpass phase characteristic can, however, still be considered approximately flat over the ECG frequency spectrum, since the maximum variation from the zero baseline is equal to 13° for frequencies above 0.67 Hz. As regards the response of the recursive FIR highpass filter to a 3 mV$\times$100 ms rectangular pulse, the undershoot occurring after the termination of the input waveform is equal to 0.23 mV. As shown in Figure 5.7, this value exceeds the 0.1 mV limit set by the EN 60601-2-51:2003 standard [9]. Moreover, given the sharp reduction in the pulse response undershoot occurring at approximately 1.3 s, the slope of the pulse response also fails to comply with the requirements specified in Section 5.2 for the highpass ECG filter.

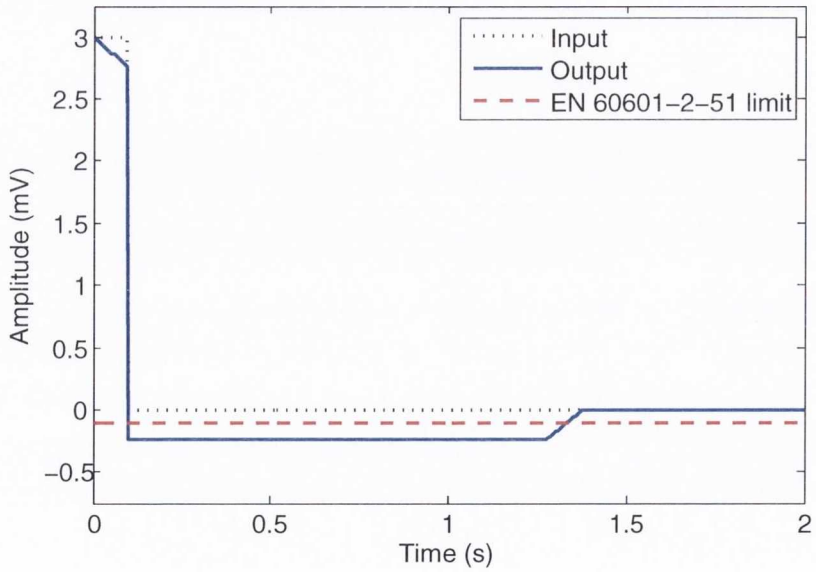


Figure 5.7: Response of the recursive filter proposed by Ahlstrom and Tompkins to a 3 mV$\times$100 ms rectangular pulse. The maximum allowable undershoot after the end of the input signal is illustrated by the dashed line.

5.4.2 FIR filter with a reduced number of impulse response coefficients (Van Alste et al., 1985)

An FIR filter was developed by Van Alste et al. [68, 94] for the concurrent removal of baseline wander and powerline interference. The filter amplitude response is defined to be periodic with narrow stopband notches at 0 Hz and at harmonics of the mains frequency of 50 Hz. The periodisation of the frequency spectrum allows the number of coefficients in the impulse response to be kept to a minimum.

The general difference equation for an FIR filter given by Eq. (5.2) can be rewritten to make the relationship between the coefficient of the impulse response and the sampling period T explicit:

$$y(nT) = \sum_{i=0}^{N} x\left[(n-i)T\right] b(iT), \tag{5.5}$$

where the sampling frequency $f_s = 1/T$ was chosen by Van Alste et al. to be 250 Hz. If the number of filter coefficients is reduced so that the time interval between them is a multiple of T, the output signal can be rewritten as:

$$y(nT) = \sum_{i=0}^{M} x\left[(n-ik)T\right] b(ikT), \tag{5.6}$$

where $M = N/k$ and kT is the interval between successive impulse samples. Van Alste et al. selected k to be equal to 5, so that the period of the filter magnitude response would be decreased from 250 Hz to exactly 50 Hz. They also noticed that, since the impulse response of an FIR filter needs to be symmetrical for its phase response to be linear [113], the number of computations needed for data processing could be further reduced. They managed, therefore, to achieve a reduction of approximately 10 in the number of multiplications and of about 5 in the number of additions, when compared to the original impulse response $b(nT)$.

The determination of the coefficients of the filter impulse response is quite convoluted and involves a window design and some adjustments to reduce the passband ripple and increase the stopband attenuation. Van Alste et al. initially obtained the coefficients $b(nkT)$ by truncating the inverse Fourier transform of the desired periodic spectrum of the filter. In order to reduce the overshoot introduced into the amplitude characteristic by this operation, the impulse response was then multiplied by a Kaiser window, which allowed the passband ripple to be lowered to ± 0.5 dB. The impulse response coefficients were further modified to achieve complete attenuation at frequencies which are multiples of 50 Hz. The magnitude response of the FIR filter obtained though this process is shown in Figure 5.8 for M = 50. The 3dB-cutoff frequency is equal to 0.98 Hz and the amplitude of the in-band ripple

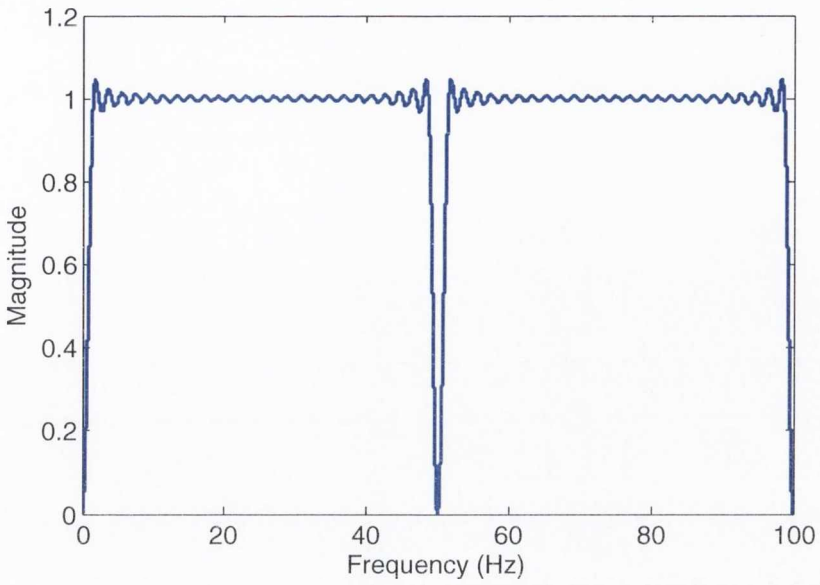


Figure 5.8: Magnitude response of the non-recursive filter designed by Van Alste et al..

is measured to be less than $\pm 5\%$. Even though the 3dB-point is slightly higher than the 0.67 Hz limit specified by the international standards for diagnostic electrocardiographic equipment, the magnitude characteristic of such a filter can be considered quite satisfactory. On the other hand, the time domain requirements that the highpass filter needs to satify to guarantee undistorted ECG measurement detailed in Section 5.2 are not fulfilled. From the filter response to a 3 mV$\times$100 ms rectangular pulse in Figure 5.9, it can be seen that the maximum displacement from the isoelectric line is almost 5 times larger than that allowed. It should be pointed out that the 0.5 s delay between input and output signals evident in the time domain characteristic is a consequence of shifting the impulse response to obtain a causal filter. The impulse response of the filter was, in fact, centered around the origin of the time axis after the windowing operation.

5.4.3 FIR filter implemented without the use of multipliers (Raita-aho et al., 1994)

Raita-aho et al. [69] also relied on the periodisation of the frequency spectrum to design a filter that eliminates the powerline interference as well as the baseline drift. The transfer function of their highpass filter is based on that of the first order lowpass integer filter described by Eq. (5.3). In order to reduce the large passband ripple characterising the magnitude response of this type of filter, Raita-aho et al. cascaded two identical recursive

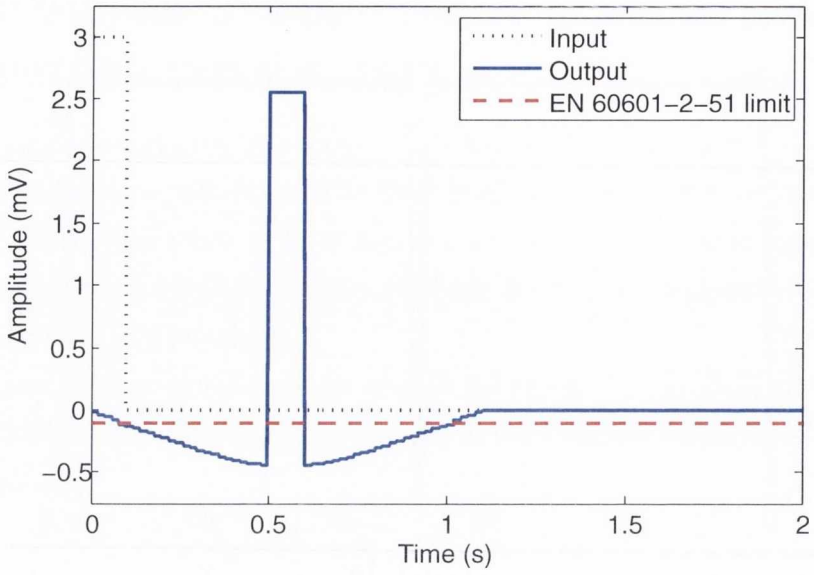


Figure 5.9: Pulse response of the non-recursive filter proposed by Van Alste et al..

filter sections, scaled to have unity gain at zero frequency:

$$G_{LP}(z) = \left[\frac{H_{LP}(z)}{N}\right]^2. \tag{5.7}$$

The maximum passband overshoot of the filter is thus reduced from 0.22 to $(0.22)^2 \approx 0.05$, as shown in Figure 5.10. The highpass counterpart of $G_{LP}(z)$ was determined as:

$$G_{HP}(z) = z^{-(N-1)} - G_{LP}(z). \tag{5.8}$$

If the sampling frequency is selected to be 200 Hz, the filter magnitude response can be periodicised to eliminate the powerline interference occurring at 50 Hz:

$$F_{HP}(z) = G_{HP}(z^4). \tag{5.9}$$

Raita-aho et al. chose N = 80, so that the system would produce an attenuation of 0.5 dB at 0.5 Hz, and proposed a recursive implementation that does not contain any multiplier. The amplitude characteristic of the filter described by Eq. (5.9) is illustrated in Figure 5.11 and a detail of its low-frequency response is shown in Figure 5.10. The passband ripple is equal to 0.42 dB and the 3dB-cutoff frequency is measured to be 0.36 Hz. It can thus be concluded that the magnitude response of the recursive FIR filter designed by Raita-aho et al. satisfies the requirements described in Section 5.2. On the other hand, it can be seen in Figure 5.12 that the 100 µV limit set by the EN 60601-2-51:2003 standard for the

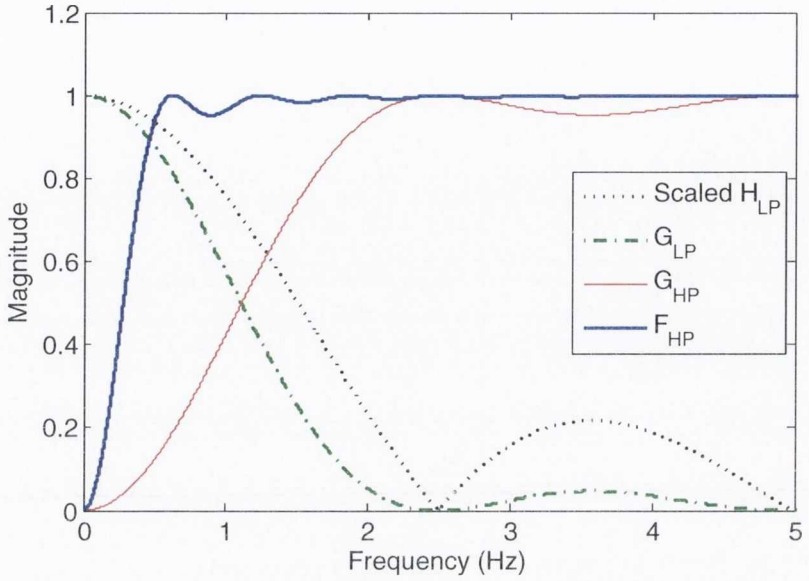


Figure 5.10: Low-frequency amplitude characteristic of the recursive FIR filter proposed by Raita-aho et al. and of the intermediate filters used in its design.

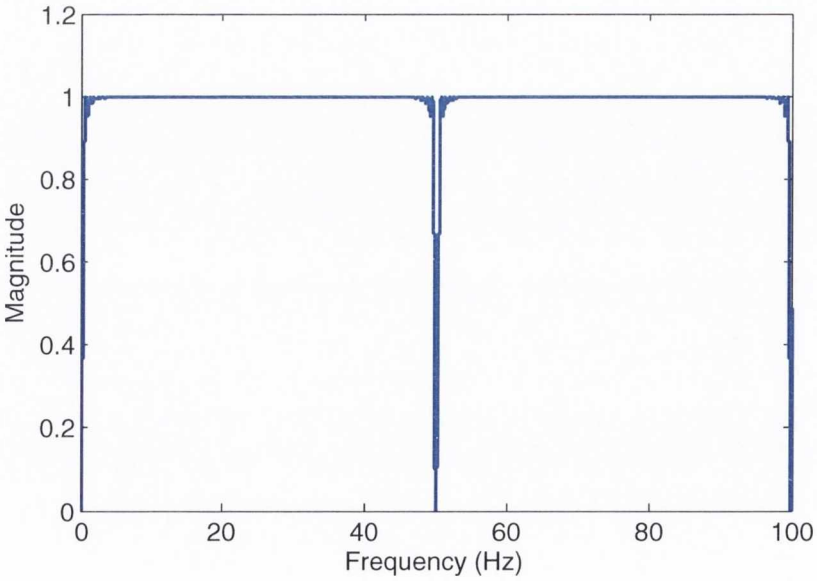


Figure 5.11: Magnitude response of the recursive FIR filter designed by Raita-aho et al..

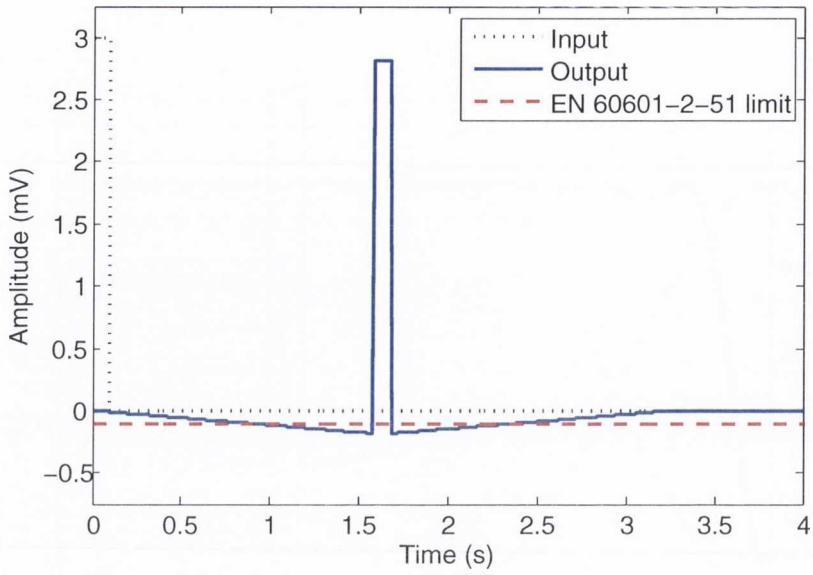


Figure 5.12: Response of the recursive FIR filter designed by Raita-aho et al. to a 3 mV$\times$100 ms rectangular pulse.

displacement occurring after the application of a 3 mV$\times$100 ms rectangular input pulse is exceeded, even though only marginally.

If the filter proposed by Raita-aho et al. is modified by increasing N to approximately 180, the 3dB-cutoff frequency is reduced to 0.16 Hz, but the offset and slope conditions set for the pulse response in the European standard are satisfied. Despite the improvement, the system still cannot be considered a suitable solution for the design of the highpass filter for diagnostic electrocardiographic applications. The sampling frequency is much lower than the minimum limit specified by both the 1990 AHA recommendations and the EN 60601-2-51:2003 standard, i.e. 500 Hz, and the stopband notches aiming at eliminating power line interference are likely to introduce distortion into the ECG signal, as discussed in Section 2.4.1.

5.4.4 Moving average filter

Numerous methodologies based on the moving average filter have been proposed since the early 1990's for the reduction of low-frequency artifacts [70, 140, 142, 146, 147] and this classic family of FIR filters is also often used as a benchmark for comparing the performance of more complex techniques for the removal of baseline wander from ECG recordings [134, 136]. A highpass moving average filter is defined by the difference equation:

$$y(nT) = x(nT) - \frac{1}{N} \sum_{i=-(N-1)/2}^{(N-1)/2} x((n+i)T), \tag{5.10}$$

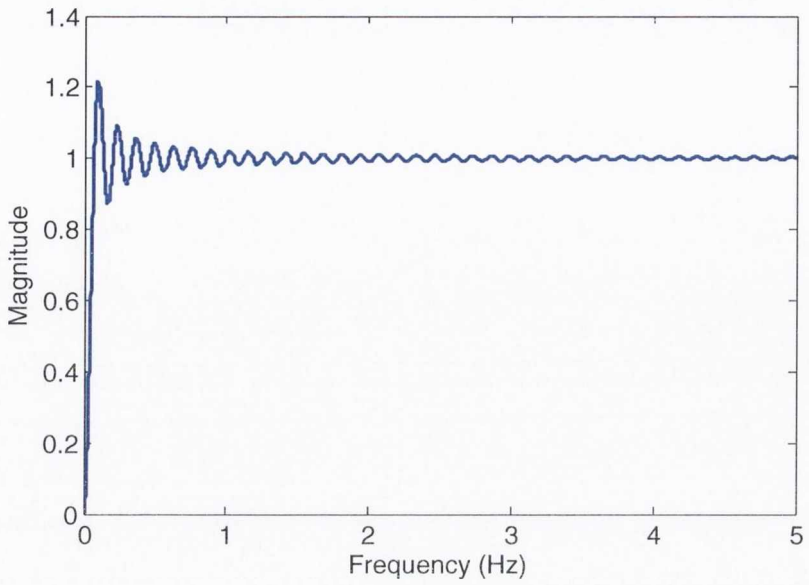


Figure 5.13: Amplitude response of a highpass moving average filter with a window length N = 7601 for a sampling frequency of 500 Hz.

where N is an odd number and represents the length of the observation window. This parameter, together with the sampling period T, determines the filter cutoff frequency.

Leski and Henzel [134] analysed the performance of the highpass moving average filter with respect to the signals included in the CTS test database described in the EN 60601-2-51:2003 European standard. They proved that the maximum distortion introduced into the noise-free test signals by the moving average filter decreases as the width of the observation window increases. They also concluded that, in order for the maximum error introduced by the highpass filter into the standardised test signals to be restricted to 25 μV, $(N-1)/2$ needs to be at least equal to 3800 for a sampling frequency of 500 Hz. The amplitude response of the highpass moving average filter defined by these parameters is illustrated in Figure 5.13. The magnitude shows a passband ripple as large as 20% of the steady state output value and the 3dB-point passband limit is measured to be 0.05 Hz. It can thus be concluded that, even though the distortion introduced by this filter on the ECG signal is negligible, it does not offer any advantage over a 0.05 Hz single-pole highpass network. Due to the large overshoot in its magnitude characteristic, the moving average filter can also give rise to noise or interference amplification at frequencies lower than the ECG spectrum.

5.4.5 Averaging $D \times N$ filter (Tabakov et al., 2008)

Tabakov et al. [70, 148] designed a filter that eliminates baseline wander and powerline interference simultaneously, by deriving the system difference equation from that of the

moving average filter presented in Eq. (5.10). The output signal of the $D \times N$ filter is defined as:

$$y(nT) = x(nT) - \frac{1}{N} \sum_{i=-(N-1)/2}^{(N-1)/2} x((n+iD)T), \tag{5.11}$$

where N is odd and is the number of averaged samples and D describes the distance, measured in number of samples, between the averaged samples. Comparing Eqs. (5.11) and (5.6), it appears clear that D and k perform the same function, that is, the periodisation of the filter spectrum. Zeros occur in the amplitude characteristic of the $D \times N$ filter at multiples of the frequency D/T and the number of ripples between zeros is determined by the value of N. For a sampling frequency of 250 Hz, Tabakov et al. [70] suggested D and N be made equal to 10 and 17, respectively. The magnitude response of the $D \times N$ filter for such parameters is illustrated in Figure 5.14, from which it can easily be noticed that a passband ripple as high as 20% is present. The choice of parameters by Tabakov et al. leads to a cutoff frequency of 1.11 Hz and to a complete rejection of integer multiples of a frequency of 25 Hz. These filter characteristics are not compatible with the ECG highpass filter requirements presented in Section 5.2. Both the 3dB-point and the ripple are higher than the values recommended in the 1990 AHA report and specified by the international standards for diagnostic electrocardiographs. Furthermore, the placement of a transmission zero at 25 Hz generates significant distortion in the ECG signal due to the presence of fundamental components of the QRS complex at this frequency, as shown in Figure 2.14. From the analysis of the time domain characteristics of the 10×17 filter, it also emerges that the conditions on the response to the 3 mV$\times$100 ms input pulse are not satisfied. The undershoot occurring after the termination of the rectangular pulse largely exceeds the 100 µV limit, as illustrated in Figure 5.15. Moreover, due to the abrupt changes in the amplitude of the output signal, the requirement on the maximum allowable recovery slope is not fulfilled either.

5.4.6 Frequency and time domain constrained filter (Henzel, 2005)

In 2005, Henzel [112, 149] devised a procedure for designing an FIR filter that simultaneously satisfied frequency and time domain specifications, as required by the AHA recommendations and the international standard for electrocardiographic instrumentation. He constrained the amplitude of the highpass filter to have a ripple lower than $\pm$10% for frequencies higher than 0.67 Hz. Moreover, the offset from the isolectric line in the response of the filter to an input triangular wave 1.5 mV high and 80 ms wide was restricted to 20 µV. Even though the magnitude requirement specified by Henzel is identical to the one established by the current European standard for diagnostic electrocardiographs, the constraint

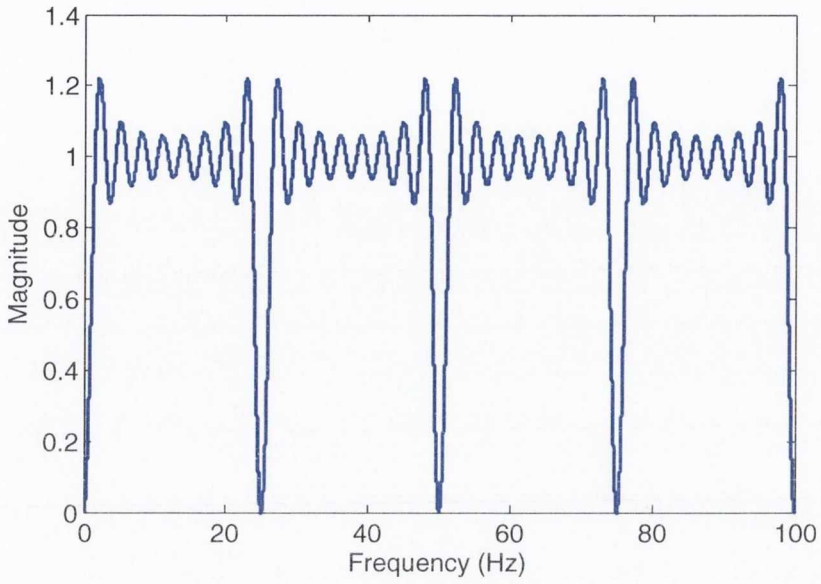


Figure 5.14: Amplitude characteristic of the averaging 10×17 filter proposed by Tabakov et al. for a sampling frequency of 250 Hz.

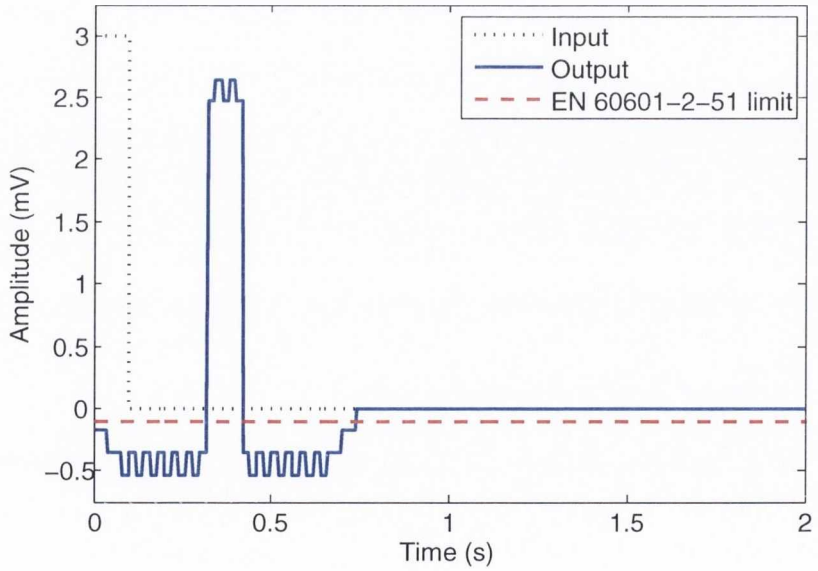


Figure 5.15: Response of the 10×17 averaging filter described by Tabakov et al. to a 3 mV×100 ms rectangular input pulse.

imposed on the displacement from the isolectric line is slightly stricter than those reported in Table 3.3 for current standards and recommendations.

The optimisation algorithm proposed by Henzel is based on the minimisation of the difference between the filter actual time and frequency domain characteristics and the desired amplitude and pulse responses. No requirement seems to have been established for the slope of the pulse response. Unfortunately, not enough information with regard to the design goals has been provided and it is unclear which are the features of the desired amplitude and pulse responses and for which frequency and time values they have been specified [112, 149]. From the magnitude characteristic of the optimised filter illustrated in Figure 5.16, it appears that the 3dB-cutoff frequency has been selected at approximately 0.5 Hz. This specification, combined with the strict bounds set for the displacement from the isoelectric line in the pulse response, provides a possible explanation for the very high number of coefficients required for the FIR filter. The minimum length of the filter impulse response was, in fact, found by Henzel to be 891, for a sampling frequency of 500 Hz [112].

From the magnitude response shown in Figure 5.16, other characteristics of this optimised filter can be deduced. A negligible ripple is present over the filter passband. The stopband limit is located at about 0.25 Hz and the amplitude of the optimised filter at zero frequency is exactly equal to the stopband ripple, that is, -40 dB. The response of the proposed filter to a 1.5 mV$\times$80 ms triangular pulse is depicted in Figure 5.17. The limit established by Henzel for the displacement from the isolectric line is exactly met by the designed filter. The recovery slope of the response to the triangular input pulse has also been evaluated. Figure 5.17 shows that the bound selected by Henzel for the slope in the regions outside the triangular wave is not exceeded. This 100 μV/s limit appears to be in line with the values recommended by the 1990 AHA report or by the American standard ANSI/AAMI EC11:1991/(R)2001/(R)2007 [15], when related to the area of the input pulse.

5.5 Analogue implementations for the reduction of low-frequency noise and interference

A single-pole highpass network is generally employed for the removal of baseline drift from electrocardiographic recordings when the morphology of the ECG signal needs to be preserved. Such a highpass filter was first proposed in 1966 by Berson and Pipberger [16], who selected 0.05 Hz as the 3dB-cutoff point to ensure that the distortion of the low frequency components of the ECG signal caused by the system was negligible. Since the amplitude characteristic of this 0.05 Hz first order network was employed in 1967 by the AHA to define the recommendations for the low-frequency response of ECG devices [23], the research of

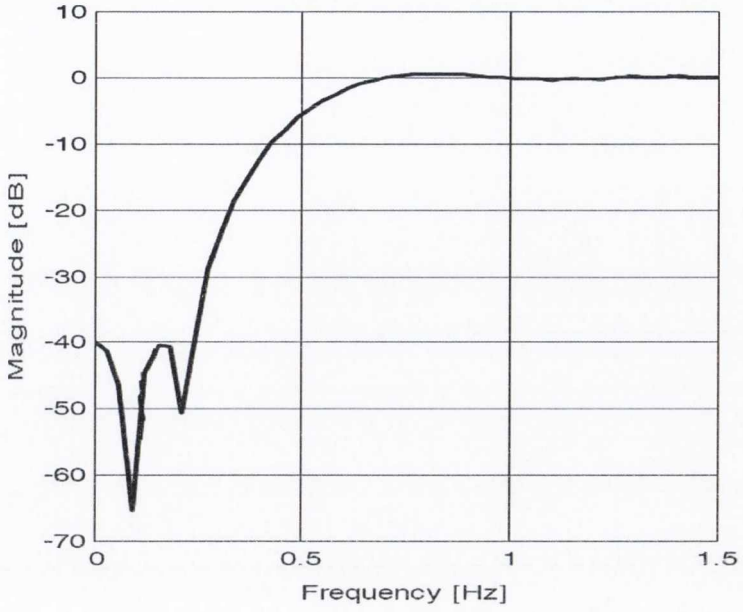


Figure 5.16: Magnitude characteristic of the filter designed by Henzel by constraining its frequency and time domain responses (modified from [112]).

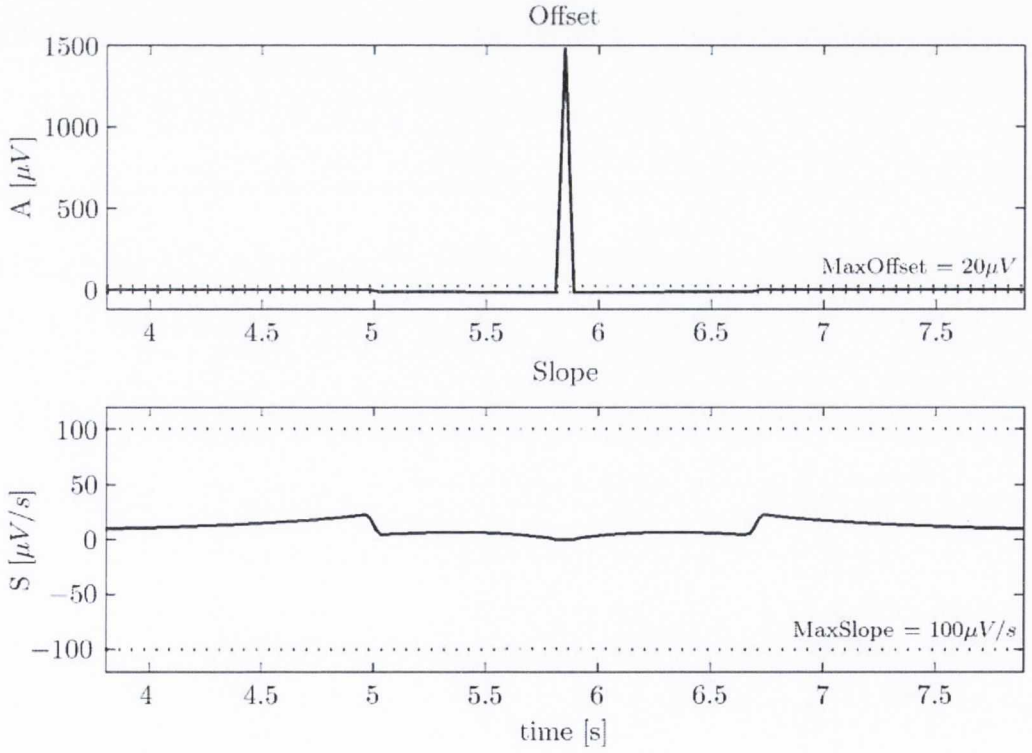


Figure 5.17: Response of the filter proposed by Henzel to a 1.5 mV×80 ms input triangular wave (modified from [149]). The slope of the pulse response is shown in the bottom panel. The limits selected by Henzel for the offset and slope outside the triangular wave are represented by the dotted lines.

other possible solutions for the removal of baseline wander from diagnostic electrocardiographic measurements was severely hindered. When, in 1990, the AHA recommendations were modified by relaxing the constraints set on the filter magnitude characteristic [19], the focus of baseline drift suppression studies had shifted towards digital algorithms. Therefore, up to this time, the only analogue filter implementation for diagnostic ECG recordings consisted of a single-pole network with cutoff frequency at approximately 0.05 Hz.

A simple RC highpass network having 3dB-cutoff frequency equal to 0.05 Hz was, for example, realised for an integrated ECG recording device by Abacherli et al. [92] in 2006, whereas Vehkaoja and Lekkala [95] employed a single-pole filter with 0.08 Hz 3dB-point for the wearable biopotential measurement device they designed in 2004. Both Yen et al. [150] and Mihel and Magjarevic [151] constructed first order highpass networks with a 3dB-cutoff point of approximately 0.11 Hz for their portable ECG processors, in 2003 and 2008, respectively.

Very often, the first order filter is directly incorporated into the front-end instrumentation amplifier. A solution based on a single off-chip capacitor that allows the filter 3dB-bandwidth to be varied between 0.05 and 0.07 Hz was proposed in 2005 by Shojaei-Baghini et al. [152]. The choice of capacitors in the differential front-end design presented in 2011 by Assambo [57] also leads to a single-pole highpass filter having a cutoff frequency equal to 0.05 Hz.

Some manufacturers of monitoring and analysing electrocardiographic devices are also known to use first order networks for the suppression of low-frequency noise and of the skin-electrode polarisation potentials. In 2006, it was reported [18] that the LabSystem PRO EP recording system by Bard (Murray Hill, NJ) employed a first order filter, whose cutoff frequency could be chosen as 0.05, 0.1, 0.5 or 1 Hz. Philips Medical Systems (Andover, MA) and GE Healthcare (Freiburg, Germany) also appear to use simple highpass RC networks in their diagnostic ECG equipment [67, 153, 154]. Even though these manufacturers do not actually state that they employ single-pole highpass networks in their devices, this characteristic of the filter can be inferred by the very low cutoff frequency disclosed. The 3dB-point of the highpass filter embedded in GE Healthcare products, for both resting and stress test ECG recordings, can adopt different values up to a maximum of 0.16 Hz.

Few other analogue circuits for removing low-frequency artifacts from the electrocardiogram have been devised. A baseline clamping circuit for centering the baseline of a pulse signal at about 0 V was independently proposed by Robinson and McFee in the early 1960's [155]. The working principle of this simple network consists in making the time during which the input wave is positive equal to the time for which it is negative. It has been claimed that the clamping circuit can be used to eliminate any DC offset from the electrocardiogram and even correct small baseline drift. However, an analysis of the distortion introduced into the

input signal was not carried out to prove whether the proposed circuit is suitable for use with electrocardiographic recordings. Another hardware technique for baseline drift correction in low-frequency applications was described by Bertolaccini et al. [156] in 1985. This analogue circuit can, however, only be employed to correct linear baseline drifts and the identification of an initial time interval in which no input signal is present is essential to its operation. Since the baseline wander of the ECG signal cannot be considered linear and especially because of the need to accurately identify the position of the isoelectric segments in the recording, the baseline corrector circuit does not appear suitable for electrocardiographic applications.

5.6 Lowpass-to-highpass transformations

In this section, attention will be directed towards the classic techniques for the design of analogue highpass filters. Two lowpass-to-highpass transformations are analysed and the distortion introduced in the frequency and time domain responses when the highpass transfer function is derived from the lowpass prototype is evaluated. As a practical example, these transforms are applied to a lowpass second order Bessel filter. For this particular transfer function, the group delay variation in the passband is approximately 20% and the step response overshoot is lower than 0.5%, as summarised in Table 4.3.

5.6.1 Classic H(1/s) transformation

A normalised highpass filter can be obtained from the lowpass prototype, having 3dB-cutoff frequency of ω = 1 rad/s, when the variable s is substituted with its reciprocal $1/s$ in the transfer function. Therefore, if the lowpass prototype has a pole or a zero at s_k, the highpass filter will have a pole or a zero at $1/s_k$ [157]. This conventional transform preserves the magnitude and phase characteristics of the original lowpass filter. The attenuation values are transposed to reciprocal frequencies, whereas the values of the phase response are both transposed and changed in sign. However, the quality of some lowpass filters, such as the Bessel, to have linear phase response in-band is lost since the passband of the normalised highpass filter extends from ω = 1 rad/s to infinite frequency. Moreover, the group delay does not retain the properties of its lowpass counterpart. In fact, even though the group delay of the lowpass filter is approximately flat in-band, that of the corresponding highpass system starts to decrease sharply at a frequency lower than the cutoff frequency, as shown in Figure 5.18(b). Furthermore, the highpass transient responses cannot be derived from the lowpass time domain characteristics and the features of the lowpass impulse and step responses are not preserved [84]. The highpass time domain responses show

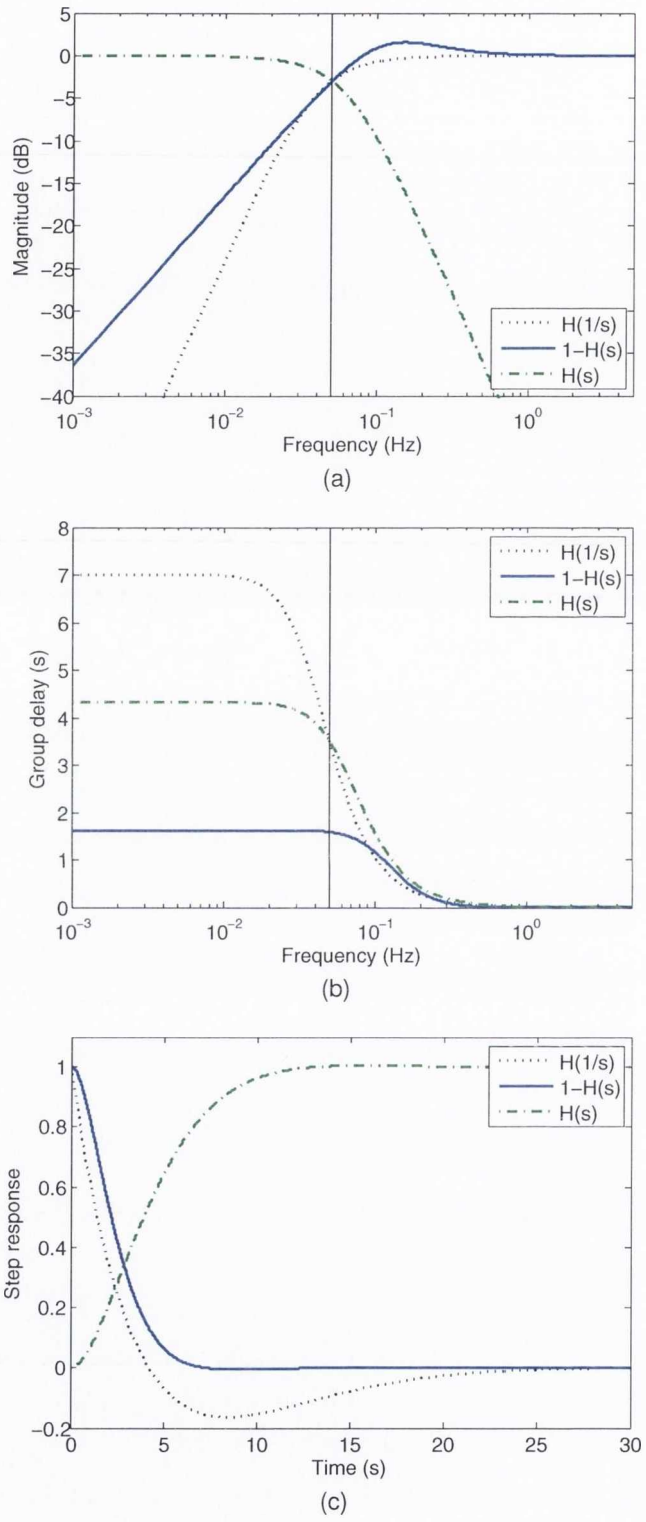


Figure 5.18: Amplitude characteristic, group delay and step response of highpass Bessel filters of order n = 2, obtained using the classic H(1/s) transformation and the 1-H(s) transform proposed by Blinchikoff and denormalised to have a 3 dB loss at 0.05 Hz. For comparison purposes, the responses of the second order lowpass Bessel filter with 3dB-cutoff at 0.05 Hz, H(s), are also shown.

marked overshoots, even when those of the corresponding lowpass responses are limited. This is, for example, the case for the highpass Bessel filter of order n = 2, whose step response is represented by the dotted line in Figure 5.18(c). In fact, whereas the step response overshoot of the lowpass filter has been shown in Section 4.4.1 to be negligible, it should be noticed that the highpass filter undershoot is larger than 15% of the input signal level.

5.6.2 1-H(s) transformation

In 1970, Blinchikoff [158] codified a different approach for transforming lowpass filters into highpass. The highpass transfer function is obtained as the frequency domain complement of the lowpass prototype:

$$H_{HP}(s) = 1 - H_{LP}(s). \tag{5.12}$$

This type of lowpass-to-highpass transformation is quite popular for digital applications, in which the low-frequency noise, determined by passing the input signal through a lowpass filter, is subtracted from the original signal. For example, the transfer function of the highpass moving average filter described in Section 5.4.4 is obtained from its lowpass counterpart using this method.

The 1-H(s) transform enables the highpass filter to preserve the transient properties of the lowpass transfer function, in terms of shape, overshoot and settling time of the impulse and step responses. In fact, the highpass impulse response is the negative of the impulse response of the lowpass filter, except for the unit impulse at t = 0 s, and the step response is the time domain complement of that of the lowpass filter. Therefore, it is possible to define a highpass filter with little or no overshoot in its transient response, provided the original lowpass filter displays such time domain performance. On the other hand, overshoot is introduced into the magnitude response, which proves to be quite distorted, as illustrated in Figure 5.18(a). Furthermore, unless the highpass filter needs to satisfy stringent transient requirements, the formula in Eq. (5.12) is generally not employed for networks of order higher than n = 2. In fact, independent of the filter order, the attenuation at frequencies close to zero is limited to 20 dB/decade for highpass filters obtained from an all-pole lowpass transfer function [158]. This characteristic of the amplitude response of highpass filters derived using the method proposed by Blinchikoff can be appreciated from Figure 5.19, where the magnitude of Bessel filters of different order is shown. It should also be noted that the amplitude of the overshoot occurring in the magnitude response increases with the filter order. The magnitude peak is limited to 1.6 dB for the transformed second order Bessel filter, but it rises to 3.7 and 4.4 dB for n = 4 and n = 6, respectively.

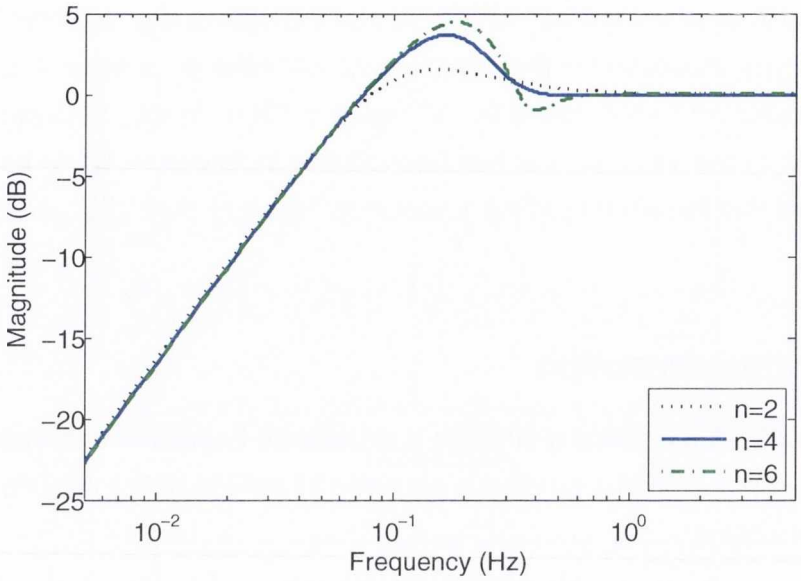


Figure 5.19: Magnitude response of highpass Bessel filters of different order, obtained through the 1-H(s) transformation and denormalised so that the 3dB-point corresponds to 0.05 Hz.

5.6.3 Discussion

Neither of the transformations presented is suitable for designing a highpass filter that simultaneously satisfies the magnitude and pulse response requirements specified by the 1990 AHA recommendations [19] and the current European standard for diagnostic ECG recording [9] and that has better rejection performance than a 0.05 Hz single-pole system. In fact, as shown in Figure 5.19, the amplitude characteristic of the highpass filter determined through the 1-H(s) technique shows a peak that is as high as 1.6 dB even for a second order Bessel filter. On the other hand, the undershoot occurring after the application of a 3 mV$\times$100 ms rectangular pulse at the input of a conventional highpass filter, having all the zeros located at infinite frequency, exceeds the 100 µV limit, when the filter 3dB-cutoff point is set at frequencies equal or higher than 0.05 Hz. The inability of the H(1/s)-transformed filters to fulfil the constraint imposed on the displacement from the isoelectric line is illustrated in Figure 5.20 for the second order Bessel system. Table 5.1 shows that, for both kinds of lowpass-to-highpass transformation, the undershoot present in the highpass pulse response has a larger maximum amplitude when the order of the filter is increased. Indeed, the 100 µV bound established for the pulse response offset is exceeded even by the filters obtained from the Bessel prototype through the 1-H(s) transform if $n \geq 3$.

As regards the phase response, the second order highpass filters analysed do not appear to have particularly critical characteristics. It can be noticed from Figure 5.21 that the deviation from zero of the phase response of the second order Bessel filter determined using the 1-H(s) method is smaller than that of a first order network with the same cutoff, for

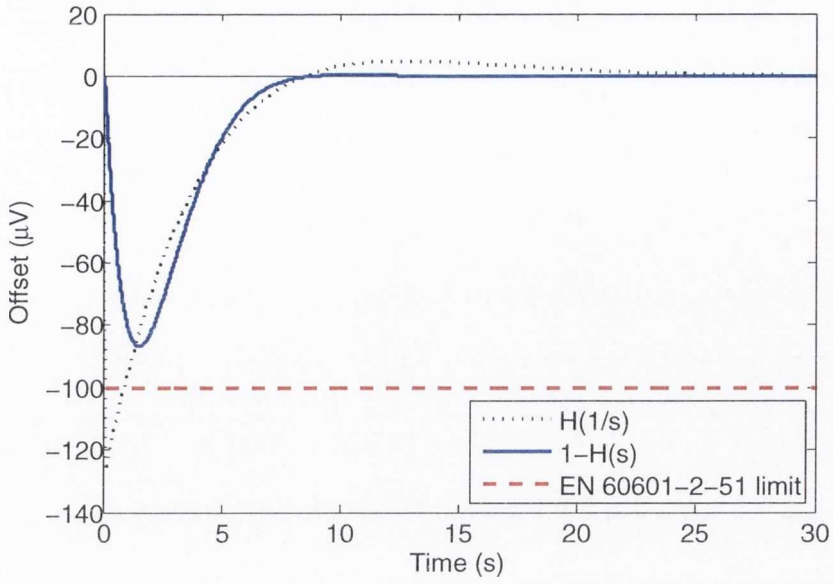


Figure 5.20: Displacement from the isoelectric line occurring in the response of highpass Bessel filters of order n = 2 and 0.05 Hz cutoff frequency after the application of a 3 mV$\times$100 ms rectangular input pulse. The maximum allowable undershoot is represented by the dashed line.

Table 5.1: Maximum displacement from the isoelectric line occurring in the pulse response of highpass Bessel filters of different orders, when their 3dB-cutoff frequency is equal to 0.05 Hz.

	Offset (μV)	
Order n	H(1/s)	1-H(s)
2	127	87
3	163	104
4	195	122
5	224	139
6	249	156

frequencies higher than approximately three times the 3dB-point, i.e. 0.15 Hz in this case. Moreover, the value of the phase response of the conventional highpass Bessel filter having order n = 2 and a 3dB-cutoff frequency equal to 0.05 Hz is only marginally larger than that of the single-pole system over the ECG spectrum, that is, for frequencies higher than 0.67 Hz.

In summary, the characteristics desired for the ECG highpass filter should be midway between those of a filter obtained using the traditional H(1/s) transform and those derived through 1-H(s) transformation. In fact, the reduced steepness of the magnitude response of the 1-H(s) filter allows the amplitude of the undershoot in its pulse response to be limited compared with that of a traditional H(1/s)-transformed highpass filter. On the other hand, in order to avoid the amplification of low-frequency noise, the filter magnitude characteristic

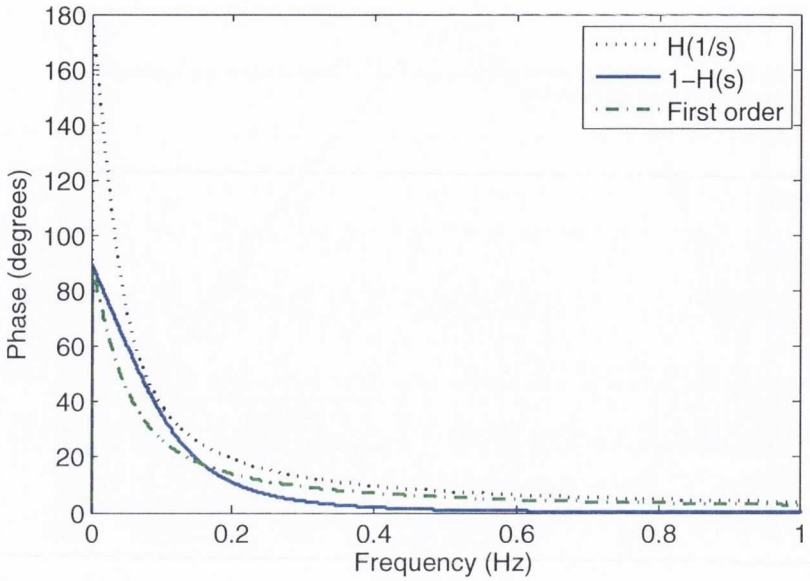


Figure 5.21: Phase response of highpass Bessel filters of order $n = 2$, obtained using the classic H(1/s) transformation and the 1-H(s) transformation and denormalised to have 3 dB attenuation at 0.05 Hz. For comparison purposes, the phase characteristic of a single-pole highpass network with the same cutoff frequency is also shown.

should not present a ripple higher than 0.5 dB, even at frequencies lower than the ECG spectrum. Moreover, the amplitude response of the desired highpass filter should ideally show an attenuation larger than that of a first order RC network in the transition region. In the following section, some compensation techniques to improve the characteristics of the highpass filters obtained by both the traditional lowpass-to-highpass transform and the 1-H(s) transformation are explored.

5.7 Analogue compensation techniques

5.7.1 Allpass network

A classic compensation technique for analogue filters consists in delay equalisation using allpass networks [159]. Allpass filters are characterised by a flat unity amplitude response over the whole spectrum. They can thus be employed to modify the phase characteristic of the system they are cascaded with, without introducing any change in its magnitude response. In this specific case, the allpass phase compensation method is only applicable to a highpass filter determined using the traditional H(1/s) transform. Its amplitude characteristic can, in fact, be designed to satisfy the passband ripple constraint defined by the 1990 AHA report [19]. As discussed in Section 3.5.2, increasing the phase linearity of the filter will allow the time domain characteristics to be improved as well. Therefore, the undershoot

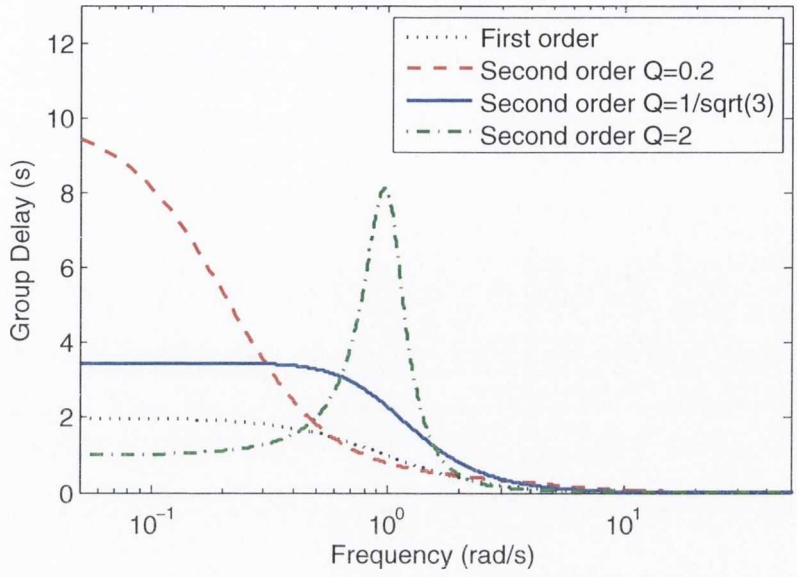


Figure 5.22: Group delay of first and second order allpass filters for ω_0 = 1 rad/s.

occurring in the response of the H(1/s)-transformed filter after the application of an input rectangular pulse might also be reduced.

The transfer function of a first order allpass filter is given by:

$$H_1(s) = \pm\frac{s-\omega_0}{s+\omega_0}, \tag{5.13}$$

where ω_0 is the frequency at which the phase is shifted by 90°. The sign in Eq. (5.13) defines the value of the phase response at zero frequency. In fact, if the sign is positive, the phase decreases from 180° to 0° as the frequency increases, whereas if the sign is negative, the phase decreases from 0° to -180° as the frequency increases. Second order allpass implementations are also possible and their transfer function is described by:

$$H_2(s) = \frac{s^2 - \dfrac{\omega_0}{Q} + \omega_0^2}{s^2 + \dfrac{\omega_0}{Q} + \omega_0^2}, \tag{5.14}$$

where ω_0 is the frequency at which the phase shift is 180°, that is, half of the total phase shift introduced by the circuit, and the quality factor Q determines the shape of the phase response. The higher the value of Q, the steeper the curve is at ω_0. For values of Q larger than $1/\sqrt{3}$, the group delay response shows a peak occurring at at approximately the critical frequency ω_0, as illustrated in Figure 5.22.

If the allpass network is to be effective in compensating the response of the highpass filter, the allpass phase response should be such as to increase the phase linearity of the

overall system. In other words, the group delay of the network obtained by cascading the highpass and allpass filters needs to be flatter than the group delay of the original filter. From Figures 5.18(b) and 5.22, it can be noticed that the highpass filter, the first order allpass and the second order allpass networks for $Q \leq 1/\sqrt{3}$ have a monotonically decreasing group delay characteristic. Since the delay of the system obtained by cascading the allpass and highpass filters is determined as the sum of the group delay responses of the two cascaded networks, a flatter group delay characteristic cannot be achieved by combining the above mentioned networks. On the other hand, the fact that the group delay response of second order allpass filters having $Q > 1/\sqrt{3}$ is increasing for frequencies lower than approximately ω_0 can be exploited to increase the group delay flatness of the network to which it is cascaded. However, even though the use of such a second order allpass network could provide a good solution for equalising the group delay of a narrow-band filter, it is not suitable for the phase correction of a highpass filter. In fact, even considering the ECG front-end filter to be band-limited at 150 Hz, a very high value would have to be chosen for the critical frequency ω_0, yielding no actual benefit in terms of the response of the highpass filter.

5.7.2 Pole-zero network

Another possibility for the compensation of the highpass response consists in cascading the filter with a pole-zero network, which will introduce modifications in both the amplitude and the phase characteristic of the original filter. The transfer function of a pole-zero network is defined by:

$$H(s) = \frac{s + \omega_z}{s + \omega_p}, \tag{5.15}$$

where ω_z and ω_p are the frequencies of the zero and the pole, respectively, and $\omega_z \neq \omega_p$. Depending on the relative frequency of the pole and zero, the system can be classified as a lead or a lag network. If the pole frequency is higher than that of the zero, Eq. (5.15) describes a lead network. When the $\omega_z > \omega_p$, the transfer function identifies a lag network, instead.

Lead and lag networks can be easily realised by three-element RC circuits, as illustrated in Figure 5.23. The transfer functions of the networks shown are, respectively, equal to:

$$H_{Lead}(s) = \frac{s + \omega'}{s + \dfrac{\omega'}{\alpha}} \tag{5.16}$$

and

$$H_{Lag}(s) = \alpha \frac{s + \omega''}{s + \alpha\omega''}, \tag{5.17}$$

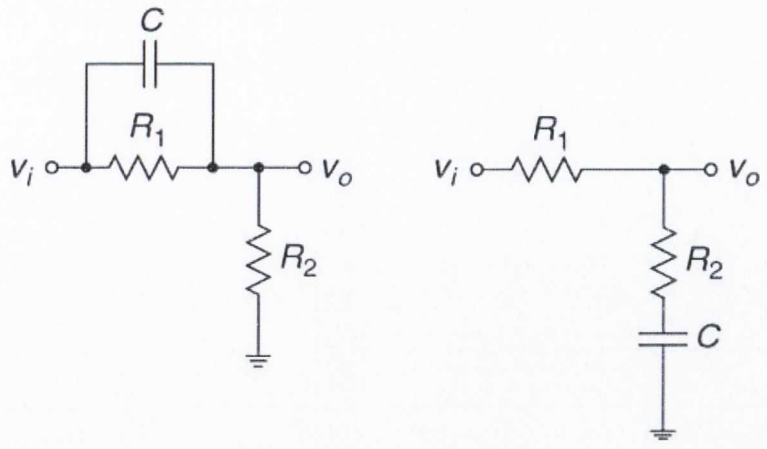


Figure 5.23: Passive implementation of lead (left) and lag (right) networks [160].

where ω' and ω'' identify the frequency of the zero for the lead and the lag network, respectively. In both cases, $\alpha = R_2/(R_1 + R_2)$ [160], which implies $0 < \alpha < 1$. The magnitude and phase responses corresponding to these transfer functions are depicted in Figure 5.24 for $\alpha = 0.2$, having normalized the frequency of the zero to be 1 rad/s. It can be noticed that the lead network is characterised by a low-frequency attenuation that is exactly equal to α. This parameter also represents the high-frequency loss of the lag circuit. As for the phase response, the lead network introduces a positive shift, whereas the phase characteristic of the lag network is negative over the whole spectrum. In both cases, the amplitude of the peak in the phase response is determined only by the value of α. It can be shown that the maximum absolute value of the phase shift is given by [161]:

$$|\theta|_{max} = \tan^{-1}\left(\frac{1}{\sqrt{\alpha}}\right) - \tan^{-1}\left(\sqrt{\alpha}\right). \tag{5.18}$$

Let us now consider the lead network with regard to the compensation of the highpass filter response. Since the magnitude of this network is unity at high frequencies, no change will be introduced in the asymptotic high-frequency amplitude of the system to which the lead circuit is cascaded. On the other hand, the lead network will enhance the attenuation of the original filter for frequencies lower than that of its pole, ω'/α. Since in this case a highpass filter is the starting point for the compensation, the lead network will cause the steepness of the filter magnitude response to increase at low frequencies. A sharper low-frequency cutoff will, in turn, determine a larger undershoot in the response of the highpass filter to an input rectangular pulse, as discussed in Section 5.2. It can thus be concluded that a lead network is not suitable for improving the adherence of the frequency and time domain characteristics of the highpass filter to the requirements set by the international standards.

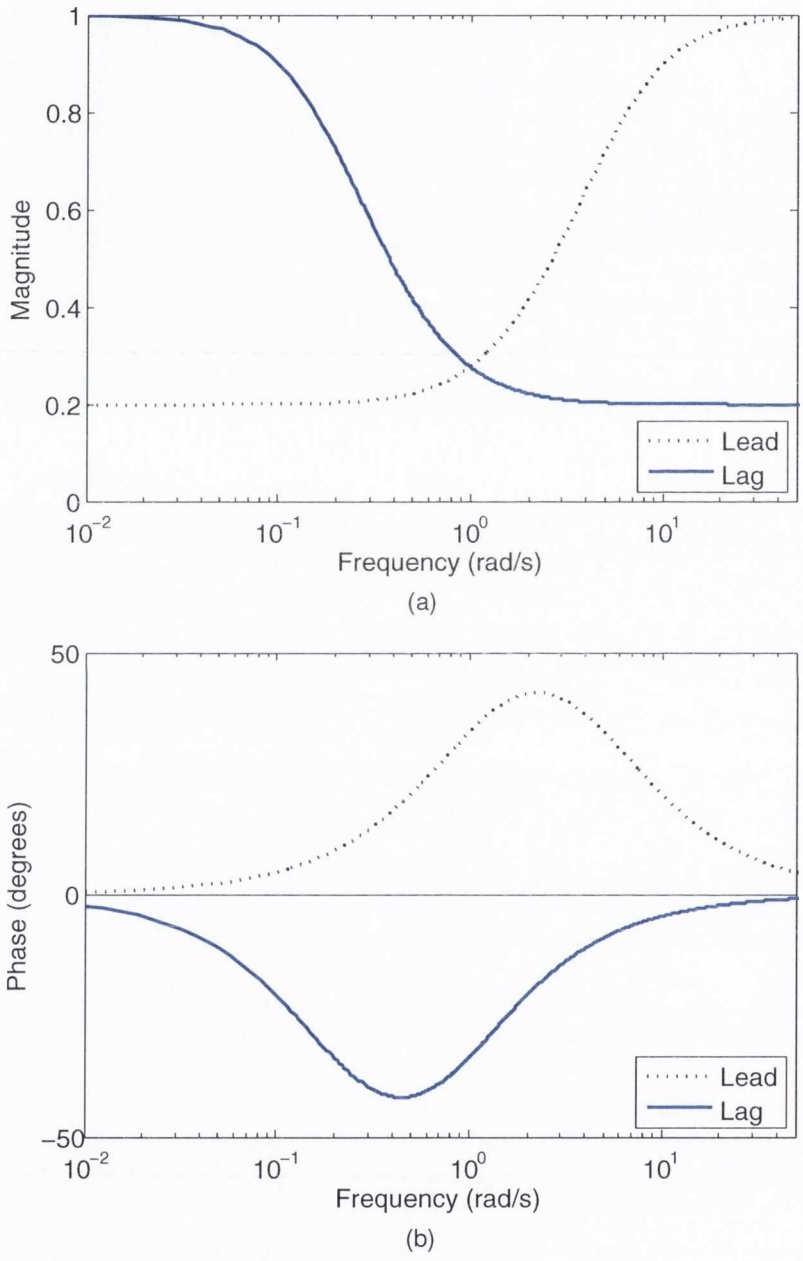


Figure 5.24: Magnitude (a) and phase (b) response of a lead and a lag network for $\alpha = 0.2$ and $\omega' = \omega'' = 1$ rad/s.

As regards the lag network, it can be seen from Figure 5.24(a) that this circuit can actually be used to decrease the steepness of the magnitude response of a H(1/s)-transformed highpass filter cascaded with it. The lag network will, however, also cause a reduction of the high-frequency gain, which, if the ratio between pole and zero frequencies is extremely large, would have to be compensated by designing the front-end amplifier to have a larger gain. In terms of phase response, this pole-zero network can be employed to decrease the phase shift introduced by the highpass filter at low frequencies (see Figure 5.21). This phase equalisation property of the lag network has been verified by Gleeson [31]. The goal of the study was to reduce the passband phase shift of a highpass filter obtained using the conventional H(1/s) transform to the level of that of a 0.05 Hz single-pole filter. Gleeson, however, failed to find a lag network that would allow such a compensation, without introducing a peak in the magnitude response larger than the 0.5 dB limit recommended in the 1990 AHA report. The choice of highpass filter as a third order system with 3dB-cutoff located at 0.3 Hz can be identified as a possible cause of the inability to determine appropriate values for the parameters of the lag network. The bandpass limit and the order of the filter result in the phase shift being extremely large in the low-frequency range of the ECG spectrum. If a second order filter with a lower cutoff frequency had been selected instead, it might have been possible to find a lag network able to reduce the low-frequency phase shift of the filter below the reference level set by the 0.05 Hz first order system.

In summary, even though a lag network can be used for the compensation of the frequency and time domain characteristics of a conventional highpass filter, this solution to the highpass design problem does not appear to be optimal. First of all, the combination of filter and pole-zero network not only attenuates the out-of-band low-frequency noise, but it also reduces the amplitude of the ECG signal. Moreover, the outcome of the compensation is highly dependent on the choice of highpass filter. In fact, the optimisation of the parameters of the lag network, ω'' and α, can succeed in reducing the undershoot occurring in the system response after the application of a rectangular input pulse only if the order and the 3dB-cutoff frequency of the highpass filter are limited.

5.7.3 Lag-lead network

A lag-lead network can be obtained by cascading a lead and a lag network if the location of poles and zeros is properly chosen. The frequencies of the zeros need, in fact, to be located between the frequencies of the poles. A simple implementation of the lag-lead network consists in the passive circuit shown in Figure 5.25, whose transfer function is

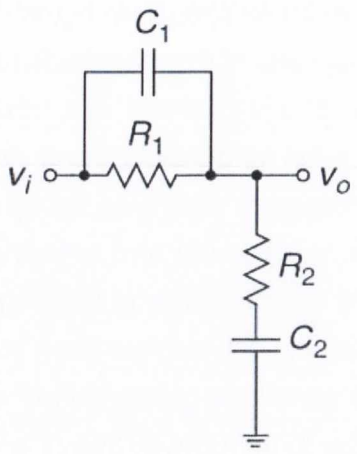


Figure 5.25: Passive realisation of a lag-lead network.

given by [162]:

$$H_{Lag-Lead}(s) = \frac{(s+\omega_1)(s+\omega_2)}{\left(s+\frac{\omega_1}{\beta}\right)(s+\beta\omega_2)}, \tag{5.19}$$

where

$$\omega_1 = \frac{1}{R_1 C_1} \quad \text{and} \quad \omega_2 = \frac{1}{R_2 C_2} \tag{5.20}$$

and the following relation must be satisfied for $0 < \beta < 1$:

$$\frac{1}{R_1 C_1} + \frac{1}{R_2 C_1} + \frac{1}{R_2 C_2} = \frac{1}{\beta}\frac{1}{R_1 C_1} + \beta\frac{1}{R_2 C_2}. \tag{5.21}$$

The amplitude and phase responses of such a lag-lead system are depicted in Figure 5.26 for ω_1 = 1 rad/s and ω_2 = 3 rad/s, when $C_1 = C_2$. Since capacitors of equal value have been selected, Eq. (5.21) can be simplified and the parameter β is calculated to be:

$$\beta = \frac{\omega_1 + 2\omega_2 - \sqrt{\omega_1^2 + 4\omega_2^2}}{2\omega_2} = 0.15. \tag{5.22}$$

It should be noticed that a minimum occurs in the magnitude characteristic of the lag-lead network at frequency $\sqrt{\omega_1\omega_2}$, i.e. the geometric mean of the frequencies of the zeros. At the same frequency, the phase shift introduced by the network changes in sign from negative to positive. The amplitude of the minimum in the magnitude response and the deviation of the phase characteristic from zero are, however, simultaneously dependent on the ratio between the frequency of the zeros and β. If the zeros are located very far apart and the value of β is large, the peaks in the magnitude and phase response are reduced. However, due to the relationship in Eq. (5.21), the frequencies of the zeros and the parameter β

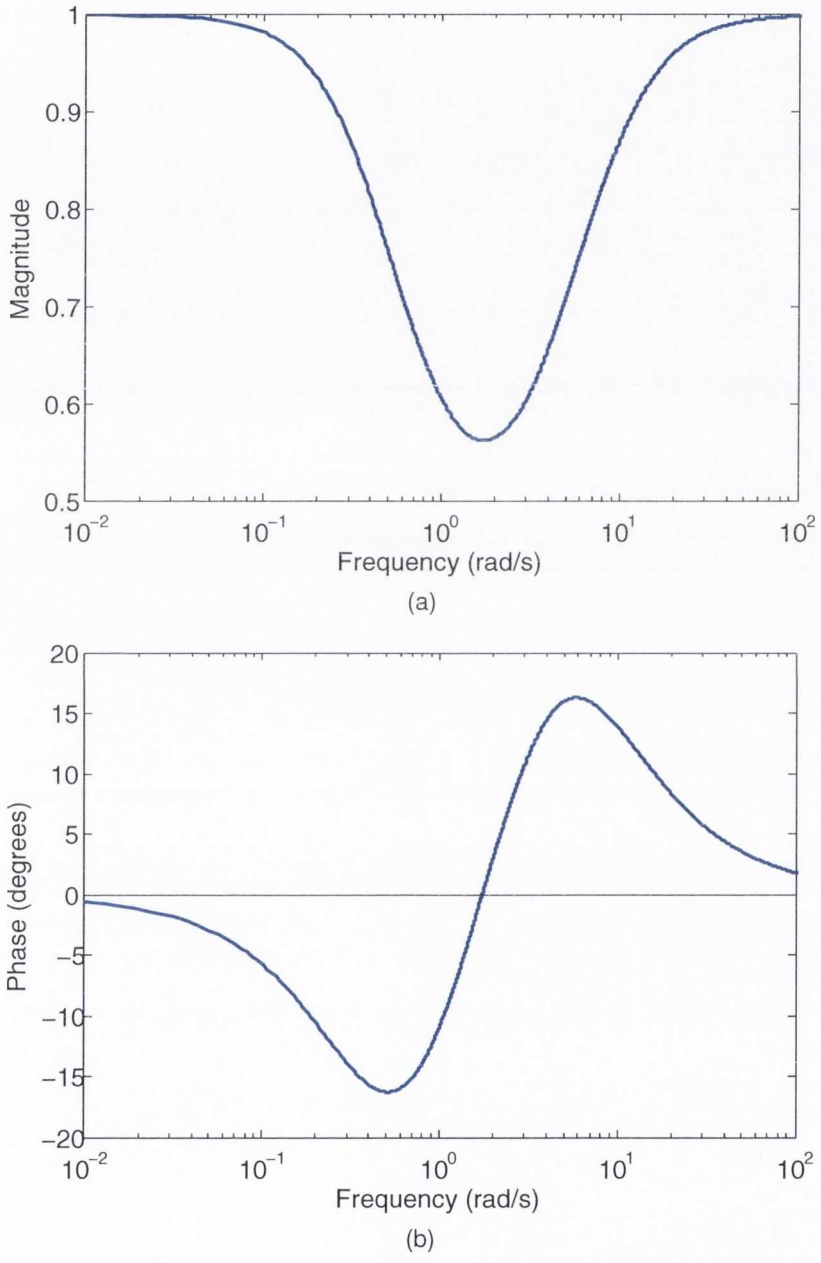


Figure 5.26: Magnitude (a) and phase (b) response of a passive lag-lead network for ω_1 = 1 rad/s and ω_2 = 3 rad/s, when $C_1 = C_2$.

cannot be chosen independently for the passive circuit in Figure 5.25.

Since a lag-lead network causes the input signal to be attenuated over a finite frequency interval but does not alter the transmission at low and high frequencies, this type of circuit can be employed to compensate the overshoot occurring in the amplitude response of highpass filters derived through the 1-H(s) transformation. Let us, for example, consider the system obtained from a second order Bessel prototype. When the 3dB-cutoff frequency the highpass filter is 0.05 Hz, its magnitude characteristic presents a peak at f_k = 0.15 Hz, as illustrated in Figure 5.19. To decrease the extent of this overshoot, a lag-lead network having a minimum located at approximately f_k can be cascaded to the highpass filter.

In order to design a passive lag-lead network for the compensation of the magnitude response of the 1-H(s) highpass filter, different combinations of values for the resistances and capacitances in Figure 5.25 have been selected. For each set of parameters, the response of the system obtained by cascading the lag-lead network and the filter has been tested for compliance with the requirements specified in Section 5.2 for the ECG filter. The first step in the selection of the passive circuit components consists in fixing the parameter C_1. Different values for the resistor R_1 are then chosen so that the zero of the lead network, ω_1, is close to the frequency of the peak in the amplitude response of the highpass filter. Since $2\pi f_k \approx 1$ rad/s, ω_1 is varied between approximately 0.5 and 2 rad/s. For each ω_1, the target value for ω_2, named ω_2', is determined though the relationship:

$$\omega_2' = \frac{(2\pi f_k)^2}{\omega_1}, \tag{5.23}$$

which sets the frequency of the minimum in the magnitude response of the lag-lead network to be equal to that of the peak occurring in the amplitude characteristic of the filter. Various combinations of C_2 and R_2, for which the zero of the lag network, ω_2, approximates the desired ω_2', are finally selected. An example of this procedure is shown in Table 5.2 for C_1 = 100 nF. It should be noticed that, for any given couple of ω_1 and ω_2, the depth of the valley in the magnitude response of the lag-lead network, that is, the amount of compensation applied to the amplitude characteristic of the highpass filter, is determined by the value of parameter β, which is, in turn, defined by the choice of C_2 and R_2.

Regarding the choice of components in Table 5.2, it should be noted that through-hole capacitors with a 1% tolerance are currently available for capacitance values up to 100 nF [163] and that through-hole resistors with a 1% tolerance are also produced according to the E6 series for values up to 100 MΩ [164]. Components characterised by high values of resistance or capacitance and low tolerances are, however, quite bulky. In order to decrease the physical dimensions of both resistors and capacitors, the design of the lag-lead circuit can be modified by selecting capacitances one order of magnitude larger and resistances

Table 5.2: Sets of parameters defining the passive lag-lead network that were tested to compensate the magnitude response of the highpass filter (C_1 = 100 nF).

	R_1 = 22 MΩ ω_1 = 0.45 rad/s ω_2' = 2.06 rad/s			R_1 = 15 MΩ ω_1 = 0.67 rad/s ω_2' = 1.40 rad/s			R_1 = 10 MΩ ω_1 = 1 rad/s ω_2' = 0.94 rad/s			R_1 = 6.8 MΩ ω_1=1.47 rad/s ω_2' = 0.64 rad/s		
C_2 (nF)	R_2 (MΩ)	ω_2 (rad/s)	β	R_2 (MΩ)	ω_2 (rad/s)	β	R_2 (MΩ)	ω_2 (rad/s)	β	R_2 (MΩ)	ω_2 (rad/s)	β
100	4.7	2.13	0.10	6.8	1.47	0.20	10	1.00	0.38	15	0.67	0.61
68	6.8	2.16	0.12	10	1.47	0.24	15	0.98	0.45	22	0.67	0.69
47	10	2.13	0.14	15	1.42	0.28	22	0.97	0.52	33	0.64	0.76
33	15	2.02	0.16	22	1.38	0.33	33	0.92	0.60	47	0.64	0.82
22	22	2.07	0.17	33	1.38	0.36	47	0.97	0.64	68	0.67	0.86
15	33	2.02	0.19	47	1.42	0.38	68	0.98	0.69	100	0.67	0.90

one order of magnitude smaller. The drawback of this approach is that capacitors with 5% tolerance need to be used. The employment of larger capacitances is also essential if a surface-mount implementation of the lag-lead network is required. In fact, even though surface-mount capacitors with 2% tolerance are on the market for values up to 220 nF [165], only few denominations of surface-mount resistors are manufactured for resistances larger than 10 MΩ [166].

The combinations of capacitance and resistance values that allow the magnitude and pulse response constraints presented in Section 5.2 to be satisfied by the cascade of the highpass filter and the passive lag-lead network are given in Table 5.3 for C_1 = 100 nF and C_1 = 68 nF. Other sets of component values may be successfully employed to compensate the magnitude response of the highpass filter if a smaller value of C_1 is chosen as the starting point for the lag-lead network design. It should, however, be noted that the resistance of both R_1 and R_2 increases as the capacitance C_1 is decreased. Therefore, a trade-off exists between the values of resistors and capacitors in the lag-lead network and, in particular, the lower limit for C_1 is set by the maximum resistance allowable for R_2.

The magnitude characteristic and the undershoot and recovery slope of the pulse response are illustrated in Figures 5.27 and 5.28 for the systems obtained by cascading the second order Bessel 1-H(s) highpass filter and each of the lag-lead networks designed for C_1 = 100 nF, whose component values are presented in Table 5.3. No substantial difference between the various compensating networks can be noticed in the frequency and time domain characteristics of the cascaded system. Each lag-lead network manages to reduce the overshoot present in the magnitude characteristic of the original highpass filter to less than 0.5 dB, without causing the pulse response of the overall system to exceed the limit set for the displacement from the isolectric line. Moreover, the absolute value of the recovery slope measured after the end of the rectangular input is actually reduced by cascading the

Table 5.3: Combinations of component values that allow the standards' requirements for ECG filtering to be fulfilled by the responses of the cascade of the lag-lead network and the highpass filter.

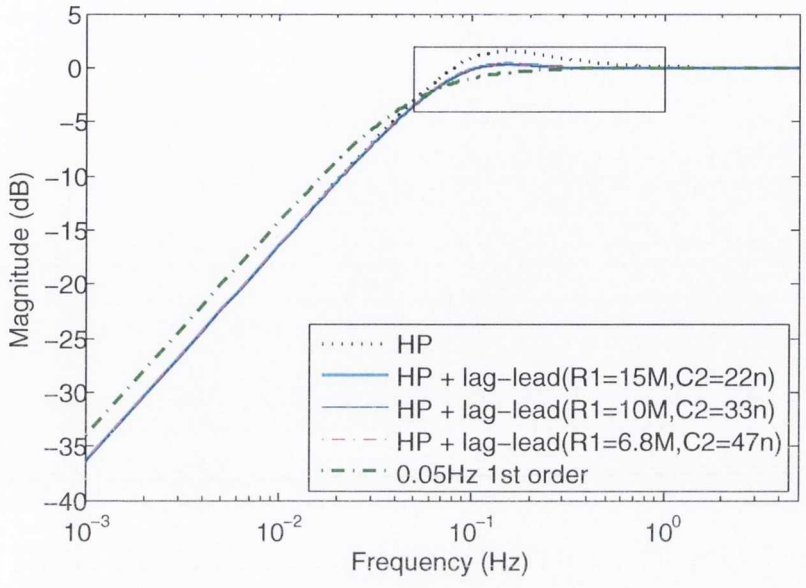
	C_1 = 100 nF		C_1 = 68 nF	
R_1 (MΩ)	R_2 (MΩ)	C_2 (nF)	R_2 (MΩ)	C_2 (nF)
22	- -	- -	47	15
15	33	22	47	22
10	33	33	47	33
6.8	33	47	- -	- -

lag-lead network to the 1-H(s) filter, as can be seen in Figure 5.28(b).

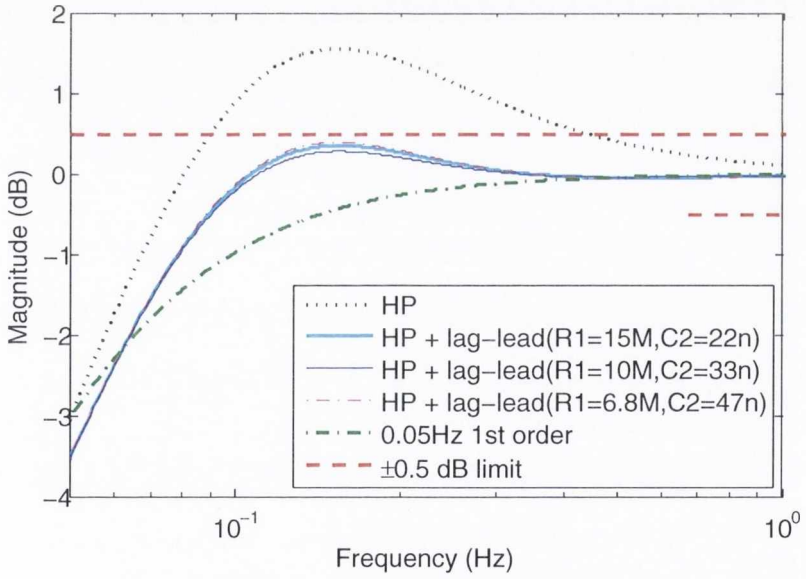
It should, however, be noted that even though a properly selected lag-lead network can be used to compensate the magnitude response of a highpass filter obtained through the 1-H(s) transformation, this is not an optimal solution for the design of the ECG highpass filter. The compensation is, in fact, dependent on the initial choice of highpass filter. If the overshoot present in the magnitude response of the highpass filter is too large, it might not be possible to determine the parameters of a lag-lead network that will reduce the highpass amplitude peak to less than 0.5 dB and at the same time allow the time domain constraints for the pulse response of the overall system to be satisfied. Furthermore, Figure 5.27 shows that the cascaded system does not provide any considerable benefit when compared with a first order 0.05 Hz filter. The 3dB-cutoff frequency of the system obtained by cascading the highpass filter and any of the compensating lag-lead networks is equal to 0.053 Hz, the slope of its magnitude response is limited to 20 dB/decade at frequencies close to zero and the rejection achieved at low frequencies is only 2 dB higher than that of the reference single-pole network. Therefore, despite its increased complexity, the cascade between the 1-H(s) Bessel filter and the lag-lead circuit does not guarantee a rejection of baseline wander and low-frequency artifacts much greater than a simple 0.05 Hz RC network can provide.

5.8 Conclusion

In the first section of this chapter, the requirements defined for the highpass ECG filter according the 1990 AHA recommendations [19] and the European standard for diagnostic recording equipment (EN 60601-2-51:2003) [9] have been summarised. In particular, it has been highlighted how the specifications set on the response of the highpass filter to an input rectangular pulse greatly limit both the steepness of its amplitude response and the frequency of its 3dB-cutoff point.



(a)



(b) Detail of the boxed portion of (a)

Figure 5.27: Amplitude characteristic of the system obtained by cascading a second order Bessel 1-H(s) highpass filter and a compensating lag-lead network. The responses determined by the employment of various lag-lead networks having C_1 = 100 nF and R_2 = 33 MΩ and different value combinations for R_1 and C_2, as well as the original magnitude of the 1-H(s) filter are illustrated. The amplitude characteristic of a 0.05 Hz first order filter is also shown for comparison purposes. The boxed portion of (a) is shown in detail in (b), where the requirements specified on the amplitude characteristic are represented by the dashed lines.

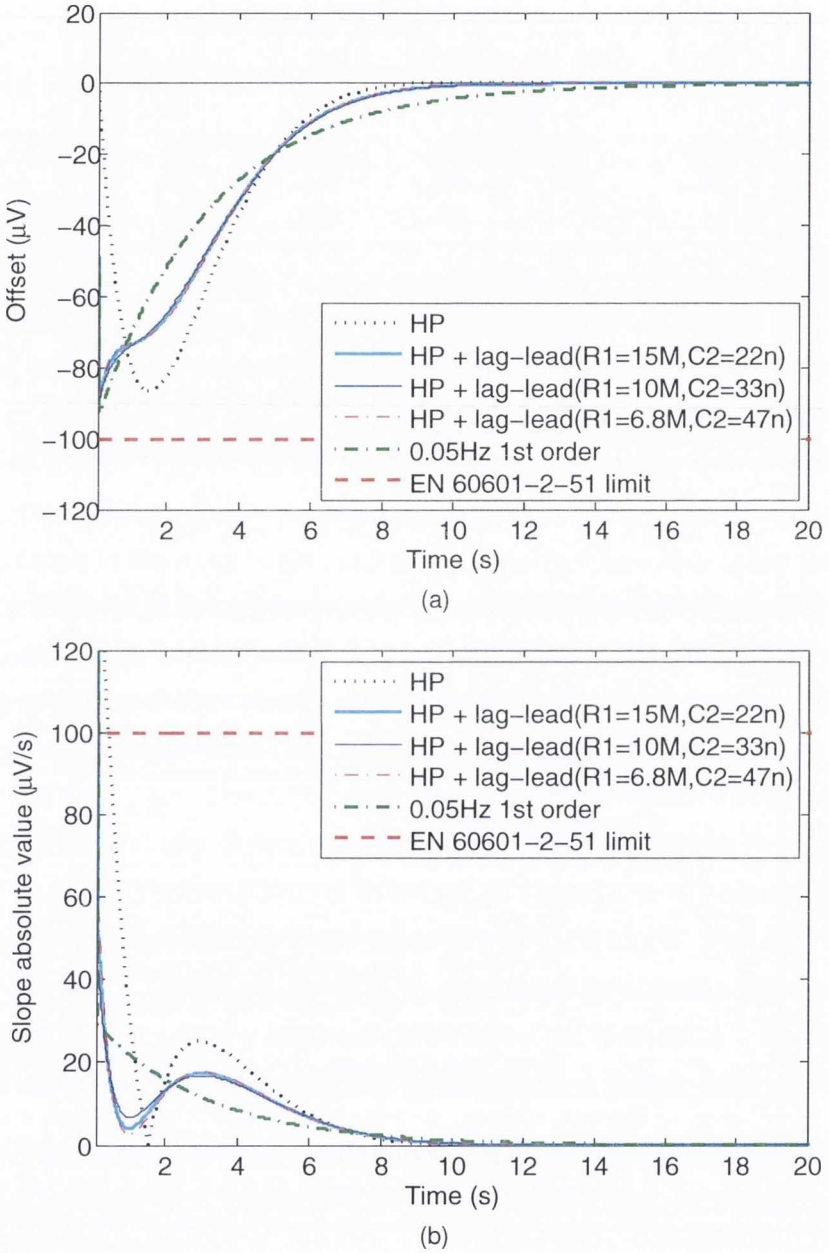


Figure 5.28: Displacement from the isoelectric line (a) and absolute value of the recovery slope (b) of the response of the system obtained by cascading a second order Bessel 1-H(s) highpass filter and a compensating lag-lead network after the application of a 3 mV$\times$100 ms rectangular input pulse. The bounds established by the European standard for the maximum allowable undershoot and slope are represented by the dashed lines.

Some of the most common digital solutions proposed over the years for the elimination of low-frequency artifacts from the ECG signal have then been briefly discussed. The majority of these techniques, however, are not appropriate for low-power applications like ambulatory ECG measurement. Extensive calculations are generally required since complex tasks, such as identifying the peak of the QRS complex, recognising some morphological characteristics of the input signal or determining the frequency content of the current section of the electrocardiographic record, need to be performed. Other less computationally demanding techniques, such as the adaptive filter described by Thakor and Zhu [116], are known to introduce distortion into the ECG signal and cannot be employed in diagnostic measurement devices.

Among the digital methods for baseline wander removal, special attention has been dedicated to FIR filters. These filters can be easily designed to have linear phase and do not require particularly intensive calculations compared to other digital techniques. Furthermore, the specifications detailed for the highpass ECG filter by standards and recommendations constitute the only *a priori* information needed for their design. The frequency and time domain characteristics of the classic FIR filters described in 1985 by Ahlstrom and Tompkins [111] and Van Alste et al. [68] and of the filters more recently presented by Raita-aho et al. [69] and Tabakov et al. [70] have been tested for compliance with the requirements established for the ECG filter. However, none of the proposed transfer functions is able to fulfil the constraints set on the response to a rectangular 3 mV$\times$100 ms input pulse. Since the filters proposed by Van Alste et al., Raita-aho et al. and Tabakov et al. have linear phase, this finding proves, once more, that the linearity of the phase response is not a sufficient condition to guarantee that the filter does not alter the morphology of the ECG signal.

An FIR filter complying with the specifications detailed in the current European standard for diagnostic ECG equipment has been found. Henzel [149] describes an algorithm for the determination of the impulse response coefficients of a filter fulfilling both magnitude and pulse constraints. The design outline provided is, however, lacking in detail and the optimisation procedure though which the filter transfer function was determined cannot be reproduced from the article.

In the remainder of the chapter, attention has been directed towards the analogue domain. It has been stressed how a simple single-pole highpass network is usually employed to eliminate the DC offset and very low-frequency noise components from diagnostic ECG records. Some examples of first order filters actually implemented in ECG measurement devices have also been presented.

Using a second order Bessel system as a example, it has then been shown that the highpass ECG filter cannot be directly designed through lowpass-to-highpass transformations. The characteristics of higher order analogue filters obtained employing either the traditional

H(1/s) or the 1-H(s) transform do not fulfil the frequency and time domain requirements defined by the AHA recommendations and the international standards. In particular, it has been highlighted that the magnitude response of the filters derived using the traditional H(1/s) transform is too steep in the transition region to allow the pulse response constraints to be satisfied. On the other hand, highpass filters determined through the 1-H(s) transformation present a peak in their magnitude characteristic that exceeds the maximum ripple of 0.5 dB permitted in the 1990 AHA report.

In the last part of this chapter, the use of some classic compensation techniques to improve the frequency and time domain characteristics of the highpass filters derived through the H(1/s) and 1-H(s) transformations has been analysed. It has first been shown that an allpass filter cannot be employed to increase the linearity of the phase response of the highpass filter. Secondly, the possibility of decreasing the steepness of the magnitude response of a traditional H(1/s)-transformed filter, and therefore reducing the undershoot occurring in the pulse response, has been explored. A lag network appears to be suitable for this purpose, but it introduces unwanted additional attenuation at high frequencies, which could degrade the quality of the ECG signal. Moreover, the outcome of the compensation procedure seems to be highly dependent on the initial choice of highpass filter. Finally, a lag-lead network has been designed to compensate the peak present in the magnitude response of a second order Bessel filter obtained using the 1-H(s) transform. Cascading this circuit with the filter allows the constraints specified for the highpass ECG filter to be satisfied by the amplitude characteristic of the overall system and it does not cause any detrimental change to the pulse response. It should, however, be pointed out that, in terms of rejection of low-frequency noise and interference, the cascaded system is not substantially different from a single-pole 0.05 Hz highpass filter.

In summary, the transfer function of an analogue highpass filter having magnitude response more selective than that of a single-pole 0.05 Hz RC network, and yet preserving the shape of the input signal, could not be determined using lowpass-to-highpass transformations and conventional compensation techniques. It was, therefore, decided to adopt a different approach and to investigate the possibility of designing the analogue highpass filter directly from the specifications detailed in the EN 60601-2-51:2003 European standard and the 1990 AHA report.

Chapter 6

Highpass filter design

6.1 Introduction

Filters are traditionally designed by approximating an ideal response by means of a realisable function. Specific properties of the desired response need to be preserved by the approximation and the mathematical technique employed for this task is usually chosen based on these properties [84]. For example, the Butterworth and Bessel transfer functions presented in Sections 4.3.1 and 4.3.3 are derived using a Taylor approximation, which minimises the error between ideal and real responses at a single point. On the other hand, the transfer functions of the Chebyshev filter (see Appendix A.2.1) and of the linear phase with equiripple error and the equiripple impulse overshoot filters described in Sections 4.3.4 and 4.3.5 are obtained through a Chebyshev approximation, which aims at reducing the maximum deviation between the desired and the actual response for any point within a selected interval.

Even though Taylor and Chebyshev approximation techniques were originally very popular and most of the classic lowpass filter transfer functions were derived using them, the least-square approximation has become increasingly widespread in recent years and it has been employed to design filters having specific characteristics in both the frequency and the time domains [167, 168]. The first step in these multi-criteria filter approximations consists in identifying an ideal magnitude response, that is, the stopband and passband limits, the stopband attenuation and the passband ripple. Other objectives, such as limited deviation from a linear phase characteristic and minimal overshoot in the time domain response, are also specified. The error between each pair of real and ideal responses is evaluated and the weighted average of these errors is then minimised, subject to possible further constraints.

A similar multi-criteria approximation was used by Henzel [112] to design a highpass digital filter (see Section 5.4.6) that satisfies the requirements of the European standard

EN 60601-2-51:2003 for diagnostic electrocardiographic applications [9]. The ideal magnitude characteristic and the desired response to a defined input waveform were specified for a set of frequency points and time instants, respectively. Acceptable ripples were established for the magnitude response in the passband and stopband and for the overshoot and undershoot occurring in the pulse response. Since both the magnitude characteristic and the time domain response of a linear phase FIR filter can be expressed as a linear combination of the impulse response coefficients, Henzel was able to formulate the design problem in terms of a linear regression model, the solution to which was derived using a constrained optimisation procedure [149]. A filter characterised by a relatively steep magnitude response was obtained with the number of impulse response coefficients being close to 900.

In this thesis, a different approach has been adopted for the design the analogue highpass filter for the front-end of ECG recording equipment and, instead of attempting to approximate desired time and frequency domain responses, it was decided to maximise its low-frequency rejection. It has, in fact, been shown that the time domain requirements impose very stringent limitations on the amplitude characteristic of the highpass system and that the steepness of the magnitude response and the frequency of the 3dB-cutoff are severely restricted by these specifications (see Section 5.2). Therefore, it does not appear feasible to define an ideally steep amplitude characteristic and then attempt to find an analogue filter of limited complexity that approximates it and, at the same time, satisfies the pulse response requirements set by the European standard. On the other hand, since the stopband attenuation and the frequency range of the transition region are not specified by any of the standards and recommendations regulating electrocardiographic devices [9, 15, 19, 62–64, 77], it should be possible to optimise the low-frequency attenuation of a highpass system of given order that fulfils both the time and the frequency domain specifications. An optimisation procedure is developed by the author where the time and frequency domain specifications which the highpass ECG filter must fulfil are expressed as constraints in the algorithm, as was previously proposed by Koca et al. [169] for the design of lowpass analogue filters.

The similarities between the design methodology proposed in this work and that described by Henzel are limited to the fact that the passband ripple and the displacement from the isolectric line occurring after the application of a defined input pulse to the ECG filter are restricted to satisfy the EN 60601-2-51:2003 standard and that a constrained optimisation technique is used to derive the filter parameters. On the other hand, whereas the stopband and passband limits of the analogue filter under design are not specified, the transition region of the FIR filter is fixed by Henzel before the design of the highpass system is attempted. Furthermore, since the relation between the magnitude and pulse character-

istics and the transfer function parameters is more complex for the analogue system than the FIR filter, the design cannot be simplified to a linear regression problem and the same algorithm cannot be employed for analogue filters of different orders. Therefore, in order to keep the complexity of the optimisation to a minimum, attention is focused only on second and third order filters. This choice also allows a simple implementation of the front-end highpass filter that can be employed in low-power electrocardiographic equipment.

This chapter thus focuses on the derivation of the transfer functions of second and third order filters that satisfy the magnitude and pulse response requirements described in Section 5.2 and are characterised by a low-frequency rejection higher than that of the reference 0.05 Hz first order network. Different approaches have been explored for the maximisation of the low-frequency attenuation of the highpass filters:

- Optimisation of the stopband limit with the 3dB-cutoff frequency fixed at 0.05 Hz;
- Optimisation of the stopband limit;
- Optimisation of the 3dB-cutoff frequency;
- Optimisation of the overall low-frequency attenuation.

At first, the optimisation procedure is employed to maximise the frequency of the stopband limit of the second and third order filters having a fixed 3dB-cutoff frequency of 0.05 Hz, so as to verify whether an analogue highpass filter of order higher than one can achieve a low-frequency attenuation significantly greater than that of the reference single-pole system. The maximisation of the stopband limit is subsequently performed without imposing any condition on the filter 3dB-point. Since the result of this latter optimisation approach is not satisfactory, the procedure is altered in order to allow the maximisation of the 3dB-cutoff frequency of the second and third order systems to be attempted. Finally, the goal of the optimisation process is modified so that, instead of concentrating on the frequency at which a specific attenuation is achieved, the overall rejection of the filter can be maximised. A brief discussion about the convergence of the optimisation algorithm implemented in MATLAB® (The MathWorks, Inc.) concludes the chapter.

6.2 Optimisation procedure

Let us consider the general transfer function for a unity gain filter of order n, having l_p pairs of complex conjugate poles, m_p real poles, l_z pairs of complex conjugate zeros and m_z real

zeros:

$$H(s) = \frac{\prod_{k=1}^{l_z} (s+\gamma_k+j\delta_k)(s+\gamma_k-j\delta_k) \prod_{i=1}^{m_z} (s+z_i)}{\prod_{k=1}^{l_p} (s+\alpha_k+j\beta_k)(s+\alpha_k-j\beta_k) \prod_{i=1}^{m_p} (s+p_i)}, \tag{6.1}$$

where $n = 2l_p + m_p = 2l_z + m_z$ for the transfer function to describe a highpass filter. To guarantee the stability of the filter described by Eq. (6.1), the location of the poles is restricted to the left-half of the s-plane, that is, the following conditions must be satisfied:

$$\alpha_k > 0 \qquad \text{for} \quad 1 \leq k \leq l_p \tag{6.2}$$

and

$$p_i > 0 \qquad \text{for} \quad 1 \leq i \leq m_p. \tag{6.3}$$

Since the high DC offset voltages generated at the skin-electrode interface can cause saturation of the front-end amplifier of the electrocardiographic recording system (see Section 2.2.4), it is essential that the signal component at zero frequency is completely suppressed by the ECG filter. In other words, at least one transmission zero needs to be fixed at ω = 0 rad/s. The general transfer function described by Eq. (6.1) thus reduces to:

$$H(s) = \frac{s \prod_{k=1}^{l_z} (s+\gamma_k+j\delta_k)(s+\gamma_k-j\delta_k) \prod_{i=1}^{m_z-1} (s+z_i)}{\prod_{k=1}^{l_p} (s+\alpha_k+j\beta_k)(s+\alpha_k-j\beta_k) \prod_{i=1}^{m_p} (s+p_i)}. \tag{6.4}$$

The magnitude response of the network described by Eq. (6.4) is then easily derived as:

$$|H(\omega)| = \frac{\omega^2 \prod_{k=1}^{l_z} \sqrt{\left({\gamma_k}^2 + {\delta_k}^2 - \omega^2\right)^2 + \left(2\gamma_k\,\omega\right)^2} \prod_{i=1}^{m_z-1} \sqrt{{z_i}^2+\omega^2}}{\prod_{k=1}^{l_p} \sqrt{\left({\alpha_k}^2 + {\beta_k}^2 - \omega^2\right)^2 + \left(2\alpha_k\,\omega\right)^2} \prod_{i=1}^{m_p} \sqrt{{p_i}^2+\omega^2}}. \tag{6.5}$$

In the remainder of this work, attention will be concentrated on the second and third order systems and the design of highpass filters having better low-frequency attenuation than the 0.05 Hz single-pole network usually employed in diagnostic electrocardiographic applications will be attempted. The transfer function of second and third order filters that act as DC blockers and have unity gain at high frequencies can be, respectively, expressed

as:

$$H_2(s) = \frac{s^2 + a_1 s}{s^2 + b_1 s + b_0} \tag{6.6}$$

and

$$H_3(s) = \frac{s^2 + a_1 s + a_0}{s^2 + b_1 s + b_0} \frac{s}{s + p_0}. \tag{6.7}$$

This type of representation allows generality to be maintained since it is not required to specify whether the poles and zeros defined by the quadratic trinomials are real or complex conjugate pairs. All the coefficients in Eqs. (6.6) and (6.7) are defined to be real. Moreover, the conditions given in Eqs. (6.2) and (6.3) that ensure the stability of the system are rewritten as:

$$b_1 > 0 \qquad \text{and} \qquad b_0 > 0 \tag{6.8}$$

and, in addition for the third order filter,

$$p_0 > 0. \tag{6.9}$$

6.2.1 Objective function

In order to optimise the out-of-band rejection of the second and third order filters described by Eqs. (6.6) and (6.7), the maximisation of either the stopband limit or the 3dB-cutoff point is performed. In both cases, the goal of the optimisation procedure involves maximising the frequency at which a specified degree of attenuation, H_c, is achieved by the highpass system, that is, the frequency ω_c for which the following condition is satisfied:

$$|H(\omega_c)| = H_c \qquad \text{with} \quad H_c < 1. \tag{6.10}$$

For the second order filter, an analytical solution to Eq. (6.10) can be easily determined. The magnitude characteristic of the system described by the transfer function $H_2(s)$, given in Eq. (6.6), is:

$$|H_2(\omega)| = \sqrt{\frac{\omega^4 + {a_1}^2\omega^2}{\left(b_0 - \omega^2\right)^2 + {b_1}^2\omega^2}} = \sqrt{\frac{\omega^2\left(\omega^2 + {a_1}^2\right)}{\omega^4 + \left({b_1}^2 - 2b_0\right)\omega^2 + {b_0}^2}}. \tag{6.11}$$

Substituting Eq. (6.11) into Eq. (6.10) and solving for ω_c leads to:

$$\left(1 - {H_c}^2\right){\omega_c}^4 + \left[{a_1}^2 - {H_c}^2\left({b_1}^2 - 2b_0\right)\right]{\omega_c}^2 - {H_c}^2{b_0}^2 = 0. \tag{6.12}$$

If the coefficients in the above equation are renamed as:

$$A = 1 - {H_c}^2 \tag{6.13}$$

$$B = {a_1}^2 - {H_c}^2 \left({b_1}^2 - 2b_0\right) \tag{6.14}$$

$$C = -{H_c}^2 {b_0}^2, \tag{6.15}$$

the solutions of Eq. (6.12) can be written using the simple quadratic formula:

$${\omega_c}^2 = \frac{-B \pm \sqrt{B^2 - 4AC}}{2A} \tag{6.16}$$

Since $A > 0$ and $C < 0$,

$$AC < 0 \qquad \text{and} \qquad B^2 - 4AC > B^2, \tag{6.17}$$

that is, the radicand is positive and the square root is always real. Because:

$$\frac{-B - \sqrt{B^2 - 4AC}}{2A} < 0, \tag{6.18}$$

only one of the solutions for ${\omega_c}^2$ is admissible. Therefore, the frequency at which the amplitude response of the filter is equal to H_c is uniquely defined outside the passband of the second order highpass filter and can be expressed as:

$$\omega_c = \frac{\sqrt{-\left[{a_1}^2 - {H_c}^2\left({b_1}^2 - 2b_0\right)\right] + \sqrt{\left[{a_1}^2 - {H_c}^2\left({b_1}^2 - 2b_0\right)\right]^2 + 4{H_c}^2\left(1 - {H_c}^2\right){b_0}^2}}}{\sqrt{2\left(1 - {H_c}^2\right)}}. \tag{6.19}$$

Let us now consider the third order case. The amplitude response of the system expressed by Eq. (6.7) is given by:

$$|H_3(\omega)| = \sqrt{\frac{\left(a_0 - \omega^2\right)^2 + {a_1}^2\omega^2}{\left(b_0 - \omega^2\right)^2 + {b_1}^2\omega^2}} \sqrt{\frac{\omega^2}{\omega^2 + {p_0}^2}}. \tag{6.20}$$

Even though it is possible to employ this formula to analytically determine the frequency at which the critical attenuation is achieved by the filter, its expression is dependent on the sign of the discriminant of Eq. (6.10), when rewritten in terms of ${\omega_c}^2$. Moreover, in order to guarantee that the critical frequency is positive, a further condition needs to be imposed on the ω_c expression. Therefore, given the complexity involved in analytically solving Eq. (6.10) for a third order system, the value of ω_c is obtained graphically using MATLAB®.

6.2.2 Constraints definition

As discussed in Section 5.2, certain conditions need to be imposed on the amplitude response of the highpass ECG filter to guarantee that the 1990 AHA recommendations [19] and the European standard EN 60601-2-51:2003 for diagnostic electrocardiographic devices [9] are satisfied. In the first place, any overshoot that may occur in the filter magnitude response is not allowed to exceed 0.5 dB. In other words,

$$|H(\omega)|_{dB} \leq R_p \qquad \forall \omega, \tag{6.21}$$

where $|H(\omega)|$, defined by Eq. (6.5), is expressed in decibels and R_p = 0.5 dB. Furthermore, in order for the passband ripple to be limited to $\pm$0.5 dB, a lower boundary has to be specified for the filter amplitude characteristic over the ECG spectrum:

$$|H(\omega)|_{dB} \geq -R_p \qquad \text{for} \quad \omega \geq \omega_0, \tag{6.22}$$

with $\omega_0 = 2\pi f_0$, where f_0 = 0.67 Hz is the upper limit specified for the transition region by the EN 60601-2-51:2003 standard.

The time domain specifications of the ECG filter have been analysed in detail in Section 3.4 and the limitations that such requirements impose on the system magnitude response have been discussed in Section 5.2. Now, a rigorous definition of the constraints that the pulse response of the highpass filter needs to satisfy in order to adhere to the EN 60601-2-51:2003 European standard is established.

Let us first consider the offset condition. According to the standard, it is required that the displacement from the isoelectric line occurring in the filter response after the application of an input rectangular pulse of k = 3 mV amplitude and t_0 = 100 ms duration is limited to d = 100 µV. Based on the offset illustration provided in the standard itself (see Figure 3.6), it appears that this condition only applies to negative displacements, whereas no constraint is defined for the pulse response overshoot. The lack of a specification for the positive displacement is probably due to the fact that the offset specification set by the standard was most likely derived from the response of a single-pole 0.05 Hz filter to a rectangular input [63], which, as shown in Section 3.4.2, only presents a negative displacement following the pulse. In contrast with the behaviour of first order filters, the response of higher order systems to an input rectangular pulse can present a positive overshoot, as illustrated in Figures 5.2(a) and 5.20. The amplitude of this overshoot is, however, considerably lower than that of the undershoot occurring immediately after the termination of the input pulse. Therefore, if the same constraint is set for both the positive and negative displacements, the condition on the overshoot would be met by any filter already fulfilling the undershoot

requirement. Since overshoot and ringing in the time domain responses are effectively distortion introduced by the system into the signal [83] and should be kept to a minimum, a more stringent requirement is thus set for the positive displacement.

The system response to a rectangular input of duration t_0 and amplitude k is given by:

$$y(t) = k\,[g(t) - g(t - t_0)], \tag{6.23}$$

where $g(t)$ is the filter response to a unit step function. The displacement occurring after the termination of the pulse is equal to $y(t)$ and the requirement on the undershoot can thus be written as:

$$k\,[g(t) - g(t - t_0)] \geq -d \qquad \text{for} \quad t \geq t_0, \tag{6.24}$$

that is,

$$g(t) - g(t - t_0) \geq -\frac{d}{k} \qquad \text{for} \quad t \geq t_0 \tag{6.25}$$

where, according to the values stated in the EN 60601-2-51:2003 standard, d/k = 0.033. The constraint on the positive displacement that may be present in the filter response to a rectangular pulse can, on the other hand, be formulated as:

$$g(t) - g(t - t_0) \leq \epsilon\frac{d}{k} \qquad \text{for} \quad t \geq t_0, \tag{6.26}$$

where $\epsilon < 1$ determines the amplitude of the allowable overshoot. In the analysis performed in this chapter, this condition will be considered optional, that is, the optimisation procedure will be initially carried out ignoring the constraint given in Eq. (6.26). If, however, a significant overshoot occurs in the response of the optimised filter, the influence of a restricted positive displacement will be evaluated.

As regards the condition on the steepness of the slope following the rectangular pulse, it appears from Figure 3.6 that the European standard is concerned only with an excessively large positive slope. This constraint can be expressed as:

$$k\,[h(t) - h(t - t_0)] \leq m \qquad \text{for} \quad t \geq t_0, \tag{6.27}$$

where $h(t)$ is the filter impulse response and m is the maximum slope allowable for the response after the pulse. However, since artifactual ST segment elevation and depression are equally detrimental to diagnostic ECG analysis [4, 8], it seems more appropriate to

impose a symmetrical constraint on the recovery slope:

$$k\,|h(t) - h(t - t_0)| \leq m \qquad \text{for} \quad t \geq t_0, \tag{6.28}$$

which can be rewritten as:

$$|h(t) - h(t - t_0)| \leq \frac{m}{k} \qquad \text{for} \quad t \geq t_0. \tag{6.29}$$

Because the EN 60601-2-51:2003 standard specifies different values for the slope over separate intervals, two conditions arise from the constraint given by Eq. (6.29):

$$|h(t) - h(t - t_0)| \leq \frac{m_1}{k} \qquad \text{for} \quad t_0 \leq t < t_1 \tag{6.30}$$

and

$$|h(t) - h(t - t_0)| \leq \frac{m_2}{k} \qquad \text{for} \quad t \geq t_1, \tag{6.31}$$

where m_1 = 250 µV/s, m_2 = 100 µV/s and t_1 = 300 ms.

6.2.3 Further constraints

The magnitude response of the second order highpass filter under analysis can be shown to be monotonically increasing outside the passband (see Appendix A.1). On the other hand, further conditions need to be imposed on the magnitude characteristic of filters of order $n \geq 3$ to limit the amplitude of the ripples in both the stopband and passband and to avoid the presence of any peak in the transition region. In particular, the amplitude of the maxima located in the stopband of the filter cannot exceed the minimum stopband attenuation A_s, whereas the passband minima are not allowed to be less than -0.5 dB. In other words,

$$|H(\omega_{max})|_{dB} \leq -A_s \qquad \text{for} \quad \omega_{max} \leq \omega_s \tag{6.32}$$

and

$$|H(\omega_{min})|_{dB} \geq -R_p \qquad \text{for} \quad \omega_{min} \geq \omega_p, \tag{6.33}$$

where ω_s and ω_p represent the stopband and passband limits, respectively, as illustrated in Figure 6.1, and ω_{max} and ω_{min} identify the frequencies at which maxima and minima occur in the magnitude response. A change in the sign of the first derivative of the filter amplitude characteristic is employed to numerically determine the location of these extreme points.

In order to avoid ripples in the transition region, the system magnitude response is required to be monotonically increasing over this frequency interval. The derivative of the

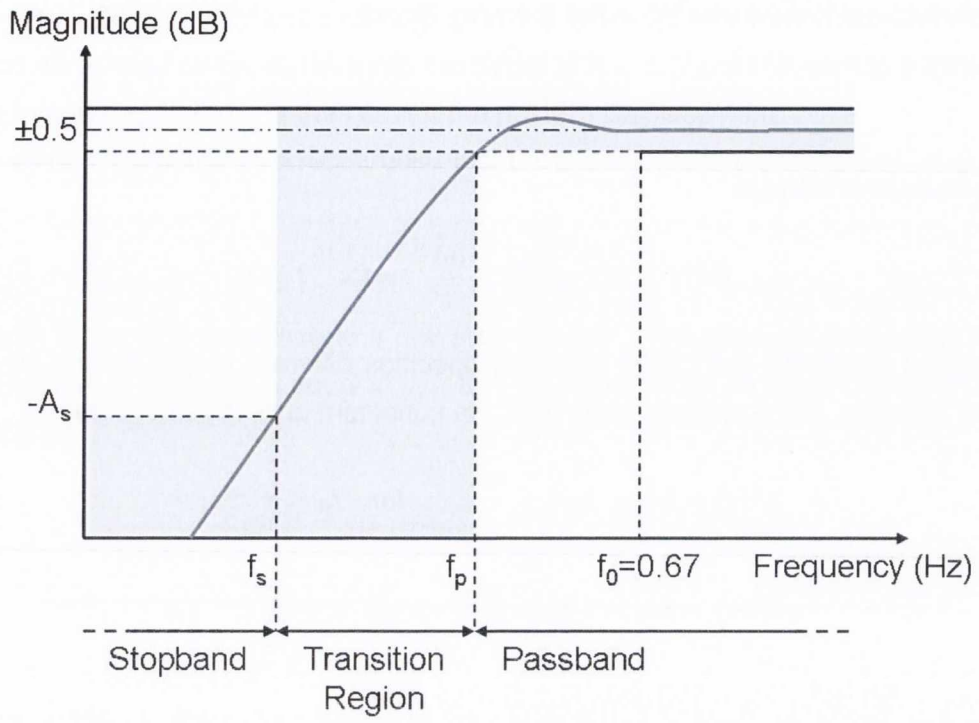


Figure 6.1: Mask showing the limits imposed on the filter magnitude response during the optimisation process. The area allowable for the amplitude characteristic is shaded.

amplitude characteristic is therefore constrained to be positive:

$$\frac{d\,|H(\omega)|_{dB}}{d\,\omega} \geq 0 \qquad \text{for} \quad \omega_s \leq \omega \leq \omega_p. \tag{6.34}$$

6.2.4 Algorithm description

A constrained numerical optimisation is implemented in MATLAB® 7.4.0 (R2007a) using the function `fmincon` available in the Optimization Toolbox™ [170]. `fmincon` attempts to find a minimum of a scalar function subject to a set of equality and inequality constraints:

$$\min_{\boldsymbol{x}} f(\boldsymbol{x}) \qquad \text{subject to} \begin{cases} c_i(\boldsymbol{x}) = 0 & \text{for} \quad i = 1, \ldots, m_e \\ c_i(\boldsymbol{x}) \leq 0 & \text{for} \quad i = m_e + 1, \ldots, m, \end{cases} \tag{6.35}$$

where $\boldsymbol{x}$ is a vector constituted by the design parameters, $f(\boldsymbol{x})$ is the objective function that returns a scalar value and $\boldsymbol{c}(\boldsymbol{x})$ is a vector of length m containing the values of the equality and inequality constraints. In the case under analysis, the design parameters are given by

the coefficients of the filter transfer function (see Eqs. (6.6) and (6.7)), that is:

$$\boldsymbol{x}^T = [a_1\ b_1\ b_0], \tag{6.36}$$

for the second order filter, and

$$\boldsymbol{x}^T = [a_1\ a_0\ b_1\ b_0\ p_0], \tag{6.37}$$

for the third order filter. Since the optimisation aims at maximising the critical frequency, ω_c, at which a desired attenuation is reached by the filter, the objective function selected for minimisation using `fmincon` is given by:

$$f(\boldsymbol{x}) = -\omega_c. \tag{6.38}$$

For the second order system, ω_c is described by Eq. (6.19), whereas for the third order one it is numerically measured as discussed in Section 6.2.1. The inequality constraints in Eq. (6.35) are obtained by rewriting Eqs. (6.21), (6.22), (6.25), (6.26), (6.30) and (6.31) as:

$$c_1(\boldsymbol{x}) = |H(\omega)|_{dB} - R_p \qquad \forall\,\omega \tag{6.39}$$

$$c_2(\boldsymbol{x}) = -|H(\omega)|_{dB} - R_p \qquad \omega \geq \omega_0 \tag{6.40}$$

$$c_3(\boldsymbol{x}) = -[g(t) - g(t-t_0)] - \frac{d}{k} \qquad t \geq t_0 \tag{6.41}$$

$$c_4(\boldsymbol{x}) = [g(t) - g(t-t_0)] - \epsilon\frac{d}{k} \qquad t \geq t_0 \tag{6.42}$$

$$c_5(\boldsymbol{x}) = |h(t) - h(t-t_0)| - \frac{m_1}{k} \qquad t_0 \leq t < t_1 \tag{6.43}$$

$$c_6(\boldsymbol{x}) = |h(t) - h(t-t_0)| - \frac{m_2}{k} \qquad t \geq t_1. \tag{6.44}$$

For the third order system, the following constraints, derived from Eqs. (6.32), (6.33) and (6.34), are also applied:

$$c_7(\boldsymbol{x}) = |H(\omega_{max})|_{dB} + A_s \qquad \omega_{max} \leq \omega_s \tag{6.45}$$

$$c_8(\boldsymbol{x}) = -|H(\omega_{min})|_{dB} - R_p \qquad \omega_{min} \geq \omega_p \tag{6.46}$$

$$c_9(\boldsymbol{x}) = -\frac{d\,|H(\omega)|_{dB}}{d\,\omega} \qquad \omega_s \leq \omega \leq \omega_p. \tag{6.47}$$

The functions and parameters used in the definition of these constraints (Eqs. (6.39) to (6.47)) are specified in Sections 6.2.2 and 6.2.3.

To solve the constrained non-linear optimisation problem, `fmincon` employs a sequential quadratic programming (SQP) method, that is, the function solves a linear quadratic

programming (QP) subproblem at each iteration. SQP methods are based on the solution of the Kuhn-Tucker equations, which constitute the necessary conditions for optimality in a constrained optimisation problem [170, 171]. Using the notation in Eq. (6.35), the Lagrange function can be obtained as a linear combination of the objective and the constraints functions:

$$L(\boldsymbol{x}, \boldsymbol{\lambda}) = f(\boldsymbol{x}) + \sum_{i=1}^{m} \lambda_i c_i(\boldsymbol{x}), \tag{6.48}$$

where $\boldsymbol{\lambda}$ is the vector of length m given by the Lagrange multipliers. Each scalar multiplier, λ_i, is associated with one constraint. The Kuhn-Tucker equations can then be expressed as:

$$\begin{aligned} &\nabla_{\boldsymbol{x}} L(\boldsymbol{x}, \boldsymbol{\lambda}) = 0 \\ &\lambda_i c_i(\boldsymbol{x}) = 0 \qquad \text{for} \quad i = m_e + 1, \ldots, m \\ &\lambda_i \geq 0 \qquad \text{for} \quad i = m_e + 1, \ldots, m \end{aligned} \tag{6.49}$$

in addition to the constraints in Eq. (6.35).

At each iteration of the SQP algorithm, the first step consists of approximating the Hessian of the Lagrangian function in Eq. (6.48), where the term Hessian indicates the matrix of second-order partial derivatives [172]:

$$\boldsymbol{H} = \nabla_{\boldsymbol{x}}^2 L(\boldsymbol{x}, \boldsymbol{\lambda}). \tag{6.50}$$

A quasi-Newton method is used for updating the Hessian matrix through the formula [170]:

$$\boldsymbol{H}_k = \boldsymbol{H}_{k-1} + \frac{\boldsymbol{q}_k \boldsymbol{q}_k{}^T}{\boldsymbol{q}_k{}^T \boldsymbol{s}_k} - \frac{\boldsymbol{H}_{k-1}{}^T \boldsymbol{H}_{k-1}}{\boldsymbol{s}_k{}^T \boldsymbol{H}_{k-1} \boldsymbol{s}_k}, \tag{6.51}$$

where

$$\boldsymbol{s}_k = \boldsymbol{x}_k - \boldsymbol{x}_{k-1} \tag{6.52}$$

and

$$\boldsymbol{q}_k = \nabla_{\boldsymbol{x}} L(\boldsymbol{x}_k, \boldsymbol{\lambda}_k) - \nabla_{\boldsymbol{x}} L(\boldsymbol{x}_{k-1}, \boldsymbol{\lambda}_{k-1}). \tag{6.53}$$

Using this approximated Hessian, a quadratic programming subproblem is then obtained by linearising the non-linear constraints in Eq. (6.35). The aim of the QP subproblem is to determine the search direction $\boldsymbol{d}_k$ for the SQP algorithm [170, 173]:

$$\min_{\boldsymbol{d}_k} \frac{1}{2} \boldsymbol{d}_k{}^T \boldsymbol{H}_k \boldsymbol{d}_k + \nabla f(\boldsymbol{x}_k)^T \boldsymbol{d}_k$$

$$\text{subject to} \begin{cases} \nabla c_i(\boldsymbol{x}_k)^T \boldsymbol{d}_k + c_i(\boldsymbol{x}_k) = 0 & \text{for} \quad i = 1, \ldots, m_e \\ \nabla c_i(\boldsymbol{x}_k)^T \boldsymbol{d}_k + c_i(\boldsymbol{x}_k) \leq 0 & \text{for} \quad i = m_e + 1, \ldots, m, \end{cases} \tag{6.54}$$

The solution of the QP subproblem returns the search direction $\boldsymbol{d}_k$, which is used to generate a further iteration of the SQP algorithm by updating $\boldsymbol{x}_k$ as:

$$\boldsymbol{x}_{k+1} = \boldsymbol{x}_k + \alpha_k \boldsymbol{d}_k. \tag{6.55}$$

The parameter α_k defining the size of the step in the search direction is selected by a line search procedure so that a sufficient decrease in a merit function is produced. Details of the merit function used by `fmincon` are available in [170].

6.2.5 Starting point

The set of parameters describing a standard highpass filter is used as the starting point of the optimisation procedure. Butterworth and Chebyshev filters with passband ripple equal to 0.5 dB are employed for the second order filter. For the third order filter, an Elliptic filter having a passband ripple of $\pm$0.5 dB and a stopband ripple equal to the required attenuation A_s is selected to determine the initial values of the design variables. The characteristics of lowpass Butterworth filters are described in Section 4.3.1, whereas the features of Chebyshev and Elliptic filters are briefly discussed in Appendix A.2. The highpass transfer function of these filters is obtained using the classic H(1/s) transformation described in Section 5.6.1. The transfer function of the second order Chebyshev filter is renormalised to achieve unity gain at high frequencies.

Since the SQP technique employed by the `fmincon` function is gradient-based and it can lead to local solutions [170], it is essential to assess the convergence of the algorithm. The optimisation procedure is repeated starting from different initial conditions, which are obtained by setting the 3dB-point of the standard highpass filters at various frequencies between 0.01 Hz and 0.15 Hz. If the 3dB-cutoff frequency is selected to be 0.05 Hz, the responses of the Butterworth, Chebyshev and Elliptic filters do not satisfy the constraint on the maximum undershoot allowable after the application of a 3 mV$\times$100 ms rectangular pulse, as also previously highlighted in Section 5.6.3 for a Bessel filter. As illustrated in Figures 6.2 and 6.3, for the condition on the negative displacement to be fulfilled by these traditional filters, the 3dB-cutoff frequency must be lower or equal to 0.037 Hz for the second order systems and 0.021 Hz for the third order ones. Choosing a 3dB-cutoff lower than these limits allows the optimisation starting point to satisfy all the constraints defined in the previous section and the set of initial parameters to be included in the solution space. The convergence of the optimisation procedure is therefore tested using starting points that are both inside and outside the feasible region. The optimum solution is selected from all of the outcomes of the maximisation procedure as the set of design parameters that leads

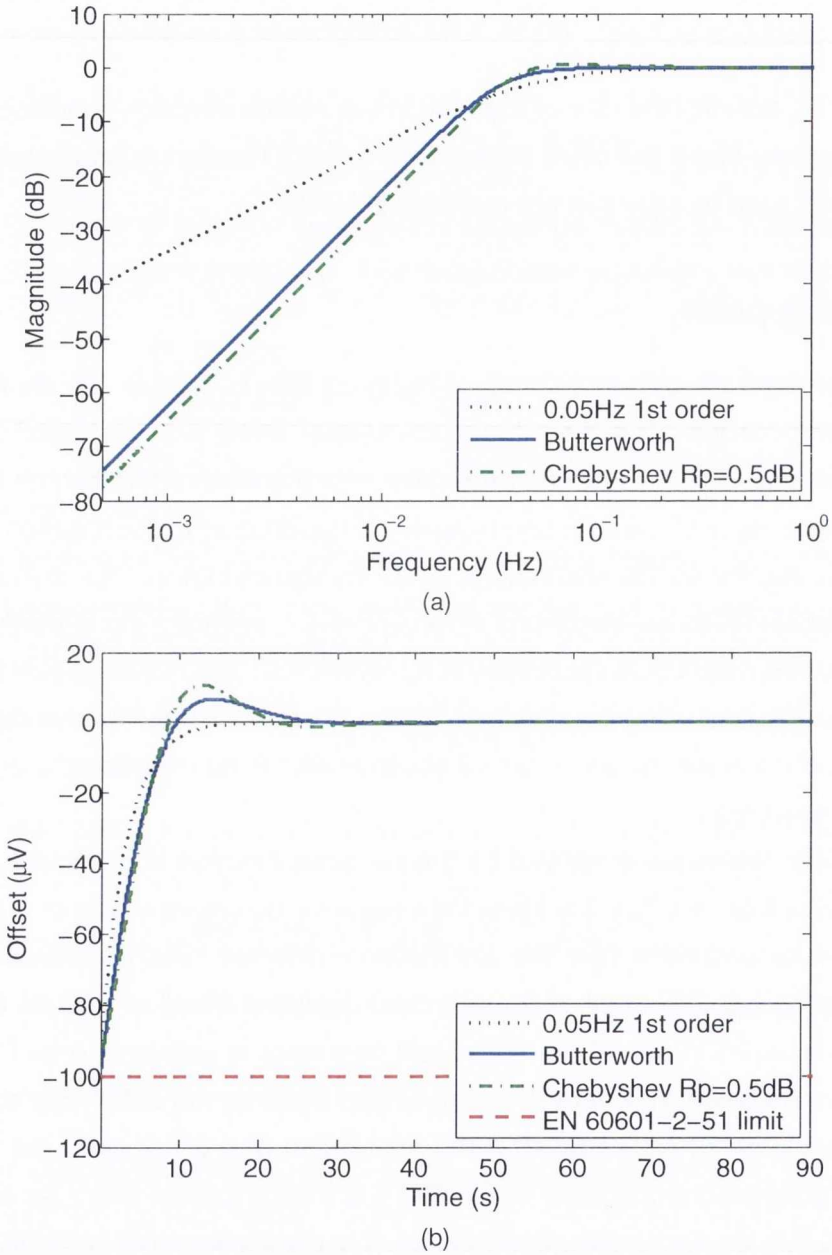


Figure 6.2: (a) Magnitude characteristic of second order Butterworth and Chebyshev filters having 3dB-cutoff frequency equal to 0.037 Hz and (b) displacement from the isoelectric line occurring after the application of a 3 mV$\times$100 ms rectangular pulse at their inputs. The responses of a 0.05 Hz first order filter are also illustrated for comparison purposes. The dashed line in (b) represents the bound established for the maximum allowable undershoot by the European standard for diagnostic electrocardiographic devices.

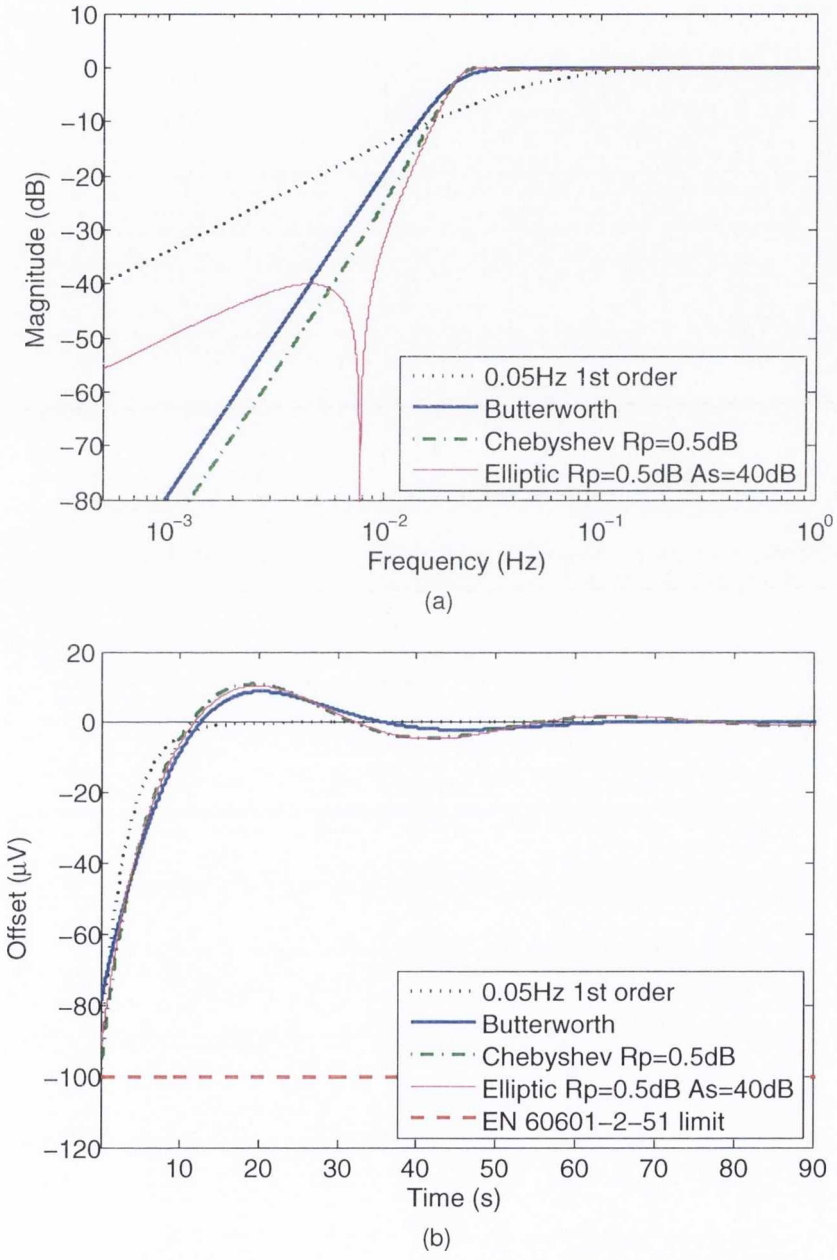


Figure 6.3: (a) Magnitude characteristic of third order Butterworth, Chebyshev and Elliptic filters having 3dB-cutoff frequency equal to 0.021 Hz and (b) displacement from the isoelectric line occurring after the application of a 3 mV$\times$100 ms rectangular pulse at their inputs.

to the highest critical frequency ω_c. The chosen solution is not guaranteed to be a global optimum, but just the highest of the local maxima.

6.3 Optimisation of the stopband limit with the 3dB-cutoff frequency being fixed at 0.05 Hz

In order to verify the possibility of designing a second or third order filter having better rejection properties than the 0.05 Hz RC network usually employed as the front-end highpass filter in electrocardiographic applications, the 3dB-cutoff frequency of the system undergoing optimisation is initially fixed at 0.05 Hz and the frequency of the stopband limit is maximised. From Eqs. (6.11) and (6.20), which define the amplitude characteristic of the second and third order filters, respectively, a relationship can be easily determined between the design parameters and the frequency of the 3dB-point, that is, one of the parameters can be derived from the other filter variables. The expression linking the 3dB-cutoff frequency and the transfer function parameters is given, for the second order filter, by:

$$b_1{}^2 = \omega_{3dB}{}^2 + 2\left(a_1{}^2 + b_0\right) - \frac{b_0{}^2}{\omega_{3dB}{}^2} \tag{6.56}$$

and, for the third order filter, by:

$$p_0{}^2 = \omega_{3dB}{}^2 \left[2\,\frac{\left(a_0 - \omega_{3dB}{}^2\right)^2 + a_1{}^2\,\omega_{3dB}{}^2}{\left(b_0 - \omega_{3dB}{}^2\right)^2 + b_1{}^2\,\omega_{3dB}{}^2} - 1 \right], \tag{6.57}$$

where ω_{3dB} = 2π 0.05 rad/s.

In order to maximise the stopband limit, the critical frequency ω_c is selected as the highest frequency at which the minimum stopband attenuation A_s is reached. Moreover, either Eq. 6.56 or Eq. 6.57 is rewritten so that all terms are on one side and it is added as a constraint to the optimisation algorithm. The minimum stopband attenuation of the second and third order systems is selected to be 40 dB, that is, the amplitude of the interference is reduced to less than 1% of its input value by the filter in the stopband. In the absence of detailed information on the noise and interference introduced into ECG measurements at frequencies lower than 0.05 Hz (see Section 2.4), such an attenuation appears to be adequate for the application.

The magnitude response of the 0.05 Hz second and third order filters resulting from the optimisation of the stopband limit and that of the reference single-pole filter are shown in Figure 6.4. The frequencies at which the amplitude characteristic reaches a range of attenuation values are reported in Table 6.1, together with the location of the poles and

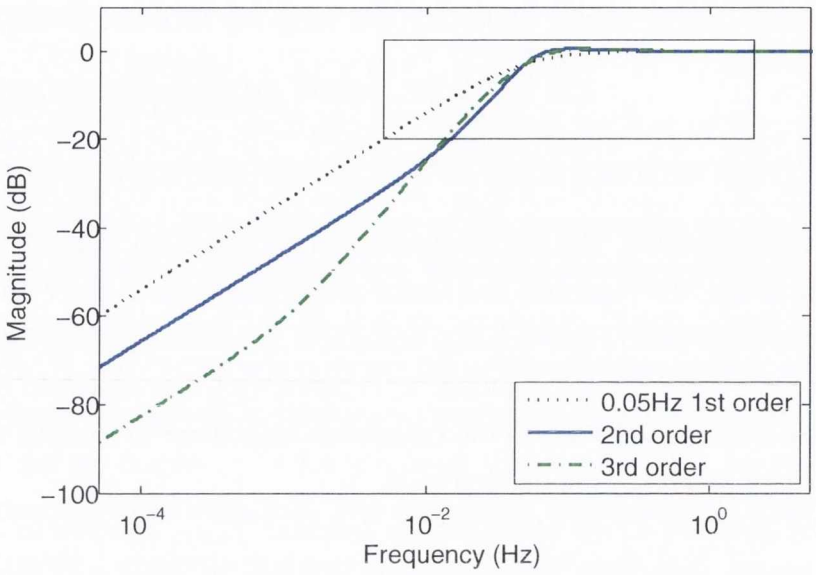
Table 6.1: Results obtained by optimising the stopband limit of the 0.05 Hz second and third order filters for A_s = 40 dB.

Order n	f_{20dB} (mHz)	f_{40dB} (mHz)	f_{60dB} (mHz)	p (rad/s)	z (rad/s)
2	14.9	**1.9**	0.19	-0.2266 $\pm j$ 0.3039	0
					-0.1194
3	13.5	**4.0**	1.04	-0.2125	0
				-0.4063 $\pm j$ 0.2281	-0.6969
					-0.0078

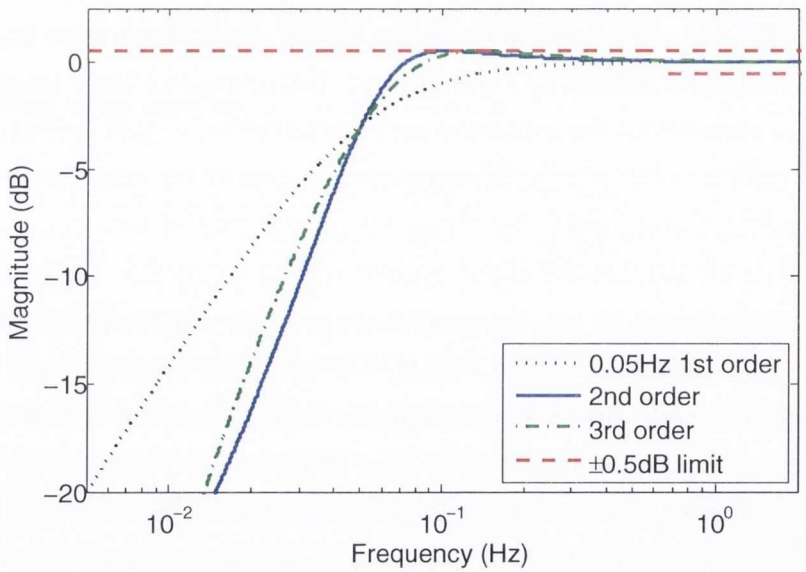
zeros of the optimised systems. The displacement from the isoelectric line and the absolute value of the slope of the filter response to a rectangular input pulse of 3 mV amplitude and 100 ms duration are depicted in Figures 6.5(a) and 6.5(b), respectively. From Figure 6.5 and from the magnitude response detail illustrated in Figure 6.4(b), it is clear that the outcome of the optimisation process satisfies all the constraints described in Section 6.2.2, which are indicated in these graphs by the dashed lines.

The frequency at which 40 dB attenuation is reached, f_{40dB}, is equal to 0.5 mHz for the reference 0.05 Hz single-pole network. From the data in Table 6.1, it can be seen that the corresponding frequencies are 4 and 8 times higher for the second order and third order filters, respectively. The advantage of the higher order filters over the single-pole system is made even more evident by Figure 6.4(a). The optimised filters yield consistently larger attenuations throughout the stopband and the transition region, without introducing excessively high peaks in the passband response. It should be noted that the rejection provided by the second and third order filters for frequencies of between 0.01 and 0.05 Hz is quite similar, with the second order system having marginally better performance. For frequencies lower than 0.01 Hz, the magnitude response of the second order filter is characterised by a 20 dB/decade slope, that is, the same as the single-pole network, but it yields an attenuation approximately 10 dB higher than that of the reference filter. The third order system provides greater rejection than the second order filter for frequencies lower than 0.01 Hz. Nonetheless, the slope of its magnitude response is also limited to 20 dB/decade at very low frequencies.

Regarding the time constraints that need to be satisfied by the optimised filter, it can be noticed from Figure 6.5(a) that the pulse response undershoot is particularly critical. In fact, for both the optimised filters the maximum displacement from the isoelectric line is exactly equal to the bound. Moreover, the upper limit of the magnitude characteristic is also tightly matched by the optimised systems, as shown in Figure 6.4(b). These two constraints thus appear to be the deciding factors in determining the limit of the optimisation. On the other hand, the constraint on the trailing slope, shown in Figure 6.5(b), does not appear to be



(a)



(b) Detail of the boxed portion of (a).

Figure 6.4: Magnitude response of the 0.05 Hz second and third order filters, optimised for a stopband attenuation of 40 dB. The boxed portion of (a) is shown in detail in (b), where the bounds imposed as limits on the filter amplitude characteristic in the optimisation process are represented by the dashed lines.

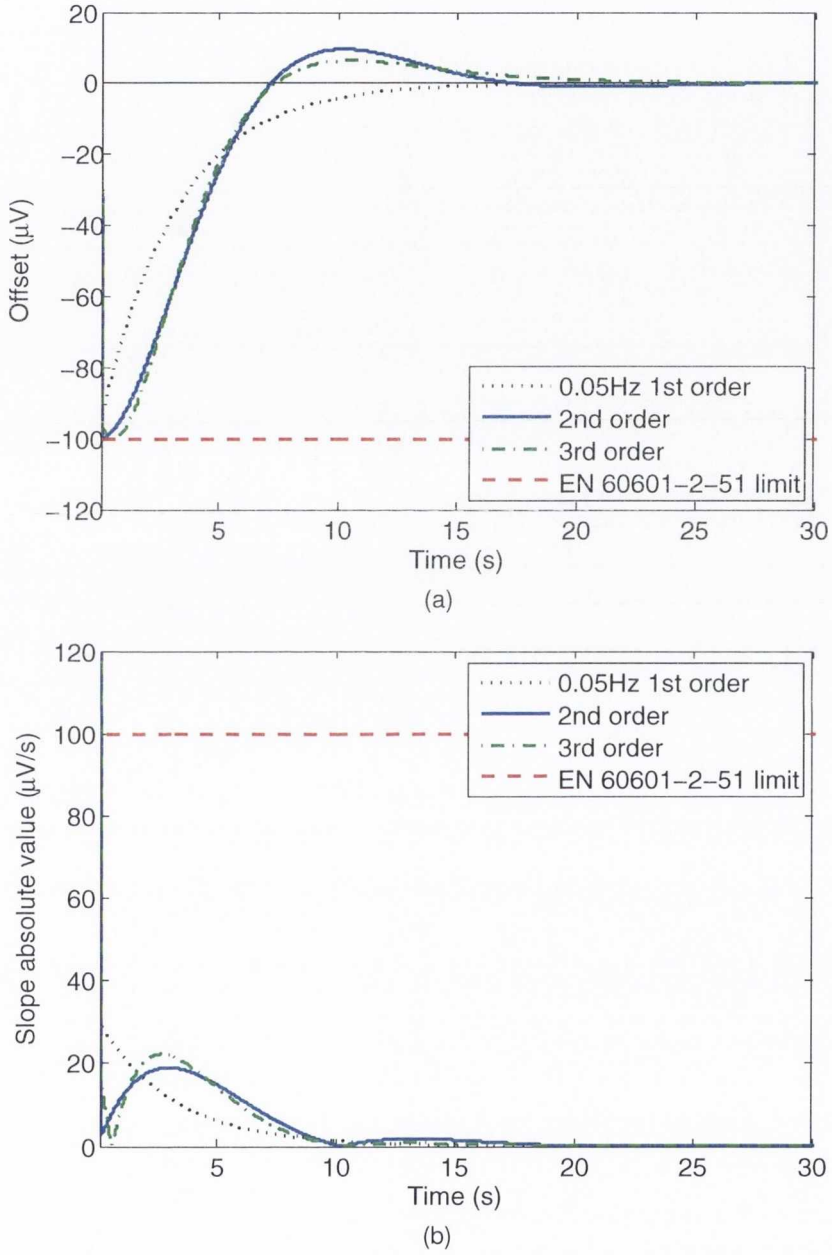


Figure 6.5: (a) Displacement from the isoelectric line and (b) absolute value of the recovery slope after the application of a 3 mV$\times$100 ms rectangular pulse at the input of the 0.05 Hz second and third order optimised filters. The dashed lines represent the bounds established by the European standard EN 60601-2-51:2003.

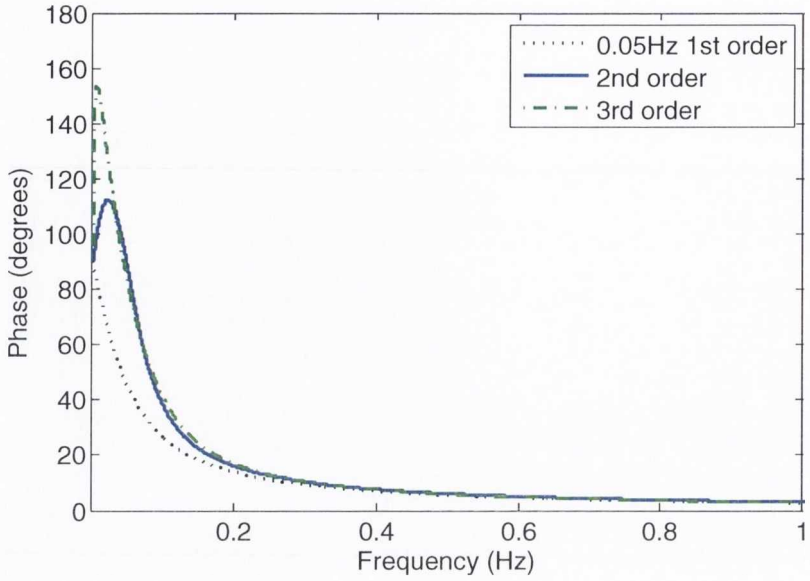


Figure 6.6: Phase response of the 0.05 Hz second and third order filters, optimised for a stopaband attenuation A_s = 40 dB.

critical since this curve is well within the bound for all of the filter orders.

The phase response of the optimised filters is compared with that of the 0.05 Hz single-pole filter in Figure 6.6. Despite its shape being more complex for the second and third order filters due to the presence of zeros and a larger number of poles, the curve approaches that of the reference system as the frequency increases. It should be noted that the phase responses are practically indistinguishable at 0.5 Hz and above. Therefore, the phase shift introduced by the optimised filters over the ECG spectrum is limited, even though no explicit condition is imposed on the phase response in the optimisation process.

The stopband limit is also maximised for other values of minimum attenuation, i.e. 20 and 60 dB. For the second order filter, when A_s = 20 dB the optimisation procedure converges to the same result obtained for a minimum stopband attenuation of 40 dB, as illustrated in Table 6.2. On the other hand, for A_s = 60 dB the optimisation of the 0.05 Hz second order filter leads to a solution that is characterised by two real poles. One of these poles is identified by a frequency of approximately 0.05 Hz, whereas the other is located one order of magnitude lower. The amplitude responses of the second order filters optimised for different values of minimum stopband attenuation are compared in Figure 6.7(a), where it appears evident that the magnitude characteristic of the system obtained for A_s = 60 dB is virtually identical to that of a simple 0.05 Hz highpass network for frequencies higher than 0.01 Hz. Looking at Tables A.1, A.2 and A.3 in Appendix A.3, it can be seen that there exists a single solution having complex conjugate poles, irrespective of the selected stopband attenuation. In this case, all the degrees of freedom available in the optimisation process are

Table 6.2: Optimisation results obtained for the 0.05 Hz second and third order filters for different levels of minimum stopband attenuation. The stopband limit, which is maximised in the optimisation process, is highlighted.

A_s (dB)	f_{20dB} (mHz)	f_{40dB} (mHz)	f_{60dB} (mHz)	p (rad/s)	z (rad/s)
			2nd order		
20	**14.9**	1.9	0.19	-0.2266 $\pm j$ 0.3039	0
					-0.1194
40	14.9	**1.9**	0.19	-0.2266 $\pm j$ 0.3039	0
					-0.1194
60	6.1	1.5	**0.46**	-0.3118	0
				-0.0271	-0.0004
			3rd order		
20	**23.6**	0.2	0.02	-0.0181	0
				-0.1892 $\pm j$ 0.2967	-0.0311 $\pm j$ 0.1180
40	13.4	**4.0**	1.04	-0.2125	0
				-0.4063 $\pm j$ 0.2281	-0.6969
					-0.0078
60	13.1	4.0	**1.24**	-0.1842	0
				-0.4158 $\pm j$ 0.2393	-0.6953
					-0.0007

employed by limiting the peak occurring in the magnitude response and the maximum negative undershoot of the pulse response and by fixing the frequency of the 3dB-point through the equality constraint described by Eq. (6.56). Hence, the slope of the amplitude response in the transition region is determined by these characteristics. Furthermore, it should be pointed out that, for each value of minimum stopband attenuation, a different solution characterised by real poles is obtained for the design of the second order highpass filter. For A_s = 40 dB this solution is sub-optimal, whereas for A_s = 60 dB the highest frequency for the stopband limit is achieved when the real-pole transfer function is selected.

As regards the third order filter, the stopband limits and the location of poles and zeros are summarised in Table 6.2 and the magnitude response is presented in Figure 6.7(b) for different attenuations. From this figure, it can be seen that the filter obtained by optimising the 60dB-point is not substantially different from that obtained for A_s = 40 dB. On the other hand, the filter optimised for A_s = 20 dB shows a side lobe in the stopband and the frequency of the 20dB-point is comparatively much higher than is the case for the other two filters. It may, also, be argued that such an attenuation level is not sufficient since some noise components might be only reduced to 10% of their actual value in the stopband. A better knowledge of the disturbances present in the ECG measurement at such low frequencies would be beneficial in the choice of a suitable attenuation level.

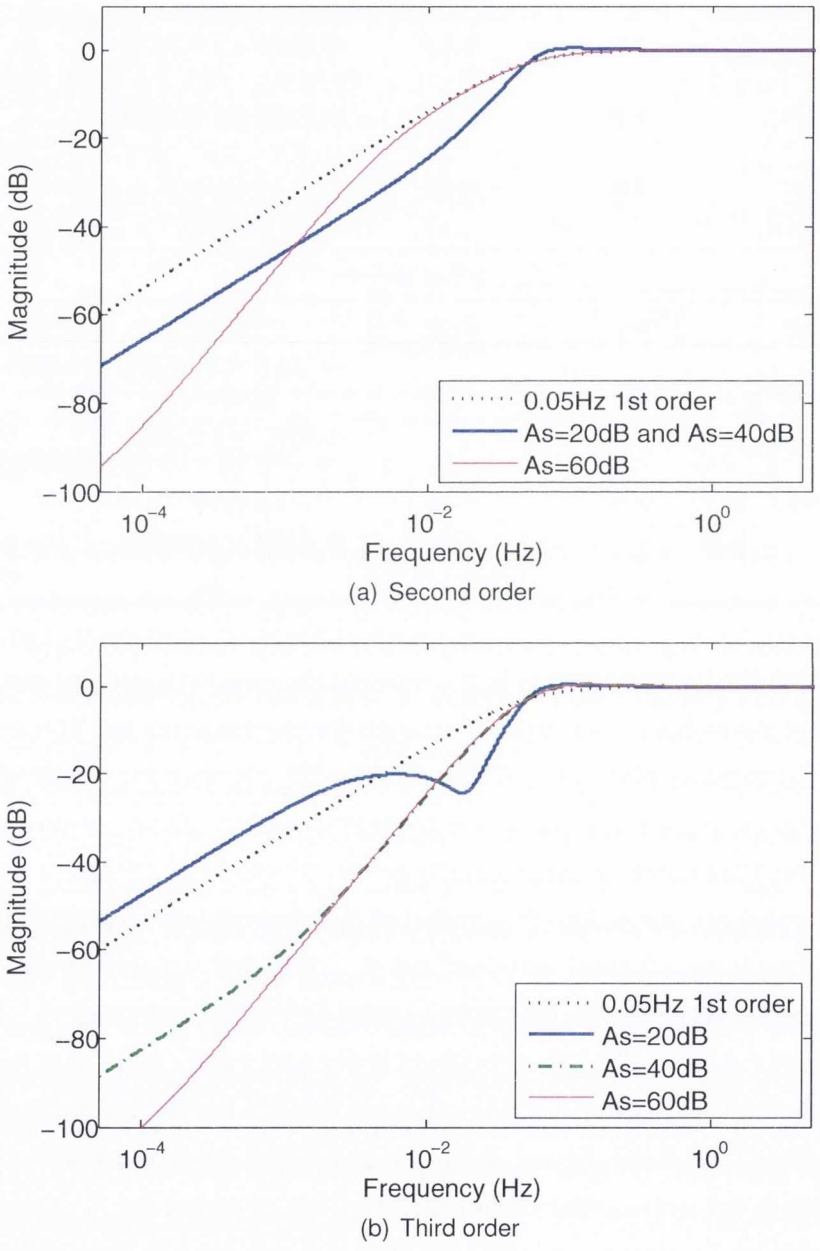


Figure 6.7: Magnitude response of the 0.05 Hz second and third order filters optimised for different values of stopband attenuation.

Let us finally analyse how the outcome of the optimisation procedure is affected by limiting the overshoot occurring in the response to an input rectangular pulse of 3 mV amplitude and 100 ms duration. For this study, the minimum stopband attenuation is selected as 40 dB. It can be seen from Figure 6.5(a) that a positive displacement as high as 10 μV is present in the pulse response of the optimised filters, when no condition is imposed on its maximum allowable amplitude. The optimisation of the 0.05 Hz filters is thus repeated introducing the additional constraint described by Eq. (6.26), where ϵ is, in turn, selected to be 0.05 and 0.02. In other words, a maximum overshoot equal to 5 and 2 μV, respectively, is allowed in the pulse response.

For the second order filter, the optimisation procedure leads to the same result for both $\epsilon = 0.05$ and $\epsilon = 0.02$, as reported in Table 6.3, where this solution is compared with the one originally determined for the unrestricted case. The transfer function obtained when the maximum allowable pulse response overshoot is smaller or equal to 5 μV is characterised by two real poles, one of which is located at approximately 0.05 Hz. Its magnitude response is, indeed, coincident with that of the 0.05 Hz single-pole network for frequencies higher than 0.01 Hz, as illustrated in Figure 6.8(a), and its pulse response, shown in Figure 6.8(b), does not present any significant ringing. Finally, from the analysis of the Tables A.1, A.4 and A.5 in Appendix A.3, it emerges that the solution obtained when the pulse response overshoot is limited to less than 5 μV is the same as the sub-optimal result, characterised by real poles, occurring when the pulse overshoot is left unconstrained.

The results obtained for the third order system are also summarised in Table 6.3 and the magnitude and pulse responses associated with them are illustrated in Figure 6.9. It can be seen that both the stopband limit, f_{40dB}, and the rejection of the filter in the transition region decrease as the requirement placed on the pulse overshoot gets more stringent. Furthermore, even though the filter transfer function contains a pair of complex conjugate poles when the positive displacement occurring in the pulse response is left unconstrained, the optimum system is characterised by three real poles for $\epsilon = 0.05$ and $\epsilon = 0.02$.

6.4 Optimisation of the stopband limit

In the previous section, it has been shown that 0.05 Hz second and third order filters that comply with international standards and recommendations for ECG monitoring applications and have better rejection properties than the reference 0.05 Hz single-pole network can be designed by maximising the stopband limit. In order to evaluate the possibility of determining the transfer function of other highpass systems that provide a larger out-of-band attenuation than these filters, the optimisation procedure is repeated without imposing any

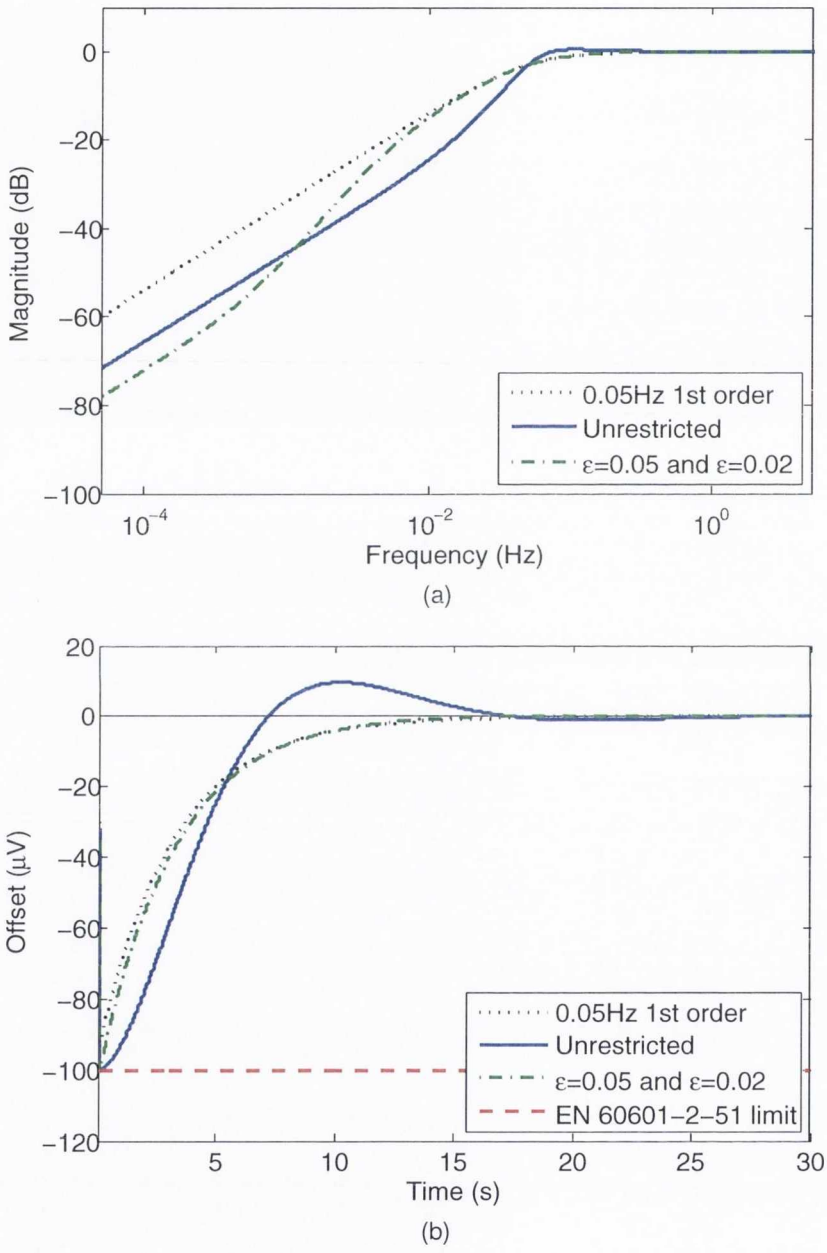


Figure 6.8: (a) Amplitude characteristic and (b) displacement from the isoelectric line occurring after the application of a 3 mV×100 ms rectangular input pulse for the 0.05 Hz second order filters optimised for different values of maximum allowable pulse response overshoot.

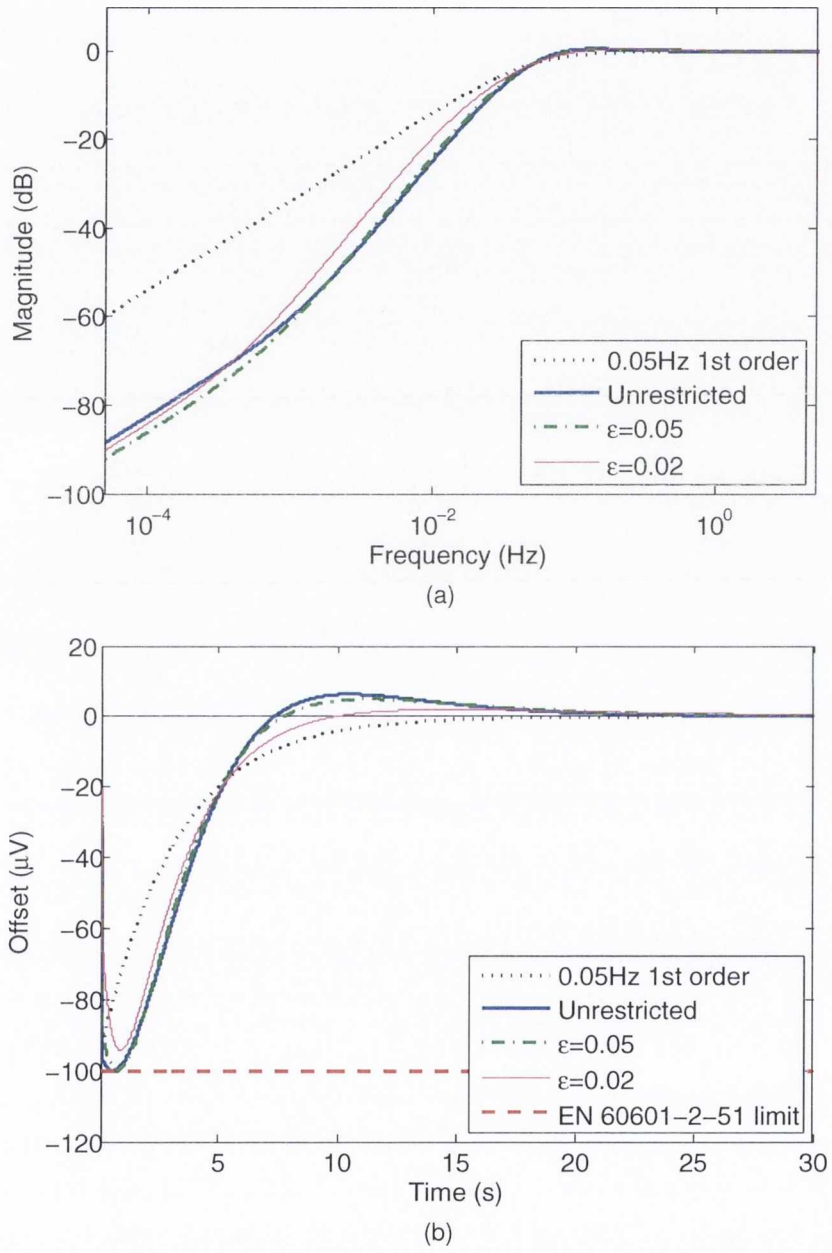


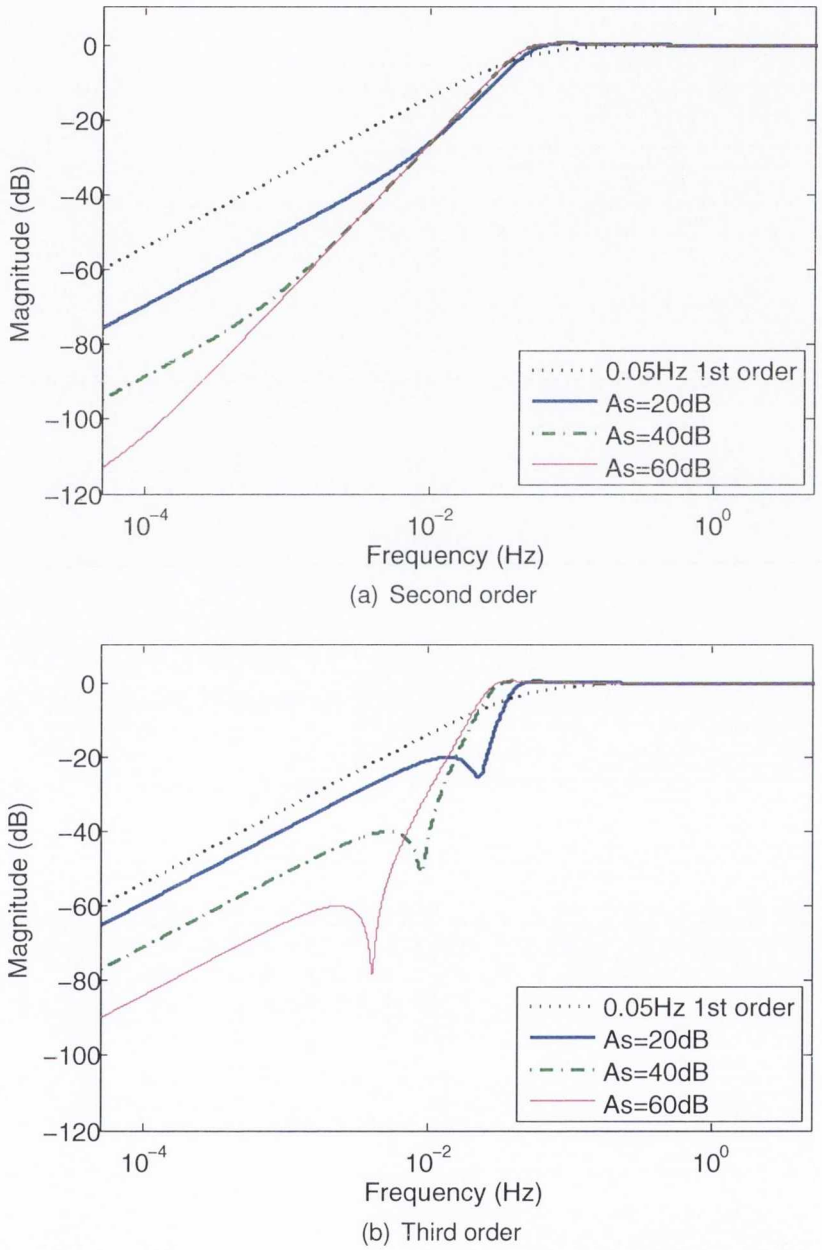
Figure 6.9: (a) Amplitude characteristic and (b) displacement from the isoelectric line occurring after the application of a 3 mV$\times$100 ms rectangular input pulse for the 0.05 Hz third order filters optimised for different values of maximum allowable pulse response overshoot.

Table 6.3: Results obtained by optimising the stopband limit of the 0.05 Hz second and third order filters (A_s = 40 dB) for different values of maximum allowable pulse response overshoot.

Overshoot (μV)	f_{20dB} (mHz)	f_{40dB} (mHz)	f_{60dB} (mHz)	p (rad/s)	z (rad/s)
			2nd order		
9.6	14.9	**1.9**	0.19	-0.2266 $\pm j$ 0.3039	0
(unrestricted)					-0.1194
5	6.3	**1.6**	0.35	-0.3111	0
				-0.0313	-0.0038
2	6.3	**1.6**	0.35	-0.3111	0
				-0.0313	-0.0038
			3rd order		
6.4	13.5	**4.0**	1.04	-0.2125	0
(unrestricted)				-0.4063 $\pm j$ 0.2281	-0.6969
					-0.0078
5	12.8	**3.9**	1.12	-0.8245	0
				-0.3413	-1.1035
				-0.2333	-0.0046
2	9.7	**2.8**	0.83	-1.5060	0
				-0.3893	-1.7813
				-0.0946	-0.0030

condition on the 3dB-cutoff frequency. The optimisation of the stopband limit is performed for different values of desired attenuation, i.e. 20, 40 and 60 dB. The location of poles and zeros of the optimised second and third order filters is reported in Table 6.4 and the frequencies at which given levels of attenuation are reached by the filter amplitude are also presented.

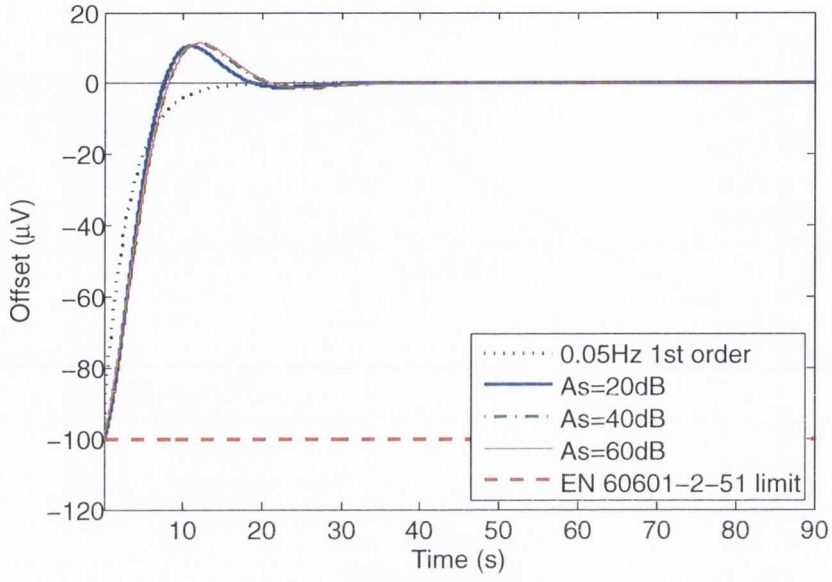
The frequency and time domain characteristics of the optimised systems are illustrated in Figures 6.10 to 6.12, from which it can be verified that the pulse responses of the filters obtained through the maximisation of the stopband limit satisfy the requirements established by the European standard for diagnostic electrocardiographic recording [9]. From the data in Table 6.4, as well as from these figures, it can be seen that the results derived when A_s is selected as either 40 or 60 dB are quite similar. The only relevant difference is given by the location of the zeros, which affects the filter magnitude response at very low frequencies. From Table 6.4, it should also be noted that the frequency of the 3dB-point decreases as the minimum required stopband attenuation increases. All of the optimised filters are characterised by a 3dB-cutoff frequency lower than 0.05 Hz and a particularly low value of less than 0.03 Hz is obtained for the third order system when A_s is chosen as 40 and 60 dB. As expected, the frequency of the stopband limit is increased with respect to the value achieved when the filter 3dB-cutoff is fixed at 0.05 Hz, which appears clear by comparing



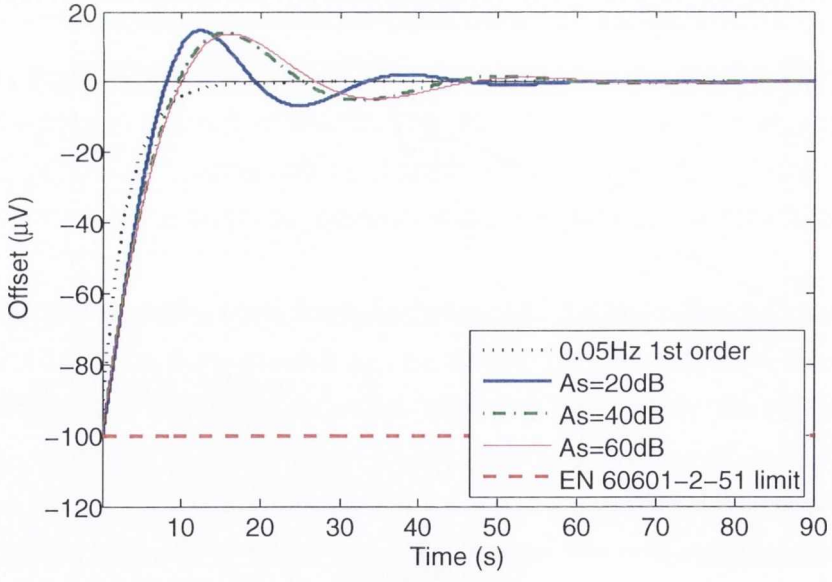
(a) Second order

(b) Third order

Figure 6.10: Amplitude response of the second and third order filters obtained by optimising the stopband limit for different values of minimum required attenuation.

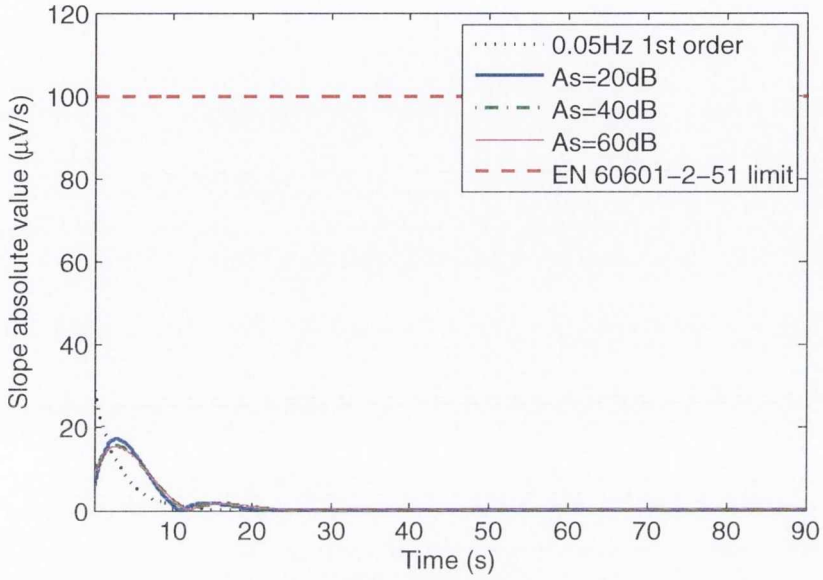


(a) Second order

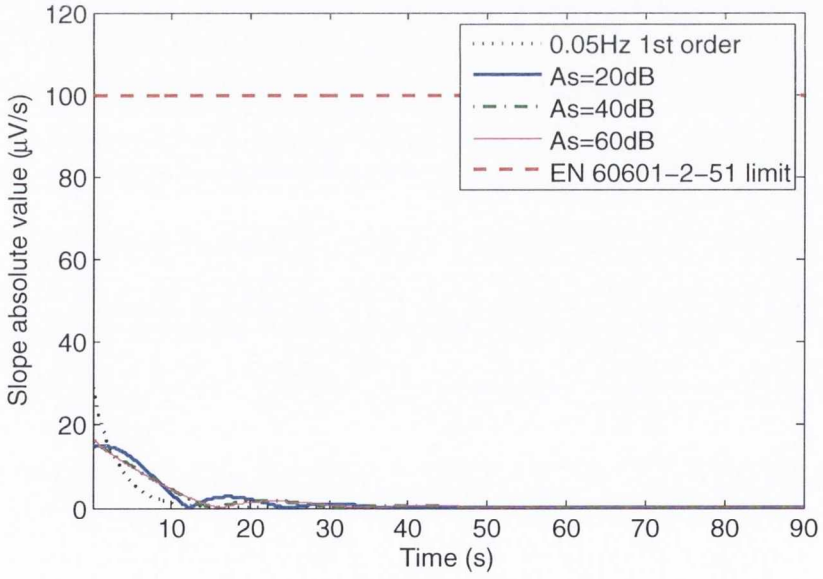


(b) Third order

Figure 6.11: Displacement from the isoelectric line occurring after the application of a 3 mV$\times$100 ms rectangular pulse at the input of the second and third order filters obtained by optimising the stopband limit for different values of minimum required attenuation.



(a) Second order



(b) Third order

Figure 6.12: Absolute value of the slope following the application of a 3 mV×100 ms rectangular pulse at the input of the second and third order filters obtained by optimising the stopband limit for different values of minimum required attenuation.

Table 6.4: Optimisation results obtained for the second and third order filters for different levels of minimum stopband attenuation. The stopband limit, which is maximised in the optimisation process, is highlighted.

A_s (dB)	f_{3dB} mHz)	f_{20dB} (mHz)	f_{40dB} (mHz)	f_{60dB} (mHz)	p (rad/s)	z (rad/s)
			2nd order			
20	45.2	**15.5**	2.9	0.30	-0.1967 $\pm j$ 0.2729	0
						-0.0592
40	39.7	14.6	**4.6**	1.37	-0.1699 $\pm j$ 0.2393	0
						-0.0050
60	39.2	14.4	4.6	**1.46**	-0.1676 $\pm j$ 0.2361	0
						-0.0005
			3rd order			
20	38.2	**26.1**	0.9	0.09	-0.2021	0
					-0.0820 $\pm j$ 0.2364	-0.0151 $\pm j$ 0.1465
40	27.2	15.8	**10.4**	0.36	-0.2122	0
					-0.0650 $\pm j$ 0.1750	-0.0030 $\pm j$ 0.0573
60	25.2	13.8	7.2	**4.71**	-0.2122	0
					-0.0626 $\pm j$ 0.1639	-0.0006 $\pm j$ 0.0257

Tables 6.4 and 6.2. When the minimum stopband attenuation is 40 dB, the frequency of the stopband limit is approximately 2.5 times that obtained earlier and, for A_s = 60 dB, it is between 3 and 4 times higher. On the other hand, when A_s is equal to 20 dB, there is a very marginal difference between the stopband limits achieved by the two optimisation procedures.

It can thus be concluded that, while the stopband limit has been maximised, the transition region has also been narrowed by the optimisation procedure at the expense of a reduced 3dB-cutoff frequency. Therefore, even though the optimised filters, and in particular the third order type, have far superior attenuation characteristics than the 0.05 Hz single-pole system, the range over which this rejection is achieved is located at lower frequencies than was the case for the reference filter and the 0.05 Hz second and third order systems discussed in the previous section.

6.5 Optimisation of the 3dB-cutoff frequency

Given the unsatisfactory results obtained when the filter stopband limit is maximised, the optimisation procedure is applied to the 3dB-cutoff frequency, instead. In other words, the critical frequency ω_c is selected as the frequency at which an attenuation of 3 dB is achieved by the filter. The outcome of this process is reported in Table 6.5 for the second

Table 6.5: Results obtained by optimising the 3dB-cutoff frequency of the second order filter.

f_{3dB} (mHz)	f_{20dB} (mHz)	f_{40dB} (mHz)	f_{60dB} (mHz)	p (rad/s)	z (rad/s)
67.7	8.5	0.9	0.09	-0.6570 $\pm j$ 0.3426	0 -1.0294

order system. The optimised 3dB-point is equal to 0.068 Hz, that is, approximately 35% larger than that of the reference first order filter. The rejection achieved by this filter at low frequencies is obviously not as high as that of the systems obtained by optimising the stopband limit in the previous section (see Table 6.4). It can, however, be seen in Figure 6.13(a) that the second order filter derived by maximising the 3dB-cutoff frequency is characterised by an attenuation that is up to 4.5 dB higher than that of the 0.05 Hz single-pole filter over the stopband and most of the transition region.

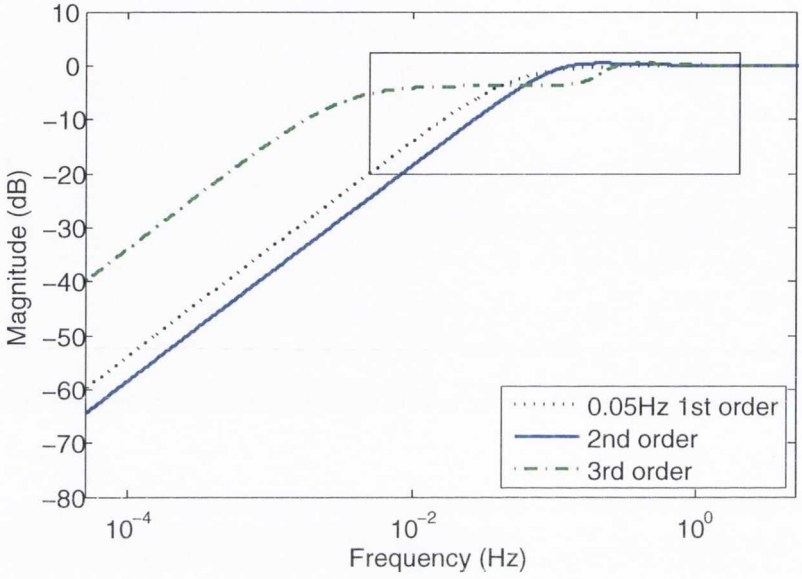
As regards the third order system, it can be noticed from Figure 6.13 that the magnitude response of the optimised filter has a staircase shape and is flat over a wide range of frequencies. In other words, the third order filter obtained by maximising the 3dB-point provides very limited attenuation, i.e. approximately 4 dB, throughout most of the transition region and, consequently, its rejection is less than that of the reference 0.05 Hz network for frequencies up to 0.043 Hz. In order to increase the low-frequency attenuation achieved by the third order system, a further constraint is imposed on the filter amplitude response during the optimisation procedure. The 0.05 Hz single-pole network is taken as a benchmark and the magnitude of the third order filter is required to be less than that of that this reference system over the transition region, as illustrated in Figure 6.14. This condition is analytically expressed as:

$$|H_3(\omega)|_{dB} \leq |H_1(\omega)|_{dB} \qquad \text{for} \quad \omega_{s_1} \leq \omega \leq \omega_{p_1}, \tag{6.58}$$

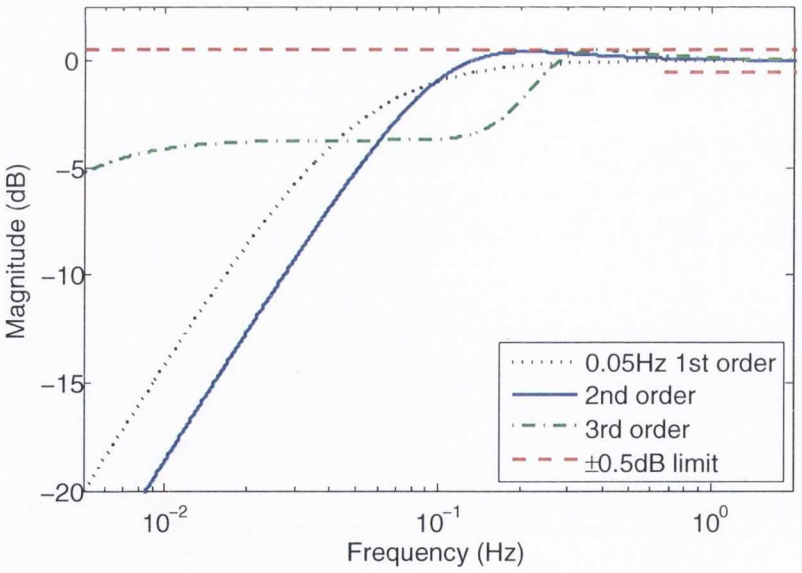
where $|H_3(\omega)|_{dB}$ and $|H_1(\omega)|_{dB}$ are the magnitudes, expressed in decibels, of the third order filter under design and of the reference 0.05 Hz single-pole network, respectively, and ω_{s_1} and ω_{p_1} represent the stopband and passband limits of the 0.05 Hz first order filter. A further inequality constraint is therefore added to the optimisation algorithm:

$$c_{10}(\boldsymbol{x}) = |H_3(\omega)|_{dB} - |H_1(\omega)|_{dB} \qquad \text{for} \quad \omega_{s_1} \leq \omega \leq \omega_{p_1}. \tag{6.59}$$

The optimisation of the 3dB-point of the third order filter is then performed for different levels of minimum stopband attenuation, i.e. A_s = 40 dB and A_s = 60 dB. Since the result is independent of the selected stopband attenuation (see Tables A.18 and A.19), the optimisation procedure is extended to investigate the case in which $A_s \rightarrow \infty$, that is, no



(a)



(b) Detail of the boxed portion of (a).

Figure 6.13: Magnitude response of the second and third order filters obtained by maximising the 3dB-cutoff frequency.

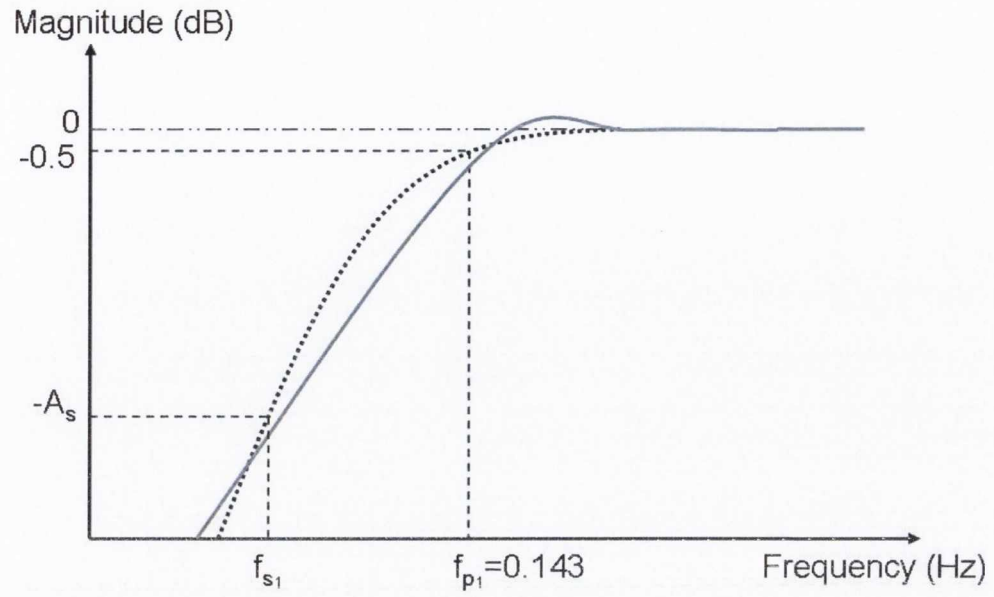


Figure 6.14: Diagram exemplifying constraint c_{10}, which requires the magnitude response of the third order filter to be lower than that of the reference 0.05 Hz single-pole system in the transition region.

ripple is allowed in the stopband of the third order filter. The constraint defined in Eq. (6.45) that limits the amplitude of the magnitude peak occurring in the stopband is omitted and constraints c_9 and c_{10}, given by Eqs. (6.47) and (6.59), are rewritten as:

$$c_9'(\boldsymbol{x}) = -\frac{d(|H_3(\omega)|_{dB})}{d\omega} \qquad \text{for} \quad \omega \leq \omega_p \tag{6.60}$$

and

$$c_{10}'(\boldsymbol{x}) = |H_3(\omega)|_{dB} - |H_1(\omega)|_{dB} \qquad \text{for} \quad \omega \leq \omega_{p_1}, \tag{6.61}$$

where ω_p and ω_{p1} are the frequencies for which $|H_3(\omega)|_{dB}$ and $|H_1(\omega)|_{dB}$ are, respectively, equal to -0.5 dB. The outcome of the optimisation when the magnitude response of the third order system is monotonically increasing over both the stopband and the transition region is identical to the one resulting for a limited stopband attenuation, which appears evident when comparing Table A.20 with Tables A.18 and A.19. It can thus be concluded that for the third order system the optimisation of the 3dB-cutoff frequency is independent of A_s, at least when its magnitude response is constrained to be lower than that of the 0.05 Hz single-pole network in the transition region.

The magnitude response of the optimised third order filter is illustrated in Figure 6.15. It can easily be noted that the attenuation provided by the third order filter is limited to only 3 dB over a wide range of frequencies in the transition region and that the magnitude of the optimised system converges to the response of the 0.05 Hz reference RC network for

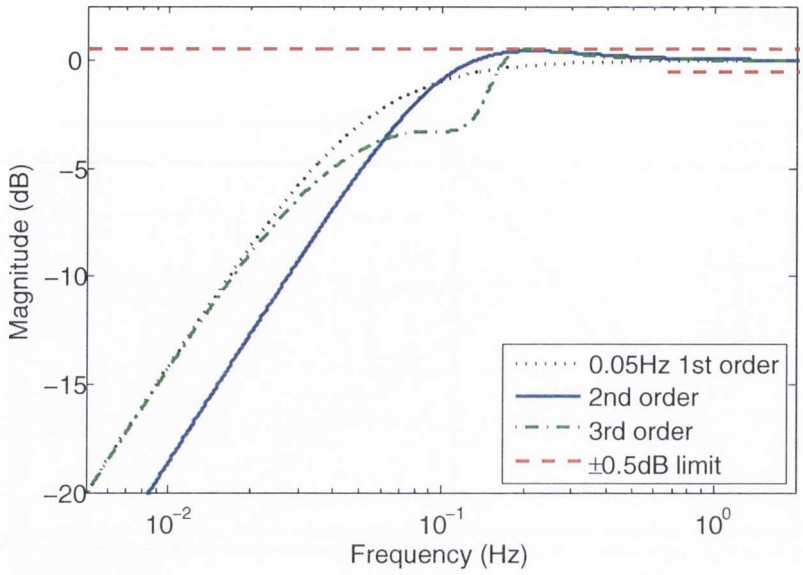


Figure 6.15: Amplitude characteristic of the third order filter obtained by maximising the 3dB-cutoff frequency when the magnitude response is constrained to be lower than that of the 0.05 Hz single-pole network in the transition region. The response of the second order filter previously determined is also shown.

attenuations higher than 10 dB.

In order to prevent the amplitude characteristic of the third order system from having a staircase shape and to increase the attenuation yielded at frequencies immediately lower than the 3dB-point, a stricter condition is imposed on the filter amplitude response in the stopband and in the transition region. The magnitude response is required to be concave between 0 rad/s and the passband limit ω_p, identified in Figure 6.1. In analytical terms, the following condition is imposed:

$$\frac{d^2(|H_3(\omega)|_{dB})}{d\omega^2} \leq 0 \qquad \text{for} \quad \omega \leq \omega_p, \tag{6.62}$$

which means that a further constraint is enforced during the optimisation procedure:

$$c_{11}(\boldsymbol{x}) = \frac{d^2(|H_3(\omega)|_{dB})}{d\omega^2} \qquad \text{for} \quad \omega \leq \omega_p. \tag{6.63}$$

The location of the poles and zeros and the frequencies at which different attenuations are achieved by this system are reported in Table 6.6, where the results obtained for the third order filter without imposing constraint c_{11} are also presented. From this table, it can be calculated that for the third order filter the frequency of the 3dB-point is 37% higher when the concavity condition is not imposed. On the other hand, as shown in Figure 6.16(b), the convergence of the amplitude curve of the concave filter to the response of the refer-

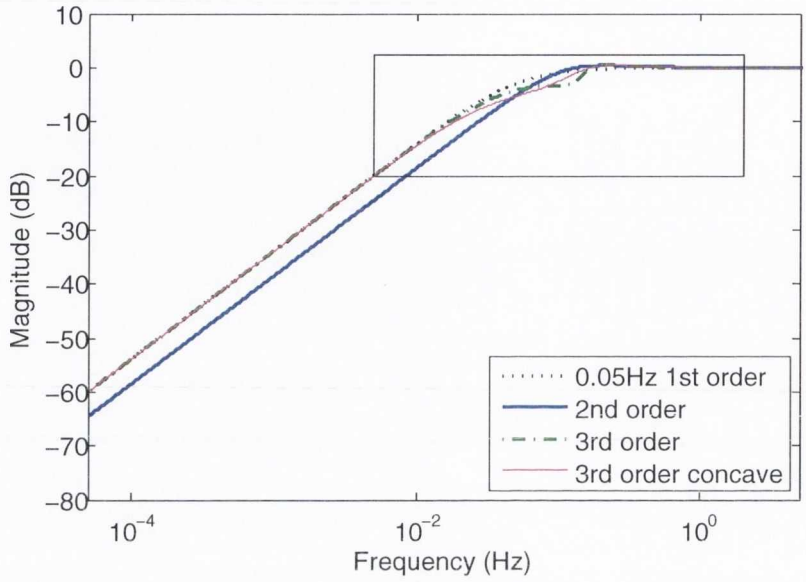
Table 6.6: Results derived by optimising the 3dB-cutoff frequency of the third order filter when the amplitude response is forced to be lower than that of the reference single-pole network.

Constraints	f_{3dB} (mHz)	f_{20dB} (mHz)	f_{40dB} (mHz)	f_{60dB} (mHz)	p (rad/s)	z (rad/s)
c_8, c'_9, c'_{10}	**122.9**	5.0	0.5	0.05	-0.2557	0
					-0.2713 $\pm j$ 0.9289	-0.2374 $\pm j$ 0.8402
c_8, c'_9, c'_{10}, c_{11}	**90.1**	5.1	0.5	0.05	-0.1887	0
(concave filter)					-0.6027 $\pm j$ 0.7332	-0.5574 $\pm j$ 0.4799

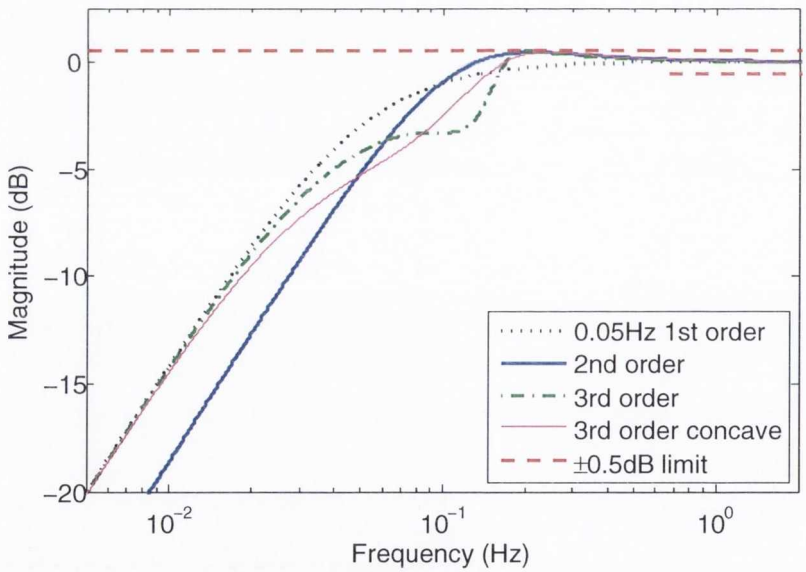
ence 0.05 Hz first order network occurs at a higher attenuation than for the monotonically increasing system.

It is important to notice that, even though in Figure 6.16 the magnitude response of the third order filter obtained by imposing constraint c_{11} does not seem to be concave outside the passband, the concavity condition is actually satisfied by the optimised system and the apparent discrepancy is due to the frequency scale of this graph being logarithmic. Figure 6.17(a), showing the amplitude characteristic of the concave filter on a linear frequency scale, helps to verify this fact. Furthermore, from Figures 6.17(b) and 6.17(c), respectively, it can be seen that the first derivative of the magnitude response of the third order concave filter is monotonically decreasing over the transition region and that its second derivative is at most equal to zero over the same interval, which eliminates any doubt about the concavity constraint being fulfilled by the optimised filter.

Figure 6.18 illustrates that the optimised filters satisfy the time constraints imposed on the response to a 3 mV$\times$100 ms input rectangular pulse. It can be noticed in Figure 6.18(a) that the condition set on the undershoot occurring after the application of the input signal is met exactly by all three filters. It can thus be concluded that this constraint plays a central role in limiting the outcome of the optimisation procedure, as previously highlighted in Section 6.3 where the optimisation of filters having a fixed 3dB-point of 0.05 Hz was analysed. In contrast to the results obtained using that procedure (see Figure 6.5(a)), no significant positive displacement occurs in the response to the rectangular pulse of the filters derived by maximising the 3dB-cutoff frequency. It is therefore unnecessary to investigate the changes affecting the optimisation procedure when the condition expressed by Eq. 6.26 limiting the pulse response overshoot is enforced. It can finally be observed from Figure 6.18(a) that a marked oscillatory behaviour is present in the response of the third order system when the amplitude characteristic is not constrained to be concave over the stopband and the transition region. Nonetheless, for both third order filters the time taken for the output signal to return to the baseline level after the application of the 3 mV$\times$100 ms rectangular pulse is quite large. It can be seen that this settling time is approximately equal to that of the ref-



(a)



(b) Detail of the boxed portion of (a).

Figure 6.16: Amplitude characteristic of the third order filter obtained by maximising the 3dB-cutoff frequency when its magnitude is constrained to be concave outside the passband. The response of the second and third order filters previously derived are illustrated for comparison purposes.

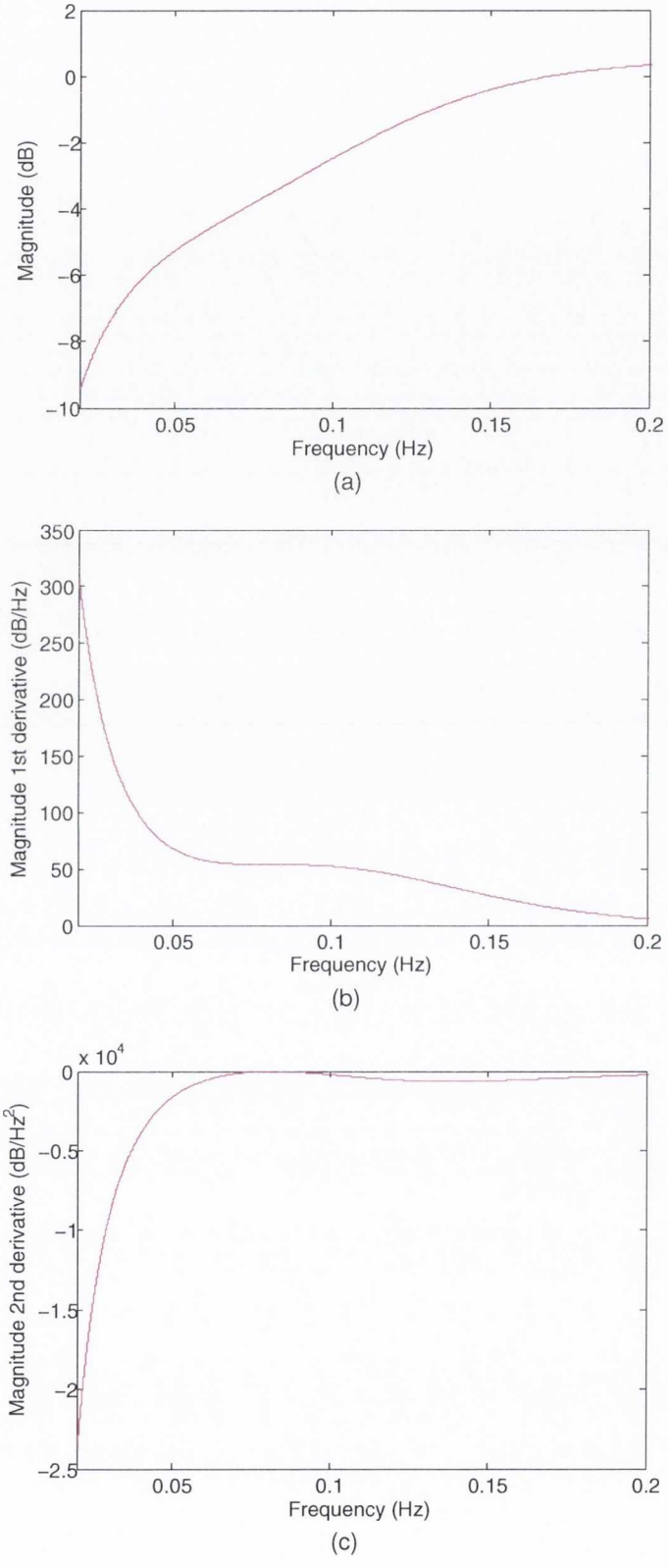


Figure 6.17: Magnitude response of the third order concave filter and its first and second derivatives, shown for a linear frequency scale.

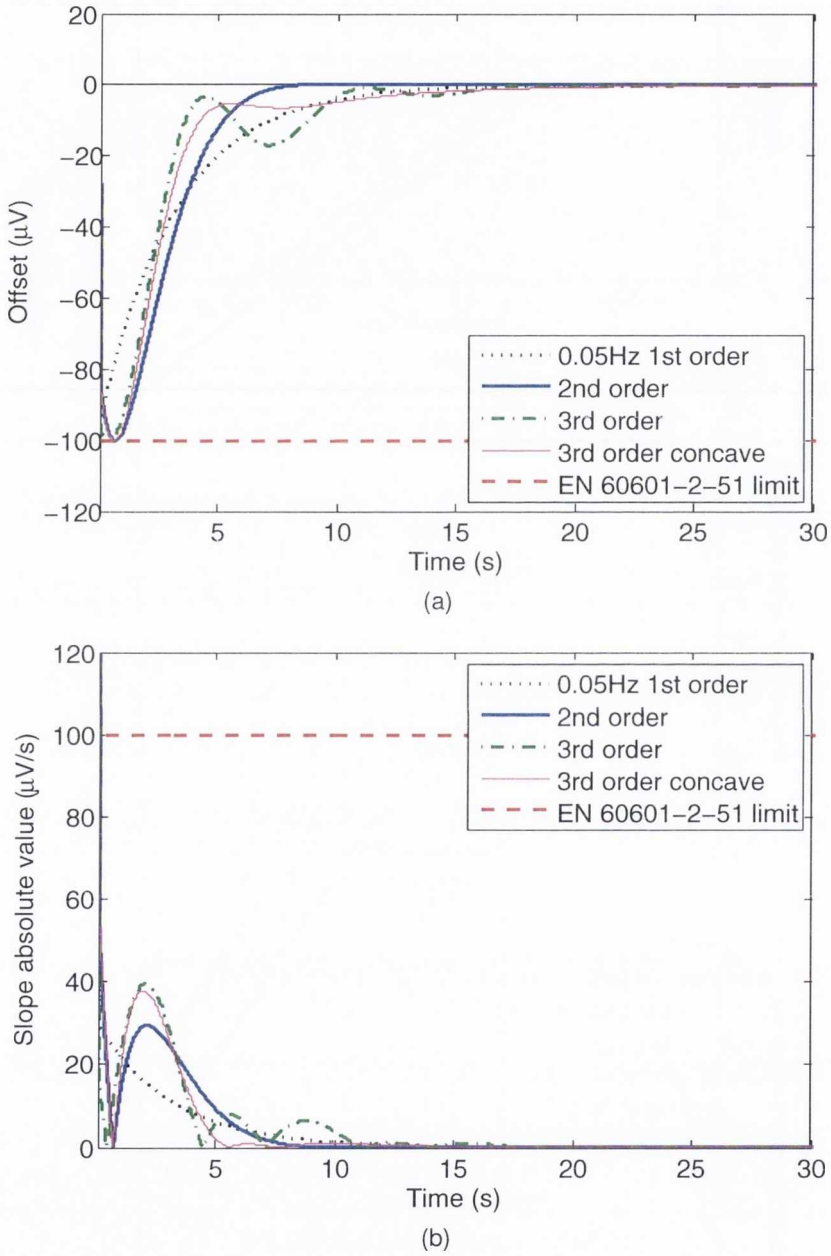


Figure 6.18: (a) Displacement from the isoelectric line and (b) absolute value of the recovery slope occurring after the application of a 3 mV$\times$100 ms rectangular pulse at the input of the second and third order filters derived by maximising the 3dB-cutoff frequency and described by the poles and zeros reported in Tables 6.5 and 6.6.

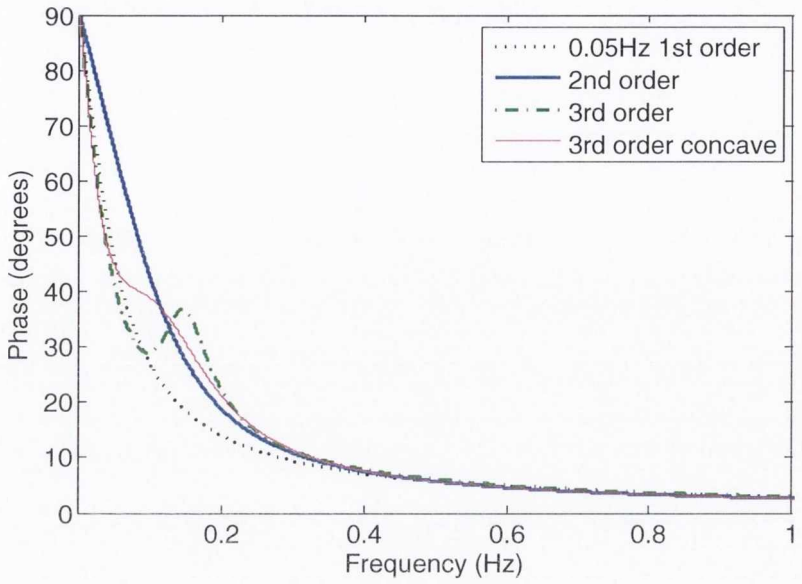


Figure 6.19: Phase response of the second and third order filters derived by maximising the 3dB-cutoff frequency.

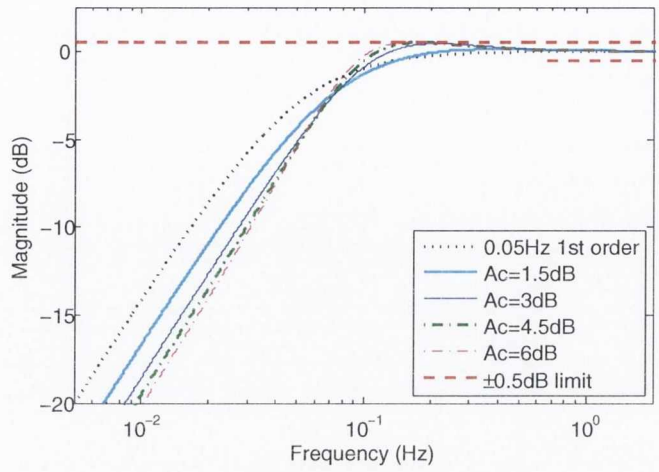
erence single-pole network, whereas it appears to be considerably shorter for the second order system.

As regards the phase of the optimised filters, it can be seen in Figure 6.19 that their responses converge to that of a 0.05 Hz single-pole filter as the frequency approaches the lower band of the ECG spectrum and that the curves are practically undistinguishable for frequencies above 0.5 Hz. The phase shift introduced by the optimised filters can therefore be considered negligible in the frequency range of the electrocardiographic signal.

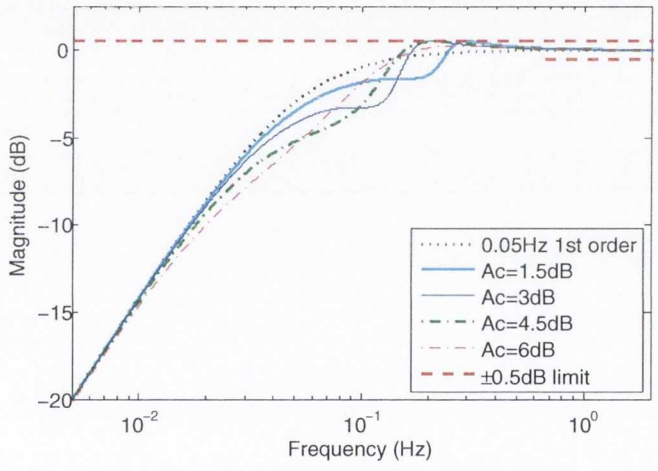
Even though in electrocardiographic applications attention is often directed exclusively to the 3dB-cutoff frequency of the highpass filter, as widely discussed in Chapters 3 and 5, it is worthwhile to evaluate the effect of choosing a different point in the system transition region as the focus of the optimisation. The procedure is, therefore, repeated by maximising the frequency at which the filter attenuation reaches, in turn, 1.5, 4.5 and 6 dB. The optimisation outcomes for the second and third order filters are summarised in Table 6.7 and the magnitude and time domain responses of the optimised systems are illustrated in Figures 6.20 to 6.22. From these figures, it can be noticed that the results obtained by optimising the frequency at which a critical attenuation, A_c, of 1.5 dB is achieved by the system are quite different from those derived for the other attenuations. This is particularly true for the second order and the third order concave filters, for which the amplitude responses derived when the critical attenuation is equal to 3, 4.5 and 6 dB, respectively, are quite similar, as clearly illustrated in Figure 6.20. It can also be noted from Table 6.7 that, when the frequency of the 6dB-point is maximised, the outcome of the optimisation procedure for the

Table 6.7: Results obtained by maximising the frequency at which different selected attenuations, A_c, are achieved by the second and third order filters in the transition region. The optimisation outcome is reported for A_c equal to 1.5, 3, 4.5 and 6 dB and the critical frequencies corresponding to them are highlighted.

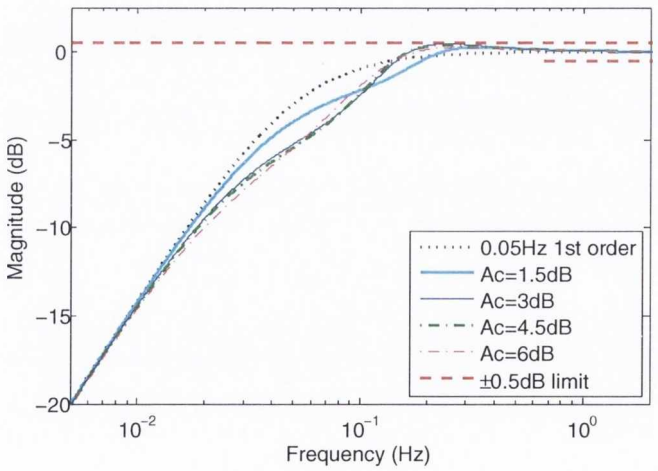
$f_{1.5dB}$ (mHz)	f_{3dB} (mHz)	$f_{4.5dB}$ (mHz)	f_{6dB} (mHz)	f_{20dB} (mHz)	f_{40dB} (mHz)	p (rad/s)	z (rad/s)
2nd order							
93.5	64.2	48.7	38.5	6.8	0.7	-2.1736	0
						-0.4545	-2.3220
87.7	**67.7**	54.5	44.7	8.5	0.9	-0.6570 $\pm j$ 0.3426	0
							-1.0294
83.1	66.9	**55.5**	46.6	9.5	1.0	-0.5012 $\pm j$ 0.4111	0
							-0.7038
79.2	65.1	55.0	**46.9**	10.2	1.0	-0.4214 $\pm j$ 0.4069	0
							-0.5299
3rd order							
194.3	58.0	39.8	30.2	5.0	0.5	-0.2834	0
						-0.3520 $\pm j$ 1.4579	-0.3404 $\pm j$ 1.3832
146.0	**122.9**	45.5	32.3	5.0	0.5	-0.2557	0
						-0.2713 $\pm j$ 0.9289	-0.2374 $\pm j$ 0.8402
124.4	101.6	**68.3**	38.9	5.1	0.5	-0.2095	0
						-0.4091 $\pm j$ 0.7789	-0.3626 $\pm j$ 0.6202
109.2	80.7	60.6	**44.8**	5.1	0.5	-0.1418	0
						-0.7168 $\pm j$ 0.4956	-0.8809
							-0.3890
3rd order concave							
135.4	69.9	43.8	31.9	5.0	0.5	-0.2527	0
						-0.7885 $\pm j$ 1.0392	-0.7678 $\pm j$ 0.8829
119.6	**90.1**	62.5	40.7	5.1	0.5	-0.1887	0
						-0.6027 $\pm j$ 0.7332	-0.5574 $\pm j$ 0.4799
116.7	89.5	**64.9**	43.1	5.1	0.5	-0.1795	0
						-0.5696 $\pm j$ 0.6780	-0.5109 $\pm j$ 0.4324
109.6	81.1	60.8	**44.7**	5.1	0.5	-0.1437	0
						-0.7173 $\pm j$ 0.5076	-0.8697
							-0.4060



(a) Second order

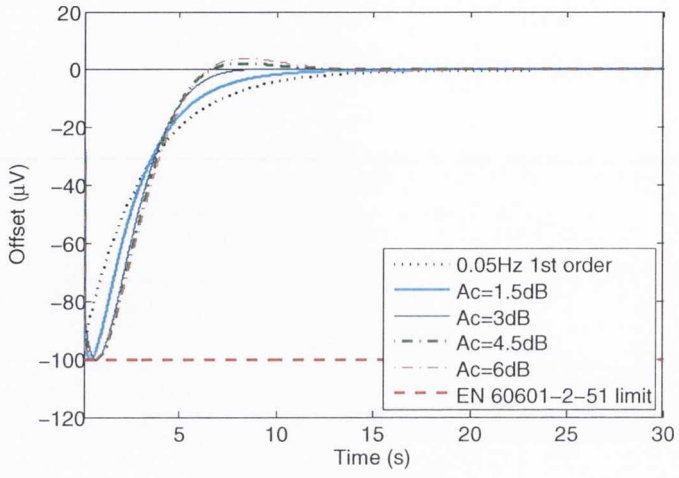


(b) Third order

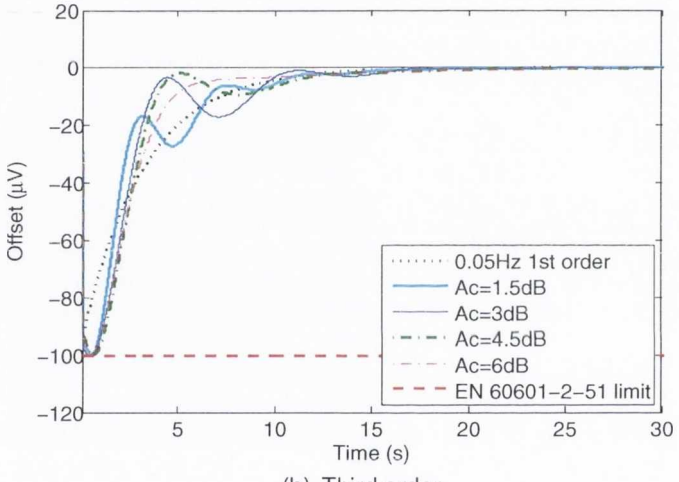


(c) Third order concave

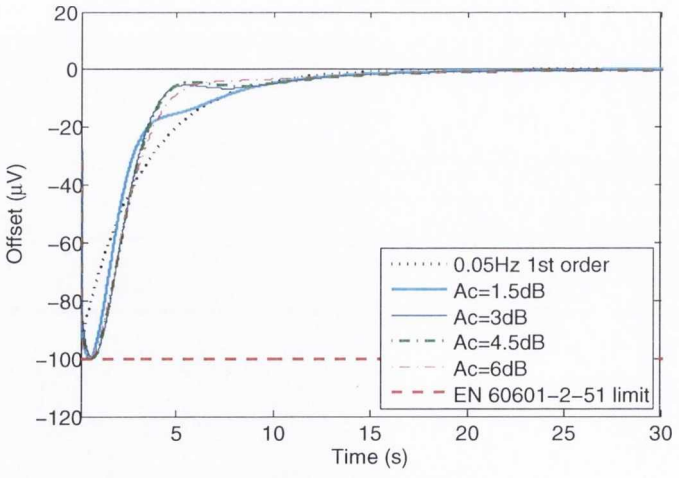
Figure 6.20: Magnitude response of the second and third order filters obtained by maximising the frequency at which different critical attenuations are reached in the transition region.



(a) Second order

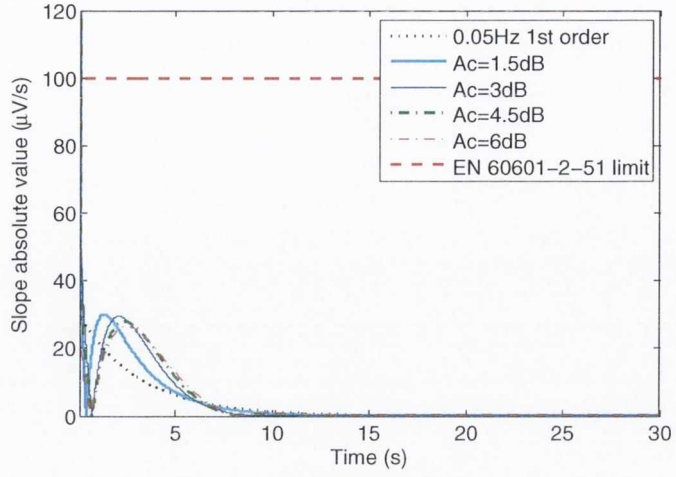


(b) Third order

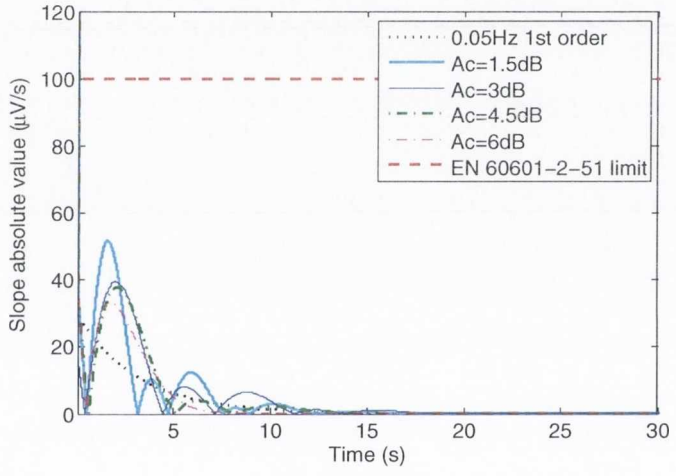


(c) Third order concave

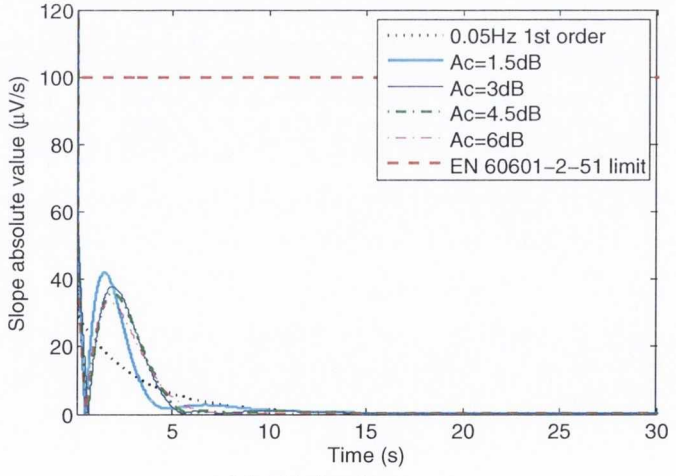
Figure 6.21: Displacement from the isoelectric line occurring after the application of a 3 mV$\times$100 ms rectangular pulse at the input of the second and third order filters derived by maximising the frequency at which different critical attenuations are reached in the transition region.



(a) Second order



(b) Third order



(c) Third order concave

Figure 6.22: Absolute value of the recovery slope occurring after the application of a 3 mV$\times$100 ms rectangular pulse at the input of the second and third order filters derived by maximising the frequency at which different critical attenuations are reached in the transition region.

third order system is substantially identical whether the constraint specifying the concavity of the magnitude response outside the passband is enforced or not.

As regards the second order filter, it can be seen from Figure 6.21(a) that the overshoot occurring in the response to a 3 mV$\times$100 ms rectangular input pulse increases when the critical attenuation gets higher. Conversely, for the third order filters, the ringing present in the pulse response decreases with increasing A_c, as is clearly visible in Figures 6.21(b) and 6.21(c). Furthermore, Figure 6.22 shows that, for all of the filters under study, the maximum absolute value of the recovery slope following the application of the input pulse decreases as the selected critical attenuation is increased.

6.6 Optimisation of the overall low-frequency attenuation

Since the ultimate goal of the highpass filter design is to determine the transfer function providing the best possible rejection of the low-frequency noise and interference associated with the electrocardiographic signal, another approach is investigated for the optimisation procedure. Instead of attempting to maximise a single critical frequency in the transition region of the filter, the overall low-frequency rejection is optimised by minimising the area subtended by the system amplitude response outside the passband. Because a 0.05 Hz single-pole RC network is considered as the reference highpass system for electrocardiographic devices, the improvement in out-of-band rejection of the second and third order filters is quantified as the difference between the area subtended by the amplitude characteristic of this first order network and that of the system being optimised. The area being maximised is illustrated in Figure 6.23. The optimisation algorithm described in Section 6.2.4 is therefore modified so that the objective function is now given by the opposite of the area comprised between the magnitude response of the 0.05 Hz reference network and that of the system under design. The modifications to the constraints adopted in the previous section for the third order systems are maintained, that is, no ripple is allowed in the stopband and the amplitude characteristic is required to be lower than that of the benchmark single-pole filter.

The results obtained through this procedure are reported in Table 6.8 and the frequency and time domain characteristics of the optimised filters are depicted in Figures 6.24 to 6.27. It can be easily verified that the filters satisfy both the magnitude and the pulse response requirements specified in the current European standard for diagnostic electrocardiographs [9] and the AHA recommendations [19]. In Figure 6.24, both the frequency and the amplitude scales are selected to be linear so that the area maximised through the optimisation process can be clearly identified. Once more, it is shown in Figure 6.25 that the phase shift

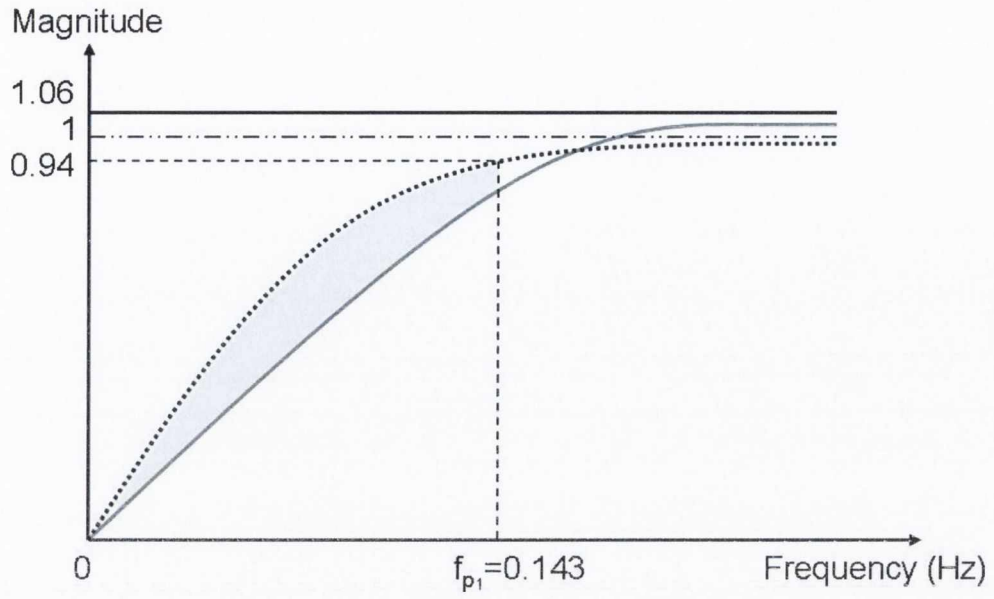


Figure 6.23: Diagram showing the area that is being maximised when the optimisation of the overall low-frequency attenuation is performed.

introduced by the optimised filters over the ECG spectrum is negligible, even though no explicit condition has been specified in the optimisation process.

When the time and frequency domain responses in Figures 6.25, 6.26 and 6.27 are compared with the corresponding plots obtained in the previous section by optimising the 3dB-cutoff point (see Figures 6.19, 6.16 and 6.18 respectively), no significant difference can be identified. The outcomes of the optimisation procedure when the 3dB-cutoff frequency or the overall low-frequency rejection of the filter are maximised thus appear to be quite similar. Let us analyse the data in Table 6.8 with respect to those shown in Table 6.7, where the results of the optimisation aimed at maximising the frequency at which different critical attenuation are reached by the system magnitude response are summarised. It can be noted that the rejection properties of the second order filter determined by minimising the area subtended by the amplitude response lie between those of the systems obtained by optimising the 3dB-cutoff point and the frequency at which A_c = 1.5 dB. Indeed, in the

Table 6.8: Results obtained by maximising the overall rejection of the filter at low frequencies.

Filter type	Area (mHz)	$f_{1.5dB}$ (mHz)	f_{3dB} (mHz)	$f_{4.5dB}$ (mHz)	f_{6dB} (mHz)	f_{20dB} (mHz)	f_{40dB} (mHz)	p (rad/s)	z (rad/s)
2nd order	**8.69**	91.6	66.9	52.2	41.9	7.6	0.8	-1.0709	0
								-0.6219	-1.3918
3rd order	**18.78**	133.5	117.7	50.4	33.5	5.0	0.5	-0.2454	0
								-0.2573 $\pm j$ 0.8306	-0.2169 $\pm j$ 0.7373
3rd order concave	**15.41**	117.3	89.9	64.7	42.8	5.1	0.5	-0.1804	0
								-0.5827 $\pm j$ 0.7005	-0.5303 $\pm j$ 0.4422

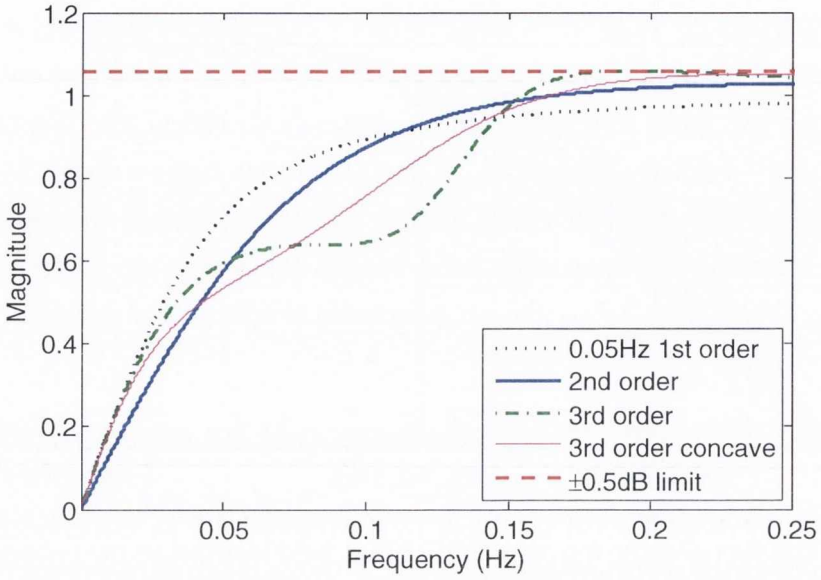


Figure 6.24: Magnitude response of the second and third order filters obtained by maximising the overall low-frequency rejection, shown for linear amplitude and frequency scales.

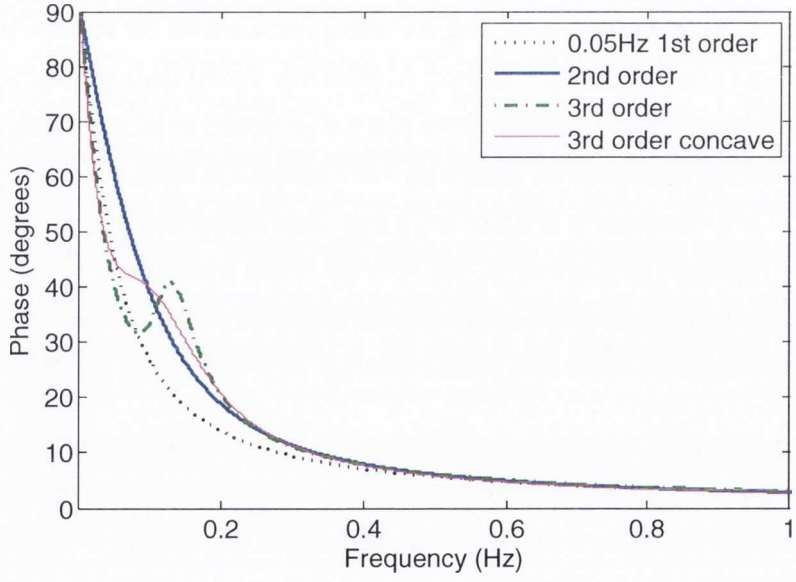
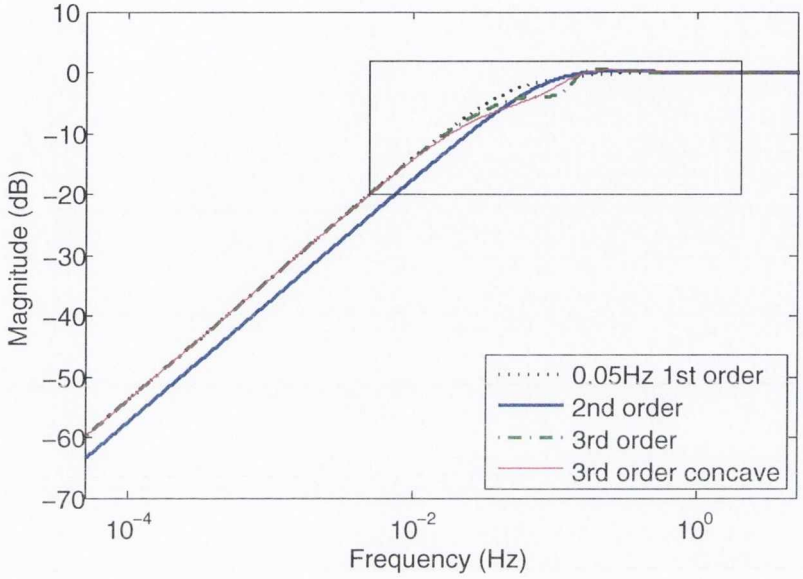
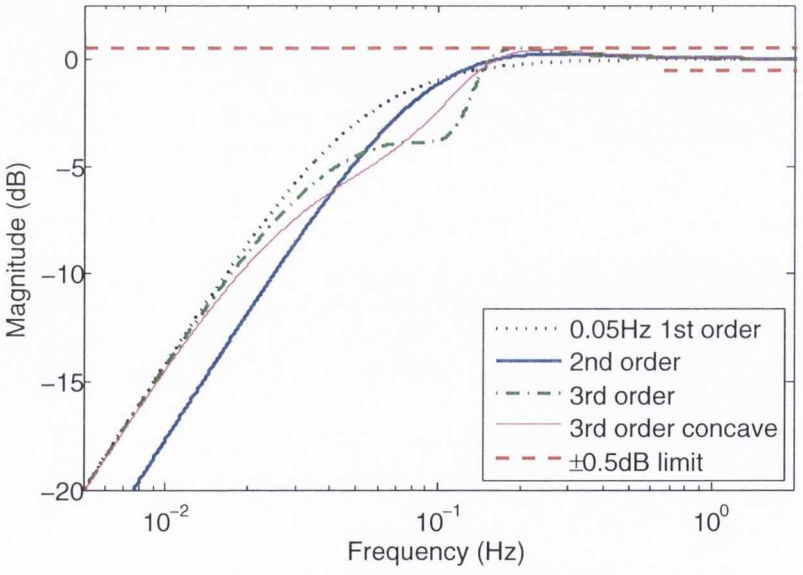


Figure 6.25: Phase response of the second and third order filters derived by maximising the overall low-frequency rejection.



(a)



(b) Detail of the boxed portion of (a).

Figure 6.26: Amplitude characteristic of the second and third order filters obtained by maximising the overall low-frequency rejection.

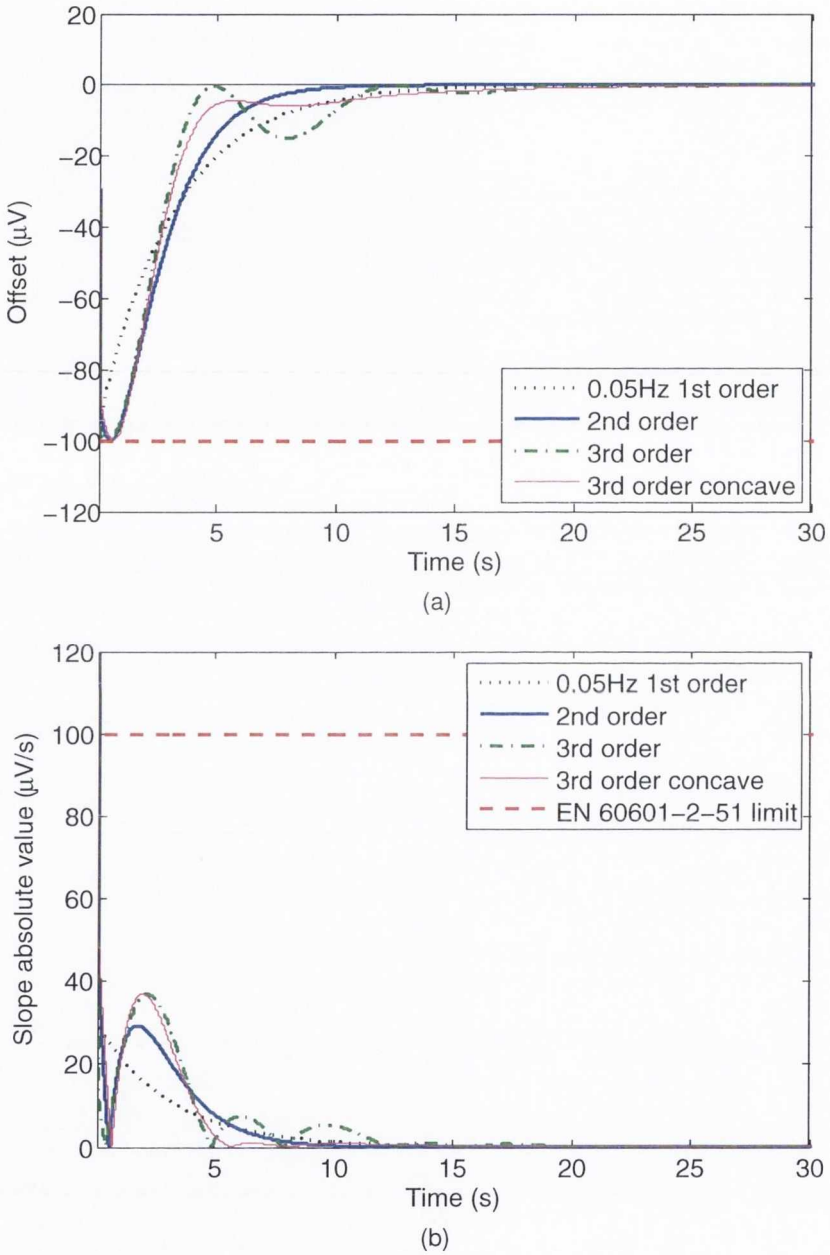


Figure 6.27: (a) Displacement from the isoelectric line and (b) absolute value of the recovery slope after the application of a 3 mV×100 ms rectangular pulse at the input of the second and third order filters obtained by maximising the overall low-frequency rejection.

latter case and when the overall low-frequency rejection is optimised, the poles of the second order filter are real. The magnitude characteristic of the third order filters derived by optimising the area, on the other hand, positions itself between those obtained when the critical attenuation to be maximised is selected as 3 and 4.5 dB. The location of the poles and zeros of the concave filter determined in the present section are actually quite close to those derived by optimising the critical frequency when A_c = 4.5 dB.

6.7 Analysis of the convergence of the optimisation algorithm

The poles and zeros describing the optimised filters reported in the previous sections have been derived from the set of parameters that leads to the best result when the optimisation procedure is repeated for different starting points. In other words, the transfer function that guarantees the highest value for the critical frequency ω_c or the area comprised between the magnitude response of the 0.05 Hz reference network and that of the system under design is selected from among all of the optimisation outcomes obtained using the starting points described in Section 6.2.5. The tables containing the full set of results are reported in Appendix A.3.

From these tables, it can be noticed that the convergence of the optimisation procedure is quite good for the second order filter. The algorithm occasionally leads to a pole-zero cancellation, which eliminates the zero located at 0 Hz and prevents the filter from blocking DC offset voltages (see Tables A.17, A.22 and A.31). The result of the optimisation procedure is sometimes sub-optimal, with this occurrence being particularly common when the 3dB-cutoff point is fixed at 0.05 Hz. As discussed in Section 6.3, for a given stopband attenuation, only two solutions exist in this case, one characterised by complex conjugate poles and the other by real poles. One of them yields a sub-optimal result for the stopband limit.

For the third order filter, the optimisation process converges more often towards local maxima. This situation is particularly common when the maximisation of the 6dB-point is performed, as shown in Tables A.27 and A.30. It should, however, be noted that, in this case, most of the sub-optimal maxima are quite close to the best result obtained through the optimisation. It is essential to point out that there are occurrences in which the algorithm does not reach any feasible solution for the third order system. These cases manifest themselves especially when the selected minimum stopband attenuation is high, as is evident by comparing Tables A.6 to A.8 and Tables A.14 to A.16. It also occurs when the magnitude response is required to be concave over the stopband and the transition region

(see, for example, Tables A.32 and A.33). Furthermore, in a significant number of cases, the optimisation procedure fails to converge when the critical frequency for which A_c = 1.5 dB is maximised, as illustrated in Tables A.25 and A.28.

The poor convergence of the optimisation algorithm for the third order filter is probably due to the presence of numerous constraints and to the fact that, since the algorithm is gradient-based and the intermediate solutions are not requested to be located inside the solution space, the optimisation process might get stuck at a point from which it is impossible to find a solution that satisfies all the constraints. It is also worth noting that, when the 3dB-point or the overall low-frequency rejection of the third order filter are optimised, none of the starting points given by the parameters of the Butterworth, Chebyshev and Elliptic filters are located inside the solution space. The condition that requires the magnitude response of the third order system to be lower than that of that the 0.05 Hz single-pole reference network over the stopband and the transition region is, indeed, not fulfilled by these classic filters.

Besides attempting to find starting points located inside the solution space, the convergence problem might be solved by using a genetic algorithm instead of a gradient-based algorithm for the optimisation procedure, as proposed by Aggarwal et al. [168]. Genetic algorithms, in fact, incorporate an element of randomness which allows them to determine the global optimum solution for most problems [173]. If the optimisation of filters of order higher than 3 is to be attempted, the author suggests that a genetic algorithm or another stochastic search optimisation method is employed. It should however be noted that, even when such an algorithm is used, pole-zero cancellations may still occur and as a consequence the order of the filter may be lowered or the zero located at 0 Hz eliminated.

6.8 Conclusion

The goal of this chapter consisted in determining the transfer function of an analogue highpass filter providing a greater out-of-band rejection than the 0.05 Hz single-pole system usually employed in electrocardiographic applications, and yet not introducing significant distortions in the ECG signal. Attention was concentrated on second and third order filters, which are characterised by a low implementation complexity and can thus be integrated into the front-end of the measurement system.

An optimisation technique aimed at maximising the low-frequency rejection of the filters under design and based directly on the requirements set by the EN 60601-2-51:2003 European standard [9] and the 1990 AHA report [19] has been developed by the author. After selecting the design parameters for the second and third order systems, the objective func-

tion has been defined as the frequency at which a set attenuation is reached by the filter magnitude response in the stopband or in the transition region. The requirements given by the European standard and the AHA recommendations have been rewritten as constraints for the optimisation procedure and further conditions have been specified on the magnitude response of the third order filter. These constraints limit the amplitude of the ripples that may occur in the stopband and in the passband and require the magnitude characteristic to be monotonically increasing in the transition region. Finally, the algorithm employed by the MATLAB® function used to performed the optimisation has been briefly presented and the selection of the starting points for the maximisation process has been discussed.

Initially, the optimisation procedure has been applied to second and third order filters having a 3dB-cutoff frequency of 0.05 Hz. Their stopband limit has been maximised for different levels of minimum stopband attenuation, consistently obtaining a low-frequency rejection higher than that of the reference 0.05 Hz single-pole network. Even when the condition imposed on the overshoot occurring in the response to a 3 mV$\times$100 ms rectangular pulse at the input of the system was tightened, the 0.05 Hz second and third order filters still attained a larger attenuation in the stopband and the transition region than their first order counterparts.

Given the positive outcome of the optimisation procedure aiming at maximising the stopband limit of the 0.05 Hz filters, it was decided to explore the effect of eliminating the constraint placed on the system 3dB-cutoff frequency. The filters thus derived are characterised by a stopband limit approximately 2 or 3 times higher than that previously obtained when the 3dB-point was fixed at 0.05 Hz. On the other hand, their 3dB-cutoff frequencies are also reduced and for the third order system is almost equal to half the original value when the minimum allowable stopband attenuation is selected as 40 or 60 dB.

Since the second and third order systems derived by maximising the stopband limit present a detrimental reduction of the 3dB-cutoff frequency when compared to the reference 0.05 Hz network, the possibility of optimising the filter 3dB-point has been investigated. The second order system obtained through this optimisation procedure is characterised by an attenuation larger than that of the single-pole network throughout the stopband and the transition region. The filter 3dB-point is equal to approximately 0.07 Hz and the rejection achieved at low frequencies is approximately 5 dB higher than that of the reference response.

In order to successfully maximise the 3dB-cutoff frequency of the third order filter, it was necessary to modify the constraints imposed during the optimisation procedure. In fact, if the amplitude characteristic of the third order system is not required to be below that of the 0.05 Hz single-pole filter outside the passband, its response tends to be flat over most of the transition region, yielding an attenuation of between 4 and 5 dB for frequencies as

low as 5 mHz. After adjusting the optimisation constraints, it was possible to determine the transfer function of a third order filter characterised by a 3dB-cutoff frequency of 0.12 Hz and having better rejection than a 0.05 Hz single-pole network throughout the stopband and the transition region. The optimisation procedure was then further modified so that the filter magnitude response is not only requested to be monotonically increasing outside the passband, but it is concave over the same interval. In this case, the 3dB-cutoff frequency of the optimised filter is equal to 0.09 Hz, that is approximately 25% lower than when the concavity condition is not imposed. Since the magnitude response of the first type of filter tends to level out at frequencies immediately lower than the 3dB-point, the concave filter may be preferred because of the larger steepness of its amplitude characteristic in the cutoff region. Moreover, even though the response of both filters to a 3 mV$\times$100 ms rectangular input pulse does not present a positive overshoot, the ringing is much smaller when the concavity condition is imposed.

Finally, the optimisation procedure was further modified so that the overall rejection at low frequencies is maximised. The attenuation achieved by the filter has been quantified in terms of the area subtended by the magnitude response curve outside the passband. The results obtained for this type of optimisation have been compared with those derived by maximising the frequency at which selected critical attenuations (1.5, 3, 4.5 and 6 dB) are achieved by the system magnitude response in the transition region. For the second order system, the outcome is quite similar to when the frequency at which the attenuation is 1.5 dB is optimised and the transfer function is characterised by real poles. The results obtained when the overall low-frequency rejection of the third order filters is optimised lie between those achieved when the critical attenuation is selected as 3 and 4.5 dB and complex conjugate pairs of poles and zeros are present in the transfer function.

Some important general conclusions can be drawn from the different types of optimisation performed. It emerges that the constraints imposed on the passband ripple and on the undershoot occurring after the application of a 3 mV$\times$100 ms rectangular input pulse are the decisive factors in the optimisation procedure and that these conditions are tightly matched for practically all of the optimised filters. Moreover, even though no specific constraint has been defined for the phase response of the system under design, the phase shift introduced by the optimised filters over the ECG spectrum is negligible and it does not significantly differ from that of the reference 0.05 Hz single-pole network. It should also be pointed out that the slope of the magnitude response of the optimised filter appears to be limited to 20 dB/decade at very low frequencies.

In this chapter, it has been shown that it is possible to design analogue highpass filters of order higher than unity that comply with international standards for diagnostic ECG monitoring applications and have better rejection properties than the 0.05 Hz single-pole system

traditionally used in the front-end of electrocardiographic equipment. When the frequency of the 3dB-point is maximised, a second order filter having a cutoff approximately 35% higher than that of the reference first order system is obtained. The 3dB-cutoff frequency of the third order filter can be as large as 2.5 times that of the benchmark network, even when its magnitude response is required to be lower than that of the reference first order system outside the passband.

Chapter 7

Validation of the highpass filter design

7.1 Introduction

In the previous chapter, second and third order highpass filters that satisfy the magnitude and pulse response requirements defined by the EN 60601-2-51:2003 European standard for recording and analysing electrocardiographs [9] and the 1990 AHA recommendations [19] were designed through an optimisation procedure. The principal aim of this chapter is to verify that the distortion introduced into the ECG signal by these filters is negligible and that they can be confidently employed at the front-end of diagnostic electrocardiographic equipment to improve the rejection of low-frequency artifacts and interference. The criteria for evaluating the distortion produced by the second and third order optimised filters are, once more, derived from the AHA recommendations and the European standard. In fact, besides specifying the frequency and pulse response requirements of the electrocardiographic filter, the 1990 AHA recommendations also establish the maximum error allowable for ECG recordings. If the electrocardiographic measurement system does not have analysing capabilities and it simply acquires the electrocardiogram to be subsequently examined by a cardiologist, the maximum deviation of the output signal from the input one at any point on the signal profile should not be larger than 25 μV or 5%, whichever is greater. A similar condition is included in the European standard for diagnostic electrocardiographic devices as well. The alternative method for testing the filter response described in Section 3.6 requires that, when a set of input calibration ECGs is employed, the output peak amplitude of R and S waves does not differ by more than 5% from the input value and the amplitude error occurring in the central portion of the ST segment does not exceed 25 μV. It is worthwhile noting that for biphasic QRS complexes the amplitude of the calibration waveforms lies between $\pm$2000 μV. The standard also states that, given the input calibration ECGs, the slope of the ST segment of the output signal shall be less that 50 μV/s.

The calibration waveforms described in the EN 60601-2-51:2003 standard thus appear to be the ideal test signals to assess the distortion generated by the second and third order highpass filters. Unfortunately, as outlined earlier in Section 3.6, a full mathematical description of such calibration ECGs is not available in the literature. Test signals characterised by the same amplitude and duration features of the calibration waveforms are therefore synthesised by the author to evaluate the distortion introduced by the optimised filters. To get a more thorough insight into the filters' performance, the amplitude error and the change in the ST segment slope produced by the highpass filters are then quantified on actual ECG recordings available on PhysioNet [174].

The ability of the optimised filters to reduce the low-frequency noise and interference present in electrocardiographic records is also evaluated, so that it can be established which system provides the best trade-off between noise reduction and time domain distortion. The power contained in ECG recordings at frequencies lower than 0.5 Hz can be considered to be out-of-band disturbance, because, as discussed in Section 2.3.3, 0.5 Hz would be the lowest frequency component of the ECG signal when the heart rate is equal to the extremely low value of 30 beats per minute. The reduction in low-frequency power achieved when the second and third order highpass filters are applied to records contained in the PhysioNet databases is measured. The performance of the different optimised filters is assessed by comparing these results with each other and to the noise reduction obtained for the reference 0.05 Hz single-pole system.

The filters selected for the analyses performed in this chapter are those derived by maximising the 3dB-cutoff frequency, the parameters of which are reported in Tables 6.5 and 6.6. As previously discussed in Section 6.6, the time and frequency domain responses of these systems are quite similar to those of the filters obtained by optimising the overall low-frequency attenuation. It should, however, be noted that, whereas the filters determined by maximising the frequency of the 3dB-point are characterised by a pair of complex conjugate poles, the transfer function of the second order filter derived through the optimisation of the low-frequency rejection contains two real poles. This real-pole system can be implemented using only passive components, which can be advantageous in low-power ambulatory applications, and it might even be possible to integrate it directly into a front-end instrumentation amplifier that has a second order transfer characteristic [57]. Therefore, the performance of the second order filter obtained by optimising the overall low-frequency rejection and described by the poles and zeros in Table 6.8 is also assessed.

7.2 Distortion analysis for synthetic ECGs

7.2.1 Input test signals

In order to evaluate the time-domain distortion produced by the optimised highpass filters, test ECG signals resembling as closely as possible the calibration waveforms described in the EN 60601-2-51:2003 European standard [9] are synthesised. Even though a full mathematical description of the calibration ECGs is not available, it is known that these signals are constructed piecewise from first and second degree polynomials and sinusoidal functions. The P and T waves of the synthetic signals are, therefore, simulated by sinusoids and the QRS complex is modelled, in the first instance, by a triangular wave. This approach was previously employed by Tabakov et al. [70] to generate test signals having properties similar to the standard calibration waveforms. Moreover, one of the test ECG waves specified by the EN 60601-2-27:2006 European standard for electrocardiographic monitoring equipment [62] is also characterised by a triangular QRS complex and by a sinusoidal T wave.

Another issue regarding the construction of the input test signals emerges from Table 3.5 in Chapter 3, where the properties of the calibration ECGs are summarised. Whereas the duration of the QT segment is provided, the duration of the ST segment or, conversely, that of the T wave is not specified. Since according to the European standard the error introduced by the electrocardiographic filter into the amplitude of the ST segment of the calibration waveforms should be measured between 20 and 80 ms after the end of the QRS complex, it is safe to assume that the length of the ST segment in the calibration ECGs should be at least 80 ms. Moreover, if the portion defined for the measurement of the error is interpreted to be symmetrical around the centre of the ST segment, the total duration of the ST segment would be equal to 100 ms. Based on these considerations, the duration of the ST segment is set to 80 ms for the test waveform corresponding to CAL20002 which is characterised by a high heart rate (120 bpm) and to 100 ms for all the other signals. Given this selection, the duration of the T wave is equal to approximately 200 ms for all waveforms, with the exception of CAL20002 for which the T wave lasts about 150 ms. That is, the duration of T wave is approximately twice that of the ST segment in all of the synthetic ECGs.

The test waveform obtained using the above methodology from the CAL20000 parameters is illustrated in Figure 7.1, while the synthetic ECGs derived for the other calibration signals are presented in Appendix B.1. Comparing these test waveforms with the calibration ECGs shown in Figure 3.16, the marked difference in the shape of the QRS complex is evident. In order for the calibration signals to be reproduced more accurately, another set of test waveforms is created by modelling the QRS complex as a sinusoid. An example

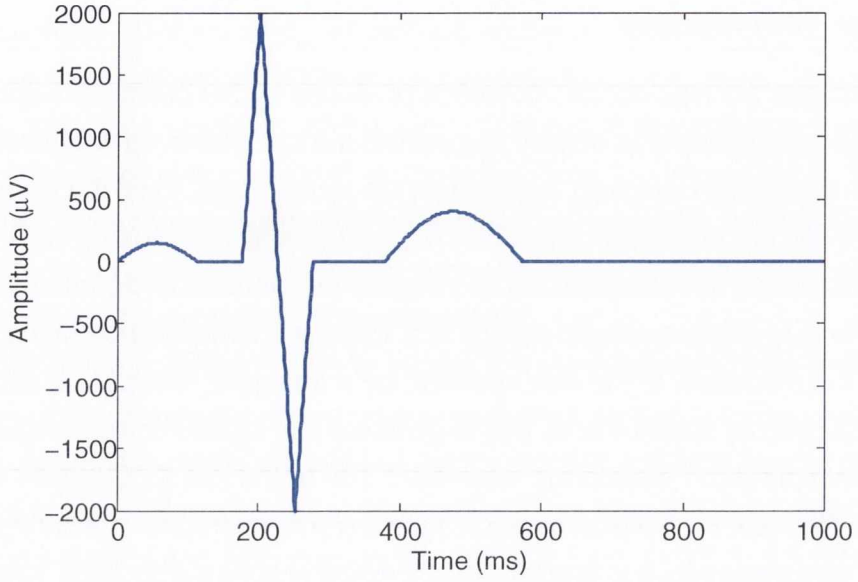


Figure 7.1: Test waveform obtained from the parameters of the CAL20000 signal when the QRS complex is modelled by a triangular wave.

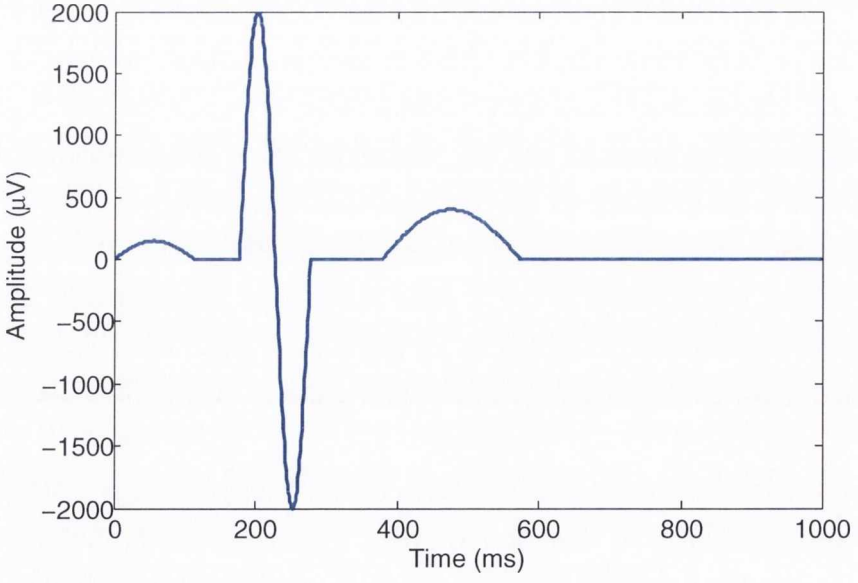


Figure 7.2: Test waveform obtained from the parameters of the CAL20000 signal when the QRS complex is modelled by a sinusoidal wave.

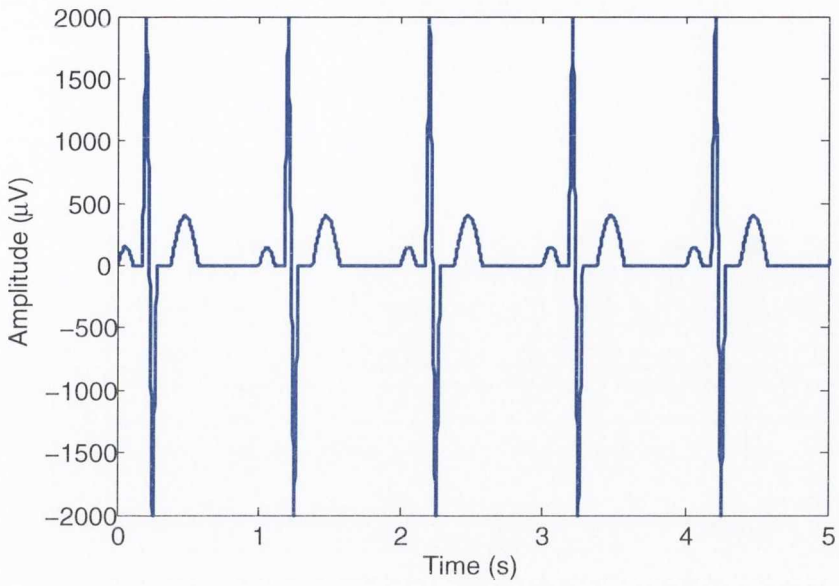


Figure 7.3: Synthetic electrocardiographic signal obtained by periodising at a heart rate of 60 bpm the test ECG derived from the parameters of the CAL20000 waveform when the QRS complex is modelled by a triangular wave (see Figure 7.1).

of this second type of synthetic electrocardiographic waveforms is shown in Figure 7.2 for the CAL20000 parameters. The test signals used to analyse the distortion produced by the highpass filters are then simply generated by periodising the synthetic ECGs, each one according to the heart rate of the corresponding calibration waveform, as illustrated in Figure 7.3.

7.2.2 Results and discussion

As shown in Table 7.1, the second and third order highpass filters obtained through the optimisation procedure are characterised by large settling times, which lead to prolonged initial transients in the output signals. In order for the distortion introduced by the highpass filters to be evaluated correctly, it is essential that the output signal is measured after the

Table 7.1: Settling times of the second and third order filters obtained through the optimisation procedure and of the reference 0.05 Hz single-pole network.

Filter type	1% settling time (s)
0.05 Hz 1st order	14.7
2nd order real-pole	8.3
2nd order (3dB max)	6.0
3rd order (3dB max)	16.4
3rd order concave	20.9

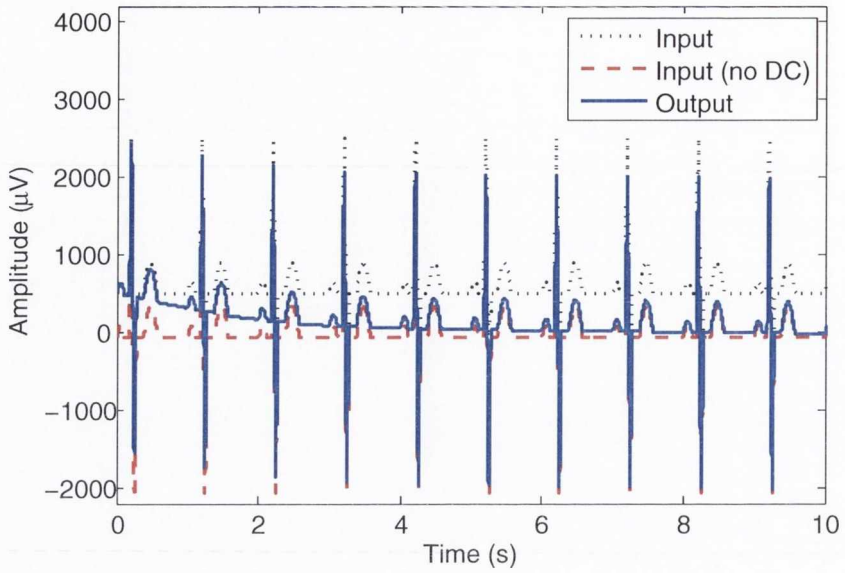


Figure 7.4: Initial transient occurring when the third order concave filter is applied to the signal generated by adding a 500 μV DC offset to the synthetic test signal derived from the CAL20000 waveform shown in Figure 7.3.

end of this transient and that its value is compared to that of the input signal after any DC offset is eliminated. It can, in fact, clearly be seen from Figure 7.4 that the output signal converges to the signal obtained by removing the DC offset from the input recording. For the purpose of representation, a large voltage offset is simulated by adding 500 μV to the synthetic input signal, making the transient more visible.

The distortion produced by the second and third order highpass filters and by the 0.05 Hz single-pole network is assessed for each of the test signals generated from the parameters of the calibration waveforms when the QRS complex is simulated using both a triangular and a sinusoidal wave. For each synthetic input signal, the average and maximum absolute error caused by the filters, the location of the maximum error and the average and maximum slope of the ST segment are evaluated over a single complete ECG waveform cycle, selected from the output signal after the termination of the initial transient. An example of the error introduced into the synthetic ECG wave is shown in Figure 7.5 for the CAL20000-derived test signal filtered using the third order concave system. In this case, the maximum error is slightly larger than 10 μV and it affects the QRS complex. From Figure 7.5, it can also be noticed that the third order concave filter introduces a positive slope in the ST segment. The average slope, calculated as the slope of the line passing through the first and last point of the ST segment, and the maximum slope, selected from the derivative of the output signal evaluated over the ST segment, are both approximately equal to 20 μV/s in this instance.

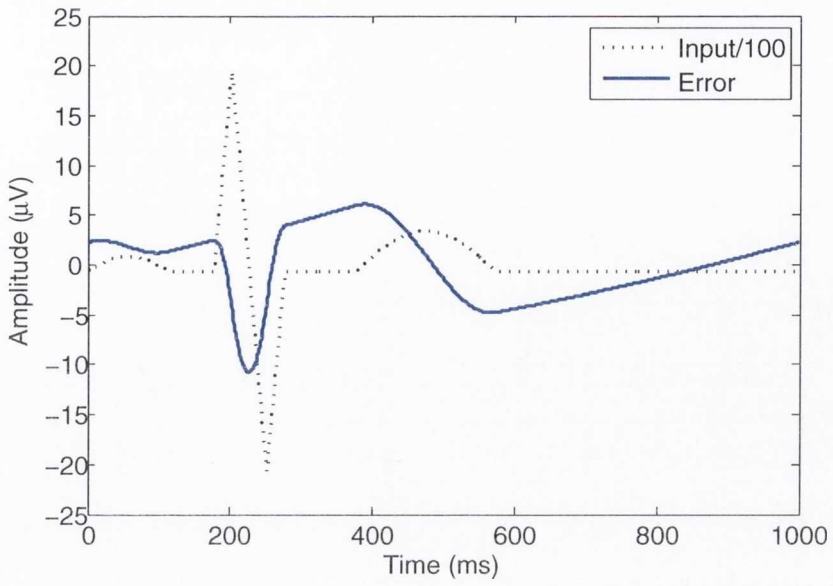


Figure 7.5: Error introduced by the third order concave filter into the test signal derived from the CAL20000 parameters. The scaled version of the input signal allows the correspondence between the error and the constituent waves and intervals of the ECG waveform to be illustrated.

The error and the ST segment slope measured when the optimised filters are applied to the synthetic ECG signals are presented in Tables 7.2 and 7.3, for triangular and sinusoidal QRS complex, respectively. It can be seen that the average error is lower than 10 μV for all of the output records and that the highest values are measured for the test signals derived from the CAL20160 waveform. Furthermore, the maximum error is in all cases well below the 25 μV limit specified in the 1990 AHA recommendations [19]. The highest readings are again associated with the synthetic ECG generated from the CAL20160 parameters. The test signal resembling the CAL20002 waveform is also accompanied by high measurements for the maximum error when the QRS complex is generated using a sinusoidal waveform. Overall, by comparing Tables 7.2 and 7.3, it appears that both the average and the maximum error are higher for the test signals that have a sinusoidal QRS complex. As regards the location of the maximum error, for most of the output signals the largest deviation from the input waveform is registered within the QRS complex. However, when the CAL20200 parameters are used to generate the input signal, the maximum error is recorded at the end of the ST segment or at the beginning of the T wave. Moreover, for the signal derived from the CAL20500 parameters mimicking a narrow QRS complex, the largest deviation between the input and output waveforms occurs at the end of the T wave.

If the results for the ST segment slope are analysed, it is clearly evident that the difference between the average and the maximum instantaneous value is very limited. It is worthwhile noting that, except for the test signals synthesised from the CAL20110 param-

Table 7.2: Distortion introduced by the second and third order highpass filters and by the 0.05 Hz single-pole network into the test signals obtained from the parameters of the calibration waveforms when the QRS complex is modelled as a triangular wave.

Filter type	Error (25 µV limit)		Location max error	Slope ST segment (50 µV/s limit)	
	avg (µV)	max (µV)		avg (µV/s)	max (µV/s)
			CAL20002		
0.05 Hz 1st order	3.3	13.5	QRS complex	27.7	28.0
2nd order real-pole	3.1	13.2	QRS complex	30.8	31.0
2nd order (3dB max)	3.0	12.5	QRS complex	29.5	29.9
3rd order (3dB max)	3.4	14.1	QRS complex	31.1	31.2
3rd order concave	2.9	12.2	QRS complex	29.3	29.8
			CAL20000		
0.05 Hz 1st order	3.3	12.1	QRS complex	17.4	17.7
2nd order real-pole	3.2	11.6	QRS complex	21.1	21.1
2nd order (3dB max)	3.0	11.0	QRS complex	20.4	20.6
3rd order (3dB max)	3.4	12.5	QRS complex	20.8	20.8
3rd order concave	3.0	10.8	QRS complex	20.5	20.7
			CAL20200		
0.05 Hz 1st order	4.9	12.3	beginning ST segment	-2.2	-2.3
2nd order real-pole	4.8	11.9	beginning T wave	7.9	8.8
2nd order (3dB max)	4.6	11.3	beginning T wave	8.5	9.2
3rd order (3dB max)	5.1	12.6	beginning T wave	4.0	4.3
3rd order concave	4.5	11.1	beginning T wave	9.5	10.3
			CAL20100		
0.05 Hz 1st order	5.3	10.5	QRS complex	37.8	38.4
2nd order real-pole	5.1	11.2	QRS complex	32.2	33.4
2nd order (3dB max)	4.8	10.7	QRS complex	30.4	31.6
3rd order (3dB max)	5.4	11.5	QRS complex	36.8	37.2
3rd order concave	4.7	10.6	QRS complex	29.3	30.7
			CAL20110		
0.05 Hz 1st order	3.8	8.7	QRS complex	**90.5**	**92.0**
2nd order real-pole	3.7	7.7	QRS complex	**83.0**	**85.4**
2nd order (3dB max)	3.5	7.2	QRS complex	**78.3**	**80.9**
3rd order (3dB max)	4.0	8.5	QRS complex	**91.2**	**92.0**
3rd order concave	3.5	7.0	QRS complex	**76.2**	**79.2**
			CAL20160		
0.05 Hz 1st order	7.0	14.0	QRS complex	-16.1	-16.3
2nd order real-pole	6.8	14.8	QRS complex	-19.9	-20.0
2nd order (3dB max)	6.4	14.2	QRS complex	-18.8	-19.0
3rd order (3dB max)	7.2	15.3	QRS complex	-18.8	-18.9
3rd order concave	6.3	14.0	QRS complex	-18.9	-19.2
			CAL20500		
0.05 Hz 1st order	3.1	6.6	end T wave	17.8	18.0
2nd order real-pole	3.0	6.1	end T wave	20.1	20.3
2nd order (3dB max)	2.9	5.7	end T wave	19.5	19.8
3rd order (3dB max)	3.2	6.6	end T wave	20.4	20.5
3rd order concave	2.8	5.6	end T wave	19.5	19.8

Table 7.3: Distortion introduced by the second and third order highpass filters and by the 0.05 Hz single-pole network into the test signals obtained from the parameters of the calibration waveforms when the QRS complex is modelled as a sinusoid.

Filter type	Error (25 μV limit)		Location max error	Slope ST segment (50 μV/s limit)	
	avg (μV)	max (μV)		avg (μV/s)	max (μV/s)
			CAL20002		
0.05 Hz 1st order	3.7	17.4	QRS complex	27.5	27.9
2nd order real-pole	3.5	16.9	QRS complex	31.1	31.3
2nd order (3dB max)	3.3	16.0	QRS complex	29.8	30.2
3rd order (3dB max)	3.8	18.0	QRS complex	31.2	31.3
3rd order concave	3.2	15.7	QRS complex	29.7	30.1
			CAL20000		
0.05 Hz 1st order	3.5	16.1	QRS complex	17.4	17.6
2nd order real-pole	3.4	15.5	QRS complex	21.3	21.4
2nd order (3dB max)	3.2	14.7	QRS complex	20.7	20.8
3rd order (3dB max)	3.6	16.7	QRS complex	20.8	20.9
3rd order concave	3.1	14.4	QRS complex	20.8	21.0
			CAL20200		
0.05 Hz 1st order	5.8	14.7	beginning ST segment	-7.7	-7.8
2nd order real-pole	5.7	13.6	beginning T wave	4.6	5.8
2nd order (3dB max)	5.4	12.8	beginning T wave	5.5	6.5
3rd order (3dB max)	6.0	14.5	beginning ST segment	-0.5	-0.8
3rd order concave	5.3	12.6	beginning T wave	6.8	7.9
			CAL20100		
0.05 Hz 1st order	6.4	12.7	QRS complex	43.2	43.9
2nd order real-pole	6.2	13.5	QRS complex	35.5	37.0
2nd order (3dB max)	5.8	12.9	QRS complex	33.4	34.9
3rd order (3dB max)	6.6	13.9	QRS complex	41.3	41.8
3rd order concave	5.7	12.8	QRS complex	32.0	33.6
			CAL20110		
0.05 Hz 1st order	4.7	11.1	QRS complex	**96.2**	**97.7**
2nd order real-pole	4.6	9.7	QRS complex	**86.4**	**89.1**
2nd order (3dB max)	4.4	9.2	QRS complex	**81.3**	**84.2**
3rd order (3dB max)	4.9	10.8	QRS complex	**95.8**	**96.7**
3rd order concave	4.3	9.1	QRS complex	**79.0**	**82.2**
			CAL20160		
0.05 Hz 1st order	8.0	16.1	QRS complex	-10.9	-11.0
2nd order real-pole	7.8	17.1	QRS complex	-16.8	-17.0
2nd order (3dB max)	7.4	16.3	QRS complex	-16.0	-16.0
3rd order (3dB max)	8.3	17.6	QRS complex	-14.5	-14.5
3rd order concave	7.2	16.2	QRS complex	-16.3	-16.3
			CAL20500		
0.05 Hz 1st order	3.1	6.6	end T wave	17.7	18.0
2nd order real-pole	3.0	6.1	end T wave	20.1	20.3
2nd order (3dB max)	2.9	5.7	end T wave	19.5	19.8
3rd order (3dB max)	3.2	6.6	end T wave	20.5	20.5
3rd order concave	2.8	5.5	end T wave	19.5	19.8

Table 7.4: Average distortion introduced by the second and third order highpass filters and by the 0.05 Hz single-pole network into the synthetic test signals.

	0.05 Hz 1st order	2nd order real-pole	2nd order (3dB max)	3rd order (3dB max)	3rd order concave
Triangular QRS complex					
avg error (μV)	4.4	4.3	4.0	4.5	3.9
% diff. with 0.05 Hz 1st order		-2.5	-8.0	3.4	-9.7
max error (μV)	11.1	10.9	10.4	11.6	10.2
% diff. with 0.05 Hz 1st order		-1.6	-6.7	4.4	-8.4
deviation avg slope ST seg. (μV/s)	29.9	30.7	29.4	31.9	29.0
% diff. with 0.05 Hz 1st order		2.6	-1.9	6.5	-3.0
Sinusoidal QRS complex					
avg error (μV)	5.0	4.9	4.6	5.2	4.5
% diff. with 0.05 Hz 1st order		-2.5	-8.0	3.4	-9.8
max error (μV)	13.5	13.2	12.5	14.0	12.3
% diff. with 0.05 Hz 1st order		-2.4	-7.4	3.8	-8.8
deviation avg slope ST seg. (μV/s)	31.5	30.8	29.5	32.1	29.2
% diff. with 0.05 Hz 1st order		-2.2	-6.5	1.8	-7.4

eters, the slope is lower than the 50 μV/s limit specified by the EN 60601-2-51:2003 European standard for the calibration waveforms. The large slope measured for the CAL20110-derived signal is most likely due to the ST segment depression characterising this synthetic ECG, as shown in Figure B.2(b). On the other hand, it should be pointed out that, even though the ST segment of the output signal is generally positive, the slope measured for the test ECGs constructed from the CAL20160 waveform, which possess an elevated ST segment (see Figure B.2(c)), is always negative. Ultimately, the highpass filters seem to introduce a negative change in slope when the ST segment is elevated and a positive change when the ST segment is either at the baseline level or depressed. Moreover, the extent of this positive change is greater when the ST segment is depressed.

Looking at Tables 7.2 and 7.3, all of the highpass filters appear to introduce approximately the same amount of distortion into the input test signals. In order to estimate the difference in performance between the optimised filters and the 0.05 Hz first order system, the results in Tables 7.2 and 7.3 are averaged across the test signals for each of the highpass filters. The outcome of this procedure is presented in Table 7.4. It can be seen, once more, that the distortion produced by the various highpass filters is not substantially different and that larger errors and changes in the ST segment slope are generated when the test signal is characterised by a sinusoidal QRS complex. It is important to notice that,

independently of the shape of the QRS complex, the error introduced by the the second order and the third order concave filters is approximately 7% to 10% lower than that of the reference single-pole network. For these two filters the deviation of the average ST segment slope from zero is also less than that produced by the 0.05 Hz first-order system. It should also be pointed out that the overall performance of the third order concave system appears to be marginally better than that of the second order filter. On the other hand, the third order filter obtained without specifying the concavity condition seems to consistently introduce the largest distortion into the test signals and both the error and the change in the ST segment slope produced by this highpass system are slightly worse than those of the reference single-pole network. As regards the second order filter characterised by real poles, it can be seen from Table 7.4 that both the average and maximum error it generates are marginally smaller than those of the reference 0.05 Hz network, whereas the changes in slope produced by these two filters are practically identical.

7.3 Distortion analysis for real ECGs

Signals from the QT database [175], available on PhysioNet [174], are selected for the analysis of the distortion caused by the optimised filters in actual ECG recordings. The main feature of this database is that its records are annotated, i.e. the waves and intervals of the ECG waveform have been manually identified and indicated by cardiologists. The QT database contains 105 two-channel records, each 15 minutes long. These records are excerpts from ambulatory ECG signals contained in other PhysioNet databases and a wide variety of morphologies for the QRS complex, T wave and ST segment are represented. For each record, between 30 and 100 normal beats are annotated. Since the slope of the ST segment is fundamental in determining the distortion introduced by the highpass filter, only the 42 records for which both the end of the QRS complex and the beginning of the T wave are identified are used to verify the performance of the optimised filters.

7.3.1 Preprocessing of the ECG records

Even though all of the records included in the QT database were selected by its investigators so that they do not contain significant baseline wander or other artifacts, being ambulatory ECG recordings, they may still present residual noise and interference at low frequencies. Since the current aim is to evaluate the distortion introduced into the signal and not the noise reduction achieved by the highpass filters, it is necessary to preprocess the ECG signals to eliminate as much of the low-frequency disturbance as possible. Bidirectional filters, previously discussed in Sections 3.5.3 and 5.3, provide a simple way of performing

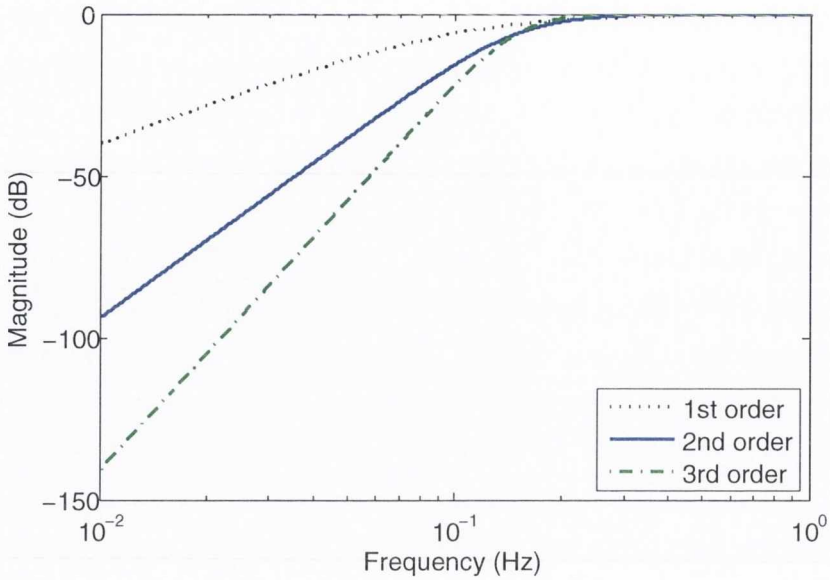


Figure 7.6: Magnitude characteristic of the highpass bidirectional filters derived from a 0.1 Hz single-pole network and from second and third order 0.15 Hz Butterworth filters.

this operation on offline recordings. In order for the preprocessing to preserve the integrity of the records of the QT database, the bidirectional filter should satisfy the requirements specified in Section 5.2 for the electrocardiographic highpass filter.

If a first order base network is used to derive the bidirectional filter, the frequency of its 3dB-point should be at most equal to 0.1 Hz for the bidirectional system to adhere to the specifications set by the EN 60601-2-51:2003 European standard [9] for the response to a 3 mV$\times$100 ms rectangular input pulse. In order to achieve a larger low-frequency rejection, a higher order base filter needs to be selected. Butterworth filters can, for example, be employed for this purpose. Due to their amplitude response being flat over the passband, Butterworth filters provide a reduction of the unwanted frequency content without altering the components of the input signal at any other frequency. Second and third order highpass Butterworth filters having a 3dB-cutoff frequency of 0.15 Hz can be used to derive bidirectional systems that fulfil the time domain specifications of the European standard. The amplitude response of these bidirectional filters and that of the system obtained from the 0.1 Hz first order highpass network are shown in Figure 7.6. Their responses to a 3 mV$\times$100 ms rectangular wave are illustrated in Figure 7.7, where it can be seen that the slope of the output signal after the termination of the input pulse is well within the limits specified by the EN 60601-2-51:2003 standard, whereas the maximum offset is very close to the 100 µV bound.

In order to select the preprocessing filter for the records in the QT database, the ability of these three bidirectional systems to reduce low-frequency noise and interference is eval-

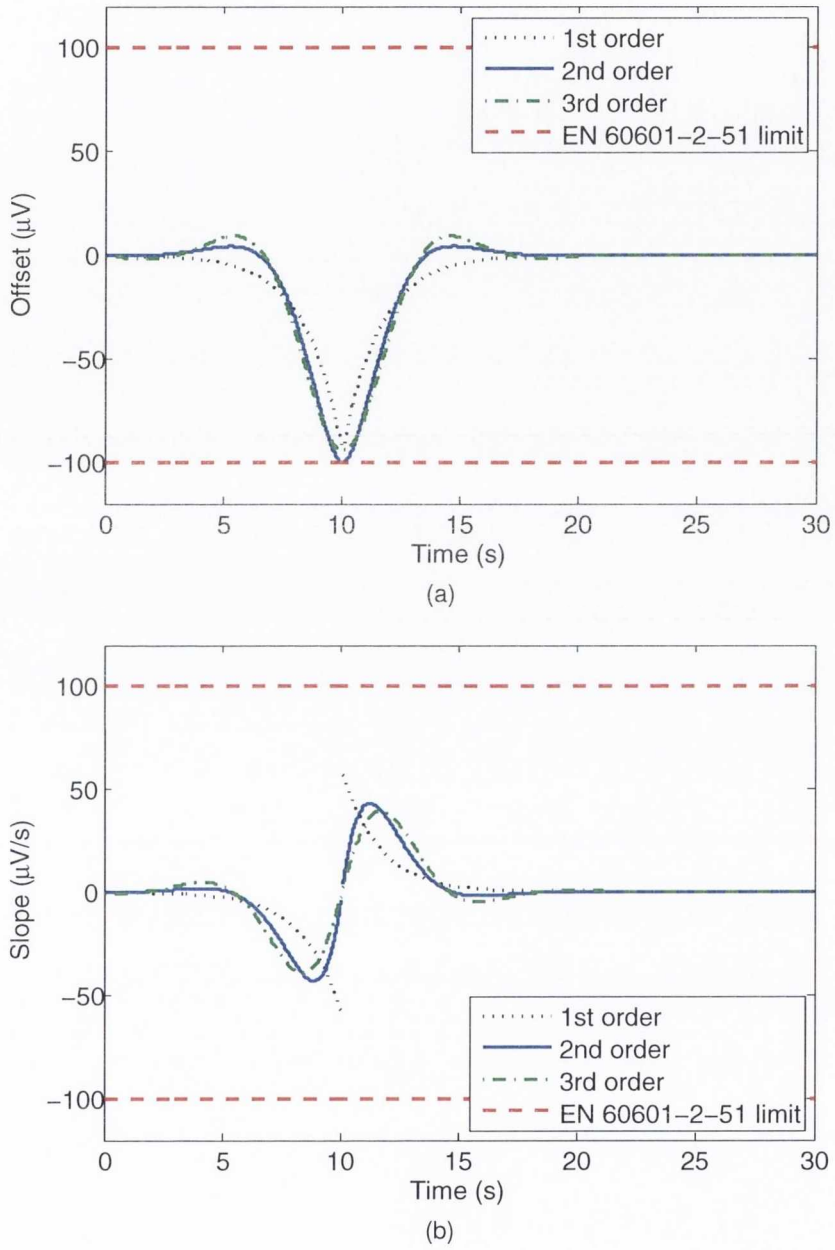


Figure 7.7: (a) Displacement from the isoelectric line and (b) slope of the response of the highpass bidirectional filters derived from a 0.1 Hz single-pole network and from second and third order 0.15 Hz Butterworth filters to a 3 mV×100 ms rectangular input pulse applied at t = 10 s. The dashed lines represent the bounds established by the European standard for diagnostic electrocardiographic devices.

uated. A two-lead record containing mainly baseline wander (bw) available on PhysioNet in the MIT-BIH Noise Stress Test database [176] is employed for this task. Its power content at frequencies lower that 0.5 Hz, which is representative of out-of-band low-frequency disturbances, is calculated before and after the application of the bidirectional filters and the reduction produced by the different highpass filters assessed.

Different techniques are available to estimate the power spectrum of a signal from a recording of limited duration. The simplest method is given by the periodogram, which is an estimate of the signal power spectral density (PSD) calculated from the square of the discrete Fourier transform of the finite data sequence [75, 106, 177]. Since the periodogram represents a biased estimate of the signal PSD [75, 177], other techniques such as the Bartlett and Welch methods are generally employed to derive the power spectrum of electrocardiographic recordings [51, 75]. In the Bartlett method, the data record is divided into different segments and the PSD is estimated by averaging the periodograms calculated for each of the segments. The Welch method represents a modification of this average periodogram procedure in which the segments are overlapping and can be windowed using different functions. Due to the fact that the discrete Fourier transform is calculated over a shorter data sequence, the resolution of the power spectrum estimate obtained using the Bartlett and Welch methods is lower that that of the periodogram [75, 177]. Since the frequency range of the low-frequency noise is very narrow and it is necessary to maintain a good resolution when calculating the power, the duration of the intervals used by these averaging techniques cannot be too short. In this case, the power of the bw record calculated through the Bartlett method is almost identical to that derived directly from the periodogram. The low-frequency power calculated using the Welch method is dependent on the shape of the window and, when the segment length is selected as one tenth that of the overall data sequence and the overlap as 50%, its value for the bw record is between 1% and 8% lower than the power calculated using the periodogram (see Appendix B.2 for further details). Given the limited difference between the methods, the power of the bw record, and that of all the other records analysed in the remainder of this chapter, is calculated using the periodogram, so that the resolution of the signal spectrum at low frequencies is not compromised.

It is also worthwhile noting that, when measuring the power of the bw record, the spectral content at zero frequency is omitted from the calculations. The power measured at 0 Hz is, in fact, simply indicative of the amplitude of the DC offset present in the signal. The bidirectional filters under analysis in this section and the highpass filters designed through the optimisation procedure are characterised by a zero at 0 Hz, which completely eliminates this DC offset. Therefore, their performance with regard to the reduction of the DC noise is identical. This approach of omitting the DC frequency content from the power calculation is

applied throughout the remainder of the chapter.

The low-frequency power of the bw record before and after the application of the bidirectional systems is presented in Table 7.5. The first and last 15 s of recordings are excluded from the calculation of both the input and the output power to account for the settling times of the filters. From Table 7.5, it can be seen that all of the filters provide a substantial reduction of the low-frequency noise. The noise power is reduced by approximately 60% by the bidirectional system derived from the 0.1 Hz first order filter, whereas the bidirectional systems obtained from the 0.15 Hz Butterworth base filters allow the noise to be lowered by almost 80%. The performance of the systems obtained from the second and third order filters is very similar. This behaviour can be explained by the fact that the bidirectional system obtained from the second order filter is characterised by a lower attenuation than that of the one derived from the third order filter at very low frequencies, but its 3dB-point is slightly higher, that is, the attenuation achieved by the former filter in the cutoff region is larger than that of the higher order system.

Table 7.5: Measurement of the power contained in bw record at frequencies lower than 0.5 Hz before and after the application of the bidirectional filters obtained from a 0.1 Hz first order system and 0.15 Hz second and third order Butterworth filters. The percentage reduction in the low-frequency noise achieved by the bidirectional filters with respect to the noise power of the input record is indicated.

	Input	Output					
		1st order		2nd order		3rd order	
	power (10^{-9} V^2)	power (10^{-9} V^2)	% reduct.	power (10^{-9} V^2)	% reduct.	power (10^{-9} V^2)	% reduct.
Lead A	200.4	79.9	-60.1	41.7	-79.2	42.0	-79.0
Lead B	29.6	12.2	-58.9	6.6	-77.8	6.7	-77.3
Average leads	115.0	46.0	-59.5	24.1	-78.5	24.4	-78.2

7.3.2 Results and discussion

After preprocessing the signals in the QT database using the bidirectional filter obtained from the 0.15 Hz second order Butterworth function, the highpass filters derived through the optimisation procedure are applied to the ECG records and the distortion produced is evaluated in terms of error and change in the slope of the ST segment. The first 45 s and the last 15 s of each record are, once more, excluded from the analysis to allow the initial transients introduced by both the bidirectional and the optimised highpass filters to be eliminated from the comparison.

Error analysis

For each of the 42 QT records being studied, the average and maximum absolute errors caused by the optimised filters and by the reference 0.05 Hz single-pole network are assessed. The percentage of samples for which the error exceeds 25 μV or 5% of the input value, which is the limit specified by the 1990 AHA recommendations [19], is calculated. It should be noted that more than 400,000 samples are analysed for each two-lead record. The complete results are presented in Appendix B.3 and a summary of the error statistics obtained by averaging the quantities of interest over the QT records is shown in Table 7.6. From this table, it can be seen that the average and the maximum errors are at their lowest for the reference 0.05 Hz single-pole network. The results obtained for the second order filters are very similar, with both the errors being approximately 25% larger than for the benchmark filter. It can also be noticed that the third order filter yields the largest distortion and its average and maximum errors are approximately 36% larger than those of the first order system. The results for the third order concave filter are somewhat intermediate between those of the second order and the third order optimised filters. Finally, the percentage of samples for which the error exceeds the limit set by the AHA recommendations is 4% for the 0.05 Hz first order system, 6% for the second order filters and just above 7% for the third order filter. Once more, the performance of the third order concave filter places itself approximately midway between those of the other highpass filters derived through the optimisation procedure.

It can be noticed from Tables B.2 to B.6, that four of the QT records under analysis are characterised by an extremely high percentage of samples for which the limit specified by the 1990 AHA recommendations is exceeded. These records (`sel39`, `sel42`, `sel47` and `sele0166`) are easily identifiable from Table B.2 reporting the error statistics for the 0.05 Hz reference filter. In fact, errors exceeding the 25 μV or 5% limit affect between 20% and 50% of the samples of these records, whereas at most 4% of the samples in the other records present an unacceptably large distortion. Records `sel39` and `sel47` are characterised by very large interference spikes (see Figure 7.8), which lead to prolonged transients in the response of the highpass filters. The large error measured for records `sel42` and `sele0166` is most likely due to rapid, yet smaller, fluctuations in the baseline level.

If records `sel39`, `sel42`, `sel47` and `sele0166` are excluded from the calculation of the average error statistics, a decrease in the error values for all of the highpass filters can be seen in Table 7.6. The percentage difference in average and maximum error between the optimised highpass filters and the 0.05 Hz single-pole network is also marginally decreased, even though it still varies between 20% and 35%. On the other hand, the percentage of samples for which the error introduced by the highpass filters exceeds the allowable limit is

Table 7.6: Statistics of the error introduced by the second and third order optimised filters and by the 0.05 Hz single-pole network into the records of the QT database.

	0.05 Hz 1st order	2nd order real-pole	2nd order (3dB max)	3rd order (3dB max)	3rd order concave
Overall (42 records)					
avg (μV)	7.3	9.0	9.0	10.0	9.4
% diff. with 0.05 Hz 1st order		22	22	36	28
max (μV)	58.4	73.6	74.4	79.5	76.8
% diff. with 0.05 Hz 1st order		26	27	36	32
% above limit	4.1	6.0	6.0	7.2	6.5
% diff. with 0.05 Hz 1st order		46	47	77	60
Excluding `sel39`, `sel42`, `sel47` and `sele0166`					
avg (μV)	5.6	6.7	6.7	7.5	7.0
% diff. with 0.05 Hz 1st order		21	20	34	26
max (μV)	45.1	55.9	56.0	60.8	58.2
% diff. with 0.05 Hz 1st order		24	24	35	29
% above limit	1.1	2.3	2.3	3.2	2.7
% diff. with 0.05 Hz 1st order		110	114	193	149

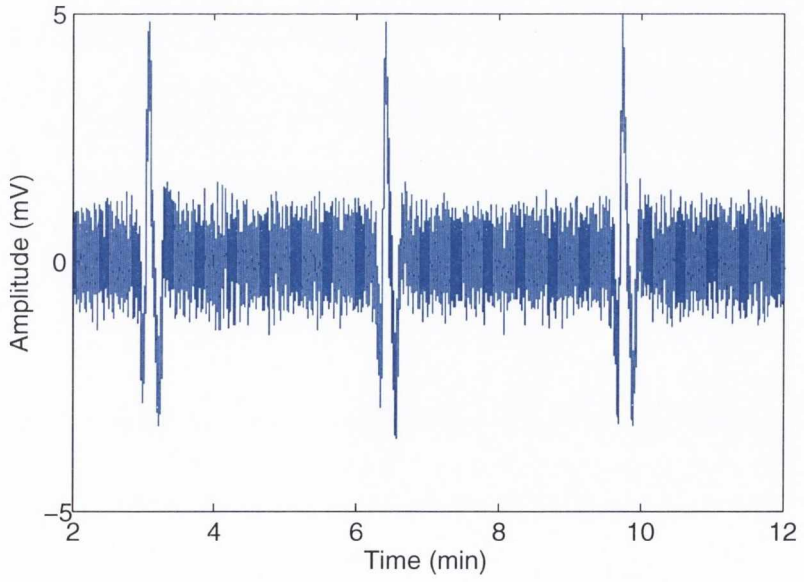


Figure 7.8: Excerpt from record `sel47` (lead A).

greatly reduced. Only 1% of the output samples are affected by an unacceptably large error when the reference network is employed, with this percentage increasing to 3% for the third order filter.

The error statistics of the signals in the QT database appear to be quite different from the ones reported in Tables 7.2 and 7.3 for synthetic ECGs. In latter case, the maximum error is much smaller than that calculated over the records of the QT database and none of the highpass filters introduces a deviation into the output signal exceeding the 25 μV limit. Furthermore, the average error measured for the synthetic signals is approximately half that evaluated for the QT records. The most significant difference between the error statistics of real and test ECGs is that the error introduced into the QT records by the reference filter is always smaller than that measured when the optimised filters are employed, whereas for synthetic signals only the third order filter appears to perform worse than the 0.05 Hz single-pole network. Moreover, when the error is evaluated on the records of the QT database, the second order filters seem to have comparable performances and to introduce the least amount of error among the optimised filters. On the other hand, when the test ECGs are employed for the analysis of the distortion, the third order concave filter appears to cause the smallest deviation between input and output signals and the performance of the second order filter having real poles is noticeably worse than that of the second order filters with complex conjugate poles.

The discrepancy in the error statistics between synthetic and real ECGs could be due to two principal causes: signal morphology and noise. Firstly, the synthetic test signals are constructed to resemble a normal ECG as measured on a healthy subject and, therefore, they reproduce only a small subset of all the morphologies possible for the electrocardiographic waveform. On the other hand, most of the records in the QT database were acquired from subjects suffering from cardiac conditions and were, indeed, selected to represent a wide variety of morphologies for the QRS complex, T wave and ST segment. Looking at Tables 7.2 and 7.3, it can be appreciated how the ECG shape influences the distortion introduced by the different highpass filters. For the test signals constructed from the parameters of the CAL20100 and CAL20160 waveforms, which are characterised by a monophasic QRS complex and isoelectric or elevated ST segment (see Figure B.2), the maximum error caused by the 0.05 Hz first order system is lower than that produced by any of the optimised filters. Nevertheless, the performance of the reference single-pole network is worse than that of the second order optimised filters and of the third order concave system for all the other test signals. As regards noise, it needs to be pointed out that, even though the records in the QT database have been filtered to eliminate low-frequency disturbances before the analysis of the distortion is performed, in-band noise, such as motion and muscle artifacts, is still present in the ECG recordings. This noise and interference is

most likely responsible for the larger average and maximum errors measured for the QT records.

Analysis of the change in the ST segment slope

For each of the selected records of the QT database, between 22 and 70 annotated ST segments are employed to evaluate the change in slope introduced by the optimised highpass filters (see Table B.7). ST segments containing less than 3 data points are excluded from the analysis. The slope of each ST segment is calculated by interpolating its data points using a straight line. After applying the selected highpass filter, the slope is recalculated and the change with respect to the original value is assessed. For each record, the average value of the absolute change in slope is computed. Moreover, the maximum difference between input and output slope is identified and the percentages of negative slope changes and of changes that exceed ± 50 μV/s are determined (see Tables B.8 to B.12). After averaging the values over the 42 records, these statistics are reported in Table 7.7. The average change lies between 31 and 36 μV/s, while the maximum slope difference between 61 and 69 μV/s. The percentage of ST segments for which a negative change in slope is introduced is quite uniform across the highpass filters and is approximately 32%. The percentage of ST segments for which the absolute value of the change is larger than 50 μV/s is approximately 20%. It is worthwhile noting that the third order filter is characterised by the highest values of average and maximum change and by the largest percentage of ST segment deviations exceeding the allowable limit. It is also the only filter whose performance is overall worse than that of the 0.05 Hz single-pole filter. The third order concave system and the second order filter have comparable performances, with an average slope change approximately 12% lower than that introduced by the 0.05 Hz first order network. For these filters, the percentage of ST segments for which the change is above the allowable limit is about 3% less than that of the reference system. The distortion introduced by the second order filter having real poles into the ST segment also appears to be lower than that caused by the 0.05 Hz single-pole network, even though the maximum change in slope is marginally lower for the latter filter.

Comparing the results in Table 7.7 with the one summarised in Tables 7.2 and 7.3 for the synthetic signals, it can be seen that the average change in the ST segment slope introduced by the highpass filters is practically equivalent for real and synthetic ECGs. In both cases, the third order concave filter is the one introducing the least amount of distortion and the third order filter is the only optimised filter producing changes in the ST segment slope larger than those of the reference 0.05 Hz system. Overall, it can be concluded that the results obtained for the real signals fully agree with the one previously determined for

Table 7.7: Statistics of the change in the ST segment slope introduced by the second and third order optimised filters and by the 0.05 Hz single-pole network into the records of the QT database.

	0.05 Hz 1st order	2nd order real-pole	2nd order (3dB max)	3rd order (3dB max)	3rd order concave
avg (μV/s)	35.2	32.8	31.1	36.4	30.8
% diff. with 0.05 Hz 1st order		-6.7	-11.5	3.4	-12.5
abs(max) (μV/s)	61.7	63.7	61.3	68.6	61.7
% diff. with 0.05 Hz 1st order		3.2	-0.6	11.1	0.0
% negative	33.6	31.7	31.1	32.6	31.6
% diff. with 0.05 Hz 1st order		-5.6	-7.5	-3.0	-5.9
% above limit	21.2	19.8	18.6	22.1	18.3
% diff. with 0.05 Hz 1st order		-6.7	-12.4	4.1	-13.7

the test ECGs.

7.4 Reduction of the low-frequency noise

Artificial signals, simulating low-frequency noise and interference, are often employed to verify the ability of highpass filters to reduce the baseline wander in ECG records. Sinusoidal waves are usually superimposed onto a known real or synthetic test record to generate the input signal, to which the output of the filter is then compared [70, 112, 120, 146]. In the case under analysis, however, once the frequency of the synthetic noise signal is selected, the rejection capability of the optimised highpass filters is already fully known. Let us, for example, consider the outcome of the filtering process when the input is given by the synthetic test signal obtained from the CAL20000 parameters illustrated in Figure 7.3 to which a 0.025 Hz sine wave with 2 mV amplitude is added. From Figure 7.9, it can been seen that the second order filters provide the best performance. This result could have been predicted directly from the magnitude response of the optimised filters shown in Figure 6.16(b) and 6.26(b), where it can be clearly seen that the attenuation achieved at 0.025 Hz by the second order filters is larger than that of the third order filters and of the reference single-pole network. Finally, it should be pointed out that simulating the low-frequency noise and interference using a very limited number of sinusoids does not seem appropriate when the spectral nature of the baseline wander is considered, which according to the noise spectrum shown in Figure 2.15 does not appear to be sinusoidal.

In order to evaluate accurately the ability of the optimised highpass filters to eliminate the baseline wander from ECG measurements, it was decided to employ the noise records

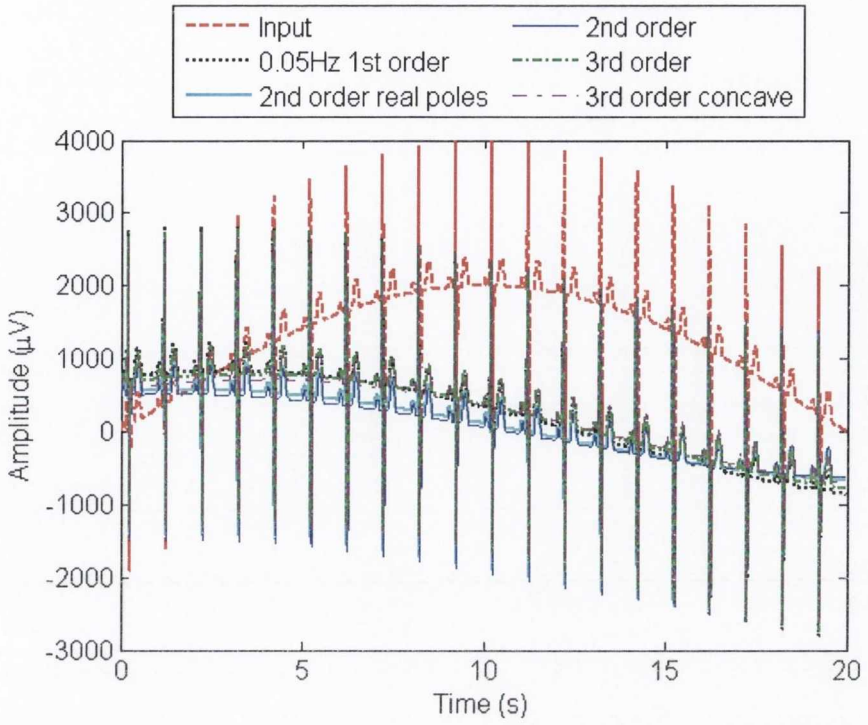


Figure 7.9: Response of the reference 0.05 Hz first order network and of the optimised highpass filters to an input signal obtained by adding a 0.025 Hz sinusoid of 2 mV amplitude to the synthetic test ECG derived from the CAL20000 parameters

contained in the MIT-BIH Noise Stress Test database [176] as test signals. Apart from the `bw` record, containing predominantly baseline wander, which was used in Section 7.3.1 to select the bidirectional filter for the preprocessing of electrocardiographic signals during the distortion analysis, two other records representative of the noise measured during ambulatory ECG recording are available in the MIT-BIH Noise Stress Test database. These records are characteristic of muscle artifacts (`ma`) and electrode motion artifacts (`em`), respectively, but they still incorporate a high level of low-frequency noise and interference, which can be evaluated as the power contained in the record at frequencies lower than 0.5 Hz. The total and low-frequency power measured for the three noise records of the MIT-BIH Noise Stress Test database are shown in Table 7.8. It can be seen that 98.5% of the total power of the `bw` record is measured at frequencies lower than 0.5 Hz. Nonetheless, even for the `ma` and `em` records, the power of the low-frequency noise and interference is quite substantial, being higher than 60% when calculated over the two leads. It should be pointed out that the noise figures presented in Table 7.8 are evaluated excluding the power of the DC component from the calculation. Moreover, in order to avoid the initial transient occurring in the response of the highpass filters under analysis, all of the noise measurements reported in the current section are performed excluding the first 30 s of each record. In other words, the output

Table 7.8: Power measured for the noise records of the MIT-BIH Noise Stress Test database.

	Lead A			Lead B			Average leads		
Record	total power (10^{-9} V^2)	power f<0.5Hz (10^{-9} V^2)	% power f<0.5Hz	total power (10^{-9} V^2)	power f<0.5Hz (10^{-9} V^2)	% power f<0.5Hz	total power (10^{-9} V^2)	power f<0.5Hz (10^{-9} V^2)	% power f<0.5Hz
bw	217.1	213.7	98.4	30.5	30.0	98.4	123.8	121.8	98.4
ma	37.5	28.9	77.1	37.2	29.0	77.9	37.4	28.9	77.5
em	536.6	224.0	41.7	41.7	34.2	82.0	289.1	129.1	61.9
Average							150.1	93.3	79.3

power is measured only on the steady state portion of the signal and the input power is calculated over the corresponding set of data, thus allowing the difference between input and output noise to be evaluated consistently.

For each of the three records in the MIT-BIH Noise Stress Test database, the power of the low-frequency disturbance is measured after applying the different highpass filters to both leads. The percentage difference between input and output noise power is also calculated and the results are indicated in Table 7.9. It can be seen that a reduction in the power measured at frequencies lower than 0.5 Hz of between 4% and 38% is achieved by the highpass filters. The only exception is given by the em record filtered using the second order system for which the low-frequency noise is marginally increased in both leads. This noise boosting is due to the fact that the frequency range of the small ripple present in the magnitude of the second order filter and that of a very large spectral component of the em record (see Figure 7.10) are quite similar. It should also be noted that, since the amplitude response of all of the optimised filters is characterised by a peak at a frequency of approximately 0.2 Hz, the noise reduction they achieve for the em record is significantly less than for the bw and ma signals. Finally, it is important to point out that, regardless of the record considered, the third order filter always provides better noise rejection than the reference 0.05 Hz single-pole filter.

Table 7.10 presents the average two-lead low-frequency power of the output signals and the noise reduction achieved by each of the highpass filters, as calculated from the rightmost columns in Table 7.9. It can be seen that, overall, the reduction in low-frequency noise and interference varies between a minimum of 5.5% for the second order filter to a maximum of 27% for the third order filter. Due to the somewhat poor performance of the highpass filters on the em record, these percentages are slightly lower than those obtained by considering the baseline wander record only (see Table 7.9). Comparing the results of the optimised filters with those of the reference first order network, the superior noise reduction performance of the third order filters is evident. The power of the low-frequency disturbances at the output of the concave filter is 4% lower than that of the 0.05 Hz single-

Table 7.9: Measurement of the power contained in the noise records of the MIT-BIH Noise Stress Test database at frequencies lower than 0.5 Hz after they have been filtered using the highpass systems under analysis. The percentage reduction in low-frequency noise achieved for each record with respect to the noise power of the input signals reported in Table 7.8 is also indicated.

Record	Lead A		Lead B		Average leads	
	power (10^{-9} V^2)	% reduct.	power (10^{-9} V^2)	% reduct.	power (10^{-9} V^2)	% reduct.
			bw			
0.05 Hz 1st order	182.0	-14.8	25.7	-14.2	103.9	-14.5
2nd order real-pole	185.1	-13.4	26.4	-12.1	105.7	-12.8
2nd order	197.6	-7.5	28.2	-6.1	112.9	-6.8
3rd order	136.4	-36.2	19.9	-33.6	78.2	-34.9
3rd order concave	160.9	-24.7	23.3	-22.3	92.1	-23.5
			ma			
0.05 Hz 1st order	24.4	-15.8	23.6	-18.4	24.0	-17.1
2nd order real-pole	24.5	-15.2	23.5	-19.0	24.0	-17.1
2nd order	25.7	-11.0	24.8	-14.3	25.3	-12.7
3rd order	20.2	-30.1	18.1	-37.6	19.1	-33.9
3rd order concave	22.2	-23.3	20.5	-29.2	21.4	-26.2
			em			
0.05 Hz 1st order	202.4	-9.6	30.8	-9.9	116.6	-9.8
2nd order real-pole	215.8	-3.6	32.9	-3.7	124.4	-3.7
2nd order	230.3	2.8	35.2	3.1	132.8	2.9
3rd order	195.1	-12.9	30.1	-11.8	112.6	-12.3
3rd order concave	208.4	-6.9	31.9	-6.7	120.1	-6.8

pole system and the other third order filter yields a reduction in the noise power 14% larger than that achieved by the reference network. On the other hand, it can be seen from Table 7.10 that the second order filters provide a smaller reduction of the low-frequency noise and interference than the 0.05 Hz reference filter. It should however be pointed out that the performance of the filter characterised by real poles does not appear to be significantly different from that of the single-pole network.

The 42 records of the QT database [175] employed in Section 7.3 to analyse the distortion introduced into the ECG signal are now used to evaluate the noise reduction capability of the optimised highpass filters. For each record, the low-frequency noise and interference are assessed in terms of the power measured for frequencies lower than 0.5 Hz (see Table B.13). The filters under study are then applied to the ECG recordings and the output noise power and the reduction of the low-frequency disturbance achieved with respect to the original signals are evaluated. For each of the highpass filters, these results are presented in

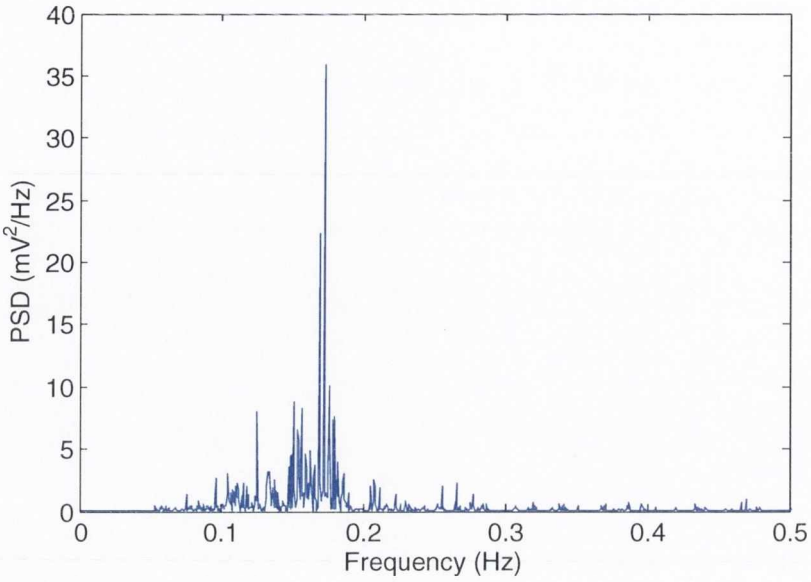


Figure 7.10: Power spectral density of the `em` record (lead A).

Appendix B.5 and, after being averaged over the 42 QT records, are summarised in Table 7.11. It can be seen that the noise power measured after filtering the ECG recordings using the optimised second and third order systems is lower than that obtained for the reference 0.05 Hz network. As was the case with the noise records of the MIT-BIH Noise Stress Test database, the third order filter provides the best rejection. It is also worth noting that, despite the noise power being lower for the output of the second order filters than of the 0.05 Hz single-pole network, the percentage noise reduction achieved by the latter filter is higher than that of the optimised second order systems. This discrepancy is easily explained by looking at Tables B.14 to B.18. For some of the QT records, the second and third order filters actually cause an small increase in the low-frequency noise power. As discussed earlier when analysing the noise reduction achieved on the MIT-BIH Noise Stress Test records, this phenomenon is linked to the 0.5 dB peak occurring in the magnitude response of the

Table 7.10: Average low-frequency power and noise reduction obtained for the noise records of the MIT-BIH Noise Stress Test database when they are filtered using the different highpass systems.

	0.05 Hz 1st order	2nd order real-pole	2nd order (3dB max)	3rd order (3dB max)	3rd order concave
power (10^{-9} V^2)	81.5	84.7	90.3	70.0	77.9
% diff. with 0.05 Hz 1st order		4	11	-14	-4
% reduction	-13.8	-11.2	-5.5	-27.0	-18.9
% diff. with 0.05 Hz 1st order		-19	-60	96	37

Table 7.11: Average low-frequency power and percentage noise reduction obtained for selected records of the QT database when they are filtered using the different highpass systems.

	0.05 Hz 1st order	2nd order real-pole	2nd order (3dB max)	3rd order (3dB max)	3rd order concave
Overall (42 records)					
power (10^{-9} V^2)	10.7	9.8	10.0	8.8	8.8
% diff. with 0.05 Hz 1st order		-9	-6	-18	-18
% reduction	-22.7	-22.2	-19.2	-27.1	-24.7
% diff. with 0.05 Hz 1st order		-2	-15	19	9
Records `sel31`, `sel39`, `sel45`, `sel47` and `sel49` only					
power (10^{-9} V^2)	69.7	61.7	63.1	53.9	53.7
% diff. with 0.05 Hz 1st order		-11	-10	-23	-23
% reduction	-35.4	-42.2	-40.7	-49.5	-49.0
% diff. with 0.05 Hz 1st order		19	15	40	38

optimised filters. It should finally be pointed out that the boosting of the noise power is restricted to records characterised by limited low-frequency disturbances. This explains why the overall noise power after the application of the second and third order filters is still lower than for the 0.05 Hz single-pole network.

Comparing the results obtained for the QT database with those of the MIT-BIH Noise Stress Test database in Table 7.10, it can be noticed that the third order filter produces the same percentage noise decrease (27%), whereas the reduction obtained by the other optimised filters and by the 0.05 Hz network is, on average, higher for the records of the QT database. Furthermore, it can be concluded that, regardless of the signals used for the evaluation, both the third order filters achieve a reduction of the low-frequency noise and interference greater than the single-pole reference network.

As highlighted in Section 7.3.1, the records included in the QT database were expressly chosen to be free from large artifacts, which leads to their average low-frequency power to be significantly smaller than that of the noise records of MIT-BIH Noise Stress Test database (see Tables 7.8 and B.13). It was, therefore, decided to re-evaluate the noise reduction capability of the highpass filters under analysis only on the records of the QT database containing large low-frequency disturbances. These records are selected from Table B.13 as `sel31`, `sel39`, `sel45`, `sel47` and `sel49` and it is interesting to note that they all originate from the MIT-BIH database containing ambulatory records of sudden death. For each of these ECG recordings, the power of low-frequency noise and interference represents more than 40% of the total power. If the low-frequency rejection provided by the highpass filters is evaluated only on these noisy records, the bottom part of Table 7.11 shows that all of

the optimised filters perform better than the reference 0.05 Hz network, in terms of both output noise power and reduction achieved with respect to the input noise. This reduction is, in fact, almost 50% for the third order filters and more than 40% for the second order systems, which is approximately double the corresponding measurements performed over the 42 records. It should also be noted that, when only the noisy records are considered, the two third order filters appear to have very similar noise rejection capabilities.

7.5 Conclusion

In this chapter, the distortion introduced into electrocardiographic recordings by the highpass filters designed to fulfil the requirements specified by the EN 60601-2-51:2003 European standard [9] and the 1990 AHA recommendations [19] has been evaluated. Attention has been directed at the filters derived by maximising the 3dB-cutoff frequency and to the second order filter having real poles obtained by optimising the overall low-frequency rejection. The difference between input and output signal and the change in the slope of the ST segment caused by these filters have been assessed with respect to guidelines proposed by the EN 60601-2-51:2003 standard and the 1990 AHA recommendations and to the performance of the reference 0.05 Hz single-pole network.

Synthetic signals constructed to resemble the calibration ECGs described in the European standard were first employed to evaluate the amplitude error and the deviation in the ST segment slope produced by the highpass filters. It emerged that the maximum deviation between the output and the input signals is always lower than the 25 μV limit specified by the AHA recommendations, that is, the amplitude distortion of the filtered ECGs can be considered negligible. As regards the change in the slope of the ST segment, the 50 μV/s limit proposed for the calibration waveforms by the EN 60601-2-51:2003 standard is fulfilled by both the optimised filters and the reference 0.05 Hz system, except for the test records characterised by a depressed ST segment. Moreover, both the error and the ST segment distortion introduced by the second order filter and by the third order concave system are lower than those produced by the 0.05 Hz first order network. On the other hand, the performance of the reference system is comparable to that of the second order filter having real poles and marginally better than that of the third order system obtained without specifying the concavity condition, in terms of both the amplitude error and the change in the ST segment slope.

The distortion analysis was then repeated on real ECG recordings taken from the QT database [175] and preprocessed using a bidirectional highpass filter to eliminate as much of the low-frequency noise and interference as possible. In this instance, the average and

maximum error introduced by the optimised filters is between 20% and 35% higher than that caused by the reference 0.05 Hz system. Nonetheless, for both the reference and the optimised filters, the percentage of samples for which the difference between input and output signal exceed 25 μV or 5% is very limited. It should finally be pointed out that the amplitude error introduced by the second order filters, even though higher than that caused by the 0.05 Hz single-pole filter, is lower than that produced by the third order optimised systems. As regards the change in the ST segment slope, no appreciable difference with the results derived using the test ECG signals can be identified, with the second order and the third order concave filters still causing the lowest distortion.

The discrepancy between the amplitude error measured for actual ECG recordings and for synthetic signals is most likely due to the varied morphology of the ECG waveforms in the QT records and the presence of residual noise and artifacts in the electrocardiographic measurements. It should also be noted that the records available on PhysioNet [174] might not provide an accurate representation of the ECG signal as it appears at the input of the recording equipment because the ECG measurement system with which they were originally acquired could have already introduced distortion into the electrocardiographic waveform.

Since it has been shown that the amount of distortion introduced by the different highpass filters is dependent on the shape of the input signal, it would be interesting to investigate how much of the error measured for the QT records is attributable to the varied geometry of ECG waveform in patients suffering from heart conditions and how much is due to the presence of noise or pre-distortion in the electrocardiographic recording. Synthetic signals that resemble the morphology of the ECG signal more closely than the waveforms employed in this chapter could be used for this purpose. Ideally, the test ECG waveforms should also be able to reproduce a wide variety of features that are characteristic of cardiac abnormalities. Alternatively, the distortion analysis could be performed only on selected portions of the PhysioNet records that can be deemed free of noise, interference and deformations not of physiological origin. This would, however, require the electrocardiographic recordings to be visually inspected in advance by a trained medical professional.

In this chapter, the ability of the optimised filters to eliminate low-frequency noise and interference from the electrocardiographic signal was evaluated as well. The power contained in the recordings at frequencies lower than 0.5 Hz was used as a measure of the out-of-band low-frequency disturbance. The reduction in this power achieved by the optimised highpass filters for the three noise records available in the MIT-BIH Noise Stress Test database [176] was assessed and compared with that produced by the 0.05 Hz single-pole network. It emerged that the third order filters provide better results than the reference system. The noise reduction analysis was then repeated on the QT database. If only the

records characterised by large low-frequency disturbances are taken into consideration, all of the optimised filters achieve a larger reduction in the low-frequency power than the reference single-pole system. In particular, the third order filters, which have comparable performances, are able to reduce the out-of-band noise by practically 50%.

When the noise reduction capability and the time domain distortion produced by the highpass filters are considered together, it emerges clearly that the third order concave filter provides the best overall performance. Its ability to eliminate the low-frequency disturbance is universally higher than that of the reference 0.05 Hz system. Furthermore, the change in the ST segment slope caused by the third order concave filter is not only the lowest among those of the optimised systems, but it is also lower than that of the 0.05 Hz single-pole filter. As regards the amplitude error, the performance of the third order concave filter, once more, emerges as the best among all of the highpass filters when the difference between input and output signals is evaluated using the synthetic ECGs. Even for the records of the QT database, the percentage of samples for which this filter introduces an error larger than the allowable limit is less than 3%. It is therefore beneficial to employ the third order concave filter at the front-end of diagnostic electrocardiographic equipment instead of the traditional 0.05 Hz single-pole network.

It should finally be noted that, throughout this chapter, the prolonged initial transients that characterise the responses of both the reference 0.05 Hz system and the optimised highpass filters in the presence of a DC offset voltage (see Figure 7.4) have been excluded from the distortion and noise reduction analysis. These transients can be considered negligible at the beginning of an ECG measurement session because in practice a delay between the placement of the electrodes and the start of the acquisition of the electrocardiogram is likely to occur and less than 30 s is needed for the filter output to stabilise at the steady state level. The long settling times of the highpass filters are more significant in the event of a loss of contact between the electrode and the body during the measurement. If the recording saturates at the full scale deflection level, the time taken for the ECG signal to reposition within the dynamic range of the electrocardiograph is dependent on the settling time of the highpass filter, which is approximately 25% longer for the third order concave system than for the reference 0.05 Hz single-pole network.

Chapter 8

Circuit topology for the third order highpass filter

8.1 Introduction

This chapter focuses on the third order concave filter designed to fulfil the highpass requirements specified by the EN 60601-2-51:2003 European standard [9] and the 1990 AHA recommendations [19] and derived by maximising the 3dB-cutoff frequency (see Section 6.5). It has been shown that the performance of this system in terms of both time domain distortion and noise rejection capability is superior to that of the other filters obtained through the optimisation procedure and that of the 0.05 Hz single-pole network usually employed as front-end highpass filter in electrocardiographic devices. It is therefore worthwhile to investigate how to implement it.

The third order concave filter is characterised by a zero at 0 Hz and a pole located at approximately 0.03 Hz and by a pair of complex conjugate zeros and another pair of complex conjugate poles (see Table 6.6). The real pole and zero can be realised using a simple first order RC section. The RC combination should be integrated into the front-end amplifier [57] to prevent large DC offsets associated with electrocardiographic measurements from saturating the instrumentation amplifier.

To realise the complex conjugate poles and zeros, on the other hand, it is necessary to select a circuit structure that allows the implementation of a general biquadratic transfer function. Most of the suitable topologies comprise three operational amplifiers [159, 178–180], but there exist a few structures that rely on a lower number of active components [159, 181, 182]. In order for the filter to be employable in ambulatory applications, its power consumption should ideally be kept to a minimum. Attention is therefore directed towards Friend's single-amplifier biquad topology [181]. Using both negative and positive feedback,

this structure provides an optimum compromise between active and passive sensitivities and it can be employed for the realisation of biquadratic section having a quality factor for the poles lower than 30 [183].

The sensitivity of Friend's structure to the manufacturing tolerance of passive components is investigated and the values of its resistors and capacitors are selected in such a way that the variability in the location of poles and zeros is minimised. A Monte Carlo simulation of the magnitude and pulse responses of the third order filter is then performed by assuming a 1% uniformly distributed tolerance for both capacitors and resistors. Based on this simulation, the limits set during the optimisation procedure on the amplitude of the passband ripple and on the undershoot occurring after the application of a 3 mV$\times$100 ms rectangular input pulse are revised, so that the variations in the filter responses due to component tolerances are accounted for. The third order concave filter is redesigned by enforcing the newly established bounds during the maximisation of the 3dB-cutoff frequency and a set of values for its implementation is finally proposed.

8.2 Analysis of the sensitivity of the time and frequency responses to changes in the filter parameters

It has previously been pointed out (see Section 6.8) that the conditions imposed during the optimisation procedure on the passband ripple and on the undershoot occurring after the application of a 3 mV$\times$100 ms rectangular input pulse are tightly matched by the highpass filters. For the third order filter under consideration, it can be seen from Figure 8.1 that the peak present in the magnitude response is marginally lower than the 0.5 dB limit set during the optimisation process and that the maximum amplitude of the pulse response undershoot is exactly equal to the allowed 100 µV bound. It is evident that manufacturing tolerances in the components can cause the 0.5 dB ripple and the 100 µV displacement limits to be exceeded by the magnitude and pulse responses of the realised filter structure.

The filter parameters to which the time and frequency domain responses are more sensitive should be identified so that their variability can be minimised through careful design of the hardware circuit. Let us therefore analyse how changes in the coefficients of the third order filter influence the maximum amplitude of the magnitude peak and that of the pulse response undershoot.

When calculating the sensitivities of a filter structure to variations in its component values, it is customary to express the filter parameters in terms of the frequency and quality factor (Q-factor) of the poles and zeros [159, 179, 182, 183]. The transfer function of the

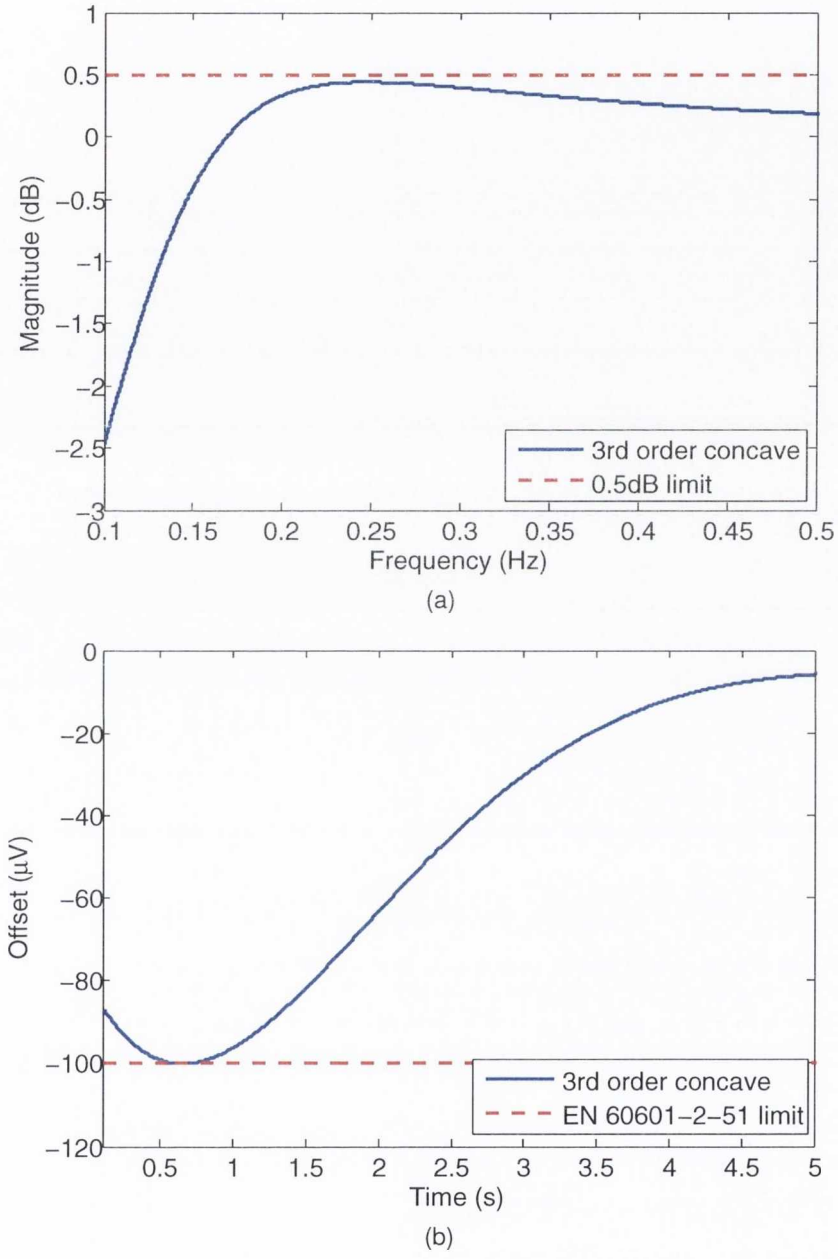


Figure 8.1: (a) Magnitude characteristic of the third order concave filter obtained by maximising the 3dB-cutoff frequency and (b) displacement from the isoelectric line occurring after the application of a 3 mV$\times$100 ms rectangular pulse at its input. The limits imposed in the optimisation process on the time and frequency responses are represented by the dashed lines.

third order highpass filter is thus rewritten as:

$$H_3(s) = \frac{s}{s+p_0}\frac{s^2+a_1 s+a_0}{s^2+b_1 s+b_0} = \frac{s}{s+p_0}\frac{s^2+\frac{\omega_z}{Q_z}s+{\omega_z}^2}{s^2+\frac{\omega_p}{Q_p}s+{\omega_p}^2}, \tag{8.1}$$

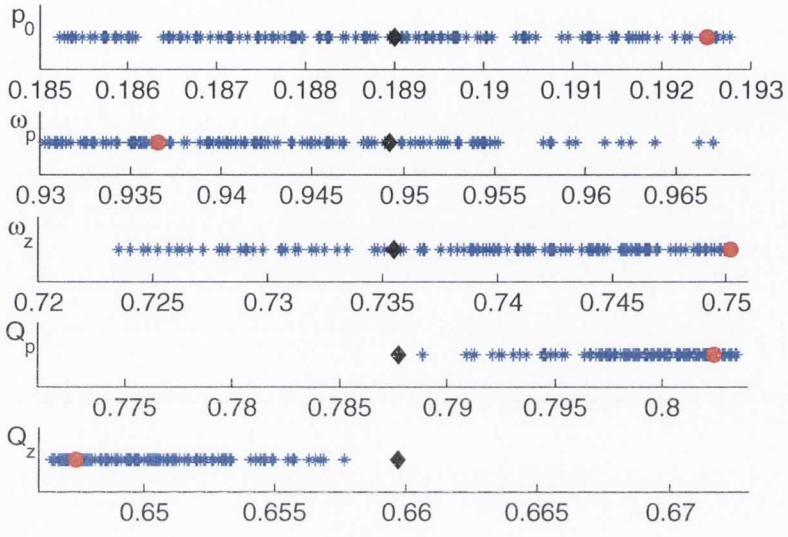
where p_0 is the frequency of the real pole, ω_p and ω_z are the frequencies of the complex conjugate poles and zeros, Q_p and Q_z are the Q-factors of the complex conjugate poles and zeros, respectively. The coefficients of the system under study are shown in Table 8.1. A Monte Carlo simulation of the time and frequency domain responses of the filter is then performed assuming a $\pm$2% uniformly distributed variation in the nominal values of p_0, ω_p, ω_z, Q_p and Q_z. This percentage variation is selected considering that through-hole resistors and capacitors are available with a 1% tolerance for values up to 100 MΩ and 100 nF, respectively [163, 164].

When 3000 simulations are run, the percentage of cases for which the 100 µV limit is exceeded by the offset occurring in the pulse response is approximately 52%, whereas the percentage of cases in which the magnitude peak is larger than 0.5 dB is equal to 25%. The maximum amplitude measured for the pulse response undershoot is approximately 115 µV and that of the magnitude peak is 0.69 dB. It should be noticed that, even though this value exceeds the $\pm$0.5 dB requirement set for the passband ripple by the 1990 AHA recommendations [19], amplitude peaks as large as 0.8 dB are acceptable according to the specifications contained in the current European and American standards for electrocardiographic equipment (see Section 3.3.1). It thus appears that changes in the values of the frequency and Q-factor of the poles and zeros are more detrimental to the filter time domain response than to its amplitude characteristic.

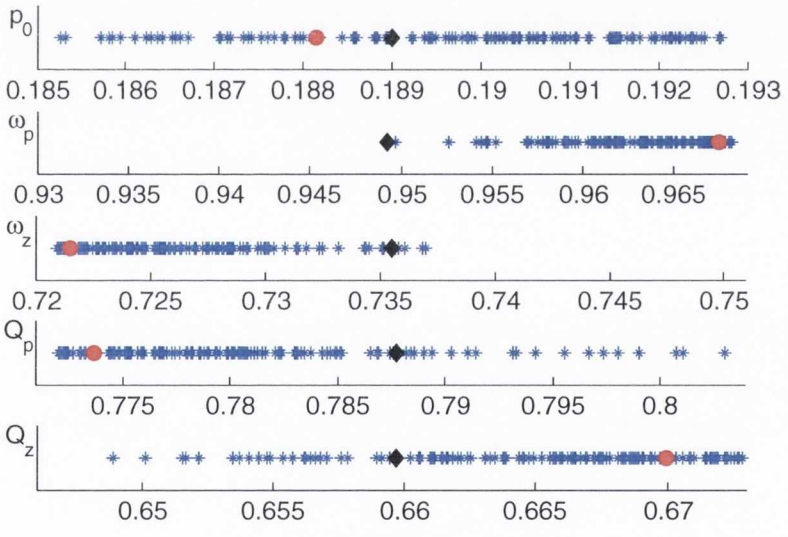
Figure 8.2 shows the distributions of the filter parameters for which either the amplitude of the magnitude peak or that of the pulse response undershoot is in the 95th percentile. In other words, the 150 sets of p_0, ω_p, ω_z, Q_p and Q_z values that lead to the largest passband peaks are shown in Figure 8.2(a) and, similarly, the 150 sets that cause the largest undershoots are illustrated in Figure 8.2(b). It can be seen that the frequency of the real pole has limited influence on the amplitude of both the magnitude peak and the pulse response

Table 8.1: Parameters of the transfer function of the third order concave filter.

p_0 (rad/s)	a_1 ((rad/s)^2)	a_0 (rad/s)	b_1 ((rad/s)^2)	b_0 (rad/s)	ω_p (rad/s)	ω_z (rad/s)	Q_p	Q_z
0.189	1.115	0.541	1.205	0.901	0.949	0.736	0.788	0.660



(a) Magnitude



(b) Undershoot

Figure 8.2: Distributions of the frequency and Q-factor of the poles and zeros of the third order filter for which either the passband peak (a) or the amplitude of the pulse response undershoot (b) is in the 95th percentile. The sets of p_0, ω_p, ω_z, Q_p and Q_z values responsible for the largest amplitude peak and undershoot are indicated by the red dots and the nominal values of the filter parameters, located at the centre of the scales, are marked by the black diamonds.

undershoot. It can also be noted that the passband peak is more sensitive to changes in Q_p and Q_z, whereas the pulse response undershoot is more sensitive to variations in the frequency of the complex conjugate poles and zeros. High values of ω_z and Q_p and low values of ω_p and Q_z are responsible for large peaks in the magnitude characteristic, whereas the opposite combination of parameters leads to the 100 µV limit imposed on the pulse response undershoot being exceeded. It should finally be remarked that variations in the parameters of the complex conjugate poles and those in the parameters of the complex conjugate zeros seem to contribute equally to the distortion of the time and frequency domain responses and therefore the variability of the frequency and Q-factor of both poles and zeros should be kept to a minimum in the implementation.

8.3 Friend's single-amplifier biquad topology

Friend's single-amplifier structure, illustrated in Figure 8.3, realises an arbitrary biquadratic function with the exception of the lowpass case [181]. Assuming an infinite open-loop gain for the operational amplifier A, the coefficients of the general transfer function:

$$H(s) = \frac{V_o(s)}{V_i(s)} = \frac{n_2 s^2 + n_1 s + n_0}{s^2 + b_1 s + b_0} = n_2 \frac{s^2 + a_1 s + a_0}{s^2 + b_1 s + b_0} \tag{8.2}$$

can be expressed in terms of the capacitances and conductances ($G = 1/R$) of the circuit components as:

$$n_2 = \frac{G_C}{G_A} \tag{8.3}$$

$$n_1 = \frac{G_C\left[C_1 G_1 + (C_1 + C_2)(G_2 + G_3)\right] - C_1 G_4 (G_A + G_B)}{C_1 C_2 G_A} - \frac{G_6 (C_1 + C_2)(G_A + G_B)}{C_1 C_2 G_A} \tag{8.4}$$

$$n_0 = \frac{G_1\left[G_C (G_2 + G_3) - G_6 (G_A + G_B)\right]}{C_1 C_2 G_A} \tag{8.5}$$

$$b_1 = \frac{(C_1 + C_2)(G_A G_2 - G_B G_3) - C_1 G_1 G_B}{C_1 C_2 G_A} \tag{8.6}$$

$$b_0 = \frac{G_1 (G_A G_2 - G_B G_3)}{C_1 C_2 G_A} \tag{8.7}$$

where

$$G_1 = G_4 + G_5 \tag{8.8}$$

$$G_3 = G_6 + G_7 \tag{8.9}$$

$$G_A = G_C + G_D. \tag{8.10}$$

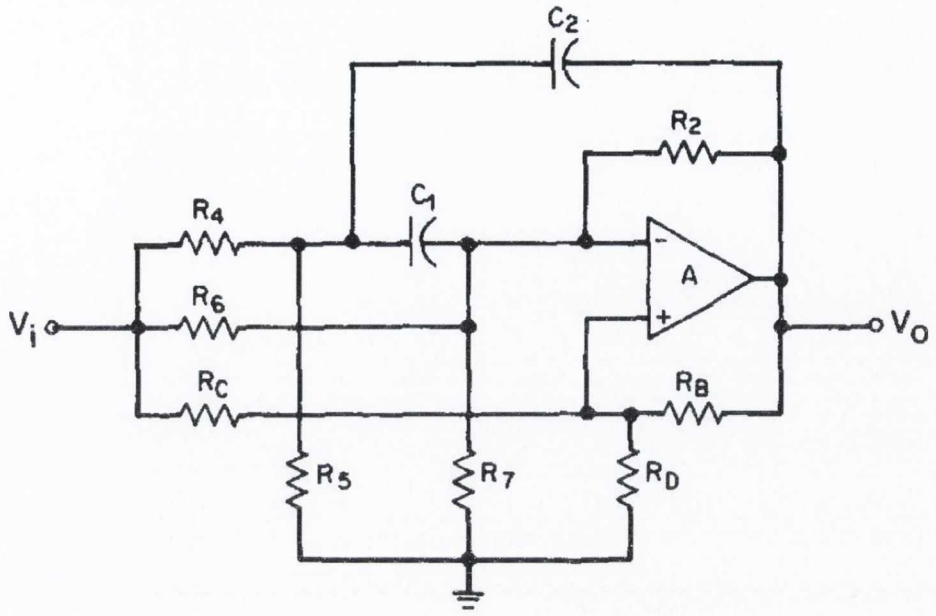


Figure 8.3: Friend's single-amplifier circuit (modified from [181]).

The value of n_2, i.e. the high-frequency gain of the transfer function, is determined by the ratio between R_C and R_D:

$$n_2 = \frac{G_C}{G_C + G_D} = \frac{1}{1 + \dfrac{G_D}{G_C}} = \frac{1}{1 + \dfrac{R_C}{R_D}} \tag{8.11}$$

and it is restricted to be less than unity [181], since the circuit cannot be simplified by eliminating either R_C or R_D. It is worthwhile noting that the third order filter implemented using Friend's biquad structure will therefore cause the amplitude of the input electrocardiographic signal to be somewhat reduced.

Given the coefficients, a_1, a_0, b_1 and b_0, of the transfer function to be implemented and having selected the values of the gain n_2 and of elements C_1, C_2, G_A and G_B, the values of all the other components in Friend's circuit can be calculated from the following equations when $b_0 > a_0$:

$$G_1 = \frac{1}{2} C_2 \frac{1}{\dfrac{G_B}{G_A}} \left[-b_1 + \sqrt{{b_1}^2 + 4\, b_0 \left(1 + \frac{C_1}{C_2} \right) \frac{G_B}{G_A}} \right] \tag{8.12}$$

$$G_4 = n_2 \frac{1}{G_1} \frac{1}{1 + \dfrac{G_B}{G_A}} \left[{G_1}^2 - a_1\, C_2\, G_1 + a_0 \left(1 + \frac{C_1}{C_2} \right) {C_2}^2 \right] \tag{8.13}$$

$$G_3 = \frac{n_2}{1-n_2}(b_0 - a_0)\frac{C_1 C_2}{G_1}\frac{1}{1+\dfrac{G_B}{G_A}} \tag{8.14}$$

$$G_2 = \frac{b_0 C_1 C_2}{G_1} + G_3\frac{G_B}{G_A} \tag{8.15}$$

$$G_5 = G_1 - G_4 \tag{8.16}$$

$$G_6 = G_3 \tag{8.17}$$

$$G_7 = 0 \tag{8.18}$$

$$G_C = n_2 G_A \tag{8.19}$$

$$G_D = (1-n_2) G_A. \tag{8.20}$$

It should be pointed out that the conductances are positive irrespective of the actual values of coefficients a_1, a_0, b_1 and b_0.

8.4 Sensitivity analysis of Friend's circuit and selection of component values

Substituting G_6 for G_3 in Eqs. (8.4) and (8.5), the coefficients of Friend's transfer function can be rewritten from Eqs. (8.4) to (8.7) as:

$$a_1 = \left(\frac{1}{C_1}+\frac{1}{C_2}\right)\left(G_2 - G_6\frac{G_B+G_D}{G_C}\right) - \frac{1}{C_2}\left(G_5 - G_4\frac{G_B+G_D}{G_C}\right) \tag{8.21}$$

$$a_0 = \frac{G_1}{C_1 C_2}\left(G_2 - G_6\frac{G_B+G_D}{G_C}\right) \tag{8.22}$$

$$b_1 = \left(\frac{1}{C_1}+\frac{1}{C_2}\right)\left(G_2 - G_6\frac{G_B}{G_A}\right) - \frac{G_1}{C_2}\frac{G_B}{G_A} \tag{8.23}$$

$$b_0 = \frac{G_1}{C_1 C_2}\left(G_2 - G_6\frac{G_B}{G_A}\right), \tag{8.24}$$

where the conditions expressed by Eqs. (8.8) and (8.10) still apply. From the above equations, the frequency and Q-factor of the complex conjugate poles and zeros (see Eq. (8.1)) can be derived as:

$$\omega_p = \sqrt{b_0} \tag{8.25}$$

$$\omega_z = \sqrt{a_0} \tag{8.26}$$

$$Q_p = \frac{\sqrt{b_0}}{b_1} \tag{8.27}$$

$$Q_z = \frac{\sqrt{a_0}}{a_1} \tag{8.28}$$

and their sensitivities with respect to the circuit passive components analytically determined using the formula [159]:

$$S_x^y = \frac{x}{y}\frac{\partial y}{\partial x}, \tag{8.29}$$

which expresses the sensitivity of y with respect to x.

Let us, for example, analyse the sensitivities of ω_p:

$$S_{C_1}^{\omega_p} = S_{C_2}^{\omega_p} = -\frac{1}{2} \tag{8.30}$$

$$S_{G_2}^{\omega_p} = \frac{1}{2}\frac{1}{1-\dfrac{G_6}{G_2}\dfrac{G_B}{G_A}} \tag{8.31}$$

$$S_{G_6}^{\omega_p} = S_{G_B}^{\omega_p} = \frac{1}{2}\frac{1}{1-\dfrac{1}{\dfrac{G_6}{G_2}\dfrac{G_B}{G_A}}} \tag{8.32}$$

$$S_{G_4}^{\omega_p} = \frac{1}{2}\frac{G_4}{G_4+G_5} \tag{8.33}$$

$$S_{G_5}^{\omega_p} = \frac{1}{2}\frac{G_5}{G_4+G_5} \tag{8.34}$$

$$S_{G_C}^{\omega_p} = -\frac{G_C}{G_C+G_D}S_{G_B}^{\omega_p} \tag{8.35}$$

$$S_{G_D}^{\omega_p} = -\frac{G_D}{G_C+G_D}S_{G_B}^{\omega_p}. \tag{8.36}$$

Using Eqs. (8.14), (8.15) and (8.17), the expression $\dfrac{G_6}{G_2}\dfrac{G_B}{G_A}$ can be rewritten as:

$$\frac{G_6}{G_2}\frac{G_B}{G_A} = \frac{1}{1+\left(\dfrac{1}{n_2}-1\right)\left(\dfrac{b_0}{b_0-a_0}\right)\left(1+\dfrac{G_A}{G_B}\right)}. \tag{8.37}$$

Since $0 < n_2 < 1$ and, for the biquadratic function under study, $b_0 > a_0$:

$$0 < \frac{G_6}{G_2}\frac{G_B}{G_A} < 1. \tag{8.38}$$

The absolute value of $S_{G_6}^{\omega_p}$ and $S_{G_B}^{\omega_p}$ is thus minimised when $\dfrac{G_6}{G_2}\dfrac{G_B}{G_A} \to 0$. In other words,

$$\left(\frac{1}{n_2}-1\right)\left(\frac{b_0}{b_0-a_0}\right)\left(1+\frac{G_A}{G_B}\right) >> 0 \tag{8.39}$$

Since b_0 and a_0 are fixed for the specific application, the highpass gain n_2 and the ratio G_B/G_A determine the value of the expression in Eq. (8.39), which is maximised when both these parameters approach zero. That is, the sensitivity of ω_p with respect to G_6 and G_B decreases as both n_2 and G_B/G_A get smaller. It should also be noticed that decreasing the value of n_2 and G_B/G_A causes $S_{G_2}^{\omega_p}$ to reduce, with its theoretical minimum being limited to 0.5. Finally, $S_{G_C}^{\omega_p}$ and $S_{G_D}^{\omega_p}$ are directly proportional to $S_{G_B}^{\omega_p}$ and, if all the resistors have the same tolerance, the combined contribution of G_C and G_D to the change in ω_p is at most equal to the variation caused by G_B. In a similar manner, even though the actual values of $S_{G_4}^{\omega_p}$ and $S_{G_5}^{\omega_p}$ depend on the coefficients of the transfer function to be implemented, the gain n_2 and the ratios G_B/G_A and C_2/C_1 (see Eqs. (8.12) and (8.13)), the combined contribution of G_4 and G_5 to the variability of ω_p is at most equal to half the tolerance of the resistive components.

The expressions for the sensitivities of ω_z, Q_p and Q_z with respect to the circuit components are more complex than those shown in Eqs. (8.30) to (8.36) for ω_p. It can however be shown that, except for $S_{C_1}^{\omega_z}$ and $S_{C_2}^{\omega_z}$ which are equal to 0.5, all of the other sensitivities depend on the coefficients of the transfer function under study, the gain n_2 and the ratio G_B/G_A and, in some cases, on the ratio C_2/C_1. In order to analyse how the sensitivities vary with n_2, G_B/G_A and C_2/C_1, they are calculated for different values of these free parameters. It should be pointed out that second order changes in the values of n_2, G_B/G_A and C_2/C_1 caused by the variability of components C_1, C_2, G_B, G_C and G_D are not taken into consideration for these calculations.

Even though most of the sensitivity factors of ω_p have been shown to decrease when n_2 is reduced, n_2 is the high-frequency gain of the filter and it cannot be selected to be excessively small if a high degree of attenuation is to be avoided. The values of n_2 used to calculate the sensitivities of poles and zeros are 0.82, 0.91 and 0.99, which correspond to R_C/R_D ratios of 2.2/10, 1/10 and 1/100, respectively. The extreme case in which the circuit gain tends to unity is represented by n_2 = 0.99. It should finally be noted that the gain sensitivity with respect to R_C and R_D is dependent on the gain itself:

$$S_{G_C}^{n_2} = -S_{G_D}^{n_2} = \frac{G_D}{G_C + G_D} = \frac{G_D}{G_A} = 1 - n_2 \tag{8.40}$$

and its value decreases for increasing n_2. As regards the ratio G_B/G_A, the values chosen for the analysis are 0.01, 0.1 and 1. It has, in fact, been shown that $S_{G_2}^{\omega_p}$, $S_{G_6}^{\omega_p}$, $S_{G_B}^{\omega_p}$, $S_{G_C}^{\omega_p}$ and $S_{G_D}^{\omega_p}$ all decrease as the ratio G_B/G_A gets smaller. The values of C_2/C_1 selected for the calculations are 0.1, 1 and 10, so that the changes produced in the sensitivities by this parameter can be fully explored.

The sensitivities of the frequency and Q-factor of the poles and zeros of Friend's transfer

function calculated using the aforementioned values for n_2, G_B/G_A and C_2/C_1 are reported in Appendix C.1. For ω_z, it can be shown that:

$$S_{C_1}^{\omega_z} = S_{C_2}^{\omega_z} = -\frac{1}{2} \tag{8.41}$$

$$S_{G_2}^{\omega_z} = \frac{1}{2} \frac{1}{1 - \frac{G_6}{G_2} \frac{1}{n_2} \left(1 - n_2 + \frac{G_B}{G_A}\right)} \tag{8.42}$$

$$S_{G_4}^{\omega_z} = \frac{1}{2} \frac{G_4}{G_4 + G_5} \tag{8.43}$$

$$S_{G_5}^{\omega_z} = \frac{1}{2} \frac{G_5}{G_4 + G_5} \tag{8.44}$$

$$S_{G_C}^{\omega_z} = -S_{G_6}^{\omega_z} = -\frac{1}{2} \frac{1}{1 - \frac{1}{\frac{G_6}{G_2} \frac{1}{n_2} \left(1 - n_2 + \frac{G_B}{G_A}\right)}} \tag{8.45}$$

$$S_{G_B}^{\omega_z} = \frac{G_B}{G_B + G_D} S_{G_6}^{\omega_z} \tag{8.46}$$

$$S_{G_D}^{\omega_z} = \frac{G_D}{G_B + G_D} S_{G_6}^{\omega_z}. \tag{8.47}$$

This means that the sensitivities with respect to the capacitors are fixed and the combined contribution of G_4 and G_5 to the variability of ω_z is at most equal to half the value of their tolerance, if resistors having the same tolerance are selected for the implementation. Moreover, $S_{G_B}^{\omega_z}$, $S_{G_C}^{\omega_z}$ and $S_{G_D}^{\omega_z}$ are directly proportional to $S_{G_6}^{\omega_z}$. Let us therefore concentrate only on $S_{G_2}^{\omega_z}$ and $S_{G_6}^{\omega_z}$. From Eqs. (8.42) and (8.45), it can be seen that they are independent of the ratio C_2/C_1 and Tables C.1 to C.3 show that their absolute values decrease as n_2 and G_B/G_A decrease.

As regards Q_p, the following equations hold:

$$S_{C_1}^{Q_p} = -S_{C_2}^{Q_p} \tag{8.48}$$

$$S_{G_2}^{Q_p} = -2\, S_{G_2}^{\omega_p}\, S_{G_1}^{Q_p} \tag{8.49}$$

$$S_{G_6}^{Q_p} = -2\, S_{G_6}^{\omega_p}\, S_{G_1}^{Q_p} \tag{8.50}$$

$$S_{G_4}^{Q_p} = \frac{G_4}{G_4 + G_5} S_{G_1}^{Q_p} \tag{8.51}$$

$$S_{G_5}^{Q_p} = \frac{G_5}{G_4 + G_5} S_{G_1}^{Q_p} \tag{8.52}$$

$$S_{G_C}^{Q_p} = -\frac{G_C}{G_C + G_D} S_{G_B}^{Q_p} \tag{8.53}$$

$$S_{G_D}^{Q_p} = -\frac{G_D}{G_C + G_D} S_{G_B}^{Q_p}. \tag{8.54}$$

The sensitivities with respect to the capacitors have the same absolute value and $S_{G_2}^{Q_p}$ and $S_{G_6}^{Q_p}$ are proportional to $S_{G_1}^{Q_p}$ and to the respective ω_p sensitivities, which have already been discussed. Moreover, the contribution of the pairs G_4, G_5 and G_C, G_D to the change in Q_p is at most equal to variation caused by G_1 and G_B, respectively. Let us therefore concentrate only on $S_{C_1}^{Q_p}$, $S_{G_1}^{Q_p}$ and $S_{G_B}^{Q_p}$. It can be seen from Tables C.1 to C.3 that $S_{C_1}^{Q_p}$ is constant with n_2 and that its value depends in a complex manner on both G_B/G_A and C_2/C_1. $S_{C_1}^{Q_p}$ is negative for C_2/C_1 = 0.01 and positive otherwise and it gets more positive as G_B/G_A is increased. $S_{G_1}^{Q_p}$, where G_1 does not refer to an actual component in the circuit but only to the sum of G_4 and G_5, is also constant with respect to n_2, but it decreases for decreasing G_B/G_A and increasing C_2/C_1. In a similar manner, $S_{G_B}^{Q_p}$ decreases when the ratio G_B/G_A is made smaller and the ratio C_2/C_1 larger. Its value is, however, directly dependent on n_2.

Whereas for ω_p and ω_z it was easy to conclude that their sensitivities decrease as n_2 and G_B/G_A get smaller, the analysis of the sensitivities of Q_p is not so straightforward. Considering that the relations that determine the sensitivities of Q_z are even more complex than those of Q_p, an overall worst case figure is employed to evaluate how changes in the free parameters affect the sensitivities of poles and zeros. The maximum percentage change for the frequency and Q-factor can be calculated as:

$$\frac{\Delta y}{y}\% = \sum_{i=1}^{9} |S_i^y| \, \frac{\Delta i}{i}\% \tag{8.55}$$

where y represents, in turn, ω_p, Q_p, ω_z and Q_z and i are the nine passive components of Friend's circuit. If the biquad structure is realised using components with a 1% tolerance, the maximum percentage change that theoretically can occur in the frequency and Q-factor of the poles and zeros is simply equal to the sum of the absolute value of the sensitivities. It should be pointed out that the maximum change is calculated independently for each of the filter parameters and the percentage changes in ω_p, Q_p, ω_z and Q_z cannot all be equal to their theoretical maximum at the same time. For example, if the values of the circuit components lead to the theoretical maximum change in ω_p, it will not be possible for the percentage change in Q_p to be concurrently equal to the worst case value calculated from the sensitivities.

The theoretical maximum percentage changes in ω_p, ω_z, Q_p and Q_z calculated from the sensitivities in Appendix C.1 are shown in Table 8.2 when the manufacturing tolerance of the components is 1%. As it could have been inferred directly from the sensitivities previously discussed, the maximum percentage change in ω_p, ω_z and Q_p increases with n_2 and G_B/G_A. Moreover, $\Delta Q_p/Q_p$ appears to be at a minimum when the ratio C_2/C_1 lies between 1 and 10. The value of C_2/C_1 at which the minimum occurs seems to depend on

Table 8.2: Theoretical maximum percentage changes that can affect the frequency and Q-factor of the poles and zeros of Friend's circuit for different values of the high-frequency gain n_2 and of the ratios C_2/C_1 and G_B/G_A.

	G_B/G_A=0.01			G_B/G_A=0.1			G_B/G_A=1		
C_2/C_1	0.1	1	10	0.1	1	10	0.1	1	10
				n_2=0.82 (R_C/R_D=2.2/10)					
$\Delta\omega_p/\omega_p$ (%)	2.04	2.04	2.04	2.33	2.33	2.33	3.82	3.82	3.82
$\Delta\omega_z/\omega_z$ (%)	3.39	3.39	3.39	3.88	3.88	3.88	6.36	6.36	6.36
$\Delta Q_p/Q_p$ (%)	2.10	1.10	1.89	4.23	1.96	2.56	19.73	9.04	8.04
$\Delta Q_z/Q_z$ (%)	7.17	2.12	1.33	8.34	2.63	1.78	22.72	8.08	6.10
				n_2=0.91 (R_C/R_D=1/10)					
$\Delta\omega_p/\omega_p$ (%)	2.08	2.08	2.08	2.73	2.73	2.73	6.00	6.00	6.00
$\Delta\omega_z/\omega_z$ (%)	3.46	3.46	3.46	4.54	4.54	4.54	9.99	9.99	9.99
$\Delta Q_p/Q_p$ (%)	2.15	1.14	1.94	5.00	2.45	3.01	31.32	14.36	12.24
$\Delta Q_z/Q_z$ (%)	4.94	1.86	1.26	7.40	2.68	1.95	33.43	12.45	9.34
				n_2=0.99 (R_C/R_D=1/100)					
$\Delta\omega_p/\omega_p$ (%)	2.79	2.79	2.79	9.26	9.26	9.26	41.96	41.96	41.96
$\Delta\omega_z/\omega_z$ (%)	4.65	4.65	4.65	15.43	15.43	15.43	69.87	69.87	69.87
$\Delta Q_p/Q_p$ (%)	2.96	1.87	2.66	17.63	10.44	10.39	222.63	102.18	81.70
$\Delta Q_z/Q_z$ (%)	3.34	1.98	1.55	15.83	7.29	6.02	218.67	86.23	63.33

both n_2 and G_B/G_A. As regards the maximum percentage change in Q_z, it can be seen that its value gets lower as G_B/G_A decreases and C_2/C_1 increases. Furthermore, for low values of G_B/G_A, $\Delta Q_z/Q_z$ appears to be at a minimum for intermediate values of n_2.

The search to determine the combination of n_2, G_B/G_A and C_2/C_1 that yields the lowest maximum percentage changes in ω_p, ω_z, Q_p and Q_z can be thus restricted to a small range of values. Since the maximum percentage change in the filter parameters can be extremely high if the ratio G_B/G_A is selected as unity, only values of G_B/G_A between 0.01 and 0.1 need to be considered. Moreover, the value of C_2/C_1 can be limited to lie between 1 and 10, because $\Delta Q_p/Q_p$ is at a minimum over this interval and $\Delta Q_z/Q_z$ is decreasing with increasing C_2/C_1. Even though the maximum changes in ω_p, ω_z and Q_p decrease with n_2, the difference in the values obtained for n_2 = 0.82 and n_2 = 0.91 appears to be limited when G_B/G_A is low. Therefore, any subsequent analysis is only performed for n_2 = 0.91, which guarantees that the amplitude of the ECG signal is not excessively reduced by the limited passband gain of the highpass filter implemented using Friend's biquad.

Before proceeding to investigate further the selection of G_B/G_A and C_2/C_1 that leads to the lowest values for the theoretical maximum changes in ω_p, ω_z, Q_p and Q_z, it is worthwhile first assessing the feasibility of the implementation of the biquad function. The values of the

Table 8.3: Values of Friend's circuit components calculated for n_2 = 0.91, when C_2 = 100 nF and R_C = 1 MΩ.

	G_B/G_A=0.01		G_B/G_A=0.1	
C_2/C_1	1	10	1	10
C_1 (nF)	100	10	100	10
C_2 (nF)	100	100	100	100
R_2 (MΩ)	15.8	87.2	11.0	62.9
R_4 (MΩ)	10.1	25.8	11.7	28.3
R_5 (MΩ)	20.3	23.3	20.4	23.8
R_6 (MΩ)	4.1	22.9	4.1	23.6
R_B (MΩ)	90.9	90.9	9.1	9.1
R_C (MΩ)	1	1	1	1
R_D (MΩ)	10	10	10	10

circuit components for each of the combinations of G_B/G_A and C_2/C_1 under analysis are calculated when C_2 = 100 nF and R_C = 1 MΩ and shown in Table 8.3. It should be noticed that resistances R_2, R_4, R_5 and R_6 are easier to implement when C_2/C_1 = 1 and that the value of R_B is quite high for G_B/G_A = 0.01. It can, nonetheless, be concluded that the realisation of the components in Friend's circuit is feasible for any of the G_B/G_A and C_2/C_1 combinations.

Let us now analyse in more detail the possibility of minimising the theoretical maximum percentage changes in ω_p, ω_z, Q_p and Q_z by selecting optimum values for the ratios G_B/G_A and C_2/C_1. In Figure 8.4, the maximum theoretical change of the Q-factors of poles and zeros is represented for G_B/G_A equal to 0.01 and 0.1 and C_2/C_1 varying between 1 and 10. It can clearly be seen that the decrease in $\Delta Q_z/Q_z$ levels off for C_2/C_1 approximately equal to 3, whereas the value of $\Delta Q_p/Q_p$ keeps increasing with C_2/C_1. It can also be noticed that for G_B/G_A = 0.01 the maximum changes in Q_p and Q_z are quite similar when C_2/C_1 = 2, whereas for G_B/G_A = 0.1 $\Delta Q_p/Q_p \approx \Delta Q_z/Q_z$ when 1 < C_2/C_1 < 1.5. Since it has been shown in Section 8.2 that the amplitude of the passband peak and of the pulse response undershoot of the filter are affected in equal manner by the variability of poles and zeros, it seems appropriate to select the ratio C_2/C_1 so that the theoretical maximum changes in Q_p and Q_z are approximately the same.

The maximum percentage changes in ω_p, ω_z, Q_p and Q_z are therefore recalculated for $1 \leq C_2/C_1 \leq 3$ and G_B/G_A varying between approximately 0.01 and 0.1. The ratios G_B/G_A and C_2/C_1 used in the analysis are selected so that capacitances C_1 and C_2 and the resistance R_B can be implemented using a single physical component. The results are presented in Table 8.4, where the combinations of G_B/G_A and C_2/C_1 for which $\Delta Q_p/Q_p \approx \Delta Q_z/Q_z$ are highlighted. Even though the combination G_B/G_A = 0.009,

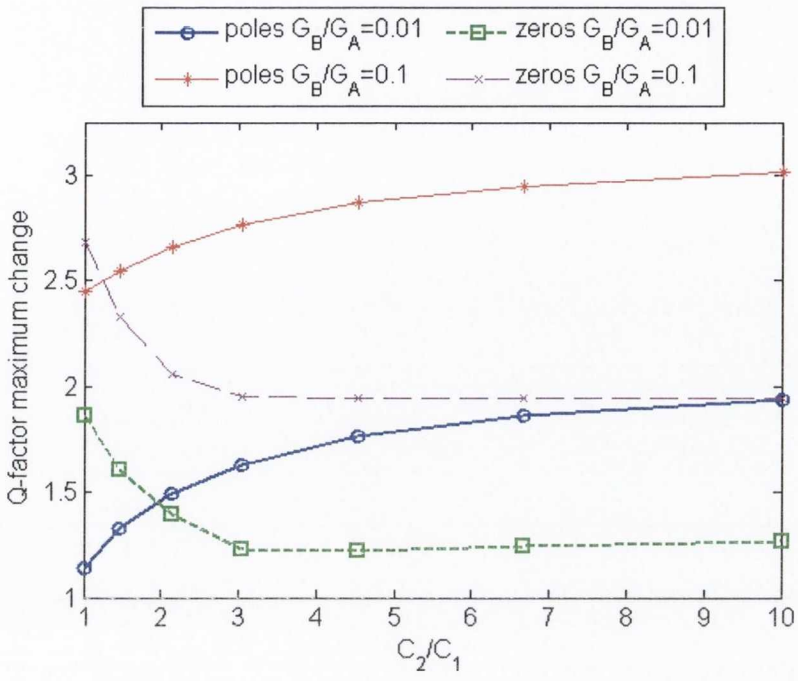


Figure 8.4: Maximum theoretical percentage change in the Q-factor of the poles and zeros of Friend's circuit for C_2/C_1 varying between 1 and 10 when n_2 = 0.91.

C_2/C_1 = 2.13 provides the overall best performance, it can be noticed that the results obtained when C_2/C_1 = 2.13 are not substantially different for values of G_B/G_A up to 0.028. The components of Friend's circuit derived for C_2/C_1 = 2.13 and $0.009 \leq G_B/G_A \leq 0.028$ are shown in Table 8.5. Since there is no appreciable difference in the values of R_2, R_4, R_5 and R_6, the circuit characterised by G_B/G_A = 0.009 can be selected for implementation, thus allowing the variability of ω_p, ω_z, Q_p and Q_z to be minimised.

8.5 Monte Carlo simulation of the highpass filter

The resistance and capacitance values derived from the design equations of Friend's circuit when C_2/C_1 = 2.13 and G_B/G_A = 0.009 can be realised by using at most two physical components and both their theoretical and implementable values are shown in Table 8.6. The values of the resistor, R_0, and the capacitor, C_0, needed for the realisation of the single-pole section of the third order filter are presented as well. The filter coefficients derived from the actual component values are also compared with the nominal values obtained from the optimisation procedure. It can be noticed that the percentage change introduced into the values of p_0, ω_p, ω_z by approximating resistances R_0, R_2, R_4, R_5 and R_6 is positive, whereas a negative variation is recorded for Q_p and Q_z. More importantly, the difference between approximated and theoretical values of the filter parameters is less than 0.6%.

Table 8.4: Theoretical maximum percentage changes that can affect the frequency and Q-factor of the poles and zeros of Friend's circuit for n_2 = 0.91, $1 \leq C_2/C_1 \leq 3$ and $0.009 \leq G_B/G_A \leq 0.091$ (C_2 = 100 nF and R_C = 1 MΩ).

G_B/G_A	0.009	0.013	0.019	0.028	0.041	0.061	0.091
R_B (MΩ)	100	68	47	33	22	15	10
			C_2/C_1=1 (C_1=100nF)				
$\Delta\omega_p/\omega_p$ (%)	2.07	2.11	2.15	2.21	2.32	2.46	2.67
$\Delta\omega_z/\omega_z$ (%)	3.45	3.51	3.58	3.69	3.86	4.09	4.44
$\Delta Q_p/Q_p$ (%)	1.13	1.19	1.28	1.39	1.59	1.87	2.31
$\Delta Q_z/Q_z$ (%)	1.85	1.89	1.94	2.01	2.13	2.31	2.60
			C_2/C_1=1.47 (C_1=68nF)				
$\Delta\omega_p/\omega_p$ (%)	2.07	2.11	**2.15**	**2.21**	**2.32**	**2.46**	**2.67**
$\Delta\omega_z/\omega_z$ (%)	3.45	3.51	**3.58**	**3.69**	**3.86**	**4.09**	**4.44**
$\Delta Q_p/Q_p$ (%)	1.31	1.37	**1.45**	**1.56**	**1.75**	**2.01**	**2.43**
$\Delta Q_z/Q_z$ (%)	1.60	1.63	**1.67**	**1.74**	**1.85**	**2.00**	**2.25**
			C_2/C_1=2.13 (C_1=37nF)				
$\Delta\omega_p/\omega_p$ (%)	**2.07**	**2.11**	**2.15**	**2.21**	2.32	2.46	2.67
$\Delta\omega_z/\omega_z$ (%)	**3.45**	**3.51**	**3.58**	**3.69**	3.86	4.09	4.44
$\Delta Q_p/Q_p$ (%)	**1.48**	**1.53**	**1.61**	**1.72**	1.90	2.15	2.54
$\Delta Q_z/Q_z$ (%)	**1.39**	**1.42**	**1.46**	**1.52**	1.62	1.76	1.99
			C_2/C_1=3.03 (C_1=33nF)				
$\Delta\omega_p/\omega_p$ (%)	2.07	2.11	2.15	2.21	2.32	2.46	2.67
$\Delta\omega_z/\omega_z$ (%)	3.45	3.51	3.58	3.69	3.86	4.09	4.44
$\Delta Q_p/Q_p$ (%)	1.62	1.67	1.75	1.85	2.02	2.27	2.65
$\Delta Q_z/Q_z$ (%)	1.23	1.25	1.29	1.34	1.45	1.61	1.87

Table 8.5: Values of Friend's circuit components calculated for n_2 = 0.91 and C_2/C_1 = 2.13, when C_2 = 100 nF and R_C = 1 MΩ.

G_B/G_A	**0.009**	0.013	0.019	0.028
R_B (MΩ)	**100**	68	47	33
C_1 (nF)	**47**	47	47	47
C_2 (nF)	**100**	100	100	100
R_2 (MΩ)	**24.85**	24.36	23.72	22.88
R_4 (MΩ)	**15.75**	15.85	15.98	16.17
R_5 (MΩ)	**21.96**	21.97	21.99	22.01
R_6 (MΩ)	**6.50**	6.50	6.51	6.52
R_B (MΩ)	**100**	68	47	33
R_C (MΩ)	**1**	1	1	1
R_D (MΩ)	**10**	10	10	10

Table 8.6: Theoretical and practical resistances and capacitances required for the implementation of the third order concave filter and corresponding values for the frequency and Q-factor of the poles and zeros.

	Theoretical	Practical	% difference
	Component values		
C_0 (nF)	100	100	
R_0 (MΩ)	52.91	52.6	-0.59
C_1 (nF)	47	47	
C_2 (nF)	100	100	
R_2 (MΩ)	24.85	24.70	-0.60
R_4 (MΩ)	15.75	15.75	-0.01
R_5 (MΩ)	21.96	22.00	0.18
R_6 (MΩ)	6.50	6.51	0.13
R_B (MΩ)	100	100	
R_C (MΩ)	1	1	
R_D (MΩ)	10	10	
	Filter parameters		
p_0 (rad/s)	0.189	0.190	0.59
ω_p (rad/s)	0.949	0.952	0.31
ω_z (rad/s)	0.736	0.740	0.48
Q_p	0.788	0.785	-0.39
Q_z	0.660	0.659	-0.18

A Monte Carlo analysis is then performed to determine the effect of the variability in the 11 passive components needed for the implementation of the third order filter on its time and frequency domain responses. A 1% uniformly distributed tolerance is simulated for the values of capacitors and resistors reported in the middle column of Table 8.6. There is no need to simulate the tolerance of every component actually used in the hardware implementation. In fact, when two or more components are needed to realise a set resistance or capacitance, the total change produced in the filter parameters due to the tolerances of the physical components is at most equal to that associated with an ideal resistor or capacitor of the required value.

The magnitude characteristic and the offset occurring after the application of a 3 mV$\times$100 ms rectangular pulse at the input of the third order filter are illustrated in Figure 8.5 for 3000 iterations of the Monte Carlo simulation. It can be seen that the variability in both the frequency and time domain responses is quite limited and that none of the simulated magnitude characteristics presents a peak higher than 0.5 dB. On the other hand, the 100 µV limit set for the pulse response undershoot is exceeded by approximately 53% of the runs, with the maximum undershoot measured to be 103.3 µV. The values of the filter parameters for this worst case are presented in Table 8.7 and their difference with respect to both the

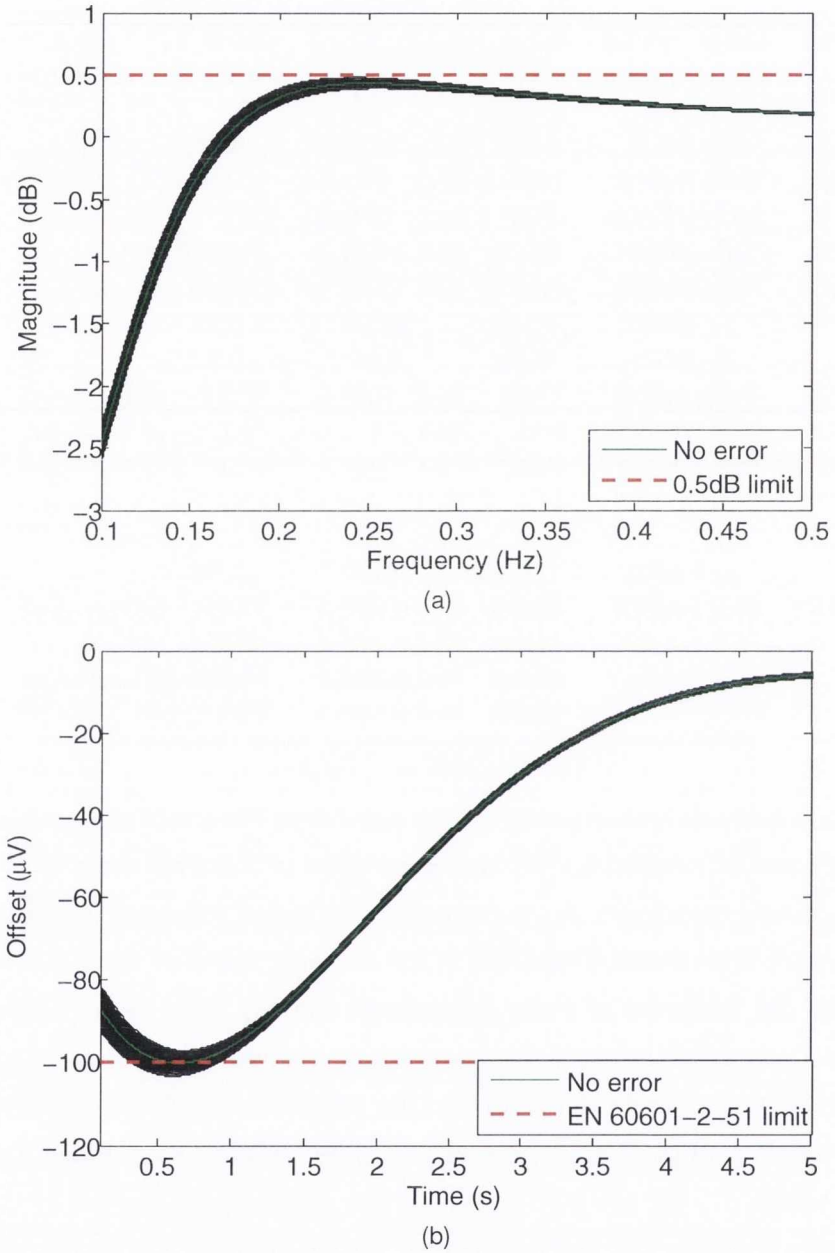


Figure 8.5: (a) Magnitude characteristic of the 3000 iterations of the third order concave filter obtained by simulating a 1% uniformly distributed tolerance in the 11 passive circuit components and (b) displacement from the isoelectric line occurring after the application of a 3 mV$\times$100 ms rectangular input pulse. The responses of the third order filter derived from the nominal component values are illustrated for comparison purposes.

Table 8.7: Frequency and Q-factor of the poles and zeros of the simulated third order filter that presents the largest pulse response undershoot.

	Values	% difference with theoretical values	% difference with practical values
p_0 (rad/s)	0.194	2.37	1.77
ω_p (rad/s)	0.945	-0.41	-0.72
ω_z (rad/s)	0.727	-1.28	-1.74
Q_p	0.788	0.00	0.39
Q_z	0.665	0.81	1.00

Table 8.8: Maximum and minimum values of the frequency and Q-factor of the poles and zeros measured from the 3000 simulations performed for the tolerance of the circuit components. The percentage difference with respect to the parameters derived from the nominal component values shown in the middle column of Table 8.6 is also calculated.

	max		min	
	Values	% diff.	Values	% diff.
p_0 (rad/s)	0.194	2.00	0.187	-1.84
ω_p (rad/s)	0.967	1.60	0.937	-1.60
ω_z (rad/s)	0.754	2.01	0.722	-2.43
Q_p	0.794	1.18	0.776	-1.10
Q_z	0.665	1.00	0.653	-0.90

theoretical and practical values shown in Table 8.6 is calculated. It can be seen that the frequencies of poles and zeros have been reduced by the component tolerances, Q_p is approximately equal to the theoretical value and marginally larger than the value derived from the realisable components, whereas Q_z is larger than both of these values. This seems to partially agree with the sensitivity analysis performed in respect of the filter parameters in Section 8.2. ω_z and Q_z are indeed smaller and larger than the nominal values, respectively. On the other hand, ω_p is expected to be larger and Q_p smaller than the nominal values if the Monte Carlo simulation carried out on the circuit components is to fully mirror the one performed directly on the frequency and Q-factor of the poles and zeros of the filter. It should finally be noted that the largest change between the simulated parameter and the nominal value occurs for p_0, which has been shown in Section 8.2 to have the least influence on the amplitude of both the magnitude peak and the pulse response undershoot. The large simulated variation in p_0 is due to the fact that the value of the real pole is linked only to R_0 and C_0 and their manufacturing tolerances reflect directly in it.

Let us finally evaluate the maximum variation affecting independently each of the filter parameters as measured from the Monte Carlo simulation. The maximum and minimum values of p_0, ω_p, ω_z, Q_p and Q_z assessed over the 3000 runs are shown in Table 8.8. As

predictable from the above considerations, the variability of p_0 is quite high. It can also be seen that the largest percentage change is measured for ω_z, whereas the Q-factors of poles and zeros present the least variation. This result is in line with what is expected from the worst case variations calculated earlier from the sensitivities of Friend's circuit to component tolerances. The theoretical maximum percentage change for Q_p and Q_z is, in fact, limited to less than 1.5%, but it can be as high as 3.5% for ω_z. It is however important to notice that the maximum change measured from the Monte Carlo simulation is between 20% and 30% lower than the theoretical worst case figure calculated from the sensitivities and shown in Table 8.4. Furthermore, since the amplitude of the peak occurring in the magnitude response has been shown to depend mainly on the variations in Q_p and Q_z (see Section 8.2), which are limited for the selected configuration of Friend's circuit, it is evident why none of the 3000 simulations leads to the 0.5 dB limit set for the passband ripple being exceeded.

8.6 Redesign of the third order highpass filter

In the previous section, it has been shown that the 100 μV limit allowed for the undershoot occurring in the response of the highpass filter to a 3 mV$\times$100 ms input rectangular pulse is exceeded by approximately half of the Monte Carlo simulations performed on the component tolerances. In order to account for the variability of the resistors and capacitors needed for the implementation of the system, the optimisation procedure aimed at maximising the 3dB-cutoff frequency of the third order concave filter (see Section 6.5) is therefore repeated specifying a stricter condition for the pulse response undershoot. By setting the bound at 95 μV instead of 100 μV, the optimisation process leads to the results shown in Appendix C.2, with the parameters characterising the third order filter being summarised in Table 8.9. By comparing these results with those presented in Table 8.1 for the initial design of the third order filter, it can be noticed that the frequency of the complex conjugate poles is reduced, while the Q-factors and the frequency of the zeros are increased. The frequency of the real pole is also approximately 10% larger than before. More importantly, the 3dB-cutoff point of the third order filter is reduced from 90.1 to 83.9 mHz. In other words, decreasing the maximum allowable undershoot by 5% causes the frequency maximised during the optimisation procedure to be reduced by approximately 7%. This reduction can be visually appreciated in Figure 8.6, where the magnitude and pulse responses of the newly derived filter are compared to those of the original design.

The variability of the frequency and Q-factor of the poles and zeros with respect to the tolerance of the components in Friend's circuit is calculated for the updated design. The

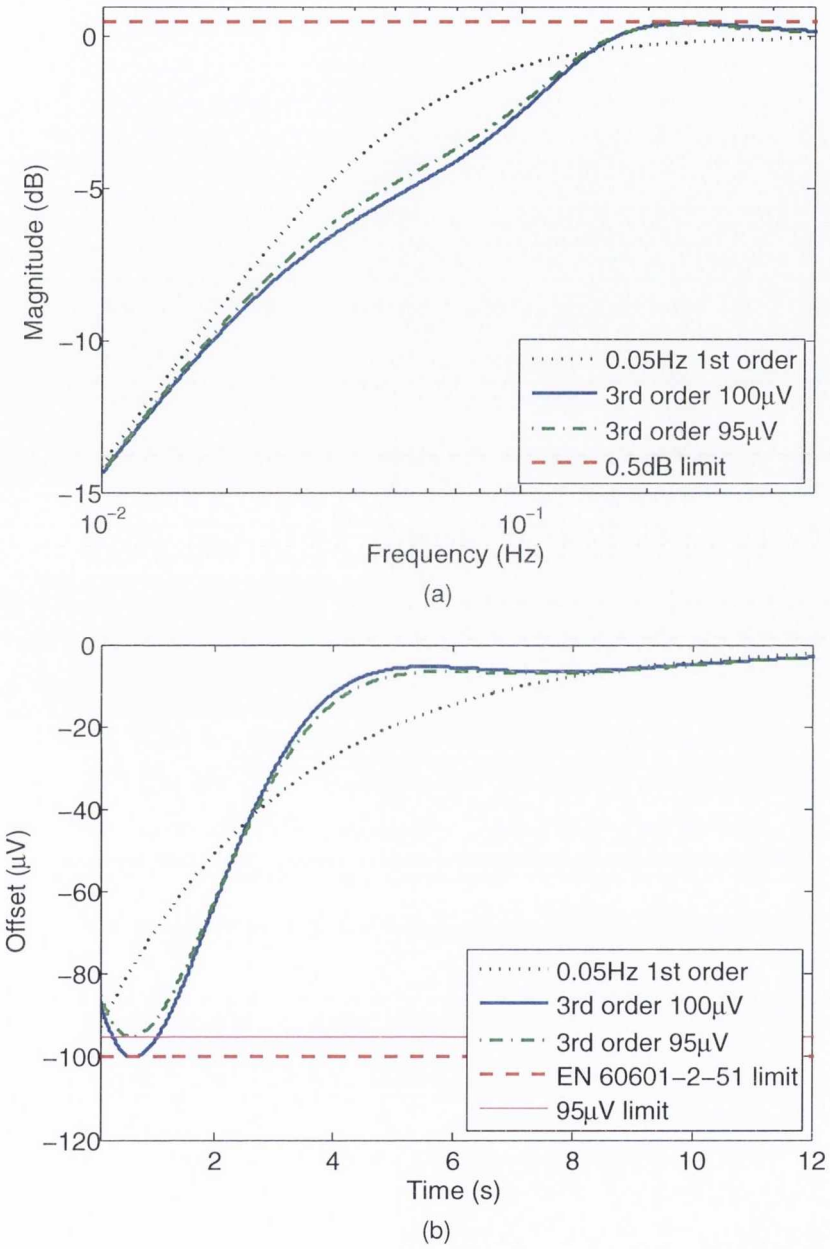


Figure 8.6: (a) Magnitude characteristic of the third order concave filter designed to have a pulse response undershoot of less than 95 μV and (b) displacement from the isoelectric line occurring after the application of a 3 mV×100 ms rectangular pulse at its input. The responses of the reference 0.05 Hz single-pole network and those of the original third order filter derived when the maximum amplitude allowed for the pulse response undershoot is equal to 100 μV are illustrated for comparison purposes.

Table 8.9: Parameters of the transfer function of the third order concave filter designed to have a pulse response undershoot of less than 95 μV.

p_0 (rad/s)	a_1 ((rad/s)^2)	a_0 (rad/s)	b_1 ((rad/s)^2)	b_0 (rad/s)	ω_p (rad/s)	ω_z (rad/s)	Q_p	Q_z
0.209	1.063	0.565	1.130	0.852	0.923	0.752	0.817	0.707

maximum percentage changes in ω_p, ω_z, Q_p and Q_z assessed for $1 \leq C_2/C_1 \leq 3$ and G_B/G_A varying between approximately 0.01 and 0.1 are shown in Table 8.10 when the gain n_2 is fixed to 0.91. It can be seen, once more, that the maximum changes in Q_p and Q_z are approximately equal for C_2/C_1 = 2.13 when $0.009 \leq G_B/G_A \leq 0.041$. The component values of Friend's circuit corresponding to these ratios are listed in Table 8.11. In this case, the values derived for C_2/C_1 = 2.13 and G_B/G_A = 0.019 seem to be the easiest to implement. Since the theoretical maximum percentage changes in the frequency and Q-factor of the poles and zeros are only marginally higher than the lowest values obtained for C_2/C_1 = 2.13 and G_B/G_A = 0.009, this choice does not significantly increase the chances of the magnitude peak and pulse response undershoot of the third order filter exceeding the limits specified by the EN 60601-2-51:2003 European standard [9] and the 1990 AHA recommendations [19] when the component tolerances are taken into consideration.

The practical values that can actually be employed in the hardware realisation of the third order concave filter designed to have a pulse response undershoot of less than 95 μV are presented in Table 8.12. It can be seen from Figure 8.7 that the time and frequency bounds set by the European standard and AHA recommendations are never exceeded when 3000 Monte Carlo simulations of the magnitude and pulse responses of this filter are performed for a 1% tolerance in the component values. The worst case value measured for the peak present in the amplitude characteristic is 0.43 dB and the pulse response undershoot is always less than 98 μV.

8.7 Conclusion

In the first section of this chapter, the sensitivity of the third order concave filter derived by maximising the 3dB-cutoff frequency has been evaluated with respect to changes in the frequency and Q-factor of its poles and zeros. Using a Monte Carlo simulation, it has been shown that that variations in the system parameters are more likely to cause significant distortion in the filter response to a 3 mV$\times$100 ms rectangular input pulse than in its magnitude characteristic. It has also been pointed out that the maximum amplitude of the undershoot occurring in the pulse response is more sensitive to changes in the frequency of the com-

Table 8.10: Theoretical maximum percentage changes that can affect the frequency and Q-factor of the complex conjugate poles and zeros of the third order filter designed to have a pulse response undershoot of less than 95 µV (n_2 = 0.91, C_2 = 100 nF and R_C = 1 MΩ).

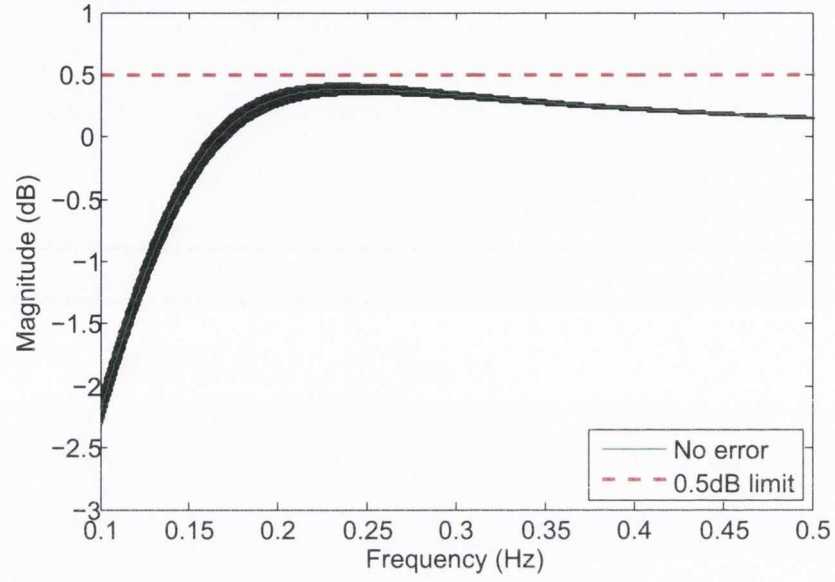
G_B/G_A	0.009	0.013	0.019	0.028	0.041	0.061	0.091
R_B (MΩ)	100.0	68.0	47.0	33.0	22.0	15.0	10.0
			C_2/C_1=1 (C_1=100nF)				
$\Delta\omega_p/\omega_p$ (%)	2.06	2.09	2.13	2.18	2.27	2.39	2.56
$\Delta\omega_z/\omega_z$ (%)	3.11	3.15	3.21	3.29	3.42	3.60	3.86
$\Delta Q_p/Q_p$ (%)	1.12	1.18	1.26	1.37	1.56	1.82	2.23
$\Delta Q_z/Q_z$ (%)	1.92	1.96	2.01	2.08	2.20	2.38	2.67
			C_2/C_1=1.47 (C_1=68nF)				
$\Delta\omega_p/\omega_p$ (%)	2.06	2.09	2.13	2.18	**2.27**	**2.39**	**2.56**
$\Delta\omega_z/\omega_z$ (%)	3.11	3.15	3.21	3.29	**3.42**	**3.60**	**3.86**
$\Delta Q_p/Q_p$ (%)	1.30	1.36	1.43	1.54	**1.71**	**1.96**	**2.34**
$\Delta Q_z/Q_z$ (%)	1.66	1.69	1.74	1.80	**1.91**	**2.07**	**2.32**
			C_2/C_1=2.13 (C_1=37nF)				
$\Delta\omega_p/\omega_p$ (%)	**2.06**	**2.09**	**2.13**	**2.18**	**2.27**	2.39	2.56
$\Delta\omega_z/\omega_z$ (%)	**3.11**	**3.15**	**3.21**	**3.29**	**3.42**	3.60	3.86
$\Delta Q_p/Q_p$ (%)	**1.47**	**1.52**	**1.59**	**1.69**	**1.86**	2.09	2.46
$\Delta Q_z/Q_z$ (%)	**1.44**	**1.47**	**1.52**	**1.58**	**1.68**	1.85	2.13
			C_2/C_1=3.03 (C_1=33nF)				
$\Delta\omega_p/\omega_p$ (%)	2.06	2.09	2.13	2.18	2.27	2.39	2.56
$\Delta\omega_z/\omega_z$ (%)	3.11	3.15	3.21	3.29	3.42	3.60	3.86
$\Delta Q_p/Q_p$ (%)	1.61	1.66	1.73	1.82	1.99	2.21	2.56
$\Delta Q_z/Q_z$ (%)	1.41	1.45	1.50	1.57	1.69	1.86	2.13

Table 8.11: Values of Friend's circuit components calculated for the third order filter designed to have a pulse response undershoot of less than 95 µV (n_2 = 0.91, C_2/C_1 = 2.13, when C_2 = 100 nF and R_C = 1 MΩ).

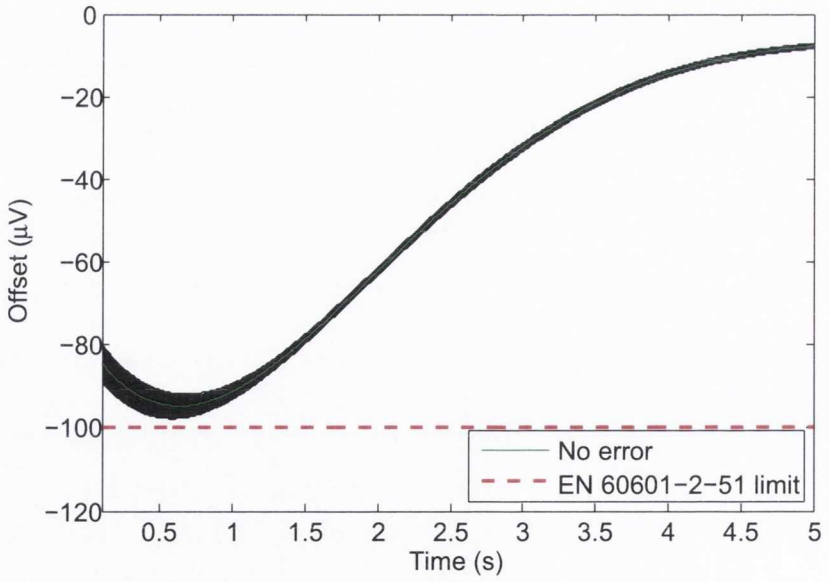
G_B/G_A	0.009	0.013	**0.019**	0.028	0.041
R_B (MΩ)	100	68	**47**	33	22
C_1 (nF)	47	47	**47**	47	47
C_2 (nF)	100	100	**100**	100	100
R_2 (MΩ)	26.63	26.16	**25.54**	24.73	23.50
R_4 (MΩ)	14.02	14.11	**14.22**	14.38	14.64
R_5 (MΩ)	25.94	25.96	**25.98**	26.01	26.06
R_6 (MΩ)	8.22	8.22	**8.22**	8.23	8.24
R_B (MΩ)	100	68	**47**	33	22
R_C (MΩ)	1	1	**1**	1	1
R_D (MΩ)	10	10	**10**	10	10

Table 8.12: Values of resistors and capacitors that can be employed for the implementation of the third order filter designed to have a pulse response undershoot of less than 95 µV.

C_0 (nF)	R_0 (MΩ)	C_1 (nF)	C_2 (nF)	R_2 (MΩ)	R_4 (MΩ)	R_5 (MΩ)	R_6 (MΩ)	R_B (MΩ)	R_C (MΩ)	R_D (MΩ)
100	47.82	47	100	25.30	14.20	25.90	8.25	47	1	10



(a)



(b)

Figure 8.7: (a) Magnitude characteristic of the 3000 iterations of the third order filter designed to have a pulse response undershoot of less than 95 µV obtained by simulating a 1% tolerance in the circuit components and (b) displacement from the isoelectric line occurring after the application of a 3 mV×100 ms rectangular input pulse.

plex conjugate poles and zeros than to variations in the Q-factors or in the frequency of the real pole.

Friend's single-amplifier biquad was then proposed for the implementation of the complex conjugate poles and zeros of the third order filter and its sensitivity to the manufacturing tolerance of passive components analysed. The theoretical maximum change that can affect the frequency and Q-factor of the poles and zeros was calculated for a 1% tolerance in both resistors and capacitors. The component values for Friend's circuit were selected to minimise the worst case theoretical variations in the location of poles and zeros. Obviously, some compromises needed to be made for the filter implementation to be feasible. For example, the maximum theoretical change that can affect the frequency of the poles and zeros and the poles' Q-factor decreases as the high-frequency gain of the biquad structure is reduced. This gain is, however, constrained to be less than unity by the circuit topology and it cannot be excessively reduced if the amplitude of the input signal is to be preserved. For the component values chosen in the filter realisation, the theoretical maximum percentage change in the poles' frequency is approximately 2%, the change in the zeros' frequency is about 3.5% and the maximum variation in the Q-factors is less than 1.5%.

A Monte Carlo simulation of the magnitude and pulse responses of the third order filter was later performed for a 1% tolerance in the component values. The amplitude characteristic was always lower than the 0.5 dB bound set for the filter passband ripple, whereas the 100 μV limit specified for the pulse response was exceeded by approximately 50% of the 3000 iterations. The maximum amplitude measured for the undershoot occurring after the application of a 3 mV$\times$100 ms rectangular input wave was limited to 103 μV. The maximum variations in the frequency and Q-factor of the complex conjugate poles and zeros evaluated over the 3000 runs were between 20% and 30% lower than their theoretical maximum values assessed from the sensitivities of Friend's circuit.

In order to allow for component tolerances, the third order concave filter was redesigned by lowering the bound specified for the maximum pulse response undershoot from 100 μV to 95 μV. The 3dB-cutoff frequency of the highpass filter derived by repeating the optimisation procedure is approximately 84 mHz, that is, 7% lower than that of the original filter. It should, however, be pointed out that this value is still 68% higher than that of the reference first order highpass filter usually employed in electrocardiographic equipment.

Chapter 9

Conclusion

9.1 Overview

The main objective of this work was to design an analogue front-end filter for portable electrocardiographic equipment, providing the highest possible rejection of out-of-band noise and interference. In order to guarantee that the morphology of the input ECG signal is not distorted, the transfer function of the filter has been devised to fulfil the requirements set by the European and American standards and the AHA recommendations for diagnostic ECG measurement systems [9, 15, 19].

At first, attention was focused on the lowpass section of the filter and a thorough analysis of the time and frequency domain responses of some classic all-pole filters was performed. It was concluded that linear phase with equiripple error and equiripple impulse overshoot characteristics represent a suitable alternative to the Bessel transfer function commonly employed for the implementation of the lowpass filter [20–22]. In fact, when the order of the system is larger than two, the passband flatness, in-band group delay variation and maximum amplitude of the step response overshoots of both Bessel and equiripple filters are well within the limits derived from the American standard ANSI/AAMI EC11:1991/(R)2001/(R)2007 [15] and the 1990 AHA recommendations [19]. The linear phase with equiripple error and equiripple impulse overshoot filters do however provide a larger attenuation than the Bessel in the transition region. This property of equiripple transfer functions appears to be particularly advantageous when considering that the lowpass filter is needed not only to eliminate high-frequency noise and interference from the input signal but also to prevent aliasing from occurring when the electrocardiographic record is digitised.

Since the requirements established by the EN 60601-2-51:2003 European standard [9] for the low-frequency time domain response of electrocardiographic recording systems are

extremely stringent, the design of the highpass filter was, on the other hand, very challenging. The possibility of compensating the characteristics of a highpass filter obtained thorough a lowpass-to-highpass transformation was initially explored. A fourth order filter satisfying both the magnitude and pulse response specifications set by the European standard and the 1990 AHA recommendations was obtained by cascading a lag-lead network to a second order system derived using the 1-H(s) transformation. Unfortunately, this filter does not provide any substantial benefit in terms of noise and interference rejection when compared with the simple 0.05 Hz single-pole highpass network traditionally employed at the front-end of diagnostic electrocardiographs.

In order to find an analogue highpass filter characterised by a magnitude response more selective than that of the traditional 0.05 Hz first order system, the derivation of the filter transfer function directly from the time and frequency domain specifications detailed in the European standard and the 1990 AHA report was attempted. A constrained optimisation procedure aimed at maximising the low-frequency rejection of second and third order highpass filters was developed. This technique was employed to maximise the stopband limit, the 3dB-cutoff frequency and the area subtended by the magnitude response of the filters. The optimisation of the stopband limit led the highpass filters to have a 3dB-cutoff frequency lower than 0.05 Hz. On the other hand, the last two approaches produced very similar results, with the 3dB-cutoff frequency of the second and third order optimised filters being as high as 0.07 Hz and 0.12 Hz, respectively. It should be noted that the conditions imposed on the passband ripple and on the negative displacement occurring after the application of the input test pulse represent the limiting factors of the optimisation procedure and that the corresponding constraints are tightly matched by the optimised filters.

The distortion introduced into synthetic and real ECG signals and the noise reduction capabilities of the optimised filters were then evaluated and compared with those produced by the reference 0.05 Hz single-pole network. It emerged that the third order filter designed to have a concave magnitude response over the transition region and characterised by a 0.09 Hz 3dB-cutoff frequency provides the best trade-off among all of the highpass filters. When evaluated on ECG records containing large low-frequency disturbances, this filter was able to provide a 50% input-output reduction of the noise power. It is also worthwhile noting that, in this case, the low-frequency out-of-band power measured in the output signals is 23% lower for the third order concave filter than for the reference 0.05 Hz single-pole system. Furthermore, the amplitude error and the change in the ST segment slope introduced into synthetic ECG waveforms by the third order optimised filter is always lower than that of the 0.05 Hz first order network.

The focus was then shifted towards the implementation of this optimal highpass filter. The employment of Friend's single-amplifier circuit [181] for the realisation of the biquadratic

section of the third order system was investigated. The passive sensitivities of this topology were evaluated and the values of its circuit components derived in such a way that the variation in the frequency and Q-factor of the poles and zeros is minimised. A Monte Carlo simulation of the magnitude and pulse responses of the proposed implementation was performed for a 1% tolerance in the circuit passive elements. Based on the results of this analysis, the optimisation procedure of the third order concave filter was repeated by constraining the pulse response undershoot to be 5% less than the requirement set by the European standard. The 3dB-cutoff frequency of this newly designed filter is approximately 7% lower than that of the original third order system, but it is still almost 70% higher than that of the reference single-pole network.

It should finally be noted that, even though the third order highpass filter proposed provides better low-frequency attenuation than the 0.05 Hz single-pole system, it is not able to reject all of the out-of-band noise and interference which corrupts ECG recordings. Therefore, digital post-processing techniques, such as those described in Section 5.3, will still be needed to remove respiratory artifacts, which occur at frequencies just below the ECG spectrum. Moreover, as discussed in Section 2.4.3, in-band noise, e.g. power line interference, muscle and motion artifacts, cannot be eliminated using linear time-invariant filters like the ones described in this work and digital techniques must be employed in the attempt to reduce this [4, 76].

9.2 Contributions of this work

Undoubtedly, the main accomplishment of this thesis consists in the design of an analogue highpass filter of limited complexity which provides low-frequency noise and interference rejection superior to that of the traditionally employed 0.05 Hz first order network without degrading the quality of the electrocardiographic signal. The derivation, testing and implementation of this filter have been extensively investigated. Attention is now drawn towards a few other contributions to the field of ECG filter design made by this work.

Even though over the years special relevance has been attributed to the phase response of the highpass filter [13, 18, 19, 24–26], in this thesis it has been proven that the phase linearity condition is not sufficient to guarantee that the morphology of the electrocardiographic signal is preserved by the recording system. It has been shown that a zero-phase bidirectional filter adhering to the magnitude response recommendations proposed in the 1990 AHA report [19] does not satisfy the time domain specifications established in the same publication. It has also been illustrated that the phase shift introduced over the ECG spectrum by the second and third order filters designed through the optimisation procedure

is negligible, despite no specific constraint being defined for their phase response. In other words, the requirement specified for the pulse response undershoot is much more stringent than the phase linearity condition and it limits both the phase shift and the low-frequency attenuation of the magnitude response of the highpass filter.

Furthermore, when the magnitude and pulse responses of a few digital FIR filters specifically designed to eliminate baseline wander were tested for compliance with the time and frequency domain specifications set by the EN 60601-2-51:2003 European standard [9] and the 1990 AHA recommendations, it emerged that only one of these systems satisfies the requirements. This surprising result highlights the difficulty of designing a highpass system suitable for diagnostic ECG applications and dispels the misconception that filters having linear or zero phase do not introduce significant time domain distortion in the electrocardiographic signal if their 3dB-cutoff point is located at frequencies lower than the ECG spectrum.

Another major achievement of his work was the proposal of a rigorous method for testing the time domain distortion and noise rejection ability of the highpass filter. The criteria employed to assess the distortion were derived from the European standard and applied to synthetic signals resembling as closely as possible the calibration waveforms defined in the same publication and to annotated ECG records available on PhysioNet [174]. It is important to note that the maximum error and change in the ST segment slope allowed are so small that they cannot actually be represented on the same scale as the ECG signal and therefore it is not possible to visually evaluate the distortion. As regards the noise rejection, it has been shown that baseline wander cannot be accurately simulated using a limited number of sinusoidal signals. A quantitative method based on the reduction of the power contained in electrocardiographic records at frequencies lower than the ECG spectrum has been employed to assess the ability of the highpass filters to eliminate out-of-band interference. This technique was applied to the three noise records and to some of the electrocardiographic recordings available on PhysioNet.

9.3 Recommendations for standards and test signals

From the review of the European and American standards and of the AHA recommendations [9, 15, 19, 62, 63], it emerged that the pulse response specifications are not consistently defined across these publications. In particular, whereas a complete geometrical definition of the input waveform is sometimes provided, in other cases the test pulse is only described by its area. Since it has been verified that the displacement occurring after the application of the input pulse and the slope of the filter response do not depend only on the

area of the test waveform, but also on its duration, it is essential that a rigorous description of the shape, amplitude and duration of the input test signal is provided by the standards. An alternative could be to define the time domain requirements of the highpass filter in terms of its impulse response. It has, in fact, been shown that both the offset and the slope of the response to a rectangular or triangular input wave can be reduced to those produced by a Dirac delta function of the same area when the duration of the test pulse is limited compared to the settling time of the highpass filter.

It has been proven that the requirement established by the current standards for the pulse response offset is based on the response of the 0.05 Hz single-pole highpass filter proposed in 1966 by Berson and Pipberger [16]. It is remarkable that, except for the work by Burri et al. [18], no other study evaluating the distortion introduced into electrocardiographic records by highpass filtering has been carried out in almost 50 years. It is advocated that an exhaustive analysis of the accuracy needed for both visual and automatic interpretation of the electrocardiogram be performed. It is hoped that, based on this study, the requirements imposed by the standards on the time domain response could be relaxed, allowing the highpass filter to provide a higher rejection of the low-frequency noise and interference.

When evaluating the most suitable transfer function for the lowpass section of the electrocardiographic filter, it emerged that no particular requirement is specified for either its phase or its step response. More importantly, besides its 3dB-cutoff frequency, no other condition is established for the attenuation of the lowpass filter in the transition region. It is therefore advocated that more detailed specifications are set in the standards for the high-frequency characteristic of the ECG filter.

The fundamental role of synthetic ECG waveforms in evaluating the amplitude error and the change in the ST segment slope caused by the highpass filter has been highlighted. In fact, even though it is possible to employ actual ECG recordings for this task, in-band noise and waveform distortion introduced by the measurement equipment can invalidate the analysis. The author feels that an extended set of test ECG signals to be used as a benchmark for comparing the performance of different electrocardiographic filters should be specified. Ideally, these synthetic waveforms should resemble the morphology of the ECG signal as closely as possible and some of the test signals should reproduce the characteristics of the ECG wave when common cardiac abnormalities are present. It is suggested that the test waveforms are included in the international electrocardiographic standards and it is hoped that it will become common practice to quantify the distortion of ECG recording devices against them.

It is also thought it would be beneficial if more recordings of noise typically affecting ECG measurements were available for testing the rejection of the electrocardiographic filter. A selection of noise recordings could be gathered to allow the performance of various

filters to be compared using a common framework. In the absence of such a set of test records, a database of ECG signals characterised by very large low-frequency noise power could be put together from the recordings already available on PhysioNet [174]. A more comprehensive testing of the noise reduction capability of the highpass filter could then be performed.

9.4 Further work

Even though the analysis performed in this thesis has been quite thorough and exhaustive, the process leading to the design of an optimal analogue filter for electrocardiographic applications cannot be deemed to be concluded. The main areas that warrant further research are the optimisation of the highpass filter, its implementation and the integration of the analogue filter into the front-end instrumentation amplifier.

Given the somewhat limited complexity of the analytical expressions of the magnitude and impulse responses of the second order highpass filter, it would be worthwhile to derive the solution space of the optimisation from the time and frequency domain constraints. It could then be verified, either analytically or graphically, if the solution obtained by maximising the frequency of the 3dB-point of the system through the numerical optimisation actually represents a global optimum. A genetic algorithm or another stochastic optimisation method should, on the other hand, be employed to check whether the results obtained for the 3dB-cutoff frequency and for the overall low-frequency rejection of the third order filter are local or global maxima. Moreover, the optimisation of a fifth order filter could also be attempted by employing these techniques.

It is also suggested that a study of the low-frequency noise content of the electrocardiographic signals be carried out. In fact, only one analysis quantifying the low-frequency noise of ECG recordings was found in the literature and it is more than 40 years old [65]. The optimisation of the highpass filter could benefit from the availability of a good spectral estimate of the out-of-band noise and interference. If the features of the noise spectrum were known in more detail, a targeted optimisation procedure could be set up. In other words, instead of maximising the 3dB-cutoff frequency or the overall low-frequency rejection of the highpass filter, the optimisation could aim at providing the largest attenuation at the frequencies where the noise power spectral density is highest.

As regards the implementation, the employment of the single-amplifier circuit proposed by Sedra et al. [182] for the realisation of the biquadratic section of the third order optimised filter should be investigated. In fact, even though the variations caused by component tolerances on the frequency and Q-factor of the poles and zeros have been shown to be limited

for Friend's circuit, the topology proposed by Sedra et al. is supposed to have even lower sensitivities for the transmission zeros. The possibility of using a double-amplifier structure, such as the one based on the generalised impedance converter (GIC) presented in [159], could also be examined. Multiple-amplifier biquads are in fact characterised by lower sensitivities than single-amplifier circuits, they allow the range of values of passive components to be reduced and provide the opportunity to tune the filter parameters, i.e. the frequency and Q-factor of the poles and zeros and the gain, more easily [180]. Obviously, these benefits will come at the price of increased power consumption and hardware complexity.

The subsequent step in the design of the analogue front-end filter should be the integration of both the highpass and the lowpass sections into the instrumentation amplifier. The time and frequency domain characteristics of the overall system should then be checked for compliance with the standards. Finally, if the structure is to be employed in electrocardiographic applications involving dry electrodes, the effect that the high impedances associated with these electrodes [35] have on the front-end magnitude and pulse responses should be evaluated. Since the impedance of the skin-electrode interface is at a maximum at zero frequency, the use of dry electrodes would mostly affect the low-frequency response of the front-end of the ECG recording system, which has already been shown to be of critical importance.

An analysis was performed by Assambo [57] to determine the minimum value of the input resistance of an AC-coupled front-end amplifier required for dry-electrode electrocardiographic applications. It emerged that, for low-frequency skin-electrode impedances of up to 4 MΩ, the effects of the skin-electrode interface on the frequency and time domain responses of the amplifier can be considered negligible when the input resistance is greater than 2 GΩ. In other words, in order to guarantee undistorted recording of the ECG signal, the resistance of the DC-blocking network needs to be several orders of magnitude higher than the impedance measured for the skin-electrode interface at zero frequency. Since the single-pole RC section of the third order filter designed in this work represents the DC-blocking network of the highpass system, similar considerations apply to it as well. For dry-electrode ECG measurements, it is therefore necessary to decrease the value of the capacitance of the RC network (see Table 8.12), so that the value of the circuit resistance can be increased to counteract the effects of the high impedance associated with the electrodes. Since resistors with a 1% tolerance are available in values up to 5 GΩ [184] and capacitors with a 1% tolerance are available in values in the region of 1 nF [185], the Monte Carlo simulations performed in Sections 8.5 and 8.6 for the third order highpass filter are still valid.

References

[1] *Global Atlas on Cardiovascular Disease Prevention and Control*, S. Mendis, P. Puska, and B. Norrving, Eds. World Health Organization, Geneva, 2011. [Online]. Available: http://www.who.int/cardiovascular_diseases/publications/atlas_cvd/en/

[2] S. Allender, P. Scarborough, V. Peto, M. Rayner, J. Leal, R. Luengo-Fernandez, and A. Gray, *European Cardiovascular Disease Statistics*, European Heart Network, Brussels, 2008. [Online]. Available: http://www.ehnheart.org/cvd-statistics.html

[3] *Mortality from Cardiovascular Disease (CVD) in 2006*, Irish Heart Foundation, Dublin, 2007. [Online]. Available: https://www.irishheart.ie/media/pub/factsheets/cvd_mortality_rates_2007.pdf

[4] L. Sornmo and P. Laguna, *Bioelectrical Signal Processing in Cardiac and Neurological Applications*. Burlington, MA: Elsevier Academic Press, 2005, ch. 6 and 7.

[5] C. Fisch, "Centennial of the String Galvanometer and the Electrocardiogram," *Journal of the American College of Cardiology*, vol. 36, no. 6, pp. 1737–1745, Nov. 2000.

[6] H. J. J. Wellens and A. P. Gorgels, "The Electrocardiogram 102 Years After Einthoven," *Circulation*, vol. 109, no. 5, pp. 562–564, Feb. 2004.

[7] A. T. Reisner, G. D. Clifford, and R. G. Mark, "The Physiological Basis of the Electrocardiogram," in *Advanced Methods And Tools for ECG Data Analysis*, G. D. Clifford, F. Azuaje, and P. E. McSharry, Eds. London: Artech House, 2006, ch. 1, pp. 1–25.

[8] D. M. Mirvis and A. L. Goldberger, "Electrocardiography," in *Braunwald's Heart Disease: A Textbook of Cardiovascular Medicine*, P. Libby, R. O. Bonow, D. L. Mann, D. P. Zipes, and E. Braunwald, Eds. Philadelphia: Saunders Elsevier, 2008, pp. 149–193.

[9] "EN 60601-2-51:2003. Medical electrical equipment. Part 2-51: Particular requirements for safety, including essential performance, of recording and analysing single channel and multichannel electrocardiographs (IEC 60601-2-51:2003)," July 2003.

[10] A. Lymberis and A. Dittmar, "Advanced Wearable Health Systems and Applications: Research and Development Efforts in the European Union," *IEEE Engineering in Medicine and Biology Magazine*, vol. 26, no. 3, pp. 29–33, May-June 2007.

[11] N. J. Holter, "New Method for Heart Studies," *Science*, vol. 134, no. 3486, pp. 1214–1220, Oct. 1961.

[12] M. H. Crawford, S. J. Bernstein, P. C. Deedwania, J. P. DiMarco, K. J. Ferrick, A. Garson, L. A. Green, H. L. Greene, M. J. Silka, P. H. Stone, C. M. Tracy, R. J. Gibbons, J. S. Alpert, K. A. Eagle, T. J. Gardner, G. Gregoratos, R. O. Russell, T. J. Ryan, and S. C. Smith, "ACC/AHA Guidelines for Ambulatory Electrocardiography: Executive Summary and Recommendations. A Report of the American College of Cardiology/American Heart Association Task Force on Practice Guidelines (Committee to Revise the Guidelines for Ambulatory Electrocardiography) Developed in Collaboration With the North American Society for Pacing and Electrophysiology," *Circulation*, vol. 100, no. 8, pp. 886–893, Aug. 1999.

[13] D. I. Tayler and R. Vincent, "Artefactual ST segment abnormalities due to electrocardiographic design," *British Heart Journal*, vol. 54, no. 2, pp. 121–128, Aug. 1985.

[14] D. I. Tayler, R. Vincent, and B. Jolley, "The importance of assessing the fidelity of electrocardiographs by using a simple calibration signal," *Journal of Medical Engineering & Technology*, vol. 32, no. 5, pp. 365–370, Sept.-Oct. 2008.

[15] "ANSI/AAMI EC11:1991/(R)2001/(R)2007. Diagnostic electrocardiographic devices," Aug. 2007.

[16] A. S. Berson and H. V. Pipberger, "The low-frequency response of electrocardiographs, a frequent source of recording errors," *American Heart Journal*, vol. 71, no. 6, pp. 779–789, June 1966.

[17] ——, "Electrocardiographic distortions caused by inadequate high-frequency response of direct-writing electrocardiographs," *American Heart Journal*, vol. 74, no. 2, pp. 208–218, Aug. 1967.

[18] H. Burri, H. Sunthorn, and D. Shah, "Simulation of anteroseptal myocardial infarction by electrocardiographic filters," *Journal of Electrocardiology*, vol. 39, no. 3, pp. 253–258, July 2006.

[19] J. J. Bailey, A. S. Berson, A. Garson, L. G. Horan, P. W. Macfarlane, D. W. Mortara, and C. Zywietz, "Recommendations for Standardization and Specifications in Automated Electrocardiography: Bandwidth and Digital Signal Processing. A Report for

Health Professionals by an Ad Hoc Writing Group of the Committee on Electrocardiography and Cardiac Electrophysiology of the Council on Clinical Cardiology, American Heart Association," *Circulation*, vol. 81, no. 2, pp. 730–739, Feb. 1990.

[20] G. D. Clifford and M. B. Oefinger, "ECG Acquisition, Storage, Transmission, and Representation," in *Advanced Methods and Tools for ECG Data Analysis*, G. D. Clifford, F. Azuaje, and P. E. McSharry, Eds. London: Artech House, 2006, ch. 2, pp. 27–53.

[21] F. Bartoli, S. Cerutti, and E. Gatti, "Digital filtering and regression algorithms for an accurate detection of the baseline in ECG signals," *Medical Informatics*, vol. 8, no. 2, pp. 71–82, Apr.-Jun. 1983.

[22] T. Desel, T. Reichel, S. Rudischhauser, and H. Hauer, "A CMOS Nine Channel ECG Measurement IC," in *Proceedings of the 2nd International Conference on ASIC*, Shanghai, Oct. 1996, pp. 115–118.

[23] C. E. Kossmann, D. A. Brody, G. E. Burch, H. H. Hecht, F. D. Johnston, C. Kay, E. Lepeschkin, H. V. Pipberger, G. Baule, A. S. Berson, S. A. Briller, G. B. Geselowitz, L. G. Horan, and O. H. Schmitt, "Recommendations for Standardization of Leads and of Specifications for Instruments in Electrocardiography and Vectorcardiography. Report of Committee on Electrocardiography, American Heart Association," *Circulation*, vol. 35, no. 3, pp. 583–602, Mar. 1967.

[24] S. Luo and P. Johnston, "A review of electrocardiogram filtering," *Journal of Electrocardiology*, vol. 43, no. 6, pp. 486–496, Nov.-Dec. 2010.

[25] D. Tayler and R. Vincent, "Signal distortion in the electrocardiogram due to inadequate phase response," *IEEE Transactions on Biomedical Engineering*, vol. 30, no. 6, pp. 352–356, June 1983.

[26] R. E. Gregg, S. H. Zhou, J. M. Lindauer, E. D. Helfenbein, and K. K. Giuliano, "What is inside the electrocardiograph?" *Journal of Electrocardiology*, vol. 41, no. 1, pp. 8–14, Jan. 2008.

[27] R. Dozio and M. J. Burke, "Second and Third Order Analogue High-Pass Filters for Diagnostic Quality ECG," in *Proceedings of the 20th IET Irish Signals and Systems Conference*, Dublin, June 2009.

[28] ——, "Optimised Design of the Front-End Analogue High-Pass Filter for a Diagnostic Quality ECG Monitoring System," in *Proceedings of the 31st Annual International Conference of the IEEE Engineering in Medicine and Biology Society*, Minneapolis, Sept. 2009, pp. 1770 –1773.

[29] J. J. Carr and J. M. Brown, *Introduction to Biomedical Equipment Technology*. Upper Saddle River, NJ: Prentice-Hall, 2001, ch. 2.

[30] L. Cromwell, F. J. Weibell, and E. A. Pfeiffer, *Biomedical Instrumentation and Measurements*. Englewood Cliffs, NJ: Prentice-Hall, 1980, ch. 3, 5 and 6.

[31] D. T. Gleeson, "Low-power ECG amplifier and detector," Master's thesis, Department of Electronic and Electrical Engineering, Trinity College Dublin, 1996.

[32] D. E. Mohrman and L. J. Heller, *Cardiovacular Physiology*. New York: McGraw Hill, 2010, ch. 1, 2 and 4.

[33] R. C. Barr, "Genesis of the Electrocardiogram," in *Comprehensive Electrocardiology: Theory and Practice in Health and Disease*, P. W. MacFarlane and T. D. V. Lawrie, Eds. Elmsford, NY: Pergamon Press, 1989, vol. 1, ch. 5, pp. 129–151.

[34] W. H. Olson, "Basic Concepts of Medical Instrumentation," in *Medical Instrumentation: Application and Design*, J. G. Webster, Ed. New York: John Wiley & Sons, 1995, ch. 1, pp. 1–55.

[35] M. R. Neuman, "Biopotential Electrodes," in *Medical Instrumentation: Application and Design*, J. G. Webster, Ed. New York: John Wiley & Sons, 1995, ch. 5, pp. 227–287.

[36] L. A. Geddes and L. E. Baker, *Principles of Applied Biomedical Instrumentation*. New York: John Wiley & Sons, 1975, ch. 9.

[37] R. D. Gatzke, "The Electrode: A Measurement System Viewpoint," in *Biomedical Electrode Technology: Theory and Practice*, D. C. Miller, A. C.and Harrison, Ed. New York: Academic Press, 1974, pp. 99–116.

[38] E. T. McAdams and J. Jossinet, "The Importance of Electrode-Skin Impedance in High Resolution Electrocardiolography," *Automedica*, vol. 13, pp. 187–208, 1991.

[39] C. Zywietz, "Technical Aspects of Electrocardiogram Recording," in *Comprehensive Electrocardiology: Theory and Practice in Health and Disease*, P. W. MacFarlane and T. D. V. Lawrie, Eds. Elmsford, NY: Pergamon Press, 1989, vol. 1, ch. 12, pp. 353–404.

[40] Y. Yamamoto, H. Isshiki, and T. Nakamura, "Instantaneous Measurement of Electrical Parameters in a Palm during Electrodermal Activity," *IEEE Transactions on Instrumentation and Measurement*, vol. 45, no. 2, pp. 483–487, Apr. 1996.

[41] D. K. Swanson and J. G. Webster, "A Model for Skin-Electrode Impedance," in *Biomedical Electrode Technology: Theory and Practice*, D. C. Miller, A. C.and Harrison, Ed. New York: Academic Press, 1974, pp. 117–128.

[42] A. Searle and L. Kirkup, "A direct comparison of wet, dry and insulating bioelectric recording electrodes," *Physiological Measurement*, vol. 21, no. 2, pp. 271–283, May 2000.

[43] J. Muhlsteff and O. Such, "Dry electrodes for monitoring of vital signs in functional textiles," in *Proceedings of the 26th Annual International Conference of the IEEE Engineering in Medicine and Biology Society*, San Francisco, Sept. 2004, pp. 2212 –2215.

[44] D. M. Thys, "The Normal ECG," in *The ECG in Anesthesia and Critical Care*, D. M. Thys and J. A. Kaplan, Eds. New York: Churchill Livingstone, 1987, ch. 1, pp. 1–15.

[45] J. Malmivuo and R. Plonsey, *Bioelectromagnetism: Principles and Applications of Bioelectric and Biomagnetic Fields*. New York: Oxford University Press, 1995, ch. 6 and 15.

[46] P. W. MacFarlane, "Lead Systems," in *Comprehensive Electrocardiology: Theory and Practice in Health and Disease*, P. W. MacFarlane and T. D. V. Lawrie, Eds. Elmsford, NY: Pergamon Press, 1989, vol. 1, ch. 11, pp. 315–352.

[47] ——, "The Coming of Age of Electrocardiology," in *Comprehensive Electrocardiology: Theory and Practice in Health and Disease*, P. W. MacFarlane and T. D. V. Lawrie, Eds. Elmsford, NY: Pergamon Press, 1989, vol. 1, ch. 1, pp. 3–40.

[48] J. C. Huhta and J. G. Webster, "60-Hz Interference in Electrocardiography," *IEEE Transactions on Biomedical Engineering*, vol. 20, no. 2, pp. 91–101, Mar. 1973.

[49] J. G. Webster, "Interference and Motion Artifact In Biopotentials," in *IEEE 1977 Region Six Conference Record*, Portland, May 1977, pp. 53–64.

[50] M. R. Neuman, "Biopotential Amplifiers," in *Medical Instrumentation: Application and Design*, J. G. Webster, Ed. New York: John Wiley & Sons, 1995, ch. 6, pp. 288–353.

[51] G. D. Clifford, "ECG Statistics, Noise, Artifacts, and Missing Data," in *Advanced Methods and Tools for ECG Data Analysis*, G. D. Clifford, F. Azuaje, and P. E. McSharry, Eds. London: Artech House, 2006, ch. 3, pp. 55–99.

[52] B. J. Drew, R. M. Califf, M. Funk, E. S. Kaufman, M. W. Krucoff, M. M. Laks, P. W. Macfarlane, C. Sommargren, S. Swiryn, and G. F. Van Hare, "Practice Standards for Electrocardiographic Monitoring in Hospital Settings: An American Heart Association Scientific Statement from the Councils on Cardiovascular Nursing, Clinical Cardiology and Cardiovascular Disease in the Young: Endorsed by the International Society of Computerized Electrocardiology and the American Association of Critical-Care Nurses," *Circulation*, vol. 110, no. 17, pp. 2721–2746, Oct. 2004.

[53] R. E. Mason and I. Likar, "A new system of multiple-lead exercise electrocardiography," *American Heart Journal*, vol. 71, no. 2, pp. 196–205, Feb. 1966.

[54] F. N. Wilson, C. E. Kossmann, G. E. Burch, E. Goldberger, A. Graybiel, H. H. Hecht, F. D. Johnston, E. Lepeschkin, and G. B. Myers, "Recommendations for Standardization of Electrocardiographic and Vectorcardiographic Leads. Report of Committee on Electrocardiography, American Heart Association," *Circulation*, vol. 10, no. 4, pp. 564–573, Oct. 1954.

[55] R. M. Griffin and J. A. Kaplan, "ECG Lead Systems," in *The ECG in anesthesia and critical care*, D. M. Thys and J. A. Kaplan, Eds. New York: Churchill Livingstone, 1987, ch. 2, pp. 17–30.

[56] G. F. Fletcher, V. F. Froelicher, L. H. Hartley, W. L. Haskell, and M. L. Pollock, "Exercise Standards. A Statement for Health Professionals from the American Heart Association," *Circulation*, vol. 82, no. 6, pp. 2286–2322, Dec. 1990.

[57] C. E. Assambo, "Amplifier front-end design in dry-electrode electrocardiography," Ph.D. dissertation, Department of Electronic and Electrical Engineering, Trinity College Dublin, June 2011.

[58] N. V. Thakor, J. G. Webster, and W. J. Tompkins, "Estimation of QRS Complex Power Spectra for Design of a QRS Filter," *IEEE Transactions on Biomedical Engineering*, vol. 31, no. 11, pp. 702–706, Nov. 1984.

[59] J. P. Marques de Sa, "Digital FIR Filtering For Removal of ECG Baseline Wander," *Journal of Clinical Engineering*, vol. 7, no. 2, pp. 235–240, July-Sept. 1982.

[60] D. P. Golden, R. A. Wolthuis, and G. W. Hoffler, "A Spectral Analysis of the Normal Resting Electrocardiogram," *IEEE Transactions on Biomedical Engineering*, vol. 20, no. 5, pp. 366–372, Sept. 1973.

[61] M. J. Burke, "A Microcontroller Based Athletic Cardiotachometer," Ph.D. dissertation, Department of Electronic and Electrical Engineering, Trinity College Dublin, 1991.

[62] "EN 60601-2-27:2006. Medical electrical equipment. Part 2-27: Particular requirements for the safety, including essential performance, of electrocardiographic monitoring equipment (IEC 60601-2-27:2005)," Apr. 2006.

[63] "EN 60601-2-47:2001. Medical electrical equipment. Part 2-47: Particular requirements for the safety, including essential performance, of ambulatory electrocardiographic systems (IEC 60601-2-47:2001)," Oct. 2001.

[64] P. Kligfield, L. S. Gettes, J. J. Bailey, R. Childers, B. J. Deal, E. W. Hancock, G. van Herpen, J. A. Kors, P. Macfarlane, D. M. Mirvis, O. Pahlm, P. Rautaharju, and G. S. Wagner, "Recommendations for the Standardization and Interpretation of the Electrocardiogram. Part I: The Electrocardiogram and Its Technology. A Scientific Statement From the American Heart Association Electrocardiography and Arrhythmias Committee, Council on Clinical Cardiology; the American College of Cardiology Foundation; and the Heart Rhythm Society. Endorsed by the International Society for Computerized Electrocardiology," *Circulation*, vol. 115, no. 10, pp. 1306–1324, Mar. 2007.

[65] D. A. Winter and B. G. Trenholm, "Reliable Triggering for Exercise Electrocardiograms," *IEEE Transactions on Biomedical Engineering*, vol. 16, no. 1, pp. 75–79, Jan. 1969.

[66] G. Friesen, T. Jannett, M. Jadallah, S. Yates, S. Quint, and H. Nagle, "A Comparison of the Noise Sensitivity of Nine QRS Detection Algorithms," *IEEE Transactions on Biomedical Engineering*, vol. 37, no. 1, pp. 85–98, Jan. 1990.

[67] *Philips DXL ECG Algorithm Physician Guide*, Philips Medical Systems, Sept. 2008, Publication number 453564106411. [Online]. Available: http://incenter.medical.philips.com/doclib/enc/fetch/2000/4504/577242/577243/577246/581606/1482581/Philips_DXL_ECG_Algorithm_Physician_s_Guide_for_PH100B%2c_Edition_3.pdf%3fnodeid%3d6066381%26vernum%3d1

[68] J. A. Van Alste and T. S. Schilder, "Removal of Base-Line Wander and Power-Line Interference from the ECG by an Efficient FIR Filter with a Reduced Number of Taps," *IEEE Transactions on Biomedical Engineering*, vol. 32, no. 12, pp. 1052–1060, Dec. 1985.

[69] T. Raita-aho, T. Saramaki, and O. Vainio, "A Digital Filter Chip for ECG Signal Processing," *IEEE Transactions on Instrumentation and Measurement*, vol. 43, no. 4, pp. 644–649, Aug. 1994.

[70] S. Tabakov, I. Iliev, and V. Krasteva, "Online Digital Filter and QRS Detector Applicable in Low Resource ECG Monitoring Systems," *Annals of Biomedical Engineering*, vol. 36, no. 11, pp. 1805–1815, Nov. 2008.

[71] H. W. Tam and J. G. Webster, "Minimizing Electrode Motion Artifact by Skin Abrasion," *IEEE Transactions on Biomedical Engineering*, vol. 24, no. 2, pp. 134–139, Mar. 1977.

[72] S. Odman, "Potential and impedance variations following skin deformation," *Medical & Biological Engineering & Computing*, vol. 19, no. 3, pp. 271–278, May 1981.

[73] J. Welch, F. Guilak, and S. D. Baker, "A Wireless ECG Smart Sensor for Broad Application in Life Threatening Event Detection," in *Proceedings of the 26th Annual International Conference of the IEEE Engineering in Medicine and Biology Society*, San Francisco, Sept. 2004, pp. 3447–3449.

[74] D. Winter, P. Rautaharju, and H. Wolf, "Measurement and characteristics of over-all noise content in exercise electrocardiograms," *American Heart Journal*, vol. 74, no. 3, pp. 324–331, Sept. 1967.

[75] D. Prutchi and M. Norris, *Design and Development of Medical Electronic Instrumentation: A Practical Perspective of the Design, Construction, and Test of Medical Devices*. Hoboken, NJ: John Wiley & Sons, 2005, ch. 2 and 5.

[76] P. E. McSharry and G. D. Clifford, "Nonlinear Filtering Techniques," in *Advanced Methods and Tools for ECG Data Analysis*, G. D. Clifford, F. Azuaje, and P. E. McSharry, Eds. London: Artech House, 2006, ch. 6, pp. 171–196.

[77] "ANSI/AAMI EC38:2007. Medical electrical equipment. Part 2-47: Particular requirements for the safety, including essential performance, of ambulatory electrocardiographic systems," Dec. 2007.

[78] H. V. Pipberger, R. C. Arzbaecher, A. S. Berson, S. A. Briller, D. A. Brody, N. C. Flowers, D. B. Geselowitz, E. Lepeschkin, G. C. Olivier, O. H. Schmitt, and M. Spach, "Recommendations for Standardization of Leads and of Specifications for Instruments in Electrocardiography and Vectocardiography. Report of the Committee on Electrocardiography, American Heart Association," *Circulation*, vol. 52, pp. 11–31, 1975.

[79] P. R. Rijnbeek, J. A. Kors, and M. Witsenburg, "Minimum Bandwidth Requirements for Recording of Pediatric Electrocardiograms," *Circulation*, vol. 104, no. 25, pp. 3087–3090, Dec. 2001.

[80] E. Heinonen, "Frequency response testing of ECG devices," *Medical and Biological Engineering and Computing*, vol. 25, no. 4, pp. 471–474, July 1987.

[81] J. J. Bailey, "The Triangular Wave Test for Electrocardiographic Devices: A Historical Perspective," *Journal of Electrocardiology*, vol. 37, pp. 71–73, Oct. 2004, suppl. 1.

[82] R. Abacherli and H. J. Schmid, "Meet the challenge of high-pass filter and ST-segment requirements with a DC-coupled digital electrocardiogram amplifier," *Journal of Electrocardiology*, vol. 42, no. 6, pp. 574–579, Nov.-Dec. 2009.

[83] A. I. Zverev, *Handbook of Filter Synthesis*. Hoboken, NJ: Wiley-Interscience, 1967, ch. 3 and 7.

[84] H. J. Blinchikoff and A. I. Zverev, *Filtering in the Time and Frequency Domains*. New York: Wiley-Interscience, 1976, ch. 2, 3 and 4.

[85] R. L. Longini, J. P. Giolma, C. Wall, and R. F. Quick, "Filtering without phase shift," *IEEE Transactions on Biomedical Engineering*, vol. 22, no. 5, pp. 432–433, Sept. 1975.

[86] P. Gibinski and A. Owczarek, "Assessment of low-frequency response of ECG recorders in relation to international requirements," *Journal of Medical Informatics & Technologies*, vol. 4, pp. 63–72, 2002.

[87] M. C. da Silva, "System for Conformity Assessment of Electrocardiographs (Sistema para Avaliacao da Conformidade de Eletrocardiografos)," Master's thesis, Postgraduate Program in Metrology, Pontifical Catholic University of Rio de Janeiro, Apr. 2008.

[88] E. S. Valchinov and N. E. Pallikarakis, "Wearable Wireless Biopotential Electrode for ECG Monitoring," in *Proceedings of the 11th Mediterranean Conference on Medical and Biomedical Engineering and Computing*, T. Jarm, P. Kramar, and A. Zupanic, Eds., vol. 16. Ljubljana: Springer, June 2007, pp. 373–376.

[89] P. H. Langner and D. B. Geselowitz, "Characteristics of the Frequency Spectrum in the Normal Electrocardiogram and in Subjects Following Myocardial Infarction," *Circulation Research*, vol. 8, no. 3, pp. 577–584, May 1960.

[90] A. L. Goldberger, V. Bhargava, V. Froelicher, and J. Covell, "Effect of Myocardial Infarction on High-frequency QRS Potentials," *Circulation*, vol. 64, no. 1, pp. 34–42, July 1981.

[91] "Marquette 12SL ECG Analysis Program," GE Healthcare, Statement of Validation and Accuracy, Feb. 2007. [Online]. Available: http://clinicalview.gehealthcare.com/download.php?obj_id=45&browser=true

[92] R. Abacherli, F. Braun, L. Zhou, M. Kraemer, J. Felblinger, and H. J. Schmid, "Electrocardiogram on a chip: overview and first experiences of an electrocardiogram manufacturer of medium size," *Journal of Electrocardiology*, vol. 39, no. 4, suppl. 1, pp. s36–s40, Oct. 2006, Proceedings of the 31st Annual ISCE Conference: Research and Technology Transfer in Computerized Electrocardiology.

[93] K. Soundarapandian and M. Berarducci, "Analog Front-End Design for ECG Systems Using Delta-Sigma ADCs," Texas Instruments, Application Report, Apr. 2010. [Online]. Available: http://focus.ti.com.cn/cn/lit/an/sbaa160a/sbaa160a.pdf

[94] J. A. Van Alste, W. Van Eck, and O. Herrmann, "ECG Baseline Wander Reduction Using Linear Phase Filters," *Computers and Biomedical Research*, vol. 19, no. 5, pp. 417 – 427, Oct. 1986.

[95] A. Vehkaoja and J. Lekkala, "Wearable Wireless Biopotential Measurement Device," in *Proceedings of the 26th Annual International Conference of the IEEE Engineering in Medicine and Biology Society*, San Francisco, Sept. 2004, pp. 2177–2179.

[96] D. S. Humpherys, *The Analysis, Design, and Synthesis of Electrical Filters*. Englewood Cliffs, NJ: Prentice-Hall, 1970, ch. 6.

[97] K. L. Su, *Time-Domain Synthesis of Linear Networks*. Englewood Cliffs, NJ: Prentice-Hall, 1971, ch. 7.

[98] A. B. Williams and F. J. Taylor, *Electronic filter design handbook*. New York: McGraw-Hill, 1995, ch. 2.

[99] J. Jess and H. W. Schussler, "A class of pulse-forming networks," *IEEE Transactions on Circuit Theory*, vol. 12, no. 2, pp. 296–299, June 1965.

[100] ——, "On the design of pulse-forming networks," *IEEE Transactions on Circuit Theory*, vol. 12, no. 3, pp. 393–400, Sept. 1965.

[101] B. D. Rakovich, D. Krstich, and M. V. Popovich, "Pulse-forming networks using generalized Laguerre polynomials," *The Radio and Electronic Engineer*, vol. 49, no. 3, pp. 157–164, Mar. 1979.

[102] M. Nasor M. Khalel, "Wavelet Analysis and Microcontroller-Based Synthesis of the Human Electrocardiogram," Ph.D. dissertation, Department of Electronic and Electrical Engineering, Trinity College Dublin, New York, Apr. 1998.

[103] H. S. Shin, C. K. Lee, S. W. Yoon, D. J. Yoon, and M. Lee, "Heart Rate Variability Analysis Using Electric Fabric in Dry-Normal Condition," in *Proceedings of the 27th Annual International Conference of the IEEE Engineering in Medicine and Biology Society*, Shanghai, Jan. 2005, pp. 3563–3566.

[104] T. Kato, A. Ueno, S. Kataoka, H. Hoshino, and Y. Ishiyama, "An Application of Capacitive Electrode for Detecting Electrocardiogram of Neonates and Infants," in *Proceedings of the 28th Annual International Conference of the IEEE Engineering in Medicine and Biology Society*, New York, Aug.-Sept. 2006, pp. 916–919.

[105] X. Liu, Y. J. Zheng, M. W. Phyu, B. Zhao, M. Je, and X. J. Yuan, "A Miniature On-Chip Multi-Functional ECG Signal Processor with 30 ţW Ultra-Low Power Consumption," in *Proceedings of the 32nd Annual International Conference of the IEEE Engineering in Medicine and Biology Society*, Buenos Aires, Aug.-Sept. 2010, pp. 2577–2580.

[106] M. Luise and G. M. Vitetta, *Teoria dei segnali.* Milan: McGraw-Hill, 1999, ch. 5.

[107] C. R. Meyer and H. N. Keiser, "Electrocardiogram Baseline Noise Estimation and Removal Using Cubic Splines and State-Space Computation Techniques," *Computers and Biomedical Research*, vol. 10, no. 5, pp. 459–470, Oct. 1977.

[108] C. D. McManus, U. Teppner, D. Neubert, and S. M. Lobodzinski, "Estimation and Removal of Baseline Drift in the Electrocardiogram," *Computers and Biomedical Research*, vol. 18, no. 1, pp. 1–9, Feb. 1985.

[109] F. Badilini, A. J. Moss, and E. L. Titlebaum, "Cubic Spline Baseline Estimation in Ambulatory ECG Recordings for the Measurement of ST Segment Displacements," in *Proceedings of the 13th Annual International Conference of the IEEE Engineering in Medicine and Biology Society*, Orlando, Nov. 1991, pp. 584–585.

[110] S. P. Arunachalam and L. F. Brown, "Real-Time Estimation of the ECG-Derived Respiration (EDR) Signal using a New Algorithm for Baseline Wander Noise Removal," in *Proceedings of the 31st Annual International Conference of the IEEE Engineering in Medicine and Biology Society*, Minneapolis, Sept. 2009, pp. 5681–5684.

[111] M. L. Ahlstrom and W. J. Tompkins, "Digital Filters for Real-Time ECG Signal Processing Using Microprocessors," *IEEE Transactions on Biomedical Engineering*, vol. 32, no. 9, pp. 708–713, Sept. 1985.

[112] N. Henzel, "Frequency and time constrained digital filter design," *Journal of Medical Informatics & Technologies*, vol. 10, pp. 103–112, 2006.

[113] J. D. Olson, "Finite impulse response filters," in *Biomedical Digital Signal Processing*, W. J. Tompkins, Ed. Englewood Cliffs, NJ: Prentice-Hall, 1993, ch. 5.

[114] L. Sornmo, "Time-Varying Filtering for Removal of Baseline Wander in Exercise ECGs," in *Proceedings of Computers in Cardiology*, Sept. 1991, pp. 145–148.

[115] S. V. Pandit, "ECG baseline drift removal through STFT," in *Proceedings of the 18th Annual International Conference of the IEEE Engineering in Medicine and Biology Society*, Amsterdam, Oct.-Nov. 1996, pp. 1405–1406.

[116] N. V. Thakor and Y. S. Zhu, "Applications of Adaptive Filtering to ECG Analysis: Noise Cancellation and Arrhythmia Detection," *IEEE Transactions on Biomedical Engineering*, vol. 38, no. 8, pp. 785–794, Aug. 1991.

[117] R. Jane, P. Laguna, N. V. Thakor, and P. Caminal, "Adaptive Baseline Wander Removal in the ECG: Comparative Analysis With Cubic Spline Technique," in *Proceedings of Computers in Cardiology*, Oct. 1992, pp. 143–146.

[118] K. L. Park, K. J. Lee, and H. R. Yoon, "Application of a wavelet adaptive filter to minimise distortion of the ST-segment," *Medical & Biological Engineering & Computing*, vol. 36, no. 5, pp. 581–586, Sept. 1998.

[119] E. Ino-Oka, S. Isoyama, Y. Shimizu, S. Sato, K. Tamaki, S. Kitaoka, N. Ishide, T. Takishima, T. Matsuo, and K. Takahashi, "A High-Pass Phaseless Filter for Eliminating Low-Frequency ECG Noise during Exercise and Its Clinical Application to Automatic Analysis of the Heart Rate and ST Segment Level," *The Tohoku Journal of Experimental Medicine*, vol. 142, no. 2, pp. 141–154, Feb. 1984.

[120] J. R. Gradwohl, E. W. Pottala, M. R. Horton, and J. J. Bailey, "Comparison of two methods for removing baseline wander in the ECG," in *Proceedings of Computers in Cardiology*, Sept. 1988, pp. 493–496.

[121] V. Shusterman, S. I. Shah, A. Beigel, and K. P. Anderson, "Enhancing the Precision of ECG Baseline Correction: Selective Filtering and Removal of Residual Error," *Computers and Biomedical Research*, vol. 33, no. 2, pp. 144–160, Apr. 2000.

[122] I. Dotsinsky and T. Stoyanov, "Optimization of bi-directional digital filtering for drift suppression in electrocardiogram signals," *Journal of Medical Engineering & Technology*, vol. 28, no. 4, pp. 178–180, July-Aug. 2004.

[123] K. Daqrouq, "ECG Baseline Wandering Reduction Using Discrete Wavelet Transform," *Asian Journal of Information Technology*, vol. 4, no. 11, pp. 989–995, Nov. 2005.

[124] R. F. von Borries, J. H. Pierluissi, and H. Nazeran, "Wavelet Transform-Based ECG Baseline Drift Removal for Body Surface Potential Mapping," in *Proceedings of the 27th Annual International Conference of the IEEE Engineering in Medicine and Biology Society*, Shanghai, Sept. 2005, pp. 3891–3894.

[125] L. Xu, D. Zhang, and K. Wang, "Wavelet-Based Cascaded Adaptive Filter for Removing Baseline Drift in Pulse Waveforms," *IEEE Transactions on Biomedical Engineering*, vol. 52, no. 11, pp. 1973–1975, Nov. 2005.

[126] M. A. Tinati and B. Mozaffary, "A Wavelet Packets Approach to Electrocardiograph Baseline Drift Cancellation," *International Journal of Biomedical Imaging*, 2006, Hindawi Publishing Corporation, Article ID 97157.

[127] O. Sayadi and M. B. Shamsollahi, "Multiadaptive Bionic Wavelet Transform: Application to ECG Denoising and Baseline Wandering Reduction," *EURASIP Journal on Advances in Signal Processing*, 2007, Hindawi Publishing Corporation, Article ID 41274.

[128] M. Blanco-Velasco, B. Weng, and K. E. Barner, "ECG signal denoising and baselinewander correction based on the empirical mode decomposition," *Computers in Biology and Medicine*, vol. 38, no. 1, pp. 1–13, Jan. 2008.

[129] C. H. H. Chu and E. J. Delp, "Impulsive noise suppression and background normalization of electrocardiogram signals using morphological operators," *IEEE Transactions on Biomedical Engineering*, vol. 36, no. 2, pp. 262–273, Feb. 1989.

[130] S. H. Oguz and M. H. Asyali, "A morphology based algorithm for baseline wander elimination in ECG records," in *Proceedings of the 1992 International Biomedical Engineering Days*, Istanbul, Aug. 1992, pp. 157–160.

[131] Y. Sun, K. Chan, and S. M. Krishnan, "ECG signal conditioning by morphological filtering," *Computers in Biology and Medicine*, vol. 32, no. 6, pp. 465–479, Nov. 2002.

[132] P. Sun, Q. Wu, A. Weindling, A. Finkelstein, and K. Ibrahim, "An Improved Morphological Approach to Background Normalization of ECG Signals," *IEEE Transactions on Biomedical Engineering*, vol. 50, no. 1, pp. 117–121, Jan. 2003.

[133] L. Keselbrener, M. Keselbrener, and S. Akselrod, "Nonlinear high pass filter for R-wave detection in ECG signal," *Medical Engineering & Physics*, vol. 19, no. 5, pp. 481–484, July 1997.

[134] J. M. Leski and N. Henzel, "ECG baseline wander and powerline interference reduction using nonlinear filter bank," *Signal Processing*, vol. 85, no. 4, pp. 781–793, Apr. 2005.

[135] P. Ciarlini and P. Barone, "A Recursive Algorithm to Compute the Baseline Drift in Recorded Biological Signals," *Computers and Biomedical Research*, vol. 21, no. 3, pp. 221–226, June 1988.

[136] M. A. Mneimneh, E. E. Yaz, M. T. Johnson, and R. J. Povinelli, "An Adaptive Kalman Filter for Removing Baseline Wandering in ECG Signals," in *Proceedings of Computers in Cardiology*, Sept. 2006, pp. 253–256.

[137] Z. Barati and A. Ayatollahi, "Baseline Wandering Removal by Using Independent Component Analysis to Single-Channel ECG data," in *Proceedings of the 2006 International Conference on Biomedical and Pharmaceutical Engineering*, Singapore, Dec. 2006, pp. 152–156.

[138] J. Mateo, C. Sanchez, C. Vaya, R. Cervigon, and J. J. Rieta, "A New Adaptive Approach to Remove Baseline Wander from ECG Recordings Using Madeline Structure," in *Proceedings of Computers in Cardiology*, Sept.-Oct. 2007, pp. 533–536.

[139] W. J. Tompkins and P. Tagare, "Basics of Digital Filtering," in *Biomedical Digital Signal Processing*, W. J. Tompkins, Ed. Englewood Cliffs, NJ: Prentice-Hall, 1993, ch. 4.

[140] R. Rossi, A. Castelli, and M. Bertinelli, "Fast FIR Filters for a Stress Test System," in *Proceedings of Computers in Cardiology*, Sept. 1991, pp. 129–132.

[141] S. Hargittai, "Efficient and Fast ECG Baseline Wander Reduction without Distortion of Important Clinical Information," in *Proceedings of Computers in Cardiology*, Sept. 2008, pp. 841–844.

[142] S. Canan, Y. Ozbay, and B. Karlik, "A method for removing low varying frequency trend from ECG signal," in *Proceedings of the 1998 2nd International Conference Biomedical Engineering Days*, Istanbul, May 1998, pp. 144–146.

[143] P. A. Lynn, "Economic linear-phase recursive digital filters," *Electronics Letters*, vol. 6, no. 5, pp. 143–145, Mar. 1970.

[144] J. D. Pfeffer, "Integer filters," in *Biomedical Digital Signal Processing*, W. J. Tompkins, Ed. Englewood Cliffs, NJ: Prentice-Hall, 1993, ch. 7.

[145] P. A. Lynn, "Recursive digital filters with linear-phase characteristics," *The Computer Journal*, vol. 15, no. 4, pp. 337–342, 1972.

[146] I. I. Christov, I. A. Dotsinsky, and I. K. Daskalov, "High-pass filtering of ECG signals using QRS elimination," *Medical & Biological Engineering & Computing*, vol. 30, no. 2, pp. 253–256, Mar. 1992.

[147] M. Dai and S. L. Lian, "Removal of Baseline Wander from Dynamic Electrocardiogram Signals," in *2nd International Congress on Image and Signal Processing 2009*, Tianjin, China, Oct. 2009, pp. 1–4.

[148] I. T. Iliev, S. D. Tabakov, and V. T. Krasteva, "Combined High-pass and Power-line Interference Rejecter Filter for ECG Signal Processing," in *Proceedings of the Technical University of Sofia*, vol. 58, no. 2, 2008, pp. 7–13.

[149] N. Henzel, "Digital filter design with constraints in time and frequency domains," in *Proceedings of the 4th International Conference on Computer Recognition Systems*, M. Kurzynski, E. Puchala, M. Wozniak, and A. Zolnierek, Eds., Rydzyna Castle, Poland, May 2005, pp. 169–176.

[150] C. J. Yen, W. Y. Chung, M. C. Chi, and S. H. Lee, "A 0.75-mW Analog Processor IC for Wireless Biosignal Monitor," in *Proceedings of the 2003 International Symposium on Low Power Electronics and Design*, Seoul, Aug. 2003, pp. 443–448.

[151] J. Mihel and R. Magjarevic, "FPGA based two-channel ECG sensor node for wearable applications," in *Proceedings of the 4th European Conference of the International Federation for Medical and Biological Engineering*, J. Vander Sloten, P. Verdonck, M. Nyssen, and J. Haueisen, Eds., vol. 22. Antwerp: Springer, Nov. 2008, pp. 1208–1211.

[152] M. Shojaei-Baghini, R. K. Lal, and D. K. Sharma, "A Low-Power and Compact Analog CMOS Processing Chip for Portable ECG Recorders," in *Proceedings of the 2005 IEEE Asian Solid-State Circuits Conference*, Hsinchu, Taiwan, Nov. 2005, pp. 473–476.

[153] "MAC 400 Resting ECG System," GE Healthcare, Brochure, 2036097-002-2007.10-V2.0. [Online]. Available: http://www.gehealthcare.com/euen/cardiology/docs/MAC_400_bro_e.pdf

[154] "CASE (Cardiac Assessment System for Exercise Testing)," GE Healthcare, Specifications, 2009836-002/V4/1109. [Online]. Available: http://www.gehealthcare.com/euen/cardiology/docs/CASE_specs_e.pdf

[155] R. McFee and G. Baule, "Research in electrocardiography and magnetocardiography," *Proceedings of the IEEE*, vol. 60, no. 3, pp. 290–321, Mar. 1972.

[156] M. Bertolaccini, D. Dotti, and G. Padovini, "A precision baseline offset and drift corrector for low-frequency applications," *IEEE Transactions on Instrumentation and Measurement*, vol. 34, no. 3, pp. 405–412, Sept. 1985.

[157] K. L. Su, *Analog Filters*. London: Chapman & Hall, 1996, ch. 10.

[158] H. J. Blinchikoff, "Low-Transient High-Pass Filters," *IEEE Transactions on Circuit Theory*, vol. 17, no. 4, pp. 663–667, Nov. 1970.

[159] R. Schaumann and M. E. Van Valkenburg, *Design of Analog Filters*. New York: Oxford University Press, 2001, ch. 5, 11 and 12.

[160] M. Thompson, "Review of feedback systems," in *Analog Circuits (World Class Designs)*, R. A. Pease, Ed. Oxford: Newnes, 2008, ch. 1.

[161] P. Bolzern, R. Scattolini, and N. Schiavoni, *Fondamenti di controlli automatici*. Milan: McGraw Hill, 1998, ch. 12.

[162] N. S. Nise, *Control Systems Engineering*. Hoboken, NJ: John Wiley & Sons, 2004, ch. 9.

[163] "MKP 1837 - Metallized Polypropylene Film Capacitor," Vishay Roederstein, Datasheet. [Online]. Available: http://www.vishay.com/docs/26017/26017.pdf

[164] "HB Series - High Value / High Voltage Resistors," Tyco Electronics, Datasheet. [Online]. Available: http://passives.te.com/documents/webservice/fetch.ashx?fileid=10363&docId=7070

[165] "ECHU(X) - Stacked Metallized PPS Film Chip Capacitor," Panasonic, Datasheet. [Online]. Available: http://industrial.panasonic.com/www-data/pdf/ABD0000/ABD0000CE13.pdf

[166] "CRHV - Thick Film Chip Resistors, High Voltage," Vishay Techno, Datasheet. [Online]. Available: http://www.vishay.com/docs/68002/crhv.pdf

[167] N. Damera-Venkata and B. Evans, "An Automated Framework for Multicriteria Optimization of Analog Filter Designs," *IEEE Transactions on Circuits and Systems II: Analog and Digital Signal Processing*, vol. 46, no. 8, pp. 981–990, Aug. 1999.

[168] V. Aggarwal, W. O. Jin, and U.-M. O'Reilly, "Filter Approximation Using Explicit Time and Frequency Domain Specifications," in *Proceedings of the 8th Annual Conference on Genetic and Evolutionary Computation*, Seattle, July 2006, pp. 753–760.

[169] O. Koca, H. Karl, and R. Weigel, "A Novel Method Based Upon Nonlinear Optimization for Analog Filter Design with Mask Constraints," in *Proceedings of the 2007 International Symposium on Signals, Systems and Electronics*, Montreal, July-Aug. 2007, pp. 9–12.

[170] *Optimization Toolbox User's Guide*, Version 3.1.1 (release 2007a) ed., The MathWorks, Inc., Natick, MA, 2007.

[171] A. Ravindran, K. M. Ragsdell, and G. V. Reklaitis, *Engineering Optimization: Methods and Applications*. Hoboken, NJ: John Wiley & Sons, 2006, ch. 5.

[172] J. S. Arora, *Introduction to Optimum Design*. San Diego, CA: Elsevier Academic Press, 2004, ch. 4.

[173] S. S. Rao, *Engineering Optimization: Theory and Practice*. New York: Wiley-Interscience, 1996, ch. 7 and 12.

[174] A. L. Goldberger, L. A. N. Amaral, L. Glass, J. M. Hausdorff, P. C. Ivanov, R. G. Mark, J. E. Mietus, G. B. Moody, C.-K. Peng, and H. E. Stanley, "PhysioBank, PhysioToolkit, and PhysioNet: Components of a New Research Resource for Complex Physiologic Signals," *Circulation*, vol. 101, no. 23, pp. e215–e220, June 2000.

[175] P. Laguna, R. G. Mark, A. Goldberg, and G. B. Moody, "A Database for Evaluation of Algorithms for Measurement of QT and Other Waveform Intervals in the ECG," in *Proceedings of Computers in Cardiology*, Sept. 1997, pp. 673–676.

[176] G. B. Moody, W. E. Muldrow, and R. G. Mark, "A Noise Stress Test for Arrhythmia Detectors," in *Proceedings of Computers in Cardiology*, Sept. 1984, pp. 381–384.

[177] A. V. Oppenheim and R. W. Schafer, *Digital Signal Processing*. Englewood Cliffs, NJ: Prentice-Hall, 1975, ch. 11.

[178] P. E. Fleischer and J. Tow, "Design Formulas for Biquad Active Filters Using Three Operational Amplifiers," *Proceedings of the IEEE*, vol. 61, no. 5, pp. 662–663, May 1973.

[179] J. C. Berka and M. Herpy, "Novel Active RC Building Block with Optimal Sensitivity," *Electronics Letters*, vol. 17, no. 23, pp. 887–888, Nov. 1981.

[180] N. J. Fliege, "Multiple-Amplifier Biquads," in *The Circuits and Filters Handbook*, W.-K. Chen, Ed. Salem, MA: CRC Press, 1995, ch. 77, pp. 2385–2409.

[181] J. Friend, C. Harris, and D. Hilberman, "STAR: An Active Biquadratic Filter Section," *IEEE Transactions on Circuits and Systems*, vol. 22, no. 2, pp. 115–121, Feb. 1975.

[182] A. Sedra, M. Ghorab, and K. Martin, "Optimum Configurations for Single-Amplifier Biquadratic Filters," *IEEE Transactions on Circuits and Systems*, vol. 27, no. 12, pp. 1155–1163, Dec. 1980.

[183] M. S. Ghausi, "Analog Active Filters," *IEEE Transactions on Circuits and Systems*, vol. 31, no. 1, pp. 13–31, Jan. 1984.

[184] "Slim-Mox - Precision Thick Film Planar Resistors," Ohmite, Datasheet. [Online]. Available: http://www.ohmite.com/cat/res_slimmox.pdf

[185] "FSC/EX - Precision Capacitors," LCR Components, Datasheet. [Online]. Available: http://www.farnell.com/datasheets/30215.pdf

[186] *Signal Processing Toolbox User's Guide*, Version 6.7 (release 2007a) ed., The MathWorks, Inc., Natick, MA, 2007.

Publications

- R. Dozio and M. J. Burke, "Optimised Design of the Front-End Analogue High-Pass Filter for a Diagnostic Quality ECG Monitoring System", in *Proceedings of the 31st Annual International Conference of the IEEE Engineering in Medicine and Biology Society*, Minneapolis, Sept. 2009, pp. 1770-1773.

- R. Dozio and M. J. Burke, "Second and Third Order Analogue High-Pass Filters for Diagnostic Quality ECG", in *Proceedings of the 20th IET Irish Signals and Systems Conference*, Dublin, June 2009.

- R. Dozio, A. Baba, C. Assambo, M. J. Burke, "Time Based Measurement of the Impedance of the Skin-Electrode Interface for Dry Electrode ECG Recording", in *Proceedings of the 29th Annual International Conference of the IEEE Engineering in Medicine and Biology Society*, Lyon, Aug. 2007, pp. 5001-5004.

- C. Assambo, A. Baba, R. Dozio, M. J. Burke, "Parameter Estimation of the Skin-Electrode Interface Model for High-Impedance Bio-Electrodes", *WSEAS Transactions on Biology and Biomedicine*, vol. 3, no. 8, pp. 573-580, Aug. 2006 (publication date backdated by WSEAS).

- C. Assambo, A. Baba, R. Dozio, M. J. Burke, "Determination of the Parameters of the Skin-Electrode Impedance Model for ECG Measurement", in *Proceedings of the 6th WSEAS International Conference on Electronics, Hardware, Wireless and Optical Communications*, Corfu, Feb. 2007, pp. 90-95.

Appendix A

A.1 Study of the first derivative of the magnitude response of the second order filter

The trend of the magnitude response of the second order filter and the presence of a peak in its amplitude characteristic can be easily determined by analysing the sign of its first derivative, which can be calculated from Eq. (6.11) to be:

$$\frac{d\,|H_2(\omega)|}{d\,\omega} = \frac{\left({b_1}^2 - {a_1}^2 - 2b_0\right)\omega^4 + 2{b_0}^2\omega^2 + {a_1}^2{b_0}^2}{\sqrt{\left(\omega^2 + {a_1}^2\right)\left[\omega^4 + \left({b_1}^2 - 2b_0\right)\omega^2 + {b_0}^2\right]^3}}. \tag{A.1}$$

Since the denominator of Eq. (A.1) is always defined and positive, the analysis can be restricted to the numerator. That is,

$$\frac{d\,|H_2(\omega)|}{d\,\omega} \geq 0 \tag{A.2}$$

reduces to:

$$\left({b_1}^2 - {a_1}^2 - 2b_0\right)\omega^4 + 2{b_0}^2\omega^2 + {a_1}^2{b_0}^2 \geq 0. \tag{A.3}$$

The biquadratic inequality in the previous equation can be rewritten as:

$$D\omega^4 + E\omega^2 + F \geq 0 \qquad \text{with} \begin{cases} D = {b_1}^2 - {a_1}^2 - 2b_0 \\ E = 2{b_0}^2 > 0 \\ F = {a_1}^2{b_0}^2 \geq 0. \end{cases} \tag{A.4}$$

The shape of the magnitude characteristic is, therefore, dependent on the sign of the parameter D. For $D \geq 0$, the inequality in Eq. (A.4) is always satisfied, that is, the amplitude response of the filter is monotonically increasing at all frequencies. On the other hand, for

$D < 0$, one real solution is obtained for the following equation:

$$D\omega^4 + E\omega^2 + F = 0. \tag{A.5}$$

In fact,

$$\omega^2 = \frac{E \pm \sqrt{E^2 - 4DF}}{-2D}, \tag{A.6}$$

where the denominator and the radicand are both positive and

$$E^2 - 4DF > E^2. \tag{A.7}$$

Since

$$\frac{E - \sqrt{E^2 - 4DF}}{-2D} < 0 \tag{A.8}$$

and cannot be accepted as a solution to Eq. (A.5), the frequency at which the first derivative of the magnitude response is null is given by:

$$\omega_k = \sqrt{\frac{{b_0}^2 + \sqrt{{b_0}^4 + \left(2b_0 - {a_1}^2 - {b_1}^2\right){a_1}^2{b_0}^2}}{2b_0 - {a_1}^2 - {b_1}^2}}. \tag{A.9}$$

Thus,

$$\frac{d\,|H_2(\omega)|}{d\,\omega} > 0 \qquad \text{for} \quad 0 \leq \omega < \omega_k \tag{A.10}$$

and

$$\frac{d\,|H_2(\omega)|}{d\,\omega} < 0 \qquad \text{for} \quad \omega > \omega_k, \tag{A.11}$$

that is, $|H_2(\omega)|$ is increasing for $0 \leq \omega < \omega_k$ and decreasing for $\omega > \omega_k$. Therefore, for $D < 0$, the amplitude response of the second order filter presents a peak at frequency ω_k, before decreasing to its high-frequency value of unity:

$$\lim_{\omega \to \infty} |H_2(\omega)| = 1. \tag{A.12}$$

Overall, it can be concluded that the magnitude response of the second order highpass filter is always monotonically increasing outside the passband.

A.2 Chebyshev and Elliptic lowpass filters

A.2.1 Chebyshev filter

The all-pole Chebyshev transfer function is obtained when the ideal rectangular magnitude response is approximated in an equiripple manner over the passband. The normalised Chebyshev magnitude characteristic is equal to [84]:

$$|H(\omega)| = \frac{1}{\sqrt{1+\epsilon^2 C_n^2(\omega)}}, \tag{A.13}$$

where the value of ϵ determines the ripple height and $C_n(\omega)$ is the Chebyshev polynomial of the first kind of order n:

$$C_n(\omega) = \begin{cases} \cos(n\cos^{-1}\omega) & \text{for } \omega \leq 1 \\ \cosh(n\cosh^{-1}\omega) & \text{for } \omega > 1, \end{cases} \tag{A.14}$$

which can alternatively be expressed using the recursive formula:

$$C_n(\omega) = 2\omega C_{n-1}(\omega) - C_{n-2}(\omega) \quad \text{with} \quad C_0(\omega) = 1 \quad \text{and} \quad C_1(\omega) = \omega. \tag{A.15}$$

The filter magnitude response at zero frequency is equal to unity for n odd ($C_n(0) = 0$). On the other hand, for n even, $C_n(0) = \pm 1$ and

$$|H(0)| = \frac{1}{\sqrt{1+\epsilon^2}}, \tag{A.16}$$

that is, the amplitude at 0 rad/s is equal to the maximum deviation from unity in the passband. For normalised Chevyshev filters, the frequency ω = 1 rad/s does not correspond to the 3dB-point, but to the edge of the equiripple approximation, as shown in Figure A.1. For frequencies lower than 1 rad/s, the magnitude oscillates between zero and the maximum allowed attenuation set by ϵ. Outside the passband, the magnitude decreases monotonically, with a slope that is much steeper than the one associated with the Butterworth characteristic (see Section 4.3.1). The Chebyshev response is, indeed, the one delivering the fastest possible rate of attenuation near the cutoff frequency from the class of all-pole transfer functions. The steepness of the magnitude characteristic is dependent on both the order of the filter and the height of the passband ripple. Larger ripple determines higher attenuation for any specified out-of-band frequency [83]. Conversely, the responses of a Chebyshev filter reduce to their Butterworth counterparts when the maximum attenuation allowed in passband goes to zero.

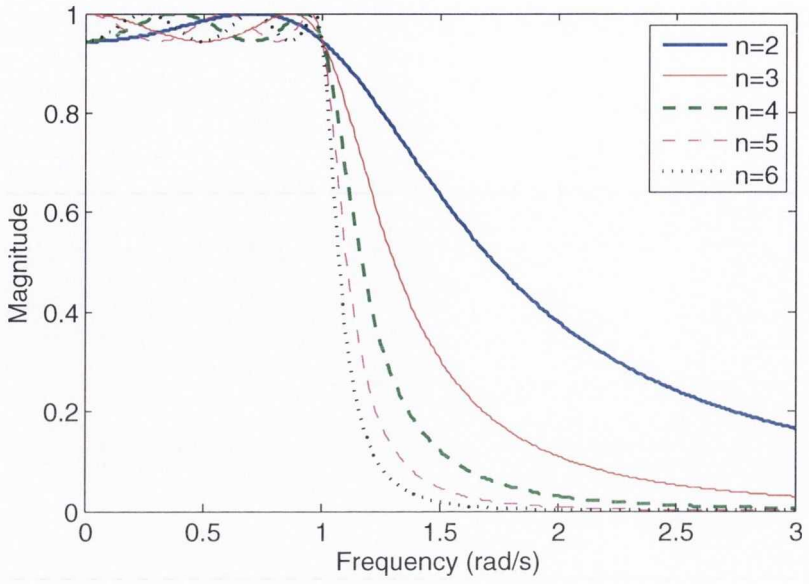


Figure A.1: Amplitude characteristic of normalised Chebyshev filters with passband ripple equal to 0.5 dB.

A.2.2 Elliptic filter

Elliptic filters, sometimes named Cauer filters, are non all-pole networks renowned for the fact that the slope of their magnitude response at the cutoff is the steepest attainable for a given order [98]. The amplitude of a normalised Elliptic filter is defined by:

$$|H(\omega)| = \frac{1}{\sqrt{1+\epsilon^2 Z_n^2(\omega)}}, \tag{A.17}$$

where ϵ determines the height of the passband ripple and $Z_n(\omega)$ is the Zolotarev function of order n. A reciprocal relationship exists between the poles and zeros of $Z_n(\omega)$, which determines an equiripple behaviour for the magnitude of Elliptic filters in both the passband and the stopband. As for the Chebyshev filters, the attenuation at ω = 1 rad/s and the loss at zero frequency for even order filters correspond to the passband ripple, as can be seen from Figure A.2(a). Moreover, all the peaks in the stopband are equal to the minimum attenuation required for the stopband, as shown in Figure A.2(b).

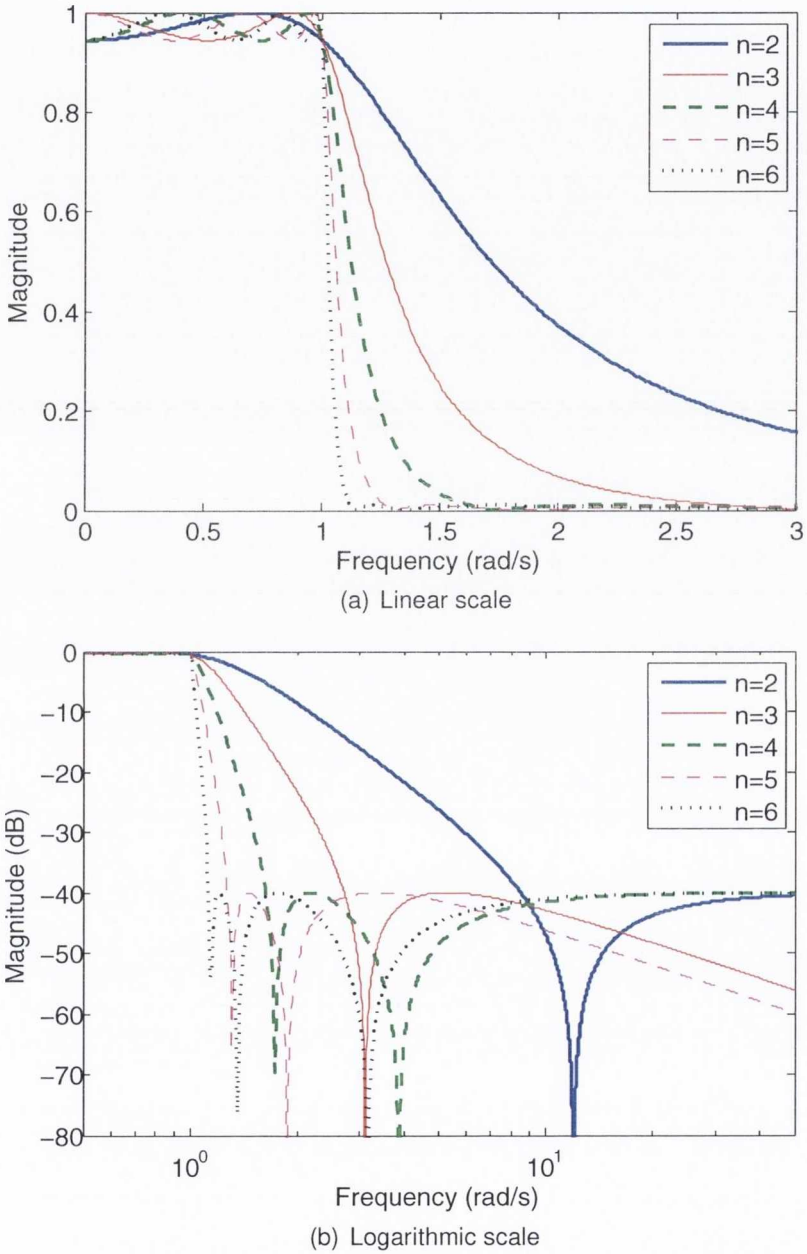


Figure A.2: Magnitude characteristic of normalised Elliptic filters having a passband ripple of 0.5 dB and a minimum stopband attenuation of 40 dB.

A.3 Complete results of the optimisation procedure

For each of the tables in this section, the set of parameters that yields the highest value for the objective function is reported as the optimum result in Chapter 6. Sometimes, more than one set of design variables lead to the same optimum result. In this case, the set that occurs more frequently in the table under consideration is selected. If all of the parameter sets that give the highest value for the objective function are different, the design variables used in Chapter 6 are highlighted. This set is chosen by considering more decimal places for the value of the objective function than shown in the table.

A.3.1 Optimisation of the 0.05 Hz second order filter

Table A.1: Results obtained by optimising the stopband limit of the 0.05 Hz second order filter when A_s = 40 dB for different starting points.

START f_{3dB} (mHz)	f_{40dB} (mHz)	a_1 (rad/s)	b_1 (rad/s)	b_0 ((rad/s)^2)	p (rad/s)	z (rad/s)	
				Butterworth			
30	1.55	0.0038	0.3424	0.0097	-0.3111 -0.0313	0 -0.0038	sub-optimal
40	1.55	0.0038	0.3424	0.0097	-0.3111 -0.0313	0 -0.0038	sub-optimal
50	1.91	0.1194	0.4532	0.1437	-0.2266 $\pm j$ 0.3039	0 -0.1194	
60	1.91	0.1194	0.4532	0.1437	-0.2266 $\pm j$ 0.3039	0 -0.1194	
70	1.91	0.1194	0.4532	0.1437	-0.2266 $\pm j$ 0.3039	0 -0.1194	
				Chebyshev (R_p = 0.5 dB)			
30	1.55	0.0038	0.3424	0.0097	-0.3111 -0.0313	0 -0.0038	sub-optimal
40	1.91	0.1194	0.4532	0.1437	-0.2266 $\pm j$ 0.3039	0 -0.1194	
50	1.91	0.1194	0.4532	0.1437	-0.2266 $\pm j$ 0.3039	0 -0.1194	
60	1.91	0.1194	0.4532	0.1437	-0.2266 $\pm j$ 0.3039	0 -0.1194	
70	1.91	0.1194	0.4532	0.1437	-0.2266 $\pm j$ 0.3039	0 -0.1194	

Table A.2: Results obtained by optimising the stopband limit of the 0.05 Hz second order filter when A_s = 20 dB for different starting points.

START f_{3dB} (mHz)	f_{20dB} (mHz)	a_1 (rad/s)	b_1 (rad/s)	b_0 ((rad/s)^2)	p (rad/s)	z (rad/s)
Butterworth						
30	14.86	0.1194	0.4532	0.1437	-0.2266 $\pm j$ 0.3039	0
						-0.1194
40	14.86	0.1194	0.4532	0.1437	-0.2266 $\pm j$ 0.3039	0
						-0.1194
50	14.86	0.1194	0.4532	0.1437	-0.2266 $\pm j$ 0.3039	0
						-0.1194
60	14.86	0.1194	0.4532	0.1437	-0.2266 $\pm j$ 0.3039	0
						-0.1194
70	14.86	0.1194	0.4532	0.1437	-0.2266 $\pm j$ 0.3039	0
						-0.1194
Chebyshev (R_p = 0.5 dB)						
30	14.86	0.1194	0.4532	0.1437	-0.2266 $\pm j$ 0.3039	0
						-0.1194
40	14.86	0.1194	0.4532	0.1437	-0.2266 $\pm j$ 0.3039	0
						-0.1194
50	14.86	0.1194	0.4532	0.1437	-0.2266 $\pm j$ 0.3039	0
						-0.1194
60	14.86	0.1194	0.4532	0.1437	-0.2266 $\pm j$ 0.3039	0
						-0.1194
70	14.86	0.1194	0.4532	0.1437	-0.2266 $\pm j$ 0.3039	0
						-0.1194

Table A.3: Results obtained by optimising the stopband limit of the 0.05 Hz second order filter when A_s = 60 dB for different starting points.

START f_{3dB} (mHz)	f_{60dB} (mHz)	a_1 (rad/s)	b_1 (rad/s)	b_0 ((rad/s)^2)	p (rad/s)	z (rad/s)	
Butterworth							
30	0.46	0.0004	0.3390	0.0085	-0.3118	0	
					-0.0271	-0.0004	
40	0.46	0.0004	0.3390	0.0085	-0.3118	0	
					-0.0271	-0.0004	
50	0.19	0.1194	0.4532	0.1437	-0.2266 $\pm j$ 0.3039	0	sub-optimal
						-0.1194	
60	0.19	0.1194	0.4532	0.1437	-0.2266 $\pm j$ 0.3039	0	sub-optimal
						-0.1194	
70	0.19	0.1194	0.4532	0.1437	-0.2266 $\pm j$ 0.3039	0	sub-optimal
						-0.1194	
Chebyshev (R_p = 0.5 dB)							
30	0.46	0.0004	0.3390	0.0085	-0.3118	0	
					-0.0271	-0.0004	
40	0.19	0.1194	0.4532	0.1437	-0.2266 $\pm j$ 0.3039	0	sub-optimal
						-0.1194	
50	0.19	0.1194	0.4532	0.1437	-0.2266 $\pm j$ 0.3039	0	sub-optimal
						-0.1194	
60	0.19	0.1194	0.4532	0.1437	-0.2266 $\pm j$ 0.3039	0	sub-optimal
						-0.1194	
70	0.19	0.1194	0.4532	0.1437	-0.2266 $\pm j$ 0.3039	0	sub-optimal
						-0.1194	

Table A.4: Results obtained by optimising the stopband limit of the 0.05 Hz second order filter when A_s = 40 dB and the maximum positive overshoot allowed for the pulse response is equal to 5 μV.

START f_{3dB} (mHz)	f_{40dB} (mHz)	a_1 (rad/s)	b_1 (rad/s)	b_0 ((rad/s)^2)	p (rad/s)	z (rad/s)	
Butterworth							
30	1.55	0.0038	0.3424	0.0097	-0.3111	0	
					-0.0313	-0.0038	
40	1.26	0.1538	0.4893	0.1215	-0.2447 $\pm j$ 0.2484	0	sub-optimal
						-0.1538	
50	1.26	0.1538	0.4893	0.1215	-0.2447 $\pm j$ 0.2484	0	sub-optimal
						-0.1538	
60	1.26	0.1538	0.4893	0.1215	-0.2447 $\pm j$ 0.2484	0	sub-optimal
						-0.1538	
70	1.26	0.1538	0.4893	0.1215	-0.2447 $\pm j$ 0.2484	0	sub-optimal
						-0.1538	
Chebyshev (R_p = 0.5 dB)							
30	1.55	0.0038	0.3424	0.0097	-0.3111	0	
					-0.0313	-0.0038	
40	1.26	0.1538	0.4893	0.1215	-0.2447 $\pm j$ 0.2484	0	sub-optimal
						-0.1538	
50	1.26	0.1538	0.4893	0.1215	-0.2447 $\pm j$ 0.2484	0	sub-optimal
						-0.1538	
60	1.26	0.1538	0.4893	0.1215	-0.2447 $\pm j$ 0.2484	0	sub-optimal
						-0.1538	
70	1.26	0.1538	0.4893	0.1215	-0.2447 $\pm j$ 0.2484	0	sub-optimal
						-0.1538	

Table A.5: Results obtained by optimising the stopband limit of the 0.05 Hz second order filter when A_s = 40 dB and the maximum positive overshoot allowed for the pulse response is equal to 2 μV.

START f_{3dB} (mHz)	f_{40dB} (mHz)	a_1 (rad/s)	b_1 (rad/s)	b_0 ((rad/s)^2)	p (rad/s)	z (rad/s)	
Butterworth							
30	1.55	0.0038	0.3424	0.0097	-0.3111	0	
					-0.0313	-0.0038	
40	0.90	0.1626	0.4998	0.0917	-0.2499 $\pm j$ 0.1710	0	sub-optimal
						-0.1626	
50	0.90	0.1626	0.4998	0.0917	-0.2499 $\pm j$ 0.1710	0	sub-optimal
						-0.1626	
60	0.90	0.1626	0.4998	0.0917	-0.2499 $\pm j$ 0.1710	0	sub-optimal
						-0.1626	
70	0.90	0.1626	0.4998	0.0917	-0.2499 $\pm j$ 0.1710	0	sub-optimal
						-0.1626	
Chebyshev (R_p = 0.5 dB)							
30	1.55	0.0038	0.3424	0.0097	-0.3111	0	
					-0.0313	-0.0038	
40	0.90	0.1626	0.4998	0.0917	-0.2499 $\pm j$ 0.1710	0	sub-optimal
						-0.1626	
50	0.90	0.1626	0.4998	0.0917	-0.2499 $\pm j$ 0.1710	0	sub-optimal
						-0.1626	
60	0.90	0.1626	0.4998	0.0917	-0.2499 $\pm j$ 0.1710	0	sub-optimal
						-0.1626	
70	0.90	0.1626	0.4998	0.0917	-0.2499 $\pm j$ 0.1710	0	sub-optimal
						-0.1626	

A.3.2 Optimisation of the 0.05 Hz third order filter

Table A.6: Results obtained by optimising the stopband limit of the 0.05 Hz third order filter when A_s = 40 dB for different starting points.

START f_{3dB} (mHz)	f_{40dB} (mHz)	a_1 (rad/s)	a_0 ((rad/s)^2)	b_1 (rad/s)	b_0 ((rad/s)^2)	p_0 (rad/s)	p (rad/s)	z (rad/s)
Butterworth								
30	1.76	0.1706	0.0005	0.4335	0.0272	0.0760	sub-optimal	
40	3.98	0.8995	0.0079	0.7356	0.1244	0.4722	sub-optimal	
50	not converging							
60	3.98	0.8995	0.0079	0.7356	0.1244	0.4722	sub-optimal	
70	4.02	0.7050	0.0054	0.8127	0.2171	0.2126	-0.2126 -0.4064 $\pm j$ 0.2280	0 -0.6972 -0.0078
Chebyshev (R_p = 0.5 dB)								
30	1.76	0.1706	0.0005	0.4335	0.0272	0.0760	sub-optimal	
40	4.02	0.7047	0.0054	0.8125	0.2171	0.2125	**-0.2125** **-0.4063 $\pm j$ 0.2281**	**0** **-0.6969** **-0.0078**
50	3.98	0.8995	0.0079	0.7356	0.1244	0.4721	sub-optimal	
60	3.98	0.8995	0.0079	0.7356	0.1244	0.4722	sub-optimal	
70	4.02	0.7049	0.0054	0.8127	0.2171	0.2126	-0.2126 -0.4063 $\pm j$ 0.2281	0 -0.6971 -0.0078
Elliptic (R_p = 0.5 dB, A_s = 40 dB)								
30	0.10	0.2491	-0.0119	0.5499	0.0194	0.0397	sub-optimal	
40	not converging							
50	3.98	0.8995	0.0079	0.7356	0.1244	0.4722	sub-optimal	
60	4.02	0.7046	0.0054	0.8125	0.2171	0.2125	-0.2125 -0.4063 $\pm j$ 0.2282	0 -0.6969 -0.0078
70	3.98	0.8995	0.0079	0.7356	0.1244	0.4722	sub-optimal	

Table A.7: Results obtained by optimising the stopband limit of the 0.05 Hz third order filter when A_s = 20 dB for different starting points.

START f_{3dB} (mHz)	f_{20dB} (mHz)	a_1 (rad/s)	a_0 ((rad/s)^2)	b_1 (rad/s)	b_0 ((rad/s)^2)	p_0 (rad/s)	p (rad/s)	z (rad/s)
Butterworth								
30	12.28	0.0481	0.0037	0.1931	0	0.1931	pole-zero cancellation	
40	15.60	1.5701	0.1299	0.4636	0.1354	1.4281	sub-optimal	
50	15.60	1.5650	0.1294	0.4636	0.1354	1.4230	sub-optimal	
60	23.64	0.0623	0.0149	0.3784	0.1238	0.0182	-0.0182	0
							-0.1892 $\pm j$ 0.2967	-0.0312 $\pm j$ 0.1180
70	23.64	0.0623	0.0149	0.3784	0.1238	0.0181	-0.0181	0
							-0.1892 $\pm j$ 0.2967	-0.0311 $\pm j$ 0.1180
Chebyshev (R_p = 0.5 dB)								
30	15.60	1.5680	0.1297	0.4636	0.1354	1.4260	sub-optimal	
40	23.64	0.0623	0.0149	0.3784	0.1238	0.0181	-0.0181	0
							-0.1892 $\pm j$ 0.2967	-0.0311 $\pm j$ 0.1180
50	23.64	0.0622	0.0149	0.3784	0.1239	0.0180	-0.0180	0
							-0.1892 $\pm j$ 0.2967	-0.0311 $\pm j$ 0.1179
60	15.60	1.5530	0.1281	0.4639	0.1353	1.4108	sub-optimal	
70	15.60	1.5650	0.1294	0.4636	0.1354	1.4230	sub-optimal	
Elliptic (R_p = 0.5 dB, A_s = 20 dB)								
30	23.64	0.0623	0.0149	0.3784	0.1238	0.0181	-0.0181	0
							-0.1892 $\pm j$ 0.2967	-0.0311 $\pm j$ 0.1180
40	23.64	0.0622	0.0149	0.3784	0.1239	0.0180	-0.0180	0
							-0.1892 $\pm j$ 0.2967	-0.0311 $\pm j$ 0.1179
50	23.64	0.0623	0.0149	0.3784	0.1238	0.0182	-0.0182	0
							-0.1892 $\pm j$ 0.2967	-0.0312 $\pm j$ 0.1180
60	23.64	0.0623	0.0149	0.3784	0.1238	0.0181	-0.0181	0
							-0.1892 $\pm j$ 0.2967	-0.0311 $\pm j$ 0.1180
70	15.60	1.5647	0.1293	0.4637	0.1353	1.4226	sub-optimal	

Table A.8: Results obtained by optimising the stopband limit of the 0.05 Hz third order filter when A_s = 60 dB for different starting points.

START (f_{3dB} mHz)	f_{60dB} (mHz)	a_1 (rad/s)	a_0 ((rad/s)^2)	b_1 (rad/s)	b_0 ((rad/s)^2)	p_0 (rad/s)	p (rad/s)	z (rad/s)
Butterworth								
30	0.54	0.1712	0.0000	0.4359	0.0269	0.0743	sub-optimal	
40	0.54	0.1712	0.0000	0.4359	0.0269	0.0743	sub-optimal	
50	1.24	0.6960	0.0005	0.8315	0.2301	0.1842	-0.1842 -0.4158 $\pm j$ 0.2393	0 -0.6953 -0.0007
60	1.24	0.6960	0.0005	0.8315	0.2301	0.1842	-0.1842 -0.4158 $\pm j$ 0.2393	0 -0.6953 -0.0007
70	1.24	0.6960	0.0005	0.8315	0.2301	0.1842	-0.1842 -0.4158 $\pm j$ 0.2393	0 -0.6953 -0.0007
Chebyshev (R_p = 0.5 dB)								
30	0.54	0.1712	0.0000	0.4359	0.0269	0.0743	sub-optimal	
40	not converging							
50	not converging							
60	1.24	0.6960	0.0005	0.8315	0.2301	0.1842	-0.1842 -0.4158 $\pm j$ 0.2393	0 -0.6953 -0.0007
70	0.06	0.2541	0.2823	0.1987	0.2751	0.3567	sub-optimal	
Elliptic (R_p = 0.5 dB, A_s = 60 dB)								
30	not converging							
40	not converging							
50	not converging							
60	1.22	0.9421	0.0008	0.7258	0.1072	0.5194	sub-optimal	
70	not converging							

Table A.9: Results obtained by optimising the stopband limit of the 0.05 Hz third order filter when A_s = 40 dB and the maximum positive overshoot allowed for the pulse response is equal to 5 μV.

START f_{3dB} (mHz)	f_{40dB} (mHz)	a_1 (rad/s)	a_0 ((rad/s)^2)	b_1 (rad/s)	b_0 ((rad/s)^2)	p_0 (rad/s)	p (rad/s)	z (rad/s)
Butterworth								
30	3.86	1.1081	0.0051	0.5746	0.0796	0.8245	-0.8245	0
							-0.3413	-1.1035
							-0.2333	-0.0046
40	3.86	1.1081	0.0051	1.1658	0.2814	0.2333	-0.8245	0
							-0.3413	-1.1035
							-0.2333	-0.0046
50	3.86	1.1081	0.0051	1.0577	0.1923	0.3413	-0.8245	0
							-0.3413	-1.1035
							-0.2333	-0.0046
60	3.86	1.1081	0.0051	1.1658	0.2814	0.2333	-0.8245	0
							-0.3413	-1.1034
							-0.2333	-0.0046
70	3.86	1.1081	0.0051	1.1658	0.2814	0.2333	-0.8245	0
							-0.3413	-1.1035
							-0.2333	-0.0046
Chebyshev (R_p = 0.5 dB)								
30	1.76	0.1706	0.0005	0.4335	0.0272	0.0760	sub-optimal	
40	3.86	1.1081	0.0051	0.5746	0.0796	0.8245	-0.8245	0
							-0.3413	-1.1035
							-0.2333	-0.0046
50	3.86	1.1081	0.0051	0.5746	0.0796	0.8245	-0.8245	0
							-0.3413	-1.1035
							-0.2333	-0.0046
60	3.86	1.1081	0.0051	0.5746	0.0796	0.8245	-0.8245	0
							-0.3413	-1.1035
							-0.2333	-0.0046
70	0.55	3.5424	7.2820	3.5208	6.3593	0.3992	sub-optimal	
Elliptic (R_p = 0.5 dB, A_s = 40 dB)								
30	0.10	0.2384	-0.0119	0.5421	0.0199	0.0368	sub-optimal	
40	not converging							
50	3.86	1.1081	0.0051	1.1658	0.2814	0.2333	-0.8245	0
							-0.3413	-1.1035
							-0.2333	-0.0046
60	3.86	1.1081	0.0051	0.5746	0.0796	0.8245	-0.8245	0
							-0.3413	-1.1035
							-0.2333	-0.0046
70	3.86	1.1081	0.0051	1.1658	0.2814	0.2333	-0.8245	0
							-0.3413	-1.1035
							-0.2333	-0.0046

Table A.10: Results obtained by optimising the stopband limit of the 0.05 Hz third order filter when A_s = 40 dB and the maximum positive overshoot allowed for the pulse response is equal to 2 μV.

START f_{3dB} (mHz)	f_{40dB} (mHz)	a_1 (rad/s)	a_0 ((rad/s)^2)	b_1 (rad/s)	b_0 ((rad/s)^2)	p_0 (rad/s)	p (rad/s)	z (rad/s)
Butterworth								
30	2.80	3.3404	0.0106	0.4339	0.0335	3.0809	sub-optimal	
40	2.81	1.7641	0.0053	1.5802	0.1404	0.3906	-1.4857	0
							-0.3906	-1.7611
							-0.0945	-0.0030
50	2.81	1.8050	0.0054	1.6214	0.1446	0.3880	-1.5267	0
							-0.3880	-1.8020
							-0.0947	-0.0030
60	2.81	1.7802	0.0053	1.8914	0.5850	0.0946	-1.5019	0
							-0.3895	-1.7772
							-0.0946	-0.0030
70	2.81	1.7831	0.0053	1.5993	0.1423	0.3893	-1.5047	0
							-0.3893	-1.7801
							-0.0946	-0.0030
Chebyshev (R_p = 0.5 dB)								
30	1.76	0.1706	0.0005	0.4335	0.0272	0.0760	sub-optimal	
40	1.76	0.1706	0.0005	0.4335	0.0272	0.0760	sub-optimal	
50	2.81	1.7793	0.0053	0.4841	0.0368	1.5010	-1.5010	0
							-0.3896	-1.7763
							-0.0946	-0.0030
60	2.81	1.7842	0.0053	1.6005	0.1424	0.3893	-1.5059	0
							-0.3893	-1.7812
							-0.0946	-0.0030
70	0.90	855.75	138.44	0.4992	0.0913	855.53	sub-optimal	
Elliptic (R_p = 0.5 dB, A_s = 40 dB)								
30	0.10	0.2420	-0.0119	0.5447	0.0197	0.0379	sub-optimal	
40	2.81	1.7843	0.0053	1.8952	0.5862	0.0946	**-1.5060**	**0**
							-0.3893	**-1.7813**
							-0.0946	**-0.0030**
50	2.81	1.7870	0.0053	1.8978	0.5870	0.0946	-1.5087	0
							-0.3891	-1.7840
							-0.0946	-0.0030
60	2.81	1.7917	0.0054	1.6080	0.1432	0.3888	-1.5134	0
							-0.3888	-1.7887
							-0.0946	-0.0030
70	2.81	1.8969	0.0057	1.7134	0.1540	0.3828	-1.6182	0
							-0.3828	-1.8939
							-0.0952	-0.0030

A.3.3 Optimisation of the stopband limit

Table A.11: Outcome of the stopband optimisation procedure for the second order filter when A_s = 20 dB for different starting points.

START f_{3dB} (mHz)	f_{20dB} (mHz)	a_1 (rad/s)	b_1 (rad/s)	b_0 ((rad/s)^2)	p (rad/s)	z (rad/s)
Butterworth						
10	15.47	0.0592	0.3935	0.1132	-0.1967 $\pm j$ 0.2729	0 -0.0592
20	15.47	0.0592	0.3935	0.1132	-0.1967 $\pm j$ 0.2729	0 -0.0592
30	15.47	0.0592	0.3935	0.1132	-0.1967 $\pm j$ 0.2729	0 -0.0592
40	15.47	0.0592	0.3935	0.1132	-0.1967 $\pm j$ 0.2729	0 -0.0592
50	15.47	0.0592	0.3935	0.1132	-0.1967 $\pm j$ 0.2729	0 -0.0592
Chebyshev (R_p = 0.5 dB)						
10	15.47	0.0592	0.3935	0.1132	-0.1967 $\pm j$ 0.2729	0 -0.0592
20	15.47	0.0592	0.3935	0.1132	-0.1967 $\pm j$ 0.2729	0 -0.0592
30	15.47	0.0592	0.3935	0.1132	-0.1967 $\pm j$ 0.2729	0 -0.0592
40	15.47	0.0592	0.3935	0.1132	-0.1967 $\pm j$ 0.2729	0 -0.0592
50	15.47	0.0592	0.3935	0.1132	-0.1967 $\pm j$ 0.2729	0 -0.0592

Table A.12: Outcome of the stopband optimisation procedure for the second order filter when A_s = 40 dB for different starting points.

START f_{3dB} (mHz)	f_{40dB} (mHz)	a_1 (rad/s)	b_1 (rad/s)	b_0 ((rad/s)^2)	p (rad/s)	z (rad/s)
Butterworth						
10	4.63	0.0050	0.3398	0.0861	-0.1699 $\pm j$ 0.2393	0 -0.0050
20	4.63	0.0050	0.3398	0.0861	-0.1699 $\pm j$ 0.2393	0 -0.0050
30	4.63	0.0050	0.3398	0.0861	-0.1699 $\pm j$ 0.2393	0 -0.0050
40	4.63	0.0050	0.3398	0.0861	-0.1699 $\pm j$ 0.2393	0 -0.0050
50	4.63	0.0050	0.3398	0.0861	-0.1699 $\pm j$ 0.2393	0 -0.0050
Chebyshev (R_p = 0.5 dB)						
10	4.63	0.0050	0.3398	0.0861	-0.1699 $\pm j$ 0.2393	0 -0.0050
20	4.63	0.0050	0.3398	0.0861	-0.1699 $\pm j$ 0.2393	0 -0.0050
30	4.63	0.0050	0.3398	0.0861	-0.1699 $\pm j$ 0.2393	0 -0.0050
40	4.63	0.0050	0.3398	0.0861	-0.1699 $\pm j$ 0.2393	0 -0.0050
50	4.63	0.0050	0.3398	0.0861	-0.1699 $\pm j$ 0.2393	0 -0.0050

Table A.13: Outcome of the stopband optimisation procedure for the second order filter when A_s = 60 dB for different starting points.

START f_{3dB} (mHz)	f_{60dB} (mHz)	a_1 (rad/s)	b_1 (rad/s)	b_0 ((rad/s)^2)	p (rad/s)	z (rad/s)
Butterworth						
10	1.46	0.0005	0.3353	0.0839	-0.1676 $\pm j$ 0.2361	0 -0.0005
20	1.46	0.0005	0.3353	0.0839	-0.1676 $\pm j$ 0.2361	0 -0.0005
30	1.46	0.0005	0.3353	0.0839	-0.1676 $\pm j$ 0.2361	0 -0.0005
40	1.46	0.0005	0.3353	0.0839	-0.1676 $\pm j$ 0.2361	0 -0.0005
50	1.46	0.0005	0.3353	0.0839	-0.1676 $\pm j$ 0.2361	0 -0.0005
Chebyshev (R_p = 0.5 dB)						
10	1.46	0.0005	0.3353	0.0839	-0.1676 $\pm j$ 0.2361	0 -0.0005
20	1.46	0.0005	0.3353	0.0839	-0.1676 $\pm j$ 0.2361	0 -0.0005
30	1.46	0.0005	0.3353	0.0839	-0.1676 $\pm j$ 0.2361	0 -0.0005
40	1.46	0.0005	0.3353	0.0839	-0.1676 $\pm j$ 0.2361	0 -0.0005
50	1.46	0.0005	0.3353	0.0839	-0.1676 $\pm j$ 0.2361	0 -0.0005

Table A.14: Outcome of the stopband optimisation procedure for the third order filter when A_s = 20 dB for different starting points.

START f_{3dB} (mHz)	f_{20dB} (mHz)	a_1 (rad/s)	a_0 ((rad/s)^2)	b_1 (rad/s)	b_0 ((rad/s)^2)	p_0 (rad/s)	p (rad/s)	z (rad/s)
Butterworth								
10	25.96	0.0247	0.0215	0.1404	0.0579	0.2204	sub-optimal	
20	26.06	0.0303	0.0217	0.1641	0.0626	0.2020	-0.2020	0
							-0.0820 $\pm j$ 0.2364	-0.0151 $\pm j$ 0.1465
30	15.91	2.0467	0.1079	0.4173	0.1183	1.9527	sub-optimal	
40	15.91	2.0470	0.1080	0.4173	0.1183	1.9530	sub-optimal	
50	15.91	2.0468	0.1080	0.4173	0.1183	1.9528	sub-optimal	
Chebyshev (R_p = 0.5 dB)								
10	26.06	0.0303	0.0217	0.1640	0.0626	0.2021	**-0.2021**	**0**
							-0.0820 $\pm j$ 0.2364	**-0.0151 $\pm j$ 0.1465**
20	26.06	0.0302	0.0217	0.1633	0.0625	0.2027	-0.2027	0
							-0.0816 $\pm j$ 0.2363	-0.0151 $\pm j$ 0.1466
30	26.06	0.0302	0.0217	0.1638	0.0626	0.2022	-0.2022	0
							-0.0819 $\pm j$ 0.2363	-0.0151 $\pm j$ 0.1465
40	5.55	0.0624	0.8314	0.0557	0.8352	0.3456	sub-optimal	
50	15.91	2.0452	0.1079	0.4173	0.1183	1.9511	sub-optimal	
Elliptic (R_p = 0.5 dB, A_s = 20 dB)								
10	not converging							
20	15.91	2.0467	0.1079	0.4173	0.1183	1.9527	sub-optimal	
30	26.06	0.0303	0.0217	0.1639	0.0626	0.2022	-0.2022	0
							-0.0819 $\pm j$ 0.2364	-0.0151 $\pm j$ 0.1465
40	26.06	0.0303	0.0217	0.1644	0.0627	0.2016	-0.2016	0
							-0.0822 $\pm j$ 0.2365	-0.0151 $\pm j$ 0.1465
50	15.91	2.0463	0.1083	0.4174	0.1183	1.9524	sub-optimal	

Table A.15: Outcome of the stopband optimisation procedure for the third order filter when A_s = 40 dB for different starting points.

START f_{3dB} (mHz)	f_{40dB} (mHz)	a_1 (rad/s)	a_0 ((rad/s)^2)	b_1 (rad/s)	b_0 ((rad/s)^2)	p_0 (rad/s)	p (rad/s)	z (rad/s)
Butterworth								
10	10.43	0.0061	0.0033	0.1312	0.0350	0.2110	-0.2110	0
							-0.0656 $\pm j$ 0.1753	-0.0030 $\pm j$ 0.0573
20	10.43	0.0067	0.0033	0.1304	0.0350	0.2123	-0.2123	0
							-0.0652 $\pm j$ 0.1754	-0.0033$\pm j$ 0.0574
30	10.43	0.0060	0.0033	0.1299	0.0348	0.2122	-0.2122	0
							-0.0650 $\pm j$ 0.1750	-0.0030 $\pm j$ 0.0573
40	0.63	0.2098	0.2265	0.2325	0.2866	0.3131	sub-optimal	
50	0.66	0.6029	0.4990	0.4673	0.4309	0.4770	sub-optimal	
Chebyshev (R_p = 0.5 dB)								
10	10.43	0.0060	0.0033	0.1310	0.0350	0.2111	-0.2111	0
							-0.0655 $\pm j$ 0.1753	-0.0030 $\pm j$ 0.0573
20	10.43	0.0060	0.0033	0.1300	0.0349	0.2122	-0.2122	0
							-0.0650 $\pm j$ 0.1750	-0.0030 $\pm j$ 0.0573
30	0.56	0.0685	0.4917	0.0617	0.5006	0.3454	sub-optimal	
40	10.43	0.0060	0.0033	0.1299	0.0348	0.2121	-0.2121	0
							-0.0650 $\pm j$ 0.1750	-0.0030 $\pm j$ 0.0573
50	10.43	0.0060	0.0033	0.1295	0.0348	0.2125	-0.2125	0
							-0.0648 $\pm j$ 0.1749	-0.0030 $\pm j$ 0.0573
Elliptic (R_p = 0.5 dB, A_s = 40 dB)								
10	10.43	0.0060	0.0033	0.1299	0.0348	0.2122	-0.2122	0
							-0.0649 $\pm j$ 0.1750	-0.0030 $\pm j$ 0.0573
20	10.43	0.0060	0.0033	0.1299	0.0348	0.2121	-0.2121	0
							-0.0650 $\pm j$ 0.1750	-0.0030 $\pm j$ 0.0573
30	10.43	0.0060	0.0033	0.1297	0.0348	0.2123	-0.2123	0
							-0.0649 $\pm j$ 0.1750	-0.0030 $\pm j$ 0.0573
40	10.43	0.0060	0.0033	0.1296	0.0348	0.2125	-0.2125	0
							-0.0648 $\pm j$ 0.1749	-0.0030 $\pm j$ 0.0573
50	10.43	0.0060	0.0033	0.1299	0.0348	0.2122	-0.2122	0
							-0.0650 $\pm j$ 0.1750	-0.0030 $\pm j$ 0.0573

Table A.16: Outcome of the stopband optimisation procedure for the third order filter when A_s = 60 dB for different starting points.

START f_{3dB} (mHz)	f_{60dB} (mHz)	a_1 (rad/s)	a_0 ((rad/s)^2)	b_1 (rad/s)	b_0 ((rad/s)^2)	p_0 (rad/s)	p (rad/s)	z (rad/s)
Butterworth								
10	4.67	0.0017	0.0007	0.1019	0.0272	0.2363	sub-optimal	
20	4.71	0.0013	0.0007	0.1249	0.0308	0.2125	-0.2125 -0.0625 $\pm j$ 0.1639	0 -0.0006 $\pm j$ 0.0257
30	0.35	12004	591.36	0.3829	0.1078	12004	sub-optimal	
40	not converging							
50	not converging							
Chebyshev (R_p = 0.5 dB)								
10	4.71	0.0013	0.0007	0.1252	0.0308	0.2122	-0.2122 -0.0626 $\pm j$ 0.1639	0 -0.0006 $\pm j$ 0.0257
20	4.71	0.0013	0.0007	0.1249	0.0308	0.2125	-0.2125 -0.0625 $\pm j$ 0.1639	0 -0.0006 $\pm j$ 0.0257
30	0.06	0.1026	0.4704	0.0941	0.4859	0.3469	sub-optimal	
40	0.06	0.1102	0.7220	0.0980	0.7303	0.3509	sub-optimal	
50	0.06	0.1235	0.5899	0.1057	0.5885	0.3571	sub-optimal	
Elliptic (R_p = 0.5 dB, A_s = 60 dB)								
10	4.71	0.0013	0.0007	0.1249	0.0308	0.2125	-0.2125 -0.0625 $\pm j$ 0.1639	0 -0.0006 $\pm j$ 0.0257
20	4.71	0.0013	0.0007	0.1252	0.0308	0.2122	-0.2122 -0.0626 $\pm j$ 0.1639	0 -0.0006 $\pm j$ 0.0257
30	4.71	0.0013	0.0007	0.1252	0.0308	0.2122	-0.2122 -0.0626 $\pm j$ 0.1639	0 -0.0006 $\pm j$ 0.0257
40	4.71	0.0013	0.0007	0.1253	0.0308	0.2121	-0.2121 -0.0627 $\pm j$ 0.1640	0 -0.0006 $\pm j$ 0.0257
50	not converging							

A.3.4 Optimisation of the 3dB-cutoff frequency

Table A.17: Results derived by maximising the 3dB-cutoff frequency of the second order filter for different starting points.

START f_{3dB} (mHz)	f_{3dB} (mHz)	a_1 (rad/s)	b_1 (rad/s)	b_0 ((rad/s)^2)	p (rad/s)	z (rad/s)
Butterworth						
10	77.95	0.3591	0.7043	0	pole-zero cancellation	
30	77.95	0.3591	0.7043	0	pole-zero cancellation	
50	77.95	0.3591	0.7043	0	pole-zero cancellation	
70	67.71	1.0294	1.3140	0.5491	-0.6570 $\pm j$ 0.3426	0 -1.0294
90	67.71	1.0294	1.3140	0.5490	-0.6570 $\pm j$ 0.3426	0 -1.0294
110	67.71	1.0296	1.3142	0.5491	-0.6571 $\pm j$ 0.3425	0 -1.0296
130	67.71	1.0295	1.3141	0.5491	-0.6570 $\pm j$ 0.3426	0 -1.0295
150	67.71	1.0294	1.3141	0.5491	-0.6570 $\pm j$ 0.3426	0 -1.0294
Chebyshev (R_p = 0.5 dB)						
10	77.95	0.3591	0.7043	0	pole-zero cancellation	
30	67.71	1.0291	1.3138	0.5490	-0.6569 $\pm j$ 0.3427	0 -1.0291
50	67.71	1.0296	1.3142	0.5491	-0.6571 $\pm j$ 0.3425	0 -1.0296
70	67.71	1.0294	1.3141	0.5491	-0.6570 $\pm j$ 0.3426	0 -1.0294
90	67.71	1.0294	1.3140	0.5490	-0.6570 $\pm j$ 0.3426	0 -1.0294
110	67.71	1.0295	1.3141	0.5491	-0.6571 $\pm j$ 0.3426	0 -1.0295
130	67.71	1.0295	1.3141	0.5491	-0.6571 $\pm j$ 0.3426	0 -1.0295
150	67.71	1.0297	1.3143	0.5492	-0.6572 $\pm j$ 0.3425	0 -1.0297

Table A.18: Results derived by maximising the 3dB-cutoff frequency of the third order filter when A_s = 40 dB for different starting points. Constraints c_7, c_8, c_9 and c_{10} are enforced.

START f_{3dB} (mHz)	f_{3dB} (mHz)	a_1 (rad/s)	a_0 ((rad/s)^2)	b_1 (rad/s)	b_0 ((rad/s)^2)	p_0 (rad/s)	p (rad/s)	z (rad/s)
Butterworth								
10	76.20	1.9892	0.5221	1.2037	0.1553	1.0563	sub-optimal	
30	76.20	1.9892	0.5231	1.2038	0.1555	1.0566	sub-optimal	
50	76.20	1.9893	0.5233	1.2038	0.1555	1.0567	sub-optimal	
70	not converging							
90	122.94	0.4747	0.7623	0.5426	0.9365	0.2557	-0.2557 -0.2713 $\pm j$ 0.9289	0 -0.2374 $\pm j$ 0.8402
110	122.94	0.4747	0.7623	0.5426	0.9365	0.2557	-0.2557 -0.2713 $\pm j$ 0.9289	0 -0.2374 $\pm j$ 0.8402
130	122.94	0.4747	0.7623	0.5426	0.9365	0.2557	-0.2557 -0.2713 $\pm j$ 0.9289	0 -0.2374 $\pm j$ 0.8402
150	122.94	0.4747	0.7623	0.5426	0.9365	0.2557	-0.2557 -0.2713 $\pm j$ 0.9289	0 -0.2374 $\pm j$ 0.8402
Chebyshev (R_p = 0.5 dB)								
10	not converging							
30	not converging							
50	122.94	0.4747	0.7623	0.5426	0.9365	0.2557	-0.2557 -0.2713 $\pm j$ 0.9289	0 -0.2374 $\pm j$ 0.8402
70	122.94	0.4747	0.7623	0.5426	0.9365	0.2557	-0.2557 -0.2713 $\pm j$ 0.9289	0 -0.2374 $\pm j$ 0.8402
90	122.94	0.4747	0.7623	0.5426	0.9365	0.2557	-0.2557 -0.2713 $\pm j$ 0.9289	0 -0.2374 $\pm j$ 0.8402
110	122.94	0.4747	0.7623	0.5426	0.9365	0.2557	-0.2557 -0.2713 $\pm j$ 0.9289	0 -0.2374 $\pm j$ 0.8402
130	122.94	0.4747	0.7623	0.5426	0.9365	0.2557	-0.2557 -0.2713 $\pm j$ 0.9289	0 -0.2374 $\pm j$ 0.8402
150	122.94	0.4747	0.7623	0.5426	0.9365	0.2557	-0.2557 -0.2713 $\pm j$ 0.9289	0 -0.2374 $\pm j$ 0.8402
Elliptic (R_p = 0.5 dB, A_s = 40 dB)								
10	not converging							
30	not converging							
50	122.94	0.4747	0.7623	0.5426	0.9365	0.2557	-0.2557 -0.2713 $\pm j$ 0.9289	0 -0.2374 $\pm j$ 0.8402
70	122.94	0.4747	0.7623	0.5426	0.9365	0.2557	-0.2557 -0.2713 $\pm j$ 0.9289	0 -0.2374 $\pm j$ 0.8402
90	122.94	0.4747	0.7623	0.5426	0.9365	0.2557	-0.2557 -0.2713 $\pm j$ 0.9289	0 -0.2374 $\pm j$ 0.8402
110	122.94	0.4747	0.7623	0.5426	0.9365	0.2557	-0.2557 -0.2713 $\pm j$ 0.9289	0 -0.2374 $\pm j$ 0.8402
130	122.94	0.4747	0.7623	0.5426	0.9365	0.2557	-0.2557 -0.2713 $\pm j$ 0.9289	0 -0.2374 $\pm j$ 0.8402
150	not converging							

Table A.19: Results derived by maximising the 3dB-cutoff frequency of the third order filter when A_s = 60 dB for different starting points. Constraints c_7, c_8, c_9 and c_{10} are enforced.

START f_{3dB} (mHz)	f_{3dB} (mHz)	a_1 (rad/s)	a_0 ((rad/s)^2)	b_1 (rad/s)	b_0 ((rad/s)^2)	p_0 (rad/s)	p (rad/s)	z (rad/s)
Butterworth								
10	122.94	0.4747	0.7623	0.5426	0.9365	0.2557	-0.2557 -0.2713 $\pm j$ 0.9289	0 -0.2374 $\pm j$ 0.8402
30	76.19	1.9893	0.5232	1.2039	0.1555	1.0566	sub-optimal	
50	not converging							
70	not converging							
90	122.94	0.4747	0.7623	0.5426	0.9365	0.2557	-0.2557 -0.2713 $\pm j$ 0.9289	0 -0.2374 $\pm j$ 0.8402
110	122.94	0.4747	0.7623	0.5426	0.9365	0.2557	-0.2557 -0.2713 $\pm j$ 0.9289	0 -0.2374 $\pm j$ 0.8402
130	122.94	0.4747	0.7623	0.5426	0.9365	0.2557	-0.2557 -0.2713 $\pm j$ 0.9289	0 -0.2374 $\pm j$ 0.8402
150	122.94	0.4747	0.7623	0.5426	0.9365	0.2557	-0.2557 -0.2713 $\pm j$ 0.9289	0 -0.2374 $\pm j$ 0.8402
Chebyshev (R_p = 0.5 dB)								
10	not converging							
30	not converging							
50	122.94	0.4747	0.7623	0.5426	0.9365	0.2557	-0.2557 -0.2713 $\pm j$ 0.9289	0 -0.2374 $\pm j$ 0.8402
70	122.94	0.4747	0.7623	0.5426	0.9365	0.2557	-0.2557 -0.2713 $\pm j$ 0.9289	0 -0.2374 $\pm j$ 0.8402
90	122.94	0.4747	0.7623	0.5426	0.9365	0.2557	-0.2557 -0.2713 $\pm j$ 0.9289	0 -0.2374 $\pm j$ 0.8402
110	122.94	0.4747	0.7623	0.5426	0.9365	0.2557	-0.2557 -0.2713 $\pm j$ 0.9289	0 -0.2374 $\pm j$ 0.8402
130	122.94	0.4747	0.7623	0.5426	0.9365	0.2557	-0.2557 -0.2713 $\pm j$ 0.9289	0 -0.2374 $\pm j$ 0.8402
150	122.94	0.4747	0.7623	0.5426	0.9365	0.2557	-0.2557 -0.2713 $\pm j$ 0.9289	0 -0.2374 $\pm j$ 0.8402
Elliptic (R_p = 0.5 dB, A_s = 60 dB)								
10	122.94	0.4747	0.7623	0.5426	0.9365	0.2557	-0.2557 -0.2713 $\pm j$ 0.9289	0 -0.2374 $\pm j$ 0.8402
30	not converging							
50	122.94	0.4747	0.7623	0.5426	0.9365	0.2557	-0.2557 -0.2713 $\pm j$ 0.9289	0 -0.2374 $\pm j$ 0.8402
70	122.94	0.4747	0.7623	0.5426	0.9365	0.2557	-0.2557 -0.2713 $\pm j$ 0.9289	0 -0.2374 $\pm j$ 0.8402
90	122.94	0.4747	0.7623	0.5426	0.9365	0.2557	-0.2557 -0.2713 $\pm j$ 0.9289	0 -0.2374 $\pm j$ 0.8402
110	122.94	0.4747	0.7623	0.5426	0.9365	0.2557	-0.2557 -0.2713 $\pm j$ 0.9289	0 -0.2374 $\pm j$ 0.8402
130	76.19	1.9893	0.5232	1.2038	0.1555	1.0566	sub-optimal	
150	76.19	1.9893	0.5234	1.2039	0.1556	1.0567	sub-optimal	

Table A.20: Results derived by maximising the 3dB-cutoff frequency of the third order filter when no amplitude ripple is allowed in the stopband ($A_s \rightarrow \infty$) for different starting points. Constraints c_8, c'_9 and c'_{10} are enforced.

START f_{3dB} (mHz)	f_{3dB} (mHz)	a_1 (rad/s)	a_0 ((rad/s)^2)	b_1 (rad/s)	b_0 ((rad/s)^2)	p_0 (rad/s)	p (rad/s)	z (rad/s)
Butterworth								
10	not converging							
30	76.19	1.9893	0.5232	1.2039	0.1555	1.0566	sub-optimal	
50	76.19	1.9893	0.5232	1.2039	0.1555	1.0566	sub-optimal	
70	not converging							
90	122.94	0.4747	0.7623	0.5426	0.9365	0.2557	-0.2557	0
							-0.2713 $\pm j$ 0.9289	-0.2374 $\pm j$ 0.8402
110	122.94	0.4747	0.7623	0.5426	0.9365	0.2557	-0.2557	0
							-0.2713 $\pm j$ 0.9289	-0.2374 $\pm j$ 0.8402
130	122.94	0.4747	0.7623	0.5426	0.9365	0.2557	-0.2557	0
							-0.2713 $\pm j$ 0.9289	-0.2374 $\pm j$ 0.8402
150	122.94	0.4747	0.7623	0.5426	0.9365	0.2557	-0.2557	0
							-0.2713 $\pm j$ 0.9289	-0.2374 $\pm j$ 0.8402
Chebyshev (R_p = 0.5 dB)								
10	77.27	1.3482	0.2860	1.5385	0.7365	0.1220	sub-optimal	
30	122.94	0.4747	0.7623	0.5426	0.9365	0.2557	-0.2557	0
							-0.2713 $\pm j$ 0.9289	-0.2374 $\pm j$ 0.8402
50	122.94	0.4747	0.7623	0.5426	0.9365	0.2557	-0.2557	0
							-0.2713 $\pm j$ 0.9289	-0.2374 $\pm j$ 0.8402
70	122.94	0.4747	0.7623	0.5426	0.9365	0.2557	-0.2557	0
							-0.2713 $\pm j$ 0.9289	-0.2374 $\pm j$ 0.8402
90	122.94	0.4747	0.7623	0.5426	0.9365	0.2557	-0.2557	0
							-0.2713 $\pm j$ 0.9289	-0.2374 $\pm j$ 0.8402
110	122.94	0.4747	0.7623	0.5426	0.9365	0.2557	-0.2557	0
							-0.2713 $\pm j$ 0.9289	-0.2374 $\pm j$ 0.8402
130	122.94	0.4747	0.7623	0.5426	0.9365	0.2557	-0.2557	0
							-0.2713 $\pm j$ 0.9289	-0.2374 $\pm j$ 0.8402
150	122.94	0.4747	0.7623	0.5426	0.9365	0.2557	-0.2557	0
							-0.2713 $\pm j$ 0.9289	-0.2374 $\pm j$ 0.8402
Elliptic (R_p = 0.5 dB, A_s = 40 dB)								
10	122.94	0.4747	0.7623	0.5426	0.9365	0.2557	-0.2557	0
							-0.2713 $\pm j$ 0.9289	-0.2374 $\pm j$ 0.8402
30	122.94	0.4747	0.7623	0.5426	0.9365	0.2557	-0.2557	0
							-0.2713 $\pm j$ 0.9289	-0.2374 $\pm j$ 0.8402
50	122.94	0.4747	0.7623	0.5426	0.9365	0.2557	-0.2557	0
							-0.2713 $\pm j$ 0.9289	-0.2374 $\pm j$ 0.8402
70	122.94	0.4747	0.7623	0.5426	0.9365	0.2557	-0.2557	0
							-0.2713 $\pm j$ 0.9289	-0.2374 $\pm j$ 0.8402
90	122.94	0.4747	0.7623	0.5426	0.9365	0.2557	-0.2557	0
							-0.2713 $\pm j$ 0.9289	-0.2374 $\pm j$ 0.8402
110	122.94	0.4747	0.7623	0.5426	0.9365	0.2557	-0.2557	0
							-0.2713 $\pm j$ 0.9289	-0.2374 $\pm j$ 0.8402
130	122.94	0.4747	0.7623	0.5426	0.9365	0.2557	-0.2557	0
							-0.2713 $\pm j$ 0.9289	-0.2374 $\pm j$ 0.8402
150	76.19	1.9898	0.5240	1.2043	0.1558	1.0568	sub-optimal	

Table A.21: Results derived by maximising the 3dB-cutoff frequency of the third order filter having concave magnitude characteristic outside the passband for different starting points. Constraints c_8, c'_9, c'_{10} and c_{11} are enforced.

START f_{3dB} (mHz)	f_{3dB} (mHz)	a_1 (rad/s)	a_0 ((rad/s)^2)	b_1 (rad/s)	b_0 ((rad/s)^2)	p_0 (rad/s)	p (rad/s)	z (rad/s)
Butterworth								
10	69.80	1.9039	0.1646	0.6150	0.0325	1.5914	sub-optimal	
30	76.19	1.9893	0.5231	1.2038	0.1555	1.0566	sub-optimal	
50	76.19	1.9893	0.5231	1.2038	0.1555	1.0566	sub-optimal	
70	not converging							
90	90.08	1.1148	0.5410	1.2053	0.9008	0.1887	-0.1887	0
							-0.6027 $\pm j$ 0.7332	-0.5574 $\pm j$ 0.4799
110	70.46	0.7608	0.2789	0.8784	0.4004	0.2185	sub-optimal	
130	not converging							
150	90.08	1.1135	0.5393	1.2043	0.8990	0.1885	-0.1885	0
							-0.6022 $\pm j$ 0.7324	-0.5568 $\pm j$ 0.4789
Chebyshev (R_p = 0.5 dB)								
10	90.08	1.1145	0.5406	1.2051	0.9004	0.1886	-0.1886	0
							-0.6025 $\pm j$ 0.7330	-0.5572 $\pm j$ 0.4797
30	76.19	1.9893	0.5232	1.2039	0.1556	1.0566	sub-optimal	
50	90.08	1.1154	0.5415	1.2057	0.9016	0.1887	-0.1887	0
							-0.6028 $\pm j$ 0.7336	-0.5577 $\pm j$ 0.4801
70	90.08	1.1146	0.5407	1.2052	0.9005	0.1886	-0.1886	0
							-0.6026 $\pm j$ 0.7331	-0.5573 $\pm j$ 0.4798
90	90.08	1.1155	0.5416	1.2058	0.9017	0.1887	-0.1887	0
							-0.6029 $\pm j$ 0.7336	-0.5578 $\pm j$ 0.4801
110	90.08	1.1168	0.5435	1.2068	0.9035	0.1890	-0.1890	0
							-0.6034 $\pm j$ 0.7345	-0.5584 $\pm j$ 0.4813
130	89.54	1.1125	0.5065	1.2034	0.8776	0.1816	sub-optimal	
150	90.08	1.1175	0.5440	1.2072	0.9043	0.1890	-0.1890	0
							-0.6036 $\pm j$ 0.7348	-0.5587 $\pm j$ 0.4814
Elliptic (R_p = 0.5 dB, A_s = 40 dB)								
10	not converging							
30	90.08	1.1152	0.5412	1.2055	0.9012	0.1887	-0.1887	0
							-0.6028 $\pm j$ 0.7334	-0.5576 $\pm j$ 0.4799
50	90.08	1.1159	0.5424	1.2061	0.9023	0.1889	-0.1889	0
							-0.6031 $\pm j$ 0.7339	-0.5580 $\pm j$ 0.4808
70	90.08	1.1150	0.5411	1.2054	0.9010	0.1887	-0.1887	0
							-0.6027 $\pm j$ 0.7333	-0.5575 $\pm j$ 0.4799
90	90.08	1.1148	0.5410	1.2053	0.9008	0.1887	-0.1887	0
							-0.6027 $\pm j$ 0.7332	-0.5574 $\pm j$ 0.4799
110	90.08	1.1162	0.5425	1.2063	0.9026	0.1888	-0.1888	0
							-0.6031 $\pm j$ 0.7340	-0.5581 $\pm j$ 0.4806
130	not converging							
150	76.19	1.9920	0.5232	1.2054	0.1556	1.0566	sub-optimal	

A.3.5 Optimisation of selected points in the filter transition region

Table A.22: Results derived by maximising the frequency at which an attenuation of 1.5 dB is achieved by the second order filter for different starting points.

START f_{3dB} (mHz)	$f_{1.5dB}$ (mHz)	a_1 (rad/s)	b_1 (rad/s)	b_0 ((rad/s)^2)	p (rad/s)	z (rad/s)
Butterworth						
10	162.52	0.9148	1.2697	0	pole-zero cancellation	
30	162.52	0.9148	1.2697	0	pole-zero cancellation	
50	162.52	0.9148	1.2697	0	pole-zero cancellation	
70	162.52	0.9148	1.2697	0	pole-zero cancellation	
90	162.52	0.9148	1.2697	0	pole-zero cancellation	
110	162.52	0.9148	1.2697	0	pole-zero cancellation	
130	162.52	0.9148	1.2697	0	pole-zero cancellation	
150	93.52	2.3223	2.6284	0.9881	-2.1738 -0.4546	0 -2.3223
Chebyshev (R_p = 0.5 dB)						
10	162.52	0.9148	1.2697	0	pole-zero cancellation	
30	162.52	0.9148	1.2697	0	pole-zero cancellation	
50	162.52	0.9148	1.2697	0	pole-zero cancellation	
70	93.52	2.3224	2.6285	0.9881	-2.1740 -0.4545	0 -2.3224
90	162.52	0.9148	1.2697	0	pole-zero cancellation	
110	162.52	0.9148	1.2697	0	pole-zero cancellation	
130	162.52	0.9148	1.2697	0	pole-zero cancellation	
150	93.52	2.3220	2.6282	0.9880	**-2.1736** **-0.4545**	**0** **-2.3220**

Table A.23: Results derived by maximising the frequency at which an attenuation of 4.5 dB is achieved by the second order filter for different starting points.

START f_{3dB} (mHz)	$f_{4.5dB}$ (mHz)	a_1 (rad/s)	b_1 (rad/s)	b_0 ((rad/s)^2)	p (rad/s)	z (rad/s)
Butterworth						
10	40.13	282.50	282.75	96.076	sub-optimal	
30	55.49	0.7038	1.0023	0.4202	-0.5012 $\pm j$ 0.4111	0 -0.7038
50	55.49	0.7038	1.0023	0.4202	-0.5012 $\pm j$ 0.4111	0 -0.7038
70	55.49	0.7038	1.0024	0.4202	-0.5012 $\pm j$ 0.4111	0 -0.7038
90	55.49	0.7038	1.0023	0.4202	-0.5012 $\pm j$ 0.4111	0 -0.7038
110	55.49	0.7038	1.0023	0.4202	-0.5012 $\pm j$ 0.4111	0 -0.7038
130	55.49	0.7038	1.0023	0.4202	-0.5012 $\pm j$ 0.4111	0 -0.7038
150	55.49	0.7038	1.0023	0.4202	-0.5012 $\pm j$ 0.4111	0 -0.7038
Chebyshev (R_p = 0.5 dB)						
10	55.49	0.7038	1.0024	0.4202	-0.5012 $\pm j$ 0.4111	0 -0.7038
30	55.49	0.7038	1.0023	0.4202	-0.5012 $\pm j$ 0.4111	0 -0.7038
50	55.49	0.7038	1.0023	0.4202	-0.5012 $\pm j$ 0.4111	0 -0.7038
70	55.49	0.7038	1.0023	0.4202	-0.5012 $\pm j$ 0.4111	0 -0.7038
90	55.49	0.7038	1.0023	0.4202	-0.5012 $\pm j$ 0.4111	0 -0.7038
110	55.49	0.7038	1.0023	0.4202	-0.5012 $\pm j$ 0.4111	0 -0.7038
130	55.49	0.7038	1.0023	0.4202	-0.5012 $\pm j$ 0.4111	0 -0.7038
150	55.49	0.7038	1.0023	0.4202	-0.5012 $\pm j$ 0.4111	0 -0.7038

Table A.24: Results derived by optimising the 6dB-point of the second order filter for different starting points.

START f_{3dB} (mHz)	f_{6dB} (mHz)	a_1 (rad/s)	b_1 (rad/s)	b_0 ((rad/s)^2)	p (rad/s)	z (rad/s)
Butterworth						
10	31.38	213.61	213.85	72.719	sub-optimal	
30	46.95	0.5299	0.8428	0.3432	-0.4214 $\pm j$ 0.4069	0
						-0.5299
50	46.95	0.5299	0.8428	0.3432	-0.4214 $\pm j$ 0.4069	0
						-0.5299
70	46.95	0.5299	0.8428	0.3432	-0.4214 $\pm j$ 0.4069	0
						-0.5299
90	46.95	0.5299	0.8428	0.3432	-0.4214 $\pm j$ 0.4069	0
						-0.5299
110	46.95	0.5299	0.8428	0.3432	-0.4214 $\pm j$ 0.4069	0
						-0.5299
130	46.95	0.5299	0.8428	0.3432	-0.4214 $\pm j$ 0.4069	0
						-0.5299
150	46.95	0.5299	0.8428	0.3432	-0.4214 $\pm j$ 0.4069	0
						-0.5299
Chebyshev (R_p = 0.5 dB)						
10	46.95	0.5299	0.8428	0.3432	-0.4214 $\pm j$ 0.4069	0
						-0.5299
30	46.95	0.5299	0.8428	0.3432	-0.4214 $\pm j$ 0.4069	0
						-0.5299
50	46.95	0.5299	0.8428	0.3432	-0.4214 $\pm j$ 0.4069	0
						-0.5299
70	46.95	0.5299	0.8428	0.3432	-0.4214 $\pm j$ 0.4069	0
						-0.5299
90	46.95	0.5299	0.8428	0.3432	-0.4214 $\pm j$ 0.4069	0
						-0.5299
110	46.95	0.5299	0.8428	0.3432	-0.4214 $\pm j$ 0.4069	0
						-0.5299
130	46.95	0.5299	0.8428	0.3432	-0.4214 $\pm j$ 0.4069	0
						-0.5299
150	46.95	0.5299	0.8428	0.3432	-0.4214 $\pm j$ 0.4069	0
						-0.5299

Table A.25: Results derived by maximising the frequency at which an attenuation of 1.5 dB is achieved by the the third order filter ($A_s \rightarrow \infty$) for different starting points.

START f_{3dB} (mHz)	$f_{1.5dB}$ (mHz)	a_1 (rad/s)	a_0 ((rad/s)^2)	b_1 (rad/s)	b_0 ((rad/s)^2)	p_0 (rad/s)	p (rad/s)	z (rad/s)
Butterworth								
10	116.03	2.6691	1.3378	1.5897	0.3082	1.3637	sub-optimal	
30	not converging							
50	116.03	2.6694	1.3380	1.5898	0.3082	1.3638	sub-optimal	
70	not converging							
90	not converging							
110	86.23	5396.1	2806.2	5396.2	3107.7	0.2837	sub-optimal	
130	194.26	0.6808	2.0292	0.7040	2.2495	0.2834	-0.2834 -0.3520 $\pm j$ 1.4579	0 -0.3404 $\pm j$ 1.3832
150	194.26	0.6808	2.0292	0.7040	2.2495	0.2834	-0.2834 -0.3520 $\pm j$ 1.4579	0 -0.3404 $\pm j$ 1.3832
Chebyshev (R_p = 0.5 dB)								
10	not converging							
30	194.26	0.6808	2.0292	0.7040	2.2495	0.2834	-0.2834 -0.3520 $\pm j$ 1.4579	0 -0.3404 $\pm j$ 1.3832
50	194.26	0.6808	2.0292	0.7040	2.2495	0.2834	-0.2834 -0.3520 $\pm j$ 1.4579	0 -0.3404 $\pm j$ 1.3832
70	194.26	0.6808	2.0292	0.7040	2.2495	0.2834	-0.2834 -0.3520 $\pm j$ 1.4579	0 -0.3404 $\pm j$ 1.3832
90	194.26	0.6808	2.0292	0.7040	2.2495	0.2834	-0.2834 -0.3520 $\pm j$ 1.4579	0 -0.3404 $\pm j$ 1.3832
110	194.26	0.6808	2.0292	0.7040	2.2495	0.2834	-0.2834 -0.3520 $\pm j$ 1.4579	0 -0.3404 $\pm j$ 1.3832
130	194.26	0.6808	2.0292	0.7040	2.2495	0.2834	-0.2834 -0.3520 $\pm j$ 1.4579	0 -0.3404 $\pm j$ 1.3832
150	194.26	0.6808	2.0292	0.7040	2.2495	0.2834	-0.2834 -0.3520 $\pm j$ 1.4579	0 -0.3404 $\pm j$ 1.3832
Elliptic (R_p = 0.5 dB, A_s = 40 dB)								
10	not converging							
30	194.26	0.6808	2.0292	0.7040	2.2495	0.2834	-0.2834 -0.3520 $\pm j$ 1.4579	0 -0.3404 $\pm j$ 1.3832
50	not converging							
70	not converging							
90	194.26	0.6808	2.0292	0.7040	2.2495	0.2834	-0.2834 -0.3520 $\pm j$ 1.4579	0 -0.3404 $\pm j$ 1.3832
110	116.03	2.6694	1.3380	1.5898	0.3082	1.3638	sub-optimal	
130	194.26	0.6808	2.0292	0.7040	2.2495	0.2834	-0.2834 -0.3520 $\pm j$ 1.4579	0 -0.3404 $\pm j$ 1.3832
150	194.26	0.6808	2.0292	0.7040	2.2495	0.2834	-0.2834 -0.3520 $\pm j$ 1.4579	0 -0.3404 $\pm j$ 1.3832

Table A.26: Results derived by maximising the frequency at which an attenuation of 4.5 dB is achieved by the the third order filter ($A_s \rightarrow \infty$) for different starting points.

START f_{3dB} (mHz)	$f_{4.5dB}$ (mHz)	a_1 (rad/s)	a_0 ((rad/s)^2)	b_1 (rad/s)	b_0 ((rad/s)^2)	p_0 (rad/s)	p (rad/s)	z (rad/s)
Butterworth								
10	45.52	5.2317	-0.0012	5.0666	0.0000	0.4049	sub-optimal	
30	68.28	0.7252	0.5162	0.8182	0.7740	0.2095	-0.2095	0
							-0.4091 $\pm j$ 0.7789i	-0.3626 $\pm j$ 0.6202
50	64.80	0.7613	0.5339	0.8443	0.7918	0.2153	sub-optimal	
70	68.28	0.7249	0.5162	0.8179	0.7740	0.2095	-0.2095	0
							-0.4089 $\pm j$ 0.7789	-0.3624 $\pm j$ 0.6204
90	68.28	0.7253	0.5162	0.8183	0.7741	0.2095	-0.2095	0
							-0.4091 $\pm j$ 0.7789	-0.3626 $\pm j$ 0.6202
110	68.28	0.7242	0.5162	0.8172	0.7738	0.2096	-0.2096	0
							-0.4086 $\pm j$ 0.7790	-0.3621 $\pm j$ 0.6206
130	55.40	1.6660	0.2232	1.8861	0.8217	0.0854	sub-optimal	
150	68.28	0.7254	0.5162	0.8185	0.7741	0.2095	-0.2095	0
							-0.4092 $\pm j$ 0.7789	-0.3627 $\pm j$ 0.6202
Chebyshev (R_p = 0.5 dB)								
10	54.74	1.7317	0.2056	0.7084	0.0486	1.3279	sub-optimal	
30	68.28	0.7252	0.5162	0.8182	0.7740	0.2095	-0.2095	0
							-0.4091 $\pm j$ 0.7789	-0.3626 $\pm j$ 0.6202
50	68.28	0.7252	0.5162	0.8182	0.7741	0.2095	-0.2095	0
							-0.4091 $\pm j$ 0.7789	-0.3626 $\pm j$ 0.6202
70	68.28	0.7252	0.5162	0.8182	0.7741	0.2095	-0.2095	0
							-0.4091 $\pm j$ 0.7789	-0.3626 $\pm j$ 0.6202
90	68.28	0.7250	0.5162	0.8181	0.7740	0.2095	-0.2095	0
							-0.4090 $\pm j$ 0.7789	-0.3625 $\pm j$ 0.6203
110	68.28	0.7250	0.5162	0.8180	0.7740	0.2095	-0.2095	0
							-0.4090 $\pm j$ 0.7789	-0.3625 $\pm j$ 0.6203
130	68.28	0.7253	0.5162	0.8183	0.7741	0.2095	-0.2095	0
							-0.4092 $\pm j$ 0.7789	-0.3627 $\pm j$ 0.6202
150	68.28	0.7240	0.5163	0.8170	0.7738	0.2096	-0.2096	0
							-0.4085 $\pm j$ 0.7790	-0.3620 $\pm j$ 0.6207
Elliptic (R_p = 0.5 dB, A_s = 40 dB)								
10	40.14	0.6658	0.0810	0.7919	0.1479	0.2124	sub-optimal	
30	50.35	11.751	21.705	9.9944	4.4876	2.1295	sub-optimal	
50	68.27	0.7141	0.5169	0.8071	0.7714	0.2105	-0.2105	0
							-0.4035 $\pm j$ 0.7801	-0.3571 $\pm j$ 0.6241
70	68.28	0.7252	0.5162	0.8182	0.7740	0.2095	-0.2095	0
							-0.4091 $\pm j$ 0.7789	-0.3626 $\pm j$ 0.6202
90	68.28	0.7251	0.5162	0.8181	0.7740	0.2095	-0.2095	0
							-0.4091 $\pm j$ 0.7789	-0.3625 $\pm j$ 0.6203
110	68.28	0.7272	0.5161	0.8202	0.7745	0.2093	-0.2093	0
							-0.4101 $\pm j$ 0.7787	-0.3636 $\pm j$ 0.6196
130	68.26	0.7413	0.5151	0.8344	0.7780	0.2080	-0.208	0
							-0.4172 $\pm j$ 0.7771	-0.3707 $\pm j$ 0.6146
150	56.91	1.7735	0.3327	1.0850	0.1082	0.9657	sub-optimal	

Table A.27: Results derived by optimising the 6dB-point of the third order filter ($A_s \rightarrow \infty$) for different starting points.

START f_{3dB} (mHz)	f_{6dB} (mHz)	a_1 (rad/s)	a_0 ((rad/s)^2)	b_1 (rad/s)	b_0 ((rad/s)^2)	p_0 (rad/s)	p (rad/s)	z (rad/s)
Butterworth								
10	43.71	1.7014	0.2922	0.9758	0.0904	1.0151	sub-optimal	
30	44.75	1.2699	0.3427	1.4336	0.7594	0.1418	-0.1418 -0.7168 $\pm j$ 0.4956	0 -0.8809 -0.3890
50	43.64	1.6371	0.2536	0.8885	0.0759	1.0495	sub-optimal	
70	43.66	1.7198	0.2970	1.1552	0.1095	0.8521	sub-optimal	
90	42.96	1.9595	3.6982	1.7916	3.4871	0.5046	sub-optimal	
110	41.55	2.5928	4.7078	2.4394	4.4218	0.4898	sub-optimal	
130	43.69	1.7030	0.2904	1.1384	0.1068	0.8544	sub-optimal	
150	42.98	1.8670	3.2620	1.7012	3.0934	0.5013	sub-optimal	
Chebyshev (R_p = 0.5 dB)								
10	34.49	0.1318	0.0222	0.1766	0.0238	0.2938	sub-optimal	
30	43.32	1.6771	0.2332	0.7876	0.0615	1.1920	sub-optimal	
50	31.39	197.22	0.0008	0.3407	0.0000	197.13	sub-optimal	
70	not converging							
90	43.74	1.6750	0.2823	1.0841	0.1003	0.8839	sub-optimal	
110	43.71	1.6834	0.2811	1.1296	0.1043	0.8465	sub-optimal	
130	43.48	1.7534	0.2783	0.8463	0.0731	1.1964	sub-optimal	
150	not converging							
Elliptic (R_p = 0.5 dB, A_s = 40 dB)								
10	33.44	0.7345	0.0138	1.0561	0.2647	0.0164	sub-optimal	
30	34.78	13.209	5.5354	0.7930	0.1713	12.700	sub-optimal	
50	42.45	0.1076	0.0699	0.1415	0.0721	0.3047	sub-optimal	
70	44.72	1.3337	0.3305	1.5031	0.7730	0.1343	sub-optimal	
90	44.51	1.1609	0.3804	1.3072	0.7566	0.1580	sub-optimal	
110	43.48	1.6558	0.2425	0.8276	0.0674	1.1301	sub-optimal	
130	43.68	1.7046	0.2890	1.1515	0.1077	0.8430	sub-optimal	
150	43.62	1.6993	0.2744	1.2026	0.1092	0.7898	sub-optimal	

Table A.28: Results derived by maximising the frequency at which an attenuation of 1.5 dB is achieved by the the third order filter having concave magnitude characteristic outside the passband for different starting points.

START f_{3dB} (mHz)	$f_{1.5dB}$ (mHz)	a_1 (rad/s)	a_0 ((rad/s)^2)	b_1 (rad/s)	b_0 ((rad/s)^2)	p_0 (rad/s)	p (rad/s)	z (rad/s)
Butterworth								
10	116.03	2.6694	1.3379	1.5898	0.3082	1.3638	sub-optimal	
30	not converging							
50	116.03	2.6694	1.3379	1.5898	0.3082	1.3638	sub-optimal	
70	94.31	45.652	103.56	2.6958	1.0226	43.359	sub-optimal	
90	not converging							
110	not converging							
130	135.49	1.5335	1.3650	1.5753	1.6975	0.2526	-0.2526 -0.7877 $\pm j$ 1.0378	0 -0.7668 $\pm j$ 0.8815
150	135.49	1.5364	1.3704	1.5778	1.7033	0.2527	-0.2527 -0.7889 $\pm j$ 1.0397	0 -0.7682 $\pm j$ 0.8833
Chebyshev (R_p = 0.5 dB)								
10	not converging							
30	135.49	1.5371	1.3735	1.5787	1.7058	0.2530	-0.2530 -0.7893 $\pm j$ 1.0406	0 -0.7685 $\pm j$ 0.8848
50	135.49	1.5373	1.3723	1.5786	1.7053	0.2528	-0.2528 -0.7893 $\pm j$ 1.0403	0 -0.7687 $\pm j$ 0.8840
70	135.49	1.5343	1.3667	1.5761	1.6992	0.2527	-0.2527 -0.7880 $\pm j$ 1.0384	0 -0.7672 $\pm j$ 0.8821
90	135.49	1.5383	1.3743	1.5795	1.7074	0.2529	-0.2529 -0.7897 $\pm j$ 1.0410	0 -0.7692 $\pm j$ 0.8847
110	135.49	1.5373	1.3724	1.5786	1.7053	0.2528	-0.2528 -0.7893 $\pm j$ 1.0404	0 -0.7686 $\pm j$ 0.8841
130	135.49	1.5369	1.3714	1.5783	1.7044	0.2528	-0.2528 -0.7891 $\pm j$ 1.0400	0 -0.7685 $\pm j$ 0.8837
150	135.49	1.5349	1.3681	1.5766	1.7006	0.2527	-0.2527 -0.7883 $\pm j$ 1.0388	0 -0.7675 $\pm j$ 0.8827
Elliptic (R_p = 0.5 dB, A_s = 40 dB)								
10	not converging							
30	135.49	1.5364	1.3705	1.5778	1.7034	0.2528	-0.2528 -0.7889 $\pm j$ 1.0397	0 -0.7682 $\pm j$ 0.8834
50	135.49	1.5355	1.3690	1.5771	1.7017	0.2527	**-0.2527** **-0.7885 $\pm j$ 1.0392**	**0** **-0.7678 $\pm j$ 0.8829**
70	not converging							
90	not converging							
110	135.49	1.5358	1.3692	1.5773	1.7021	0.2527	-0.2527 -0.7886 $\pm j$ 1.0393	0 -0.7679 $\pm j$ 0.8829
130	not converging							
150	135.49	1.5339	1.3660	1.5757	1.6984	0.2527	-0.2527 -0.7879 $\pm j$ 1.0381	0 -0.7670 $\pm j$ 0.8819

Table A.29: Results derived by maximising the frequency at which an attenuation of 4.5 dB is achieved by the the third order filter having concave magnitude characteristic outside the passband for different starting points.

START f_{3dB} (mHz)	$f_{4.5dB}$ (mHz)	a_1 (rad/s)	a_0 ((rad/s)^2)	b_1 (rad/s)	b_0 ((rad/s)^2)	p_0 (rad/s)	p (rad/s)	z (rad/s)
Butterworth								
10	not converging							
30	64.93	1.0209	0.4474	1.1386	0.7831	0.1795	-0.1795	0
							-0.5693 $\pm j$ 0.6775	-0.5104 $\pm j$ 0.4323
50	64.86	0.9996	0.4331	1.1233	0.7581	0.1795	sub-optimal	
70	62.56	0.9366	0.4148	1.0652	0.6908	0.1915	sub-optimal	
90	64.93	1.0208	0.4473	1.1385	0.7829	0.1795	-0.1795	0
							-0.5692 $\pm j$ 0.6774	-0.5104 $\pm j$ 0.4322
110	64.93	1.0208	0.4474	1.1385	0.7830	0.1795	-0.1795	0
							-0.5693 $\pm j$ 0.6774	-0.5104 $\pm j$ 0.4323
130	45.79	0.5443	0.1434	0.6556	0.1988	0.2267	sub-optimal	
150	62.78	1.2207	0.4915	1.3176	0.8938	0.1727	sub-optimal	
Chebyshev (R_p = 0.5 dB)								
10	46.10	5.6233	2.4494	0.8683	0.1998	5.0344	sub-optimal	
30	54.56	1.4039	2.0574	1.2588	2.0223	0.4789	sub-optimal	
50	64.81	1.0223	0.4450	1.1413	0.7799	0.1793	sub-optimal	
70	64.93	1.0221	0.4483	1.1394	0.7845	0.1795	-0.1795	0
							-0.5697 $\pm j$ 0.6782	-0.5111 $\pm j$ 0.4325
90	64.92	1.0275	0.4521	1.1432	0.7909	0.1796	sub-optimal	
110	64.93	1.0217	0.4480	1.1392	0.7841	0.1795	**-0.1795**	**0**
							-0.5696 $\pm j$ 0.6780	**-0.5109 $\pm j$ 0.4324**
130	64.93	1.0219	0.4481	1.1393	0.7842	0.1795	-0.1795	0
							-0.5697 $\pm j$ 0.6780	-0.5110 $\pm j$ 0.4325
150	54.79	0.9613	0.9070	0.9094	1.0524	0.3650	sub-optimal	
Elliptic (R_p = 0.5 dB, A_s = 40 dB)								
10	43.40	0.6106	0.0439	0.8830	0.2098	0.0658	sub-optimal	
30	64.93	1.0221	0.4483	1.1394	0.7845	0.1795	-0.1795	0
							-0.5697 $\pm j$ 0.6782	-0.5110 $\pm j$ 0.4325
50	64.89	1.0370	0.4576	1.1502	0.8005	0.1796	sub-optimal	
70	64.93	1.0225	0.4486	1.1397	0.7850	0.1795	-0.1795	0
							-0.5699 $\pm j$ 0.6784	-0.5113 $\pm j$ 0.4326
90	64.90	1.0214	0.4478	1.1389	0.7834	0.1797	sub-optimal	
110	64.93	1.0220	0.4482	1.1394	0.7844	0.1795	-0.1795	0
							-0.5697 $\pm j$ 0.6781	-0.5110 $\pm j$ 0.4325
130	43.97	16.0903	11.3376	15.6926	6.5520	0.6655	sub-optimal	
150	56.91	1.7641	0.3277	1.0661	0.1054	0.9767	sub-optimal	

Table A.30: Results derived by optimising the 6dB-point of the third order filter having concave magnitude characteristic outside the passband for different starting points.

START f_{3dB} (mHz)	f_{6dB} (mHz)	a_1 (rad/s)	a_0 ((rad/s)^2)	b_1 (rad/s)	b_0 ((rad/s)^2)	p_0 (rad/s)	p (rad/s)	z (rad/s)
Butterworth								
10	not converging							
30	43.04	1.6576	0.2091	1.3041	0.0993	0.6616	sub-optimal	
50	42.92	1.9961	3.6427	1.8283	3.4356	0.5040	sub-optimal	
70	43.12	1.6598	2.6953	1.4987	2.5864	0.4957	sub-optimal	
90	43.39	1.0196	0.4278	1.1455	0.7589	0.1771	sub-optimal	
110	41.17	3.7559	7.9436	3.6054	7.3922	0.4908	sub-optimal	
130	43.12	1.7222	2.8744	1.5588	2.7460	0.4984	sub-optimal	
150	43.11	1.7214	2.8767	1.5581	2.7482	0.4983	sub-optimal	
Chebyshev (R_p = 0.5 dB)								
10	31.96	0.1191	0.0048	0.4165	0.0366	0.0412	sub-optimal	
30	44.75	1.2757	0.3531	1.4346	0.7722	0.1437	-0.1437 -0.7173 $\pm j$ 0.5076	0 -0.8697 -0.4060
50	35.88	5.2347	0.0012	0.4091	0.0000	5.0409	sub-optimal	
70	not converging							
90	43.93	1.7520	2.8161	1.5992	2.7964	0.4827	sub-optimal	
110	43.13	1.6975	2.8004	1.5347	2.6798	0.4976	sub-optimal	
130	43.10	1.6034	2.5353	1.4450	2.4447	0.4925	sub-optimal	
150	43.13	1.7050	2.8235	1.5414	2.7008	0.4977	sub-optimal	
Elliptic (R_p = 0.5 dB, A_s = 40 dB)								
10	33.58	0.8891	0.0138	1.2134	0.3233	0.0135	sub-optimal	
30	43.07	1.7406	2.8854	1.5774	2.7558	0.4981	sub-optimal	
50	35.91	0.9568	0.1267	1.1839	0.3626	0.1098	sub-optimal	
70	44.72	1.2387	0.3582	1.3951	0.7627	0.1476	sub-optimal	
90	44.74	1.2487	0.3419	1.4125	0.7500	0.1432	sub-optimal	
110	43.10	1.5891	2.5030	1.4315	2.4158	0.4919	sub-optimal	
130	39.70	2.2023	0.6292	0.9857	0.1578	1.4686	sub-optimal	
150	43.73	1.6832	0.2848	1.1006	0.1023	0.8746	sub-optimal	

A.3.6 Optimisation of the overall low-frequency attenuation

Table A.31: Results obtained by optimising the overall low-frequency rejection of the second order filter for different starting points.

START f_{3dB} (mHz)	Area (mHz)	a_1 (rad/s)	b_1 (rad/s)	b_0 ((rad/s)^2)	p (rad/s)	z (rad/s)
Butterworth						
10	7.35	0.1427	0.4842	0	pole-zero cancellation	
30	8.69	1.3918	1.6928	0.6660	-1.0709	0
					-0.6219	-1.3918
50	8.69	1.3917	1.6927	0.6660	-1.0708	0
					-0.6220	-1.3917
70	8.69	1.3918	1.6928	0.6660	-1.0709	0
					-0.6219	-1.3918
90	7.35	0.1427	0.4842	0	pole-zero cancellation	
110	8.69	1.3918	1.6928	0.6660	-1.0709	0
					-0.6219	-1.3918
130	8.69	1.3919	1.6929	0.6661	-1.0710	0
					-0.6219	-1.3919
150	8.69	1.3918	1.6928	0.6660	-1.0708	0
					-0.6220	-1.3918
Chebyshev (R_p = 0.5 dB)						
10	7.35	0.1427	0.4842	0	pole-zero cancellation	
30	7.35	0.1427	0.4842	0	pole-zero cancellation	
50	8.69	1.3917	1.6927	0.6660	-1.0707	0
					-0.6220	-1.3917
70	8.69	1.3918	1.6928	0.6660	-1.0709	0
					-0.6219	-1.3918
90	7.35	0.1427	0.4842	0	pole-zero cancellation	
110	8.69	1.3918	1.6928	0.6660	-1.0709	0
					-0.6219	-1.3918
130	8.69	1.3919	1.6929	0.6661	-1.0710	0
					-0.6219	-1.3919
150	8.69	1.3918	1.6928	0.6660	-1.0709	0
					-0.6219	-1.3918

Table A.32: Results obtained by optimising the overall low-frequency rejection of the third order filter ($A_s \rightarrow \infty$) for different starting points.

START f_{3dB} (mHz)	Area (mHz)	a_1 (rad/s)	a_0 ((rad/s)^2)	b_1 (rad/s)	b_0 ((rad/s)^2)	p_0 (rad/s)	p (rad/s)	z (rad/s)
Butterworth								
10	7.38	3.1733	-0.0004	3.0340	0	0.4298	pole-zero cancellation	
30	18.79	0.4338	0.5907	0.5147	0.7562	0.2454	-0.2454 -0.2573 $\pm j$ 0.8306	0 -0.2169 $\pm j$ 0.7373
50	not converging							
70	11.91	1.8199	0.3925	1.1153	0.1247	0.9890	sub-optimal	
90	3.35	128.85	4151.32	61.048	21.171	68.217	sub-optimal	
110	4.35	14.453	4.3351	0.6710	0.1098	14.022	sub-optimal	
130	8.57	16.272	33.034	16.154	30.742	0.4666	sub-optimal	
150	18.79	0.4338	0.5907	0.5147	0.7562	0.2454	-0.2454 -0.2573 $\pm j$ 0.8307	0 -0.2169 $\pm j$ 0.7373
Chebyshev (R_p = 0.5 dB)								
10	18.79	0.4338	0.5907	0.5147	0.7562	0.2454	-0.2454 -0.2573 $\pm j$ 0.8306	0 -0.2169 $\pm j$ 0.7373
30	3.54	67280	62093	67279	26047	0.8735	sub-optimal	
50	not converging							
70	2.54	368.07	1.1129	368.40	124.54	0.0037	sub-optimal	
90	not converging							
110	8.90	10.881	23.662	10.760	22.033	0.4708	sub-optimal	
130	not converging							
150	2.37	2437.9	-2.8478	2438.2	821.08	0.0011	sub-optimal	
Elliptic (R_p = 0.5 dB, A_s = 40 dB)								
10	not converging							
30	18.79	0.4339	0.5906	0.5147	0.7562	0.2454	-0.2454 -0.2574 $\pm j$ 0.8306	0 -0.2169 $\pm j$ 0.7373
50	18.79	0.4338	0.5907	0.5147	0.7562	0.2454	-0.2454 -0.2573 $\pm j$ 0.8307	0 -0.2169 $\pm j$ 0.7373
70	8.45	31.170	70.533	29.274	13.342	2.2842	sub-optimal	
90	3.10	59.549	0.5053	59.792	20.539	0.0077	sub-optimal	
110	8.44	36.243	82.192	36.179	76.674	0.4631	sub-optimal	
130	7.94	7160.4	16384	7160.4	15357	0.4529	sub-optimal	
150	18.79	0.4338	0.5907	0.5147	0.7562	0.2454	-0.2454 -0.2573 $\pm j$ 0.8306	0 -0.2169 $\pm j$ 0.7373

Table A.33: Results obtained by optimising the overall low-frequency rejection of the third order filter having concave magnitude characteristic outside the passband for different starting points.

START f_{3dB} (mHz)	Area (mHz)	a_1 (rad/s)	a_0 ((rad/s)^2)	b_1 (rad/s)	b_0 ((rad/s)^2)	p_0 (rad/s)	p (rad/s)	z (rad/s)
Butterworth								
10	15.40	1.0606	0.4767	1.1653	0.8300	0.1804	-0.1804 -0.5826 $\pm j$ 0.7004	0 -0.5303 $\pm j$ 0.4421
30	not converging							
50	6.59	6.5755	0.5777	0.4804	0.0285	6.3588	sub-optimal	
70	not converging							
90	not converging							
110	not converging							
130	8.07	151.98	338.03	151.93	316.18	0.4561	sub-optimal	
150	not converging							
Chebyshev (R_p = 0.5 dB)								
10	not converging							
30	not converging							
50	not converging							
70	5.98	18.736	25.357	17.669	7.2803	1.3870	sub-optimal	
90	11.91	1.8226	0.3926	1.1160	0.1246	0.9901	sub-optimal	
110	8.54	21.357	48.884	21.264	45.620	0.4642	sub-optimal	
130	15.40	1.0604	0.4766	1.1652	0.8299	0.1804	-0.1804 -0.5826 $\pm j$ 0.7003	0 -0.5302 $\pm j$ 0.4421
150	8.29	9.3874	15.661	2.4734	0.9299	7.2490	sub-optimal	
Elliptic (R_p = 0.5 dB, A_s = 40 dB)								
10	not converging							
30	11.91	1.8205	0.3928	1.1155	0.1247	0.9894	sub-optimal	
50	15.40	1.0607	0.4768	1.1654	0.8302	0.1804	**-0.1804** **-0.5827 $\pm j$ 0.7005**	**0** **-0.5303 $\pm j$ 0.4422**
70	13.46	1.1129	0.4532	1.2232	0.7604	0.1983	sub-optimal	
90	15.29	1.1273	0.5529	1.2134	0.9167	0.1895	sub-optimal	
110	8.54	20.413	47.766	18.280	8.2626	2.5038	sub-optimal	
130	15.40	1.0613	0.4773	1.1658	0.8310	0.1804	-0.1804 -0.5829 $\pm j$ 0.7008	0 -0.5307 $\pm j$ 0.4423
150	15.40	1.0610	0.4770	1.1656	0.8306	0.1804	-0.1804 -0.5828 $\pm j$ 0.7007	0 -0.5305 $\pm j$ 0.4423

Appendix B

B.1 Synthetic ECG waveforms

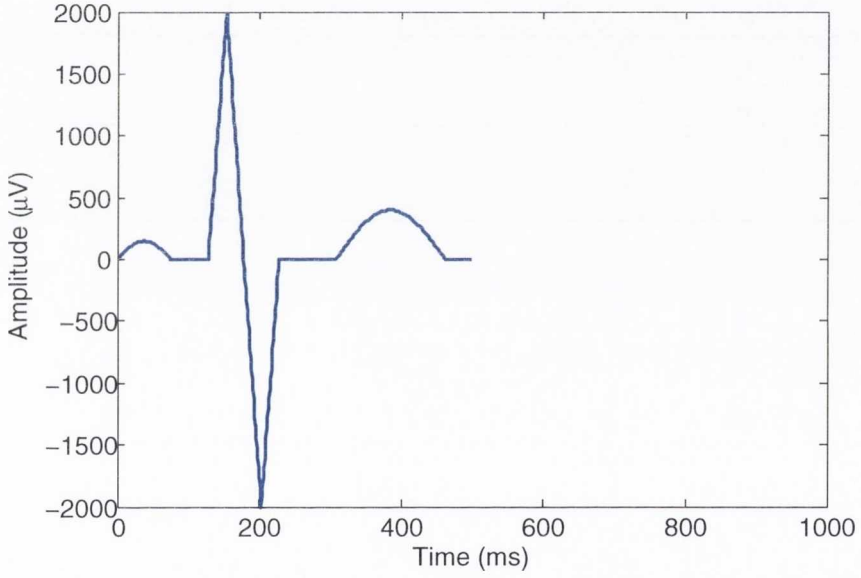
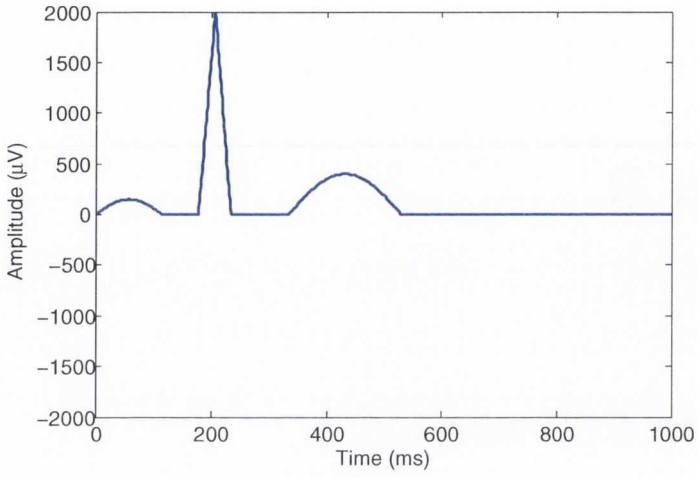
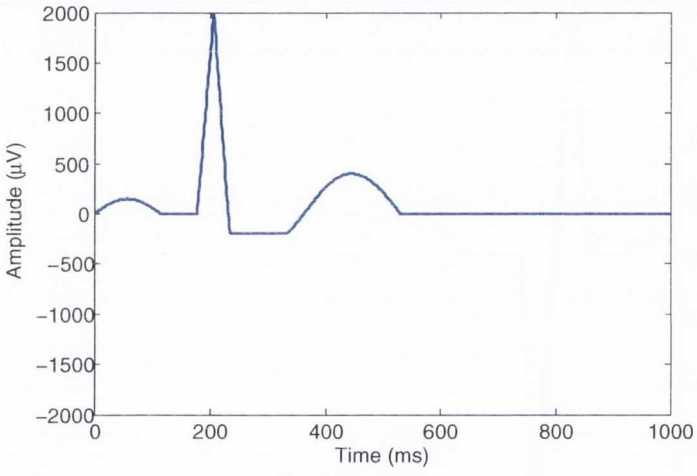


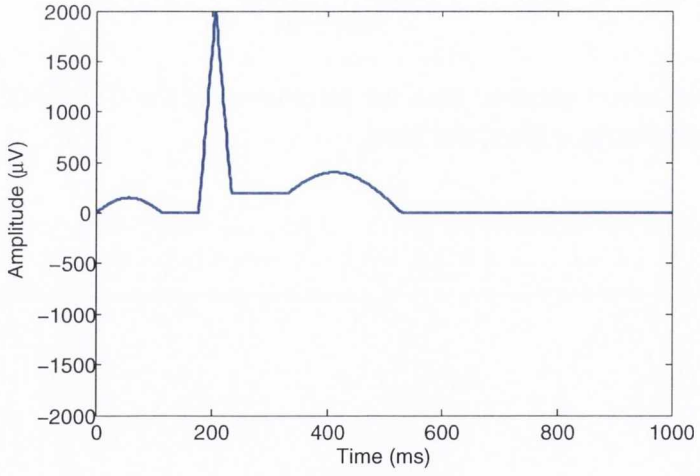
Figure B.1: Test waveform obtained from the parameters of the CAL20002 signal when the QRS complex is modelled by a triangular wave.



(a) CAL20100



(b) CAL20110



(c) CAL20160

Figure B.2: Test waveforms obtained from the parameters of the CAL20100, CAL20110 and CAL20160 signals when the QRS complex is modelled by a triangular wave.

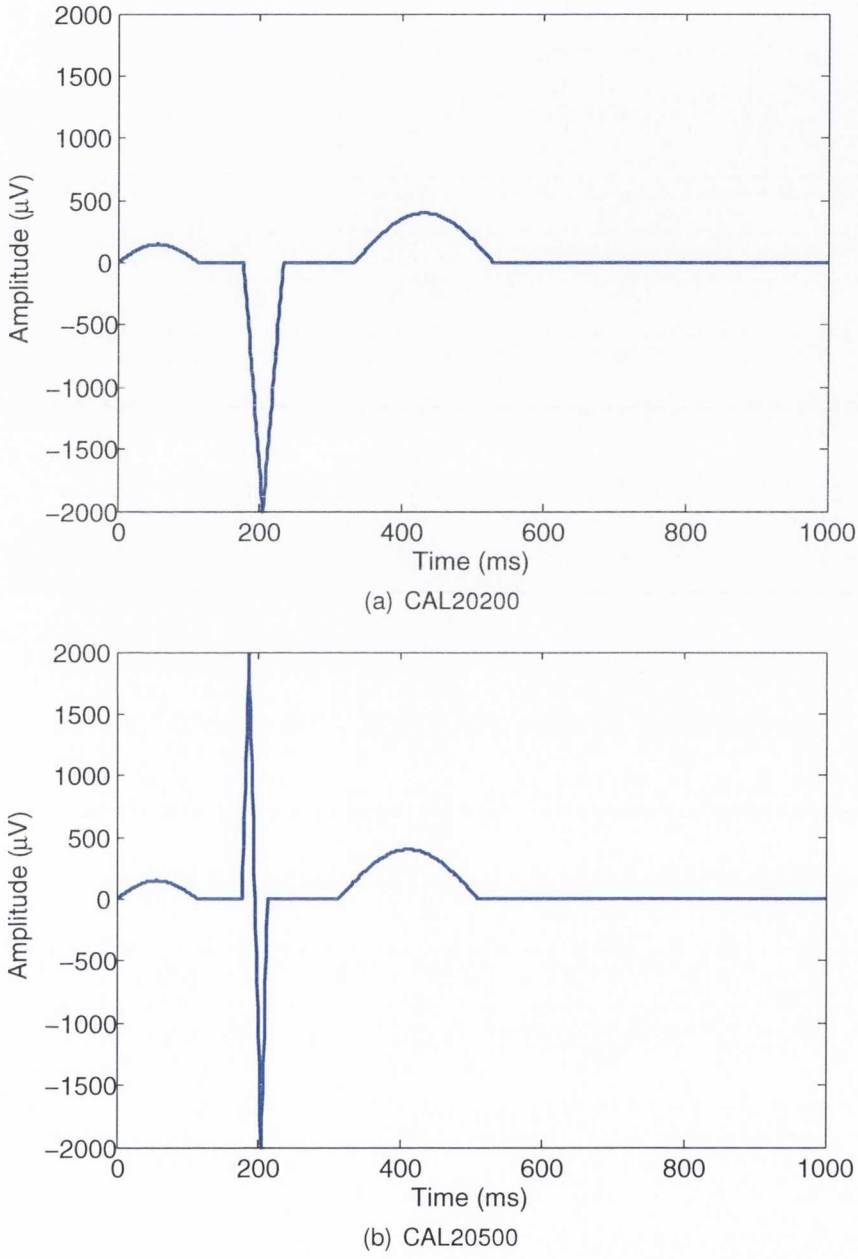


Figure B.3: Test waveforms obtained from the parameters of the CAL20200 and CAL20500 signals when the QRS complex is modelled by a triangular wave.

B.2 Power spectrum of the bw record

The power contained in the bw record of the MIT-BIH Noise Stress Test database [176] at frequencies lower than 0.5 Hz is calculated through the periodogram and the Bartlet and Welch methods [177]. When calculating the power spectral density using the Bartlet method, two different lengths are employed for the segments in which the bw record is divided, $N/10$ and $N/20$, where N is the total length of the recorded signal. When employing the Welch method, the length of the window is fixed to $N/10$, but three different shapes are selected for it, rectangular, triangular and Hamming, which is the MATLAB® default [186] and was used for electrocardiographic signals by Clifford [51]. An overlap of 50% between segments, which is the MATLAB® default employed by Clifford, is selected.

Table B.1: Power content of the bw record at frequencies lower than 0.5 Hz measured using different techniques.

	Periodogram	Bartlett		Welch ($N/10$, 50% overlap)		
		$N/10$	$N/20$	Rectang.	Triang.	Hamming
		Lead A				
power (10^{-9} V^2)	213.7	213.6	213.0	211.0	196.7	197.7
% diff. with periodogram		-0.0	-0.3	-1.3	-7.9	-7.5
		Lead B				
power (10^{-9} V^2)	30.0	30.0	29.9	29.4	29.6	29.5
% diff. with periodogram		-0.1	-0.2	-2.0	-1.4	-1.7

B.3 Error introduced by the highpass filters into selected records of the QT database

The average and maximum absolute errors and the percentage of samples for which the deviation of the output signal from the input one is larger than 25 μV or 5%, which is the limit specified by the 1990 AHA recommendations [19], are calculated for each channel of 42 selected records of the QT database. Since the recordings are not performed on the same two leads for all of the QT records, average results for each lead are not calculated. The results of the two leads are instead averaged to obtain an overall figure for each record.

Table B.2: Error introduced when the reference 0.05 Hz single-pole system is applied to selected records of the QT database.

	Lead A			Lead B			Average leads		
Record	avg (μV)	max (μV)	% exc. limit	avg (μV)	max (μV)	% exc. limit	avg (μV)	max (μV)	% exc. limit
sel14172	7.4	31.1	0.4	8.0	47.2	1.5	7.7	39.2	1.0
sel16539	5.1	33.4	0.1	3.1	12.8	0	4.1	23.1	0.0
sel16786	6.4	26.7	0.0	3.8	15.4	0	5.1	21.1	0.0
sel16795	6.0	20.9	0	6.3	21.8	0	6.1	21.4	0
sel17152	4.4	20.8	0	4.1	19.1	0	4.2	19.9	0
sel17453	4.7	24.6	0	3.3	11.2	0	4.0	17.9	0
sel223	7.8	88.1	1.9	6.1	37.1	0.7	7.0	62.6	1.3
sel301	4.4	29.8	0.0	6.8	73.1	2.1	5.6	51.5	1.0
sel30	4.5	41.7	0.6	5.3	43.7	1.3	4.9	42.7	0.9
sel31	5.7	50.4	3.5	6.7	47.1	1.2	6.2	48.8	2.3
sel32	6.2	119.8	3.3	5.4	168.4	1.5	5.8	144.1	2.4
sel33	8.2	44.6	2.4	7.2	35.2	0.6	7.7	39.9	1.5
sel34	11.4	107.0	6.9	4.5	38.7	0.3	8.0	72.8	3.6
sel38	8.3	36.8	0.7	5.0	23.7	0	6.6	30.2	0.4
sel39*	22.7	279.8	29.6	22.7	168.1	33.8	22.7	224.0	31.7
sel40	7.0	45.4	0.7	7.4	59.8	1.9	7.2	52.6	1.3
sel41	3.8	29.1	0.0	6.0	36.6	0.5	4.9	32.8	0.3
sel42*	29.9	133.2	37.8	17.9	137.7	20.1	23.9	135.4	29.0
sel43	5.1	26.3	0.0	7.3	52.4	1.6	6.2	39.4	0.8
sel44	6.9	42.4	0.8	9.8	59.1	4.3	8.4	50.7	2.5
sel45	10.2	91.8	7.5	4.8	39.9	0.6	7.5	65.8	4.0
sel46	5.2	46.1	0.4	7.1	68.5	2.8	6.2	57.3	1.6
sel47*	40.3	346.3	56.2	25.2	246.2	39.0	32.8	296.3	47.6
sel48	4.9	63.9	0.4	4.5	62.0	0.9	4.7	62.9	0.7
sel49	6.9	117.8	3.5	5.3	33.8	0.4	6.1	75.8	2.0
sel50	7.2	103.4	2.2	9.5	134.1	5.6	8.3	118.7	3.9
sel51	1.7	17.5	0	2.2	27.0	0.0	2.0	22.3	0.0
sel52	5.2	101.4	3.0	3.8	74.2	1.0	4.5	87.8	2.0
sel821	3.2	18.6	0	3.6	13.2	0	3.4	15.9	0
sel840	3.4	30.9	0.1	3.2	39.9	0.3	3.3	35.4	0.2
sele0106	3.1	42.4	0.2	4.1	36.4	0.1	3.6	39.4	0.1
sele0114	3.4	30.3	0.0	5.3	25.8	0.0	4.4	28.0	0.0
sele0116	5.6	24.9	0	6.8	29.3	0.3	6.2	27.1	0.1
sele0124	3.1	19.0	0	3.2	21.9	0	3.2	20.5	0
sele0136	4.6	21.0	0	3.6	17.4	0	4.1	19.2	0
sele0166*	9.3	56.1	4.0	24.0	107.5	39.9	16.7	81.8	21.9
sele0210	3.3	19.7	0	3.5	24.4	0	3.4	22.0	0
sele0211	3.3	19.6	0	4.5	43.9	0.3	3.9	31.8	0.1
sele0303	2.0	22.1	0	3.9	29.1	0.0	2.9	25.6	0.0
sele0409	9.3	52.2	2.3	9.5	50.5	4.9	9.4	51.4	3.6
sele0609	4.3	34.2	0.0	6.9	39.4	0.6	5.6	36.8	0.3
sele0612	9.8	44.2	2.2	9.7	77.3	4.2	9.7	60.8	3.2
Average							7.3	58.4	4.1
Average excl. *							5.6	45.1	1.1

Table B.3: Error introduced when the second order filter characterised by real poles is applied to selected records of the QT database.

Record	Lead A			Lead B			Average leads		
	avg (μV)	max (μV)	% exc. limit	avg (μV)	max (μV)	% exc. limit	avg (μV)	max (μV)	% exc. limit
sel14172	9.2	37.5	2.0	9.7	56.3	4.5	9.5	46.9	3.2
sel16539	6.3	41.1	0.2	3.6	14.8	0	4.9	27.9	0.1
sel16786	6.7	30.3	0.0	4.4	17.6	0	5.6	23.9	0.0
sel16795	6.4	22.8	0	6.9	24.6	0	6.6	23.7	0
sel17152	5.8	25.9	0.0	4.5	22.4	0	5.2	24.1	0.0
sel17453	5.8	28.6	0.0	3.6	12.5	0	4.7	20.5	0.0
sel223	8.6	112.2	2.7	6.8	39.6	1.2	7.7	75.9	2.0
sel301	4.6	31.4	0.0	8.4	83.5	3.9	6.5	57.4	1.9
sel30	5.8	53.6	1.7	6.9	55.9	2.9	6.3	54.7	2.3
sel31	7.4	68.4	5.6	7.8	60.0	2.6	7.6	64.2	4.1
sel32	7.9	153.6	4.7	7.0	213.0	2.3	7.5	183.3	3.5
sel33	10.0	59.2	5.5	8.7	41.7	2.3	9.3	50.5	3.9
sel34	14.7	139.7	13.9	6.0	50.4	1.3	10.4	95.1	7.6
sel38	9.5	44.6	2.5	6.3	30.6	0.1	7.9	37.6	1.3
sel39*	30.2	389.0	40.7	29.8	232.9	46.1	30.0	310.9	43.4
sel40	7.7	54.7	1.6	8.7	75.7	3.8	8.2	65.2	2.7
sel41	4.7	35.5	0.1	7.5	45.1	2.0	6.1	40.3	1.0
sel42*	30.0	144.9	36.8	21.3	175.6	26.5	25.7	160.3	31.7
sel43	6.6	33.4	0.6	9.5	70.0	5.0	8.1	51.7	2.8
sel44	8.1	52.1	1.8	11.7	66.6	8.2	9.9	59.3	5.0
sel45	13.8	127.3	14.4	6.4	53.8	1.8	10.1	90.5	8.1
sel46	6.5	53.1	1.6	8.7	76.4	5.1	7.6	64.8	3.3
sel47*	52.5	459.6	64.9	33.6	327.3	51.6	43.1	393.5	58.2
sel48	5.7	78.7	0.6	5.8	82.7	1.6	5.8	80.7	1.1
sel49	8.7	143.2	6.5	6.8	45.1	1.8	7.8	94.1	4.2
sel50	8.4	126.1	3.9	11.4	165.9	9.2	9.9	146.0	6.6
sel51	2.0	20.8	0	2.7	35.5	0.2	2.3	28.1	0.1
sel52	6.5	127.4	4.7	5.0	92.6	1.5	5.7	110.0	3.1
sel821	3.9	22.5	0	3.8	14.8	0	3.9	18.7	0
sel840	4.2	37.5	0.3	4.0	47.3	0.5	4.1	42.4	0.4
sele0106	3.6	55.8	0.4	4.7	42.1	0.1	4.1	49.0	0.3
sele0114	3.8	36.9	0.1	5.7	30.5	0.0	4.8	33.7	0.1
sele0116	6.6	31.4	0.1	8.0	36.1	1.1	7.3	33.8	0.6
sele0124	3.5	24.3	0	4.2	29.3	0.1	3.8	26.8	0.0
sele0136	5.8	26.6	0	3.9	18.9	0	4.8	22.8	0
sele0166*	12.0	75.2	10.0	31.3	132.6	52.2	21.6	103.9	31.1
sele0210	4.1	25.0	0	4.5	32.2	0.1	4.3	28.6	0.1
sele0211	4.0	24.4	0	5.8	59.6	0.5	4.9	42.0	0.3
sele0303	2.2	21.9	0	4.0	31.4	0.0	3.1	26.7	0.0
sele0409	10.3	63.5	4.6	12.0	63.6	10.5	11.1	63.5	7.6
sele0609	4.8	34.6	0.1	8.3	49.5	2.1	6.5	42.0	1.1
sele0612	12.0	53.6	7.1	12.4	98.2	9.4	12.2	75.9	8.3
Average							9.0	73.6	6.0
Average excl. *							6.7	55.9	2.3

Table B.4: Error introduced when the second order filter is applied to selected records of the QT database.

Record	Lead A			Lead B			Average leads		
	avg (μV)	max (μV)	% exc. limit	avg (μV)	max (μV)	% exc. limit	avg (μV)	max (μV)	% exc. limit
sel14172	9.2	37.6	2.0	9.7	55.1	4.5	9.4	46.3	3.3
sel16539	6.4	40.7	0.2	3.5	14.6	0	4.9	27.7	0.1
sel16786	6.4	30.0	0.0	4.4	17.2	0	5.4	23.6	0.0
sel16795	6.2	22.2	0	6.6	24.4	0	6.4	23.3	0
sel17152	6.1	25.6	0.0	4.5	22.4	0	5.3	24.0	0.0
sel17453	5.9	28.4	0.0	3.5	12.3	0	4.7	20.4	0.0
sel223	8.3	113.0	2.5	6.6	39.5	0.9	7.5	76.3	1.7
sel301	4.4	30.0	0.0	8.5	78.2	4.0	6.5	54.1	2.0
sel30	5.9	52.9	1.9	7.0	55.4	3.0	6.4	54.2	2.5
sel31	7.7	72.9	6.3	7.8	62.8	2.9	7.8	67.9	4.6
sel32	8.0	156.4	4.8	7.1	209.2	2.4	7.6	182.8	3.6
sel33	10.0	63.3	6.0	8.7	40.4	2.2	9.3	51.9	4.1
sel34	14.7	140.7	13.9	6.1	51.5	1.4	10.4	96.1	7.7
sel38	9.2	44.0	2.1	6.4	30.7	0.1	7.8	37.3	1.1
sel39*	31.2	412.8	41.0	30.4	244.9	46.4	30.8	328.8	43.7
sel40	7.6	55.7	1.6	8.7	76.5	4.1	8.1	66.1	2.9
sel41	4.8	35.3	0.2	7.6	47.1	2.1	6.2	41.2	1.2
sel42*	28.6	142.7	34.3	21.2	174.4	26.2	24.9	158.6	30.2
sel43	6.7	34.1	0.7	9.7	70.8	5.5	8.2	52.5	3.1
sel44	7.9	51.4	1.6	11.4	64.1	7.6	9.6	57.8	4.6
sel45	14.3	131.9	15.2	6.6	56.2	2.1	10.4	94.1	8.6
sel46	6.5	53.8	2.0	8.7	72.6	5.2	7.6	63.2	3.6
sel47*	53.3	476.0	64.8	34.3	339.6	52.1	43.8	407.8	58.4
sel48	5.7	78.5	0.6	5.9	82.7	1.7	5.8	80.6	1.2
sel49	9.0	144.9	7.1	6.9	48.0	2.1	7.9	96.4	4.6
sel50	8.2	126.6	3.6	11.2	167.4	9.0	9.7	147.0	6.3
sel51	1.9	20.7	0	2.6	35.7	0.2	2.3	28.2	0.1
sel52	6.5	125.9	4.7	5.0	90.1	1.5	5.8	108.0	3.1
sel821	3.9	22.5	0	3.7	14.6	0	3.8	18.5	0
sel840	4.2	37.4	0.3	4.0	46.4	0.5	4.1	41.9	0.4
sele0106	3.5	56.3	0.5	4.5	41.3	0.1	4.0	48.8	0.3
sele0114	3.8	36.6	0.1	5.5	29.4	0.0	4.6	33.0	0.1
sele0116	6.5	31.6	0.1	7.9	36.2	1.1	7.2	33.9	0.6
sele0124	3.4	24.5	0	4.3	30.4	0.1	3.8	27.5	0.1
sele0136	5.8	26.8	0.0	3.8	18.4	0	4.8	22.6	0.0
sele0166*	12.1	77.4	10.2	31.4	128.7	52.6	21.8	103.1	31.4
sele0210	4.1	25.9	0.0	4.6	32.8	0.1	4.3	29.3	0.1
sele0211	4.1	25.0	0	5.9	60.1	0.7	5.0	42.5	0.3
sele0303	2.1	20.8	0	3.8	31.6	0.0	3.0	26.2	0.0
sele0409	10.1	62.8	4.5	12.1	65.6	10.8	11.1	64.2	7.7
sele0609	4.6	32.5	0.1	8.2	49.3	2.1	6.4	40.9	1.1
sele0612	11.7	52.3	6.5	12.5	101.2	9.2	12.1	76.7	7.8
Average							9.0	74.4	6.0
Average excl. *							6.7	56.0	2.3

Table B.5: Error introduced when the third order filter is applied to selected records of the QT database.

Record	Lead A			Lead B			Average leads		
	avg (μV)	max (μV)	% exc. limit	avg (μV)	max (μV)	% exc. limit	avg (μV)	max (μV)	% exc. limit
sel14172	10.5	43.1	4.4	11.0	63.4	7.5	10.8	53.2	5.9
sel16539	7.1	45.2	0.5	3.8	15.6	0	5.4	30.4	0.2
sel16786	7.1	29.7	0.1	4.7	19.2	0	5.9	24.5	0.0
sel16795	6.8	25.6	0.0	7.4	27.0	0.1	7.1	26.3	0.0
sel17152	6.4	28.0	0.0	4.9	24.0	0	5.7	26.0	0.0
sel17453	6.3	29.2	0.0	3.8	13.4	0	5.1	21.3	0.0
sel223	9.2	128.5	3.5	7.2	43.0	1.5	8.2	85.8	2.5
sel301	5.0	33.1	0.0	9.6	91.2	6.0	7.3	62.2	3.0
sel30	6.5	58.8	2.6	8.0	63.0	3.9	7.3	60.9	3.3
sel31	7.7	66.1	6.5	8.6	62.1	3.5	8.1	64.1	5.0
sel32	9.4	159.5	6.2	8.1	234.3	2.7	8.7	196.9	4.5
sel33	10.7	57.3	7.6	9.5	44.3	4.1	10.1	50.8	5.8
sel34	16.7	150.2	18.8	7.1	54.2	2.1	11.9	102.2	10.5
sel38	10.1	50.8	3.8	7.2	35.3	0.3	8.6	43.0	2.1
sel39*	32.3	401.4	45.0	33.5	237.1	49.9	32.9	319.2	47.4
sel40	8.5	56.1	2.2	9.7	87.4	5.0	9.1	71.8	3.6
sel41	5.1	39.0	0.2	8.5	49.6	3.8	6.8	44.3	2.0
sel42*	32.0	159.6	39.6	24.4	195.9	31.6	28.2	177.8	35.6
sel43	7.5	35.7	1.4	10.9	85.7	8.1	9.2	60.7	4.7
sel44	8.5	58.4	2.3	12.3	71.3	9.8	10.4	64.9	6.0
sel45	15.9	145.2	19.4	7.4	58.0	2.6	11.6	101.6	11.0
sel46	7.4	51.9	2.2	9.8	94.7	6.5	8.6	73.3	4.3
sel47*	59.9	478.0	68.3	39.2	343.2	56.9	49.6	410.6	62.6
sel48	6.4	85.0	0.9	6.7	94.6	2.3	6.5	89.8	1.6
sel49	9.1	154.6	6.6	7.6	45.7	2.4	8.3	100.1	4.5
sel50	9.3	129.5	5.2	12.8	170.3	11.4	11.0	149.9	8.3
sel51	2.1	22.3	0	3.0	41.5	0.3	2.6	31.9	0.1
sel52	7.6	140.4	5.8	5.8	99.0	2.1	6.7	119.7	4.0
sel821	4.3	24.5	0	4.1	16.6	0	4.2	20.6	0
sel840	4.6	39.4	0.3	4.4	49.8	0.6	4.5	44.6	0.5
sele0106	3.9	62.1	0.7	4.9	40.2	0.2	4.4	51.2	0.4
sele0114	4.1	42.4	0.2	6.1	32.1	0.1	5.1	37.3	0.1
sele0116	7.2	36.2	0.3	8.7	38.1	2.2	8.0	37.1	1.3
sele0124	3.8	27.3	0.0	4.9	31.7	0.2	4.4	29.5	0.1
sele0136	6.4	31.0	0.1	4.2	21.4	0	5.3	26.2	0.0
sele0166*	13.7	85.6	14.7	35.5	156.9	57.4	24.6	121.2	36.1
sele0210	4.7	29.7	0.2	5.2	37.0	0.4	4.9	33.3	0.3
sele0211	4.6	27.3	0.0	6.6	66.6	1.3	5.6	46.9	0.7
sele0303	2.4	22.7	0	4.3	34.4	0.0	3.3	28.6	0.0
sele0409	11.5	74.8	7.1	14.0	73.3	14.6	12.7	74.0	10.9
sele0609	5.2	35.4	0.1	9.3	53.6	3.7	7.3	44.5	1.9
sele0612	12.5	56.9	9.6	14.2	106.2	13.5	13.4	81.6	11.6
Average							10.0	79.5	7.2
Average excl. *							7.5	60.8	3.2

Table B.6: Error introduced when the third order concave filter is applied to selected records of the QT database.

Record	Lead A			Lead B			Average leads		
	avg (μV)	max (μV)	% exc. limit	avg (μV)	max (μV)	% exc. limit	avg (μV)	max (μV)	% exc. limit
sel14172	9.9	39.8	2.9	10.3	59.2	5.9	10.1	49.5	4.4
sel16539	6.7	42.8	0.3	3.6	14.9	0	5.1	28.8	0.2
sel16786	6.4	29.0	0.0	4.6	17.7	0	5.5	23.4	0.0
sel16795	6.2	22.9	0	6.8	25.1	0.0	6.5	24.0	0.0
sel17152	6.3	27.3	0.0	4.6	22.8	0	5.4	25.1	0.0
sel17453	6.1	28.7	0.0	3.6	12.4	0	4.8	20.6	0.0
sel223	8.5	121.5	2.6	6.8	41.1	1.1	7.7	81.3	1.9
sel301	4.5	30.0	0.0	9.0	84.0	4.9	6.7	57.0	2.4
sel30	6.2	56.8	2.3	7.4	59.5	3.4	6.8	58.1	2.9
sel31	7.6	69.7	6.3	7.9	59.9	3.0	7.8	64.8	4.6
sel32	8.6	157.6	5.3	7.6	226.9	2.6	8.1	192.2	4.0
sel33	10.2	58.9	6.4	9.1	42.7	3.1	9.7	50.8	4.7
sel34	16.0	147.6	17.0	6.7	53.6	1.7	11.3	100.6	9.4
sel38	9.6	46.9	2.8	6.8	33.1	0.2	8.2	40.0	1.5
sel39*	31.9	407.6	42.9	32.1	245.2	48.6	32.0	326.4	45.8
sel40	7.7	54.1	1.8	9.0	81.6	4.5	8.4	67.9	3.1
sel41	4.9	36.6	0.2	7.9	46.7	2.8	6.4	41.7	1.5
sel42*	28.3	146.9	33.5	22.4	186.7	27.7	25.4	166.8	30.6
sel43	7.1	33.7	1.0	10.3	78.9	6.8	8.7	56.3	3.9
sel44	8.2	55.5	1.9	11.9	65.9	8.8	10.1	60.7	5.3
sel45	15.0	140.6	17.1	6.9	56.8	2.3	11.0	98.7	9.7
sel46	6.9	50.9	1.9	9.2	81.2	5.8	8.0	66.1	3.8
sel47*	56.6	478.1	67.1	36.7	341.5	54.8	46.6	409.8	61.0
sel48	5.9	80.9	0.7	6.2	90.3	2.1	6.1	85.6	1.4
sel49	9.0	156.2	6.9	7.2	46.2	2.3	8.1	101.2	4.6
sel50	8.6	127.1	4.2	11.9	168.0	9.9	10.3	147.5	7.1
sel51	2.0	21.2	0	2.7	38.7	0.2	2.4	29.9	0.1
sel52	7.0	133.3	5.3	5.4	96.8	1.9	6.2	115.0	3.6
sel821	4.1	23.5	0	3.8	14.9	0	3.9	19.2	0
sel840	4.4	38.4	0.3	4.2	48.4	0.5	4.3	43.4	0.4
sele0106	3.7	59.8	0.6	4.7	40.4	0.2	4.2	50.1	0.4
sele0114	3.8	39.0	0.1	5.6	30.8	0.0	4.7	34.9	0.1
sele0116	6.8	33.3	0.1	8.2	37.2	1.4	7.5	35.3	0.8
sele0124	3.5	25.8	0.0	4.6	31.3	0.1	4.0	28.6	0.1
sele0136	6.2	28.5	0.1	3.8	19.2	0	5.0	23.9	0.0
sele0166*	13.0	81.2	12.6	34.1	142.8	56.3	23.6	112.0	34.4
sele0210	4.3	27.0	0.1	4.8	34.9	0.3	4.6	31.0	0.2
sele0211	4.2	25.1	0.0	6.2	64.9	0.8	5.2	45.0	0.4
sele0303	2.1	20.3	0	3.8	32.7	0.0	3.0	26.5	0.0
sele0409	10.4	67.1	5.3	12.9	67.8	12.3	11.7	67.5	8.8
sele0609	4.8	32.3	0.1	8.8	52.3	2.8	6.8	42.3	1.4
sele0612	12.4	55.0	8.6	13.5	101.3	11.6	13.0	78.1	10.1
Average							9.4	76.8	6.5
Average excl. *							7.0	58.2	2.7

B.4 Change in the ST segment slope introduced by the highpass filters into the records of the QT database

The slope of each ST segment containing 3 or more data points is evaluated before and after the application of the highpass filters. For each channel, the largest slope change is identified and the average change calculated from the absolute difference between input and output slopes. The percentages of negative slope changes and of changes that exceed the 50 μV/s limit proposed by the EN 60601-2-51:2003 European standard [9] are computed.

Table B.7: Number and length of the annotated ST segments employed in the analysis of the change in slope introduced by the highpass filters into the records of the QT database.

		length (samples)		
Record	# ST segments	avg	min	max
sel14172	50	21.6	14	28
sel16539	30	32.6	25	40
sel16786	30	23.9	13	44
sel16795	29	23.6	18	36
sel17152	30	16.5	6	24
sel17453	30	22.9	12	31
sel223	31	41.9	31	53
sel301	30	31.8	22	38
sel30	30	34.1	26	41
sel31	30	46.1	21	61
sel32	30	31.2	24	40
sel33	30	79.0	72	86
sel34	30	27.9	20	37
sel38	30	11.6	6	21
sel39	30	28.8	25	32
sel40	27	6.3	3	10
sel41	29	7.4	3	13
sel42	30	14.7	11	19
sel43	30	13.8	7	19
sel44	22	22.5	16	30
sel45	30	20.9	15	26
sel46	30	27.8	10	42
sel47	29	9.0	3	16
sel48	30	27.3	22	35
sel49	30	9.1	4	14
sel50	30	25.5	12	42
sel51	30	60.6	54	68
sel52	30	23.8	16	30
sel821	30	24.2	16	35
sel840	70	22.9	13	38
sele0106	30	34.0	26	45
sele0114	30	18.7	12	26
sele0116	30	44.5	30	56
sele0124	50	20.0	9	27
sele0136	30	42.8	36	49
sele0166	36	32.5	22	43
sele0210	30	25.1	18	32
sele0211	30	16.3	7	32
sele0303	30	39.0	32	44
sele0409	30	16.0	12	20
sele0609	30	34.2	25	41
sele0612	30	26.9	17	42
Average	31.7	27.1	18.7	35.9

Table B.8: Change in the ST segment slope produced when the reference 0.05 Hz single-pole filter is applied to the records of the QT database.

Record	Lead A				Lead B				Average leads			
	avg (μV/s)	% neg	max (μV/s)	% exc. limit	avg (μV/s)	% neg	max (μV/s)	% exc. limit	avg (μV/s)	% neg	abs(max) (μV/s)	% exc. limit
sel14172	25.7	2.0	46.9	0.0	13.8	86.0	-32.3	0.0	19.8	44.0	39.6	0.0
sel16539	19.4	3.3	40.3	0.0	19.0	100.0	-33.9	0.0	19.2	51.7	37.1	0.0
sel16786	47.4	0.0	59.3	33.3	21.6	100.0	-34.2	0.0	34.5	50.0	46.8	16.7
sel16795	7.7	96.6	-17.8	0.0	40.3	100.0	-53.6	10.3	24.0	98.3	35.7	5.2
sel17152	32.2	0.0	45.4	0.0	69.7	100.0	-86.6	100.0	51.0	50.0	66.0	50.0
sel17453	39.9	0.0	56.4	13.3	10.6	100.0	-17.7	0.0	25.2	50.0	37.1	6.7
sel223	71.4	3.2	-117.1	100.0	15.1	87.1	-44.7	0.0	43.3	45.2	80.9	50.0
sel301	101.2	0.0	111.4	100.0	91.6	0.0	111.7	100.0	96.4	0.0	111.6	100.0
sel30	21.3	0.0	33.6	0.0	22.2	3.3	47.5	0.0	21.8	1.7	40.5	0.0
sel31	25.7	3.3	64.8	6.7	35.6	100.0	-49.4	0.0	30.6	51.7	57.1	3.3
sel32	9.6	26.7	29.0	0.0	14.2	93.3	-31.1	0.0	11.9	60.0	30.1	0.0
sel33	9.8	73.3	-21.2	0.0	10.6	53.3	-29.9	0.0	10.2	63.3	25.5	0.0
sel34	34.8	20.0	110.6	16.7	8.6	36.7	-31.5	0.0	21.7	28.3	71.1	8.3
sel38	20.8	83.3	-55.0	3.3	10.3	73.3	-27.2	0.0	15.6	78.3	41.1	1.7
sel39	72.6	26.7	229.4	60.0	61.3	20.0	227.9	56.7	66.9	23.3	228.6	58.3
sel40	26.9	100.0	-65.7	3.7	24.3	100.0	-56.0	3.7	25.6	100.0	60.8	3.7
sel41	12.0	96.6	-28.8	0.0	17.8	96.6	-48.4	0.0	14.9	96.6	38.6	0.0
sel42	198.3	0.0	235.7	100.0	20.5	30.0	51.9	3.3	109.4	15.0	143.8	51.7
sel43	6.8	93.3	-15.0	0.0	18.3	0.0	40.2	0.0	12.6	46.7	27.6	0.0
sel44	32.5	13.6	80.6	22.7	45.6	18.2	107.3	40.9	39.1	15.9	93.9	31.8
sel45	33.6	3.3	52.7	13.3	7.1	56.7	-26.3	0.0	20.3	30.0	39.5	6.7
sel46	12.5	23.3	-35.8	0.0	17.9	83.3	-42.0	0.0	15.2	53.3	38.9	0.0
sel47	78.1	27.6	261.3	55.2	49.8	31.0	102.5	51.7	63.9	29.3	181.9	53.4
sel48	62.5	0.0	85.1	86.7	23.8	100.0	-38.0	0.0	43.2	50.0	61.6	43.3
sel49	20.7	0.0	29.9	0.0	9.8	30.0	31.5	0.0	15.2	15.0	30.7	0.0
sel50	40.8	3.3	63.8	20.0	49.3	3.3	74.5	60.0	45.0	3.3	69.1	40.0
sel51	12.7	0.0	19.4	0.0	15.5	0.0	25.8	0.0	14.1	0.0	22.6	0.0
sel52	28.0	0.0	39.0	0.0	9.2	80.0	-22.3	0.0	18.6	40.0	30.6	0.0
sel821	3.7	40.0	9.8	0.0	13.8	3.3	-25.8	0.0	8.7	21.7	17.8	0.0
sel840	12.2	7.1	26.9	0.0	5.2	75.7	-16.5	0.0	8.7	41.4	21.7	0.0
sele0106	7.3	83.3	-20.2	0.0	33.1	0.0	45.0	0.0	20.2	41.7	32.6	0.0
sele0114	6.3	23.3	16.2	0.0	8.3	90.0	-23.6	0.0	7.3	56.7	19.9	0.0
sele0116	22.7	0.0	31.8	0.0	8.5	70.0	-15.7	0.0	15.6	35.0	23.7	0.0
sele0124	25.8	0.0	37.4	0.0	10.8	2.0	26.6	0.0	18.3	1.0	32.0	0.0
sele0136	18.9	6.7	33.3	0.0	24.3	0.0	38.4	0.0	21.6	3.3	35.9	0.0
sele0166	40.3	0.0	73.1	41.7	57.9	27.8	152.5	52.8	49.1	13.9	112.8	47.2
sele0210	20.6	0.0	29.2	0.0	29.3	0.0	42.0	0.0	24.9	0.0	35.6	0.0
sele0211	72.8	0.0	94.2	96.7	46.8	0.0	66.5	33.3	59.8	0.0	80.3	65.0
sele0303	37.2	0.0	44.1	0.0	80.7	0.0	87.6	100.0	59.0	0.0	65.9	50.0
sele0409	180.7	0.0	190.9	100.0	142.5	0.0	166.4	100.0	161.6	0.0	178.6	100.0
sele0609	61.2	0.0	72.6	86.7	61.6	0.0	99.8	70.0	61.4	0.0	86.2	78.3
sele0612	45.8	0.0	76.4	40.0	19.3	13.3	44.0	0.0	32.6	6.7	60.2	20.0
Average									35.2	33.6	61.7	21.2

Table B.9: Change in the ST segment slope produced when the second order filter characterised by real poles is applied to the records of the QT database.

Record	Lead A				Lead B				Average leads			
	avg (μV/s)	% neg	max (μV/s)	% exc. limit	avg (μV/s)	% neg	max (μV/s)	% exc. limit	avg (μV/s)	% neg	abs(max) (μV/s)	% exc. limit
sel14172	32.3	0.0	60.1	2.0	9.7	58.0	29.2	0.0	21.0	29.0	44.6	1.0
sel16539	19.4	3.3	44.7	0.0	14.1	100.0	-30.2	0.0	16.7	51.7	37.4	0.0
sel16786	41.1	0.0	53.8	6.7	16.5	100.0	-30.9	0.0	28.8	50.0	42.3	3.3
sel16795	5.3	75.9	-15.2	0.0	33.0	100.0	-50.2	3.4	19.1	87.9	32.7	1.7
sel17152	28.3	0.0	44.1	0.0	61.6	100.0	-80.9	86.7	45.0	50.0	62.5	43.3
sel17453	35.9	0.0	57.5	13.3	6.8	83.3	-13.8	0.0	21.4	41.7	35.7	6.7
sel223	63.7	3.2	-163.0	67.7	13.0	67.7	-47.4	0.0	38.4	35.5	105.2	33.9
sel301	92.9	0.0	104.9	100.0	84.2	0.0	104.8	96.7	88.6	0.0	104.9	98.3
sel30	18.8	0.0	34.6	0.0	20.3	6.7	48.3	0.0	19.6	3.3	41.5	0.0
sel31	25.2	10.0	76.3	6.7	28.7	100.0	-45.9	0.0	27.0	55.0	61.1	3.3
sel32	10.1	36.7	30.0	0.0	12.5	90.0	-31.4	0.0	11.3	63.3	30.7	0.0
sel33	11.8	63.3	29.4	0.0	13.3	50.0	-35.7	0.0	12.5	56.7	32.6	0.0
sel34	37.9	30.0	115.0	26.7	11.0	36.7	-40.6	0.0	24.4	33.3	77.8	13.3
sel38	18.6	73.3	-49.0	0.0	10.6	66.7	-28.1	0.0	14.6	70.0	38.5	0.0
sel39	93.9	33.3	297.9	63.3	70.5	23.3	266.7	60.0	82.2	28.3	282.3	61.7
sel40	16.5	81.5	-61.0	3.7	15.3	88.9	-51.8	3.7	15.9	85.2	56.4	3.7
sel41	8.9	89.7	-25.3	0.0	13.5	79.3	-43.9	0.0	11.2	84.5	34.6	0.0
sel42	145.3	0.0	189.2	100.0	33.7	16.7	77.6	20.0	89.5	8.3	133.4	60.0
sel43	6.0	83.3	-14.4	0.0	15.6	13.3	42.3	0.0	10.8	48.3	28.3	0.0
sel44	29.5	22.7	82.8	27.3	43.5	22.7	107.2	36.4	36.5	22.7	95.0	31.8
sel45	33.0	6.7	61.1	13.3	8.3	50.0	-29.3	0.0	20.7	28.3	45.2	6.7
sel46	13.8	40.0	-44.5	0.0	16.6	83.3	-53.1	3.3	15.2	61.7	48.8	1.7
sel47	86.3	37.9	272.1	65.5	57.3	34.5	122.5	55.2	71.8	36.2	197.3	60.3
sel48	57.4	0.0	79.3	70.0	21.2	100.0	-37.0	0.0	39.3	50.0	58.2	35.0
sel49	12.9	0.0	24.1	0.0	13.1	33.3	40.3	0.0	13.0	16.7	32.2	0.0
sel50	33.6	3.3	55.4	10.0	41.0	6.7	67.0	43.3	37.3	5.0	61.2	26.7
sel51	10.7	0.0	18.5	0.0	13.0	0.0	25.8	0.0	11.8	0.0	22.1	0.0
sel52	24.5	0.0	38.3	0.0	9.5	76.7	-22.1	0.0	17.0	38.3	30.2	0.0
sel821	5.0	20.0	11.6	0.0	9.5	6.7	-24.0	0.0	7.2	13.3	17.8	0.0
sel840	14.0	4.3	29.2	0.0	4.9	55.7	-14.7	0.0	9.4	30.0	22.0	0.0
sele0106	5.8	60.0	-16.8	0.0	33.8	0.0	46.0	0.0	19.8	30.0	31.4	0.0
sele0114	9.5	6.7	22.0	0.0	9.4	90.0	-25.0	0.0	9.5	48.3	23.5	0.0
sele0116	19.8	3.3	30.8	0.0	9.4	73.3	-16.6	0.0	14.6	38.3	23.7	0.0
sele0124	25.4	0.0	35.1	0.0	11.4	4.0	31.9	0.0	18.4	2.0	33.5	0.0
sele0136	17.2	6.7	34.0	0.0	19.8	0.0	33.6	0.0	18.5	3.3	33.8	0.0
sele0166	40.4	8.3	82.1	41.7	68.6	27.8	172.6	47.2	54.5	18.1	127.4	44.4
sele0210	20.2	0.0	31.1	0.0	26.3	0.0	42.0	0.0	23.3	0.0	36.5	0.0
sele0211	68.8	0.0	92.8	93.3	43.0	0.0	64.7	23.3	55.9	0.0	78.8	58.3
sele0303	34.2	0.0	40.2	0.0	74.0	0.0	80.6	100.0	54.1	0.0	60.4	50.0
sele0409	170.2	0.0	181.8	100.0	131.9	0.0	161.7	100.0	151.0	0.0	171.8	100.0
sele0609	54.6	0.0	68.2	73.3	53.2	0.0	99.2	60.0	53.9	0.0	83.7	66.7
sele0612	37.2	0.0	73.7	40.0	19.1	16.7	41.4	0.0	28.2	8.3	57.6	20.0
Average									32.8	31.7	63.7	19.8

Table B.10: Change in the ST segment slope produced when the second order filter is applied to the records of the QT database.

Record	Lead A				Lead B				Average leads			
	avg (μV/s)	% neg	max (μV/s)	% exc. limit	avg (μV/s)	% neg	max (μV/s)	% exc. limit	avg (μV/s)	% neg	abs(max) (μV/s)	% exc. limit
sel14172	31.3	0.0	60.0	2.0	9.3	52.0	29.8	0.0	20.3	26.0	44.9	1.0
sel16539	18.6	3.3	43.6	0.0	12.8	100.0	-28.1	0.0	15.7	51.7	35.9	0.0
sel16786	38.8	0.0	50.9	3.3	15.1	96.7	-29.1	0.0	26.9	48.3	40.0	1.7
sel16795	4.6	72.4	-13.6	0.0	30.3	100.0	-47.2	0.0	17.4	86.2	30.4	0.0
sel17152	26.5	0.0	42.3	0.0	57.7	100.0	-76.3	80.0	42.1	50.0	59.3	40.0
sel17453	33.8	0.0	55.8	6.7	6.1	83.3	-12.4	0.0	20.0	41.7	34.1	3.3
sel223	59.8	3.2	158.9	61.3	12.3	67.7	-45.7	0.0	36.0	35.5	102.3	30.6
sel301	87.1	0.0	99.3	100.0	79.2	0.0	98.1	96.7	83.1	0.0	98.7	98.3
sel30	17.7	0.0	33.2	0.0	19.3	6.7	45.2	0.0	18.5	3.3	39.2	0.0
sel31	24.4	13.3	77.7	10.0	26.6	100.0	-44.0	0.0	25.5	56.7	60.9	5.0
sel32	9.9	33.3	28.7	0.0	12.0	80.0	-29.7	0.0	10.9	56.7	29.2	0.0
sel33	11.7	60.0	30.1	0.0	13.2	43.3	-35.3	0.0	12.5	51.7	32.7	0.0
sel34	36.4	30.0	108.7	26.7	11.0	40.0	-39.7	0.0	23.7	35.0	74.2	13.3
sel38	17.6	73.3	-47.3	0.0	10.4	63.3	-26.0	0.0	14.0	68.3	36.7	0.0
sel39	98.7	33.3	311.2	60.0	69.2	23.3	267.3	56.7	84.0	28.3	289.3	58.3
sel40	15.0	81.5	-58.1	3.7	13.9	81.5	-49.0	0.0	14.5	81.5	53.5	1.9
sel41	8.3	86.2	-24.5	0.0	12.5	79.3	-40.5	0.0	10.4	82.8	32.5	0.0
sel42	132.5	0.0	175.8	100.0	34.0	16.7	79.3	20.0	83.3	8.3	127.5	60.0
sel43	5.7	80.0	-13.2	0.0	14.8	13.3	40.2	0.0	10.3	46.7	26.7	0.0
sel44	27.6	22.7	79.7	22.7	40.5	22.7	102.8	31.8	34.1	22.7	91.3	27.3
sel45	31.3	6.7	60.9	13.3	8.2	50.0	-28.6	0.0	19.8	28.3	44.7	6.7
sel46	13.9	43.3	-43.3	0.0	15.5	76.7	-53.8	3.3	14.7	60.0	48.5	1.7
sel47	83.4	37.9	251.1	65.5	55.5	37.9	126.0	55.2	69.5	37.9	188.5	60.3
sel48	53.9	0.0	75.7	56.7	19.8	100.0	-34.8	0.0	36.9	50.0	55.3	28.3
sel49	11.5	0.0	22.8	0.0	13.0	30.0	39.6	0.0	12.3	15.0	31.2	0.0
sel50	30.7	3.3	51.5	3.3	37.7	6.7	63.2	26.7	34.2	5.0	57.4	15.0
sel51	9.9	0.0	17.7	0.0	12.1	0.0	24.9	0.0	11.0	0.0	21.3	0.0
sel52	22.9	0.0	36.9	0.0	9.2	76.7	-20.5	0.0	16.0	38.3	28.7	0.0
sel821	4.9	20.0	11.4	0.0	8.6	6.7	-22.1	0.0	6.8	13.3	16.8	0.0
sel840	13.6	4.3	28.0	0.0	4.7	54.3	-13.8	0.0	9.1	29.3	20.9	0.0
sele0106	5.4	56.7	-15.8	0.0	32.1	0.0	43.2	0.0	18.8	28.3	29.5	0.0
sele0114	9.4	6.7	21.9	0.0	8.6	90.0	-22.9	0.0	9.0	48.3	22.4	0.0
sele0116	18.8	3.3	29.6	0.0	9.3	73.3	-16.5	0.0	14.0	38.3	23.0	0.0
sele0124	24.3	0.0	32.7	0.0	11.0	4.0	31.1	0.0	17.6	2.0	31.9	0.0
sele0136	16.1	10.0	32.9	0.0	18.4	0.0	31.1	0.0	17.3	5.0	32.0	0.0
sele0166	39.0	11.1	81.3	38.9	67.1	25.0	163.1	47.2	53.0	18.1	122.2	43.1
sele0210	19.3	0.0	30.3	0.0	24.8	0.0	41.0	0.0	22.0	0.0	35.6	0.0
sele0211	65.0	0.0	87.7	90.0	40.6	0.0	60.8	16.7	52.8	0.0	74.3	53.3
sele0303	32.1	0.0	37.8	0.0	69.4	0.0	76.2	100.0	50.8	0.0	57.0	50.0
sele0409	160.5	0.0	172.3	100.0	124.2	0.0	153.2	100.0	142.4	0.0	162.8	100.0
sele0609	51.2	0.0	64.9	66.7	49.7	0.0	94.5	60.0	50.4	0.0	79.7	63.3
sele0612	34.7	0.0	69.6	36.7	18.7	16.7	37.7	0.0	26.7	8.3	53.7	18.3
Average									31.1	31.1	61.3	18.6

Table B.11: Change in the ST segment slope produced when the third order filter is applied to the records of the QT database.

Record	Lead A				Lead B				Average leads			
	avg (μV/s)	% neg	max (μV/s)	% exc. limit	avg (μV/s)	% neg	max (μV/s)	% exc. limit	avg (μV/s)	% neg	abs(max) (μV/s)	% exc. limit
sel14172	31.4	2.0	62.7	2.0	12.3	68.0	-29.7	0.0	21.9	35.0	46.2	1.0
sel16539	20.8	3.3	45.9	0.0	16.8	100.0	-34.1	0.0	18.8	51.7	40.0	0.0
sel16786	46.7	0.0	59.2	30.0	19.5	100.0	-34.3	0.0	33.1	50.0	46.7	15.0
sel16795	6.1	82.8	-16.1	0.0	37.6	100.0	-55.7	10.3	21.8	91.4	35.9	5.2
sel17152	31.7	0.0	46.1	0.0	68.5	100.0	-88.1	100.0	50.1	50.0	67.1	50.0
sel17453	39.9	0.0	65.7	16.7	8.5	93.3	-16.9	0.0	24.2	46.7	41.3	8.3
sel223	71.1	3.2	-168.3	87.1	14.8	74.2	-51.4	3.2	42.9	38.7	109.8	45.2
sel301	101.4	0.0	114.7	100.0	92.1	0.0	114.2	96.7	96.7	0.0	114.4	98.3
sel30	21.0	0.0	37.1	0.0	22.5	6.7	50.1	3.3	21.7	3.3	43.6	1.7
sel31	28.0	10.0	80.3	13.3	33.1	100.0	-50.8	3.3	30.6	55.0	65.6	8.3
sel32	11.7	33.3	32.8	0.0	14.4	86.7	-35.7	0.0	13.1	60.0	34.3	0.0
sel33	12.6	63.3	31.9	0.0	14.7	50.0	39.6	0.0	13.7	56.7	35.7	0.0
sel34	39.6	20.0	118.8	36.7	11.8	43.3	-43.4	0.0	25.7	31.7	81.1	18.3
sel38	20.7	76.7	-54.8	6.7	12.8	70.0	-30.8	0.0	16.8	73.3	42.8	3.3
sel39	105.7	30.0	-307.1	63.3	79.3	20.0	270.8	66.7	92.5	25.0	289.0	65.0
sel40	21.4	96.3	-70.1	3.7	19.7	92.6	-61.1	3.7	20.5	94.4	65.6	3.7
sel41	10.7	89.7	-27.7	0.0	15.9	86.2	-48.1	0.0	13.3	87.9	37.9	0.0
sel42	176.0	0.0	222.1	100.0	33.5	20.0	75.1	26.7	104.8	10.0	148.6	63.3
sel43	6.9	90.0	-15.4	0.0	17.7	13.3	48.0	0.0	12.3	51.7	31.7	0.0
sel44	31.8	18.2	87.9	27.3	46.4	18.2	114.5	31.8	39.1	18.2	101.2	29.5
sel45	35.5	6.7	63.9	26.7	9.2	50.0	-32.2	0.0	22.3	28.3	48.1	13.3
sel46	15.7	40.0	-48.7	0.0	18.7	83.3	-61.7	3.3	17.2	61.7	55.2	1.7
sel47	90.5	31.0	272.3	69.0	64.2	34.5	132.8	62.1	77.3	32.8	202.5	65.5
sel48	62.5	0.0	87.8	76.7	23.4	100.0	-40.5	0.0	43.0	50.0	64.1	38.3
sel49	17.1	0.0	29.4	0.0	13.7	33.3	41.3	0.0	15.4	16.7	35.4	0.0
sel50	38.0	3.3	61.9	20.0	46.3	6.7	77.5	50.0	42.1	5.0	69.7	35.0
sel51	12.0	0.0	20.5	0.0	14.7	0.0	28.8	0.0	13.4	0.0	24.7	0.0
sel52	27.4	0.0	43.4	0.0	10.5	76.7	-23.4	0.0	18.9	38.3	33.4	0.0
sel821	4.6	30.0	11.6	0.0	11.9	6.7	-25.3	0.0	8.3	18.3	18.5	0.0
sel840	14.1	4.3	29.4	0.0	5.5	62.9	-17.1	0.0	9.8	33.6	23.3	0.0
sele0106	6.5	70.0	-19.7	0.0	35.3	0.0	47.8	0.0	20.9	35.0	33.7	0.0
sele0114	8.5	6.7	22.2	0.0	9.1	86.7	-26.3	0.0	8.8	46.7	24.3	0.0
sele0116	22.5	3.3	35.5	0.0	10.4	73.3	19.6	0.0	16.5	38.3	27.6	0.0
sele0124	27.2	0.0	37.6	0.0	12.1	10.0	35.5	0.0	19.7	5.0	36.6	0.0
sele0136	19.0	6.7	38.2	0.0	22.9	0.0	38.0	0.0	21.0	3.3	38.1	0.0
sele0166	43.4	11.1	89.3	41.7	73.8	27.8	177.2	50.0	58.6	19.4	133.3	45.8
sele0210	21.6	0.0	32.5	0.0	29.1	0.0	47.1	0.0	25.4	0.0	39.8	0.0
sele0211	74.6	0.0	98.7	96.7	47.4	0.0	69.4	40.0	61.0	0.0	84.1	68.3
sele0303	37.3	0.0	43.4	0.0	80.8	0.0	87.8	100.0	59.1	0.0	65.6	50.0
sele0409	184.2	0.0	196.8	100.0	143.7	0.0	175.9	100.0	164.0	0.0	186.4	100.0
sele0609	60.4	0.0	75.4	80.0	59.7	0.0	111.4	66.7	60.1	0.0	93.4	73.3
sele0612	43.3	0.0	81.9	40.0	22.1	13.3	44.9	0.0	32.7	6.7	63.4	20.0
Average									36.4	32.6	68.6	22.1

Table B.12: Change in the ST segment slope produced when the third order concave filter is applied to the records of the QT database.

Record	Lead A				Lead B				Average leads			
	avg (μV/s)	% neg	max (μV/s)	% exc. limit	avg (μV/s)	% neg	max (μV/s)	% exc. limit	avg (μV/s)	% neg	abs(max) (μV/s)	% exc. limit
sel14172	31.6	0.0	61.3	4.0	9.7	46.0	32.0	0.0	20.7	23.0	46.6	2.0
sel16539	18.4	3.3	43.3	0.0	12.0	100.0	-27.8	0.0	15.2	51.7	35.5	0.0
sel16786	37.5	0.0	49.6	0.0	14.3	96.7	-28.7	0.0	25.9	48.3	39.2	0.0
sel16795	4.5	72.4	-13.0	0.0	28.9	100.0	-46.9	0.0	16.7	86.2	29.9	0.0
sel17152	25.7	0.0	41.1	0.0	55.9	100.0	-74.9	70.0	40.8	50.0	58.0	35.0
sel17453	32.9	0.0	56.5	10.0	5.9	83.3	-12.3	0.0	19.4	41.7	34.4	5.0
sel223	58.2	3.2	-172.0	58.1	12.6	67.7	-46.8	0.0	35.4	35.5	109.4	29.0
sel301	84.8	0.0	97.1	100.0	77.1	0.0	96.8	96.7	80.9	0.0	96.9	98.3
sel30	17.2	3.3	33.4	0.0	19.0	6.7	45.7	0.0	18.1	5.0	39.6	0.0
sel31	24.1	10.0	76.3	6.7	25.3	100.0	-42.9	0.0	24.7	55.0	59.6	3.3
sel32	10.5	36.7	-29.5	0.0	11.7	80.0	-30.6	0.0	11.1	58.3	30.1	0.0
sel33	12.5	63.3	32.5	0.0	14.3	46.7	38.2	0.0	13.4	55.0	35.3	0.0
sel34	37.6	30.0	108.7	26.7	11.6	40.0	-43.3	0.0	24.6	35.0	76.0	13.3
sel38	18.1	66.7	-49.7	0.0	10.9	63.3	-27.8	0.0	14.5	65.0	38.7	0.0
sel39	99.3	26.7	304.4	63.3	71.7	20.0	261.0	60.0	85.5	23.3	282.7	61.7
sel40	14.4	81.5	-58.0	3.7	13.6	77.8	-49.5	0.0	14.0	79.6	53.7	1.9
sel41	7.9	86.2	-23.7	0.0	12.2	72.4	-39.9	0.0	10.1	79.3	31.8	0.0
sel42	124.5	0.0	169.4	100.0	36.0	16.7	79.5	30.0	80.2	8.3	124.5	65.0
sel43	5.7	80.0	-13.4	0.0	14.9	23.3	42.6	0.0	10.3	51.7	28.0	0.0
sel44	27.6	36.4	80.6	22.7	40.3	27.3	105.1	36.4	33.9	31.8	92.8	29.5
sel45	31.1	6.7	60.7	10.0	8.6	50.0	-29.4	0.0	19.9	28.3	45.1	5.0
sel46	14.5	43.3	-46.4	0.0	15.9	76.7	-58.5	3.3	15.2	60.0	52.5	1.7
sel47	87.0	41.4	255.4	65.5	59.0	37.9	129.0	55.2	73.0	39.7	192.2	60.3
sel48	52.4	0.0	75.5	53.3	19.2	100.0	-35.0	0.0	35.8	50.0	55.3	26.7
sel49	10.5	3.3	22.0	0.0	13.8	30.0	41.3	0.0	12.2	16.7	31.7	0.0
sel50	29.4	3.3	49.7	0.0	36.5	6.7	62.0	20.0	32.9	5.0	55.8	10.0
sel51	9.5	3.3	17.2	0.0	11.6	6.7	24.5	0.0	10.6	5.0	20.9	0.0
sel52	22.2	3.3	37.6	0.0	9.3	76.7	-20.7	0.0	15.8	40.0	29.2	0.0
sel821	5.1	20.0	11.8	0.0	8.1	13.3	-21.6	0.0	6.6	16.7	16.7	0.0
sel840	13.6	4.3	27.8	0.0	5.0	51.4	-13.9	0.0	9.3	27.9	20.9	0.0
sele0106	5.6	53.3	-16.1	0.0	31.6	0.0	43.0	0.0	18.6	26.7	29.6	0.0
sele0114	9.7	6.7	22.5	0.0	8.7	90.0	-23.6	0.0	9.2	48.3	23.1	0.0
sele0116	18.3	3.3	30.0	0.0	9.6	73.3	18.3	0.0	13.9	38.3	24.1	0.0
sele0124	23.9	0.0	32.3	0.0	11.0	10.0	33.0	0.0	17.4	5.0	32.6	0.0
sele0136	16.0	10.0	33.7	0.0	17.6	0.0	30.6	0.0	16.8	5.0	32.2	0.0
sele0166	38.9	11.1	83.1	38.9	70.1	27.8	171.5	47.2	54.5	19.4	127.3	43.1
sele0210	18.9	0.0	30.0	0.0	24.2	3.3	40.2	0.0	21.5	1.7	35.1	0.0
sele0211	63.6	0.0	86.6	90.0	39.6	0.0	60.2	16.7	51.6	0.0	73.4	53.3
sele0303	31.3	0.0	37.0	0.0	67.5	0.0	74.5	100.0	49.4	0.0	55.8	50.0
sele0409	156.8	0.0	169.5	100.0	121.0	0.0	152.0	100.0	138.9	0.0	160.8	100.0
sele0609	49.6	0.0	63.9	56.7	48.0	3.3	96.0	56.7	48.8	1.7	79.9	56.7
sele0612	33.2	0.0	70.6	36.7	19.2	20.0	39.1	0.0	26.2	10.0	54.8	18.3
Average									30.8	31.6	61.7	18.3

B.5 Noise reduction achieved by the highpass filters for selected records of the QT database

The power contained in the records of the QT database at frequencies lower than 0.5 Hz, which is indicative of the out-of-band noise and interference occurring at low frequencies, is measured after applying the different highpass filters. The percentage difference between this output power and the low-frequency input power is also calculated.

Table B.13: Power measured for selected records of the QT database.

	Lead A			Lead B			Average leads		
Record	total power (10^{-9} V^2)	power f<0.5Hz (10^{-9} V^2)	% power f<0.5Hz	total power (10^{-9} V^2)	power f<0.5Hz (10^{-9} V^2)	% power f<0.5Hz	total power (10^{-9} V^2)	power f<0.5Hz (10^{-9} V^2)	% power f<0.5Hz
sel14172	66.9	2.1	3.1	52.3	2.4	4.6	59.6	2.2	3.8
sel16539	55.7	1.2	2.2	19.9	0.3	1.4	37.8	0.8	1.8
sel16786	182.4	0.6	0.3	17.9	0.5	2.9	100.2	0.5	1.6
sel16795	58.2	0.5	0.9	40.3	0.6	1.4	49.3	0.5	1.2
sel17152	32.3	1.4	4.4	61.0	0.4	0.7	46.6	0.9	2.6
sel17453	115.5	1.2	1.0	36.2	0.3	0.7	75.9	0.7	0.9
sel223	171.3	5.4	3.1	64.6	3.5	5.4	118.0	4.4	4.3
sel301	252.7	0.4	0.2	85.5	5.6	6.6	169.1	3.0	3.4
sel30	20.1	6.3	31.6	20.4	3.9	19.4	20.2	5.1	25.5
sel31*	48.9	38.3	78.4	41.7	6.9	16.6	45.3	22.6	47.5
sel32	18.4	4.4	23.8	16.7	4.3	25.9	17.6	4.4	24.9
sel33	35.2	19.8	56.1	16.1	2.8	17.3	25.7	11.3	36.7
sel34	54.5	7.9	14.5	2.7	1.4	51.9	28.6	4.6	33.2
sel38	80.7	2.8	3.5	12.4	1.5	11.9	46.6	2.1	7.7
sel39*	356.3	330.6	92.8	105.4	77.9	73.9	230.9	204.3	83.3
sel40	64.2	3.4	5.2	51.7	4.3	8.3	58.0	3.8	6.8
sel41	20.8	5.8	28.0	36.8	4.4	11.9	28.8	5.1	19.9
sel42	1440.2	5.9	0.4	214.5	19.0	8.8	827.3	12.4	4.6
sel43	9.7	4.5	46.0	22.3	5.2	23.3	16.0	4.8	34.7
sel44	58.0	3.0	5.2	114.4	6.2	5.4	86.2	4.6	5.3
sel45*	53.2	28.0	52.6	6.3	4.8	75.3	29.7	16.4	63.9
sel46	24.7	3.3	13.5	30.3	5.3	17.6	27.5	4.3	15.5
sel47*	547.8	435.9	79.6	144.0	121.9	84.7	345.9	278.9	82.1
sel48	50.4	3.5	7.0	18.6	3.8	20.6	34.5	3.7	13.8
sel49*	63.0	29.4	46.6	10.5	4.7	44.6	36.7	17.0	45.6
sel50	45.3	3.1	6.8	71.7	5.8	8.2	58.5	4.5	7.5
sel51	7.2	0.1	1.8	11.0	0.3	2.5	9.1	0.2	2.1
sel52	35.6	3.2	8.9	4.7	1.7	35.3	20.2	2.4	22.1
sel821	14.1	0.6	4.3	33.4	0.3	0.8	23.8	0.4	2.5
sel840	24.2	0.8	3.5	12.5	0.8	6.6	18.4	0.8	5.0
sele0106	11.0	1.1	10.3	59.9	0.7	1.2	35.5	0.9	5.8
sele0114	16.8	1.3	7.8	26.7	0.9	3.5	21.8	1.1	5.6
sele0116	41.6	1.5	3.6	16.7	2.8	16.8	29.2	2.2	10.2
sele0124	61.9	0.5	0.8	4.8	1.0	21.7	33.4	0.8	11.2
sele0136	24.4	4.2	17.2	59.2	0.5	0.8	41.8	2.3	9.0
sele0166	60.5	4.8	7.9	137.7	26.6	19.4	99.1	15.7	13.7
sele0210	14.4	1.0	6.8	29.9	1.4	4.8	22.2	1.2	5.8
sele0211	71.2	1.6	2.2	51.4	4.9	9.5	61.3	3.2	5.9
sele0303	38.3	0.1	0.4	88.2	0.4	0.5	63.3	0.3	0.4
sele0409	218.8	3.3	1.5	127.9	6.1	4.8	173.4	4.7	3.1
sele0609	63.9	0.5	0.8	63.9	2.0	3.1	63.9	1.2	1.9
sele0612	78.6	4.3	5.4	31.1	5.2	16.8	54.9	4.7	11.1
Average							80.7	15.8	16.5
Average * only							137.7	107.8	64.5

Table B.14: Low-frequency power and noise reduction obtained for selected records of the QT database when they are filtered using the 0.05 Hz single-pole reference network.

	Lead A		Lead B		Average leads	
Record	power (10^{-9} V^2)	% reduction	power (10^{-9} V^2)	% reduction	power (10^{-9} V^2)	% reduction
sel14172	1.9	-8.1	2.2	-8.6	2.0	-8.4
sel16539	1.1	-10.9	0.2	-16.1	0.7	-13.5
sel16786	0.5	-17.2	0.5	-11.1	0.5	-14.2
sel16795	0.4	-18.6	0.5	-11.1	0.5	-14.8
sel17152	1.2	-16.9	0.4	-18.1	0.8	-17.5
sel17453	1.0	-13.2	0.2	-17.4	0.6	-15.3
sel223	2.7	-50.5	1.6	-55.4	2.1	-52.9
sel301	0.3	-30.0	3.7	-33.3	2.0	-31.7
sel30	3.6	-43.6	3.0	-24.2	3.3	-33.9
sel31*	19.9	-48.0	4.5	-34.5	12.2	-41.2
sel32	4.0	-8.3	4.0	-8.3	4.0	-8.3
sel33	11.7	-40.8	2.4	-13.0	7.1	-26.9
sel34	7.5	-5.1	1.3	-8.3	4.4	-6.7
sel38	2.7	-4.1	1.4	-8.8	2.0	-6.4
sel39*	184.6	-44.2	57.8	-25.8	121.2	-35.0
sel40	2.3	-30.1	3.5	-18.2	2.9	-24.2
sel41	3.3	-44.0	3.4	-23.2	3.3	-33.6
sel42	5.5	-7.0	17.9	-5.9	11.7	-6.4
sel43	3.1	-29.9	4.3	-17.7	3.7	-23.8
sel44	2.9	-3.7	5.9	-4.2	4.4	-3.9
sel45*	17.2	-38.4	3.3	-31.2	10.2	-34.8
sel46	2.6	-22.6	4.4	-17.6	3.5	-20.1
sel47*	300.3	-31.1	89.8	-26.3	195.1	-28.7
sel48	2.4	-32.3	2.9	-25.7	2.6	-29.0
sel49*	16.3	-44.4	3.2	-30.5	9.8	-37.5
sel50	2.9	-4.8	5.5	-5.4	4.2	-5.1
sel51	0.1	-6.5	0.3	-6.8	0.2	-6.7
sel52	3.0	-4.9	1.6	-6.0	2.3	-5.4
sel821	0.5	-14.8	0.2	-18.1	0.4	-16.4
sel840	0.7	-15.3	0.7	-10.4	0.7	-12.9
sele0106	0.6	-50.4	0.6	-16.1	0.6	-33.2
sele0114	0.6	-53.1	0.7	-30.7	0.6	-41.9
sele0116	1.0	-35.2	1.6	-44.1	1.3	-39.7
sele0124	0.3	-38.7	0.8	-25.8	0.5	-32.3
sele0136	1.3	-69.2	0.3	-43.6	0.8	-56.4
sele0166	4.5	-7.3	25.1	-5.7	14.8	-6.5
sele0210	0.7	-24.1	1.0	-29.8	0.9	-27.0
sele0211	1.1	-32.8	3.1	-36.4	2.1	-34.6
sele0303	0.1	-27.4	0.2	-52.0	0.2	-39.7
sele0409	2.6	-20.8	5.3	-13.4	4.0	-17.1
sele0609	0.5	-4.9	1.9	-5.1	1.2	-5.0
sele0612	4.1	-4.1	4.8	-7.3	4.5	-5.7
Average					10.7	-22.7
Average * only					69.7	-35.4

Table B.15: Low-frequency power and noise reduction obtained for selected records of the QT database when they are filtered using the second order filter having real poles.

	Lead A		Lead B		Average leads	
Record	power (10^{-9} V^2)	% reduction	power (10^{-9} V^2)	% reduction	power (10^{-9} V^2)	% reduction
sel14172	2.0	-1.3	2.4	-2.2	2.2	-1.8
sel16539	1.2	-5.4	0.3	-11.2	0.7	-8.3
sel16786	0.5	-13.8	0.5	-5.0	0.5	-9.4
sel16795	0.4	-15.5	0.5	-4.1	0.5	-9.8
sel17152	1.2	-13.7	0.4	-14.8	0.8	-14.3
sel17453	1.1	-8.6	0.2	-13.0	0.7	-10.8
sel223	2.5	-53.0	1.5	-57.5	2.0	-55.3
sel301	0.3	-32.7	3.7	-34.8	2.0	-33.8
sel30	3.0	-52.7	2.9	-27.6	2.9	-40.2
sel31*	15.4	-59.7	4.0	-42.3	9.7	-51.0
sel32	4.3	-1.9	4.2	-2.9	4.3	-2.4
sel33	9.5	-52.1	2.5	-10.5	6.0	-31.3
sel34	8.1	2.9	1.4	-2.0	4.8	0.5
sel38	2.9	3.0	1.4	-3.6	2.2	-0.3
sel39*	158.2	-52.1	56.1	-28.0	107.2	-40.1
sel40	2.2	-35.8	3.5	-19.1	2.8	-27.4
sel41	2.6	-55.1	3.2	-26.4	2.9	-40.8
sel42	5.8	-0.9	19.2	1.1	12.5	0.1
sel43	2.9	-35.7	4.3	-17.5	3.6	-26.6
sel44	3.1	2.7	6.3	2.0	4.7	2.4
sel45*	15.6	-44.3	3.1	-35.7	9.3	-40.0
sel46	2.5	-26.0	4.4	-18.5	3.4	-22.2
sel47*	265.0	-39.2	83.5	-31.6	174.2	-35.4
sel48	2.1	-41.0	2.7	-31.0	2.4	-36.0
sel49*	13.5	-54.2	3.0	-34.7	8.3	-44.4
sel50	3.1	1.4	5.9	1.0	4.5	1.2
sel51	0.1	-0.9	0.3	-1.0	0.2	-1.0
sel52	3.2	2.4	1.7	0.8	2.5	1.6
sel821	0.5	-11.1	0.2	-13.7	0.4	-12.4
sel840	0.7	-11.8	0.8	-5.5	0.8	-8.7
sele0106	0.5	-51.9	0.6	-12.7	0.6	-32.3
sele0114	0.5	-59.3	0.7	-31.0	0.6	-45.2
sele0116	1.0	-36.2	1.5	-45.7	1.2	-40.9
sele0124	0.3	-39.5	0.8	-25.5	0.5	-32.5
sele0136	1.2	-71.2	0.3	-46.2	0.7	-58.7
sele0166	4.8	-0.4	27.3	2.5	16.0	1.1
sele0210	0.7	-25.6	0.9	-34.6	0.8	-30.1
sele0211	1.0	-39.0	2.7	-45.7	1.8	-42.3
sele0303	0.1	-29.3	0.2	-56.6	0.1	-43.0
sele0409	2.7	-17.4	5.5	-9.6	4.1	-13.5
sele0609	0.5	1.8	2.0	2.4	1.3	2.1
sele0612	4.4	4.0	5.2	-0.5	4.8	1.7
Average					9.8	-22.2
Average * only					61.7	-42.2

Table B.16: Low-frequency power and noise reduction obtained for selected records of the QT database when they are filtered using the second order filter.

	Lead A		Lead B		Average leads	
Record	power (10^{-9} V^2)	% reduction	power (10^{-9} V^2)	% reduction	power (10^{-9} V^2)	% reduction
sel14172	2.1	3.7	2.5	3.1	2.3	3.4
sel16539	1.2	-0.2	0.3	-7.2	0.8	-3.7
sel16786	0.5	-8.8	0.5	-0.9	0.5	-4.8
sel16795	0.5	-10.0	0.6	0.8	0.5	-4.6
sel17152	1.3	-7.3	0.4	-9.8	0.9	-8.5
sel17453	1.1	-3.5	0.2	-8.7	0.7	-6.1
sel223	2.6	-52.1	1.5	-56.9	2.0	-54.5
sel301	0.3	-30.6	3.8	-32.7	2.0	-31.7
sel30	3.0	-52.8	2.9	-25.4	3.0	-39.1
sel31*	15.3	-60.2	4.1	-40.9	9.7	-50.5
sel32	4.5	3.5	4.4	1.6	4.5	2.5
sel33	9.4	-52.4	2.6	-7.1	6.0	-29.7
sel34	8.5	7.6	1.5	3.4	5.0	5.5
sel38	3.0	5.9	1.5	0.8	2.2	3.4
sel39*	161.6	-51.1	58.2	-25.2	109.9	-38.2
sel40	2.2	-34.7	3.7	-15.0	2.9	-24.8
sel41	2.6	-55.7	3.3	-24.2	2.9	-39.9
sel42	6.0	2.8	20.1	5.8	13.1	4.3
sel43	2.9	-34.5	4.5	-14.2	3.7	-24.3
sel44	3.1	5.2	6.5	4.7	4.8	4.9
sel45*	16.1	-42.5	3.2	-33.4	9.6	-38.0
sel46	2.5	-23.6	4.5	-15.8	3.5	-19.7
sel47*	269.7	-38.1	86.1	-29.4	177.9	-33.8
sel48	2.1	-40.6	2.7	-29.1	2.4	-34.9
sel49*	13.5	-53.9	3.2	-32.5	8.3	-43.2
sel50	3.2	4.7	6.1	4.7	4.7	4.7
sel51	0.1	2.6	0.3	3.0	0.2	2.8
sel52	3.4	6.5	1.7	5.1	2.6	5.8
sel821	0.6	-6.3	0.2	-10.0	0.4	-8.1
sel840	0.8	-7.5	0.8	-1.8	0.8	-4.7
sele0106	0.6	-50.4	0.7	-9.8	0.6	-30.1
sele0114	0.5	-59.0	0.7	-29.7	0.6	-44.4
sele0116	1.0	-33.7	1.6	-43.6	1.3	-38.7
sele0124	0.3	-37.7	0.8	-22.2	0.6	-29.9
sele0136	1.2	-70.6	0.3	-44.8	0.8	-57.7
sele0166	5.0	4.8	28.7	7.7	16.9	6.3
sele0210	0.8	-22.2	1.0	-32.5	0.9	-27.3
sele0211	1.0	-38.0	2.7	-45.6	1.8	-41.8
sele0303	0.1	-27.6	0.2	-56.1	0.1	-41.8
sele0409	2.8	-14.3	5.8	-5.3	4.3	-9.8
sele0609	0.6	5.4	2.1	6.7	1.3	6.1
sele0612	4.6	7.6	5.5	4.7	5.0	6.2
Average					10.0	-19.2
Average * only					63.1	-40.7

Table B.17: Low-frequency power and noise reduction obtained for selected records of the QT database when they are filtered using the third order filter.

	Lead A		Lead B		Average leads	
Record	power (10^{-9} V^2)	% reduction	power (10^{-9} V^2)	% reduction	power (10^{-9} V^2)	% reduction
sel14172	2.1	0.4	2.3	-4.7	2.2	-2.2
sel16539	1.1	-14.3	0.2	-16.2	0.7	-15.3
sel16786	0.4	-30.5	0.5	-7.4	0.4	-19.0
sel16795	0.3	-37.8	0.5	-3.6	0.4	-20.7
sel17152	0.8	-42.3	0.3	-31.7	0.6	-37.0
sel17453	0.9	-24.1	0.2	-22.1	0.6	-23.1
sel223	2.5	-53.5	1.5	-56.8	2.0	-55.2
sel301	0.3	-36.4	3.4	-39.0	1.9	-37.7
sel30	3.0	-53.0	2.6	-33.5	2.8	-43.2
sel31*	14.4	-62.5	3.3	-51.9	8.8	-57.2
sel32	4.1	-6.2	4.0	-8.2	4.0	-7.2
sel33	8.8	-55.3	2.3	-15.9	5.6	-35.6
sel34	8.2	4.3	1.3	-7.0	4.8	-1.4
sel38	2.9	3.2	1.4	-8.0	2.1	-2.4
sel39*	133.4	-59.7	49.3	-36.7	91.3	-48.2
sel40	2.0	-39.7	2.8	-35.3	2.4	-37.5
sel41	2.5	-56.6	2.9	-32.9	2.7	-44.7
sel42	5.6	-4.0	18.7	-1.3	12.2	-2.7
sel43	2.7	-40.0	4.0	-23.3	3.3	-31.6
sel44	3.1	2.0	6.2	0.3	4.6	1.2
sel45*	13.5	-51.8	2.6	-44.6	8.0	-48.2
sel46	2.2	-35.0	4.0	-25.5	3.1	-30.3
sel47*	234.3	-46.2	73.1	-40.0	153.7	-43.1
sel48	2.0	-44.2	2.4	-36.7	2.2	-40.4
sel49*	12.1	-58.7	2.6	-43.3	7.4	-51.0
sel50	3.1	-0.2	5.8	-1.2	4.4	-0.7
sel51	0.1	-5.1	0.3	-5.2	0.2	-5.2
sel52	3.2	1.6	1.6	-1.1	2.4	0.3
sel821	0.4	-25.8	0.2	-18.2	0.3	-22.0
sel840	0.6	-23.5	0.8	-9.5	0.7	-16.5
sele0106	0.5	-54.3	0.6	-15.6	0.6	-35.0
sele0114	0.5	-59.9	0.7	-30.6	0.6	-45.2
sele0116	0.9	-37.0	1.5	-48.5	1.2	-42.8
sele0124	0.3	-40.9	0.7	-31.9	0.5	-36.4
sele0136	1.3	-69.8	0.3	-47.1	0.8	-58.4
sele0166	4.7	-3.0	27.7	3.8	16.2	0.4
sele0210	0.6	-35.1	0.9	-40.8	0.7	-38.0
sele0211	0.9	-42.7	2.6	-46.9	1.8	-44.8
sele0303	0.1	-32.8	0.2	-56.6	0.1	-44.7
sele0409	2.6	-19.4	5.1	-16.2	3.9	-17.8
sele0609	0.5	0.5	2.0	3.5	1.3	2.0
sele0612	4.5	5.4	5.0	-4.7	4.7	0.3
Average					8.8	-27.1
Average * only					53.9	-49.5

Table B.18: Low-frequency power and noise reduction obtained for selected records of the QT database when they are filtered using the third order concave filter.

	Lead A		Lead B		Average leads	
Record	power (10^{-9} V^2)	% reduction	power (10^{-9} V^2)	% reduction	power (10^{-9} V^2)	% reduction
sel14172	2.1	0.4	2.4	-2.4	2.2	-1.0
sel16539	1.1	-7.5	0.3	-11.2	0.7	-9.4
sel16786	0.4	-19.5	0.5	-3.8	0.5	-11.7
sel16795	0.4	-23.1	0.6	-2.2	0.5	-12.6
sel17152	1.1	-23.6	0.3	-20.1	0.7	-21.9
sel17453	1.0	-13.2	0.2	-14.7	0.6	-14.0
sel223	2.5	-53.6	1.5	-57.1	2.0	-55.3
sel301	0.3	-35.7	3.5	-37.9	1.9	-36.8
sel30	2.8	-56.0	2.6	-33.3	2.7	-44.6
sel31*	13.2	-65.5	3.4	-50.8	8.3	-58.1
sel32	4.3	-2.7	4.1	-4.4	4.2	-3.6
sel33	8.2	-58.4	2.4	-13.1	5.3	-35.8
sel34	8.3	5.7	1.4	-3.0	4.9	1.4
sel38	3.0	5.7	1.4	-4.8	2.2	0.4
sel39*	136.2	-58.8	51.6	-33.8	93.9	-46.3
sel40	2.0	-40.7	3.1	-28.8	2.5	-34.8
sel41	2.3	-60.2	3.0	-32.0	2.6	-46.1
sel42	5.9	-0.4	19.3	1.9	12.6	0.7
sel43	2.6	-41.1	4.1	-21.5	3.4	-31.3
sel44	3.1	4.8	6.4	3.6	4.8	4.2
sel45*	13.9	-50.3	2.7	-42.7	8.3	-46.5
sel46	2.2	-33.3	4.1	-23.8	3.1	-28.6
sel47*	227.9	-47.7	74.0	-39.3	150.9	-43.5
sel48	1.9	-47.3	2.4	-37.8	2.1	-42.5
sel49*	11.7	-60.2	2.7	-41.3	7.2	-50.7
sel50	3.1	2.7	6.0	1.8	4.5	2.2
sel51	0.1	-1.0	0.3	-1.5	0.2	-1.2
sel52	3.3	4.2	1.7	1.8	2.5	3.0
sel821	0.5	-16.4	0.2	-13.8	0.4	-15.1
sel840	0.7	-15.7	0.8	-6.0	0.7	-10.9
sele0106	0.5	-53.4	0.6	-12.9	0.6	-33.2
sele0114	0.5	-61.4	0.7	-30.5	0.6	-46.0
sele0116	0.9	-36.7	1.5	-47.3	1.2	-42.0
sele0124	0.3	-39.7	0.7	-28.7	0.5	-34.2
sele0136	1.2	-70.3	0.3	-47.0	0.8	-58.7
sele0166	4.8	-0.1	28.0	5.1	16.4	2.5
sele0210	0.7	-31.6	0.9	-40.1	0.8	-35.9
sele0211	0.9	-43.5	2.4	-50.0	1.7	-46.7
sele0303	0.1	-32.0	0.2	-57.0	0.1	-44.5
sele0409	2.7	-17.5	5.4	-12.1	4.1	-14.8
sele0609	0.5	3.4	2.0	4.7	1.3	4.0
sele0612	4.6	7.6	5.2	-0.8	4.9	3.4
Average					8.8	-24.7
Average * only					53.7	-49.0

Appendix C

C.1 Sensitivity of Friend's circuit

Table C.1: Sensitivities of the frequency and Q-factor of the poles and zeros of Friend's circuit with respect to component tolerances for n_2 = 0.82 (R_C/R_D = 2.2/10).

	G_B/G_A=0.01			G_B/G_A=0.1			G_B/G_A=1		
C_2/C_1	0.1	1	10	0.1	1	10	0.1	1	10
				ω_p					
S_{C_1}	-0.50	-0.50	-0.50	-0.50	-0.50	-0.50	-0.50	-0.50	-0.50
S_{C_2}	-0.50	-0.50	-0.50	-0.50	-0.50	-0.50	-0.50	-0.50	-0.50
$\boldsymbol{S_{G_2}}$	**0.51**	**0.51**	**0.51**	**0.58**	**0.58**	**0.58**	**0.95**	**0.95**	**0.95**
S_{G_4}	0.39	0.30	0.21	0.37	0.29	0.21	0.30	0.24	0.19
S_{G_5}	0.11	0.20	0.29	0.13	0.21	0.29	0.20	0.26	0.32
$\boldsymbol{S_{G_6}}$	**-0.01**	**-0.01**	**-0.01**	**-0.08**	**-0.08**	**-0.08**	**-0.45**	**-0.45**	**-0.45**
S_{G_B}	-0.01	-0.01	-0.01	-0.08	-0.08	-0.08	-0.45	-0.45	-0.45
S_{G_C}	0.01	0.01	0.01	0.07	0.07	0.07	0.37	0.37	0.37
S_{G_D}	0.00	0.00	0.00	0.01	0.01	0.01	0.08	0.08	0.08
$\sum \lvert S \rvert$	2.04	2.04	2.04	2.33	2.33	2.33	3.82	3.82	3.82
				ω_z					
S_{C_1}	-0.50	-0.50	-0.50	-0.50	-0.50	-0.50	-0.50	-0.50	-0.50
S_{C_2}	-0.50	-0.50	-0.50	-0.50	-0.50	-0.50	-0.50	-0.50	-0.50
$\boldsymbol{S_{G_2}}$	**0.85**	**0.85**	**0.85**	**0.97**	**0.97**	**0.97**	**1.59**	**1.59**	**1.59**
S_{G_4}	0.39	0.30	0.21	0.37	0.29	0.21	0.30	0.24	0.19
S_{G_5}	0.11	0.20	0.29	0.13	0.21	0.29	0.20	0.26	0.32
$\boldsymbol{S_{G_6}}$	**-0.35**	**-0.35**	**-0.35**	**-0.47**	**-0.47**	**-0.47**	**-1.09**	**-1.09**	**-1.09**
S_{G_B}	-0.02	-0.02	-0.02	-0.17	-0.17	-0.17	-0.92	-0.92	-0.92
S_{G_C}	0.35	0.35	0.35	0.47	0.47	0.47	1.09	1.09	1.09
S_{G_D}	-0.33	-0.33	-0.33	-0.30	-0.30	-0.30	-0.17	-0.17	-0.17
$\sum \lvert S \rvert$	3.39	3.39	3.39	3.88	3.88	3.88	6.36	6.36	6.36
				Q_p					
$\boldsymbol{S_{C_1}}$	**-0.40**	**0.01**	**0.42**	**-0.37**	**0.06**	**0.47**	**-0.21**	**0.36**	**0.83**
S_{C_2}	0.40	-0.01	-0.42	0.37	-0.06	-0.47	0.21	-0.36	-0.83
S_{G_2}	-0.57	-0.52	-0.52	-1.13	-0.71	-0.66	-5.08	-2.33	-1.84
$\boldsymbol{S_{G_1}}$	**0.56**	**0.51**	**0.51**	**0.97**	**0.61**	**0.56**	**2.66**	**1.22**	**0.97**
S_{G_4}	0.44	0.31	0.22	0.71	0.35	0.23	1.58	0.58	0.36
S_{G_5}	0.13	0.20	0.29	0.25	0.26	0.33	1.08	0.65	0.61
S_{G_6}	0.01	0.01	0.01	0.16	0.10	0.09	2.42	1.11	0.88
$\boldsymbol{S_{G_B}}$	**0.07**	**0.02**	**0.02**	**0.63**	**0.21**	**0.16**	**4.58**	**1.83**	**1.34**
S_{G_C}	-0.06	-0.02	-0.01	-0.51	-0.17	-0.13	-3.75	-1.50	-1.10
S_{G_D}	-0.01	0.00	0.00	-0.11	-0.04	-0.03	-0.83	-0.33	-0.24
$\sum \lvert S \rvert$ excl. S_{G_1}	2.10	1.10	1.89	4.23	1.96	2.56	19.73	9.04	8.04
				Q_z					
$\boldsymbol{S_{C_1}}$	**-0.44**	**-0.17**	**0.09**	**-0.41**	**-0.14**	**0.13**	**-0.31**	**0.06**	**0.36**
S_{C_2}	0.44	0.17	-0.09	0.41	0.14	-0.13	0.31	-0.06	-0.36
$\boldsymbol{S_{G_2}}$	**-0.32**	**-0.27**	**-0.26**	**-0.88**	**-0.43**	**-0.37**	**-4.93**	**-1.96**	**-1.43**
$\boldsymbol{S_{G_4}}$	**1.64**	**0.49**	**0.29**	**1.64**	**0.52**	**0.30**	**2.29**	**0.76**	**0.45**
$\boldsymbol{S_{G_5}}$	**-1.45**	**-0.33**	**-0.13**	**-1.19**	**-0.30**	**-0.11**	**-0.74**	**-0.15**	**0.00**
S_{G_6}	0.13	0.11	0.11	0.42	0.21	0.18	3.38	1.34	0.98
S_{G_B}	0.07	0.02	0.01	0.60	0.16	0.10	4.55	1.59	1.06
$\boldsymbol{S_{G_C}}$	**-1.38**	**-0.29**	**-0.18**	**-1.69**	**-0.44**	**-0.28**	**-5.37**	**-1.87**	**-1.25**
S_{G_D}	1.31	0.28	0.17	1.09	0.29	0.18	0.82	0.29	0.19
$\sum \lvert S \rvert$	7.17	2.12	1.33	8.34	2.63	1.78	22.72	8.08	6.10

Table C.2: Sensitivities of the frequency and Q-factor of the poles and zeros of Friend's circuit with respect to component tolerances for n_2 = 0.91 (R_C/R_D = 1/10).

	G_B/G_A=0.01			G_B/G_A=0.1			G_B/G_A=1		
C_2/C_1	0.1	1	10	0.1	1	10	0.1	1	10
				ω_p					
S_{C_1}	-0.50	-0.50	-0.50	-0.50	-0.50	-0.50	-0.50	-0.50	-0.50
S_{C_2}	-0.50	-0.50	-0.50	-0.50	-0.50	-0.50	-0.50	-0.50	-0.50
$\boldsymbol{S_{G_2}}$	**0.52**	**0.52**	**0.52**	**0.68**	**0.68**	**0.68**	**1.50**	**1.50**	**1.50**
S_{G_4}	0.43	0.33	0.24	0.41	0.32	0.23	0.33	0.26	0.21
S_{G_5}	0.07	0.17	0.26	0.09	0.18	0.27	0.17	0.24	0.29
$\boldsymbol{S_{G_6}}$	**-0.02**	**-0.02**	**-0.02**	**-0.18**	**-0.18**	**-0.18**	**-1.00**	**-1.00**	**-1.00**
S_{G_B}	-0.02	-0.02	-0.02	-0.18	-0.18	-0.18	-1.00	-1.00	-1.00
S_{G_C}	0.02	0.02	0.02	0.17	0.17	0.17	0.91	0.91	0.91
S_{G_D}	0.00	0.00	0.00	0.02	0.02	0.02	0.09	0.09	0.09
$\sum \lvert S \rvert$	2.08	2.08	2.08	2.73	2.73	2.73	6.00	6.00	6.00
				ω_z					
S_{C_1}	-0.50	-0.50	-0.50	-0.50	-0.50	-0.50	-0.50	-0.50	-0.50
S_{C_2}	-0.50	-0.50	-0.50	-0.50	-0.50	-0.50	-0.50	-0.50	-0.50
$\boldsymbol{S_{G_2}}$	**0.87**	**0.87**	**0.87**	**1.14**	**1.14**	**1.14**	**2.50**	**2.50**	**2.50**
S_{G_4}	0.43	0.33	0.24	0.41	0.32	0.23	0.33	0.26	0.21
S_{G_5}	0.07	0.17	0.26	0.09	0.18	0.27	0.17	0.24	0.29
$\boldsymbol{S_{G_6}}$	**-0.37**	**-0.37**	**-0.37**	**-0.64**	**-0.64**	**-0.64**	**-2.00**	**-2.00**	**-2.00**
S_{G_B}	-0.04	-0.04	-0.04	-0.33	-0.33	-0.33	-1.83	-1.83	-1.83
S_{G_C}	0.37	0.37	0.37	0.64	0.64	0.64	2.00	2.00	2.00
S_{G_D}	-0.33	-0.33	-0.33	-0.30	-0.30	-0.30	-0.17	-0.17	-0.17
$\sum \lvert S \rvert$	3.46	3.46	3.46	4.54	4.54	4.54	9.99	9.99	9.99
				Q_p					
$\boldsymbol{S_{C_1}}$	**-0.40**	**0.01**	**0.42**	**-0.37**	**0.06**	**0.47**	**-0.21**	**0.36**	**0.83**
S_{C_2}	0.40	-0.01	-0.42	0.37	-0.06	-0.47	0.21	-0.36	-0.83
S_{G_2}	-0.59	-0.53	-0.53	-1.32	-0.83	-0.77	-7.97	-3.66	-2.89
$\boldsymbol{S_{G_4}}$	**0.56**	**0.51**	**0.51**	**0.97**	**0.61**	**0.56**	**2.66**	**1.22**	**0.97**
S_{G_5}	0.49	0.34	0.24	0.79	0.39	0.26	1.75	0.64	0.40
S_{G_6}	0.08	0.17	0.27	0.18	0.22	0.31	0.91	0.58	0.57
S_{G_B}	0.02	0.02	0.02	0.35	0.22	0.20	5.31	2.44	1.93
$\boldsymbol{S_{G_B}}$	**0.09**	**0.03**	**0.03**	**0.82**	**0.33**	**0.27**	**7.47**	**3.16**	**2.39**
S_{G_C}	-0.08	-0.03	-0.02	-0.74	-0.30	-0.24	-6.79	-2.87	-2.18
S_{G_D}	-0.01	0.00	0.00	-0.07	-0.03	-0.02	-0.68	-0.29	-0.22
$\sum \lvert S \rvert$ excl. S_{G_1}	2.15	1.14	1.94	5.00	2.45	3.01	31.32	14.36	12.24
				Q_z					
$\boldsymbol{S_{C_1}}$	**-0.44**	**-0.17**	**0.09**	**-0.41**	**-0.14**	**0.13**	**-0.31**	**0.06**	**0.36**
S_{C_2}	0.44	0.17	-0.09	0.41	0.14	-0.13	0.31	-0.06	-0.36
$\boldsymbol{S_{G_2}}$	**-0.33**	**-0.27**	**-0.27**	**-1.02**	**-0.50**	**-0.43**	**-7.74**	**-3.08**	**-2.25**
$\boldsymbol{S_{G_4}}$	**1.09**	**0.43**	**0.28**	**1.27**	**0.48**	**0.30**	**2.18**	**0.75**	**0.45**
$\boldsymbol{S_{G_5}}$	**-0.90**	**-0.27**	**-0.12**	**-0.82**	**-0.26**	**-0.10**	**-0.63**	**-0.13**	**0.00**
S_{G_6}	0.14	0.11	0.11	0.57	0.28	0.24	6.19	2.46	1.80
S_{G_B}	0.08	0.02	0.01	0.75	0.23	0.16	7.37	2.71	1.88
$\boldsymbol{S_{G_C}}$	**-0.80**	**-0.21**	**-0.15**	**-1.44**	**-0.44**	**-0.31**	**-8.04**	**-2.95**	**-2.05**
S_{G_D}	0.72	0.19	0.14	0.68	0.21	0.15	0.67	0.25	0.17
$\sum \lvert S \rvert$	4.94	1.86	1.26	7.40	2.68	1.95	33.43	12.45	9.34

Table C.3: Sensitivities of the frequency and Q-factor of the poles and zeros of Friend's circuit with respect to component tolerances for n_2 = 0.99 (R_C/R_D = 1/100).

	G_B/G_A=0.01			G_B/G_A=0.1			G_B/G_A=1		
C_2/C_1	0.1	1	10	0.1	1	10	0.1	1	10
				ω_p					
S_{C_1}	-0.50	-0.50	-0.50	-0.50	-0.50	-0.50	-0.50	-0.50	-0.50
S_{C_2}	-0.50	-0.50	-0.50	-0.50	-0.50	-0.50	-0.50	-0.50	-0.50
$\boldsymbol{S_{G_2}}$	**0.47**	**0.36**	**0.26**	**0.45**	**0.35**	**0.25**	**0.36**	**0.28**	**0.22**
S_{G_4}	0.70	0.70	0.70	2.32	2.32	2.32	10.49	10.49	10.49
S_{G_5}	-0.20	-0.20	-0.20	-1.82	-1.82	-1.82	-9.99	-9.99	-9.99
$\boldsymbol{S_{G_6}}$	**0.03**	**0.14**	**0.24**	**0.05**	**0.15**	**0.25**	**0.14**	**0.22**	**0.28**
S_{G_B}	-0.20	-0.20	-0.20	-1.82	-1.82	-1.82	-9.99	-9.99	-9.99
S_{G_C}	0.20	0.20	0.20	1.80	1.80	1.80	9.89	9.89	9.89
S_{G_D}	0.00	0.00	0.00	0.02	0.02	0.02	0.10	0.10	0.10
$\sum \lvert S \rvert$	2.79	2.79	2.79	9.26	9.26	9.26	41.96	41.96	41.96
				ω_z					
S_{C_1}	-0.50	-0.50	-0.50	-0.50	-0.50	-0.50	-0.50	-0.50	-0.50
S_{C_2}	-0.50	-0.50	-0.50	-0.50	-0.50	-0.50	-0.50	-0.50	-0.50
$\boldsymbol{S_{G_2}}$	**1.16**	**1.16**	**1.16**	**3.86**	**3.86**	**3.86**	**17.47**	**17.47**	**17.47**
S_{G_4}	0.47	0.36	0.26	0.45	0.35	0.25	0.36	0.28	0.22
S_{G_5}	0.03	0.14	0.24	0.05	0.15	0.25	0.14	0.22	0.28
$\boldsymbol{S_{G_6}}$	**-0.66**	**-0.66**	**-0.66**	**-3.36**	**-3.36**	**-3.36**	**-16.97**	**-16.97**	**-16.97**
S_{G_B}	-0.33	-0.33	-0.33	-3.05	-3.05	-3.05	-16.80	-16.80	-16.80
S_{G_C}	0.66	0.66	0.66	3.36	3.36	3.36	16.97	16.97	16.97
S_{G_D}	-0.33	-0.33	-0.33	-0.30	-0.30	-0.30	-0.17	-0.17	-0.17
$\sum \lvert S \rvert$	4.65	4.65	4.65	15.43	15.43	15.43	69.87	69.87	69.87
				Q_p					
$\boldsymbol{S_{C_1}}$	**-0.40**	**0.01**	**0.42**	**-0.37**	**0.06**	**0.47**	**-0.21**	**0.36**	**0.83**
S_{C_2}	0.40	-0.01	-0.42	0.37	-0.06	-0.47	0.21	-0.36	-0.83
S_{G_2}	-0.79	-0.71	-0.71	-4.47	-2.83	-2.61	-55.80	-25.62	-20.26
$\boldsymbol{S_{G_1}}$	**0.56**	**0.51**	**0.51**	**0.97**	**0.61**	**0.56**	**2.66**	**1.22**	**0.97**
S_{G_4}	0.53	0.37	0.26	0.86	0.42	0.28	1.91	0.70	0.43
S_{G_5}	0.04	0.14	0.25	0.10	0.19	0.28	0.75	0.53	0.53
S_{G_6}	0.22	0.20	0.20	3.51	2.22	2.05	53.14	24.39	19.29
$\boldsymbol{S_{G_B}}$	**0.29**	**0.21**	**0.21**	**3.97**	**2.33**	**2.11**	**55.30**	**25.12**	**19.76**
S_{G_C}	-0.28	-0.21	-0.21	-3.93	-2.31	-2.09	-54.75	-24.87	-19.56
S_{G_D}	0.00	0.00	0.00	-0.04	-0.02	-0.02	-0.55	-0.25	-0.20
$\sum \lvert S \rvert$ excl. S_{G_1}	2.96	1.87	2.66	17.63	10.44	10.39	222.63	102.18	81.70
				Q_z					
$\boldsymbol{S_{C_1}}$	**-0.44**	**-0.17**	**0.09**	**-0.41**	**-0.14**	**0.13**	**-0.31**	**0.06**	**0.36**
S_{C_2}	0.44	0.17	-0.09	0.41	0.14	-0.13	0.31	-0.06	-0.36
$\boldsymbol{S_{G_2}}$	**-0.44**	**-0.36**	**-0.36**	**-3.48**	**-1.71**	**-1.47**	**-54.17**	**-21.55**	**-15.76**
$\boldsymbol{S_{G_4}}$	**0.60**	**0.38**	**0.27**	**0.94**	**0.44**	**0.29**	**2.07**	**0.74**	**0.45**
$\boldsymbol{S_{G_5}}$	**-0.41**	**-0.23**	**-0.11**	**-0.49**	**-0.22**	**-0.10**	**-0.52**	**-0.12**	**0.00**
S_{G_6}	0.25	0.21	0.20	3.03	1.49	1.28	52.62	20.93	15.31
S_{G_B}	0.19	0.11	0.11	3.21	1.44	1.20	53.80	21.18	15.39
$\boldsymbol{S_{G_C}}$	**-0.38**	**-0.23**	**-0.21**	**-3.53**	**-1.58**	**-1.32**	**-54.33**	**-21.39**	**-15.54**
S_{G_D}	0.19	0.11	0.10	0.32	0.14	0.12	0.53	0.21	0.15
$\sum \lvert S \rvert$	3.34	1.98	1.55	15.83	7.29	6.02	218.67	86.23	63.33

C.2 Results of the optimisation procedure

Table C.4: Results obtained by maximising the 3dB-cutoff frequency of the third order concave filter when the undershoot occurring after the application of a 3 mV×100 ms rectangular input pulse is constrained to be less than 95 µV for different starting points.

START f_{3dB} (mHz)	f_{3dB} (mHz)	a_1 (rad/s)	a_0 ((rad/s)^2)	b_1 (rad/s)	b_0 ((rad/s)^2)	p_0 (rad/s)	p (rad/s)	z (rad/s)
Butterworth								
10	54.13	1.3031	0.1108	0.4409	0.0294	1.1828	sub-optimal	
30	83.92	1.0618	0.5644	1.1293	0.8506	0.2085	-0.2085	0
							-0.5647 $\pm j$ 0.7292	-0.5309 $\pm j$ 0.5316
50	71.32	1.8828	0.4893	1.1393	0.1529	1.0054	sub-optimal	
70	not converging							
90	83.92	1.0626	0.5651	1.1299	0.8516	0.2085	-0.2085	0
							-0.5649 $\pm j$ 0.7297	-0.5313 $\pm j$ 0.5318
110	83.92	1.0613	0.5640	1.1290	0.8501	0.2084	-0.2084	0
							-0.5645 $\pm j$ 0.7290	-0.5307 $\pm j$ 0.5314
130	not converging							
150	83.92	1.0616	0.5643	1.1292	0.8504	0.2085	-0.2085	0
							-0.5646 $\pm j$ 0.7291	-0.5308 $\pm j$ 0.5315
Chebyshev (R_p = 0.5 dB)								
10	not converging							
30	83.92	1.0619	0.5645	1.1294	0.8508	0.2085	-0.2085	0
							-0.5647 $\pm j$ 0.7293	-0.5310 $\pm j$ 0.5316
50	83.92	1.0623	0.5649	1.1297	0.8513	0.2085	-0.2085	0
							-0.5648 $\pm j$ 0.7296	-0.5312 $\pm j$ 0.5317
70	83.92	1.0619	0.5645	1.1294	0.8507	0.2085	-0.2085	0
							-0.5647 $\pm j$ 0.7293	-0.5309 $\pm j$ 0.5316
90	59.98	1.0433	0.3506	1.1248	0.4627	0.2380	sub-optimal	
110	83.92	1.0623	0.5648	1.1296	0.8512	0.2085	-0.2085	0
							-0.5648 $\pm j$ 0.7295	-0.5311 $\pm j$ 0.5317
130	83.92	1.0626	0.5651	1.1298	0.8516	0.2085	-0.2085	0
							-0.5649 $\pm j$ 0.7297	-0.5313 $\pm j$ 0.5318
150	83.92	1.0626	0.5651	1.1299	0.8516	0.2085	-0.2085	0
							-0.5649 $\pm j$ 0.7297	-0.5313 $\pm j$ 0.5318
Elliptic (R_p = 0.5 dB, A_s = 40 dB)								
10	83.92	1.0617	0.5643	1.1292	0.8505	0.2085	-0.2085	0
							-0.5646 $\pm j$ 0.7292	-0.5308 $\pm j$ 0.5315
30	83.92	1.0619	0.5645	1.1294	0.8508	0.2085	-0.2085	0
							-0.5647 $\pm j$ 0.7293	-0.5310 $\pm j$ 0.5316
50	not converging							
70	83.92	1.0617	0.5644	1.1293	0.8506	0.2085	-0.2085	0
							-0.5646 $\pm j$ 0.7292	-0.5309 $\pm j$ 0.5315
90	83.92	1.0628	0.5653	1.1300	0.8519	0.2085	-0.2085	0
							-0.5650 $\pm j$ 0.7298	-0.5314 $\pm j$ 0.5319
110	83.92	1.0619	0.5645	1.1294	0.8508	0.2085	-0.2085	0
							-0.5647 $\pm j$ 0.7293	-0.5310 $\pm j$ 0.5316
130	not converging							
150	71.22	1.9553	0.5375	1.1777	0.1641	1.0290	sub-optimal	